DUAL S- AND K_U-BAND TRACKING FEED FOR A TDRS REFLECTOR ANTENNA

Tradeoff Study

J.C. Pullara, C.W. Bales, G.P. Kefalas and M. Uyehara
Martin Marietta Aerospace Corporation
P.O. Box 5837
Prlando, Florida 32805

August 1974
Final Report (Phase I) for Period August 1973 - June 1974

Prepared for

NASA
GODDARD SPACE FLIGHT CENTER
Greenbelt, Maryland 20771

Report No. Final (Phase I)	2. Government Accession No.	3. Recipient's Catalog No.
Title and Subtitle DUAL S- AND K_U-BAND TRACKING FEED FOR A TDRS REFLECTOR ANTENNA		5. Report Date August 1974 6. Performing Organization Code
Author(s) Joseph C. Pullara, C. William Bales, George P. Kefalas, and Masao Uyehara		8. Performing Organization Report No. OR 13,225
Performing Organization Name and Address Martin Marietta Aerospace Corporation P.O. Box 5837 Orlando, Florida 32805		10. Work Unit No. 11. Contract or Grant No. NAS5-20415
Sponsoring Agency Name and Address NASA, L.R. Dod (Project Manager) GODDARD SPACE FLIGHT CENTER Greenbelt, Maryland 20771		13. Type of Report and Period Covered Phase I Final Report August 1973 - June 1974 14. Sponsoring Agency Code
Supplementary Notes		

Abstract

This report presents the results of a trade study designed to identify a synchronous satellite antenna system suitable for receiving and transmitting data from lower orbiting satellites at both S- and K_U-bands simultaneously as part of the Tracking and Data Relay Satellite System (TDRSS). The study addresses all related problems associated with maintaining a data link between two satellites with a K_U-band half-power beamwidth of 0.4 dB. Specifically, the study addresses data link maintenance techniques, beam pointing accuracies, gimbal and servo errors, solar heating, angle tracking schemes, acquisition problems and aids, tracking accuracies versus SNR, antenna feed designs, equipment designs, weight and power budgets, and detailed candidate antenna system designs.

Key Words (Selected By Author(s)) Satellite antenna Dual frequency Erectable reflectors Beam steering Auto tracking Acquisition Monopulse feed	18. Distribution Statement		
Security Classif. (of this report) Unclassified	20. Security Class. (of this page) Unclassified	21. No. of Pages 350	22. Price*

PREFACE

The purpose of this task is to define the optimum antenna system for the synchronous altitude Tracking and Data Relay Satellite (TDRS) Antenna for communication with lower orbit user spacecraft, and to demonstrate its performance through evaluation of a breadboard model of the antenna. The antenna system shall include the reflector, feeds, pointing mechanism, and tracking subsystems. This effort is divided into two phases. Phase I (reported herein) is a tradeoff study of conceptual antenna systems to determine one or more preferred designs for optimization of communication capability consistent with minimizing the equipment and complexity of TDRS. Phase II is the detailed hardware design, fabrication, test, and delivery of the preferred design for a reflector with minimum diameter of 12.5 feet.

The S- and K_u-band beams simultaneously generated in the 12.5 foot reflector antenna must be steered throughout a 30-degree cone centered on the local radius. Four S-band options were addressed relating to the capability to independently steer the S-band beam relation to the K_u-band beam and the auto tracking capability of the S-band feed system. The tradeoff study involved detailed analysis on beam pointing via ground commands, auto tracking, acquisition, SNR impact, angle sensing feed systems, mechanical designs, weight, and power consumption.

The preferred candidate recommended for Phase II breadboard design and testing is a 12.5 foot erectable reflector system of the cassegrain design. The K_u-band feed is located at the secondary focal point and is comprised of a five horn array. The center horn is optimized to achieve the required gain and is used only for data reception and transmission. The other four horns are configured as a monopulse array for angle sensing and auto tracking. The tracking array is defocused in order to generate a wider field of view required for acquisition of the user satellites. The S-band feed is a simple cupped helix antenna located at the primary focal point of the reflector. Both feeds can operate simultaneously due to the dual frequency characteristics of the dichroic subreflector. Both S- and K_u-band beams are fixed with respect to the reflector and are steered by gimballed movement of the complete reflector relative to the satellite.

CONTENTS

ILLUSTRATIONS

ILLUSTRATIONS (Continued)

ILLUSTRATIONS (Continued)

ILLUSTRATIONS (Continued)

TABLES

TABLES (Continued)

1.0 INTRODUCTION

This document is the Phase I Final Report for work performed under NASA Contract No. NAS5-20415, the Dual S- and K_u-Band Tracking Feed for a TDRS Reflector Antenna. This report covers the period from 21 August 1973 to 7 June 1974. The following is a brief background of the Tracking and Data Relay Satellite System (TDRSS) concept (Reference 1).

NASA's current method of tracking and receiving data from spacecraft consists of a series of ground stations located around the world. This network of stations, in addition to an aircraft and a ship, is called the Spaceflight Tracking and Data Network (STDN) and is managed and operated by Goddard Space Flight Center (GSFC). The major functions of the STDN are to:

1. Track spacecraft and relay launch and trajectory data in real time from spacecraft to control centers;
2. Relay commands from control centers to spacecraft;
3. Relay telemetry and TV signals both in real-time and in store-and-forward modes from spacecraft to control centers;
4. Relay voice communications between control centers and spacecraft;
5. Augment recovery communications, as required.

Although the STDN provides sophisticated tracking and data acquisition support to earth orbiting spacecraft, it does have such limitations as spacecraft access time, geographic coverage, and information bandwidth, which impose design and operational constraints on the user spacecraft. To reduce these limitations, as well as to minimize the overall cost of tracking and data acquisition, NASA has investigated the use of a TDRSS to augment the STDN.

The TDRSS concept consists of two geosynchronous satellites, 130 degrees apart in longitude, which will relay tracking, telemetry, and command data between the Earth-orbiting user spacecraft, and a ground terminal located at White Sands Test Facility, New Mexico. This concept also provides two spare satellites: one in orbit, and the other in configuration for a rapid launch. A "bent-pipe" concept is used in the design of the telecommunications service system, i.e., all communication signals received at the TDRSS are translated in frequency and retransmitted, making possible almost continuous reception of data in real time.

The purpose of this task is to determine the optimum antenna system, using a dual S- and K_u-band tracking feed for the synchronous

altitude TDRSS reflector antenna, for communication with lower orbit user spacecraft. The overall TDRSS antenna system to be optimized consists of the reflector, feed, pointing mechanism, and tracking subsystems.

The total task effort is divided into two phases. Phase I is a tradeoff study to determine one or more preferred antenna system designs consistent with minimization of TDRSS equipment and equipment complexity. Phase II, which follows, will address the design, fabrication, test, and delivery of a preferred breadboard antenna subsystem (feed and reflector) design for a reflector with a minimum diameter of 12.5 feet. This report addresses Phase I only.

The antenna system must produce two simultaneous beams: one at S-band and one at K_u-band. These beams must be steerable throughout a 30 degree cone centered about the local nadir without any compromise to RF performance criteria. An antenna system that will provide independent and simultaneous S- and K_u-band beam steering is desirable. It is recognized that this capability may entail some degradation in RF performance along with additional complexity; therefore, this study will be aimed at providing numerical values on degradation and complexity from which meaningful trades and selections can be made.

The basic intent of this study is to select S- and K_u-band reflector/feed candidates for various S-band feed options, which comprise techniques, components, and materials that will provide trouble-free operation for five years in space. Furthermore, design, fabrication, and testing of these candidates should be possible in sufficient time to assure a TDRS launch by 1978. The following S-band feed options are considered:

1. Option I - The S-band beam is fixed to the reflector axis and has no auto tracking capability;
2. Option II - The S-band beam is fixed to the reflector axis and has the capability of generating auto tracking error signals;
3. Option III - The S-band beam is steerable with respect to the reflector axis via ground command, i.e., has no auto tracking capability;
4. Option IV - The S-band beam is steerable with respect to the reflector axis via auto tracking.

The study is limited to reflector/feed combinations and is further restricted to reflector configurations which are of proven design for erection and operation in a space environment. In particular, identification of an antenna system compatible with a 12.5-foot diameter reflector designed, fabricated, and tested by Radiation, Inc. is desirable. If testing verifies the claims, this reflector would represent the state of the art in erectable space-qualified reflectors suitable for K_u-band operation.

The major TDRSS constraints and characteristics which influenced the Phase I tradeoff study are summarized in Table I. The criteria for evaluating and screening candidate antenna systems are presented in Table II ("Musts") and Table III ("Wants"). The "Musts" are non-negotiable requirements; failure to fulfill any one of these requirements automatically eliminates the candidate from further consideration. The "Want" requirements are negotiable; therefore, their desirability is reflected in the relative weight associated with each item. The listing of "Musts" and "Wants" was developed from the Statement of Work and several discussions with the NASA Technical Officer.

This report provides a comprehensive summary of the work performed in Phase I. A summary of this Phase I report is contained in section 2.0, including a brief description of the resulting preferred candidate antenna system for each of the S-band feed options. Each of the selected antenna systems has a K_u-band data-beam and independent K_u-band auto tracking beams fixed on the reflector axis.

A detailed description of the preferred TDRS antenna system candidate for each of the above options is given in section 3.0. Design and performance capabilities and characteristics of each candidate are referenced to a defined set of TDRSS baseline characteristics, and the criteria for their selection are given. The supporting analyses which provide the justification for the selection of the preferred antenna candidates, and the tradeoff data and tools by which further selection could be made by the TDRSS designer, are contained in section 4.0. Finally, this contractor's recommendations for further analytical and/or developmental efforts are given in section 5.0.

TABLE I

Basic TDRSS Requirements, Objectives, and Constraints

Requirements

Select a candidate S- and K_u-band antenna system for each of S-band feed Options I, II, III, and IV

Circular polarization

Frequency:

S-band
2200-2300 MHz (receive)
2025-2120 MHz (transmit)

K_u-band
14.4-15.35 GHz (receive)
13.4-14.2 GHz (transmit)

TABLE I (Continued)

Autotrack on CW beacon signal from user with SNR defined in IF bandwidth:

10 dB (max) in 1.0 MHz bandwidth at K_u-band

-14 dB (max) in 150 kHz bandwidth at S-band

Antenna gain (on-axis)

S-band:

35.4 dB (transmit)
36.0 dB (receive)

K_u-band:

52.0 dB (transmit)
52.6 dB (receive)

Objectives

Perform a trade study to select the best S- and K_u-band angle sensing and auto tracking techniques

Devise methods to perform onboard non-coherent processing at K_u-band; coherent processing via the ground station at S-band

Attempt to restrict the data channel losses, exclusive of those in the antenna, to:

0.5 dB due to angular beam pointing errors
2.0 dB due to component losses

Investigate the performance of four designation methods:

Direct ground station designation

S-band auto tracking system

K_u-band pencil beam search

K_u-band command beam broadening

Constraints

Reflector diameter: 12.5 ft

Delta 2914 launch vehicle envelope

User spacecraft orbital parameters

TDRS spacecraft stabilization

TABLE II

Musts for TDRS S/K_u Antenna System

1. Simultaneous Operation at S- and K_u-Bands

2. On-axis gain:
   (Receive)

   36 dB at S-band

   52.6 dB at K_u-band

   (Minimum aperture 12.5 feet diameter)

3. Reflector/feed antenna type

4. Compatible with TDRSS concept

   Synchronous satellite

   Delta launch vehicle (deployable)

5. K_u-band autotrack

6. $\pm$ 15 degrees Scan sector relative to local nadir

7. Five-year life

8. RF Power:

   50 watts S-band
   2 watts K_u-band

9. Circular polarization (S/K_u)

10. Provide a mode of operation to maintain the on-axis gain throughout 30 degree scan sector (not necessarily simultaneously)

11. Transmit and receive simultaneously:

S-band	2025-2120 MHz (transmit)	2200-2300 MHz (receive)
K_u-band	13.4-14.2 GHz (transmit)	14.4-15.35 GHz (receive)

12. Compatible with existing space-erectable reflector designs

TABLE III

Wants for TDRSS S/K_u Antenna System

	Weights
1. Compatible with Radiation, Inc., 12.5 foot reflector	10
2. Minimum risk, i.e., little that is not already state-of-the-art	10
3. Uninterrupted communications within the scan sector	10
4. Automatic, simple, and reliable K_u-band acquisition mode	10
5. Independent S and K_u-band beam steering	9
6. Maximum gain versus off-axis beam steering	8
7. Minimum spacecraft complexity and components	7
8. Minimum weight	3
9. Minimum power consumption	3
10. Minimum mechanical movement	5

2.0 SUMMARY

This Phase I tradeoff study resulted in the selection of a preferred conceptual antenna system design, with the optimized communication capability and minimized TDRS equipment complexity for each of the S-band feed options. The baseline performance and operational characteristics of the preferred antenna candidates are referenced to the TDRSS requirements, objectives, and constraints set forth in Table I, and as derived from the Statement of Work, its attachments, and from technical discussions and direction of the NASA program manager. The candidate antennas were selected with due consideration of data link performance, state of the art and availability of space-qualified designs, TDRSS equipment simplicity/operational flexibility/operational redundancy, and reliability of establishing and maintaining a data link. A tabular description of the preferred antenna candidates follows.

Option I Preferred Candidate

1. Dual reflector cassegrain configuration
2. 12.5-foot parabolic reflector
3. 17-inch dichroic hyperbolic subreflector
4. S-band feed at primary focal point
5. K_u-band dedicated data feed at secondary focal point
6. K_u-band defocused tracking feed at secondary focal point
7. S- and K_u-band colinear data beams, fixed relative to reflector axis, and pointed by two-axis gimbal
8. K_u-band data link maintenance via K_u-band autotrack monoscan receiver
9. S-band data link maintenance via programmed ground command.

Option II Preferred Candidate

1. Dual reflector cassegrain configuration
2. 12.5-foot parabolic reflector
3. 17-inch dichroic hyperbolic subreflector
4. S-band tracking feed at primary focal point
5. K_u-band dedicated data feed at secondary focal point
6. K_u-band defocused tracking feed at secondary focal point

7 S- and K_u-band colinear data beams, fixed relative to reflector axis, and pointed by two-axis gimbal

8 K_u-band data link maintenance via K_u-band autotrack monoscan receiver

9 S-band data link maintenance via S-band autotrack receiver (two-channel Σ/Δ monopulse with coherent angle sensor at ground station).

Option III Preferred Candidate

1 Dual reflector cassegrain configuration

2 12.5-foot (diameter) spherical reflector with 11-foot radius

3 17-inch dichroic subreflector, shaped for correction of K_u-band spherical aberration

4 S-band feed movable about primary focal point

5 K_u-band dedicated data feed fixed at secondary focal surface

6 K_u-band defocused tracking feed fixed at secondary focal point

7 S- and K_u-band data beams steerable simultaneously and independently; K_u-band data beam fixed relative to reflector axis and pointed by two-axis gimbal; S-band beam pointed by moving feed on spherical focal surface

8 K_u-band data link maintenance via K_u-band autotrack monoscan receiver

9 S-band data link maintenance via programmed ground command.

Option IV Preferred Candidate

1 Dual reflector cassegrain configuration

2 12.5-foot (diameter) spherical reflector with 11-foot radius

3 17-inch dichroic subreflector, shaped for correction of K_u-band spherical aberration

4 S-band shared data/tracking feed movable about primary focal surface

5 K_u-band dedicated data feed fixed at secondary focal point

6 K_u-band defocused tracking feed fixed at secondary focal point

7 S- and K_u-band data beams steerable simultaneously and independently; K_u-band data beam fixed relative to reflector axis and pointed by two-axis gimbal; S-band beam pointed by moving feed on spherical focal surface

8 K_u-band data link maintenance via K_u-band autotrack monoscan receiver

9 S-band data link maintenance via S-band autotrack receiver (at ground station).

For data link maintenance via S-band auto tracking (in Options II and IV), successful closing of the tracking loop is preceded by reflector pointing using commands from the ground station. In the case of data link maintenance via K_u-band auto tracking (all options), the same designation method can be employed; however, two other methods are also available. In Option II, the S-band auto tracking system can be utilized for aided designation if the user provides an S-band beacon. A less desirable aided designation alternative is the use of a systematic spatial search with a K_u-band pencil beam formed either by the dedicated data channel or the defocused K_u-band tracking system.

Various angle sensing techniques were investigated and evaluated for S- and K_u-band auto tracking. These techniques were evaluated and compared on the basis of their thermal noise contribution to data beam pointing error, insertion loss and intermodulation effects introduced to the data signal, relative complexity and power consumption, compatibility with a suitable tracking feed, and adaptability to coherent angle tracking at the ground station. As a result, the following baseline angle sensors are recommended:

1 S-band - 2-Channel Σ and Δ monopulse with a dual-mode four-arm spiral feed/comparator assembly at primary focal point of reflector;

2 K_u-band - Single-channel monoscan with a five-horn feed/comparator assembly at secondary focal point of reflector; focused central element feeds dedicated data channel, and defocused peripheral elements for wide FOV angle sensor.

The need for coherent angle tracking in the S-band is dictated by the user's EIRP, which delivers a low carrier-to-noise ratio at the TDRS input. Investigations showed that coherent angle tracking via a ground station receiver will require somewhat complex and sophisticated equipment aboard the TDRS for preconditioning of the Σ and Δ downlink signals and for detecting the uplink error signals. If a coherent angle tracking receiver using swept phase-lock techniques can be made sufficiently reliable for use aboard the TDRS (rather than at the ground station), relatively less TDRS equipment will be required.

Although tradeoffs between Options I, II, III, and IV are outside the scope of this study, the results of this task clearly show that Options II and IV need not be considered further for the TDRSS because S-band auto tracking is required neither as a designation aid (for K_u-band data-beam

pointing) nor for S-band data-beam pointing. In fact, early considerations of these factors and the relative complexity required to implement Option IV dictated the limited treatment of Option IV in this program. Therefore, the remaining choice between Options I and III would be dictated by the importance of simultaneous and independent beamsteering for the TDRSS.

The necessary design tools and data for tradeoffs between options and within each option were generated to enable the TDRSS designer sufficient flexibility in selecting an option and in varying its performance with respect to the baseline characteristics. In particular, the contributions to data beam pointing error are defined and analytical expressions are provided wherever applicable. Tradeoff data of data beam pointing error as a function of servo noise bandwidth, with carrier-to-noise ratio (proportional to user beacon power) and servo torque disturbance as variables, were generated for both S- and K_u-band auto tracking modes of data link maintenance.

Finally, based upon the analyses and results of the Phase I tradeoff study, specific areas of additional activity are recommended in support of the forthcoming design and fabrication effort (Phase II), depending upon the final choice of S-band feed option (See section 5.0).

3.0 PREFERRED ANTENNA SYSTEM CANDIDATES

In this section a preferred TDRS antenna system candidate is presented for each of the four possible options described earlier. The design, performance, capabilities, and characteristics of these candidates are referenced to the baseline characteristics of the TDRSS (reference 2) as summarized in Table I. It will be shown that each of the candidates can be made to operate within the constraints of the TDRSS characteristics and each of the designs are within the current state of the art. These candidates were selected based on performance, current state of the art designs, TDRSS equipment simplicity, operational flexibility, redundant modes of operation, user equipment simplicity, and reliability of establishing and maintaining a data link. The supporting analysis contained in section 4.0 provides the justification for the selection of these candidates and the tools by which further trades could be made either within an option or between options. From these supporting analyses trades could be made on the following:

1. Safety margin of the acquisition beamwidth versus auto tracking SNR
2. Autotrack SNR and accuracy versus user transmit power
3. S-band steering angle versus gain degradation.

3.1 Option I Candidate

3.1.1 Candidate Description

The preferred candidate for an Option I antenna system is shown in the sketch of Figure 1. This antenna is a dual reflector cassegrain system with a main parabolic reflector of 12.5-foot diameter and a dichroic hyperbolic subreflector 17 inches in diameter. The K_u-band feed located at the secondary focal point and the S-band feed positioned at the primary focal point produce colinear beams fixed with respect to the parabolic axis. The S- and K_u-band beams are pointed by means of a two axis gimbal which in essence points the complete antenna system.

A block diagram of the K_u-band feed system is shown in Figure 2. The center horn is aligned with the parabolic axis and is dedicated only to the reception and transmission of data; as such, it is optimized for maximum gain. The K_u-band auto tracking beams are provided by the four horn monopulse array. The four horn array is set slightly behind the focal plane to achieve a 1.5 to 1 beam broadening by feed defocusing. The widened beamwidth (about 0.6 degree) provides an FOV of about 1.2 degree and thus assures acquisition or a user satellite via ground command. A monoscan (TDM pseudomonopulse) angle sensing system is employed to achieve auto tracking of the user and thus maintain an efficient and continuous data link as long as the user is within view of the TDRS. The defocused K_u-band antenna tracking feed network achieves an

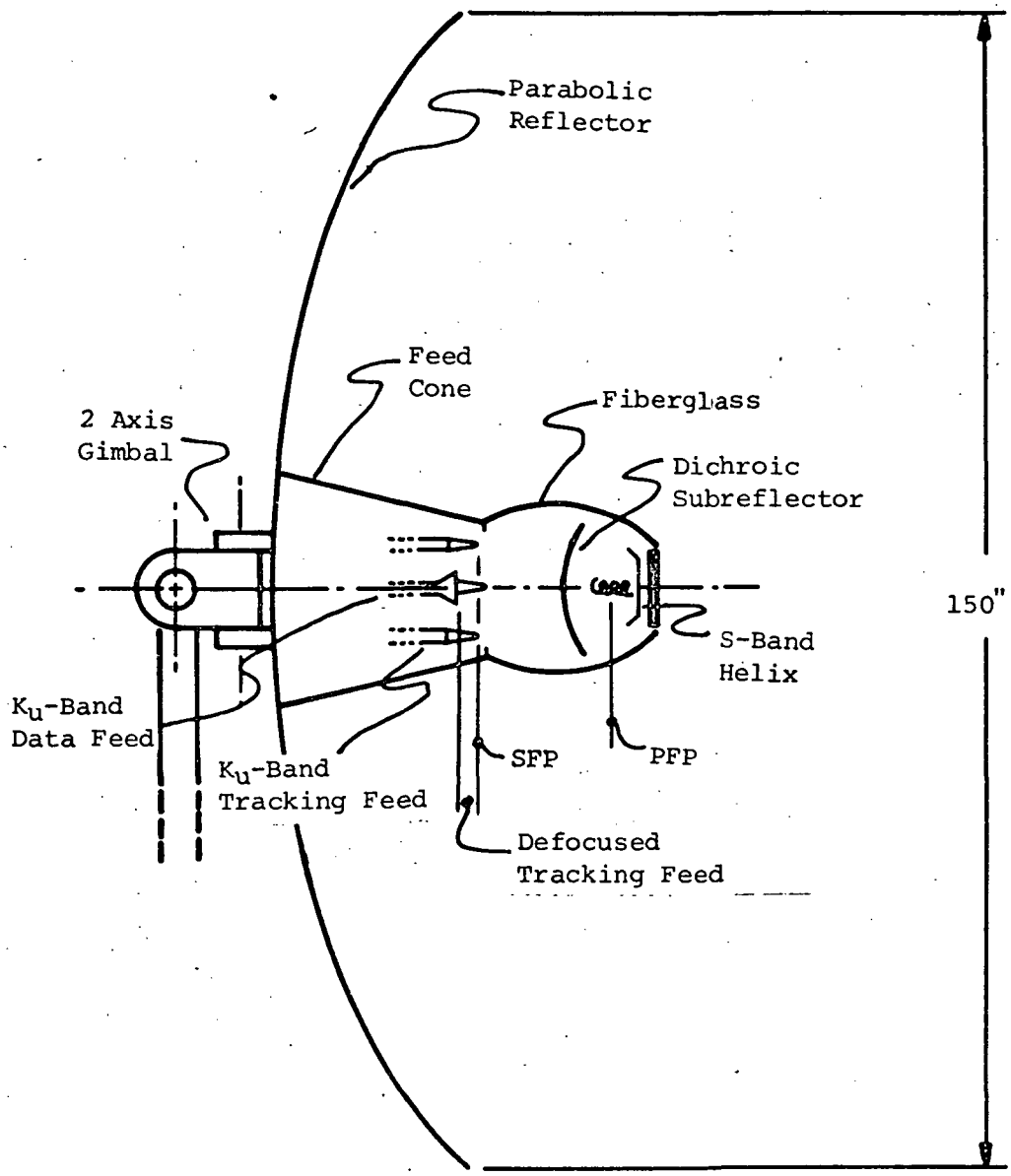

Figure 1. Preferred Candidate for Option I

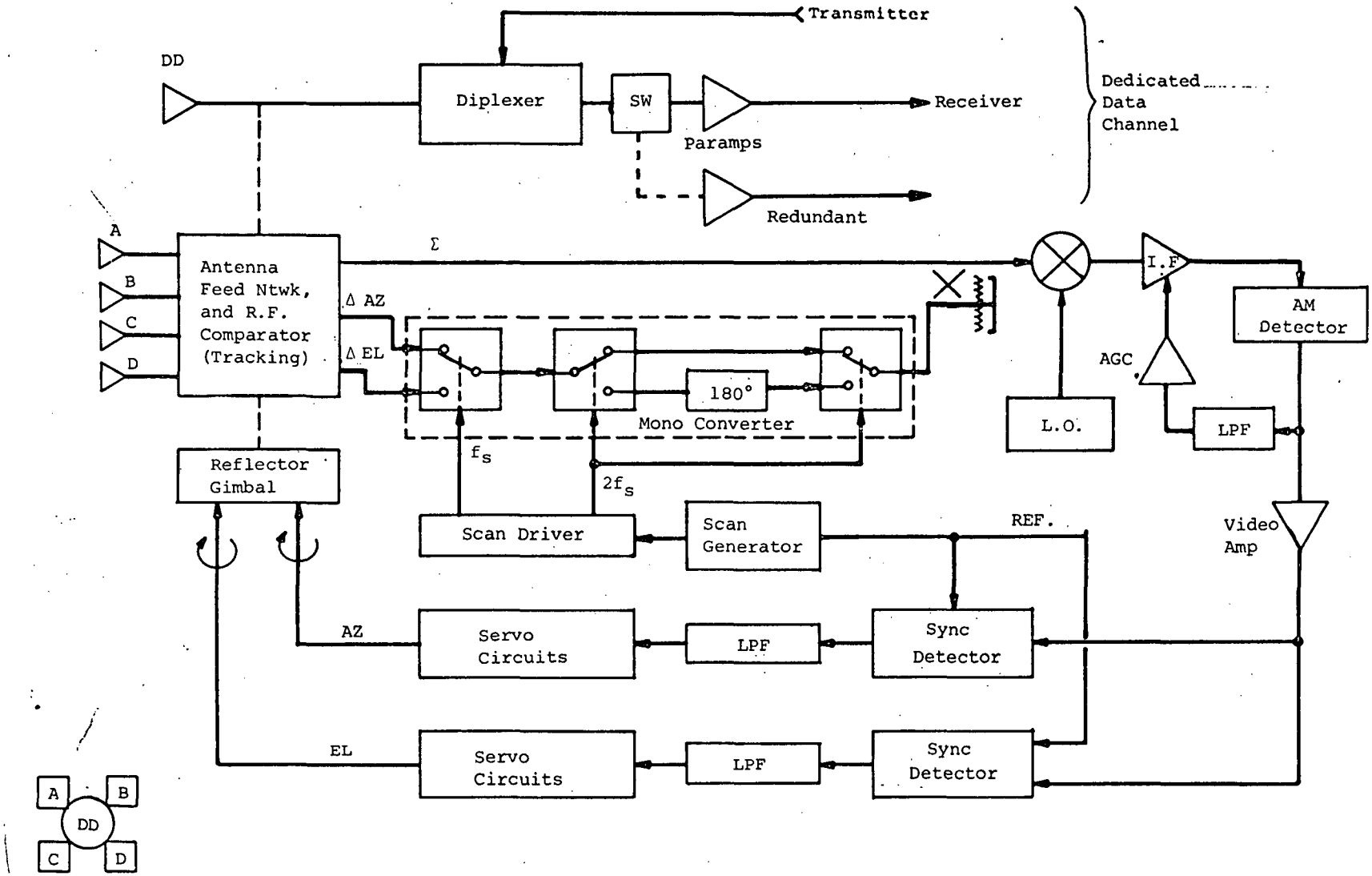

Figure 2. Block Diagram of the K_u-Band Feed System

SNR of about 5.7 dB (in a 1 MHz noise bandwidth), which is sufficient to point the data-beam toward the user to within an accuracy of ± 0.8 degree (3σ). This results in a ≤ 0.5 dB loss to the data signal, and, therefore, no provisions are made for refocusing the K_u-band tracking feed after initial acquisition.

The K_u-band data channel paramplifier, the S-band preamplifier, and the K_u-band tracking channel paramplifier and receiver are all contained in the feed cone behind the K_u-band feed. This location reduces the effect of RF transmission losses which would otherwise be experienced through 10 feet of waveguide/coax in bringing the received signal to the satellite equipment enclosure. Furthermore, locating these components in the feed cone reduces the requirements on multiple or multichannel rotary joints in the antenna gimbal. As envisioned, only one dual-channel K_u-band rotary joint is required in each of the two gimbal axes to carry the K_u-band transmit and post-paramplifier receive data signals between the feed and the satellite enclosure.

3.1.2 Operation and Capabilities

The operation and capabilities of the Option I antenna system depend on the characteristics and capabilities of the user satellites (see Table IV). Three user configurations have been postulated although more combinations could have been developed. It was assumed, however, that other combinations were either not very probable or that the added capabilities were obvious; e.g., if another user configuration has both K_u- and S-band data transmitters, then the added capability would be simultaneous S- and K_u-band two-way data links.

The step-track autotrack technique referred to in Table IV is a backup capability for K_u-band autotrack and can be implemented with ground terminal equipment with little or no impact on the TDRS antenna design. This technique operates by periodically stepping the TDRS antenna (via ground command) $\pm$ a small angular increment in each axis. By monitoring the small change in received signal level and applying an appropriate algorithm, an estimation of the source position, direction, and velocity can be made. (In a similar way, an operator can manually track a slow moving target.) This scheme is proposed as a backup, since at K_u-band it would require more movement of the antenna system (impacting TDRS attitude control, fuel consumption, power consumption, and gimbal wear), it is more susceptible to signal fluctuation, and is not believed capable of the tracking accuracies needed to maintain the high performance capacity of the K_u-band data link.

Other backup tracking and acquisition schemes for the K_u-band data link are given in Table IV, even though they are not as desirable as the preferred technique. However, in the event of a malfunction in the

preferred technique equipment, the backup system could be employed with reduced data link performance. No additional equipment is required on the ground or on the TDRS to implement the backup schemes.

Table V presents a recommended step by step procedure for establishing and maintaining a K_u-band data link for the Option I candidate antenna system. It should be noted that this procedure assumes that the user's K_u-band antenna is no larger than 2 feet in diameter and that it can be accurately command pointed so that the TDRS will be within its half-power beamwidth (2.5 degrees).

TABLE IV

TDRS Operational Capabilities of Option I Candidate

User Equipment	TDRS Operational Capabilities
User A S-band receiver K_u-band data transmitter and receiver	•K_u-band two-way data link •S- and K_u-band command link •K_u-band data link maintenance K_u-band autotrack (preferred) Ground controlled step-track (backup) •Designation for K_u-band autotrack Defocused (wide FOV) tracking feed (preferred) Scanning search (backup)
User B S-band data transmitter and receiver No K_u-band	•S-band two-way data link •S-band command link •S-band data link maintenance Preprogrammed ground commands (preferred) Ground controlled step-track (backup)

TABLE IV (Continued)

User C S-band beacon transmitter and receiver K_u-band data transmitter and receiver	• K_u-band two-way data link • S and K_u-band command links • K_u-band data link maintenance K_u-band autotrack (preferred) Ground controlled step-track on K_u-band signal (primary backup) Ground controlled step-track on S-band signal (reduced K_u-band data link performance) • Designation for K_u-band autotrack Defocused (wide FOV) tracking feeds (preferred) Scanning search (primary backup) Manual search on maximizing S-band signal
Multiple Users A and B or C and B	• Autotrack on User A or User C and maintain maximum performance K_u-band data link • Establish simultaneous S-band data link with User B with degraded performance dependent on the separation of the two satellites within the S-band beam

TABLE V

Designation and K_u-Band Autotrack Sequence (Option I)

Assumptions:

User has S-band command receiver with omnidirectional antenna.

User has K_u-band autotrack capability with 24-inch reflector with a 2.5 degree half-power beamwidth.

All commands are initiated at the ground terminal and transmitted through TDRS to user.

Automatic verification at ground terminal.

Sequence:

Step 1 - Ground computes TDRS/user relative look angles and commands TDRS to point antenna at the user ($\pm$0.45 degree accuracy).

Step 2 - User is commanded through S-band link to point its K_u-band antenna at TDRS (sufficient FOV and pointing accuracy to assure illumination of TDRS).

Step 3 - User is commanded (S-band) to turn on K_u-band transmitter (unmodulated).

Step 4 - a) If TDRS sees user K_u signal and if it meets criteria for autotrack, then TDRS automatically locks up and autotracks user.
b) If TDRS does not receive adequate signal conditions for autotrack, then ground initiates a TDRS antenna scanning search program until a lockup is achieved.

Step 5 - When TDRS autotrack is verified, TDRS is commanded to turn on K_u-band transmitter (unmodulated).

Step 6 - User locks up on TDRS and maintains autotrack.

Step 7 - TDRS S-band transmitter is turned off.

Step 8 - K_u-band data link is established and is ready for HDR transmission.

*Step 9 - When operation is complete, user is commanded to point K_u-band antenna to new coordinates of next anticipated contact. If user will not be picked up by second TDRS, then the last command will include directions to turn off the transmitter.

---

* Step 9 provides added insurance of re-establishing a link with the user should problems develop in the S-band link and conserves power otherwise consumed in turning on the TDRS S-band transmitter for initial user contact.

3.1.3 Performance

3.1.3.1 RF Performance for K_u- and S-Band

The details of the RF losses for Option I are presented in Tables VI and VII for the K_u-band and the S-band, respectively. The rationale and/or equations used to obtain the values as presented in the budget tables is as follows:

Aperture area gain $= \left(\frac{\pi D}{\lambda}\right)^2$

where D = diameter of main reflector in inches

λ = wavelength in inches.

Amplitude taper loss (Reference 3). Parameters assumed: 10 dB taper (A=0.3, B=0.7 and P=1.5).

Spillover loss (Reference 4).

Blockage values were calculated from following equation (References 5, 6, and 7):

*Loss $= 20 \log (1-\alpha)\left(1-\alpha \frac{1-q}{1+q}\right)$

where q = edge taper in voltage (=0.3)

α = area ratio of the blocking aperture to the unblocked aperture.

Subreflector S-band loss and K_u-band reflectivity values are experimental data (Reference 8).

Phase loss value was estimated (Reference 9).

Surface tolerance loss obtained from the following equation (Reference 10):

$$\frac{G}{G_o} = \text{loss in gain (dB)} = 10 \log\{\exp[-(\frac{4\pi d}{\lambda})^2]\}$$

where d = rms surface tolerance in inches

λ = wavelength in inches.

Mesh reflectivity loss and cross-polarization loss values (Reference 11).

Ogive (radome) loss (Reference 12).

---

* For K_u-band, optimizing the hyperbola subreflector shape increased the efficiency by 10 percentage points (Reference 23).

TABLE VI

RF Performance: K_u-Band (Options I, II, III, and IV)

Performance Factors	Dedicated Data Channel		Tracking Channel
	Transmit	Receive	Receive
Frequency (GHz)	13.7	14.9	14.9
Aperture diameters (meters)	3.81	3.81	3.81
Aperture area gain (dB)	54.41	55.50	55.50
Amplitude taper loss (dB)	0.53	0.53	0.53
Spillover loss (dB)	0.71	0.71	0.71
Blockage loss (dB)	0.23	0.23	0.23
Phase loss (dB)	0.05	0.05	0.05
Cross-polarization loss (dB)	0.05	0.05	0.05
Ogive loss (dB)	0.25	0.25	0.25
Subreflector reflectivity loss (dB)	0.50	0.50	0.50
Surface tolerance loss (dB)	0.37	0.44	0.44
Mesh reflectivity loss (dB)	0.09	0.09	0.09
Polyrod I^2R loss (dB)	0.09	0.13	0.13
Polarizer loss (dB)	0.20	0.20	0.20
Comparator loss (dB)	NA	NA	0.50
VSWR loss (dB), 1.30:1	0.07	0.07	0.07
Loss due to defocus (dB) 1.5 x BW	0	0	4.3
Total overall loss (dB)	3.14	3.25	8.05
Overall efficiency (percent)	48.5	47.3	15.7
Antenna peak gain (dB)*	51.3	52.3	47.5
Diplexer loss (dB)	0.60	0.60	NA
Azimuth rotary joint loss (dB)	0.10	NA	NA
Elevation rotary joint loss (dB)	0.10	NA	NA
Loss due to 10 feet WG to S/C (dB)	0.90	NA	NA
Redundancy switch loss (dB)	NA	0.20	NA
Half power beamwidth (degrees)	0.38	0.35	0.57
Polarization sense	Circular	Circular	Circular

*Assumes negligible gain degradation via mutual coupling effects caused by interfering effective apertures. Phase II measurements will determine the magnitude of these effects.

TABLE VII

RF Performance: S-Band (Option I)

Performance Factor	Transmit	Receive
Frequency (MHz)	2072.5	2250.0
Aperture diameter (meters)	3.81	3.81
Aperture area gain (dB)	38.36	39.07
Amplitude taper loss (dB)	0.46	0.46
Spillover loss (dB)	1.25	1.25
Blockage loss (dB)	0.18	0.18
Phase loss (dB)	0.13	0.13
Cross-polarization loss (dB)	0.11	0.11
Ogive loss (dB)	0.15	0.15
Subreflector loss (dB)	0.50	0.50
Surface tolerance loss (dB)	0.01	0.01
Mesh reflectivity loss (dB)	0.004	0.004
Feed antenna I^2R loss (dB)	0.05	0.05
Cable loss (dB), ant. to diplexer	0.30	0.30
VSWR loss (dB), 1.25:1	0.05	0.05
Total overall loss (dB)	3.19	3.19
Overall efficiency (percent)	48.0	48.0
Antenna peak gain (dB)	35.2	35.9
Diplexer loss (dB)	0.60	0.50
Cable loss to S/C interface (dB), 10 ft	0.75	NA
Cable wrap loss through gimbals (dB)	0.18	NA
Redundancy switch loss (dB)	NA	0.30
Half-power beamwidth (degrees)	2.53	2.33
Polarization sense	Circular	Circular

S-band cable loss from Times Wire and Cable data:

Flexi-tape, which has a loss of 0.065 dB/ft at 2.3 GHz. Cable loss values include connector-pair loss of 0.05 dB/pair. This cable is currently undergoing thermal vacuum tests for use on the GEOS (geodetic satellite).

VSWR loss calculated from the following equation (Reference 13):

$$\text{Loss} = 10 \log[1-|\Gamma|^2] \text{ , where } \Gamma \text{ is the reflection coefficient.}$$

Efficiency in percent calculated from $100 \times 10^{-(\frac{\text{loss in dB}}{10})}$

Half-power beamwidth (Reference 3): $\text{HPBW} = 1.162 \times 57.29578 \times \frac{\lambda}{D}$ degrees

where λ = wavelength in inches

D = parabola diameter in inches.

Component losses are either vendor data or estimated values.

K_u-band polyrod I^2R loss (Reference 14) is calculated as follows:

$$\text{Loss} = \frac{27.3}{\lambda} \sqrt{\varepsilon} \tan \delta \text{ dB/inch}$$

where ε = dielectric constant

λ = wavelength in inches

$\tan \delta$ = loss tangent

K_u-band polarizer and diplexer loss (Reference 15).

WR 62 (K_u-band) copper waveguide loss (Reference 16).

Loss due to defocus (Reference 17).

Comparator loss from vendor data: MDL, Needham Heights, Massachusetts.

K_u-band rotary joint loss was obtained from vendor data of an aluminum K_u-band dual axis, dual channel, rotary joint for Skylab. Vendor: MDL, Needham, Massachusetts.

Redundant switch loss value from vendor data: Microwave Associates, Burlington, Massachusetts.

S-Band antenna I^2R loss was estimated.

Table VI assumes that the degradation of gain caused by mutual coupling between data and tracking feeds is negligible. The Phase II effort will investigate these effects.

3.1.3.2 Data Beam Pointing Error

The 3σ data beam pointing accuracy and associated data signal loss for the preferred Option I candidate will be as follows for the ground command and auto tracking pointing modes:

TABLE VIII

Option I Data Beam Pointing Accuracy

Mode	3σ Pointing Accuracy (degrees)	Data Signal Loss (dB)	Reference
Ground command			
S-Band data link	±0.45	0.39	Table LII
K_u-band autotrack			
K_u-band data link	±0.054	0.22	Figure 87
S-band data link	<±0.160	<0.05	Figure 89

The above accuracies in the K_u-band autotrack mode are based on a maximum received beacon SNR = 5.7 dB, a 1 Hz servo bandwidth, and a servo torque disturbance factor of 10^{-3} sec^{-2}. Tradeoffs with variations in these parameters are given in the referenced plots. Ground command for the K_u-band data link would result in excessive (>15.2 dB) data signal loss and is therefore not considered for any of the candidates.

3.1.4 Feed Design Considerations

3.1.4.1 K_u-Band Feed System

The feed elements for the K_u-band tracking system are configured in a four element square cluster to develop the monopulse tracking signals. A separate element is centrally placed and is electrically separate from the four element cluster. This element is the dedicated data channel feed element. The four element cluster develops the azimuth and elevation tracking signals through a waveguide monopulse comparator network. This network consists basically of four hybrids for dividing the azimuth, elevation, and sum signals and outputting them to separate ports. The elevation and azimuth signals are fed to a monoscan converter network where proper combination and modulation are made of the error signals. The combination of this modulated error signal with the sum signal is then accomplished in the waveguide directional coupler, allowing the use of a single receiver instead of the conventional monopulse requirement of three separate receiver channels. The four element feed cluster is permanently defocused intentionally for the purpose of broadening the beam. The defocus will be in the axial direction, toward

the main reflector by 0.63 inch. This amount of defocus will increase the beamwidth from the focused case (0.38 degree) to the defocused case (0.57 degree). Theoretical analysis has been reported in the technical literature which showed the beam broadening to be monotonic as a function of the amount of defocus. Variations in slope, phase, and gain for a large amount of aperture phase deviation have been plotted for TDRS geometry and are presented in paragraph 4.5.4. Of specific concern here is the effect upon the monopulse tracking capability due to variations in the sum and difference pattern shapes. The monopulse sum and difference beamwidth increases and the slope decreases with defocusing.

The polyrod feed design is similar to the feed design of the 40-foot cassegrain tracking antenna for the ATS Mojave tracking facility. Further similarities between the 40-foot antenna and the TDRS antenna are presented in Table IX. These similarities are used throughout this

TABLE IX

Characteristics of ATS/Mojave and TDRS Antenna Systems

Characteristics	40-Foot ATS	12.5-Foot TDRS
f/D ratio	0.4	0.4
Main dish diameter in wavelengths	166.8 λ	181 λ
Location of feed from focal point	35.2 λ	33.9 λ
Equivalent parabola f/D ratio	1.899	1.660
Eccentricity (subreflector)	1.534	1.635

report in support of the proposed preferred candidates. Both primary and secondary patterns measured on the ATS antenna are employed to predict the FOV and tracking performance of the TDRS antenna. Other ATS measurements are employed to demonstrate predicted performance and design feasibility.

The four feed elements in the tracking feed cluster are separated by 1.6 λ. The polyrod dielectric is fabricated from teflon* whose length and diameter have been experimentally determined as 6 λ and 0.7 λ, respectively. The tapered section of the polyrod antenna is dependent upon the beamwidth, resulting in a primary illumination edge taper of 10 dB or slightly greater for optimum antenna efficiency. The polyrod will extend 1 inch into the circular feed waveguide and will consist of several step transitions for impedance matching over the frequency bandwidth of operation. The phase center of the four element monopulse feed cluster has been experimentally determined to be approximately 1.91 λ from the tip end of the polyrod.

The circular polarizer selected for use is an all metal periodic loaded pin type in circular waveguide. The input to the polarizer is in WR 62 rectangular waveguide; a two-step transition is used to match the rectangular input to the circular guide. Proper field orientation of the electric field relative to the opposing sets of "pins" of the polarizer is achieved by physical orientation of the transition at 45 degrees relative to the circular guide section pins. At the resonant frequency, a field parallel to the pins will be delayed in phase by 90 degrees with

*Satisfactory performance of teflon in space environment was confirmed by Messrs. Paul Swindall (NASA, MSFC) and L. Ferris (duPont).

respect to the field perpendicular to the pins. The following are reasons for the selection of the periodic all metal polarizer:

1 Lower polarization axial ratio is obtained over a greater bandwidth than in a dielectric design

2 Low input VSWR is easily obtained

3 Average power limitations are minimized

4 Lower insertion loss compared to dielectric polarizers.

The polarizer will be in a $0.72\lambda_o$ diameter circular waveguide, where λ_o is the band center free space wavelength. Periodic loading is provided by the thin metal pins equally spaced along the longitudinal axis of the waveguide. Ten pairs of pins spaced $0.266\lambda_o$ apart provide the necessary 90 degrees of differential phase shift.

The requirement for both S- and K_u-band simultaneous operational capability will be achieved by the utilization of a frequency sensitive or dichroic surface. The choice was made for the subreflector surface to have the property of being reflective at one frequency (K_u-band) and transparent at the second frequency (S-band). The reflective and transparent properties are dependent upon the configuration, orientation, and dimensions of the arrays of passive resonant elements. Experimental data has indicated that a crossed dipole configuration for the resonant element has provided the best RF properties for TDRS. This work was performed at NASA-GSFC during 1973, and the expected maximum reflective loss within the K_u-band of interest is 0.5 dB, while providing a 0.5 dB transmission loss at the S-band of interest.

The ogive radome for the feed-cone provides a means of supporting the dichroic subreflector without introducing strut blockages. Furthermore, the ogive must have a sufficiently high modulus of elasticity and impact strength to provide mechanical support for the S-band feed mechanism in the launch environment. Epoxy figerglass materials, such as Epon 828, can suitably be used, and it is anticipated that the thickness of the ogive can be 0.032 inch. Radiation, Inc., uses two fibreglass/epoxy skins, each 0.010 inch thick, separated by a 3/8-inch honeycomb core.

The K_u-band diplexer consists of two WR-62 rectangular waveguide sections placed side-by-side along the narrow wall to form a single unit. The diplexer has the RF property of channeling the transmit energy at 13.7 GHz to the polyrod feed element for radiation, and conversely, directing the received energy at 14.9 GHz to the parametric amplifier. Thus, the diplexer acts to isolate the transmitter from the receiver by separating these two frequencies. To provide the necessary isolation, four waveguide cavities make up a direct-coupled bandpass filter network for both the transmit and the receive channels. The projected performance indicates that each channel bandwidth be approximately 1 GHz. The maximum insertion loss is 0.6 dB with a 40 dB isolation between channels. The VSWR will be less than 1.1.

3.1.4.2 S-Band Feed Design

The S-band feed is a cupped helix (cavity-mounted helical) antenna. This type of antenna uses the size and shape of the cavity to control the beamwidth and shape of the pattern, producing a symmetrical and circularly polarized radiated field. Helix antennas have large bandwidth capabilities and greater than octave bandwidth operation is obtained by tapering the helix diameter. Since the TDRS bandwidth is only 13 percent, this is small in comparison with the helical antenna capability. Therefore, a cylindrical helix configuration was selected. In general, the band center determines the helix diameter where the circumference is made equal to the wavelength.

Figure 3 shows the variation in beamwidth with the dimension of one side of a square cavity (W). Measured values indicate that the square cavity and round cavity beamwidths are comparable. This figure shows the inverse ratio of the beamwidth to the cavity size. The half-power beamwidth required to produce a 10 dB edge taper at the main reflector is 70 degrees so that the cavity size should be 0.55λ.

The depth of the cavity is determined by the height of the 2½ turn helix and can be approximated by geometry when the helix pitch angle is chosen to be 14 degrees.

The best axial ratio and impedance match occur for the normalized frequency (normalized at the low end of the frequency band of operation) of between 1.05 to 1.2, or 15 percent bandwidth; the voltage axial ratio will be less than 1.3 and the VSWR will be less than 1.2.

A dielectric support, form-fitted to the helix, would be necessary for mechanical support. This dielectric will be constructed of a low loss dielectric material, whose thickness can be reduced to maintain low loss. The effect of the dielectric is minimal, as reported in the technical literature.

Radiation patterns from this type of antenna have indicated a parabola-on-a-pedestal illumination so that the theoretical equations for pattern generations can be applied. In this way, illumination efficiency, spillover efficiency, and gain can be compared to measured data.

The S-band diplexer will consist of two bandpass filters connected together at a common junction. Each filter will have eight resonators and will typically provide 80 dB interchannel rejection. The maximum insertion losses in the transmit and receive passbands are 0.6 dB and 0.5 dB, respectively. The size is 20 inches long by 4.8 inches wide by 2.6 inches high.

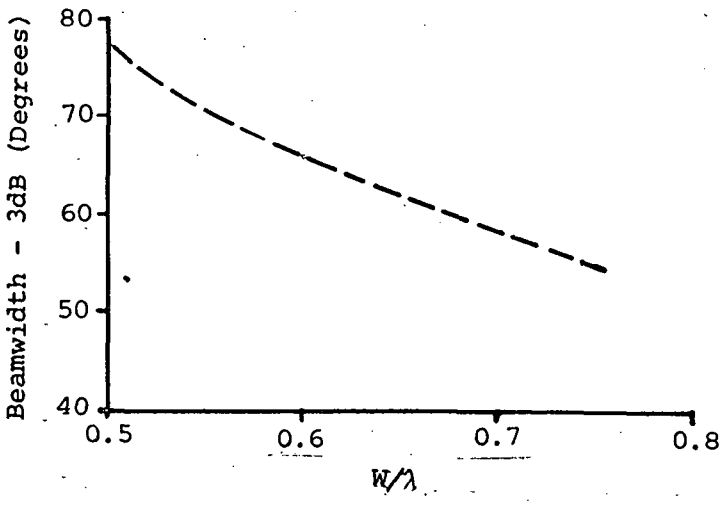

Figure 3. Variation of Beamwidths Versus Cavity Size

3.1.5 Mechanical Design

3.1.5.1 Complete Antenna System

Figure 4 shows two Option I antenna systems as they will sit on the deck of the spacecraft. Both are shown in the stowed position, the deployed position, and the intermediate attitude. From the stowed position, the folded antennas must first be rotated 90 degrees about the pitch axis prior to unfolding. The gimbal assembly as outlined in Figure 4 is only representative of the type of arrangement believed to be applicable. The gimbal assembly is envisioned as one similar to the Ball Brothers' Nimbus Attitude Pointing System, where each gimbal is driven by a 90-degree stepper motor coupled to a harmonic drive, designed in a bi-axial arrangement.

3.1.5.2 Compatibility with Delta Shroud

This configuration will be compatible with the Delta shroud, as is the Advanced Applications Flight Experiment (12.5-foot diameter) antenna presented by Radiation, Inc., in their Critical Design Review Data Package, NASA 1-11444 Sequence Number 4318-01. The height of the stowed package is the same as that given by Radiation, Inc. The DIM A (DIA A) has been increased for Option I, due to the larger subreflector, from 25.75 inches to about 29 inches. This increase should cause no problem because the critical interface point with the Delta shroud occurs higher up, nearer to the gimbal assembly and the antenna hub where there have been no changes.

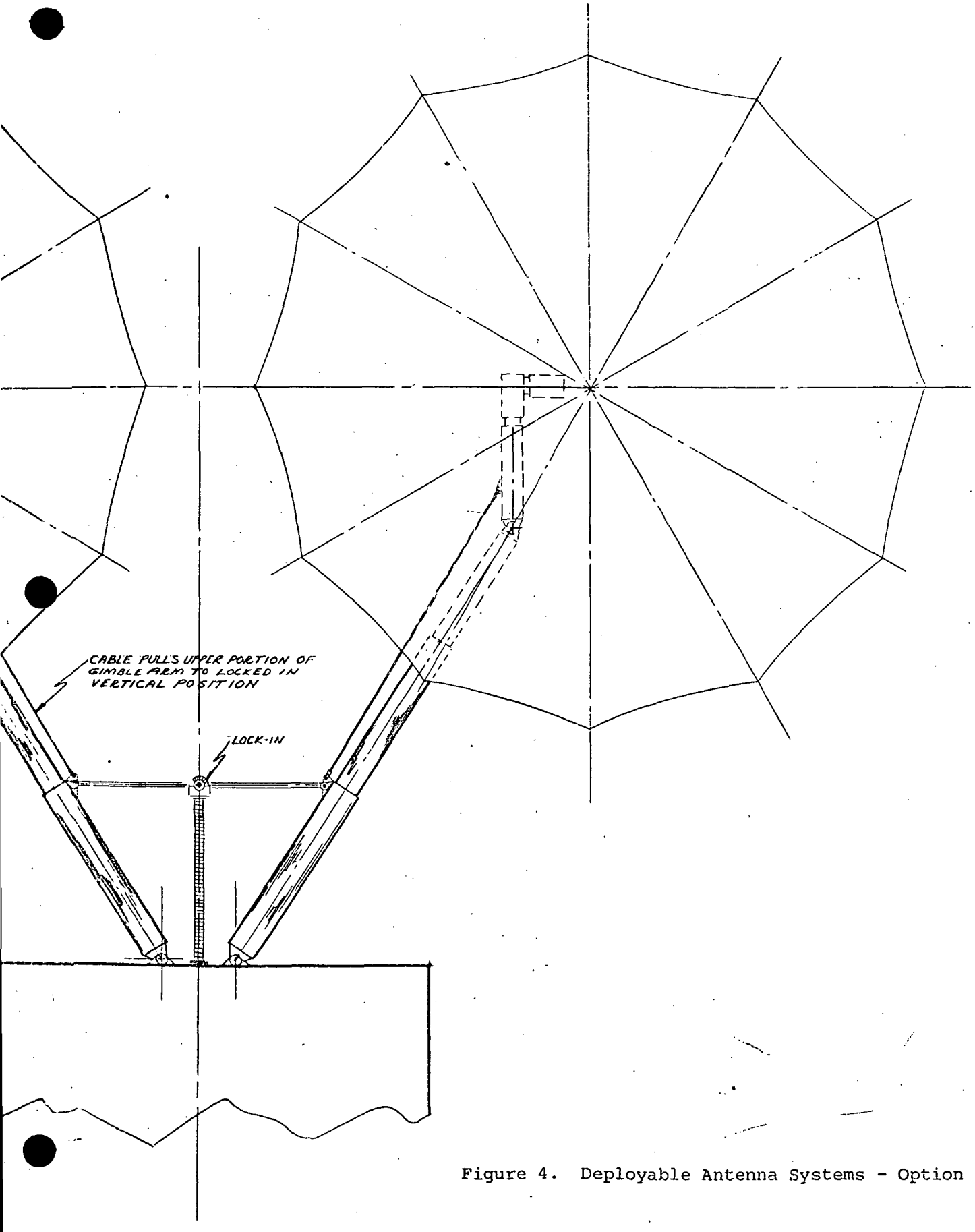

Figure 4. Deployable Antenna Systems - Option I

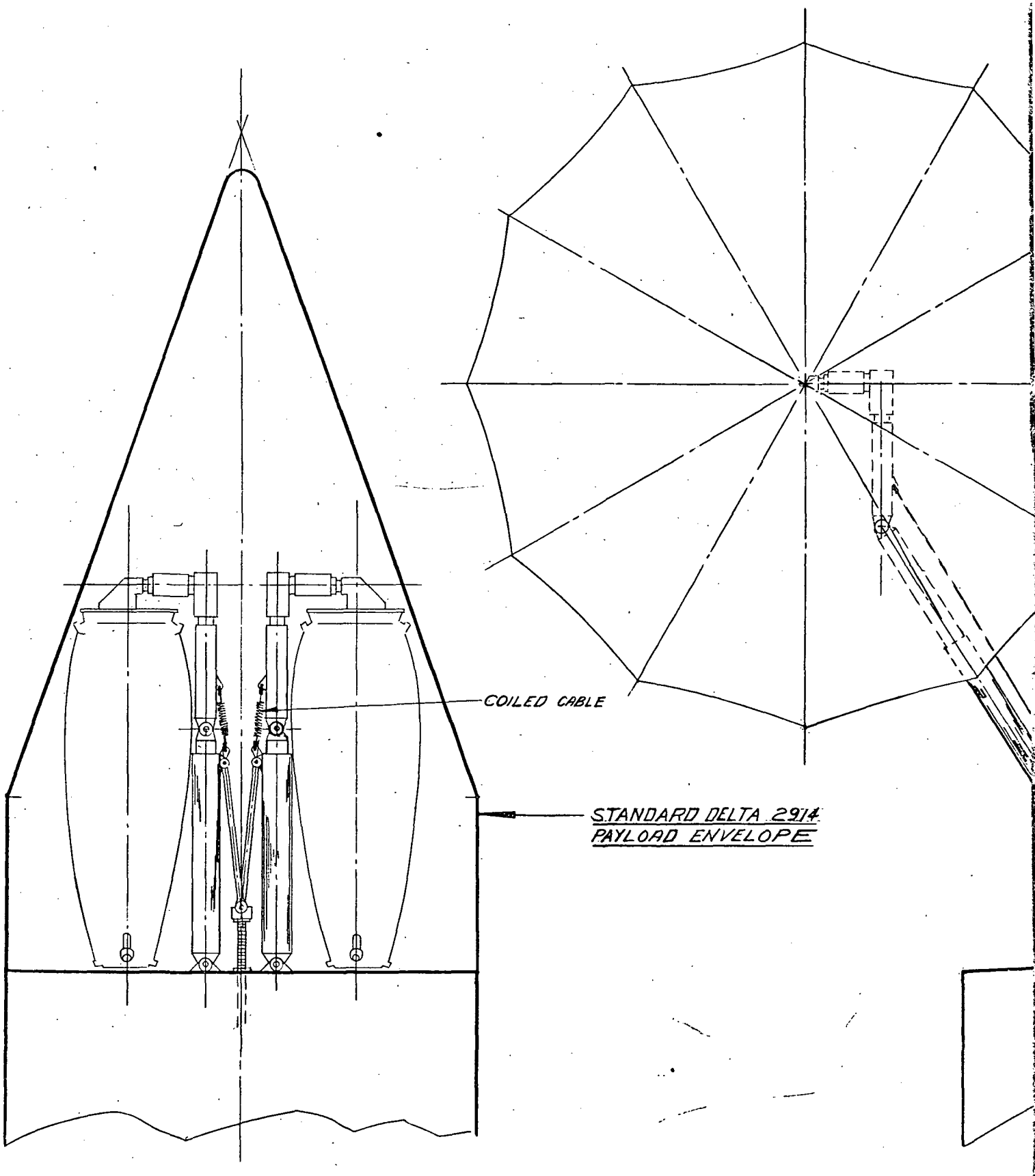
COILED CABLE
STANDARD DELTA 2914
PAYLOAD ENVELOPE

3.1.5.3 Compatibility with the Radiation, Inc. Reflector

Option I will be completely compatible with the Radiation, Inc. design scheme and will require only a few dimensional changes, as indicated in Figure 5. The exact extent of the change is seen by comparing the phantom outline of the Radiation, Inc. side view with the solid outline of Option I. The increased size and somewhat different shape was necessitated by the larger (17.5 inch diameter) dichroic subreflector. A small increase in component weight may require a slight increase in skin thickness for greater stiffness of the aluminum feed cone.

3.1.5.4 Interface

The major interface will occur at the spacecraft floor, where the rib tip restraint ring diameter has increased from 9 inches to about 14 inches, and at the gimbal assembly. The gimbal must interface, for Option I, two RF waveguides - an electric wire bundle (8 to 12 wires) and two RF flexible coaxial cables (S-band). The antenna MDS assembly area must also interface the two waveguides, wire and coaxial cables, to provide a passage way to the gimbal. An interface situation also exists between the gimbal and the antenna hub structural attachment.

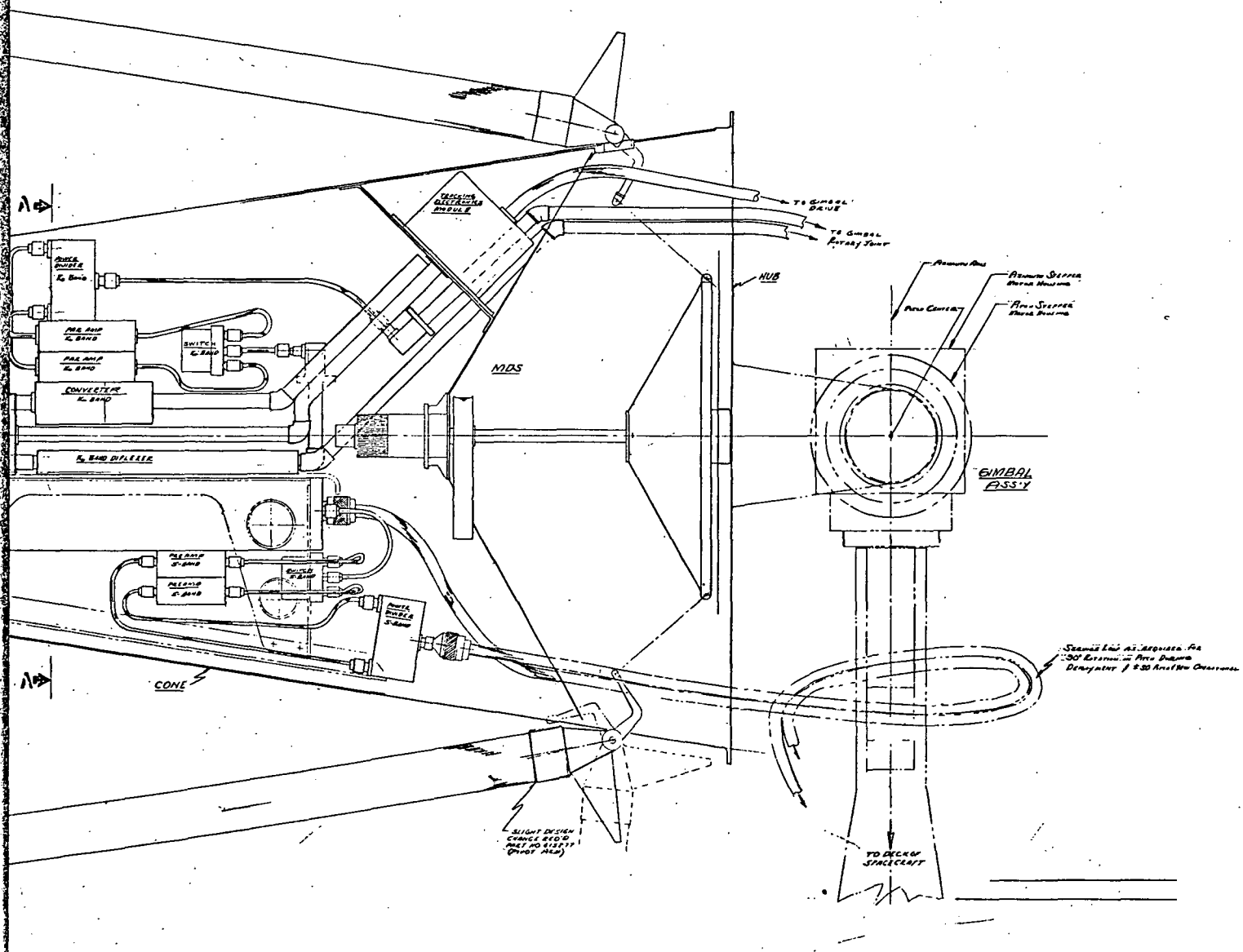

Figure 5. Detailed Drawing of S- and K -Band Feed System - Option I

of graphite fiber reinforced plastic (GFRP) for the cone structure. The GFRP is now in use on the ATS-F as the support truss that connects the reflector with its feed and is the largest graphite structure to be used in space. There are several advantages that may favor GFRP. The coefficient of thermal expansion of aluminum is 13 x 10^{-6} compared with the GFRP material's expansion ratio of almost zero. This would indicate that with GFRP the pointing accuracy could be improved due to lower thermal expansion.

GFRP has a density of 0.6 that of aluminum and a stiffness ratio of 2.5 times greater than that of aluminum. This would mean that greater rigidity and lower weight could be realized with the use of GFRP.

Studies may show that fiberglass for all three sections (cone, ogive, and upper cone) may be a possible compromise.

As is shown in Figure 5, the support structure for the monopulse system, the K_u-band feed system and the S-band feed is of the aluminum aircraft type design. However, with more detailed thermal studies it is likely that this supporting structure material would have to be made compatible with the cone structure. Once the cone material is established, this could alter the structural concept, depending upon the final cone design. Wherever feasible, structural attachments are used as bonds, provided compatibility with thermal requirements can be maintained.

3.2 Option II Candidate

3.2.1 Candidate Description

The preferred Option II candidate system is basically of the same configuration as the Option I design in that the antenna system is a dual reflector cassegrain with a K_u-band feed system at the secondary focal point and an S-band feed system at the primary focal point. With the exception of the S-band feed system, all other design characteristics are identical to the Option I design.

To satisfy the S-band autotrack provision of Option II. a two-channel monopulse tracking feed system is fixed at the primary focal point of the reflector. Figure 6 shows the block diagram of the tracking feed system. The feed element is a dual mode spiral antenna with a comparator network, which generates the sum and difference pattern required to develop the tracking error signals. The sum signal is shared with the S-band data channel and serves both the receive and transmit data functions. The unique feature of this sytems is that the S-band tracking loop is closed through the ground station. Ground loop S-band auto tracking was considered because of the limited beacon signal (SNR = -14 dB maximum in a 150 kHz noise bandwidth) available at the TDRS, based on a user transmitter beacon power of 1 watt into an omnidirectional antenna for the baseline Option II system. The advantage of closing the loop through the ground terminal is the ability to effectively increase the SNR by using a coherent phase-locked angle tracking receiver (which may not be desirable in the TDRS because

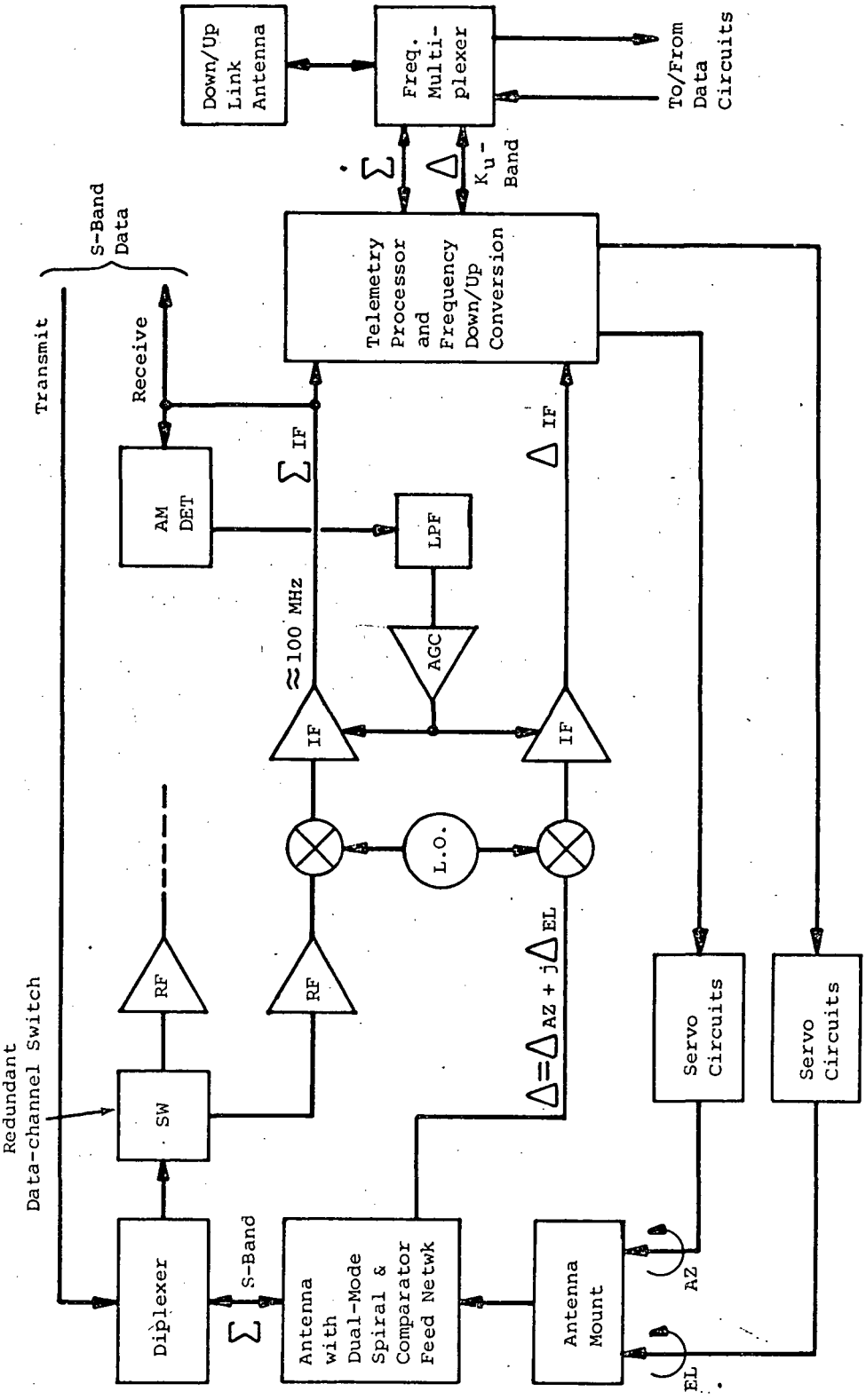

Figure 6. Block Diagram of S-Band Angle Tracking System with Shared Data Channel (TDRS Equipment Only)

of complexity and/or reliability). A more detailed discussion of the S-band auto tracking problem, the advantages of coherent auto tracking, and constraints under which the system will operate, is contained in paragraph 4.6.3.2 and Appendix I of this report.

Referring to Figure 6, the TDRS telemetry processor uses the Σ and Δ signals to phase-modulate subcarriers, which are then upconverted to the K_u-band and frequency multiplexed into the downlink antenna. The ground station equipment (Figure 7) extracts the phase-modulated K_u-band Σ and Δ signals and downconverts them to a convenient carrier for demodulation. The VCO of the phase lock loop (PLL) is frequency swept to affect a phase lock-on to the Σ signal, thereby deriving a narrow-band high SNR reference for angle error sensing at the product detectors.

The azimuth and elevation pointing error signals are proportional to the angle off boresight, and their polarity ($\pm$) is determined by the phase sensitivity of the product detectors. The quadrature characteristic of the $\Delta \mp \Delta_{Az} + j\Delta_{El}$ signal allows the exclusive extraction of Az and El error outputs from the individual product detectors. These error signals are used to modulate an uplink carrier, which is finally demodulated in the TDRS to provide pointing correction signals to the antenna.

3.2.2 Operation and Capabilities

The primary advantages of the Option II candidate as compared with Option I, are its ability to automatically maintain an S-band data link without ground station predictive (open-loop) commands and its capability to use the wide beamwidth (2.5 degrees) S-band autotrack system as an acquisition aid for the K_u-band autotrack system. Table X presents a summary of increased capability inherent in the selection of an Option II candidate. The designation and K_u-band auto tracking sequence applicable to the Option II candidate is contained in Table XI.

With regard to the postulated user and TDRS baseline scenarios, the added complexity of the TDRS antenna and ground support equipment may not warrant the selection of Option II over Option I, e.g.,

1. Auto tracking an S-band user with the Option II antenna system requires a significantly more complex array of equipment aboard the TDRS and at the ground station than would be required to point the S-band beam by pre-programmed ground command positioning;

2. It is necessary to preserve sufficient fidelity of the user S-band reference and error signals in the TDRS repeater and ground station receivers, so that sufficient bandwidth processing gain may be achieved at the ground station for adequate angle tracking SNR enhancement;

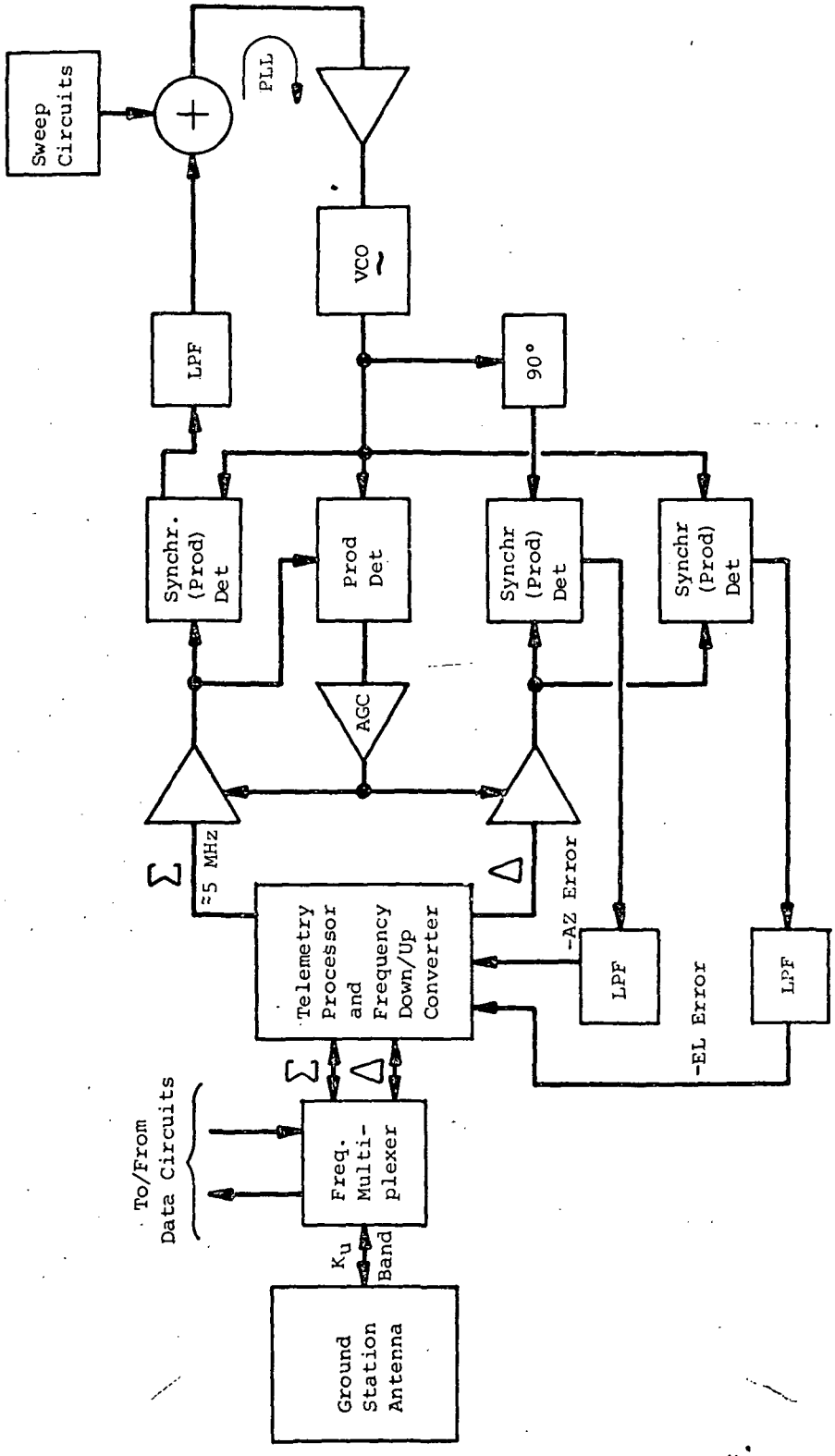

Figure 7. Ground Station Equipment for S-Band Angle Tracking

TABLE X

Additional Operational Capabilities of
Option II Candidate (Compared with Option I)

User Equipment	Additional TDRSS Operational Capabilities
User A S-band receiver K_u-band data transmitter and receiver	None
User B S-band data transmitter and receiver No - K_u-band	• S-band data link maintenance S-band autotrack
User C S-band beacon transmitter and receiver K_u-band data transmitter and receiver	• K_u-band data link maintenance S-band autotrack (backup) • Designation aid for K_u-band autotrack S-band autotrack
Multiple User A and B or C and B	None

TABLE XI

Designation and K_u-Band Autotrack Sequence (Option II)

Assumptions:

Same as Option I

User has S-band beacon transmitter (one watt) radiating into an omnidirectional antenna.

Sequence:

Step 1 - Ground station computes TDRS/user relative look angles and commands TDRS to point antenna at the user (±0.45 degree accuracy).

Step 2 - User is commanded through S-band to turn on its S-band beacon transmitter and also to point its K_u-band antenna at TDRS.

Step 3 - User is now well within the TDRS S-band FOV (± 2.65 degrees); TDRS locks up on user S-band beacon and auto tracks with an accuracy of better than ±0.35 degree.

Step 4 - User is commanded to turn on the K_u-band transmitter (unmodulated).

Step 5 - User is well within the TDRS K_u-band FOV (±0.6 degree) and can now achieve a lock-up and autotrack; TDRS K_u-band tracking accuracy is better than ±0.054 degree.

Step 6 - TDRS is commanded to turn on K_u-band transmitter (unmodulated).

Step 7 - User locks up on K_u-band signal and maintains autotrack.

Step 8 - User S-band transmitter is turned off.

Step 9 - TDRS S-band transmitter is turned off.

Step 10 - K_u-band data link is established and is ready for HDR transmission.

Step 11* - When operation is complete, user is commanded to point K_u-band antenna to new coordinates of next anticipated contact. If user will not be picked up by second TDRS, then the last command will include directions to turn off the K_u-band transmitter.

---

* Step 11 provides added insurance of re-establishing a link with the user should a problem develop in the S-band link. Acquisition can then be affected by using the defocused K_u-band TDRS feed, or scanned search, of the TDRS antenna at K_u-band. The first search through the cone of uncertainty would be sufficiently slow to allow time for a command for the user to turn on its K_u-band transmitter. The second search would be to lock up on the user's signal.

3 Pre-programmed ground command pointing of the S-band beam is sufficiently accurate to insure less than 0.42 dB data signal loss relative to the data beam peak;

4 Employment of an auto tracking S-band feed will result in about 0.73 dB data signal loss due to the presence of the comparator network (assumes shared data and sum channel);

5 S-band auto tracking is not required as a designation aid for K_u-band auto tracking. As shown in the performance description for the Option I candidate (paragraph 3.1.2), the defocused K_u-band autotrack FOV is more than adequate to assure acquisition of any K_u-band user. The loss in sum signal gain still leaves about 5 dB SNR margin to meet an overall auto tracking accuracy within $\leq$ 0.2 of the data link beamwidth (corresponds to $\leq$ 0.5 dB loss).

In spite of the above observations, the Option II preferred candidate offers a baseline for further tradeoffs on user impact and TDRSS capabilities.

3.1.3 Performance

3.1.3.1 RF Performance for K_u-Band and S-Band

The details of the RF losses for Option II are presented in Table XII for the S-band. The K_u-band RF losses are the same as Option I and are presented in Table VI. Comments associated with these values are applicable for all options and are placed immediately behind the tables in paragraph 3.1.3.1.

TABLE XII

RF Performance: Option II - S-Band

Performance Factors	Transmit	Receive
Frequency (MHz)	2072.5	2250.0
Aperture diameter (meters)	3.81	3.81
Aperture area gain (dB)	38.36	39.07
Amplitude taper loss (dB)	0.46	0.46
Spillover loss (dB)	1.25	1.25
Blockage loss (dB)	0.18	0.18
Phase loss (dB)	0.13	0.13
Cross-polarization loss (dB)	0.11	0.11
Ogive loss (dB)	0.15	0.15
Subreflector loss (dB)	0.50	0.50
Surface tolerance loss (dB)	0.01	0.01
Mesh reflectivity loss (dB)	0.004	0.004
Feed antenna I^2R loss (dB)	0.70	0.70
Comparator loss (dB)	0.50	0.50
Cable loss (dB) ant. to diplexer	0.30	0.30
VSWR loss (dB) 1.25:1	0.05	0.05
Total overall loss (dB)	4.34	4.34
Overall efficiency (percent)	36.8	36.8
Antenna peak gain (dB)	34.0	34.7
Diplexer loss (dB)	0.6	0.50
Cable loss to S/C interface (dB) 10 feet	0.75	NA

TABLE XII (Continued)

Performance Factors	Transmit	Receive
Cable wrap loss through gimbals (dB)	0.18	NA
Redundancy switch loss (dB)	NA	0.30
Half power beamwidth (degrees)	2.53	2.33
Polarization sense	Circular	Circular

3.2.3.2 Data Beam Pointing Error

The 3σ data beam pointing accuracy and associated data signal loss for the preferred Option II candidate for the ground command and auto tracking pointing modes are presented in Table XIII.

TABLE XIII

Option II Data Beam Pointing Accuracy

Mode	3σ Pointing Accuracy (degrees)	Data Signal Loss (dB)	Reference
Ground command			
S-band data link	±0.47	0.42	Table LII
K_u-band autotrack			
K_u-band data link	±0.054	0.22	Figure 87
S-band data link	±0.160	0.05	Figure 89
S-band autotrack			
S-band data link	±0.317	0.19	Figure 91

As for Option I, the above K_u-band autotrack accuracies are based on a maximum received beacon SNR = 5.7 dB at the TDRS, a 1 Hz servo bandwidth, and a 10^{-3} sec^{-2} servo torque disturbance factor. Accuracy tradeoffs with variations in these parameters are given in the referenced plots. The S-band autotrack accuracy is based on a maximum received beacon SNR = -16 dB at the ground station, a 1 Hz TDRS servo bandwidth, and negligible servo torque disturbance factor. Tradeoffs with SNR and servo bandwidth are given in the referenced plot.

3.2.4 Feed Design Considerations

3.2.4.1 K_u-Band Feed System

The feed system in Option II is the same as the Option I design.

3.2.4.2 S-Band Feed System

To satisfy the D/F requirements, a monopulse technique was chosen. A single dual-mode spiral antenna eliminates the need for four or more single mode antennas and provides two-angle tracking signals as opposed to the conventional orthogonal azimuth-elevation tracking signals obtained using the interferometer techniques of the multiple antenna systems.

The antenna itself is a planar archimedian spiral with a diameter approximately equal to $2\lambda_{LOW}/\pi$, or 3.71 inches. The spiral will be backed by a cavity $\lambda_{MID}/4$ deep, or 1.31 inch. A balun for each arm of the spiral matches it to the hybrid beam forming network. Four arms are sufficient to develop two modes, the sum and a difference modes.

This S-band antenna will be placed at the primary focus where it will illuminate the paraboloid with an edge taper of 10 dB. This illumination function can be approximated by

$$A + B\ (1-\rho^2/a^2)^{1.5}$$

where

A = the pedestal height

B = the energy illuminating the parabola with a tapered distribution

a = the aperture radius

ρ = fraction of a, corresponding to the illumination intensity at a given distance from aperture center.

3.2.5 Mechanical Design

Option II is similar to Option I, as seen by comparison of Figures 8 and 9 with 4 and 5. The exception is that Option II has an S-band spiral feed with two flexible coaxial cables leading away from it, whereas Option I has the helix S-band feed with but one coaxial cable. Other than the above, the discussions of section 3.1.5 also apply to Option II.

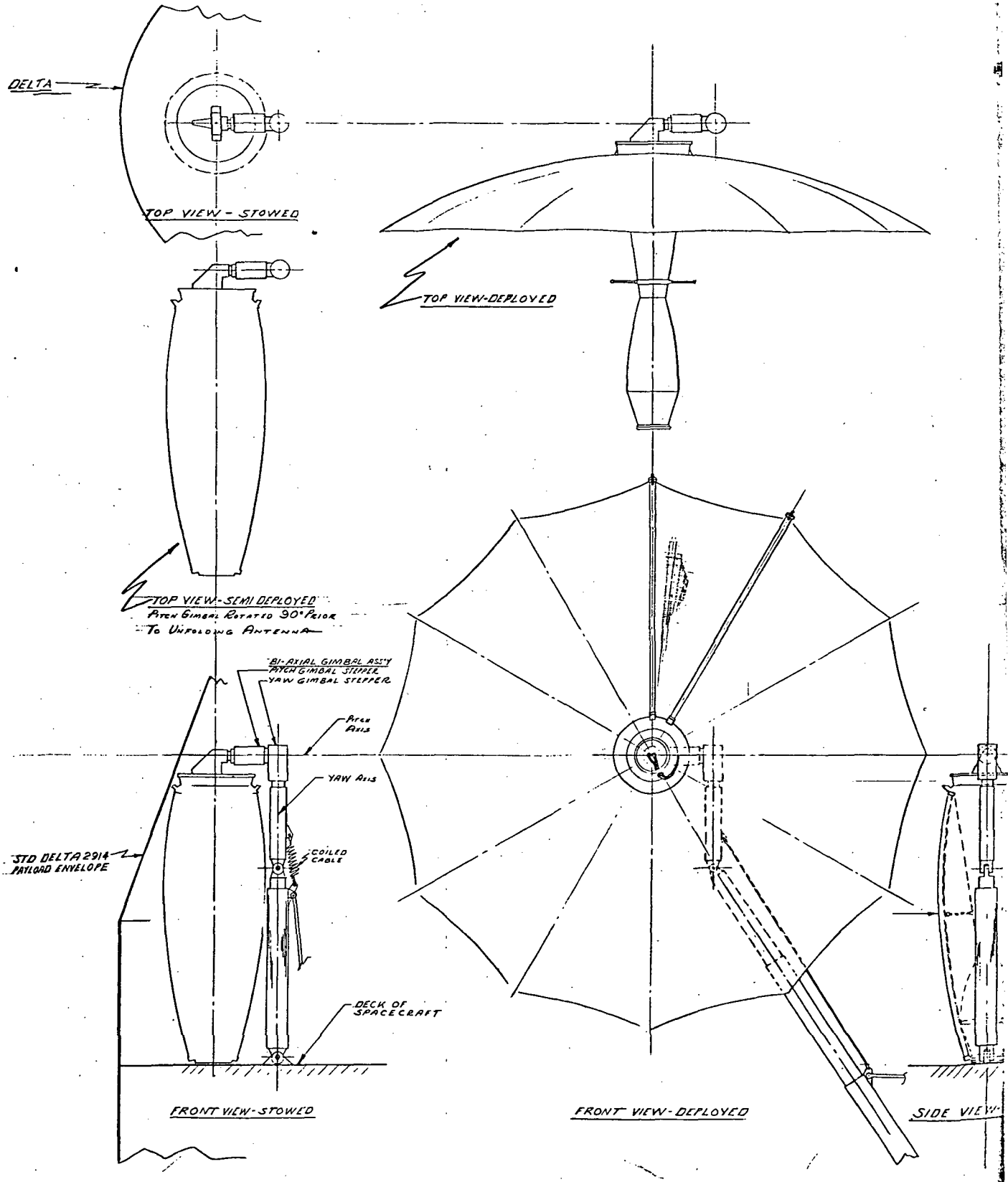

Figure 8. Deployable Antenna System - Option II

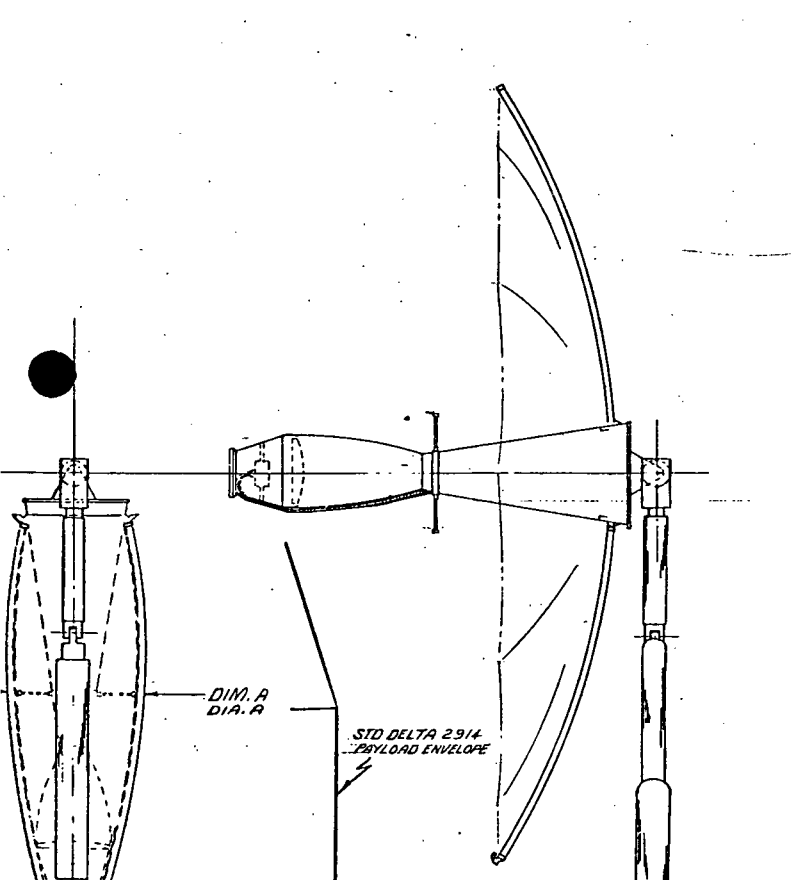
DIM. A
DIA. A
STD DELTA 2914
PAYLOAD ENVELOPE
DE VIEW- STOWED
SIDE VIEW - DEPLOYED

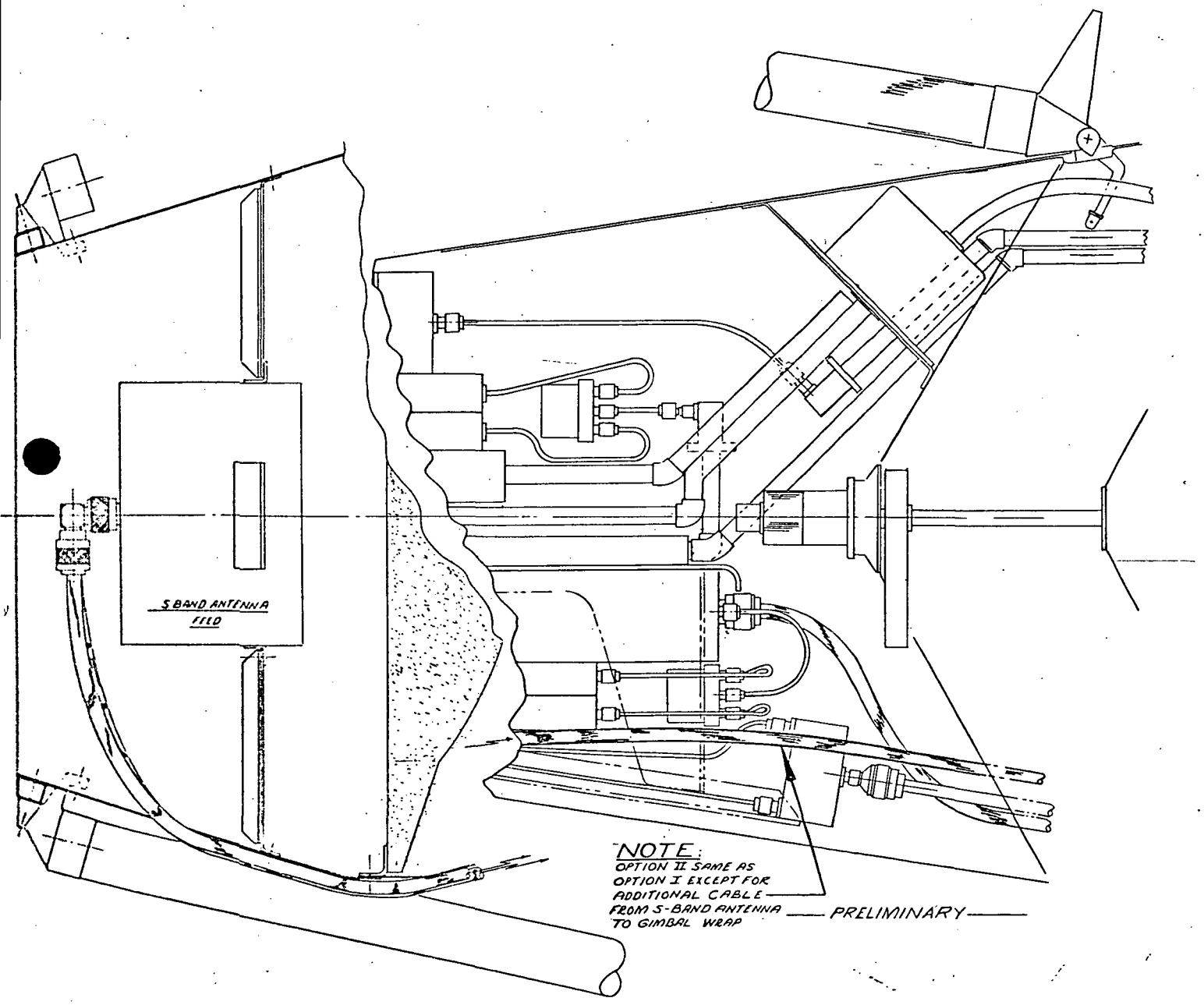

Figure 9. Detailed Drawing of the S-Band Feed System - Option II

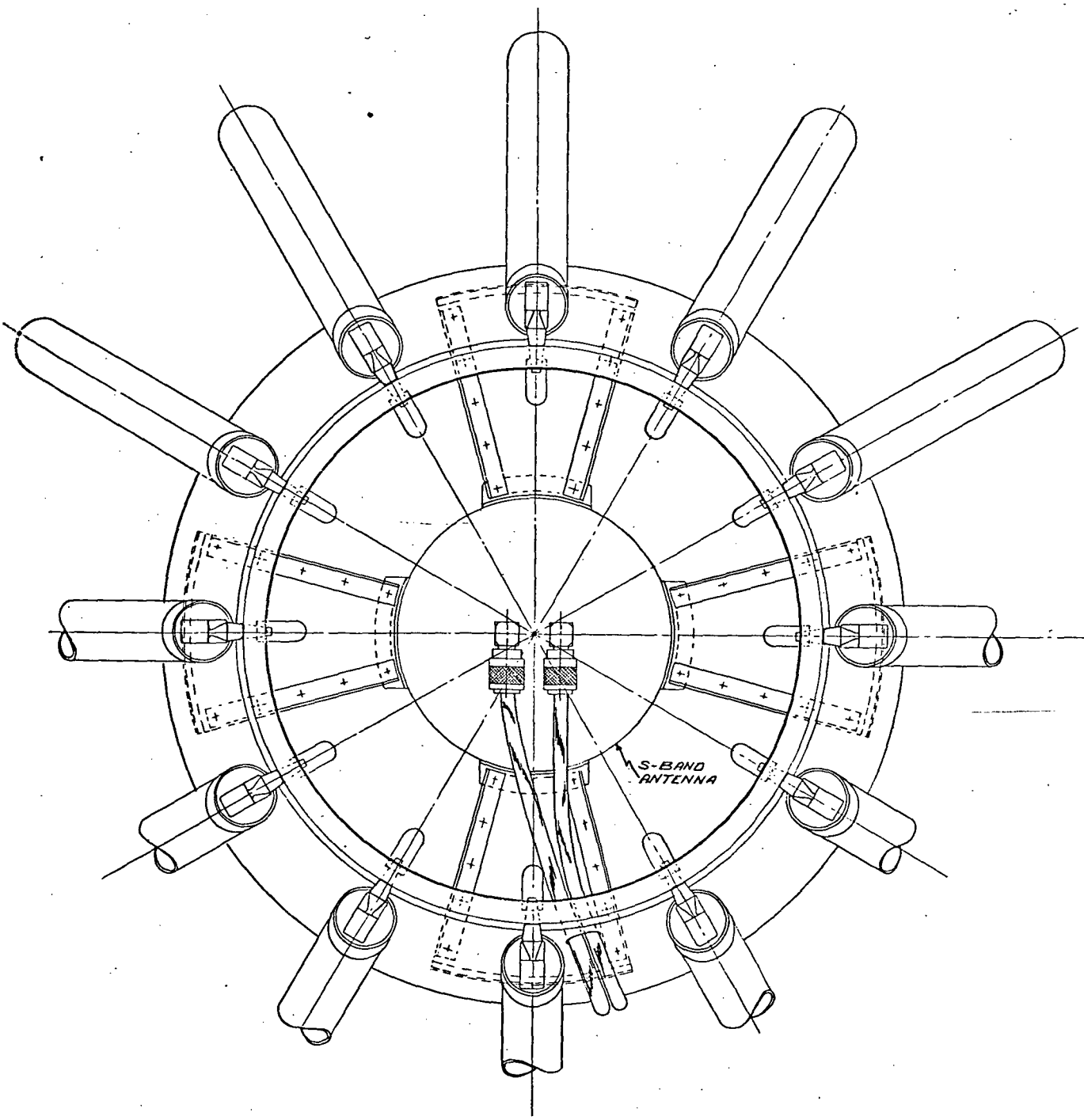
S-BAND
ANTENNA

3.3 Option III Candidate

3.3.1 Candidate Description

The requirements of the Option III system differ from those of Option I in that the S-band beam must be capable of being steered independently of the K_u-band beam. The preferred candidate which satisfies this requirements is a dual reflector cassegrain antenna, wherein the main reflector is a 12.5-foot diameter spherical section with a radius of 11 feet (Figure 10). As in Option I, the K_u-band feed is located at the secondary focus and the S-band feed is positioned at the primary (paraxial) focal point of the sphere. The subreflector is a convex reflector whose shaped surface is mathematically matched to the parameters of the dual reflector system so that it completely corrects for the phase errors (spherical aberration) inherent in a spherical reflector antenna. The K_u-band feed is essentially identical to the feed described for the preferred Option I candidate in that it employs a dedicated data channel feed surrounded by a defocused auto-track feed array. The actual dimensions of the K_u-band feed system are altered to fit the spherical dual reflector geometry. The resulting K_u-band beam is fixed with respect to the axis of the reflector system and is steered, as in Option I, by movement of the complete antenna.

The S-band feed is essentially the same cupped helix antenna described for the Option I candidate. A feed positioning mechanism (as suggested by NASA, Reference 18) and servo network are provided to position the S-band feed anywhere on the spherical surface intersecting the paraxial focal point with a radius of one-half that of the main reflector. Movement of the feed on this surface provides the means for steering the S-band beam relative to the axis of the dual reflector antenna independently of the K_u-band beam. The beam steering angle is equal to the angular displacement of the feed off the reflector axis. The preferred candidate is configured for $\pm$ 30 degrees of independent S-band beam steering capability with respect to the K_u-band beam maximum, e.g., when the K_u-band beam is pointed at $\pm$ 15 degrees relative to local nadir, then the S-band beam must be capable of steering to $\mp$30 degrees relative to the reflector axis, to service a user at $\mp$15 degrees of the nadir. This worst case design is presented as a baseline from which further trades can be made. Any compromise in the S-band beam steering angle will simplify the design of the beam steering mechanism.

The S-band feed positioning mechanism is comprised of two basic motions. Transverse motion steers the beam off-axis, and rotation about the dual reflector axis provides the capability to steer the beam anywhere within a solid cone of $\pm$ 30 degrees.

Computations involving TDRS position and attitude, position of the S-band user satellite, and the pointing angle of the reflector system are made by the ground terminal computer to provide periodic updated commands for the S-band beam pointing angle. The position mechanism is designed to respond to commands initiated at the ground terminal.

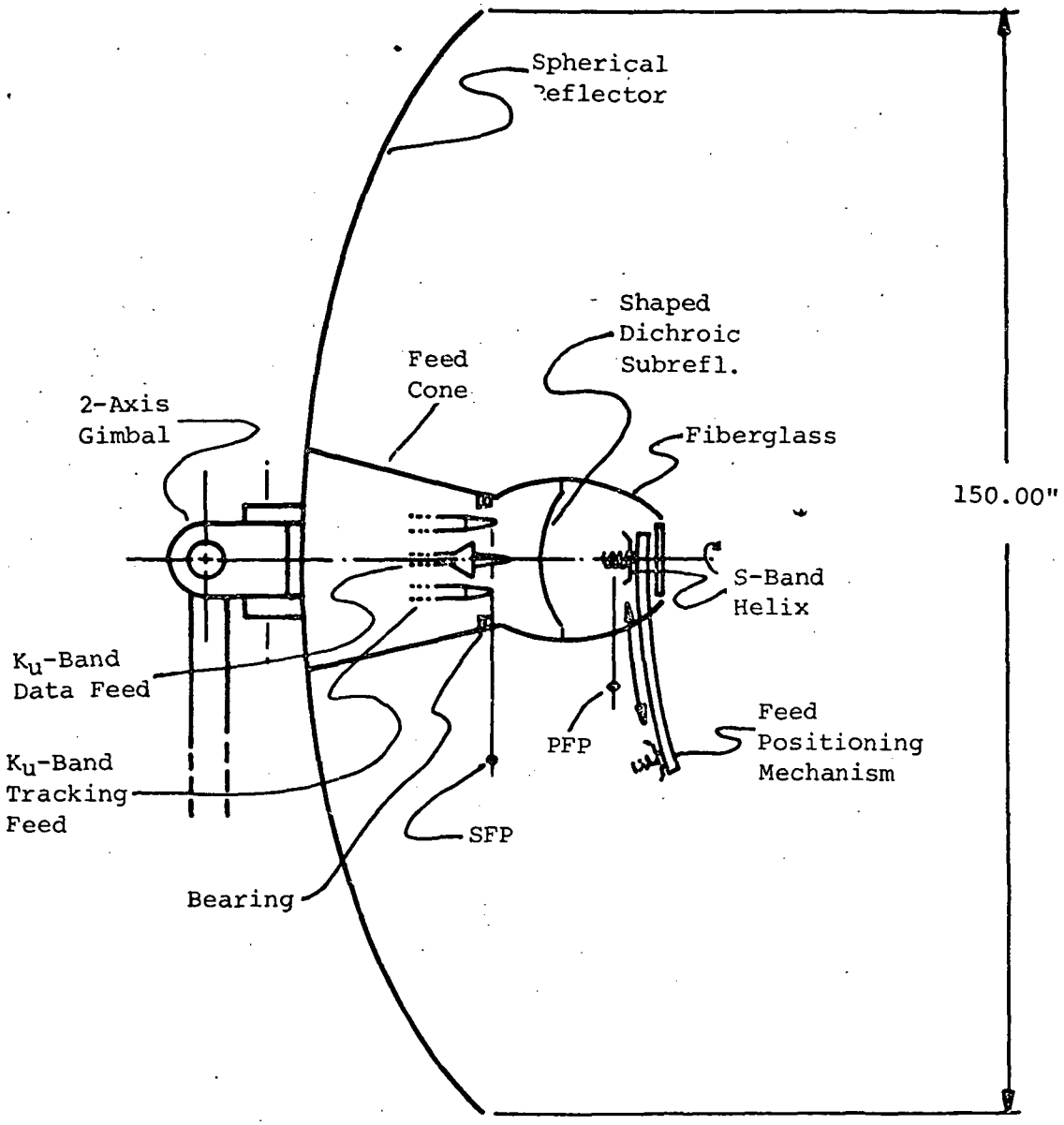

Figure 10. Preferred Candidate for Option III

3.3.2 Operation and Capabilities

The basic operation and capabilities of this candidate antenna system are presented in Table XI V and are essentially the same as for Option I with the additional flexibility of the independently steered S-band beam. The S-band beam steering capability allows the simultaneous and independent maintenance of data links with two user satellites (one at S-band and the oth at K_u-band) that are widely spaced from one another. Restrictions to the cap bility are:

1. The S-band beam must be used to establish initial contact with a K_u-band user; therefore, an S-band data link may have to be interrupted for the initiation of another K_u-band link. (This interruption can be avoided if the "new" K_u-band user was pre-commanded to point its antenna toward the new TDRS coordinates before its release during the previous orbital pass);

2. The S-band data link will suffer some degradation in SNR due to beam steering off axis. (The degradation will vary from 0 to 5.4 dB and will depend on the scan angle.)

A step by step procedure for establishing and maintaining a K_u-band data link, unique to the Option III candidate, is contained in Table XV . Again, as in the discussion of the Option I candidate, the S-band designation and data maintenance procedure is handled entirely by ground pointing commands. In Option III, however, the commands are sent to the S-band feed positioning mechanism rather than to the reflector gimbal.

3.3.3 Performance

3.3.3.1 RF Performance for K_u-Band and S-Band

The details of the RF losses for Option III are presented in Table XVI for the S-band. The K_u-band RF losses are the same as Option I and are presented in Table VI. Comments associated with these values are applicable for all options and are placed immediately behind the tables in paragraph 3.1.3.1.

3.3.3.2 Data-Beam Pointing Error

The 3σ data-beam pointing accuracy and associated data signal loss, for the preferred Option III candidate, are presented in Table XVII for the ground command and auto tracking pointing modes.

These autotrack accuracies are based on the same SNR and servo parameters as for Option I (paragraph 3.1.3.2); accuracy tradeoffs with variations in these parameters are given in the referenced plots.

TABLE XIV

Additional Operational Capabilities of Option III Candidate
(Compared with Option I)

User Equipment	Additional TDRS Operational Capabilities
User A S-band receiver K_u-band data transmitter and receiver	None
User B S-band data transmitter and receiver No K_u-band	None
User C S-band beacon transmitter and receiver K_u-band data transmitter and receiver	None
Multiple User A and B or C and B	Maintain maximum performance K_u-band data link with User A or User C. Maintain S-band data link with User B at wide angular separation from User A or User C.

TABLE XV

Designation and K_u-Band Autotrack Sequence (Option III)

Assumption:

Same as Option I

Sequence:

Step 1 - TDRS S-band feed is commanded to return to on-axis reference position (S-band beam aligned with K_u-band beam).

Steps 2 through 10 - Same as Steps 1 through 9 of Option I.

Note: When K_u-Band HDR link is established, S-band feed can be used to establish an independent S-band link with another user.

Trouble Sequence:

In the event of a malfunction, whereby the S-band feed cannot be returned to its on-axis position, then the following sequence can be employed:

Step 1 - Ground computes TDRS/User relative look angles with compensation for the known position (offset angle) of the S-band feed.

Step 2 - TDRS antenna is commanded to look at the user so that the S-band beam is illuminating the user; pointing accuracy is ±0.59 degrees (3σ), worst case for maximum scan angle.

Step 3 - User is commanded to point its K_u-band antenna at TDRS.

Step 4 - User is commanded to turn on the K_u-band transmitter.

Step 5 - Ground commands TDRS to point its antenna so that K_u-band beam illuminates the user.

Steps 6 through 11 - (Same as Steps 4 through 9 of Option I).

Note: Last step to repoint user K_u-band antenna at next anticipated contact angle is especially important in the trouble sequence in that S-band compensated pointing commands to the user may not be required again.

TABLE XVI

RF Performance: Option III--S-Band

Performance Factors	Boresight		±30 Degree Scan	
	Transmit	Receive	Transmit	Receive
Frequency (MHz)	2072.5	2250.0	2072.5	2250.0
Aperture diameter (meters)	3.81	3.81	3.81	3.81
Aperture area gain (dB)	38.36	39.07	38.36	39.07
Amplitude taper loss (dB)	0.46	0.46	0.46	0.46
Spillover loss (dB)	1.25	1.25	1.25	1.25
Blockage loss (dB)	0.23	0.23	0.18	0.18
Phase loss (dB)	0.13	0.13	0.13	0.13
Cross-polarization loss (dB)	0.11	0.11	0.11	0.11
Ogive loss (dB)	0.15	0.15	0.0	0.0
Subreflector loss (dB)	0.50	0.50	0.0	0.0
Surface tolerance loss (dB)	0.01	0.01	0.01	0.01
Mesh Reflectivity loss (dB)	0.004	0.004	0.004	0.004
Spherical aberration loss (dB)	0.30	0.30	0.03	0.03
Feed antenna I^2R loss (dB)	0.05	0.05	0.05	0.05
Cable loss (dB), ant. to diplexer	0.65	0.65	0.65	0.65
Rotary joint loss (dB)	0.15	0.15	0.15	0.15
VSWR loss (dB), 1.25:1	0.05	0.05	0.05	0.05
Off-boresight scan loss (dB)	NA	NA	5.4	5.4
Total overall loss (dB)	4.04	4.04	8.47	8.47
Overall efficiency (percent)	39.4	39.4	14.2	14.2
Antenna peak gain (dB)	34.3	35.0	29.9	30.6
Diplexer loss (dB)	0.50	0.50	0.6	0.50
Cable loss to S/C interface (dB), 10 ft	0.75	NA	0.75	NA
Cable wrap loss through gimbals (dB)	0.18	NA	0.18	NA
Redundancy switch loss (dB)	NA	0.30	NA	0.30
Half power beamwidth (degrees)	2.53	2.33	2.92	2.69
Polarization sense	Circular	Circular	Circular	Circular

TABLE XVII

Option III Data Beam Pointing Accuracy

Mode	3σ Pointing Accuracy (degrees)	Data Signal Loss (dB)	Reference
Ground command			
S-Band data link	±0.59 (max. scan angle)	0.67 (max. scan)	Table LI
	±0.45 (min. scan angle)	0.39 (min. scan)	Table LI
K_u-band autotrack			
K_u-band data link	± 0.054	0.22	Figure 87
S-band data link	< ±0.160	< 0.05	Figure 89

3.3.4 Feed Design Considerations

3.3.4.1 K_u-Band Feed System

Only slight changes are required for the Option III K_u-band feed. Since the subreflector is closer to the feed elements, the illumination angle is larger, requiring a smaller length of polyrod. The polyrod taper would also require some optimization for the new beamwidth, and the amount of defocusing for spherical reflector systems may be different from those for parabolic/hyperbolic systems.

3.3.4.2 S-Band Feed Design

Same as Option I except there is a single rotary joint installed in the cone area to prevent excessive twisting of the cables while the S-band feed is undergoing rotation movement.

The rotary joint is a coaxial type whose insertion loss is 0.15 dB maximum. Its diameter is 2 inches and its length is 1.6 inches, not including connectors. The weight is 6 ounces. Dry lubricants will be used on the ball bearings and races, and contacts will be fabricated from precious metals.

3.3.5 Mechanical Design

3.3.5.1 Complete Antenna System

The deployable Option II antenna system as it sits on the spacecraft deck is shown in Figure 11. It is depicted in the stowed position, the deployed position, and the intermediate attitude. In stowing the Option III configuration on the spacecraft deck, the S-band tracking arm must first be cycled to a position where it will protrude equally from each side of the upper cone so that both ends remain above the deck level. This is shown in Figure 11 for the stowed positions. The gimbal assembly

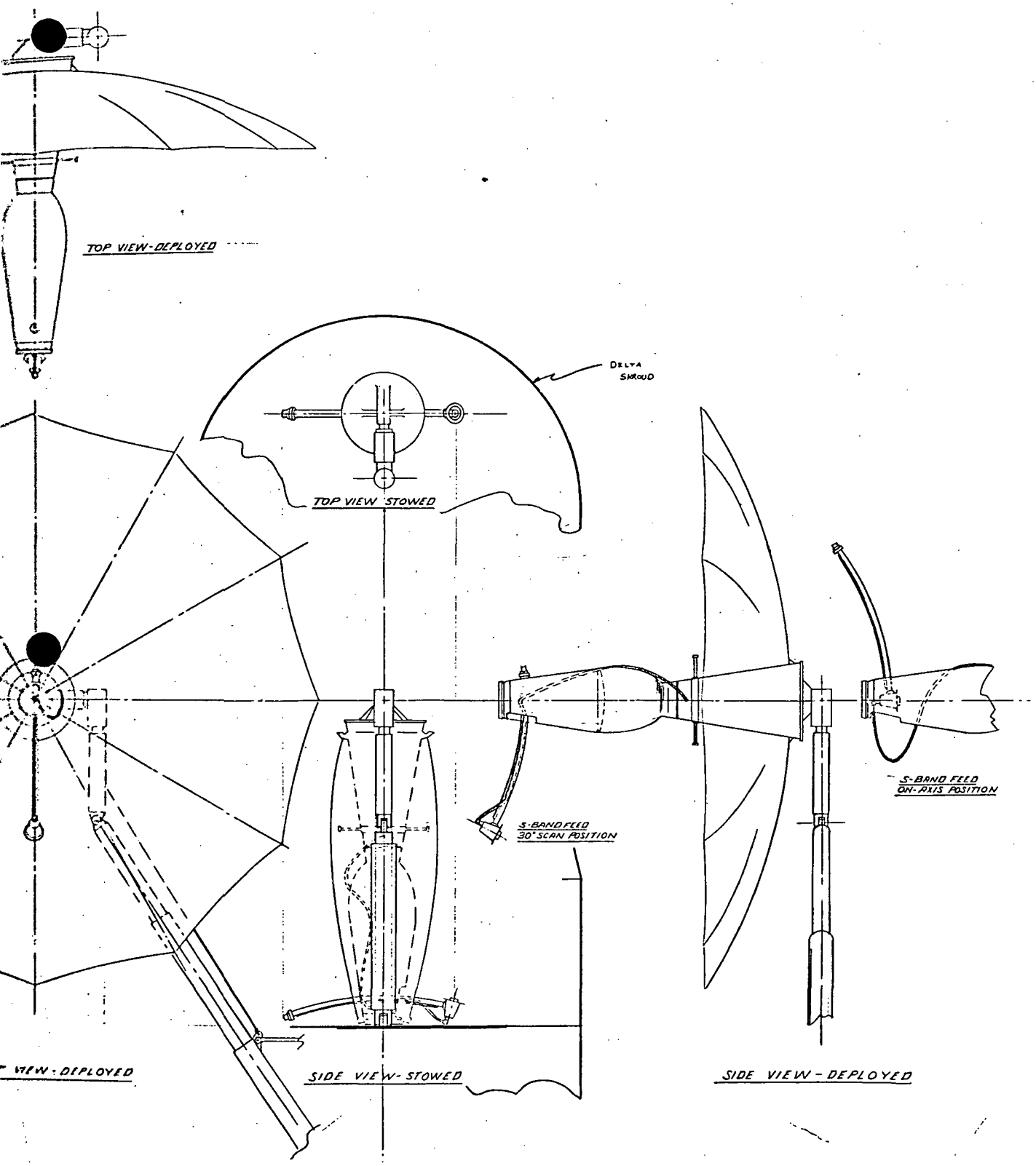

Figure 11. Deployable Antenna System - Option III

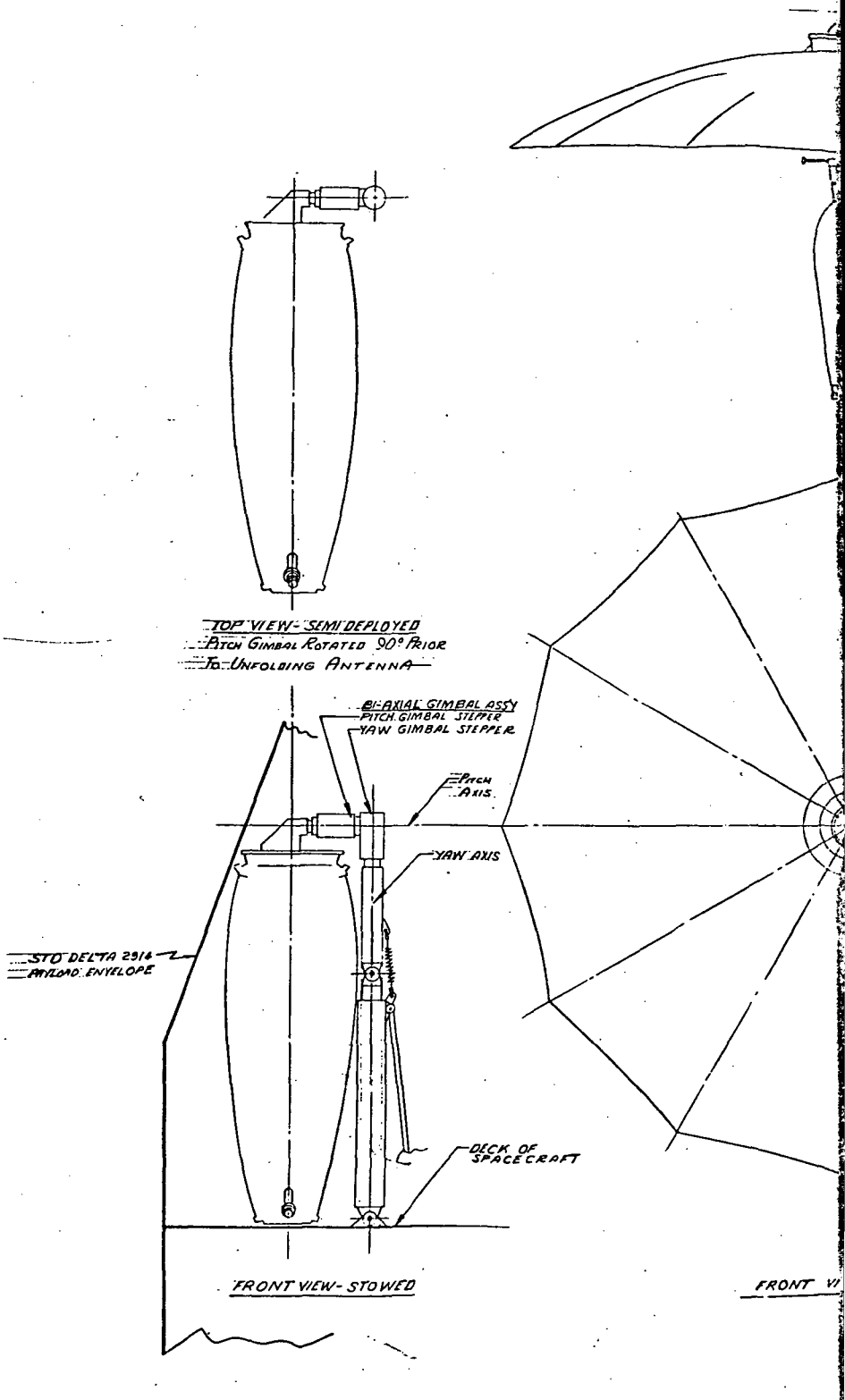
TOP VIEW - SEMI DEPLOYED
PITCH GIMBAL ROTATED 90° PRIOR
TO UNFOLDING ANTENNA
BI-AXIAL GIMBAL ASSY
PITCH GIMBAL STEPPER
YAW GIMBAL STEPPER
PITCH AXIS
YAW AXIS
STO DELTA 2914
PAYLOAD ENVELOPE
DECK OF SPACECRAFT
FRONT VIEW - STOWED
FRONT VI

shown for Option III is the same as for Options I and II, but may have to have a slightly higher torque rating than I and II due to the somewhat higher weight and inertia of Option III.

The major difference among Options I, II and Option III is, of course, the fact that the S-band feed for Option III is given a rotation and translation movement where the Option I-II S-band feed is static. Further, Option III has a spherical reflector as compared to the parabola of Options I and II. The geometry which is basic to Option III as well as Option IV is shown in Figure 12.

3.3.5.2 Compatibility with Delta Shroud

In its stowed configuration, the Option III package shape should not vary enough from the parabolic shape of Options I and II to significantly impact fit within the Delta shroud.

3.3.5.3 Compatibility with Radiation, Inc. Reflector

Configuration III uses a spherical reflector, whereas the Radiation, Inc., reflector is a prabola. However, it is possible to use the Radiation, Inc., design and configure the reflector surface to be spherical instead of parabolic.

3.3.5.4 Interface

With respect to interface, the problem is the same as for Options I and II but with some additional aspects. The S-band feed arm will have to be interfaced with the spacecraft deck to provide safe support for the arm during boost acceleration.

Further, the reflector mesh, in the area where the arm protrudes out from the upper cone, will have to drape around the arm during stow and deploy without being damaged or fouled during deployment.

3.3.5.5 Environment

The same as for Options I and II except that Option III will contain more items which may be critical to the thermal environment such as the four stepper motors that rotate the S-band feed arm, the S-band rotary joint, and the bearings upon which the ogive and upper cone are rotating.

3.3.5.6 Configuration and Components

The components for Option III are the same as for Options I and II with the following exceptions and additions discussed below.

The gimbal assembly should be similar but may need to have slightly higher torque rating about both axes due to the additional inertia of the S-band feed arm and its associated hardware and components.

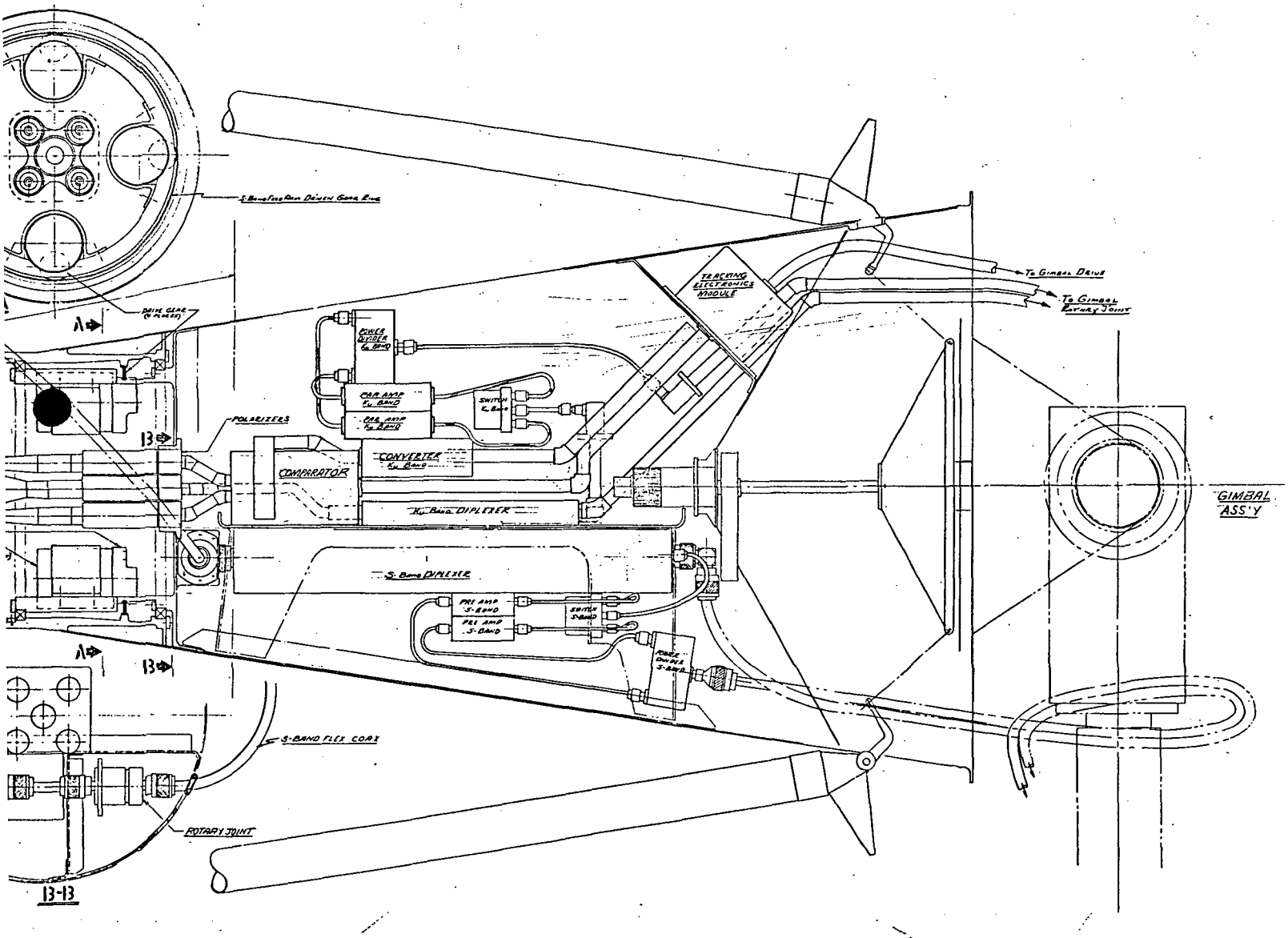

Figure 12. Detail Drawing of S- and K_u-Band Feed System - Option III

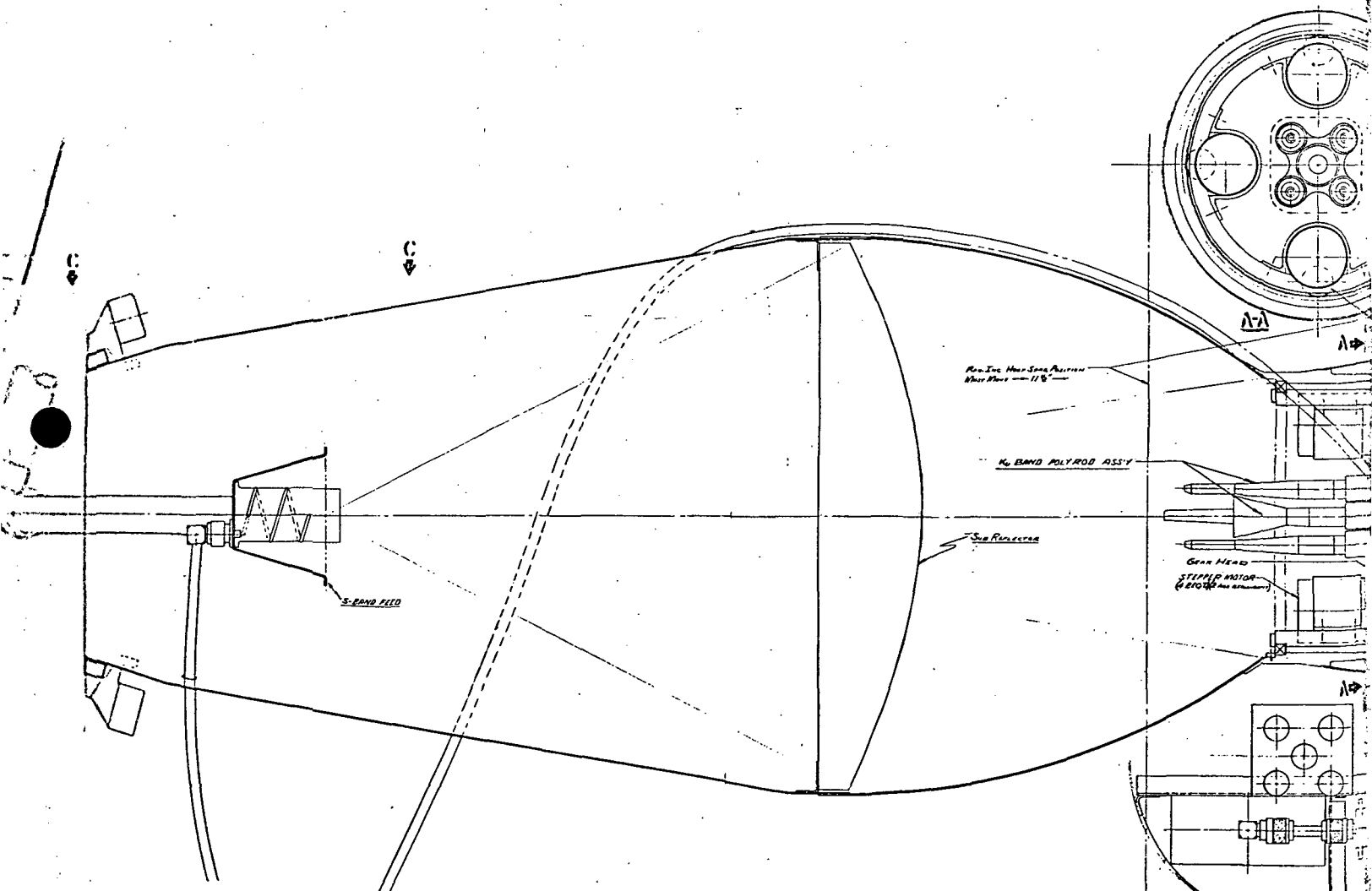
A-A
S-BAND FEED
SUB REFLECTOR
GEAR HEAD
STEPPER MOTOR
13-13

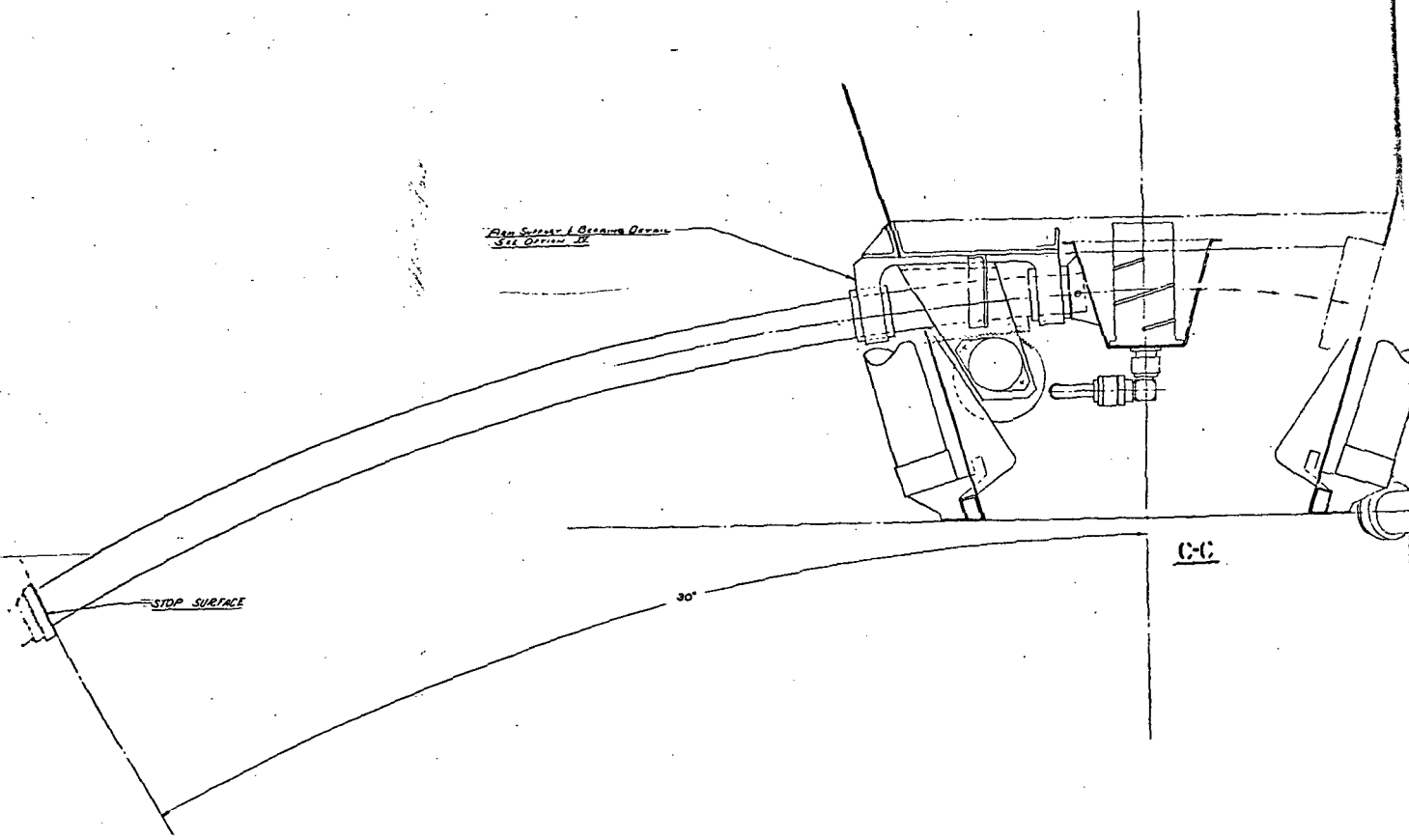
ARM SUPPORT & BEARING DETAIL
SEE OPTION II
C-C
STOP SURFACE
30°

The S-band tracking system requires a pair of curvilinear motion bearings for the tracking arm to move in. The curvilinear bearings would be similar to the Thomsom Linear Ball Bearings but would have several of the recirculating ball races fitted to a double curved surface rather than a single curvature. The curvilinear ball bushings would be a development item but are shown on Option III because of the advantages in simplicity of installation and light weight. If this type bearing should prove impractical for this application as more detailed design studies occur, it would be a simple matter to go to a track and roller design to obtain the curvilinear motion for the S-band feed.

Two stepper motors and two auto backlash drive gears are also required to drive the tracking arm. The use of stepper motors most likely will eliminate the need for position readouts, as feedback is not ordinarily required when the stepper is used properly. However, a stepper is compatible with feedback if further design studies should so indicate. Steppers are normally compatible with feedback whether analog or digital, whether for velocity or position, or both. Error is non-cumlative as long as pulse-to-step integrity is maintained. A stream of pulses can be counted into a stepper, and its fluid shaft position is known within a very small percent of one step. DC servo accuracy, in contrast, is subject to the sensitivity and phase shift of the loop. Steppers do not have null positions, bi-directional rotation is continuous. Maximum torque occurs at low pulse rates and the torquer can readily accelerate its load. When the desired position is reached and command pulses end, the stepper shaft stops. There is no need for clutches and brakes. Once stopped, there is almost no drift. Many steppers available are magnetically detected in the last position. In sum, a load can be started in either direction, moved to a position, and remain there without power drain until commanded again. Steppers are true digital actuators and do not require a digital-to-analog conversion at the input as do conventional servos. They offer close speed control and reversibility over a wide range. Starting current is low. The rotor moment of inertia is low. Multiple steppers driven from the same source maintain perfect synchronization. For driving the arm two steppers are used where one is redundant. To rotate the arm, four steppers are used where two are redundant (Section A-A, Figure 12). Each of these steppers will carry its own gear reduction head and drive a large ring gear about 8 inch diameter. The entire rotating mass will be supported on two ball bearings about 8-1/2 inches in diameter (Figure 12).

As shown in Section B-B of Figure 12, an RF rotary joint is used to minimize the cable twist in the RF flex coax from the S-band feed into the non-rotating part of the cone. Slack in the cable is intended to allow for the S-band rotation and arm translation since a rotary joint cannot be used in its most proper manner, i.e., a rotary joint could not be placed on the axis of rotation without undue disadvantage to structural configuration and/or RF function.

The supporting structure inside the cone, for the monopulse system and the polyrod assembly (Section AA, Figure 12) would most likely be a precision cast piece designed to support and give alignment to the stepper motors, drive gears, and bearings. The remaining support structure would be similar to that for Options I and II, a lightweight aircraft type aluminum assembly.

The tracking arm as shown on the Option III drawing (Figure 12) is depicted as three telescoped tubes giving a tapered effect on tube thickness and then formed to a radius of sixty or so inches. The gear rack then must attach to the arm. Further design study may indicate this to be rather impractical, in which event it would then seem well to consider that the arm should be a Vanasil casting. Vanasil is a hyperentectic of about 23 percent silicon with a coefficient of expansion that may be more compatible with TDRS accuracy requirements. Reynolds A-390 casting is also another possible material for the tracking arm.

3.4 Option IV Candidate

3.4.1 Candidate Description

The preferred candidate for the Option IV requirements is basically the same as the Option III candidate with the exception of the S-band feed system. The Option IV S-band feed system is an auto tracking feed identical to that presented in Option II. In summary, Option IV is comprised of the following:

1. Spherical dual reflector, cassegrain, 12.5 feet in diameter
2. K_u-band feed at the secondary focal point (dedicated data channel and defocused autotrack)
3. Shaped dichroic subreflector
4. S-band autotracking feed (dual mode spiral)
5. S-band auto tracking via ground station processing
6. S-band feed positioning mechanism (includes dual channel rotary joint)
7. Independent servo control system for positioning the S-band feed. The rotation of the feed arm could cause a linearly related phase variation in the S-band error channel; phase characteristic of the feed is fixed with respect to the arm.

The design of the feed positioning mechanism includes a mechanical gearing arrangement which counter-rotates the spiral antenna so that its reference is fixed with respect to the satellite. This method of preserving coordinate alignment was selected over compensation by mechanical or electrical phase shifters because of its simplicity and inherent accuracy.

3.4.2 Operation and Capabilities

This candidate antenna provides the maximum degree of flexibility of all the previous options. Table XVIII summarizes its additional capabilities (compared with Option I), as applied to specific user equipment. Most significant is the capability to autotrack an S-band user while simultaneously auto tracking a K_u-band user, when the two users are widely separated in angle. In addition, the S-band tracking feed can be used as an acquisition aid to the K_u-band auto tracking system. Table XIX gives a step by step procedure for employing the S-band feed during K_u-band acquisition and data maintenance.

TABLE XVIII

Additional Operational Capabilities of Option IV Candidate

(Compared with Option I)

User Equipment	Additional TDRS Operational Capabilities
User A S-band receiver K_u-band data transmitter and receiver	None
User B S-band data transmitter and receiver No K_u-band	• S-band data link maintenance S-band autotrack
User C S-band beacon transmitter and receiver K_u-band data transmitter and receiver	• K_u-band data link maintenance S-band autotrack (backup) • Acquisition aid for K_u-band autotrack S-band autotrack
Multiple Users A and B or C and B	• Maintain maximum performance K_u-band data link with User A or User C. • Maintain S-band data link with User B at wide angular separation from User A or User C.

TABLE XIX

Designation and K_u-Band Autotrack Sequence

(Option IV)

Assumptions:

Same as Option II

Sequence:

Step 1 - TDRS S-band feed is commanded to return to on-axis reference position (S-band beam aligned with K_u-band beam).

Steps 2 through 12 - (Same as Steps 1 through 11 of Option II).

Note: When K_u-Band HDR link is established, S-band feed can be used to establish an independent S-band link with another user.

Trouble Sequence:

In the event of a malfunction whereby the S-band feed cannot be returned to its on-axis position, then the following sequence can be employed:

Step 1 - Ground computes TDRS/user relative look angles with compensation for the known position (offset angle) of the S-band feed.

Step 2 - TDRS antenna is commanded to look at the user so that the S-band beam is illuminating the user.

Step 3 - User is commanded to point its K_u-band antenna at TDRS.

Step 4 - User is commanded to turn on the K_u-band transmitter.

Step 5 - Ground commands TDRS to point its antenna so that the K_u-band beam essentially illuminates the user.

Steps 6 through 11 - (Same as Steps 4 through 9 of Option I).

In spite of its obvious advantages for achieving maximum TDRSS flexibility and operational capabilities, it is by far the least desirable from the standpoint of complexity, weight, cost, development time, power consumption, and reliability. By viture of the same arguments presented in paragraph 3.2.2 for Option II, the inherent disadvantages of this option may not be justifiable by its additional flexibility and capabilities. This is especially significant when considering that an S-band auto tracking feed is not required to maintain an S-band data link; nor is it required for designation of a K_u-band user (assuming baseline user and TDRSS characteristics of Table I). Elimination of the S-band auto tracking feed system reduces this option to Option III.

3.4.3 Performance

3.4.3.1 RF Performance for K_u-Band and S-Band

The details of the RF losses for Option IV are presented in Table XX for the S-band. The K_u-band losses are the same as Option I and are presented in Table VI. Comments associated with these values are applicable for all options and are placed immediately behind the tables in paragraph 3.1.3.1.

3.4.4 Feed Design Considerations

3.4.4.1 K_u-Band Feed System

Same as Option III.

3.4.4.2 S-Band Feed System

Same feed antenna as Option II. Two dual channel rotary joints are required in the S-band feed system to prevent the two RF cables from twisting while the feed is tracking. The first rotary joint placed directly behind the antenna allows the antenna to maintain spatial reference with respect to the x-y coordinate axis orientation of the main reflector. The second rotary joint is located in the cone structure and is used to prevent excessive twisting of the cables while the S-band feed is undergoing rotational movement.

TABLE XX

RF Performance: Option IV--S-Band

Performance Factors	Boresight		±30° Scan	
	Transmit	Receive	Transmit	Receiv
Frequency (MHz)	2072.5	2250.0	2072.5	225
Aperture diameter (meters)	3.81	3.81	3.81	
Aperture area gain (dB)	38.36	39.07	38.36	3
Amplitude taper loss (dB)	0.46	0.46	0.46	0.46
Spillover loss (dB)	1.25	1.25	1.25	1.25
Blockage loss (dB)	0.23	0.23	0.12	0.12
Phase loss (dB)	0.13	0.13	0.13	0.13
Cross-polarization loss (dB)	0.11	0.11	0.11	0.11
Ogive loss (dB)	0.15	0.15	0.0	0.0
Subreflector loss (dB)	0.50	0.50	0.0	0.0
Surface tolerance loss (dB)	0.01	0.01	0.01	0.01
Mesh reflectivity loss (dB)	0.004	0.004	0.004	0.004
Spherical aberration Loss (dB)	0.30	0.30	0.30	0.30
Feed antenna I^2R loss (dB)	0.25	0.25	0.70	0.70
Comparator loss (dB)	0.50	0.50	0.50	0.50
Cable loss (dB) (antenna to diplexer)	0.65	0.65	0.65	0.65
Rotary joint loss (dB), T2	0.30	0.30	0.30	0.30
VSWR loss (dB), 1.25:1	0.05	0.05	0.05	0.05
Off boresight scan loss (dB)	NA	NA	5.4	5.4
Total overall loss (dB)	4.89	4.89	9.98	
Overall efficiency (percent)	32.4	32.4	10.0	1
Antenna peak gain (dB)	33.5	34.2	28.4	
Diplexer loss (dB)	0.50	0.50	0.6	
Cable loss to S/C interface (dB), 10 feet	0.75	NA	0.75	
Cable wrap loss through gimbals (dB)	0.18	NA	0.18	
Redundancy switch loss (dB)	NA	0.30	NA	
Half power beamwidth (degrees)	2.53	2.33	2.92	
Polarization sense	Circular	Circular	Circular	Circ

3.4.5 Mechanical Design

Option IV as it appears on Figures 13 and 14 is the same as Option III as it appears on Figures 11 and 12 with the exceptions and additions discussed below.

The S-band feed of Option III, which is a helix, will be replaced by a spiral feed for Option IV. Also, Option IV will use two flexible coaxial cables form the feed instead of one as for Option III. Option IV will require the S-band feed to be de-spun as the tracking arm is rotated. Figure 14 shows the spiral S-band feed being turned by two torque motors which use two feedback pots, where one is redundant in each case. An RF rotary joint on axis conducts the two flexible coaxial cables away from the spiral feed and onto the arm. This arrangement will most likely give way to the use of two stepper motors and no feedback for reasons explained in paragraph 3.3.5.

3.5 Weight Budget - All Options

Tables XXIand XXIIprovide a detailed weight breakdown by options. These are based on weights obtained from the various component vendors and/or calculated weights based upon the particular option configuration.

3.6 Performance Summary for Preferred Candidates

Tables XXIIIand XXIV comprise a summary of the performance for each of the preferred baseline candidates. Each performance factor, except data-channel RF loss, has been discussed in this section. Data channel RF loss is separately treated in paragraph 4.6.3.3. RF loss is defined as the insertion loss between the feed network output and the RF paramp input on receive and between the transmitter output to the feed network input on transmit. The feed network output and input are a common (single) port which connects to the data channel diplexer with an appropriate transmission line.

TABLE XXI

Detailed Weight Breakdown

External Structure	Weight (Pounds) Options			
	I	II	III	IV
Hub	3.1	3.1	4.3	4.3
Cone	4.5	4.5	4.7	4.7
Ogive	3.5	3.5	1.6	1.6
Upper cone	1.1	1.1	3.0	3.0
Total	12.2	12.2	13.6	13.6

TABLE XXI(Continued)

	Weight (Pounds) Options			
	I	II	III	IV
Rib Assembly				
Ribs	4.0	4.0	4.0	4.0
Midpoint pins	0.5	0.5	0.5	0.5
Standoffs	0.2	0.2	0.2	0.2
Pivot arms	1.6	1.6	1.6	1.6
Rib tip	0.7	0.7	0.7	0.7
Total	7.0	7.0	7.0	7.0
Mesh Gore Assembly				
Front	1.2	1.2	1.2	1.2
Back	0.2	0.2	0.2	0.2
Tie wires	0.1	0.1	0.1	0.1
Intercoastals	0.2	0.2	0.2	0.2
Total	1.7	1.7	1.7	1.7
Mechanical Deployment System Total	2.9	2.9	2.9	2.9
Restraint System				
Hoop and spar assembly	1.5	1.5	1.3	1.3
Top ring, cones, hardware	0.6	0.6	0.6	0.6
Pyro release system	0.4	0.4	0.4	0.4
Total	2.5	2.5	2.3	2.3
Thermal Control				
Rib insulation	0.5	0.5	0.5	0.5
Cone/hub insulation	0.8	0.8	0.8	0.8
Total	1.3	1.3	1.3	1.3
Internal Structure and Mechanism				
Stringers, total	0.3	0.3	0.2	0.2
Main platform	0.4	0.4	0.3	0.3
Legs: 2 @.1	0.2	0.2	0.1	0.1
Polyrod support ring adapter	0.5	0.5	--	--
Polarizer blkd. (precision)	0.6	0.6	--	--
Waveguide support bkt.	0.1	0.1	0.2	0.2
S-band feed support stringers and webs	0.6	0.4	--	--
S-band diagonal bracing	0.3	0.2	--	--
*Rotating Structure bearing support fittings	--	--	1.5	1.5
** Static structure bearing and motor support fittings	--	--	2.5	2.5

* Also includes ring gear

** Made integral with cone ring blkd. which supports polyrod assembly.

TABLE XXI(Continued)

Internal Structure and Mechanism (cont'd)	Weight (Pounds) Options I	II	III	IV
Rotation bearings (2) and retainers	--	--	1.2	1.2
Rotation stepper motor and gear head (4)	--	--	2.2	2.2
S-band arm and end fittings and rack	--	--	1.5	1.5
S-band feed framing structure	--	--	0.1	0.4
Bearings, curvalinear and support bkts.	--	--	1.5	1.5
Curvalinear drive steppers and support bkts	--	--	0.8	0.8
S-band feed de-spin torquers (2)	--	--	--	0.3
S-band feed de-spin pots (2) and gears	--	--	--	0.2
Total	3.0	2.7	12.1	12.9
K_u-Band System				
Polyrod antennas (teflon)	0.2	0.2	0.2	0.2
Comparator (aluminum)	0.5	0.5	0.5	0.5
Polarizers (copper)	1.0	1.0	1.0	1.0
Converter (vendor data)	1.0	1.0	1.0	1.0
Scan code generator, synch demodulation (card)	0.5	0.5	0.5	0.5
Diplexer (copper)	0.4	0.4	0.4	0.4
Paramps and redundancy switch (vendor data)	2.8	2.8	2.8	2.8
Directional coupler (copper)	0.3	0.3	0.3	0.3
Steering electronics (card)	--	0.6	--	0.6
Subreflector (honeycomb dielectric)	0.3	0.3	0.2	0.2
Coupler and phase shifter (vendor data)	0.7	0.7	0.7	0.7
Waveguides (copper, WR-62)	3.2	3.2	3.2	3.2
Hardware, bkts., flange, screws	1.5	1.5	1.5	1.5
Total	12.4	13.0	12.3	13.0
S-Band System				
Cupped helix feed (estimate)	0.3	--	0.3	--
Spiral feed (vendor data)	--	5.0	--	5.0
Diplexer (vendor data)	4.0	4.0	4.0	4.0
Rotary joints (vendor data)	--	--	0.4	0.8
Cables (vendor data)	2.4	3.9	2.9	5.0
Connectors (vendor data)	1.1	1.7	1.2	1.8
Paramps and redundancy switch (vendor data)	2.5	2.5	2.5	2.5
TOTAL	10.3	17.1	11.3	19.1

TABLE XXII

Complete System Weight Summary for Preferred Candidates

	Weight (Pounds)			
		Options		
	I	II	III	IV
External structure	12.2	12.2	13.6	13.6
Rib assembly	7.0	7.0	7.0	7.0
Mesh gore assembly	1.7	1.7	1.7	1.7
Mechanical deployment system	2.9	2.9	2.9	2.9
Restraint system	2.5	2.5	2.3	2.3
Thermal control	1.3	1.3	1.3	1.3
Internal structure and mechanism	3.0	2.7	12.1	12.9
K_u-band system	12.4	13.0	11.3	13.0
S-band system	10.3	17.1	11.3	19.1
*Antenna system total	53.3	60.4	63.5	73.8
Space Pointing Gimbal Assembly				
Gimbal structure and mechanism	17.0	18.0	19.0	20.0
Drive electronics	4.0	4.5	5.0	5.5
	21.0	22.5	24.0	25.5

*Total load on gimbal

TABLE XXIII

Preferred Candidate Antenna Gain, Aperture Efficiency, and Data Channel Loss Summary

	All Options K_u-Band			S-Band Transmit				S-Band Receive			
	Trans-mit	Received Data	Received Track	Options I	II	III	IV	Options I	II	III	IV
Gain (dB)	51.3	52.3	47.5	35.2	34.0	34.3 max 29.0 min	33.5 max 28.2 min	34.7	35.2	35.0 max 29.7 min	34.2 max 28.9 min
Efficiency (percent)	48.9	47.9	15.8	48.0	36.8	39.4 max 11.5 min	32.4 max 9.6 min	36.8	40.8	39.4 max 11.5 min	32.4 max 9.6 min
Data Channel RF Loss (dB)	1.90	0.80	NA	1.68	1.68	1.68	1.68	0.90	0.90	0.90	0.90

TABLE XXIV

Data Beam Pointing Accuracy and Resulting Data Signal Loss for Preferred Baseline Candidates

Mode	3σ Pointing Accuracy* (degrees)			Data-Signal Loss (dB)		
	I	Option II	III	I	Option II	III
Ground Command						
• S-Band Data Link	±0.45	±0.47	±0.45 (min) ±0.59 (max)	0.39	0.42	0.39 (min) 0.67 (max)
K_u-Band Autotrack						
• K_u-Band Data Link	±0.054	±0.054	±0.054	0.22	0.22	0.22
• S-Band Data Link	$\leq\pm$0.160	±0.160	$\leq\pm$0.160	<0.05	0.05	<0.05
S-Band Autotrack	NA		NA	NA		NA
• S-Band Data Link		$\pm$0.317			0.19	

* SNR = 5.7 dB
B_n = 1 Hz
$T_d/J = 10^{-3}$ sec^{-2}
} For K_u-Band Autotrack

SNR = -16 dB
B_n = 1 Hz
$T_d/J \approx 0$
} For S-Band Autotrack

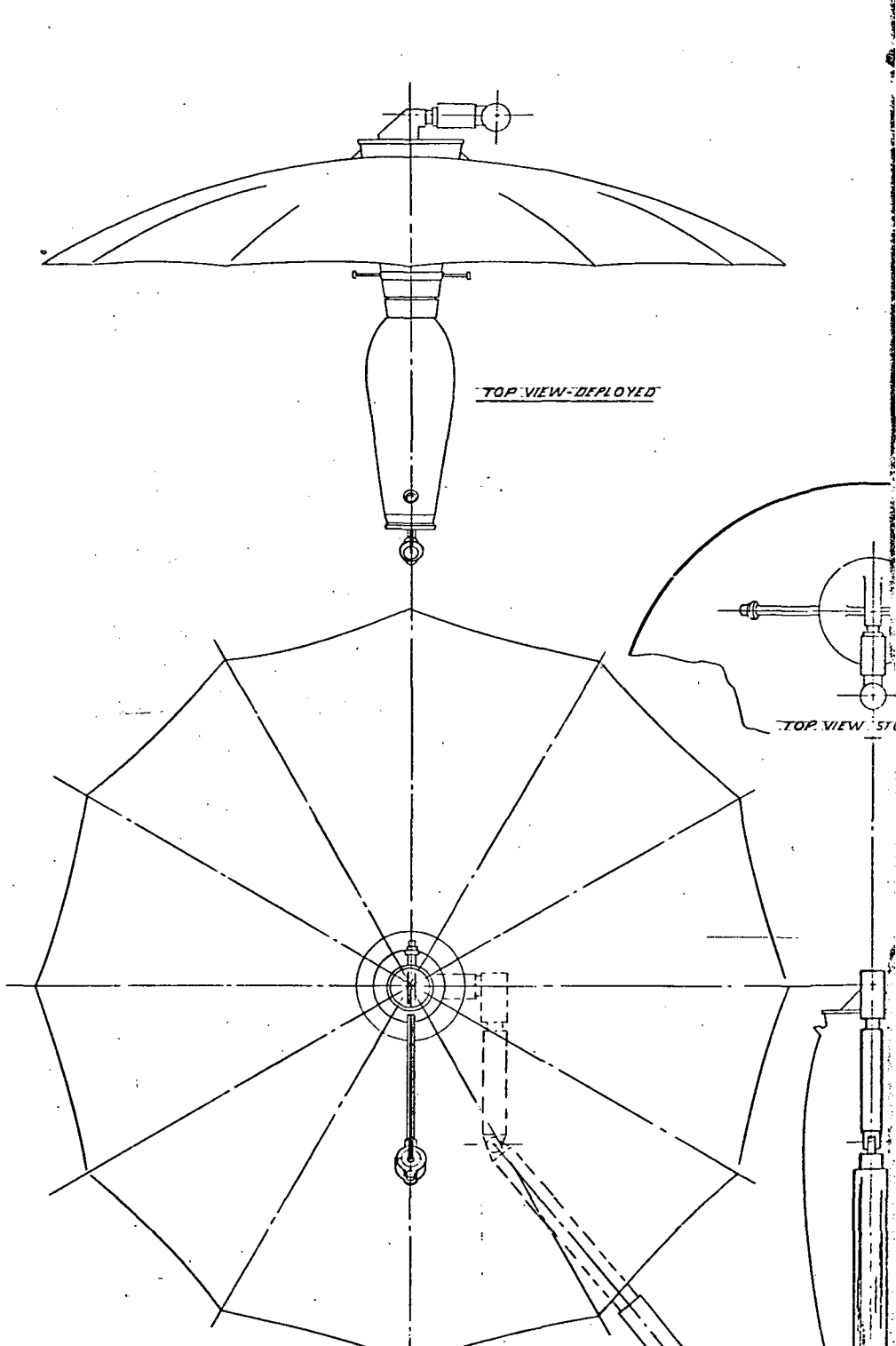

Figure 13. Deployable Antenna System - Option IV

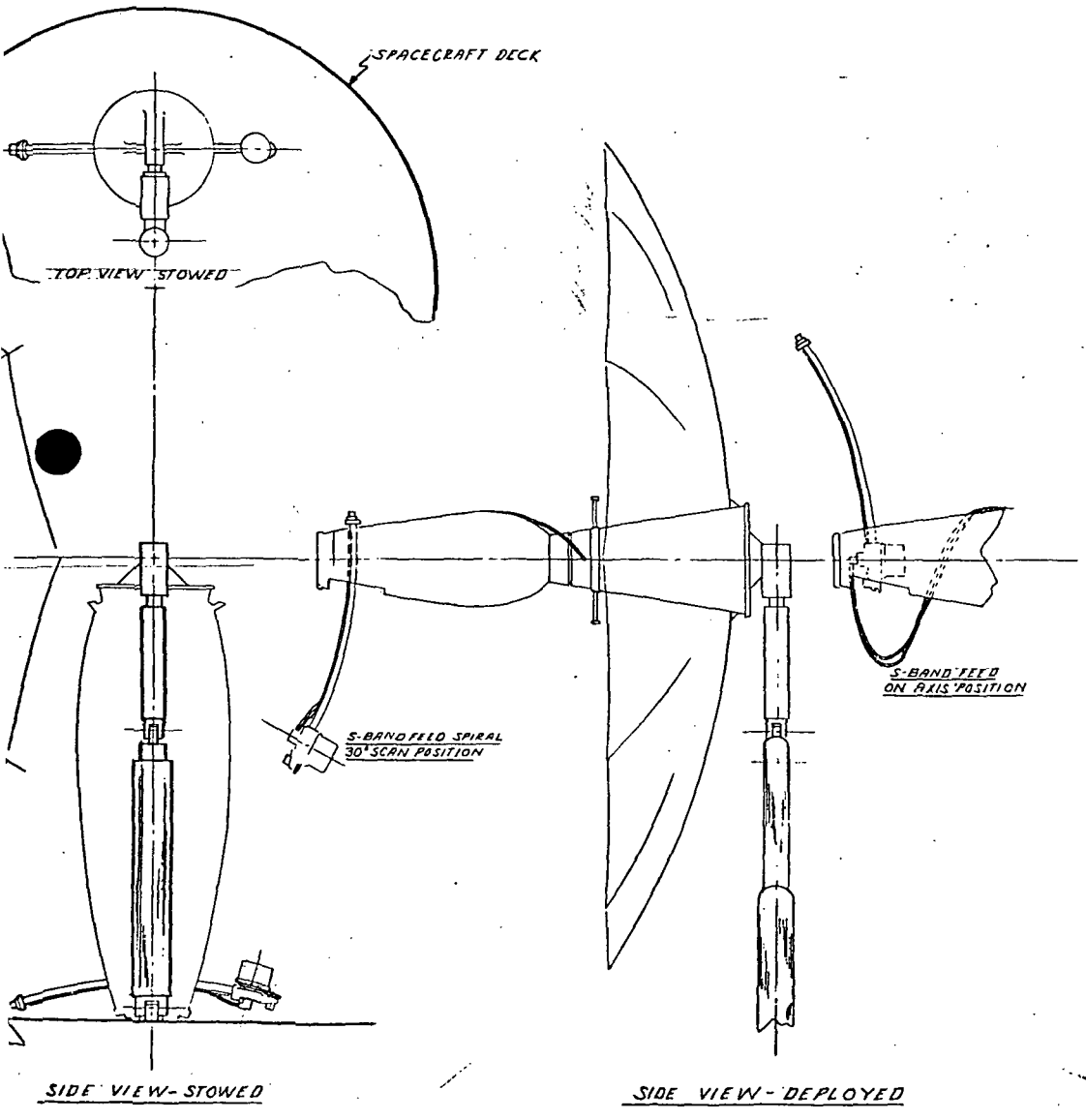
SPACECRAFT DECK
TOP VIEW STOWED
S-BAND FEED SPIRAL
30° SCAN POSITION
S-BAND FEED
ON AXIS POSITION
SIDE VIEW - STOWED
SIDE VIEW - DEPLOYED

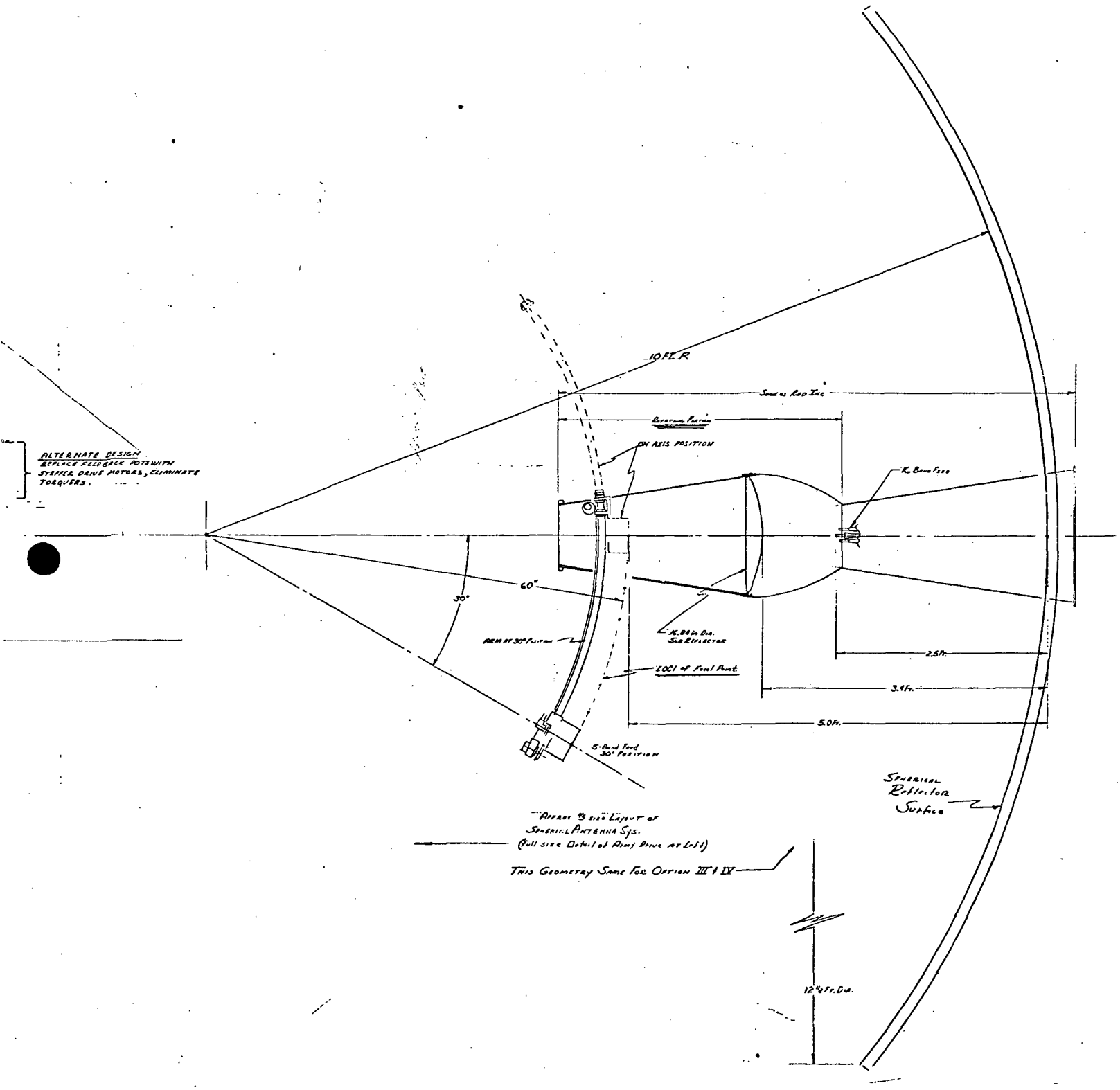

Figure 14. Detail Drawing of S-Band Feed System - Option IV

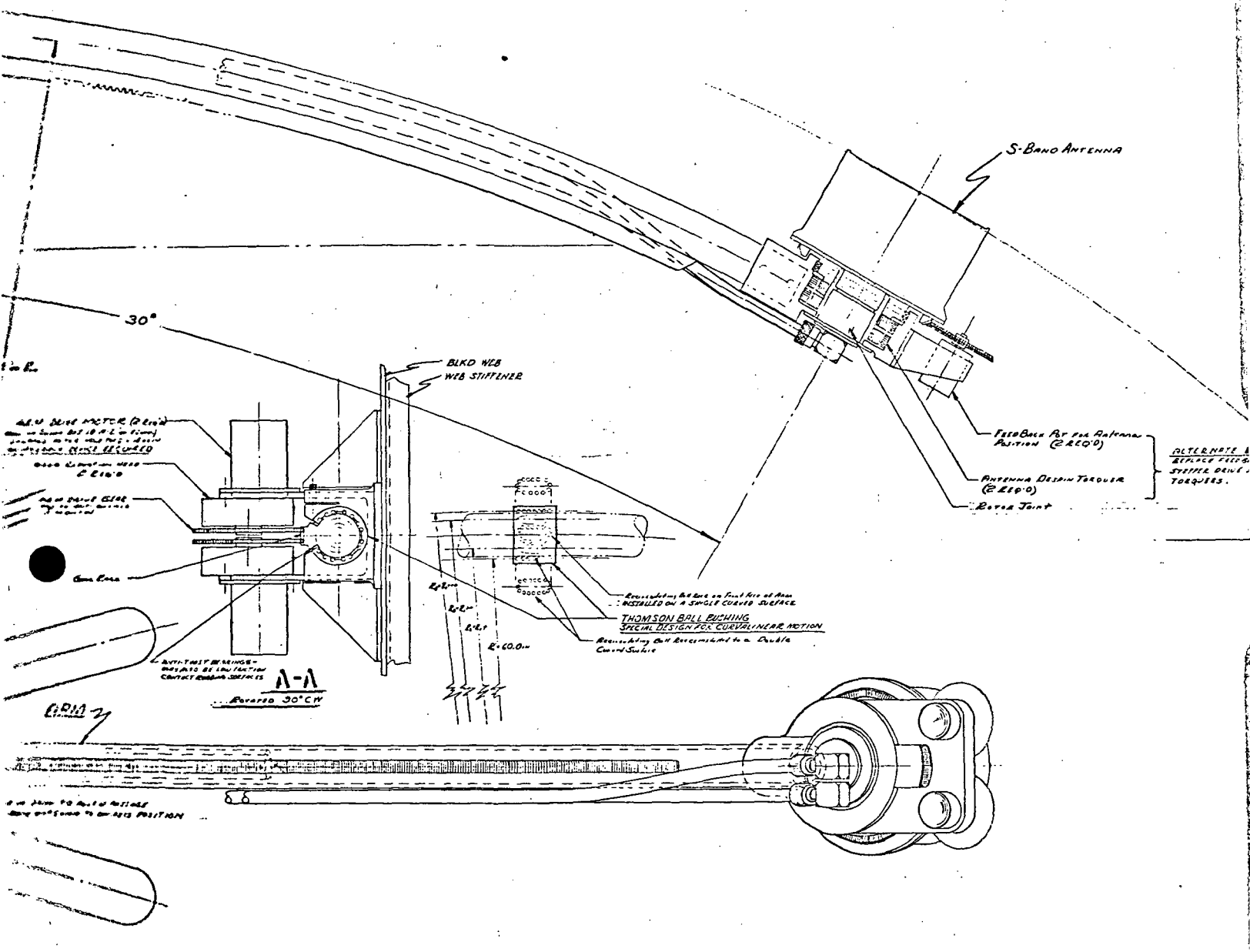
S-Band Antenna
30°
Blkd Web
Web Stiffener
Feedback Pot for Antenna Position (2 Req'd)
Antenna Design Torquer (2 Req'd)
Rotor Joint
Thomson Ball Bushing
Special Design for Curvilinear Motion
A-A
Rotated 30° CW

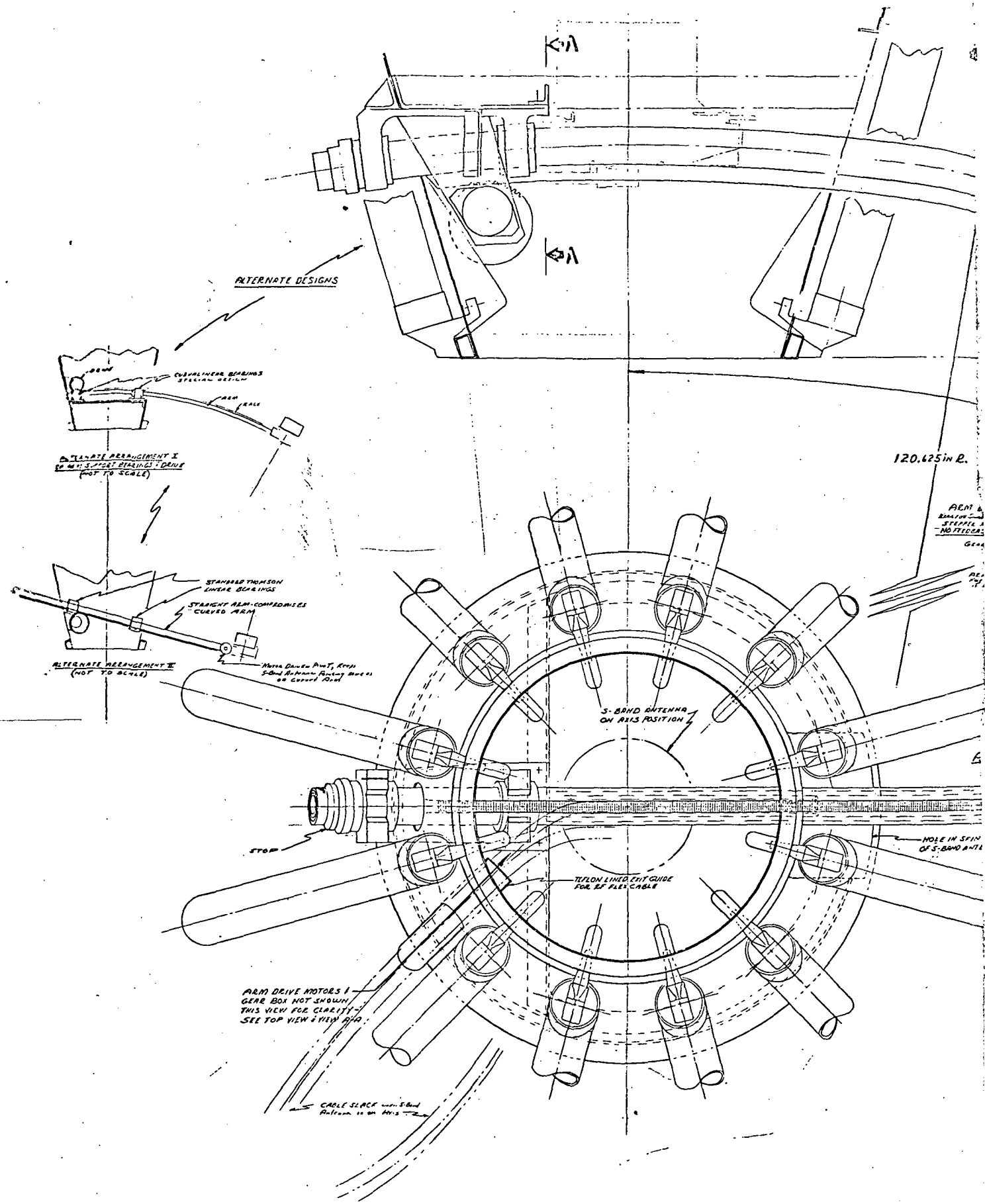
ALTERNATE DESIGNS
CURVILINEAR BEARINGS SPECIAL DESIGN
ARM
RAIL
ALTERNATE ARRANGEMENT I
(NOT TO SCALE)
120.625 in R.
STANDARD THOMSON LINEAR BEARINGS
STRAIGHT ARM-COMPROMISES CURVED ARM
ALTERNATE ARRANGEMENT II
(NOT TO SCALE)
S-BAND ANTENNA ON AXIS POSITION
STOP
TEFLON LINED EXIT GUIDE FOR RF FLEX CABLE
ARM DRIVE MOTORS I GEAR BOX NOT SHOWN, THIS VIEW FOR CLARITY - SEE TOP VIEW & VIEW A-A

4.0 SUPPORTING ANALYSES

This section provides the supporting analyses and design tradeoff data for the performance, operation, and characteristics of the preferred antenna candidates described in section 3.0. The various S-band options and their implementation and tradeoff implications are briefly outlined in section 4.1. Methods for assuring the maintenance of a data link, i.e., the continuous pointing of the data beam toward the user, are detailed in section 4.2. Various designation and aided designation techniques for the acquisition process are then considered in section 4.3. Section 4.4 establishes the contributing components of the data beam angular pointing error, for both ground command and auto tracking modes of operation, and derives the analytical expressions with which pointing error may be calculated for the various reflector/feed options. The screening of various reflector, feed network, and beam steering techniques is performed in section 4.5, wherein the selection of reflector/feed configurations are justified for the different options. Available angle tracking techniques are evaluated for both the S- and K_u-bands in section 4.6; this is followed by the selection of an optimum angle tracking receiver for each band.

The data beam pointing error expressions, derived in section 4.4, were used in section 4.7 in conjunction with the selected angle tracking receiver characteristics (section 4.6) to determine the pointing errors for the preferred candidates, and to provide tradeoff design data of pointing error as a function of servo bandwidth, torque disturbance, and user beacon power (SNR).

Finally, section 4.8 characterizes the various designation and aided designation methods of section 4.3 to determine the compatibility of the field-of-view of the angle sensing system and the angular uncertainty with which its boresight axis is positioned as a result of designation.

4.1 Basic S-Band Antenna Options and Implementation Requirements

4.1.1 S-Band Antenna Options

The basic TDRS antenna requirement centers on the need for simultaneous S- and K_u-band beams generated by a common reflector. This basic requirement leads to four S-band antenna system options; each of these options has an impact on TDRS operational flexibility, S-band performance, user requirements, ground terminal support, complexity, reliability, and weight.

Option I (S-band beam is fixed to the reflector axis and has no auto tracking capability.)

This option is by far the easiest to implement, requires the least components, and is the most reliable. However, the flexibility

of TDRS is limited to the use of either K_u- or S-band at any given time, unless two users are within the S-band beamwidth (2.5 degrees). S-band beam must be controlled by ground command and cannot be used to assist K_u-band acquisition of a K_u-band user.

Option II (S-band beam is fixed to the reflector axis and generates auto tracking error signals.)

This option is also limited to the support of only one user at any given time. This configuration does have two advantages over Option I. It can auto track the user satellite at S-band and, thus, does not require continuous ground control commands. Another advantage is that the S-band feed can be employed as an acquisition aid for K_u-band provided the K_u-band user is equipped with an S-band beacon transmitter.

Option III (S-band beam can be steered off-axis by ground command only, i.e., no autotrack.)

This option provides the capability of simultaneous support of two independent users at S- and K_u-bands. Pointing commands for the S-band beam must be initiated by the ground station. The extent of beam steering is directly related to the minimum RF performance which must be maintained at the maximum steering angle. As in Option I, S-band cannot serve as an acquisition aid for K_u-band.

Option IV (S-band can be steered off-axis with autotrack capability.)

This is the most flexible mode of operation since it provides the advantages of both Options II and III, but is the least desirable in terms of performance, complexity, cost, weight, etc.

Selection of one preferred candidate antenna system from among the four S-band options requires information and trades which are not necessarily technical nor within the scope of this program. This report does present at least one candidate for each option and will leave the final trades between options to the TDRSS designer. Sufficient technical data is presented here to provide the performance base needed for this trade analysis.

4.1.2 System Implementation and Trade Factors

This section will address the relative complexity of each option with regard to hardware implementation, interrelation of major subsystems and command and control functions. Trade factors and evaluation factors are presented.

Figure 15 presents a simplified block diagram of the major subsystem required in the implementation of the TDRS antenna system showing each of the four options. Figures 16 and 17 show more detailed diagrams of the gimbal/servo/reflector interrelationship and the K_u-band tracking

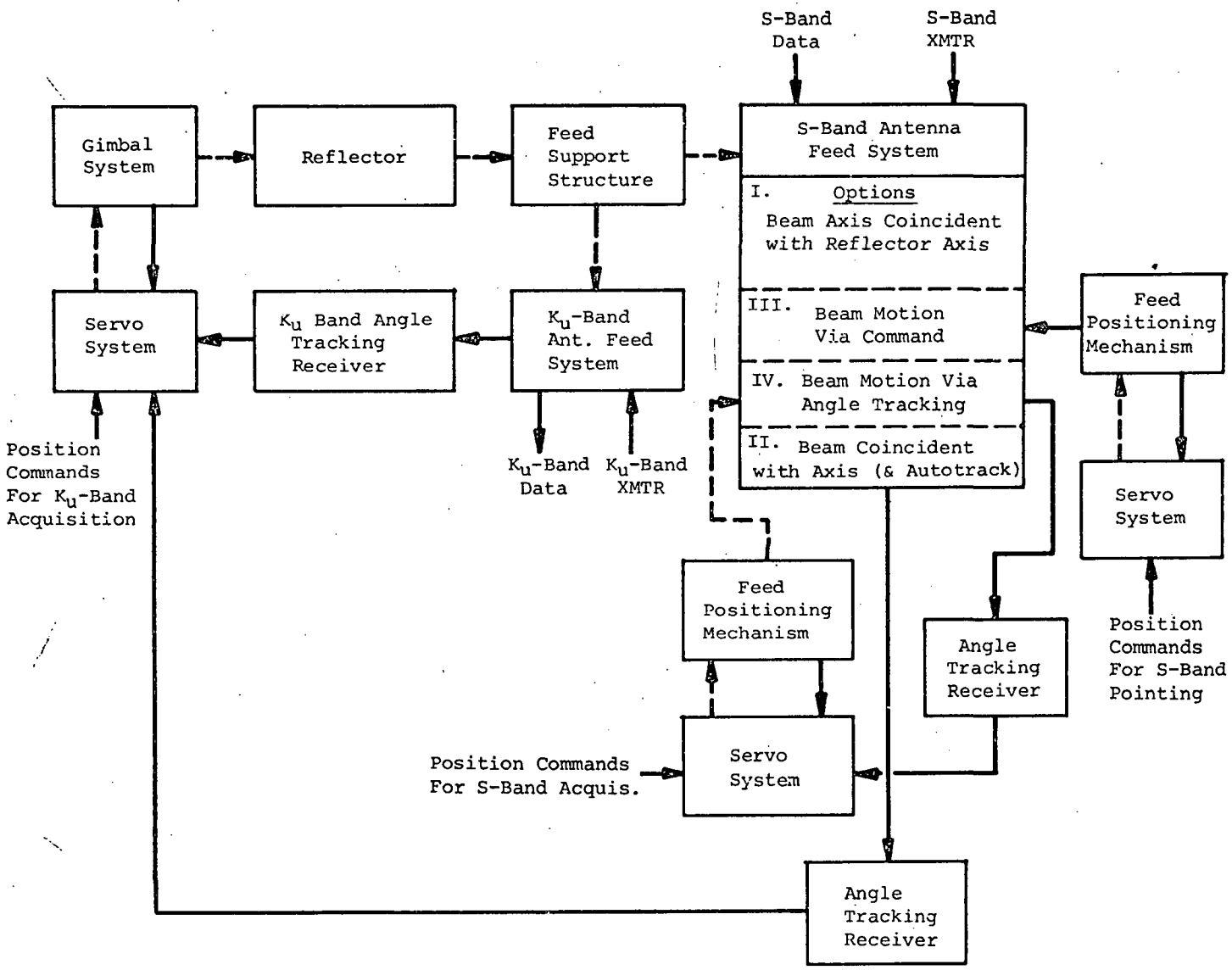

Figure 15. Simplified Block Diagram of S- and K_u Band Tracking Antenna System

Tracking Receiver

Figure 15. Simplified Block Diagram of S- and K_u Band Tracking Antenna System

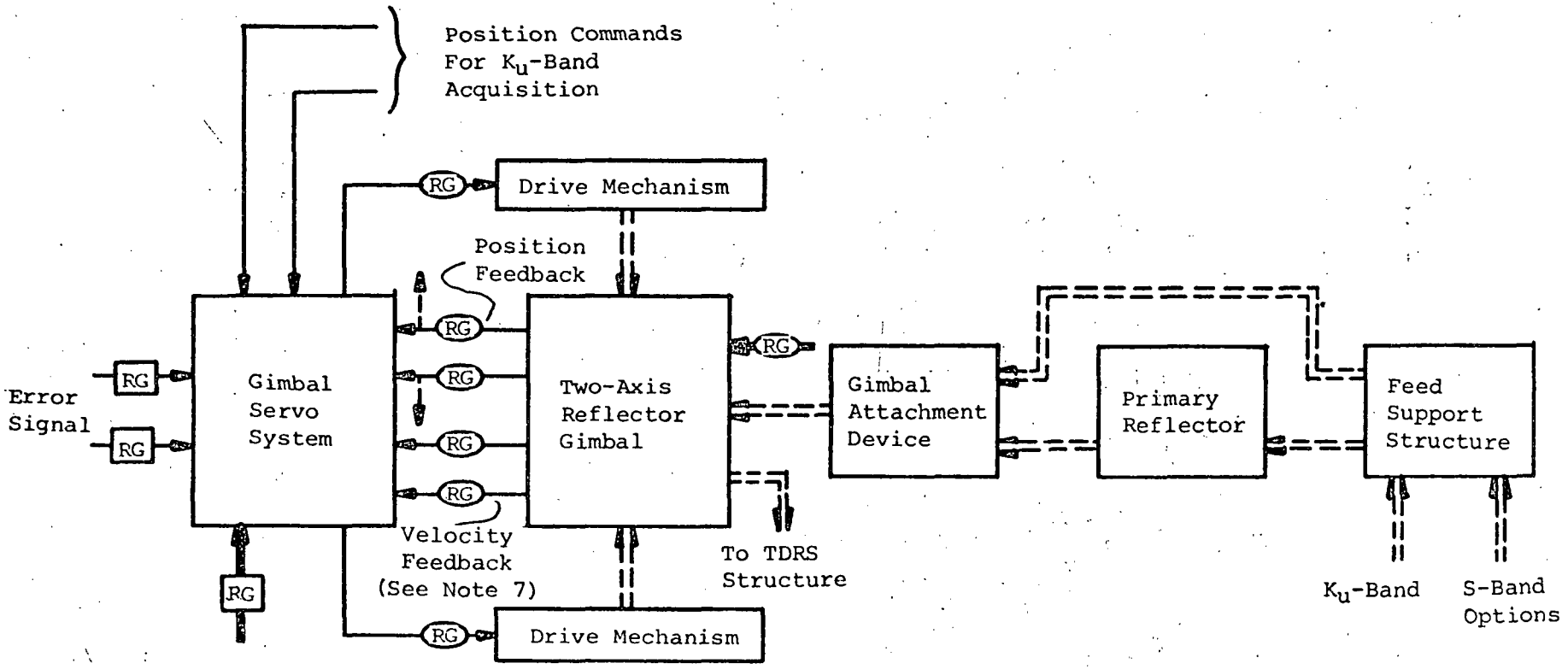

Figure 16. Gimbal/Servo/Reflector

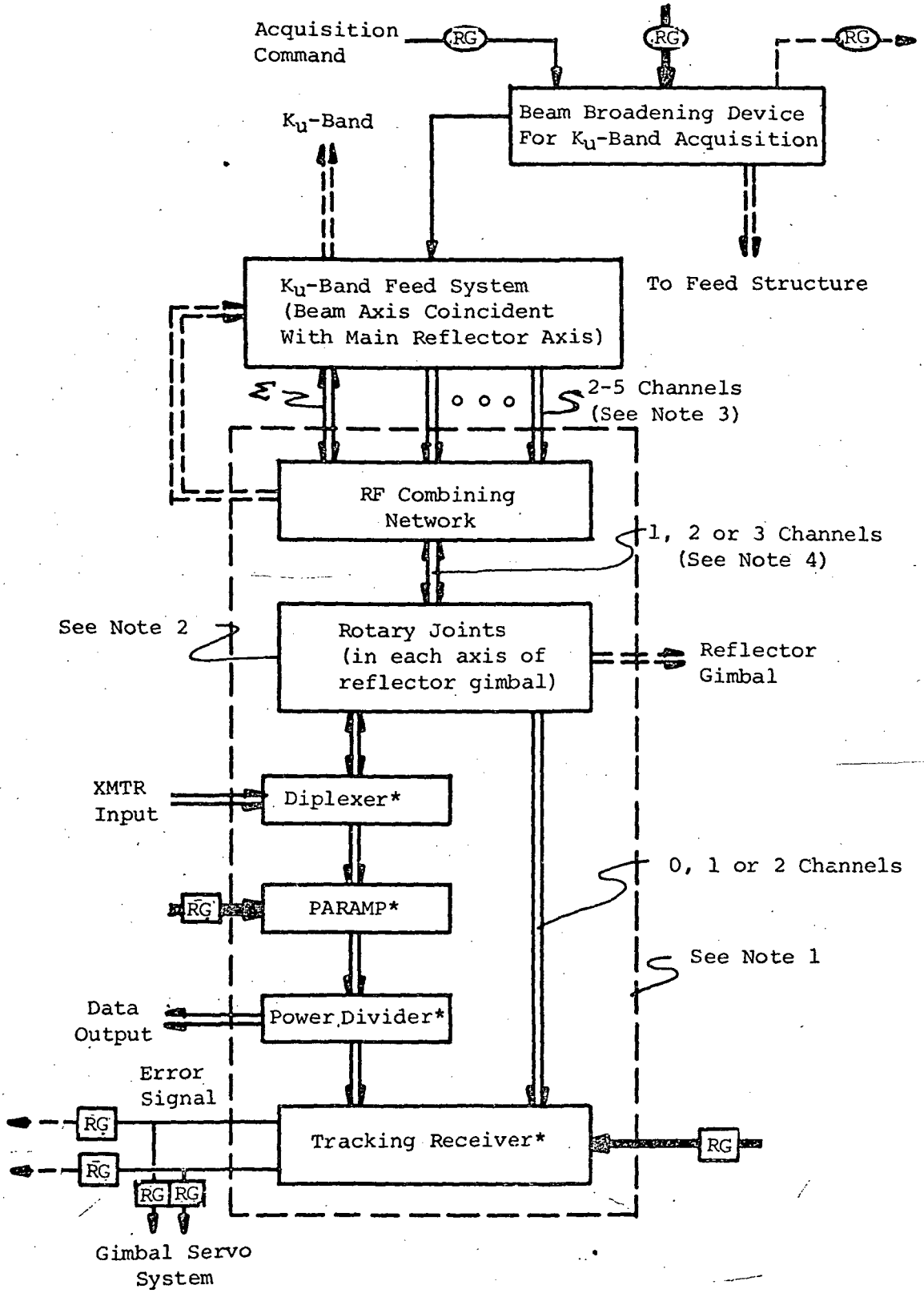

Figure 17. K_u-Band Tracking Feed System

system which are common to each of the four S-band options. The interconnecting keys and notes are explained in Figures 18 and 19.

One significant trade is readily apparent from the K_u-band block diagram (Figure 17). The location of the diplexer, paramp, and tracking receiver relative to the gimbal directly affects waveguide losses. If these devices can be mounted on the feed side of the gimbal, then losses in the data and tracking channels can be kept to a minimum and the SNR can be maximized.

The Option I S-band feed system is shown in Figure 20. This is by far the least complex of all S-band options and, as configured, would require a rotary joint in each axis of the gimbal. Again a trade should be made on the location of the S-band receiver amplifier. If the amplifier is placed on the feed side of the gimbal (to increase the SNR), then the gimbal axis could be crossed with two flexible coaxial cables, one for the transmit signal to the feed and the other for the received signal to the satellite equipment enclosure.

Figure 21 presents a block diagram of S-band Option II. The additional hardware and complexity of adding an autotrack capability is readily apparent. Similar to the K_u-band feed system, the location of the data receiver and tracking receiver must be traded for losses and number of rotary joints. In addition, consideration should be given to the selection of the S-band tracking feed. It is highly deisrable to select a tracking system so that the resultant error signals relate directly to the coordinate system of the gimbal system. For example, if the error signals are derived from a (ρ, θ) system they would need to be converted to an (x, y) system to drive the gimbal.

The feed system of Option III, as shown in Figure 22, is identical to Option I except that a mechanism is added to position the feed off axis upon commands from the ground terminal. Notice that in addition to the servo controlled feed positioning mechanism, a new requirement for either rotary joints or an RF cable wrap has been generated.

Finally, Option IV as presented in Figure 23 is a compilation of all the preceding options. An added complexity is the need for a rotary joint or cable wrap in each axis of the feed positioning mechanism and the gimbal for each tracking channel. For example, if a two channel tracking feed is employed, dual channel rotary joints or dual cable wraps would be required in each axis of the feed positioning mechanism as well as in the reflector gimbal. Some trades in S-band amplifiers and receivers are possible which would reduce the number of rotary joints, but these trades can only be applied to the gimbal axis. Any attempt to place a receiver on the feed side of the feed positioning mechanism would cause additional blockage, increase the drive motor size, and require an even larger feed positioning mechanism.

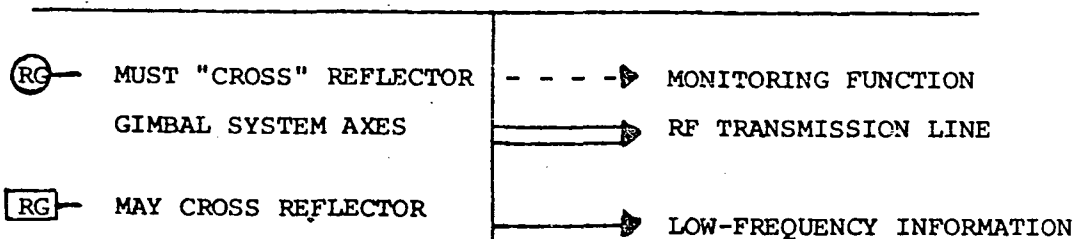

Figure 18. Interconnecting Keys to Preliminary Block Diagram of S- and K_u-Band TDRS Antenna System

(1) THE COMPONENTS SHOWN WILL ALL BE PRESENT IN THE ACTUAL SYSTEM; HOWEVER, THEY MAY NOT BE INTERCONNECTED AS SHOWN. ALSO, OTHER DEVICES, NOT SHOWN, MAY ALSO BE EMPLOYED.

(2) A COAXIAL CABLE-WRAP SYSTEM IS AN OPTION.

(3) THE OPTIONS ON THE NUMBER OF CHANNELS IS INTENDED TO INCLUDE:

NO. OF CHANNELS	ANGLE-SENSING METHOD (TYPICAL)
2	FOUR-ARM SPIRAL
3	ONE Σ AND TWO Δ CHANNELS
4	CONVENTION 4-CHANNEL SIMULT/SEQUEN. LOBING
5	ON-AXIS Σ CHANNEL AND FOUR TRACKING CHANNELS

(4) THE OPTIONS ON THE NUMBER OF CHANNELS ARE BASED, FOR EXAMPLE, ON:

ONE CHANNEL: SINGLE-CHANNEL SIMULT./SEQUENT. LOBING,
TWO CHANNELS: ONE Σ AND TWO MULTIPLEXED DIFFERENCE CHANNELS,
THREE CHANNELS: CONVENTIONAL Σ AND Δ .

(5) MAY NOT BE REQUIRED.

(6) FOR K_u-BAND BEAM BROADENING, EITHER ELECTRICAL OR MECHANICAL OR BOTH MEANS MAY BE EMPLOYED.

(7) THE NEED FOR VELOCITY FEEDBACK HAS NOT BEEN DETERMINED.

* THE LOCATION OF THESE DEVICES HAS NOT BEEN DETERMINED.

Figure 19. Notes on Preliminary Block Diagram of S- and K_u-Band TDRS Antenna System

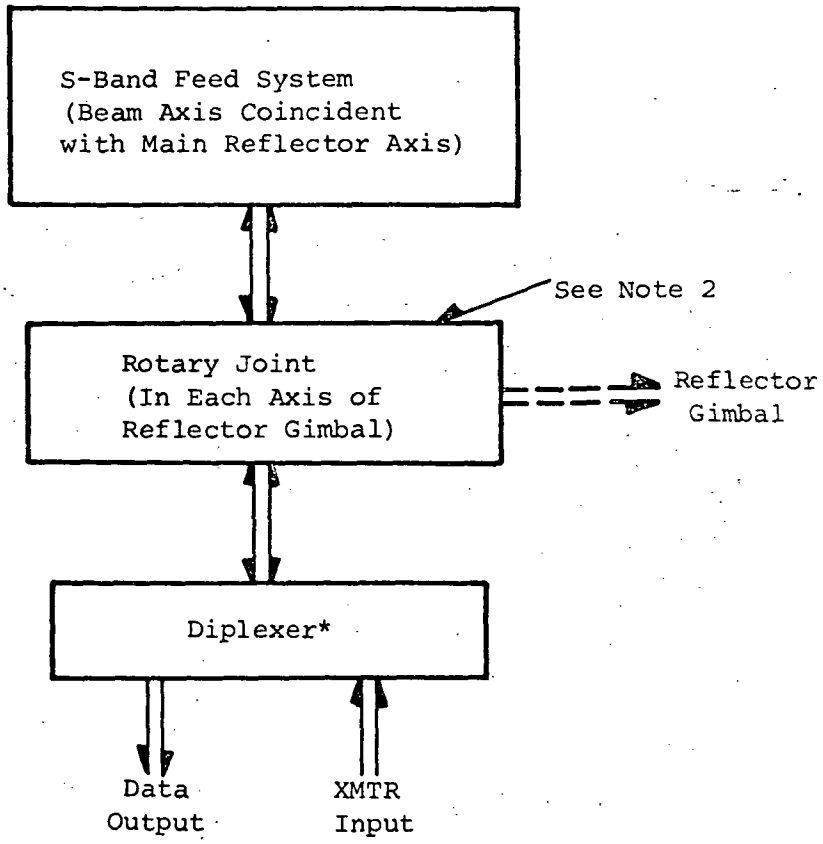

Figure 20. S-Band Feed System - Option I - Beam Fixed and Coincident with Reflector Axis

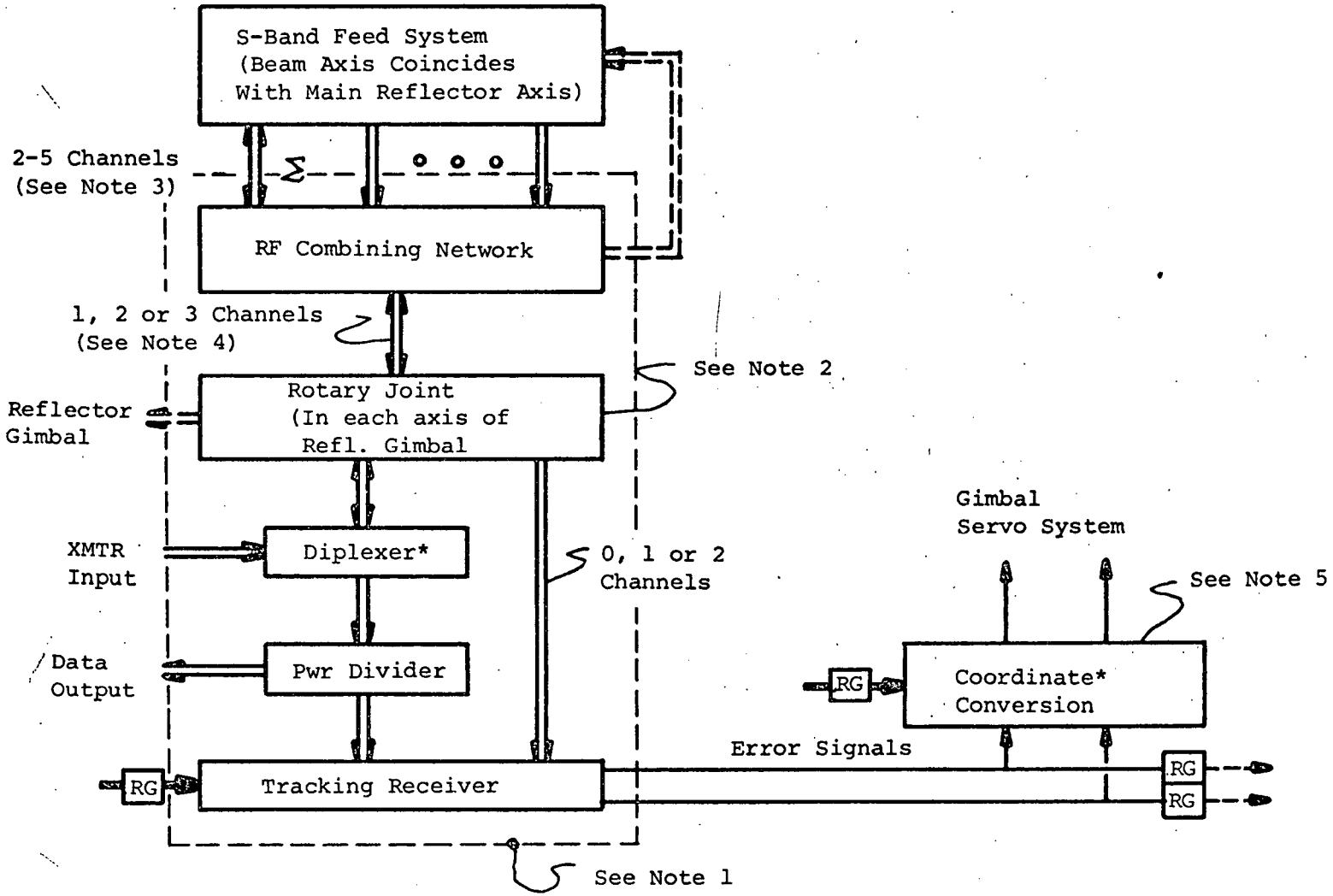

Figure 21. S-Band Feed System - Option II - Beam Fixed and Coincides with Reflector Axis (with Autotrack)

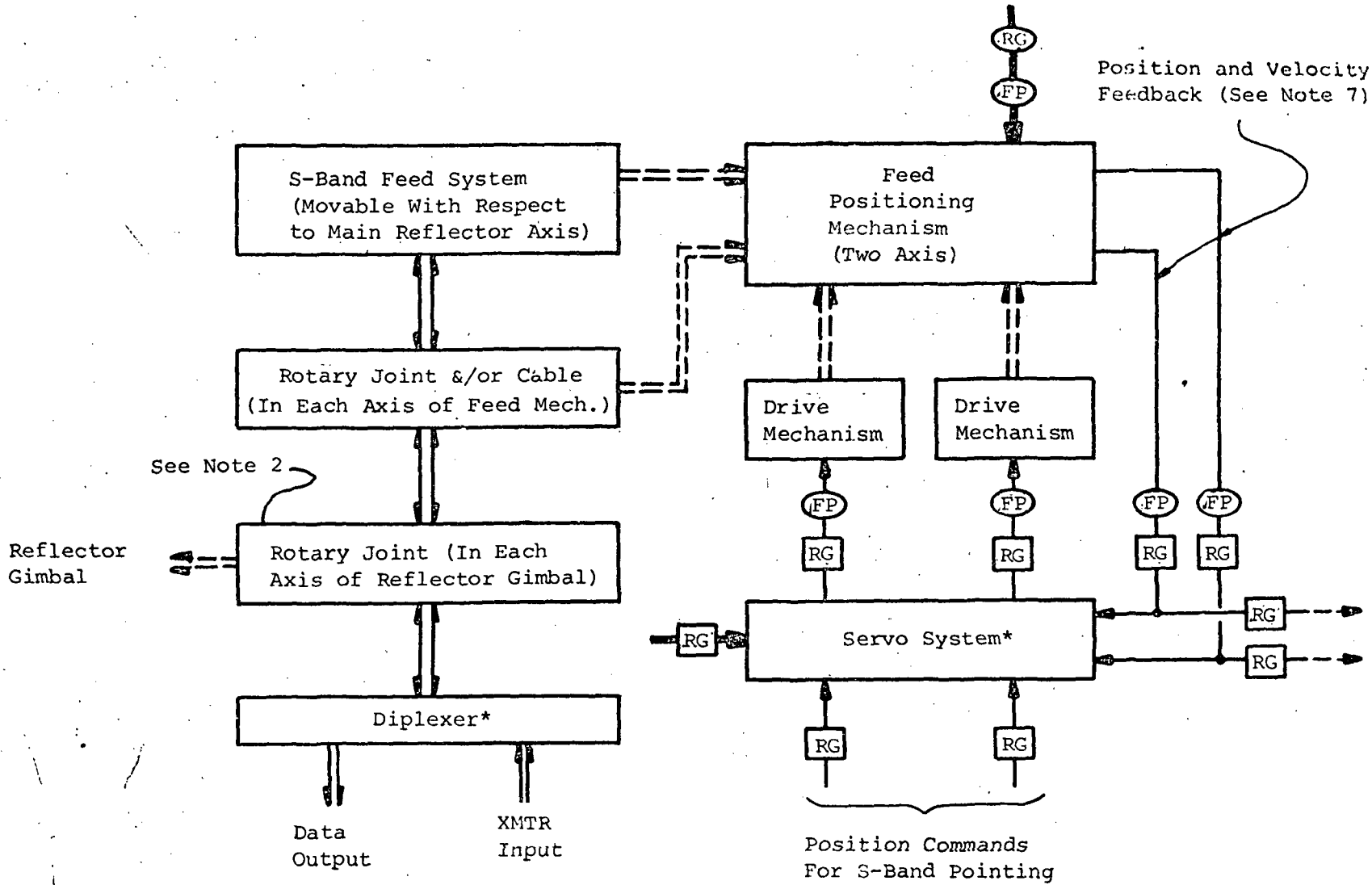

Figure 22. S-Band Feed System - Option III - Beam Steering Off-Axis by Ground Command

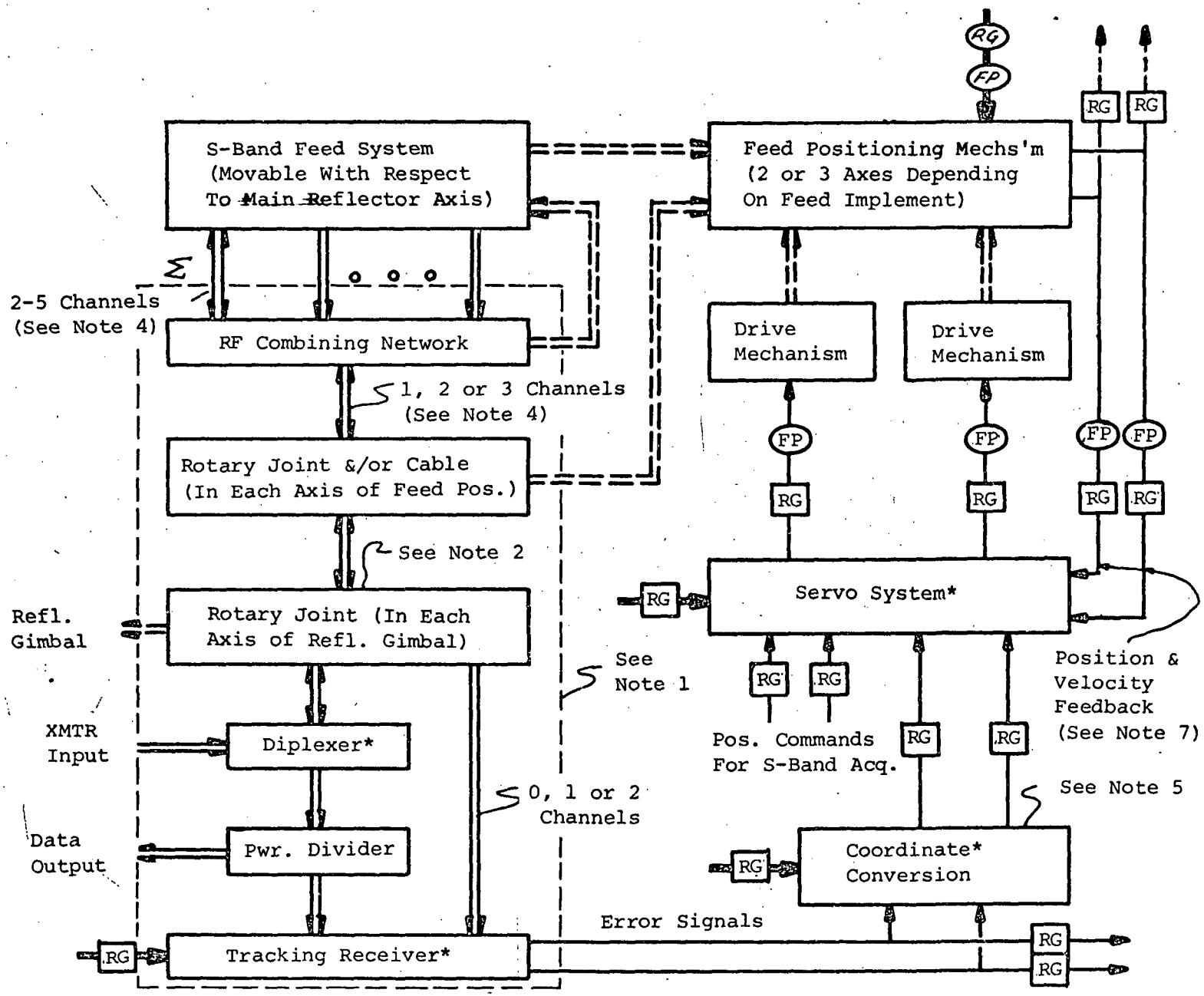

Figure 23. S-Band Feed System - Option IV - Beam Steered Off-Axis by Autotrack Function

1.3 Restricted Consideration and Treatment of Option IV

During the course of this program a decision was made to limit the treatment of Option IV for the following reasons:

1. As is evident in the block diagram of Figure 22, the additional hardware and mechanisms required to implement this option would certainly lead to a less reliable system.

2. The beamwidth at S-band is sufficiently wide to be compatible with the uncertainties in ground commanded pointing, therefore, S-band autotrack is not essential. One primary reason for considering S-band autotrack was to show how it could be used as a designation aid for K_u-band autotrack. The added complexity in the feed positioning mechanism and associated hardware lead to a less reliable system as compared to Option II. If the S-band feed fails to return to the on axis position, it would be lost as a designation aid and could jeoparize the use of the K_u-band system.

3. The primary reason for considering Option IV over Option II is to service two widely separated users simultaneously (K_u and S); however, there are currently no firm requirements for this capability.

The treatment of Option IV is therefore limited to design configurations with no detailed analysis to support the design. This was done to assure sufficient treatment of the more promising options which were more closely aligned with current TDRSS requirements. The ground work is laid for a continuation of this study if more details and analyses of Option IV are required.

4.2 Data Link Maintenance

The term data link maintenance refers to the continuous pointing of the sum channel, S- and K_u-band, transmit/receive antenna beam toward the user(s). There are two fundamental methods by which data link maintenance can be performed:

1. Reflector pointing (Options I, II, and III)

2. S-band feed positioning (Option III).

The next order of classification is:

1. S-band auto tracking

2. K_u-band auto tracking

3. ground command.

Clearly, reflector pointing can be carried out by either 1, 2, or 3, whereas, S-band positioning can be performed only by 3.

Thus, only four basic methods of performing data link maintenance are allowed by the definition of the options given in the previous section. They are listed below along with their respective abbreviations (to be used frequently in this report) and the options to which they apply:

1 Reflector pointing via K_u-band auto tracking

- a RP/K-AUTO
- b Options, I, II, and III

2 Reflector pointing via S-band auto tracking

- a RP/S-AUTO
- b Option II

3 Reflector pointing via ground command

- a RP/GC
- b Options I, II, III

4 S-band feed positioning via ground command

- a FP/GC
- b Option III.

Now that the basic methods of data link maintenance have been defined, it is of interest to relate them to the specific data link frequencies which they will support as well as the number of distinct users which can be served. Table XXV illustrates this relationship in terms of methods of data link maintenance method as a function of option, number of users served simultaneously, and data link frequencies.

It has been assumed in Table XXV that for those cases in which a single data link frequency is associated with one user, those data link maintenance methods which employ auto tracking are restricted to operation in the same frequency band. This assumption leads to the conclusion that for operation with only an S-band data link, there is no back-up method of data link maintenance for Option I; Option II (when two users are served simultaneously); and Option III.

Next, it is seen from the same table that a variation of two of the four basic data link maintenance methods (listed above) has been introduced. It applies only to Option III when a single user is being served and requires that the S-band feed be commanded to a position on the reflector axis. This variation will be denoted by a (*) following both the RP/GC and RP/K-AUTO methods of data link maintenance.

It is important to note that for those cases in which more than one method of data link maintenance can be utilized, an order of preference obviously cannot be established without additional analysis. A quantitative examination of the performance characteristics of the various methods will be performed in section 4.7.

TABLE XXV

Data Link Maintenance Methods

Characteristics of Interest	Options				
	I • Auto tracking K_u-band feed on reflector axis • Non-tracking S-band feed on reflector	II Auto tracking K_u-band and S-band feeds on reflector axis	III • Auto tracking K_u-band feed on reflector axis • Non-tracking S-band feed movable with respect to reflector		
Number of users served simultaneously	1	1	2		1
Data link frequency(s)	S-band and/or K_u-band	S-band and/or K_u-band	S-band only	K_u-band only	S-band and/or K_u-band
S-band only	RP/GC	RP/S-AUTO RP/GC	FP/GC (see Note 1)		RP/GC (*)
K_u-band only	RP/K-AUTO RP/GC	RP/K-AUTO RP/GC		RP/K-AUTO RP/GC	RP/K-AUTO RP/GC
S-band and K_u-band	RP/K-AUTO RP/GC	RP/K-AUTO RP/S-AUTO RP/GC			RP/K-AUTO (*) RP/GC (*)

RP/S-AUTO: Reflector pointing via S-band auto tracking
RP/K-AUTO: Reflector pointing via K_u-band auto tracking
FP/GC: Reflector pointing via ground command
FP/GC: S-band feed positioning via ground command
(*): S-band feed positioned on main reflector axis

NOTE 1: Pointing angles of reflector must be relayed to ground statio

Figures 24 through 29 clarify the functional operation associated with the four fundamental methods of data link maintenance and the single variation of two of them. In particular, data link maintenance methods RP/K-AUTO, RP/K-AUTO(*), RP/S-AUTO, RP/GC, RP/GC(*), and FP/GC are shown.

Consideration is given next to the problem of identifying the various data link maintenance methods for which pertinent performance characteristics are to be subsequently determined. The six methods defined above are considered unique implementations of beam pointing. However, they are neither unique in terms of the data link frequencies which they support nor in the configuration of the S-band feed system mechanization.

Table XXVIpresents the relationships between data link maintenance method, data link frequency, and S-band feed configuration. There are seen to be 10 distinct combinations of these three factors. Two are unique: RP/S-AUTO, with an S-band data link, in Option II; and FP/GC, with an S-band data link, in Option III. Also, the other eight distinct cases are subdivided as follows. When data link maintenance is performed with either RP/K-AUTO or RP/GC, the combination of data link frequency and S-band feed configuration are identical. Specifically, there is a K_u-band data link and an S-band link associated with each of the three feed options.

Summarizing, pertinent methods of maintaining "bent-pipe" data links at S- and K_u-band have been defined and characterized in a preliminary way. The next problem to be addressed is the definition of the activities which must be carried out prior to the establishment of a given data link. These activities, termed designation, are the subject of the next section.

4.3 Designation and Aided Designation

The foregoing section defined four basic methods of data link maintenance, i.e.:

1. Reflector pointing via K_u-band auto tracking (RP/K-AUTO)
2. Reflector pointing via S-band auto tracking (RP/S-AUTO)
3. Reflector pointing via ground command (RP/GC)
4. S-band feed positioning via ground command (FP/GC).

Two other straightforward variations of these methods, RP/K-AUTO(*) and RP/GC(*), require that the S-band feed be positioned on the axis of the main reflector in the case of Option III.

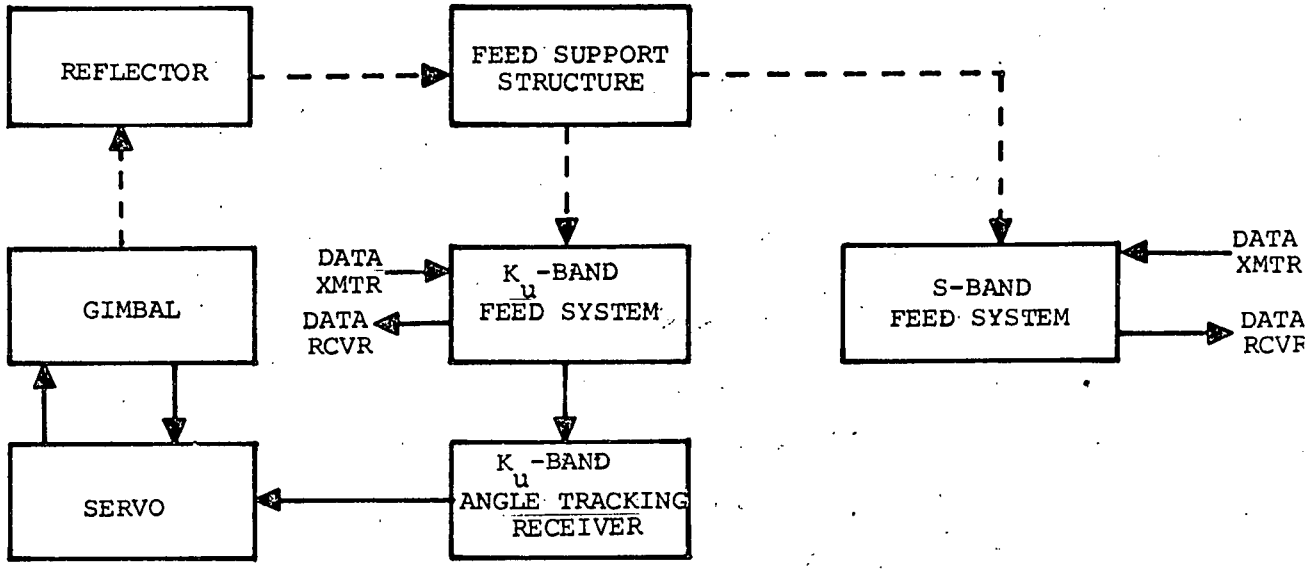

CONTROLLED ANTENNA CHARACTERISTICS(S)	DATA LINK FREQUENCIES	OPTION
POINTING DIRECTION OF ON-AXIS K_u-BAND DATA BEAMS (T/R)	K_u-BAND ONLY	I,II,III
POINTING DIRECTIONS OF ON-AXIS S-BAND AND K_u-BAND BEAMS (T/R)	S-BAND & K_u-BAND	I,II

Figure 24. Main Reflector Pointing Via K_u-Band Auto Tracking (RP/K AUTO)

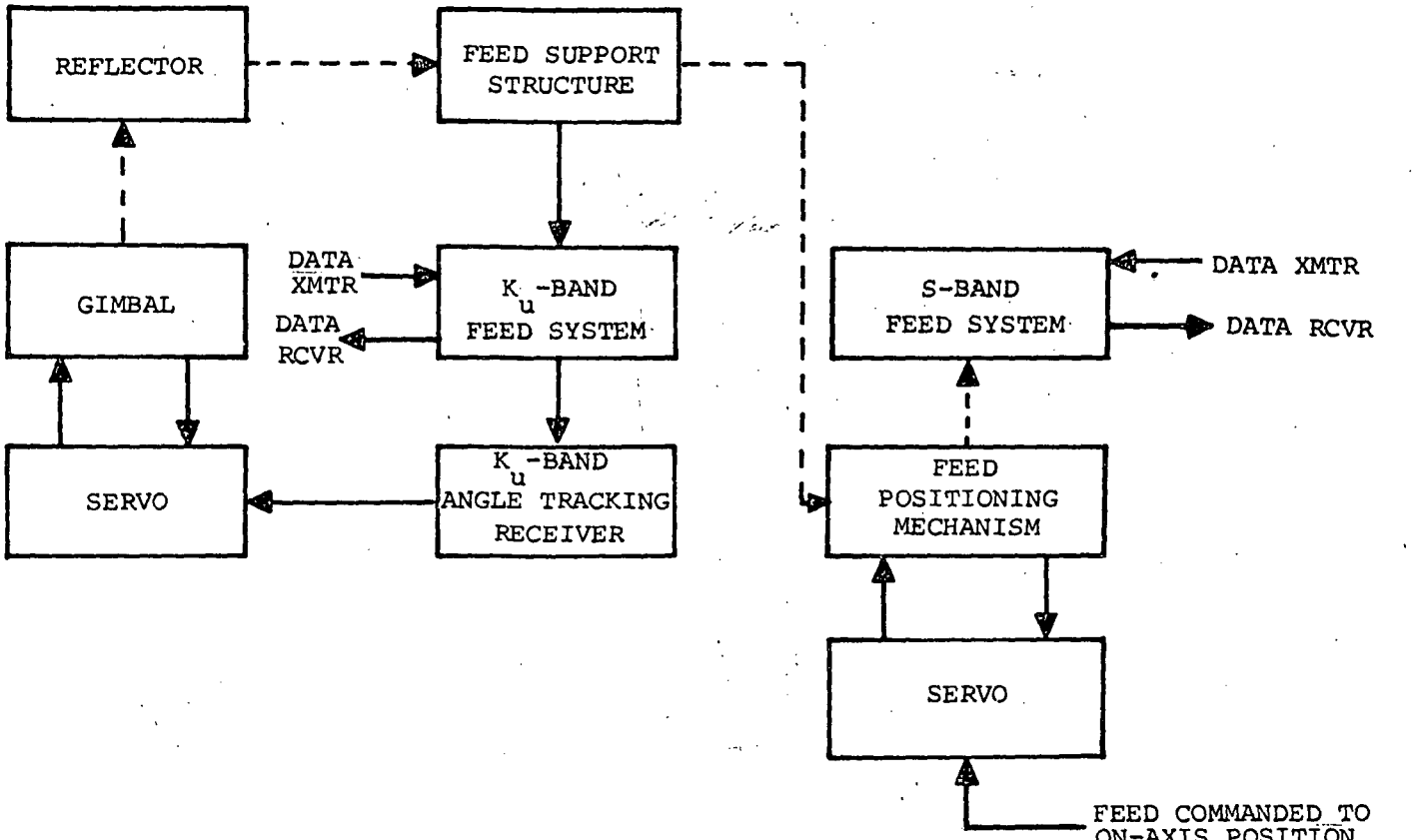

CONTROLLED ANTENNA CHARACTERISTICS: POINTING DIRECTION OF ON-AXIS S-BAND AND K_u-BAND DATA BEAMS (T/R) (WHEN S-BAND FEED IS POSITIONED ON MAIN REFLECTOR AXIS VIA GROUND COMMAND)

DATA LINK FREQUENCIES: S-BAND & K_u-BAND

OPTIONS: III

Figure 25. Main Reflector Pointing Via K_u-Band Auto Tracking (RP/K-AUTO (*))

Figure 25. Main Reflector Pointing Via K_u-Band Auto Tracking
(RP/K-AUTO (*))

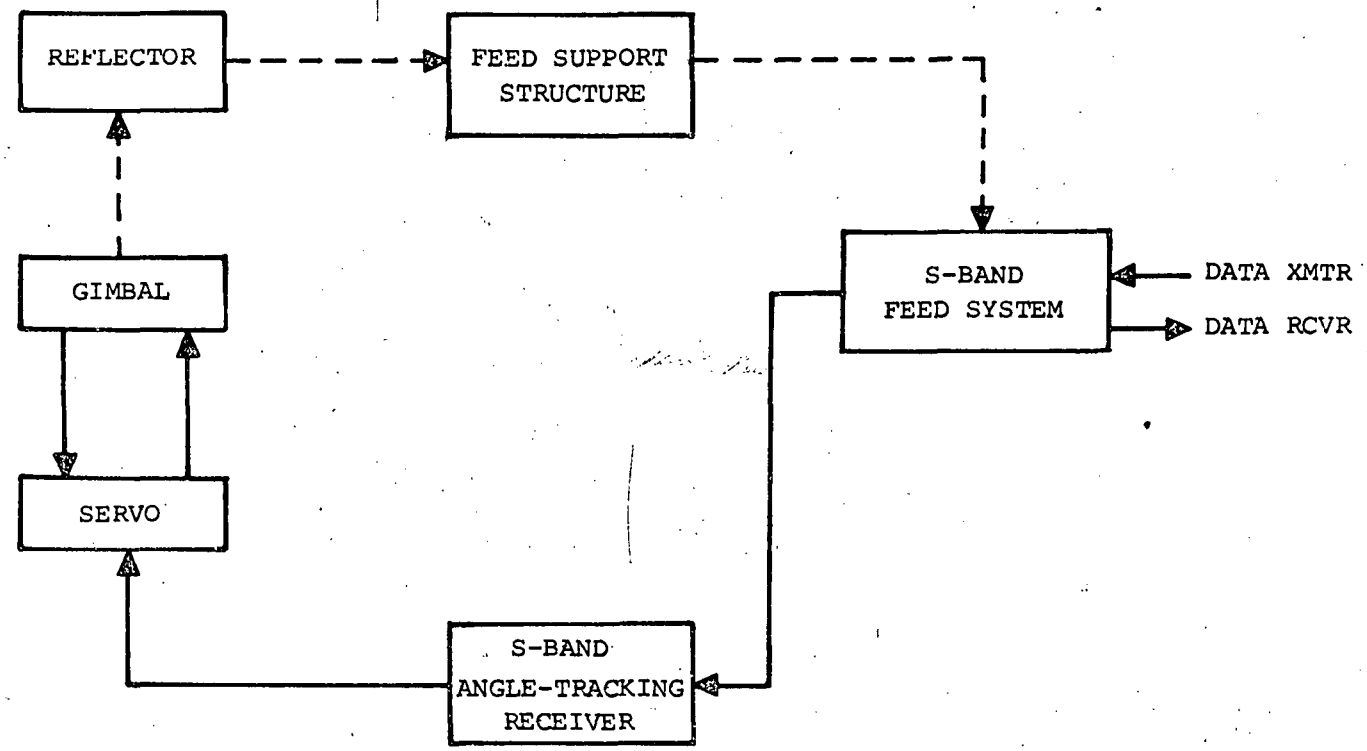

CONTROLLED ANTENNA CHARACTERISTIC: POINTING DIRECTION OF ON-AXIS S-BAND DATA BEAMS (T/R)

DATA LINK FREQUENCIES: S-BAND ONLY

OPTION: II

Figure 26. Main Reflector Pointing Via S-Band Auto Tracking
(RP/S-AUTO)

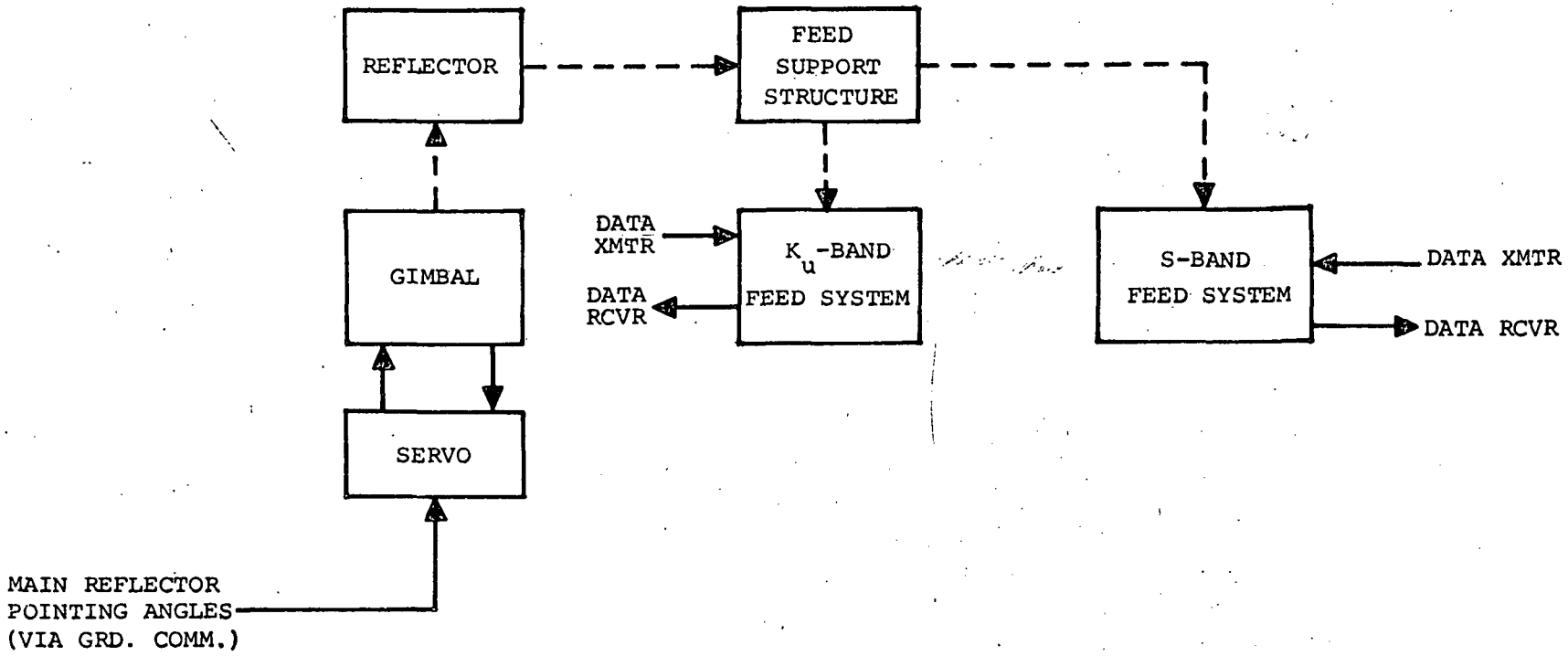

CONTROLLED ANTENNA CHARACTERISTIC(S)	DATA LINK FREQUENCIES	OPTION
POINTING DIRECTION OF ON-AXIS S-BAND DATA BEAMS (T/R)	S-BAND ONLY	I, II
POINTING DIRECTION OF ON AXIS K_u-BAND DATA BEAMS (T/R)	K_u-BAND ONLY	I, II, III
POINTING DIRECTION OF ON-AXIS S & K_u-BAND DATA BEAMS (T/R)	S & K_u-BAND	I, II

Figure 27. Main Reflector Pointing Via Ground Command (RP/GC)

Figure 27. Main Reflector Pointing Via Ground Command (RP/GC)

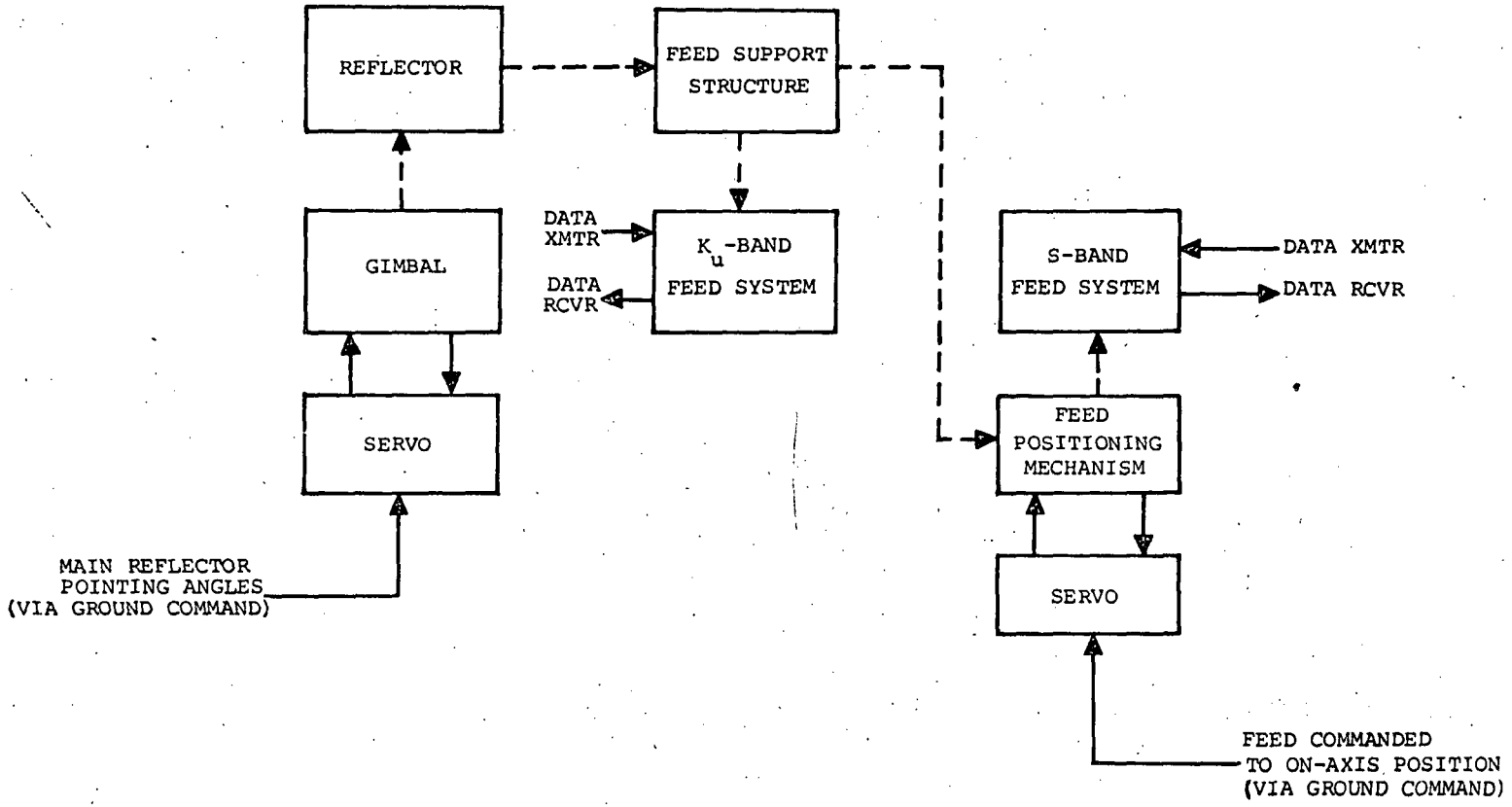

CONTROLLED ANTENNA CHARACTERISTIC(S)	DATA LINK FREQUENCIES	OPTION
POINTING DIRECTION OF ON-AXIS S-BAND DATA BEAMS (T/R)	S-BAND ONLY	III
POINTING DIRECTION OF ON-AXIS S & K_u-BAND DATA BEAMS (T/R)	S & K_u-BAND	III

Figure 28. Main Reflector Pointing Via Ground Command (RP/GC (*)

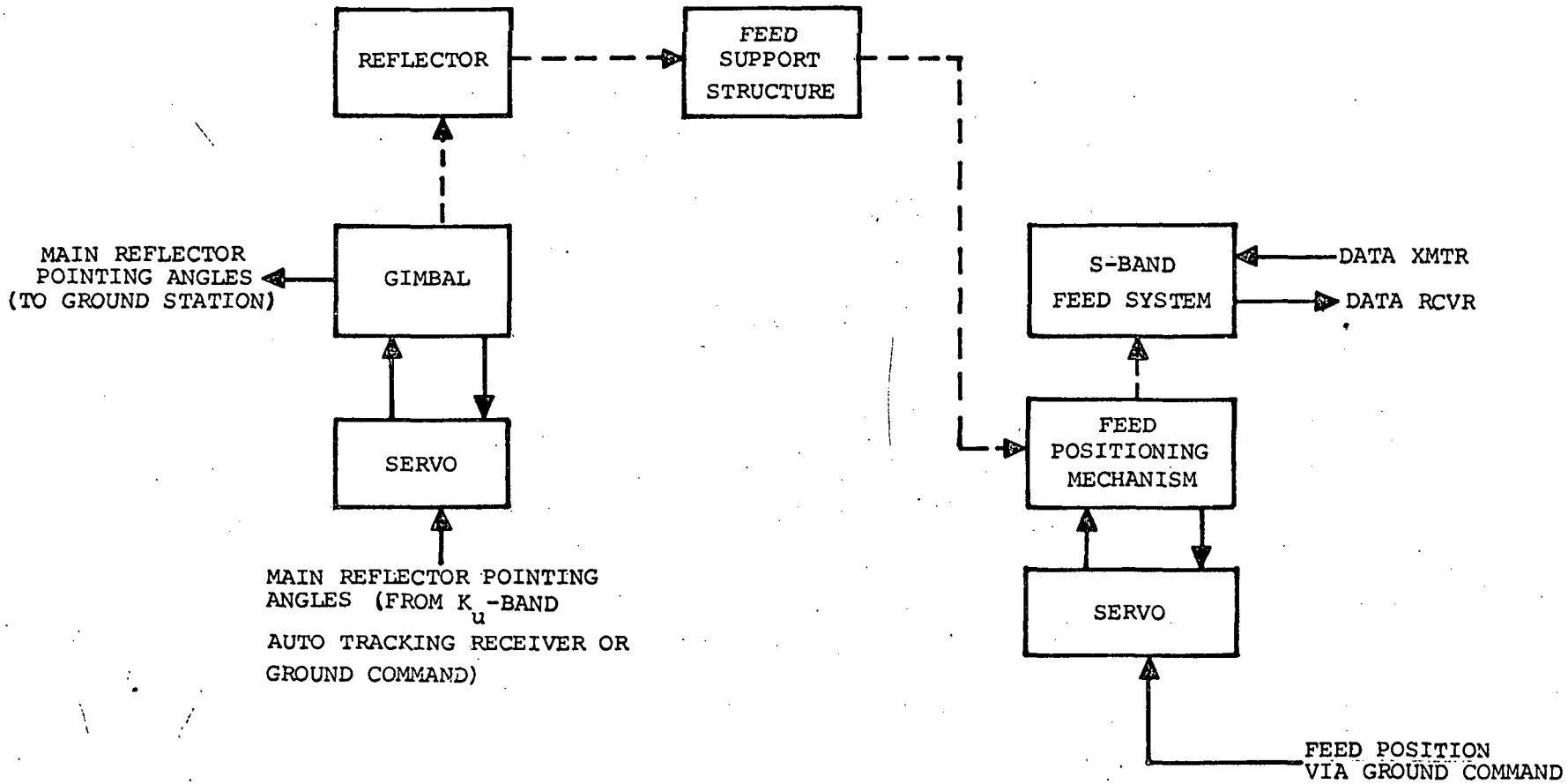

CONTROLLED ANTENNA CHARACTERISTIC: POINTING DIRECTION OF OFF-AXIS S-BAND DATA BEAMS (T/R) (WITH REFLECTOR POINTED IN A KNOWN, BUT NOT NECESSARILY FIXED ORIENTATION).

DATA LINK FREQUENCY: S-BAND

OPTION: III

Figure 29. S-Band Feed Positioning Via Ground Command (FP/GC)

Figure 29. S-Band Feed Positioning Via Ground Command (FP/GC)

TABLE XXVI

Distinct Data Link Frequencies, Maintenance Methods, and Antenna Feed Configurations

Data Link Maintenance Method	Data Link Frequency Band(s)	Option Number and Associated S-band Feed Configuration	Identification of Distinct Combinations of Data Link Maintenance Method, Data Link Frequency, and S-Band Feed Configuration
RP/K-AUTO	K_u	N/A	K_u
	S and K_u	I: on axis, non-tracking II: on axis, tracking	S-I S-II
RP/S-AUTO(*)	S and K_u	III: movable, non-tracking, positioned on reflector axis by command	S-III(*)
RP/S-AUTO	S	II: on axis, tracking	S-II
RP/GC	S	I: on axis, non-tracking	K_u
	S and K_u	II: on axis, tracking	S-I S-II
	K_u	N/A	S-III(*)
RP/GC(*)	S	III: movable, non-tracking, positioned on reflector axis by command.	
	S and K_u		
FP/GC	S	III: movable, non-tracking	S-III

Attention is now turned to the activities which must precede the establishment and operation of the data link(s). The term designation will be used to describe these activities. In the case of data link maintenance via auto tracking (1 and 2 on page 82), designation refers to the act of indirectly aiming the boresight axis of the auto tracking antenna system by pointing the reflector with an angular precision such that the tracking loop can be successfully closed. When data link maintenance is performed with either reflector pointing or S-band feed positioning via ground command (3 and 4 on page 82), then designation is direct, i.e., the ground station generates commands for the reflector pointing angles or S-band feed position and the execution of these commands maintains the data link.

Figure 30 illustrates the rudimentary functions which comprise designation. When the data link is maintained with auto tracking, there are two indicated methods of designation: one direct from the ground and the other with a designation aid. In the latter case, the designation aid acts to refine the reflector pointing angle commands relayed from the ground station, i.e., the designation aid system is intended to result in a smaller angular difference between the actual direction of signal arrival from the user and the boresight axis of the auto tracking system than does the use of direct designation.

It is asserted that the designation aid system can perform its function in only two ways:

1 The systematic search of a given spatial region (in an open-loop manner),

2 Angle-sensing in a closed loop fashion (auto tracking).

In 1, the search region is considered centered about the spatial direction which results from the ground designation commands. The designation aid system must decide, at some time during the search process, whether the searching antenna beam is pointing toward the source of radiation (the user's transmitting antenna). It must also remember either the position of the S-band feed or the main reflector pointing angles at the time at which that decision was made. The remembered values are then used for designation.

In 2 above, the designation aid system will attempt to continuously align its boresight axis with the direction of signal arrival, i.e., once the auto tracking loop in the designation aid system is closed (and allowed to stabilize), the designation process will occur directly and continuously. Then, the tracking loop associated with data link maintenance can be closed at any time.

It is important to note that there is no way of determining, without further anaylsis, if the two designation aid methods just defined are

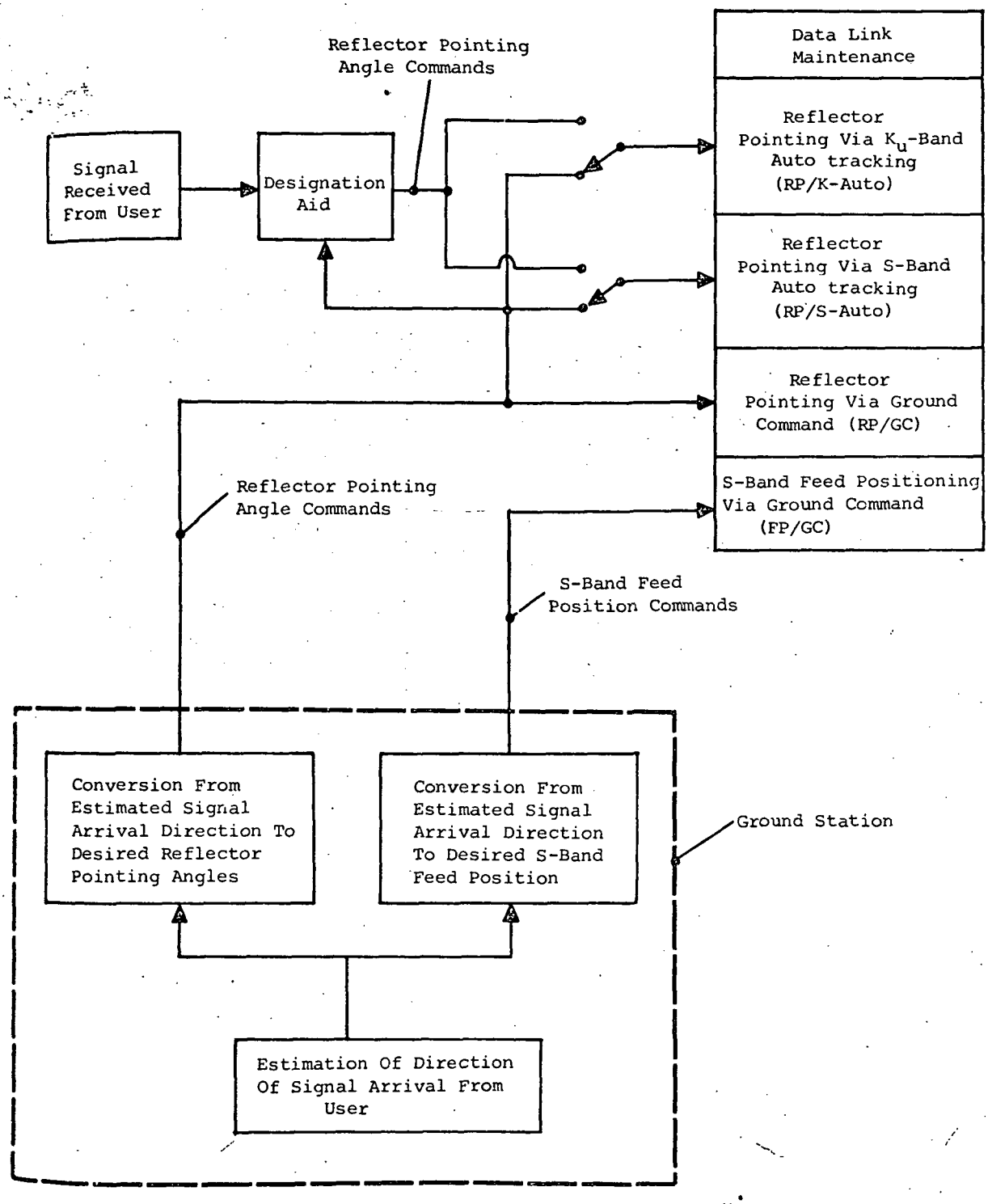

Figure 30. Basic Functions Associated with Designation

satisfactory, i.e., there is no proof that either method offers more precise designation than that obtainable directly from the ground station.

Having defined the general methods of obtaining aided designation, an examination is now made of the specific nature of these devices. In those cases in which aided designation is achieved via auto tracking, the following assumptions are made:

1 No feed systems and/or reflectors are added to the TDRS equipment solely for the purpose of aided designation;

2 Only a single angle sensing method is employed at S-band for both aided designation and data link maintenance;

3 Only a single angle sensing method is employed at K_u-band for aided designation and data link maintenance.

By "angle sensing method" (2 and 3) we mean the antenna feed systems and associated angle tracking receivers illustrated in Figures 24, 25, and 26 in conjunction with data link maintenance methods RP/K-AUTO, RP/K-AUTO(*), and RP/S-AUTO.

Based upon the material presented above and discussions with NASA personnel at GSFC, three methods of aided designation will be investigated. They are defined in Table XXVIIalong with the abbreviations by which they will be identified.

In accordance with Figure 30, it is clear that in the case of aided designation via DA/K-SEARCH, the center of the search region is defined by the reflector pointing angles obtained by way of command from the ground station. For the two cases in which aided designation is performed with an auto tracking system, the boresight axis of that system takes on a spatial direction dictated by the reflector pointing angles obtained from the ground station commands, i.e., initialization of all three designation aid methods is obtained as a result of the operation already identified as RP/GC.

To crystallize the many concepts set forth above in conjunction with designation, aided designation, and data link maintenance, Figure 31 presents a condensation of the interrelationships between these functions. It is important to note that those designation and designation aid techniques which lead to data link maintenance via auto tracking are defined to be potnetially suitable. Their actual, relative value has not yet been established.

A much more detailed version of Figure 31 is presented in Figure 32 in which many of the individual operations entailed by designation, aided designation, and data link maintenance are illustrated.

TABLE XXVII
Aided Designation Methods

Aided Designation Method	Method Of Designation
Search at K_u-band with a pencil beam antenna pattern having a half-power width consistent with the feed system and reflector employed for data link maintenance.	DA/K-SEARCH
Autotrack at S-band with the same feed system and angle tracking receiver employed for data link maintenance.	DA/S-AUTO
Autotrack at K_u-band with the same basic feed system and angle tracking receiver employed for data link maintenance (RP/K-AUTO) but with modifications to increase the field of view, on command from the ground, by an amount to be determined.	DA/K-AUTO

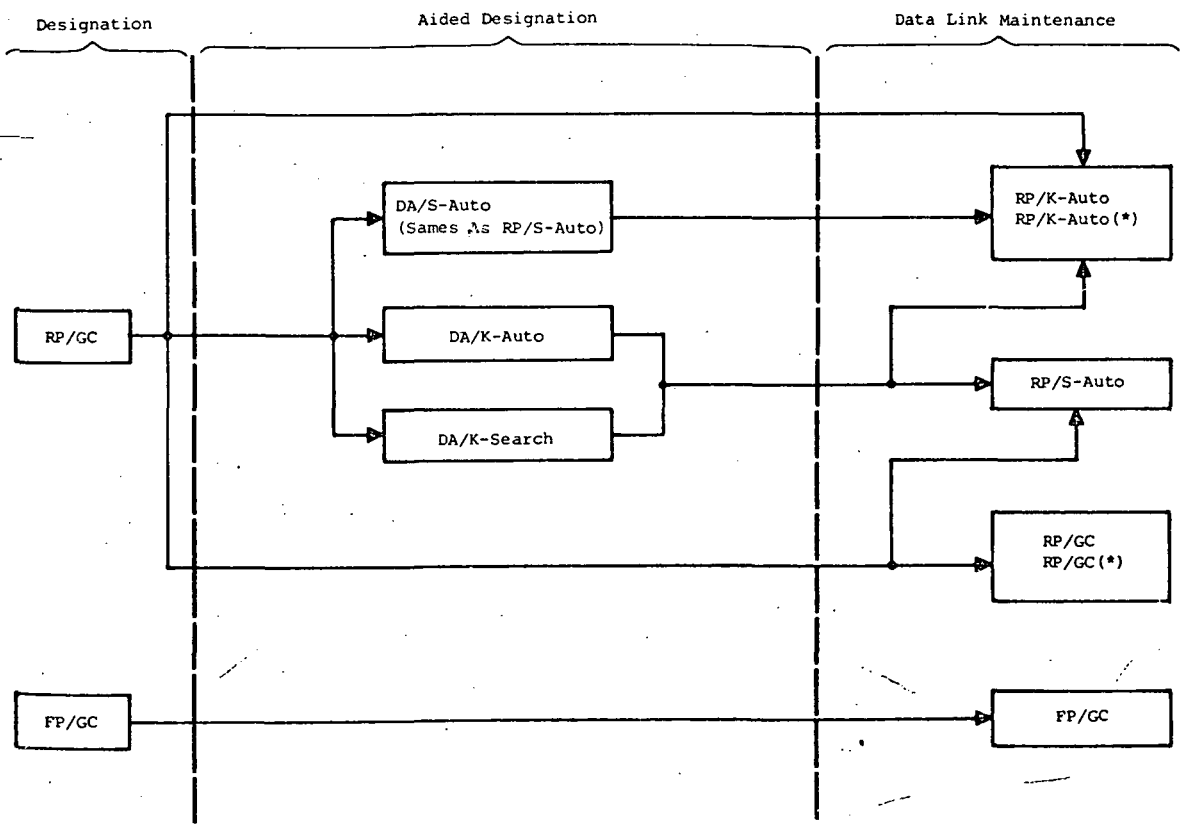

Figure 31. Summary of Methods for Designation, Aided Designation, and Data Link Maintenance

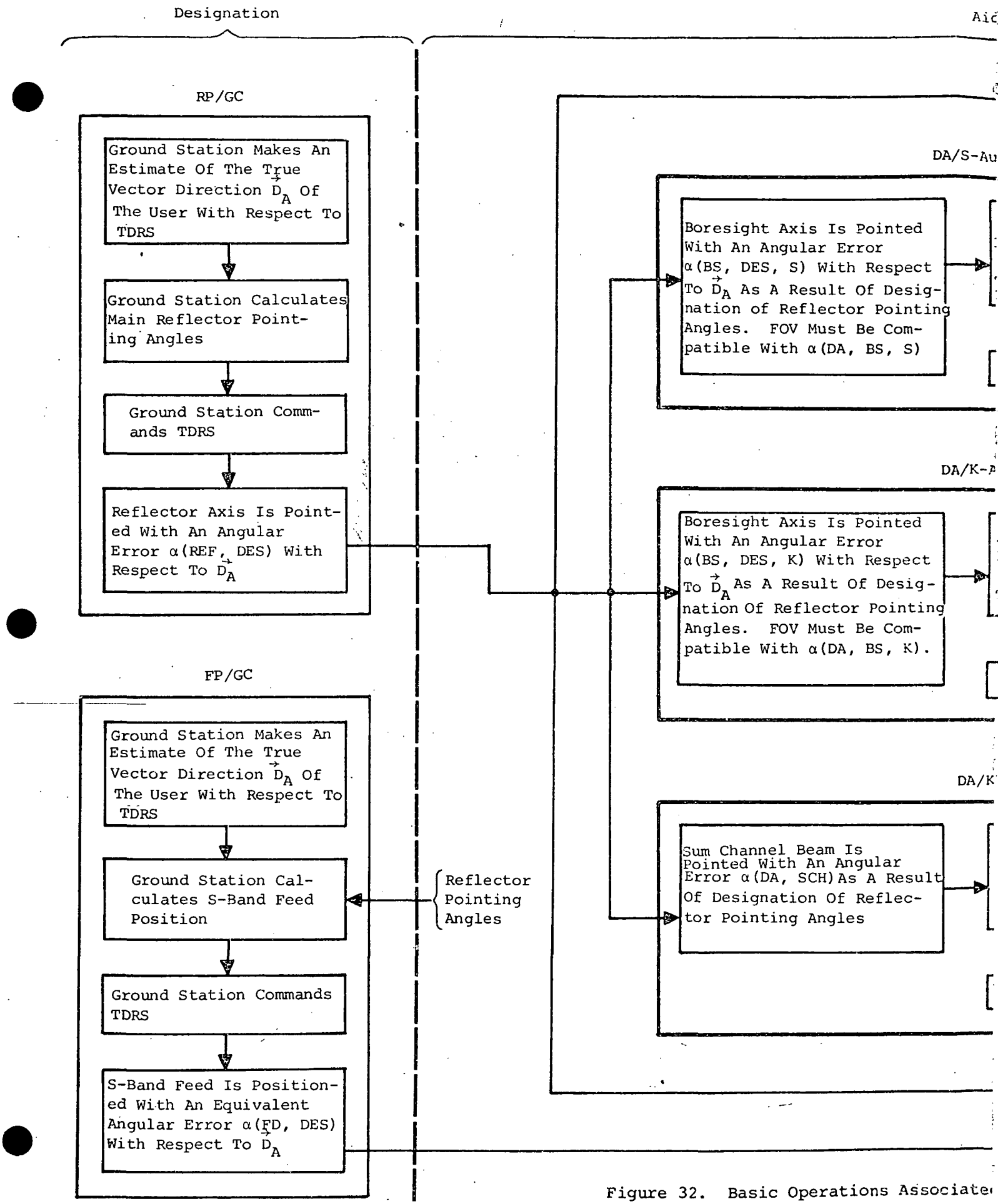

Figure 32. Basic Operations Associate
Designation, and Data Link

Aided Designation

/S-Auto (Same As RP/S-Auto)

Auto Tracking Loop Is Closed (And Allowed To Stabilize)

Grd. Station†

Boresight Axis Is Pointed With An Angular Error $\alpha'(DA, BS, S)$ With Respect To $\vec{D}_A$.

Reflector Axis Is Pointed With An Angular Error $\alpha(REF, DA, S)$ With Respect To $\vec{D}_A$.

Boresight Axis Is Pointed With An Angular Error $\alpha(BS, K)$ With Respec To $\vec{D}_A$ As A Result Of Designation Or Aided Designation. FOV Must Be Com patible with $\alpha(BS, K)$.

A/K-Auto

Autotracking Loop Is Closed (And Allowed To Stabilize)

Grd. Station†

Boresight Axis Is Pointed With An Angular Error $\alpha'(DA, BS, K)$ With Respect To $\vec{D}_A$.

Reflector Axis Is Pointed With An Angular Error $\alpha(REF, DA, K)$ With Respect To $\vec{D}_A$.

Boresight Axis Is Pointed With An Angular Error $\alpha(BS, S)$ With Respec To $\vec{D}_A$ As A Result Of Designation Or Aided Designation. FOV Must Be Compatible With $\alpha(BS, S)$.

DA/K-Search

Search Procedure Is Carried Out Until "Detection" Occurs

Grd. Station+

Reflector Pointing Angles Are Set At Redesignated Values With An Angular Error $\alpha(REF, DA, SCH)$ With Respect To $\vec{D}_A$.

RP/GC & RP/GC(*)

S-Band And/Or K_u-Band Data Beams Are Pointed Wit An Angular Error $\alpha(Data, S)$ And/Or $\alpha(Data,$ With Respect To $\vec{D}_A$

FP/GC

S-Band Data Beam Is Pointed With An Angular Error $\alpha(Data, S)$ With Respect To $\vec{D}_A$.

lated with Designation, Aided
Link Maintenance

RP/K-Auto & RP/K-Auto(*)

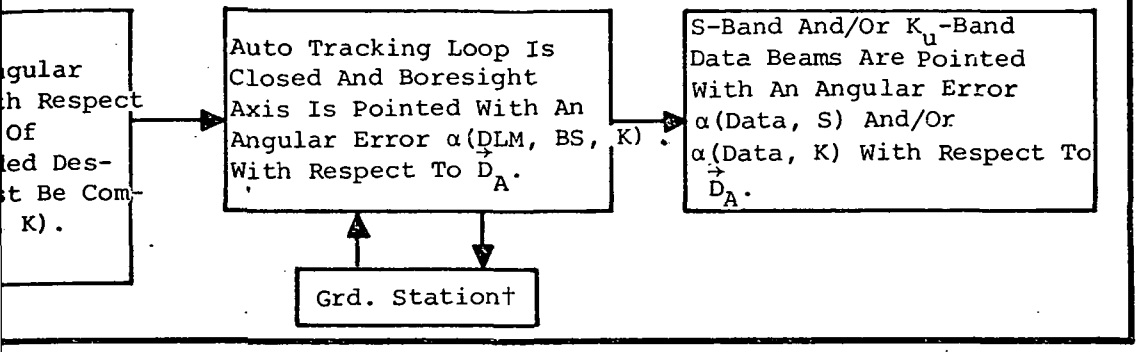

RP/S-Auto

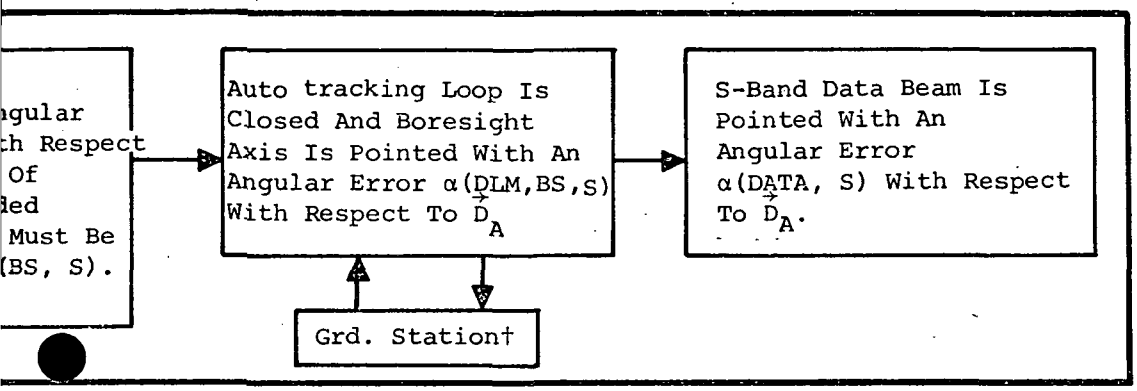

GC(*)

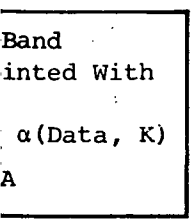

Notes:

† The auto tracking loop may be closed through the ground station.

* The search function may be carried out in conjunction with the ground st

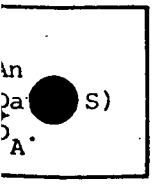

In the next section, methods for prediction of the various angular errors defined in Figure 32 will be developed in conjunction with data link maintenance. Then, in section 4.8, the angular errors associated with designation and aided designation will be analyzed.

4.4 Methods for Determining Data Channel Gain Reduction Due to Data Beam Pointing Errors

Subsequent paragraphs present the method to be employed in the determination of angular data beam pointing errors. Then, the technique for analyzing the data channel gain reduction is outlined. This is followed in section 4.4.1, 4.4.2, and 4.4.3 with a detailed examination of the data beam pointing errors.

The angular data beam pointing error is defined herein to be the angular displacement between the direction of the user spacecraft with respect to the TDRS, and the direction of the maximum of the antenna gain function associated with the data channel. Regardless of the specific data link maintenance method under consideration, there will be a sum channel to which a diplexer is connected for the purpose of segregating the data transmission/reception channels in the frequency domain. Thus, two directions of the antenna beam maxima actually exist - one associated with the transmit port of the diplexer and the other with the receive port. As a practical matter, it will be assumed that the frequency response of the antenna, diplexer, and intermediate RF components is such that the two directions conicide.

The two fundamental methods of data link maintenance have already been defined: auto tracking and ground command. When data link maintenance is performed with auto tracking (RP/K-AUTO and RP/S-AUTO), the angle-sensing system attempts to align its boresight axis with the direction of signal arrival from the user spacecraft.

In the case of data link maintenance via ground command, there are two distinct pointing schemes. With reflector pointing (RP/GC), the ground station attempts to align the reflector axis with a line connecting the TDRS and user. Alternatively, the ground station endeavors to position the S-band feed (FP/GC) so that the direction of the maximum intensity of the beam which it forms (in conjunction with the reflector) coincides with a line connecting the TDRS and user spacecraft.

The foregoing paragraphs present the definition of the data beam pointing error to be employed here as well as a description of the role of the angle-sensor and the ground station in the various data link maintenance methods. These results lead to a method of defining the various components of the data-beam pointing errors which is presented in Table XXVIII.

TABLE XXVIII

Preliminary Description of Data Beam Pointing Errors

Data Link Maintenance Method	Data Beam Pointing Error Δ Angular Displacement Between the Directions of the Data Channel Gain Maximum and the Direction of the User Spacecraft with Respect to the TDRS
RP/K-AUTO RP/K-AUTO(*) RP/S-AUTO	Angular displacement between direction of signal arrival and boresight axis of the autotracker And Angular displacement of boresight axis and direction of data channel gain maximum
RP/GC RP/GC(*)	Angular displacement of reflector axis and the line connecting the TDRS and the user And Angular displacement of the reflector axis and direction of data channel gain maximum
FP/GC	Angular displacement of the data channel gain maximum and the line connecting the TDRS and the user

The data beam pointing errors associated with each of the above defined data link maintenance methods are now discussed in turn.

RP/AUTO

The two contributors to the data beam pointing error given in Table XXVIIIare easily analyzed. In the material which follows, the angular displacement between the boresight axis of the angle sensor and the direction of signal arrival from the user will be referred to as a tracking error. The symbols adopted in Figure 32 for this error component were α (DLM, BS, K) and α (DLM, BS, S), where DLM relates the error to the data link maintenance system, BS refers to the boresight direction, and K and S define the data link frequency.

The other error contributor to be evaluated is the angular displacement of the boresight axis of the auto tracking system and the direction of the data channel gain maximum. This component will be termed a data beam offset/boresight error and a symbol will be assigned to it subsequently.

The two error contributors which result from reflector pointing via ground command are directly analogous to those discussed above in connection with auto tracking except that the reflector axis becomes the reference to which both components are referenced, as can be seen from Figure XXVIII.

The angular displacement of the reflector axis from the line connecting the TDRS and user spacecraft will be called the reflector designation error and denoted as α(REF, DES) and is done in Figure 32.

The angular difference between the reflector axis and the direction of the data channel gain maximum will be termed a data beam offset/reflector axis error. It will subsequently be given a symbolic representation.

When data link maintenance is performed by positioning the S-band feed from the ground, there is no convenient "reference" direction as is used in the two cases just discussed. However, just as there is a reflector designation error in the case of RP/GC, so there is a feed designation error in the subject case, to be termed α(FD, DES). There is also a displacement of the data beam maximum with respect to the direction associated with the designated feed position. This component will be labeled a data beam offset/feed position error.

Summarizing, the following components of data beam pointing error have been identified:

1 RP/AUTO: tracking error and data beam offset/boresight error,

2 RP/GC: reflector designation error and data beam offset/reflector-axis error,

3 FP/GC: feed designation error and data beam offset/feed position error.

Before proceeding with a detailed analysis of the various error sources, it is necessary to examine the various data beam offset errors in somewhat greater detail. To perform this examination, reference is made to Table XXIX which defines the distinct methods of data link maintenance that must be considered. The last column in Table XXIX gives ten distinct combinations of four data link maintenance methods, two data link frequencies, and three S-band feed configurations. There are, in general, ten different values of the data beam offset errors. Table XXIX defines all of the basic error components to be examined in the material which follows.

TABLE XXIX
Definition of Data Beam Pointing Error Components

Data Link Maintenance Method	Data Link Frequency Band(S)	Option Number and Associated S-Band Feed Configuration	Components of Data Beam Pointing Error, α(DATA, S) and α(DATA, K)
RP/K-AUTO	K_u	N/A	Tracking error, α(DLM, BS, K), and data beam offset/boresight error: • α(DBO, BS, K) • α(DBO, BS, S-I) • α(DBO, BS, S-II) • α(DBO, BS, S-III(*))
	S and K_u	I: on axis, non-tracking II: on axis, tracking	
RP/K-AUTO(*)	S and K_u	III: movable, non-tracking, positioned on reflector axis by command	
RP/S-AUTO	S	II: on axis, tracking	Tracking error, α(DLM, BS, S), and data beam offset/boresight error, α(DBO, BS, S-II)
RP/GC	S	I: on axis, non-tracking	Reflector designation error, α(REF, DES), and data beam offset/reflector axis error: • α(DBO, REF, K) • α(DBO, REF, S-I) • α(DBO, REF, S-II) • α(DBO, REF, S-III(*))
	S and K_u	II: on axis, tracking	
	K_u	N/A	
RP/GC(*)	S	III: movable, non-tracking, positioned on reflector axis by command	
	S and K_u		
FP/GC	S	III: movable, non-tracking	Feed designation error, α(FD, DES), and data beam offset/feed position error, α(DBO, FP, S-III)

The sole purpose of analyzing the data beam pointing errors is to determine the loss of data channel gain which results. There are two distinct angle errors which give rise to a reduction in data channel antenna gain - the angular displacement of the direction of the data beam maximum from the reflector axis and also from the line of sight to the user spacecraft. Both of these errors are analyzed in the material which follows and then used in section 4.7 in computations of the data channel gain reduction.

4.4.1 Data Beam Pointing Errors for Data Link Maintenance Using RP/AUTO

The material summarized in Table XXIX shows that when data link maintenance is performed with auto tracking, the data beam pointing error has two basic components: a tracking error and a data beam offset/boresight error. In the material which follows, these errors are evaluated in turn. Then, they are combined to yield the data beam pointing errors.

4.4.1.1 Tracking Error

A tracking error is defined above as the angular displacement of the boresight axis of the auto tracking system and the direction of signal arrival. In the material presented below, the basic sources of tracking error are first categorized and defined. Then, each error contributor is examined in detail and either assigned a numerical value based upon a typical implementation or defined by an analytical relationship. Finally, the various error contributors are combined into a single expression suitable for subsequent use.

Before proceeding with the error source characterization, the hardware associated with the RP/K-AUTO and RP/S-AUTO data link maintenance methods is defined in Figure 33. All of the basic elements illustrated contribute to the pointing error. The presence of ground station in the tracking receiver illustrates the fact that the tracking loop may be closed through the ground station.

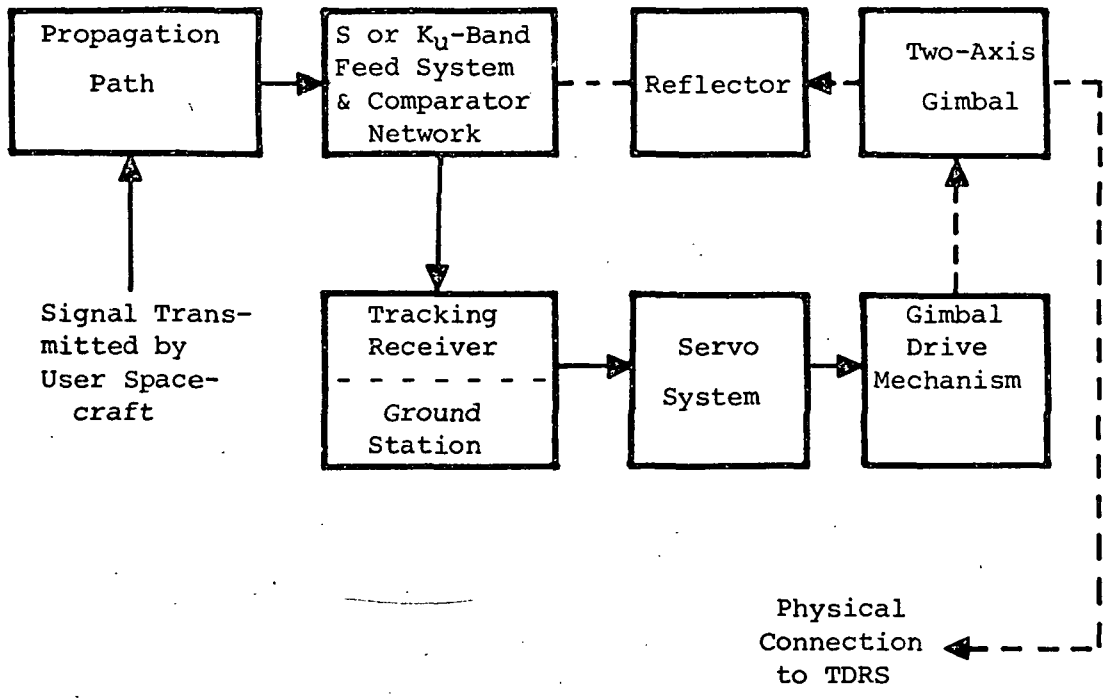

Figure 33. Data Link Maintenance Via Auto Tracking

Table XXX presents a summary list of those error source which, when suitably combined, define the angle tracking error.

TABLE XXX

Sources of Tracking Error

Propagation Path	Signal level reduction
	Random phase/amplitude modulation of signal
Antenna and Tracking Receiver	Receiver generated noise
	Error signal slope reduction
Servo System and Gimbal	Servo system offset
	Gimbal backlash
	Torque disturbances
	Servo dynamic lag

4.4.1.1.1 Individual Error Sources

Each of the tracking error contributors given in Table XXX are now examined. Some are eliminated from further consideration, others are assigned fixed numerical values, and analytical relationships are defined for the remainder.

Propagation Path Errors

There are two distinct components of tracking error which result from the propagation path from the user to the TDRS spacecraft. The first is a reduction in signal power, or equivalently, an increase in the competing noise level which results from signal attenuation due to absorption in the troposphere and polarization rotation in the ionosphere. The second error source is attributed to an increase in relative noise level associated with random phase/amplitude modulation of the signal received from the user via multipath transmission. These error sources are now considered in turn.

First, in the case of tropospheric attenuation, the propagation path between the user and the TDRS intersects the troposphere for a negligibly small fraction of the total time during which the user is in view of the TDRS. This error component is therefore taken to be non-existent.

With regard to polarization change in the ionosphere, the propagation path between those users which have orbital altitudes below about 1000 km will intersect the ionosphere for a short period of time. However, the detailed nature of the change in the transmitted polarization orientation and its influence on the power received by the TDRS tracking antenna system is beyond the scope of the study program reported herein.

Multipath transmission via the earth's surface will, of course, occur during the entire time for which a given user can communicate with a TDRS. Again, the quantitative impact of this source of tracking error is beyond the scope of this study.

Antenna and Tracking Receiver Errors

It was noted in Table XXX that the antenna and tracking receiver give rise to two tracking error components: noise generated in the tracking receiver which enters the servo system and a reduction in the error-signal slope at the receiver output terminals.

Since the tracking error contribution due to receiver noise is a random variable, the quantity of interest will be the root-mean-square (rms) value of the error. Two methods of second detection in the tracking receiver, coherent and noncoherent, will be discussed in section 4.6. In both cases, however, it will be shown that the mean-squared single-axis tracking error has the form:

$$\delta_R^2 = \Phi\beta_n$$

where

β_n = the one-sided servo noise bandwidth (to be discussed subsequently)

Φ = an angle error spectral density (in deg^2/Hz)

which depends on the tracking antenna and receiver characteristics as well as the signal power received from the user spacecraft.

The three signa value of the single axis tracking error will be utilized when the aggregate of error contributors are summed. Thus, the final two-axis value of interest is

$$\delta_R = 3\sqrt{2\Phi\beta_n} \quad . \tag{1}$$

With regard to the error signal slope reduction, it will be shown in section 4.6 that all of the angle sensing methods which satisfy the pertinent TDRS performance requirements are based upon an adaptation of the radar monopulse concept. More specifically, the RF inputs to the tracking receiver shown in Figure 33 are a sum and two orthogonal-plane difference signals developed by the antenna feed system and associated comparator network. The outputs of the tracking receiver are two error signals, each associated with an angle sensing plane. In the vicinity of the boresight axis, a given error signal is proportional to the difference between the angle of signal arrival and the antenna pointing direction as measured in the appropriate plane.

It is shown in section 4.6 that the angle error spectral density, Φ, discussed above, is inversely proportional to the square of the error signal slope. It is well known that a tracking system of the type shown in Figure 33 contains pre- and post-comparator amplitude and phase unbalances. One of the effects of thses unbalances is a reduction in the error signal slope (with respect to the no-error case), hence an increase in the angle tracking error. Appendix A contains a quantitative analysis of the error signal slope, at the receiver output terminals, as a function of the extent of pre/post-comparator unbalance. This analysis will be used in a computation of the angle error spectral density, Φ.

In summary, although error signal slope reduction is a distinct contributor to the overall tracking error, its impact is included in the category of tracking receiver noise.

Servo System and Gimbal Errors

Table XXX defines four tracking error contributions associated with the servo system and the gimbal - servo system offset, gimbal backlash, torque disturbance, and servo dynamic lag. In general, the first two error components are invariant to the servo system design philosophy and will be considered first.

In the case of servo system offset, reference is made to the non-zero output voltage of the servo system when there is no input. This error component, caused by servo system hardware imperfections, is asserted to have a value which is negligible compared to others considered here. As a result, it will not be further considered.

The entire backlash angle which exists in the gimbal gear train will be taken as a tracking error contribution. Although a numerical value is dependent on the detailed nature of the specific gimbal selected, it seems reasonable, based upon typical space qualified units, to use a two-axis value of 0.01 degree.

Attention is given next to the components of tracking error which result from torque disturbances and dynamic lag. Although a servo system design is not a requirement of the study program reported here, the servo must be characterized to formulate the subject errors as well as that associated with receiver noise. Moreover, the servo system characterization must take account of the tracking receiver being located either in the TDRS or contained in the ground station. In the latter case, the sum and two difference signals developed by the angle sensing feed system and comparator network are relayed to the ground station where error signals suitable for gimbal positioning are developed and relayed back to the TDRS. The corresponding transport delay of (the order of) 0.33 second* requires a change in the servo system design philosophy with respect to the case in which ground station processing is not performed. The servo system errors are now separately discussed for the two tracking receiver locations.

Servo Errors - Tracking Receiver Aboard TDRS

A single-loop position servo is postulated for the case in which the tracking error signals are generated by a receiver contained solely in

---

* The subject value was obtained by assuming that the TDRS is in equatorial orbit at 171 degrees west longitude; the ground station is located at 30 degrees north latitude and 100 degrees west longitude. Then, the distance from the TDRS to the ground station is approximately 27,030 nmi. and the corresponding round trip time delay is 1/3 second.

the TDRS. An obvious alternative is to add an inner velocity loop which would act to effectively eliminate torque disturbance errors. The penalty, of course, is the added weight and power associated with appropriate electronic circuits and a rate sensor, as well as a rate sensor noise contribution. On the basis of a 5 year projected life for the TDRS, it is believed that the use of a rate loop cannot be justified unless the torque disturbance error is excessive.

A block diagram of the postulated servo system is shown in Appendix B. Here, torquers have been selected in preference to stepper motors for antenna positioning, since they should require less energy to move the relatively large inertial load at an essentially uniform rate than will stepper motors which alternately accelerate and decelerate the load in response to each command.

The single-axis tracking error contribution, δ_T, which results from torque disturbances is derived in Appendix B. The two-axis value is

$$\delta_T = \frac{11.5\sqrt{2}\,T_d}{\beta_n^2\,J}\ , \text{degree} \qquad (2)$$

where

T_d = total disturbance torque, ft-lb

β_n = one-sided servo noise bandiwdth in Hz

J = equivalent inertia (ft-lb-s^2)

which depends on the inertia on the motor and load shafts as well as the gear ratio. Its relationship to these quantities is given in Appendix B. In a numerical evaluation of the torque disturbance error, the quantity T_d/J (s^{-2}) will be treated as a parameter.

The servo dynamic lag error results from the response of the servo system to movement of the user spacecraft. The servo system defined above will exhibit a dynamic lag error, δ_D, defined by

$$\delta_D = \frac{\dot{\theta}}{K_v} + \frac{\ddot{\theta}}{K_a}$$

where

$\dot{\theta}$ and $\ddot{\theta}$ = the angular velocity and acceleration, respectively, of one of the gimbal axes

K_v and K_a = the servo system error constants associated with velocity and acceleration.

For the servo system shown in Appendix B, K_v is essentially infinite, whereas $K_a \approx 2.5\ \beta_n^2$.

It is shown in Appendix C that $|\ddot{\theta}|_{max} \approx 1.25 \times 10^{-5}$ degree/second^2 and that the maximum value of the dynamic lag error is

$$\delta_D = \frac{10^{-5}}{2\beta_n^2} \text{ degrees} \qquad (3)$$

where β_n is again expressed in Hz. It is important to note that the just defined value of maximum gimbal acceleration is based upon the two gimbal axes being in alignment with the Earth's polar axis and equatorial plane. Then, when the maximum value of acceleration defined above is associated with one of the gimbal axes, $\ddot{\theta} = 0$ for the other axis. Therefore, only a single axis value of δ_D need be considered.

Servo Errors - Ground Station Processing

A block diagram of the servo system hypothesized for the case in which the auto tracking loop is closed through the ground station is shown in Appendix B. It is similar to the system described above except a velocity feedback loop has been added. Its function is to allow a small bandwidth in the outer loop and also to minimize the effect of high frequency components of torque disturbance. Thus, the transport delay of 0.33 seconds, discussed above, will not cause instability in the outer tracking loop.

In this case the tracking error contribution due to torque disturbance is reduced so markedly that $\delta_T \approx 0$. The dynamic lag error is virtually the same as that derived earlier for the case in which the tracking receiver is contained aboard the TDRS. Therefore, Equation (3) will be employed to define the dynamic lag error.

Servo Bandwidth Limitation

An inspection of Equations (1), (2), and (3) reveals that there is an optimum value of the servo noise bandwidth, β_n, which will minimize the combined error due to receiver noise, torque disturbance (where applicable), and dynamic lag error. However, there is a fundamental limitation on the value of β_n. Specifically, the closed loop servo bandwidth, B, is limited by the natural structural resonant frequencies which are coupled into the servo system. All structural resonances in the TDRS impact the system stability. However, those which occur between the feed system and the gimbal drive mechanism are the most important since they are inside the servo position loop. Although the boom which extends from the satellite body to support the gimbal system may have a rather low natural frequency, it is coupled into the loop

through the gimbal friction and is, therefore, severely attenuated. If the lowest structural resonant frequency of important is f_r, then, as an engineering rule of thumb, the closed loop servo bandwidth is bounded by

$$B \leq f_r/3.$$

In a typical well designed system of the type of interest here, it is the case that $\beta_n \approx 2B$, so that the important restriction

$$\beta_n \leq 2 f_r/3 \tag{4}$$

is obtained. According to Dr. B. C. Tankersley of Radiation, Inc. a division of Harris Intertype*, performance measurements with their 12.5-foot DRC antenna, shows that the lowest structural resonant frequency of the entire antenna assembly (ribs, mesh, and loaded cone assembly) is $\geq$ 8 Hz. The reflector structure and cone assembly are virtually decoupled from one another and the lowest structural resonant frequency is established by the reflector structure.

---

* Telephone conversation of 12 June 1974.

4.4.1.1.2 Summation of Tracking Error Components

The individual error components defined above are now combined on a root-sum-square basis. Two cases are considered-- one for which the auto tracking receiver is contained aboard the TDRS and the other with ground station processing.

The two-axis error components to be included in the tracking error are:

1 Receiver generated noise: $\delta_R = 3\sqrt{2\Phi\beta_n}$

2 Gimbal backlash: 0.01

3 Torque disturbance: $\delta_T = \begin{cases} \frac{16.3}{\beta n^2}\left(\frac{Td}{J}\right), & \text{TDRS processing} \\ 0, & \text{ground station processing} \end{cases}$

4 Dynamic lag: $\delta_D = \frac{10^{-5}}{2\beta_n^{\ 2}}$

where all values are in degrees. As noted, βn is the one-sided servo noise bandwidth, in Hz, with the restriction $\beta n \leq 2f_r/3$, where f_r is the lowest natural structural resonant frequency inside the servo loop. The factor T_d/J (1/second^2) is treated as a parameter with values in the range $10^{-7} \leq T_d/J \leq 10^{-2}$.

It is noted in Table XXIX that the two values of tracking error which are to be evaluated are α(DLM, BS, S) and α(DLM, BS, K) for S- and K_u-band auto tracking. The only quantity which depends on frequency is Φ, the angle error spectral density (degree^2/Hz).

The total tracking error is defined below:

$$\alpha(\text{DLM, BS, f}) = \begin{cases} \sqrt{10^{-4} + \delta_R^2(f) + \delta_T^2 + \delta_D^2} & \text{; TDRS processing} \quad (5) \\ \sqrt{10^{-4} + \delta_R^2(f) + \delta_D^2} & \text{; ground station processing} \quad (6) \end{cases}$$

where

$$\delta_R(f) \triangleq 3\sqrt{2\beta_n\Phi(f)}$$

(f) denotes either S- or K_u-band operation.

4.4.1.2 Data Beam Offset/Boresight Error

The subject error is associated with data link maintenance via auto tracking. It is defined as the angular displacement of the boresight

axis of the auto tracking system and the direction of the data channel gain maximum.

Table XXIX shows that there are four values of the data beam offset/boresight error to be considered for the case of RP/K-AUTO, viz., α(DBO, BS, K), α(DBO, BS, S-I), α(DBO, BS, S-II), and α(DBO, BS, S-III(*)). In the case of RP/S-AUTO, only the single value α(DBO, BS, S-II) must be evaluated. The first and last of the just defined five errors will be evaluated in a similar manner since in both cases an angle sensing feed is used for both auto tracking and data beam formation. Moreover, the other three errors result from the use of separate feeds for angle sensing and data beam formation. This logical categorization will be used in the evaluation of errors which follows.

α(DBO, BS, K)

In this case the antenna feed performs angle sensing at K_u-band. The data beam offset/boresight error therefore results solely from inherent phase/amplitude unbalance which occurs in the pre- or post-comparator circuitry. Appendix A contains an analysis of both the boresight shift and the angular displacement of the direction of the sum channel gain maximum which results from these factors. It is shown in Appendix A that boresight shift results from pre-comparator amplitude unbalance as well as pre- and post-comparator phase unbalance. The angular displacement of the sum channel maximum is influenced only by pre-comparator unbalance.

For purposes of analysis, the following baseline values of unbalance have been adopted on the basis of typical implementation results:

1	Pre-comparator phase unbalance:	± 5 degrees at S-band ±15 degrees at K_u-band
2	Pre-comparator amplitude unbalance:	±0.4 dB at S- and K_u-bands
3	Post-comparator phase unbalance:	±20 degrees at S- and K_u-bands.

The boresight shift and the angular displacement of the sum channel maximum are both influenced by the crossover level of the angle sensing antenna patterns. The crossover level is assumed to be -3 dB in the material which follows. Small variations with respect to this value will not materially influence the quoted results. Based on the results of Appendix A, and the K_u-band values given above, the single plane angular displacement of the sum channel gain maximum from the no-error boresight direction is $\pm 0.039\ \theta_{3,K}$, where $\theta_{3,K}$ is the half-power beamwidth (in degrees) of either of two squinted mirror image antenna patterns formed in one of the sensing planes. It is also the case that the single plane boresight shift is either $\pm 0.017\ \theta_{3,K}$ or $\pm 0.051\ \theta_{3,K}$, where the actual value depends on the choice of

signs in the pertinent circuit unbalances. The maximum possible angular displacement between the boresight axis and the sum channel gain maximum is $0.09\ \theta_{3,K}$. The two-axis data beam offset/boresight error will be taken to be $\sqrt{2}$ times this value, with the result $\alpha(\text{DBO, BS, K}) = 0.127\ \theta_{3,K}$

If the K_u-band angle sensing feed system employs a dedicated data channel, then there is no angular displacement of the data channel gain maximum due to circuit unbalance so that $\alpha(\text{DBO, BS, K}) = 0.051\sqrt{2}\ \theta_{3,K} = 0.072\ \theta_{3,K}$.

In the material which follows it will be assumed that the K_u-band feed contains a dedicated data channel since, as is shown in section 4.5, this is the baseline approach.

α(DBO, BS, S-II) With RP/S-AUTO

The error of interest in this case is analogous to that evaluated above except that operation is at S-band. It is assumed that the S-band angle sensing feed and associated tracking receiver can be analyzed on the basis of sum and difference auto tracking as is done in Appendix A. With the circuit unbalance values defined above, the single plane angular displacement of the sum channel gain maximum is $\pm 0.038\ \theta_{3,S}$ and the boresight shift has values of $\pm 0.005\ \theta_{3,S}$ and $\pm 0.028\ \theta_{3,S}$. Reasoning as above, the error of interest is $\alpha(\text{DBO, BS, S-II}) = 0.092\ \theta_{3,S}$. In this case and in those which follow, the value $\theta_{3,S} = 2.5$ degrees will be used. Therefore, $\alpha(\text{DBO, BS, S-II}) = 0.23$ degree.

α(DBO, BS, S-I)

In this case and for the errors α(DBO, BS, S-II) and α(DBO, BS, S-III(*)), different antenna feeds are associated with angle sensing and data beam formation. All three errors will be evaluated using the same basic technique. In particular, the angular displacement of the boresight axis of the K_u-band angle sensing feed system from the reflector axis is determined. Then, the angular offset of the data channel gain maximum (formed by the S-band feed system) with respect to the reflector axis is evaluated. These two values, when combined on an root sum square (rss) basis, yield the desired result.

The first of the two angular errors just defined is common to all three of the cases in which auto tracking is carried out at K_u-band and the data beam is formed at S-band. The basic components of the angular shift of the boresight axis from the reflector axis are:

1. Physical displacement of the K_u-band angle sensing feed from the boresight axis due to:
   - a. Improper placement during manufacture
   - b. Deflection due to solar heating
   - c. Deflection due to acceleration

2 Boresight shift of the K_u-band auto tracker due to pre-comparator unbalance.

With the aid of the physical layouts of the antenna systems given in section 4.5, it is estimated that the three sigma displacement of the K_u-band feed system from the desired position is ±0.030 inch. With a reflector focal distance of 60 inches (f/D = 0.4 and diameter = 12.5 feet) and a beam deviation factor of unity (near the reflector axis) the equivalent two-axis angular offset is 0.029 degree.

The two-axis deflection of the feed system due to solar heating (Reference 19) is taken to be 0.008 degree based upon the use of three layers of multilayer insulation of the feed cone assembly.

Next, an analysis of the deflection of the feed system due to acceleration of the antenna system of 1.25×10^{-5} degrees/second^2 indicates that this error component is negligible.

The boresight shift of the K_u-band auto tracker due to pre-comparator circuit unbalance was evaluated above, as α(DBO, BS, K), and found to have a two-axis value of $0.072\ \theta_{3,K}$ degree.

An rss combination of the three errors given above yields a value of $0.03\sqrt{1+(2.4\ \theta_{3,K})^2}$ for the angular displacement of the boresight axis of the K_u-band auto tracker and the reflector axis.

The other error component needed for a determination of α(DBO, BS, S-I) is the angular offset of the direction of the data beam maximum of the S-band feed from the reflector axis. (The designation S-I refers, of course, to the use of a non-tracking feed which is nominally located on the reflector axis.) The error contributors are:

1 Improper placement during manufacture

2 Deflection due to solar heating

3 Deflection due to acceleration

4 Displacement of the feed phase center from the physical center.

Only the first of these four components is applicable since deflection due to solar heating has already been considered in the boresight axis/reflector axis error, the effect of antenna acceleration is essentially zero and the displacement of the phase center is taken to be negligibly small.

The three sigma feed placement error is estimated to be ±0.050 inch which results in an angular error of 0.048 degree between the data beam maximum and the reflector axis. When this value is combined with a $0.03\sqrt{1+(2.4\ \theta_{3,K})^2}$ degree boresight axis/reflector axis error, the result

is $\alpha(\text{DBO, BS, S-I}) = 0.057\sqrt{1+(1.27\ \theta_{3,K})^2}$

α(DBO, BS, S-II) with RP/K-AUTO

The subject error differs from the one just discussed only by virtue of the S-band feed possessing an angle sensing capability. Therefore, it is only necessary to combine α(DBO, BS, S-I) with the angular displacement of the S-band data beam maximum which results from pre/post-comparator unbalance. The latter value was evaluated above, as a component of α(DBO, BS, S-II) with RP/S-AUTO, and found to be $0.038\sqrt{2}\theta_{3,S} = 0.134$ degree. This value, when combined with $0.057\sqrt{1+(1.27\theta_{3,K})^2}$ on an rss basis, yields $0.15\sqrt{1+(0.5_3K)^2}$.

α(DBO, BS, S-III(*))

In this case the S-band feed, which forms the data beam, is non-tracking, and is positioned on the reflector axis (with some error) via ground command. Therefore, the subject error is identical to α(DBO, BS, S-I) except for the additional error incurred in feed positioning. This added error is estimated to be $\pm$0.025 inch. The equivalent three sigma angular error is therefore $0.07\sqrt{2}$ degree, as opposed to 0.048 degree when the S-band feed is not movable. It follows then that $\alpha(\text{DBO, BS, S-III(*)}) = 0.078\sqrt{1+(0.92\theta_{3,K})^2}$ degree.

4.4.1.3 Angular Displacement Between Reflector Axis and Direction of Data Beam Maximum

The subject quantity is not explicitly needed for a determination of the data beam pointing error but is required in the computation of data channel gain. All of the ingredients are available from the material just completed.

When the K_u-band angle sensing feed forms a data beam, the direction of the maximum of that beam is displaced from the reflector axis by $\pm$0.029 degree due to physical feed placement, $\pm$0.008 degree as a result of solar heating, and an additional $\pm 0.039\ \theta_{3,K}$ degree due to pre-comparator phase/amplitude unbalance when a dedicated data channel is not employed. Therefore, the angular displacement of the data channel gain maximum from the reflector axis is $\pm$0.03 degree and $\pm 0.03\sqrt{1+(1.3\theta_{3,K})^2}$ with and without a dedicated data channel.

In the case S-I, a non-tracking S-band feed forms the data beam so that the only error of interest is its physical displacement from the reflector axis. That value is simply $\pm$0.048 degree.

When case S-II is examined, there is an additional error due to pre-comparator unbalance of $\pm 0.038\sqrt{2}\theta_{3,S} = 0.134$ degree, so that the total angular offset of the data beam maximum from the reflector axis is 0.14 degree.

For S-III, the situation is analogous to S-I except for the added physical displacement due to command positioning of the feed. The corresponding angular error is $\pm$0.072 degree.

4.4.1.4 Total Data Beam Pointing Error

The material set forth in sections 4.4.1.1, 4.4.1.2, and 4.4.1.3 is summarized in Table XXXI. All of the angular errors which influence the loss of data channel gain when data link maintenance is carried out with auto tracking are contained in Table XXXI.

4.4.2 Data Beam Pointing Errors for Data Link Maintenance Using RP/GC

When data link maintenance is performed by ground control of the reflector pointing angles, there are two basic error components: a reflector designation error and a data beam offset/reflector axis error. It is recalled that the reflector designation error is the angular displacement between the reflector axis and the line connecting the TDRS and user spacecraft. The data beam offset/reflector axis error is defined as the angular displacement of the reflector axis and the direction of the data channel gain maximum.

Table XXIX shows that the reflector designation error is defined as α(REF,DES). The data beam offset/reflector axis error has four distinct values which depend on the data link frequency and S-band feed option. They are defined as α(DBO,REF,K), α(DBO,REF,S-I), α(DBO,REF, S-II), and α(DBO,REF,S-III(*)). An evaluation of these errors follows.

4.4.2.1 Reflector Designation Error

Subsequent paragraphs categorize and define pertinent error components. Then, each error component is analyzed and assigned a numerical value. Finally, a single value of the reflector designation error is obtained by combining the various components.

The basic elements of the system which perform data link maintenance with reflector pointing via ground command are shown in Figure 34.

All of the system elements shown above, with the exception of the feed system, contribute to the reflector designation error. Table XXXIIpresents a detailed list of those contributors.

3σ Data Beam Pointing Error (± degrees)	3σ Angular Displacement Between Reflector Axis and Direction of Data Beam Maximum (± degrees)
$=\sqrt{\alpha^2(DLM,BS,K)+\alpha^2(DBO,BS,K)}$	$0.030\sqrt{1+(1.3\theta_{3,K})^2}$; without dedicated data channel 0.030; with dedicated data channel
$=\sqrt{\alpha^2(DLM,BS,K)+\alpha^2(DBO,BS,S\text{-}I)}$	0.048
$=\sqrt{\alpha^2(DLM,BS,K)+\alpha^2(DBO,BS,S\text{-}II)}$	0.14
$=\sqrt{\alpha^2(DLM,BS,K)+\alpha^2(DBO,BS,S\text{-}III(*))}$	0.072
$=\sqrt{\alpha^2(DLM,BS,S)+\alpha^2(DBO,BS,S\text{-}II)}$	0.14

TABLE XXXI

Angular Errors Associated with Data Link Maintenance via Auto Tracking

Tracking Error (± degrees)	3σ Data Beam Offset/ Boresight Error (± degrees)	3σ Data Be (±
$\sqrt{10^{-4}+\delta_R^2(K)+\delta_T^2+\delta_D^2}$; TDRS processing $\sqrt{10^{-4}+\delta_R^2(K)+\delta_D^2}$; ground station processing	$\alpha(DBO,BS,K) = \begin{cases} 0.127\theta_{3,K}; \text{ without dedicated data channel} \\ 0.072\theta_{3,K}; \text{ with dedicated data channel} \end{cases}$	$\alpha(DATA,K) = \sqrt{\alpha^2(DLM,BS}$
	$\alpha(DBO,BS,S\text{-}I) = 0.057\sqrt{1+(1.27\theta_{3,K})^2}$	$\alpha(DATA,S) = \sqrt{\alpha^2(DLM,BS}$
	$\alpha(DBO,BS,S\text{-}II) = 0.15\sqrt{1+(0.5\theta_{3,K})^2}$	$\alpha(DATA,S) = \sqrt{\alpha^2(DLM,BS,}$
	$\alpha(DBO,BS,S\text{-}III(*)) = 0.078\sqrt{1+(0.92\theta_{3,K})^2}$	$\alpha(DATA,S) = \sqrt{\alpha^2(DLM,BS,}$
$\sqrt{10^{-4}+\delta_R^2(S)+\delta_T^2+\delta_D^2}$; TDRS processing $\sqrt{10^{-4}+\delta_R^2(S)+\delta_D^2}$; ground station processing	$\alpha(DBO,BS,S\text{-}II) = 0.23$	$\alpha(DATA,S) = \sqrt{\alpha^2(DLM,BS,}$

ise error $\triangleq 3\sqrt{2\beta_n\Phi(f)}$

; K_u-band auto tracking
; S-band auto tracking

urbance error $\triangleq \frac{16.3}{\beta_n^2}\left(\frac{T_d}{J}\right)$

^2_s $^{-2}$

error $\triangleq \frac{10^{-5}}{2\beta_n^2}$

l servo noise bandwidth
$2f_r/3$

$\theta_{3,K} \triangleq$ half-power, pre-comparator angle sensing beamwidth in degrees

Data Link Maintenance Method	Data Link Frequency Band(s)	Option Number and Associated S-band Feed Configuration	3σ Tracking Er (± degrees)
RP/K-AUTO	K_u	N/A	$\alpha(DLM,BS,K) = \begin{cases} \sqrt{10^{-4}+\delta_R} \\ \text{TDRS} \\ \sqrt{10^{-4}+\delta_R} \\ \text{stati} \end{cases}$
	S and K_u	I: on-axis, non-tracking	
		II: on-axis, tracking	
RP/K-AUTO(*)	S and K_u	III: movable, non-tracking, positioned on reflector axis ground command	
RP/S-AUTO	S	II: on-axis, tracking	$\alpha(DLM,BS,S) = \begin{cases} \sqrt{10^{-4}+\delta_R} \\ \text{TDRS} \\ \sqrt{10^{-4}+\delta_R} \\ \text{stati} \end{cases}$

δ_R = receiver noise error Δ

$\Phi(f) = \begin{cases} \Phi(K); K_u\text{-band a} \\ \Phi(S); S\text{-band au} \end{cases}$

δ_T = torque disturbance err

$10^{-7} \leq T_d/J \leq 10^{-2}$ s $^{-2}$

δ_D = dynamic lag error $\Delta \frac{10}{2\beta}$

β_n = one-sided servo noi in Hz; β_n $2f_r/3$

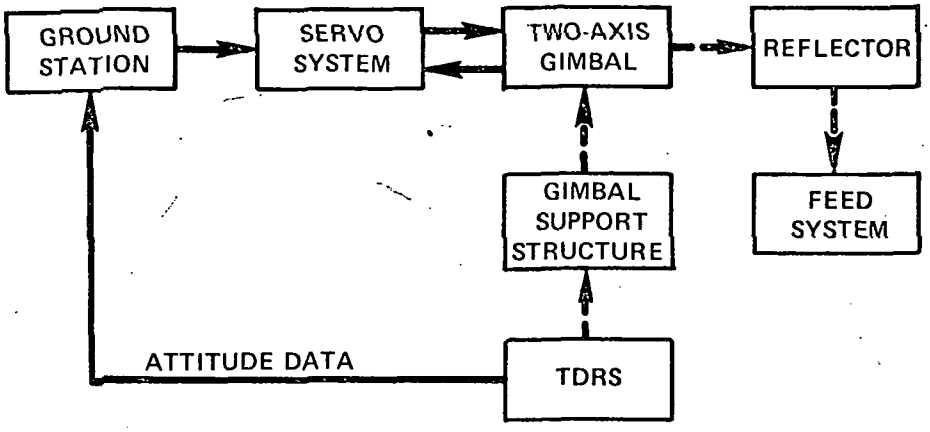

Figure 34. Data Link Maintenance Via Reflector Pointing

TABLE XXXII

Sources of Reflector Designation Errors

Non-antenna*	Ephemerides Operational time delays TDRS stabilization
Gimbal support structure*	Alignment Deflection due to solar heating Deployment mechanism
Gimbal**	Non-orthogonality of axes Backlash Deflection due to solar heating Shaft angle readout
Servo**	Offset Dynamic lag Torque disturbance
Reflector**	Natural distortion Thermal distortion Distortion due to acceleration

*Error contributions to commanded reflector pointing angles

**Error contributions to difference in actual and commanded pointing angles

4.4.2.1.1 Individual Error Sources

Each of the contributors to the reflector designation error which are listed in Table XXXIIare now examined and assigned numerical values. In those cases in which the errors are random, the 3σ values are given. Also, only two-axis errors are quoted.

Ephemerides

The uncertainty in the estimated position of the user spacecraft results in an equivalent angular error contribution of 0.02 degree (Reference 20).

Operational Time Delays

The subject term refers to the time lag associated with the angle commands delivered to the positioning servo system, i.e., even if the angle commands were carried out without error, there would be an inherent reflector designation error component incurred as a result of the tardiness of those commands.

There are at least four distinct sources of operational time delay:

1 Cueing time (prior to required ground station computation)

2 Computation time

3 Non-continuous angle command updating

4 Propagation path delay.

It will be assumed that the total operational time delay is limited to 10.0 seconds which corresponds to a designation error of 0.13 degree for the maximum user angular rate of 0.013 degree/second obtained from Appendix C.

TDRS Stabilization

Based upon instructions from GSFC personnel, the TDRS is assumed to possess three-axis stabilization. The uncertainty which the ground station experiences in the TDRS altitude is taken to be ± 0.357 degree (Reference 21). This value is based upon the combination of the following error sources:

1 Attitude determination sensor errors: ± 0.173 degree

2 Sensor alignment and thermal deformation: ± 0.087 degree

3 Short term dynamic control errors: ± 0.30 degree.

Gimbal Support Structure

Three distinct error contributions are associated with the structure by which the TDRS supports the two-axis gimbal. They are (Reference 20):

1 Alignment: 0.1 degree

2 Thermal deflection: 0.2

3 Deployment mechanisms: 0.05.

The total gimbal support structure error is therefore 0.23 degree.

Gimbal

A total of four error components are attributed to the gimbal. The non-orthogonality of the two axes contributes 0.02 degree to the reflector designation error (Reference 20). The two-axis gimbal backlash angle, discussed earlier in conjunction with the tracking error, is taken to be 0.01 degree. Deflection of the gimbal caused by solar heating is assumed to create an angular error of 0.05 degree. A shaft angle readout error is caused by bearing wobble and data gear nonlinearity/backlash in the gimbal, transducer nonlinearity, and granularity. This error source is assumed to be 0.06 degree based upon typical hardware.

The total angular error which results from the gimbal is 0.08 degree.

Servo

Two servo systems design concepts were postulated in paragraph 4.4.1.1.1 to evaluate the tracking errors incurred with data link maintenance via auto tracking. The need for two different designs resulted from differing requirements imposed by the auto tracking receiver located either aboard the TDRS or at the ground station. Both design concepts are defined in block diagram form in Appendix B.

Three potential servo error contributors require consideration. The offset error was judged to be negligibly small in the foregoing consideration of tracking errors. Dynamic lag and torque disturbance errors are assumed to be negligibly small on the basis of high gain in the position loop associated with the angle command mode. Thus, the servo system does not influence the reflector designation error.

Reflector

The reflector gives rise to three potential error sources, all associated with distortion. One source of distortion results from

assembly of the antenna system under the influence of the Earth's gravity and its subsequent use in a zero-g environment. This source can be negated by proper placement of the feed system during the check-out phase to offset the reduction in gravitational force which occurs in orbit. (This was confirmed by Dr. Thrasher of Radiation, a Division of Harris Intertype.)

The second source of distortion, which results from non-uniform solar heating of the reflector surface, exhibits a maximum value of 0.03 degree (Reference 22) when the sun is in a direction orthogonal to the reflector axis.

The third distortional effect is caused by acceleration of the antenna and is believed to be negligible.

4.4.2.1.2 Summation of Reflector Designation Error Components

Table XXXIII summarizes the error components enumerated above.

TABLE XXXIII

Summary of Reflector Designation Error Components

Error Source	Two-axis, 3σ Angular Error (degrees (±))
Ephemerides	0.02
Operational time delays	0.13
TDRS stabilization	0.357
Gimbal support structure	0.23
Gimbal	0.08
Servo	negligible
Reflector	0.03
	rss = 0.45

The rss reflector designation error is α (REF,DES) = 0.45 degree and the maximum sum error is 0.847 degree. Clearly, the only errors of importance to the rss value are those attributed to TDRS stabilization and the gimbal support structure.

4.4.2.2 Data Beam Offset/Reflector Axis Error

The subject error is defined as the angular difference between the reflector axis and the direction of the data channel gain maximum. From Table XXIX , four values are required: α(DBO, REF, K), α(DBO, REF, S-I), α(DBO, REF, S-II), and α(DBO, REF, S-III(*)). They have already been computed, in conjunction with the data beam offset/boresight errors in paragraph 4.4.1.2 and are given below in Table XXXIV where the total data beam pointing errors are presented.

4.4.2.3 Total Data Beam Pointing Errors

The results of paragraphs 4.4.2.1 and 4.4.2.2 are now utilized in the formulation of the data beam pointing errors associated with reflector pointing via ground command. Table XXXIV presents both basic error contributors as well as the combined error.

4.4.3 Data Beam Pointing Error for Data Link Maintenance Using FP/GC

For the case in which the S-band non-tracking feed is positioned in response to ground commands, there are two basic error components defined in Table XXIX : a feed designation error α(FD,DES) and a data beam offset/feed position error α(DBO, FP, S-III). The feed designation error is the angular displacement between a line connecting the user and the TDRS spacecraft and the direction of maximum gain of a hypothetical beam associated with the physical center of the feed.

The data beam offset/feed position error is the angular displacement between the directions of the gain maxima of the defined hypothetical beam and the actual data beam. This error component results solely from the displacement of the feed phase center from its physical center and is believed to be negligibly small.

Figure 35 illustrates the basic elements of the system which perform data link maintenance with feed positioning via ground command. This mode of operation is employed only when two users are being simultaneously served - one at S-band and the other at K_u-band. Thus, the K_u-band data link is maintained via either RP/K-AUTO or RP/GC, as can be seen from Table XXV . In either case, estimates of the reflector pointing angles are telemetered to the ground station for use in the computation of the desired S-band feed location with respect to the reflector axis. It is clear that a contribution to the feed designation error is made by all of the elements of Figure 35 with the exception of the gimbal servo system and the K_u-band feed.

The feed designation error is now characterized with the aid of Figure 36 which depicts the feed location problem in two-dimensional form. Table XXXV presents a detailed list of contributors to the feed designation error, α(FD, DES), in terms of the components defined

TABLE XXXIV

Data Beam Pointing Errors for RP/GC

Data Link Maintenance Method	3σ Reflector Designation Error (± degrees)	3σ Data Beam Offset/Reflector Axis Error (± degrees)	3σ Data Beam Pointing Error (± degrees)
RP/GC	$\alpha(REF,DES) = 0.45$	$\alpha(DBO,REF,K) = \begin{cases} 0.030\sqrt{1+(1.3\theta_{3,K})^2} \\ \text{without ded. data channel; 0.030 with ded. data channel.} \end{cases}$	$\alpha(DATA,K) = \begin{cases} 0.45\sqrt{1+(0.09\theta_{3,K})^2} \\ \text{without ded. data channel; 0.45 with ded. data channel.} \end{cases}$
		$\alpha(DBO,REF,S\text{-}I) = 0.048$	$\alpha(DATA,S) = 0.45$
		$\alpha(DBO,REF,S\text{-}II) = 0.14$	$\alpha(DATA,S) = 0.47$
RP/GC(*)		$\alpha(DBO,REF,S\text{-}III(*)) = 0.072$	$\alpha(DATA,S) = 0.45$

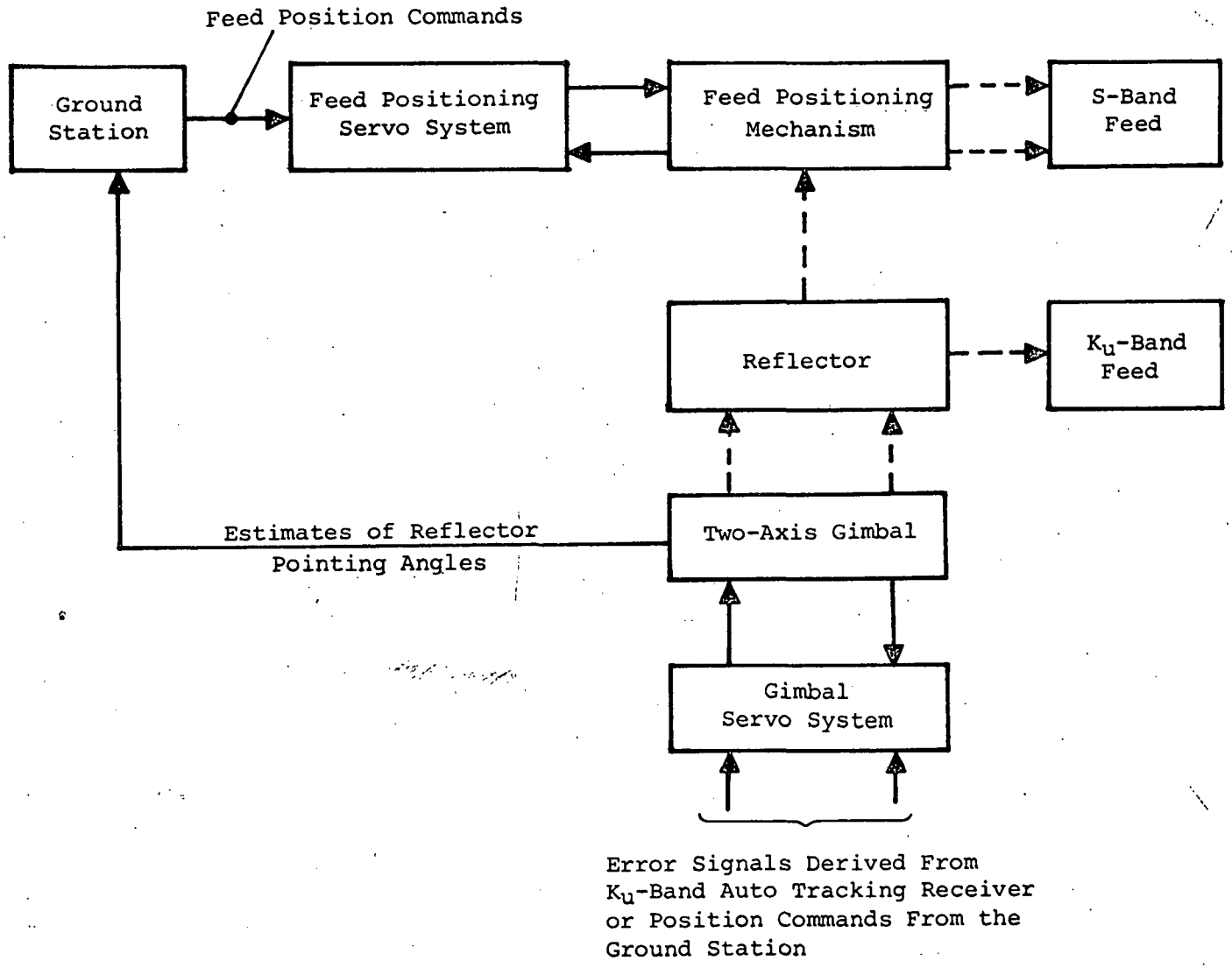

Figure 35. Data Link Maintenance Via Feed Positioning

TABLE XXXV

Sources of Feed Designation Error

Non-Antenna*	Ephemerides
	Operational time delays
	TDRS stabilization
Gimbal support structure*	Alignment
	Deflection due to solar heating
	Deployment mechanism
Gimbal*	Non-orthogonality of axes
	Backlash
	Deflection due to solar heating
	Shaft angle readout
Reflector pointing servo*	Offset
	Dynamic lag
	Torque disturbance
Reflector*	Natural distortion
	Thermal distortion
	Distortion due to acceleration
Feed positioning mechanism**	Backlash
	Deflection due to solar heating
	Position readout
	Positional granularity
Feed positioning servo**	Offset
	Dynamic lag
	Torque disturbance
Antenna feed**	Thermal distortion
	Distortion due to acceleration

* Error contributions to difference in desired and commanded feed positions.

** Error contributions to difference in commanded and actual feed positions.

Figure 35. Data Link Maintenance Via Feed Positioning

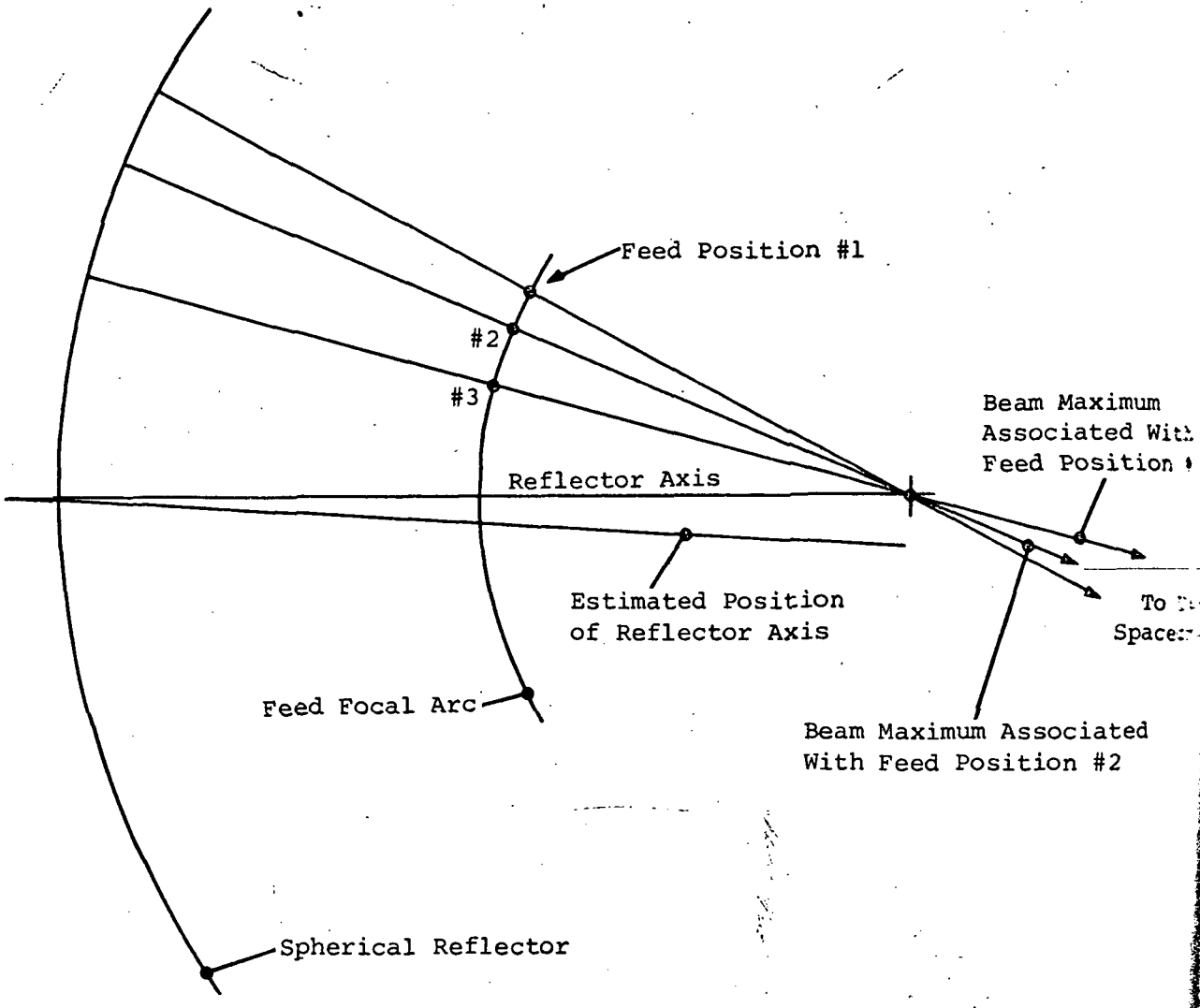

Feed Position #1: Desired Location Based on Actual Pointing Direction of Reflector Axis with Respect to Line Connecting the User and TDRS Spacecraft

Feed Position #2: Location Associated with Position Commands Computed by Ground Station

Feed Position #3: Actual Location

Figure 36. Actual/Desired Feed Location Geometry

in Figure 35. A comparison of Tables XXXV and XXXII reveals that the composite error associated with the difference in the desired and commanded feed positions has been evaluated in conjunction with the reflector designation error encountered with RP/GC and found to have a value of 0.45 degree. This value is increased to 0.47 degree as a result of the operational time delay*.

The remaining quantity of interest is the error associated with the difference in the commanded and actual feed position for which the pertinent components are given in Table XXXV . Rather than investigate each of these error components, the overall feed displacement is estimated and then converted to an equivalent angular error. The details are presented in Appendix D on the supposition that the feed is positioned, in response to ground commands, with a rotational angular error of 0.5 degree and a translational error of 0.25 inch. These values are based on a study of the S-band feed positioning mechanism, described in section 4.5, and the assertion that its errors will completely mask those attributable to the feed positioning servo and the feed distortion resulting from solar heating and acceleration. With 3σ rotational and translational errors of 0.5 degree and 0.25 inch, the equivalent angular error is shown in Appendix D to be 0.35 degree, subject to the following conditions:

1 Reflector focal length - 60 inches

2 Beam offset angle from reflector axis = 30 degrees (maximum value).

The total feed designation error has components of 0.47 and 0.35 degree, whereby α(FD, DES) = 0.59 degree. Since αDBO, FP, S-III) = 0, shown earlier, the data beam pointing error associated with FP/GC is α(DATA, S) = 0.59 degree.

4.5 Main Reflector and Feed Configurations

In this section, the complete category of high gain antennas, feed systems, and beam steering techniques will be reviewed for their application to the requirements of the S- and K_u-band high data rate (HDR) single access (SA) antenna system of the TDRSS. The specific require-

---

* The reflector designation error contains a components of 0.13 degree as a result of an operational time delay of 10 seconds and a maximum user to TDRS angular velocity of 0.013 degree/second. When two users are served simultaneously, the angular velocity of the S-band data beam has a maximum angular velocity of 0.018 degree/second so that the same operational time delay causes an error of 0.18 degree.

ments of this antenna system are outlined in the "Musts" and "Wants" presented in Tables II and III, respectively. A first screening is primarily directed to the "Musts" with the understanding that failure to meet any one of the "Musts" automatically eliminates a candidate and precludes any further consideration of that candidate. By this means the number of configurations requiring further consideration and analysis is quickly reduced to a workable number.

4.5.1 First Screening of Reflectors, Feeds, and Beam Steering Techniques

4.5.1.1 Reflector Antenna Screening

In this first screening exercise, the complete category of high gain antennas is compared to the list of "Musts". Failure to meet any one of the "Must" criteria automatically eliminates a candidate and precludes any further consideration.

The category of high gain antennas can be quickly reduced to the class of reflector antennas by Must No. 3, Reflector/Feed Antennas. Obviously, no further consideration will be given to lenses, arrays, and traveling wave antennas. Reflector antennas are classified in Table XXXVI. Appendix E presents a summary of some of the most promising reflector antenna configurations, along with the attendant advantages and disadvantages of each.

A further screening can be effected by employing Musts No. 2, 4, and 12. Must No. 2 specifies a minimum gain characteristic of a 12.5-foot diameter reflector. Must No. 4 states that the reflector must be compatible with the TDRS concept and the Delta launch vehicle. Therefore, the 12.5-foot reflector must be erectable (deployed) in space because the Delta shroud cannot physically hold two solid 12.5-foot reflectors along with the two other TDRS antennas, namely, the multiple access phased array (S-band) and the K_u-band ground tracking antenna. A thorough survey of existing space erectable antenna designs has uncovered no significant effort in phased corrected surfaces, polarized and polarizing surfaces, and horn paraboloids, thereby causing their elimination by reason of Must No. 12.

The parabolic torus is basically a parabola in one plane and a sphere in the orthogonal plane. Its only possible application to this program would be its wide angle beam steering capability in the spherical plane; however, since Must No. 6 requires beam steering in a cone ($\pm$15 degrees), there is no advantage to the combined contours as compared to the symmetrical reflectors.

Although there are no known designs of erecting a 12-foot parabolic section, it is conceivable that the space erection techniques employed by Radiation, Inc., and Lockheed could be extended to include

TABLE XXXVI
Reflector Antenna Classification

- Reflectors
  - Single-reflector surfaces
    - Symmetrical (circular)
      - Parabolic
      - Spherical
    - Asymmetrical
      - Offset paraboloid
      - Parabolic torus
      - Horn paraboloid (Note A)
  - Dual reflector surfaces
    - Cassegrain
    - Gregorian
    - Shaped (Note B)
  - Polarized and polarizing surfaces
    - Transreflector (Note C)
    - Twistreflector (Note D)
    - Rotaflector (Note E)
  - Phase corrected surfaces
    - Stepping ~ the reflector is an aggregate of smaller reflectors
    - Lensing ~ the reflecting surface is covered with a refractive material

NOTES:

A. Examples are the conical and cassegrain horn parabola.

B. Either one or both reflectors does not have a shape derived from a conic section (as in the case of a cassegrain system). Rather, the reflectors are shaped to satisfy some criterion e.g., the Abbe' sine condition or uniform illumination of the radiating aperture.

C. A polarized reflector which reflects waves of one linear polarization and transmits energy of the orthogonal linear polarization.

D. A reflector which rotates the polarization of an incident wave through a fixed angle, frequently 90 degrees.

E. A reflector which transforms incident linear polarization into reflected circular polarization.

an asymmetrical parabolic shape. Even if this were possible within the TDRS time frame, the following disadvantages would dictate elimination even though there is no violation of any "Musts":

1. Beam steering at K_u-band must be implemented by pivoting the entire feed/reflector assembly due to the intolerable losses which would be encountered in steering a 0.4 degree beam 30 degrees off-axis;

2. Independent S-band beam steering appears to be restricted and complex due to the asymmetry of the reflector.

There is no documented data or experience on beam steering effects, and the magnitude of developing a working understanding of these effects is beyond the scope of this study.

As a final result of this screening of reflector types, the only remaining candidates are presented in Table XXXVII. Notice that shaped reflectors are missing. They have not been eliminated but are included later as a method of optimizing remaining candidates.

TABLE XXXVII
Results of First Screening of Reflectors

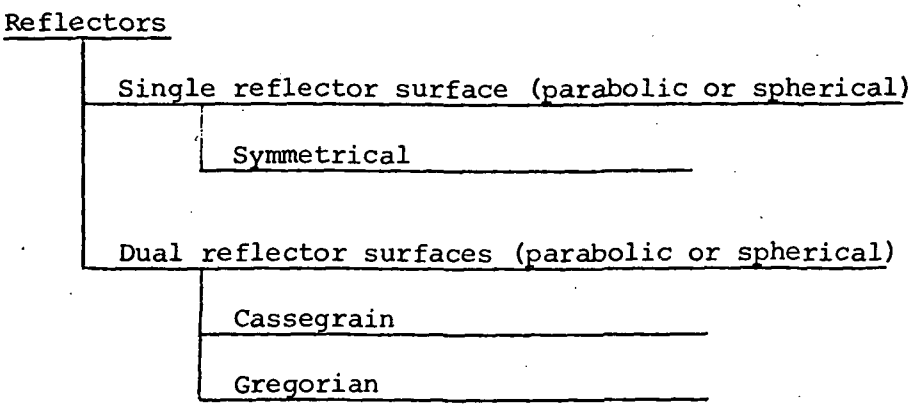

4.5.1.2 Feed/Reflector Combinations

In the preceding section, it was concluded that only three basic reflector configurations satisfied the firm requirements of the TDRS antenna system: namely, a single reflector, a double reflector cassegrain, and a double reflector Gregorian. This section will address the location of feed combinations for each reflector necessary to meet the program objectives. Must No. 1 specifies that two simultaneous beams be generated by the reflector: one at S-band and one at K_u-band. Therefore, two independent feeds must be supported by the common aperture. The first consideration is the location of the feeds relative to the focal point(s) of the reflector(s).

Obviously, the single reflector (SR) surface has but one focal point and both feeds must illuminate the reflector from that position. Both the dual reflector cassegrain (DRC) and the dual reflector Gregorian (DRG) have two focal points: the prime focal point (PFP) of the parabola and the secondary focal point (SFP) of the subreflector (Figures 37 and 38). If designed properly, a feed located at either the PFP or SFP will provide a collimated beam. In both cases placing a feed at the PFP reduces to the condition of an SR (single reflector) antenna. However, the attractive feature of the DRC or DRG is the possibility of locating a feed at each focal point simultaneously and independently. The DRG concept of two independent feeds is easy to visualize and is straightforward in basic design. The DRC will support two independent feeds only if the subreflector is dichroic, i.e., reflects SFP feed frequencies and passes PFP feed frequencies. This concept has been proven and is employed in many operational systems.

Table XXXVIII presents a summary of all possible combinations of S- and K_u-band feeds in each of the three reflector systems. Some of these combinations will be deleted based on the following discussions.

TABLE XXXVIII

Reflector/Feed Combinations

Reflector Type	Feed Combinations
SR	S/K_u at PFP
DRC	S/K_u at SFP
	S at PFP/K_u at SFP
	S at SFP/K_u at PFP
DRG	S/K_u at SFP
	S at PFP/K_u at SFP
	S at SFP/K_u at PFP

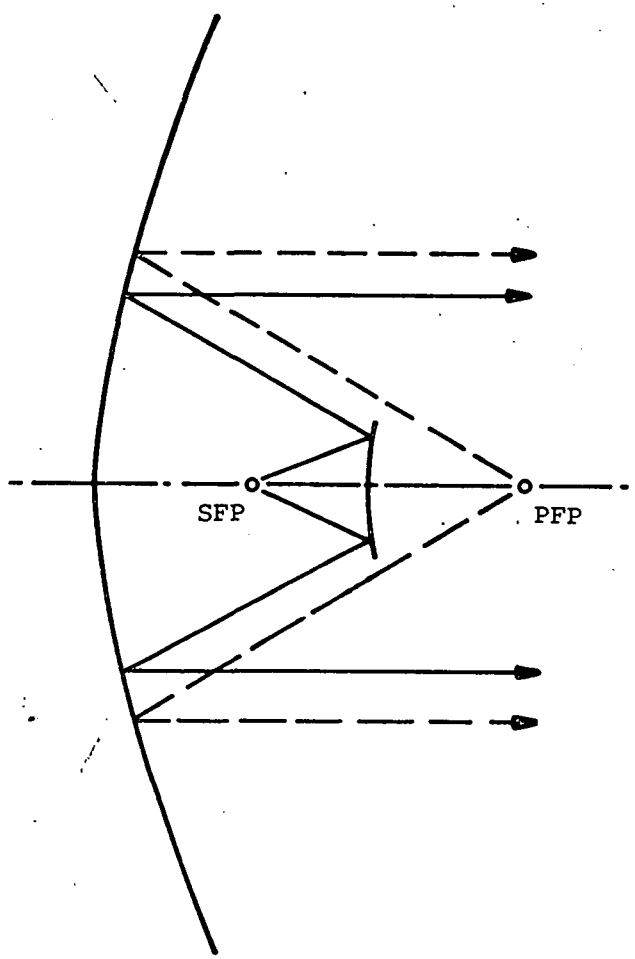

Figure 37. Dual Reflector Cassegrain

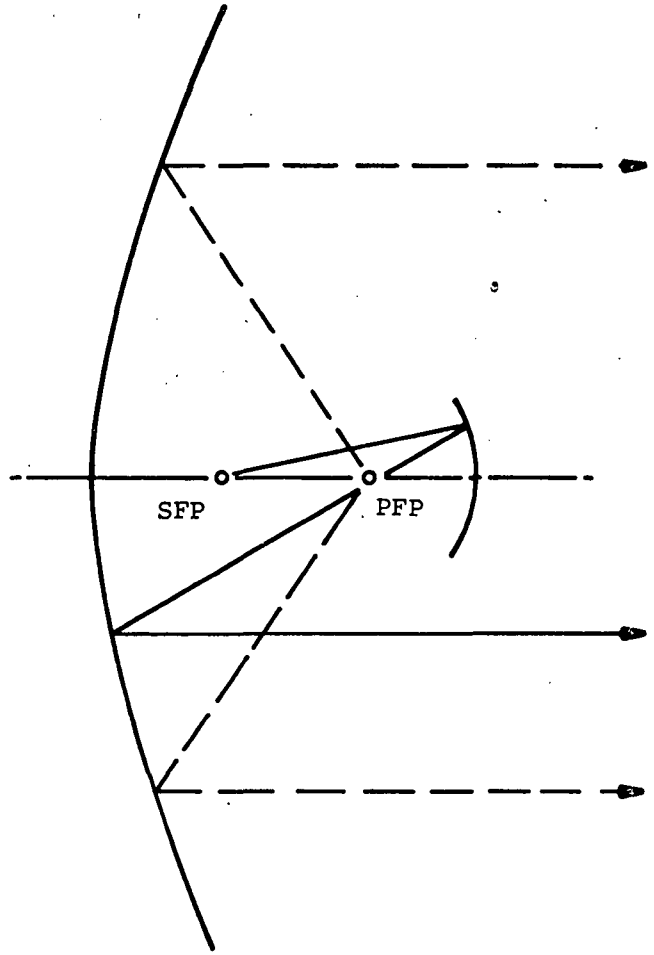

Figure 38. Dual Reflector Gregorian

An efficient cassegrain or Gregorian design requires a subreflector diameter greater than 10λ. In addition, the subreflector is nominally 10 to 15 percent of the parabolic reflector diameter to realize an acceptable blockage of the main reflector. For a 12.5-foot diameter main reflector, the subreflector would be approximately 12 to 18 inches or 2 to 3λ at S-band. These dimensions would result in a poor design with low efficiency and will not satisfy the gain requirements of Must No. 2 for an S-band feed located at the SFP, in either the DRC or DRG configurations.

Consider the DRG reflector/feed combinations. Figure 39 shows the layout of the S- and K_u-band feeds in a Gregorian design. In the most basic design, an S-band feed at the PFP (no autotrack) will be at least 3 inches in diameter. Based on a maximum subreflector diameter of 12 to 18 inches, the S-band PFP feed will cause a minimum of 17 to 25 percent blockage to the K_u-band SFP illumination of the subreflector. The divergence of the SFP illumination will cause even more blockage. The actual blockage will be dependent on the selection of the Gregorian focii. In any practical design one could expect as much as 25 to 30 percent blockage resulting in over 1 dB of gain loss. If an S-band auto tracking feed were placed at the PFP, then the nominal 6-inch diameter feed would produce 50 percent blockage or a gain loss of 3 dB. In any configuration, the gain requirement of Must No. 2 could not be realized in a 12.5-foot diameter reflector. If the S-band feed at the PFP were moved off axis to provide independent beam steering, then the blockage to the K_u-band feed would become dependent on the position of the S-band feed. The result would be asymmetrical patterns and perhaps some degree of K_u-band beam tilt.

Other negative features of the Gregorian design relate to the matching problems encountered when directing energy from one feed to another and the incompatibility with the Radiation, Inc. reflector design.

The only two remaining candidates from the initial listing of all possible configurations shown in Table XXXVIIIare SR (S/K_u at PFP) and DRC (S at PFP/K_u at SFP). All others have been eliminated for the reasons presented in the preceding paragraphs. Table XXXIX presents a listing of the advantages and disadvantages of each remaining candidate.

To eliminate the SR configuration on the grounds of a violation of one "Must", it would be necessary to show that any envisioned feed design would violate a "Must". Instead, the SR configuration will be eliminated on the basis of engineering judgment in that no feed configuration can be envisioned which will satisfy all "Musts" and yet have the features necessary to fulfill the other requirements of an operational system.

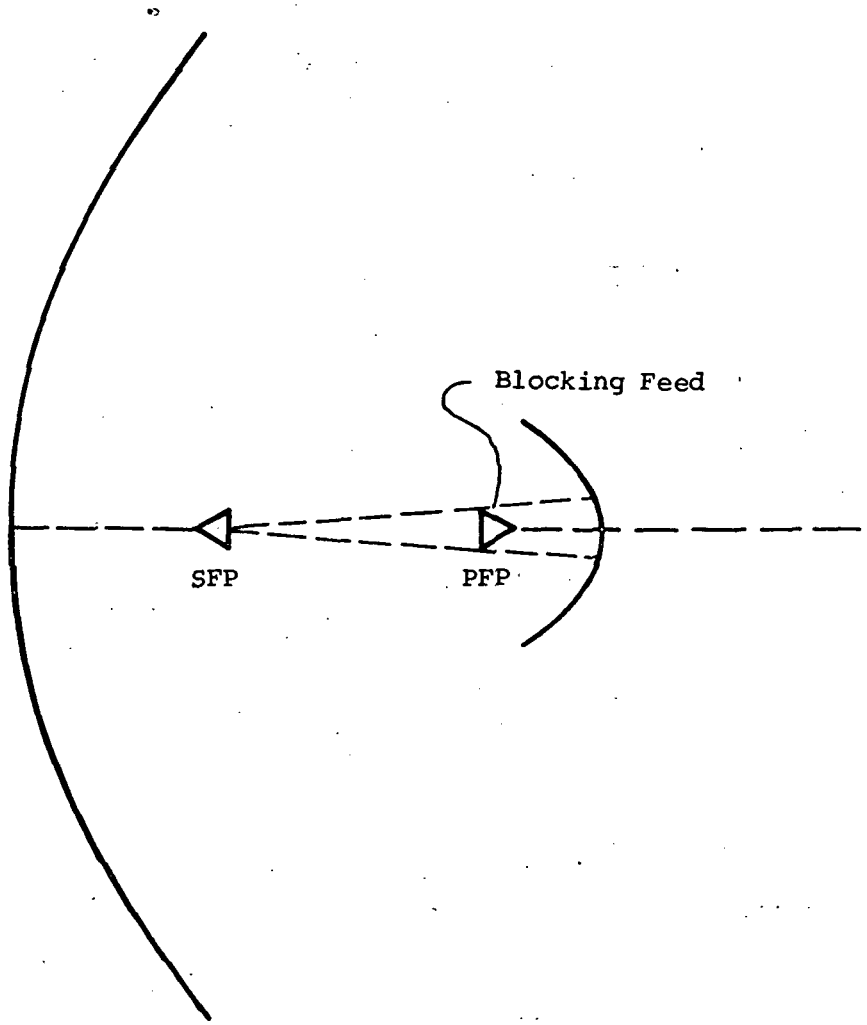

Figure 39. Dual Reflector Gregorian Feed Blockage Problem

The conclusion of this section is that only one feed/reflector configuration can satisfy the TDRS Antenna System requirements; namely, the Dual Reflector Cassegrain with the S-band feed at the primary focal point and the K_u-band feed at the secondary focal point.

TABLE XXXIX

Comparison of SR and DRC Configurations

Configuration	Advantages	Disadvantages
SR (S/K_u at PFP)	Inherently collimated beams Dichroic subreflector not required	Complex nested feed design with limited space for each Simple S-band feed not possible; must use an array 3 to 4 K_u W/G runs from feed to receiver (vertex mounted) Σ, Tx, ΔEL, ΔAZ Additional W/G losses Limitation on acquisition aid schemes at K_u-band No possibility of independent S-band beam steering
DRC (S at PFP K_u at SFP)	Simple independent feed designs Flexibility in acquisition aids at K_u-band, i.e., subreflector or feed defocusing Can employ single aperture S-band feed K_u feed located near receiver (low loss and phase stability) Can add provisions for independent S-band beam steering	Requires low loss dichroic subreflector More difficult alignment and collimation of two beams

4.5.1.3 Beam Steering Techniques

In this section all possible beam steering techniques are screened against the requirements of the antenna with particular emphasis on their application to the only feed/reflector configuration found acceptable in paragraph 4.5.1.2, namely DRC (S at PFP/K_u at SFP). From Must No. 6, each beam must be steerable up to ±15 degrees of the local nadir and from Must No. 10, the gain values specified in Must No. 2 must be maintained throughout the 30 degree cone. Must No. 2 does not apply if S- and K_u-band beams are steered simultaneously and independently since that capability is a "Want" (No. 5) and not a "Must."

All beam steering schemes can be categorized as follows:

1 Electronic (E) - No physical motion of either the feed or reflector(s);

2 Mechanical (M) - Motion of the entire primary or secondary reflectors, either separately or in combination; (the feed can either be attached to the reflector(s) and move with it or it can be attached to another reference from which the reflector(s) is moved.)

3 Electromechanical (EM) - Fixed reflectors with motion of part or all of the radiating portion of the feed.

It is readily apparent that the simplest, most accurate, and most reliable means for steering the K_u-band beam ±15 degrees is by fixing the feed to the reflector axis and mechanically moving the entire reflector system. In a parabolic reflector the degradation in gain which would result in E or EM steering of the beam ±37.5 beamwidths off axis constitutes a clear violation of Must No. 2. Electronic (E) beam steering in a spherical reflector would require a phased array of more than 1000 elements, and the complexity and inherent losses of this array could not be tolerated on TDRS. Electromechanical (EM) beam steering is possible in the spherical reflector. The only apparent advantage of EM as compared with M steering would be in moving a smaller device (feed or feed/subreflector). Examination of devices used to EM scan feeds on the Arecibo spherical reflector and other reported implementations quickly lead to the conclusion that any design for moving the K_u-band feed relative to a fixed reflector will obviously be more complex, less accurate, less reliable, and will cause more RF blockage.

Obviously, since the complete reflector system must be moved to point the K_u-band beam, the same mechanism can be employed to steer the S-band beam mechanically. This condition will satisfy all of the "Musts". However, to satisfy Want No. 5 (independent S- and K_u-band beam steering) an alternate means for steering the S-band will be addresse

To steer the secondary beam of a reflector system, it is necessary to move the feed phase center off the reflector axis in proportion to the amount of steering required. In a spherical reflector system, the beam steering angle is equal to the feed offset angle. Table XL shows the relation between the beam steering angle (θ) and the number of elements required (No.) if beam steering were by electronic means. It is assumed that the spherical focal surface (R_f = 5 feet) is completely filled with feed elements spaced $\lambda/2$ apart. E beam steering over any appreciable angle is undesirable for the following reasons:

1. Complexity in corporate feed network
2. Losses in corporate feed network, i.e., switches and transmission lines
3. S/K_u-band blockage of the main reflector by the array
4. Weight of feed array (elements, switches, drivers, and power dividers)
5. Less reliability due to part count.

TABLE XL

Electronic Beam Steering

Number of Array Elements Versus Beam Steering Angle

Angle (θ) (degrees)	N_S (Radius) Elements	No. (Focal Surface) Elements
5	2	13
10	4	50
15	5	79
20	7	155
25	9	260
30	10	340

Another variation in beam steering employs E steering along the radius of the spherical focal surface and mechanical rotation of the radial array about the reflector axis to effect beam steering anywhere in the conical area. The advantage of this hybrid technique is that

fewer feed elements are required (N_S of Table XL) to achieve a large scan angle. The problem with this technique, which is also found in the full E steering system is the loss in gain when the user is between adjacent beam peaks. This crossover loss amounts to 3 dB when the element spacing is $\lambda/2$. This effect can be reduced by feeding adjacent elements appropriately to achieve a smooth transition in phase center steering; however, this correction also requires compensation for primary feed beamwidth and gain. The simple feed has thereby developed into a more complex phased array and is thus found to be less desirable.

Finally, the most desirable beam steering technique is moving a simple single feed off axis and rotating the feed about the reflector axis, i.e., via EM. From the RF point of view, this system will produce the best performance and is the least complex. The only drawback is the complete dependence on mechanical motion in two independent axes. In a space environment, mechanical motion should be avoided as much as possible; however, EM is the only technique which presently fulfills the requirement for independent beam steering without undue complexity.

In summary, the K_u-band beam must be steered by movement of the complete reflector system; the S-band beam would also be steered by the same mechanism. If it is necessary to steer S-band independently of K_u-band, then the S-band beam must be steered by electromechanical means.

4.5.1.4 Conclusions of First Screening

Table XLI summarizes the conclusions for first screening of reflectors, feed combinations, and beam steering methods.

TABLE XLI

First Screening Summary

Reflector	Feed Combinations	Beam Steering	Options
DRC (Parabolic)	K_u at SFP S at PFP	M	I, II
DRC (Spherical)	K_u at SFP S at PFP	M EM	III, IV

For Options I and II, where the S- and K_u-band beams are colinear and aligned to the reflector axis, the only viable system is a parabolic dual reflector cassegrain system with the K_u-band feed at the secondary focal point (SFP) and the S-band feed located at the primary focal

point (PFP). Beam steering for both beams is by mechanical motion of the complete reflector system. The application of the spherical reflector system to Options I and II has no advantage, since beam steering is mechanical.

The spherical dual reflector cassegrain system is the preferred solution to Options III and IV where the S- and K_u-band beams are required to steer independently. The K_u-band feed is located at the secondary focal point and the resultant K_u beam is steered by moving the entire reflector system. The S-band feed is located at the primary focal point (paraxial focus), and its beam is steered by moving the feed relative to the reflector axis. The parabolic reflector is not considered for this case because of the intolerable degradation in gain experienced in EM steering $\pm$30 degrees off axis. (A detailed discussion of the effect of EM steering of S-band in a parabola is contained in Appendix G.) Of course, if smaller S-band beam steering angles could be tolerated, then the use of a parabolic reflector would be more attractive.

4.5.2 Design Considerations for Dual Reflector Antenna Systems

4.5.2.1 Parabolic Dual Reflectors

Total efficiencies of cassegrain antennas generally are in the vicinity of 50 percent and include illumination efficiency (or amplitude taper efficiency), spillover, blockage, and phase efficiencies. Illumination efficiencies are dependent upon the edge taper and the variation of taper over the antenna aperture. Measured tapers can be approximated by a parabola-on-a-pedestal function defined by $A + B\ (1-\rho^2)^P$ function; several values of illumination efficiencies (Reference 3) are presented in Table XLII. The spillover efficiency is a measure of the ability of the energy source to illuminate only the reflector while minimizing the radiated energy elsewhere and is typically 75 percent for 10 dB edge tapers (Reference 10 and 6). Table XLIII shows the spillover efficiencies as variations of the edge taper.

TABLE XLII

Aperture Taper Efficiency-(Percent)

A (Edge Taper)		P (Form Factor)			
Magnitude	dB	0	1.0	1.5	2.0
0	00	100.00	75.00	64.00	55.55
0.2	13.98	- - -	87.10	82.44	79.29
0.3	10.45	- - -	91.19	88.41	86.72
0.4	7.96	- - -	94.23	92.67	91.84

TABLE XLIII

Spillover Efficiencies

Fractional Edge Taper	Edge Taper (dB)	Spillover Efficiency, (Percent)	Corresponding Loss in Gain, (dB)
0.0	- - -	85	0.71
0.006	25	84	0.75
0.100	20	83	0.81
0.178	15	81	0.91
0.251	12	79	1.02
0.316	10	75	1.25
0.398	8	71	1.49

Potter (Reference 23) has shown that the spillover efficiency can be increased so that the efficiencies approach 85 percent. He accomplished this by extending the edge of the hyperbola subdish in a flare angle of approximately 18.5 degrees, resulting in a total antenna efficiency improvement from 49 percent to 55 percent. This increase has resulted in a 0.4 dB net gain, including the increased aperture blockage due to the flared portion. Figure 40 is a diagram of Potter's concept.

Cramer (Reference 24) has shown that improvement in antenna efficiencies were obtained for 17 percent increases in subdish diameter, with the subdish retaining its hyperboloidal shape. The increase in efficiency was 4 percent but this did not include the slight increase in blockage loss. For the TDRS subdish diameter, the gain represented by a 4 percent increase in efficiency is just about lost by the increase in blockage. Figure 41 shows Cramer's concept. Cramer's optimum design procedure for large cassegrain antenna configurations is described in Appendix H.

4.5.2.2 Spherical Dual Reflectors

Spherical reflector antenna systems are obvious candidates for applications requiring beam steering over wide fields of view with a fixed reflector. The natural application to the TDRS requirements is for steering the S-band feed off axis independent of the K_u-band beam such as is required in Options III and IV. Because of inherent spherical aberrations, spherical reflectors are not perfect reflecting devices, and are unlike parabolas which focus a plane wave onto a single point (focal point). The spherical reflector tends to focus a plane wave onto the paraxial focal point with some phase error. The amount of phase error is dependent on the f/D of the reflector such that as f/D increases

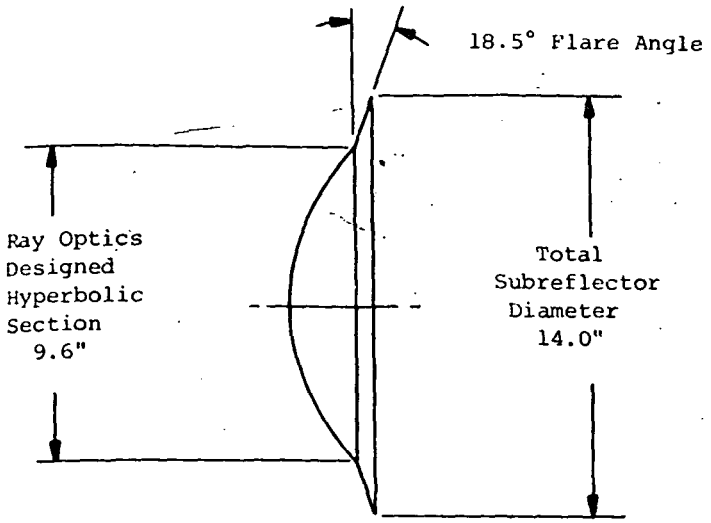

Figure 40. Potter's Concept

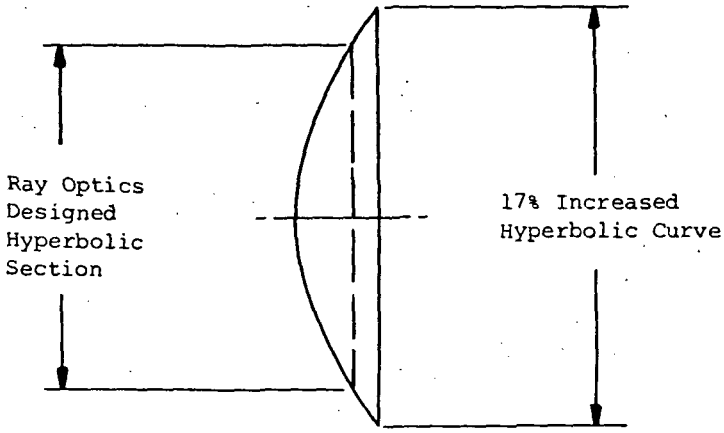

Figure 41. Cramer's Concept

the phase error decreases. The relationship between the maximum permissible illuminated aperture, the total allowable phase error and the focal length (R=2f) is given by (Reference 25):

$$\left(\frac{a}{R}\right)^4 = 14.7 \frac{(\Delta/\lambda)}{(R/\lambda)} \qquad \text{total}$$

where

$a = D/2$

D = diameter of reflector

R = radius of the sphere

Δ = total phase error

As an example, consider a spherical reflector having an effective aperture of 12.5 foot diameter. If the allowable phase error is $\lambda/16$ at 4 GHz, the required radius of the sphere would need to be 28.73 feet.

The paraxial focal point would then be R/2 = 14.37 feet, resulting in an f/D = 1.15. Under the condition of $\Delta = \lambda/16$, experimental measurements have confirmed spherical aperture efficiences equivalent to parabolic apertures while using conventional feed horns. This long focal length approach to reducing spherical aberration cannot be employed for TDRS at K_u-band because of the antenna packaging constraints of the Delta launch vehicle.

There are four ways to correct for spherical aberration:

1 Lens placed before the main reflector

2 Transverse array

3 Line feed design

4 Subreflector correction.

The correction by means of a lens placement before the main reflector is widely used in optical astronomy and is called the Schmidt camera system. For microwave applications a low loss dielectric or metal plate lens could be used; however, for large erectable antenna systems this scheme is obviously unacceptable.

The transverse array technique shown in Figure 42, requires a rather large surface with distributed radiating elements. For single beam operation, this feed structure seems unreasonably complex; furthermore, no practical design or experimental data on this scheme has been reported.

The line feed, Figure 43, is perhaps the most widely used and reported method of correcting for spherical aberrations. The line feed is designed so that the phase velocity in the feed varies to just compensate for the path length deviations experienced by non-axial rays, thereby eliminating spherical aberrations. Love (Reference 26) has reported on S, K_u-, and K_a-band line source feeds which have produced 55 percent aperture efficiencies. These feeds are linearly polarized and are 5 to 10 wavelengths long. He also reports briefly on some success in producing a split beam with a line feed which can be used for auto tracking error signal. Love (Reference 27) reported on a dual polarized line feed 42 λ long which produced a 53 percent aperture efficiency. In all cases, however, these feeds are long, complex in design, critical in fabrication, and apparently sensitive to environments which can cause dimensional changes.

For TDRS application, the most attractive spherical aberration correction technique is by subreflector correction. Several papers have been published on the theory and experimental operation of this technique. The subreflectors fall into three basic categories:

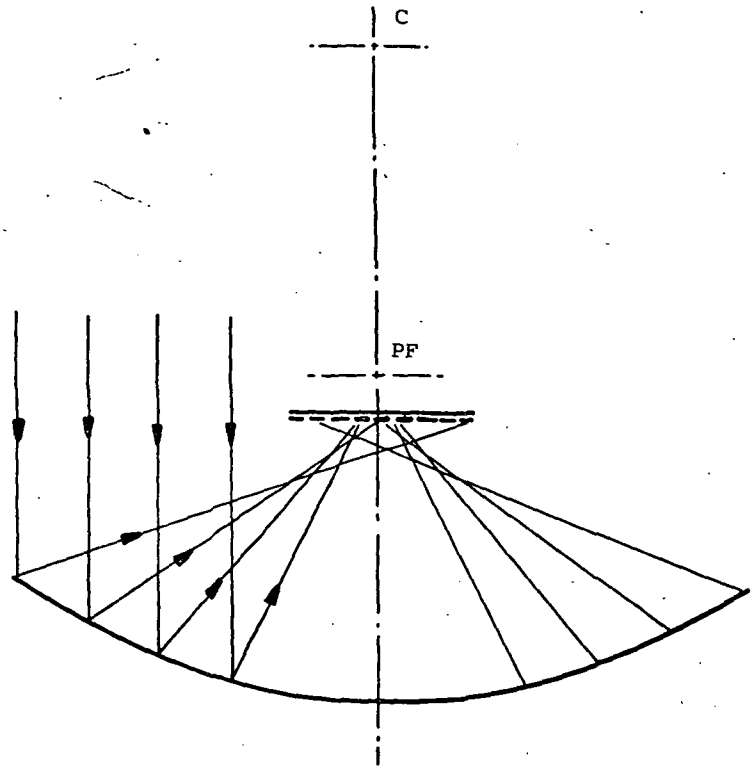

Figure 42. Transverse Feed Correction

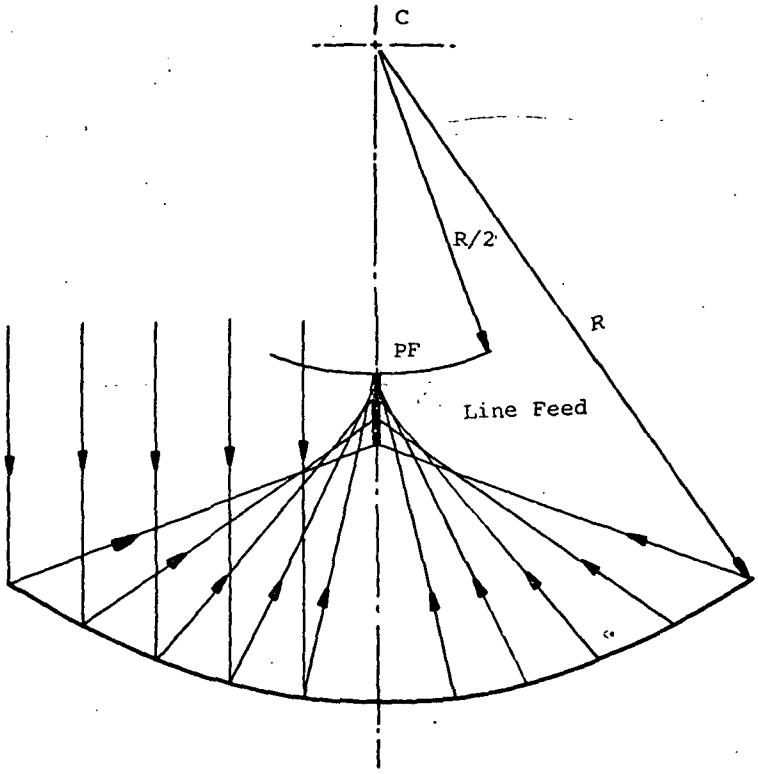

Figure 43. Line Feed Correction

1 Shaped cassegrain (convex)

2 Shaped Gregorian (concave)

3 Spherical (convex).

Subreflectors 1 and 2 can be mathematically shaped to provide complete correction to aberrations, whereas 3 can be designed to reduce the aberration to a tolerable level. Bresler (Reference 28) reports on a comparative design and measurement program which resulted in essentially equivalent performance between the shaped and simple spherical subreflector.

Ishimaru (Reference 29) presents a parametric analysis of the trade factors, such as f/D, subreflector position, subreflector diameter, and feed location and phase error which must be manipulated in the design of a spherical subreflector. Again, as with the single reflector system, the phase error is shown to decrease as a function of increasing f/D.

The following constraints were imposed on the design of a spherical dual reflector system to satisfy TDRS requirements for Options III and IV (Figure 44):

1 12.5-foot diameter to meet gain requirements;

2 Maximum paraxial focal point of 5.5 foot to fit within the Delta shroud as configured in Hughes (Reference 9) concept employing Radiation, Incorporated reflector design;

3 Feed located at least 2 feet from dish vertex to clear Radiation, Incorporated reflector deployment mechanism.

The first consideration was given to a design which would assure the required K_u-band gain (55 percent aperture efficiency). This can be achieved by placing the K_u-band feed at the SFP of the dual spherical reflector. After manipulating the design parameters described by Ishimaru, a reasonable compromise design evolved and is shown in Figure 45. Because of the TDRS constraints on f/D and the large aperture at K_u-band (180λ), it is not possible to achieve acceptable correction to the phase errors by a simple spherical subreflector. Therefore, a convex shaped subreflector is required. In accordance with the work by Bresler, this design can be made to produce the 55 percent aperture efficiency.

Examination of the S-band feed located at the PFP of the spherical reflector reveals that no correction to the feed is required to keep the phase error less than $\pm \lambda/16$. In particular, Ashmead and Pippard (Reference 30) show that if f/D = 0.5 and a single point source feed is used to illuminate a 32λ aperture, the resultant phase error would be $\pm \lambda/16$. The TDRS candidate configuration shown in Figure 45 has f/D = 0.44 and an illuminated aperture of 27.8λ where λ = 0.45 feet at 2200 MHz. In particular, the estimated loss in gain due to spherical aberrations will be less than 7 percent (0.3 dB) as shown in the curves of Figure 46.

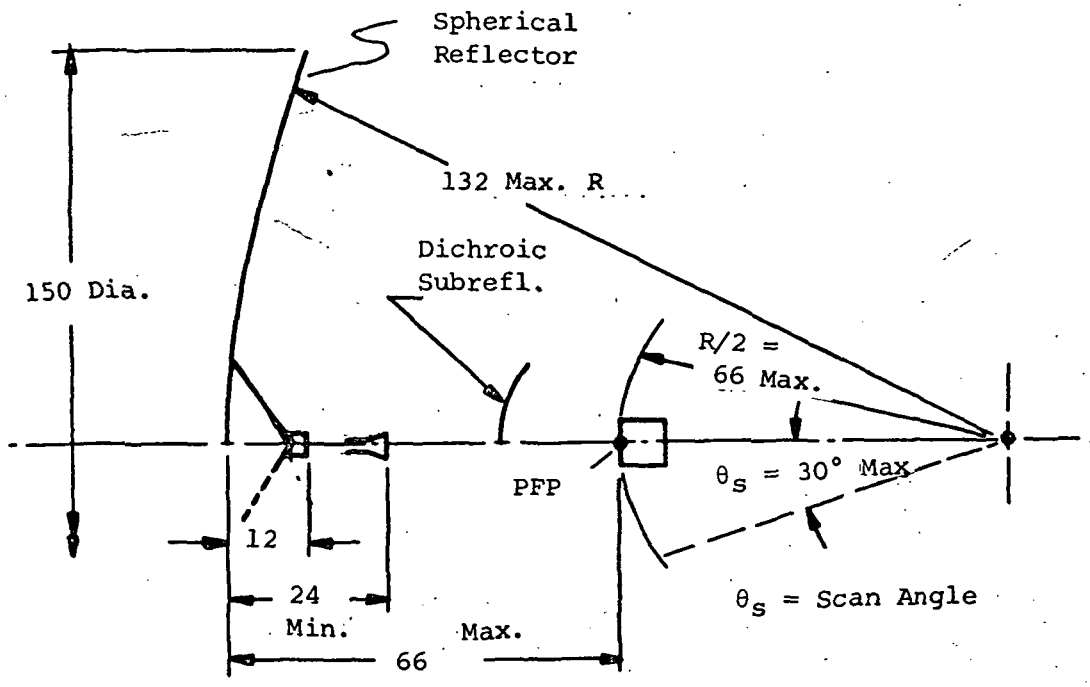

Figure 44. TDRS Constraints on Spherical Reflector Design

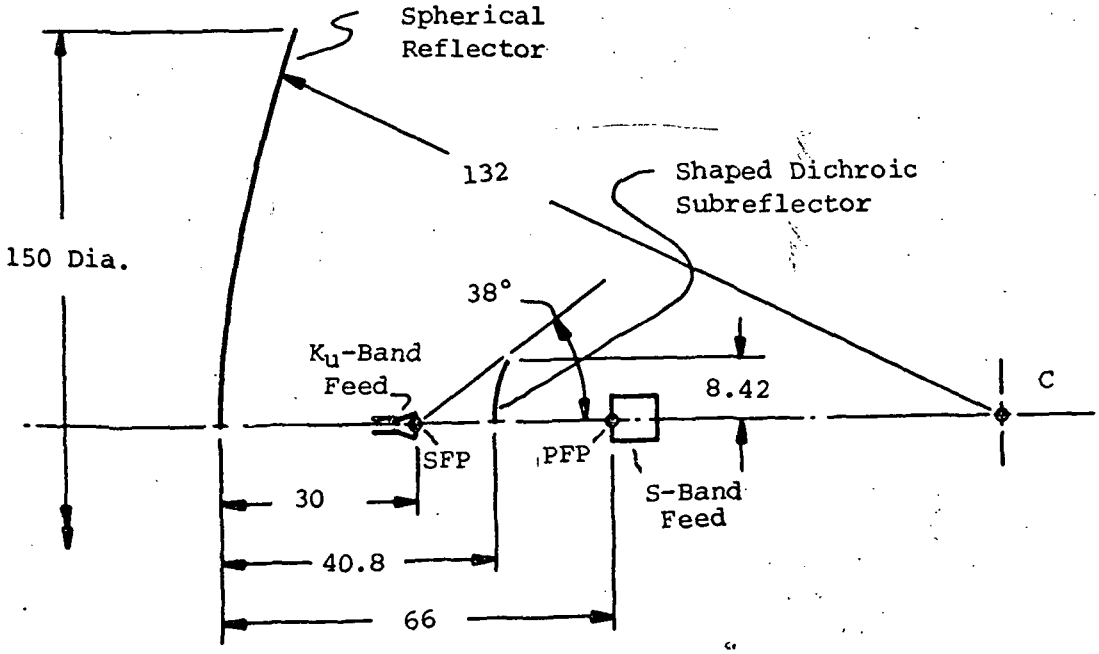

Figure 45. Compromise Design of a Spherical Dual Reflector Antenna

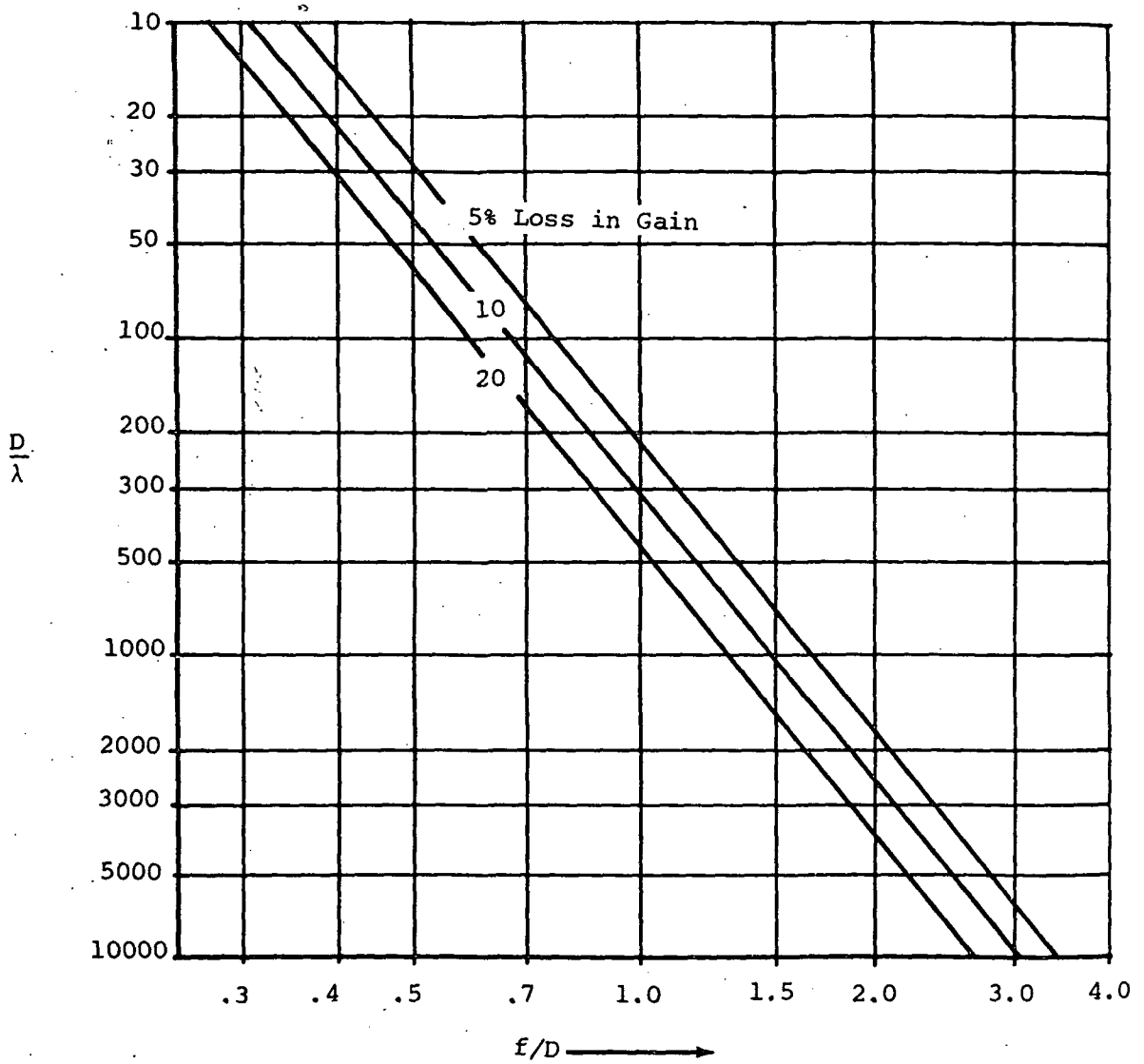

Figure 46. Loss in Gain for Spherical Reflectors

A final consideration in the application of the spherical reflector to off-axis steering is the size of the reflector in relation to the scan angle. Figure 47 shows the TDRS reflector diameter would need to be increased by 13.4 percent to maintain the required on-axis gain over ±30 degrees of S-band beam steering. Only 3.5 percent increase in diameter would be required for ±15 degrees of steering.

In addition, to the loss in effective aperture when steering a beam off axis, there is also a loss in gain due to spillover. Masterman (Reference 31) treats these combined effects in his analysis of beam steering in a spherical reflector. Of particular interest is a measurement of gain loss as a function of scan angle. Figure 48 shows the results of Masterman's measurements normalized to a reflector of fixed diameter. Superimposed on this figure is the gain loss which can be expected when steering a beam off the axis of a parabolic antenna, as presented in Appendix G of this report. The difference in gain losses between the spherical and parabolic reflectors can be mostly attributed to the phase errors experienced in moving the feed of a parabolic reflector away from the focal axis. This additional loss is not experienced in the spherical reflector because the feed is always focused for all beam scan angles. Figure 49 shows that a 5.4 dB loss in gain would result at a scan angle of 30 degrees assuming the 12.5-foot reflector was fixed in design to produce the required S-band gain on axis (0 degree scan). Notice that only 1.9 dB is lost in scanning ±15 degrees. Trading between off-axis gain, antenna diameters, and beam steering angles is dependent on TDRSS and user trades and is not considered to be within the scope of this program.

In summary, it has been shown that a spherical dual reflector antenna system is a viable candidate solution to the TDRS requirements as outlined in the "Musts" and this configuration also fulfills many of the negotiable requirements contained in the list of "Wants".

4.5.2.3 Dichroic Subreflector

Employment of a dichroic Subreflector is essential to the operation of the TDRS preferred candidate systems. In particular, the subreflector must be designed to reflect K_u-band energy and pass S-band energy. The efficiency of the reflector is related to the losses incurred in reflection at K_u-band and transmission of S-band. Losses attributed to the dichroic reflector directly reduce the gain of the antenna system and must therefore, be held to a minimum.

There are two basic categories of dichroic surface design: resonance and non-resonant. Both have been developed and are employed on many dual frequency cassegrain antenna systems. A simple example of a non-resonant dichroic surface is a wire screen whereby the electrically large mesh size allows high frequency signals to pass and the same mesh appears to be small to lower frequencies, acting as a reflector. Although this design is

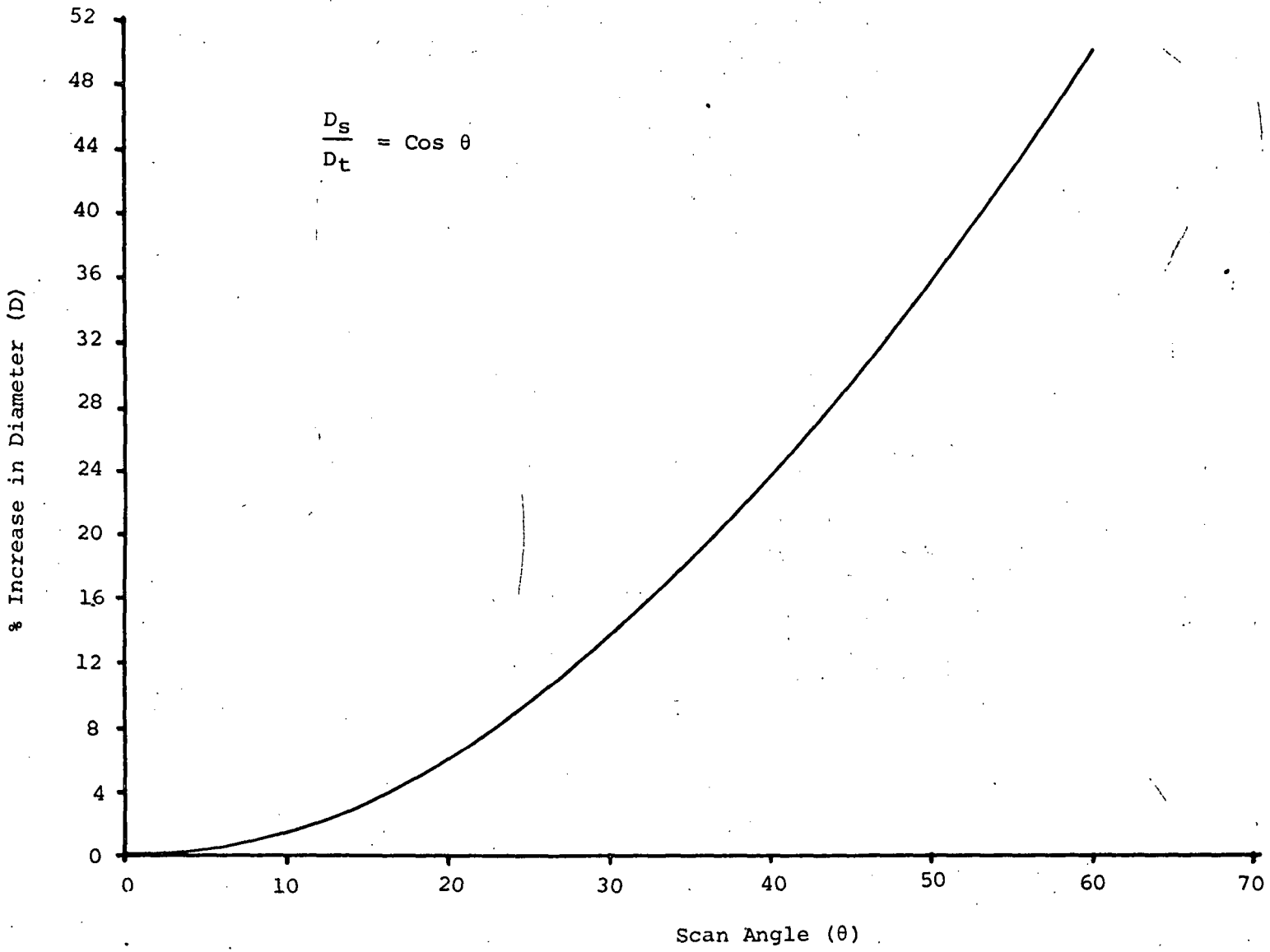

Figure 47. Increase in Total Spherical Reflector Diameter to Maintain Constant Effective Diameter

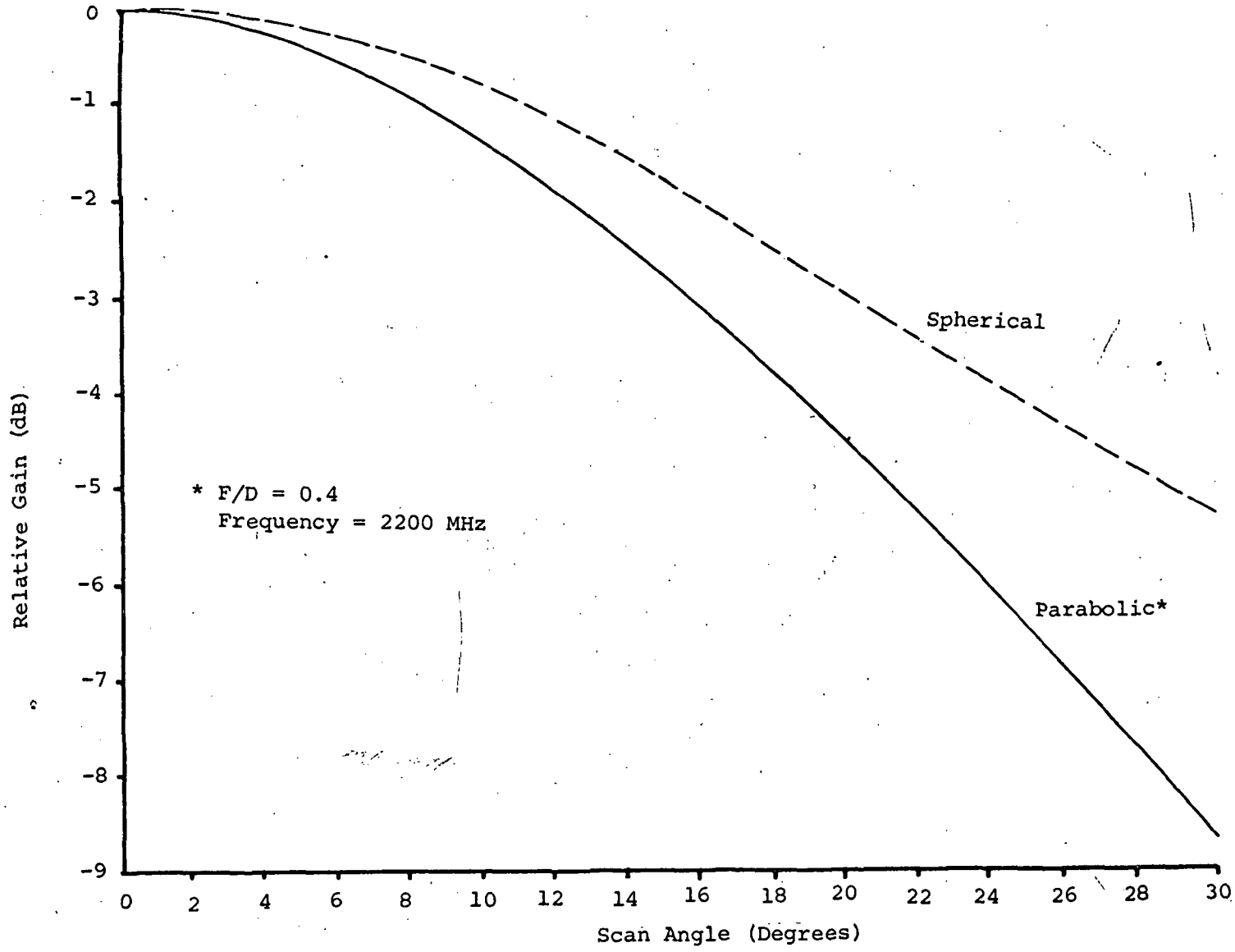

Figure 48. Relative Gain as a Function of Scan Angle

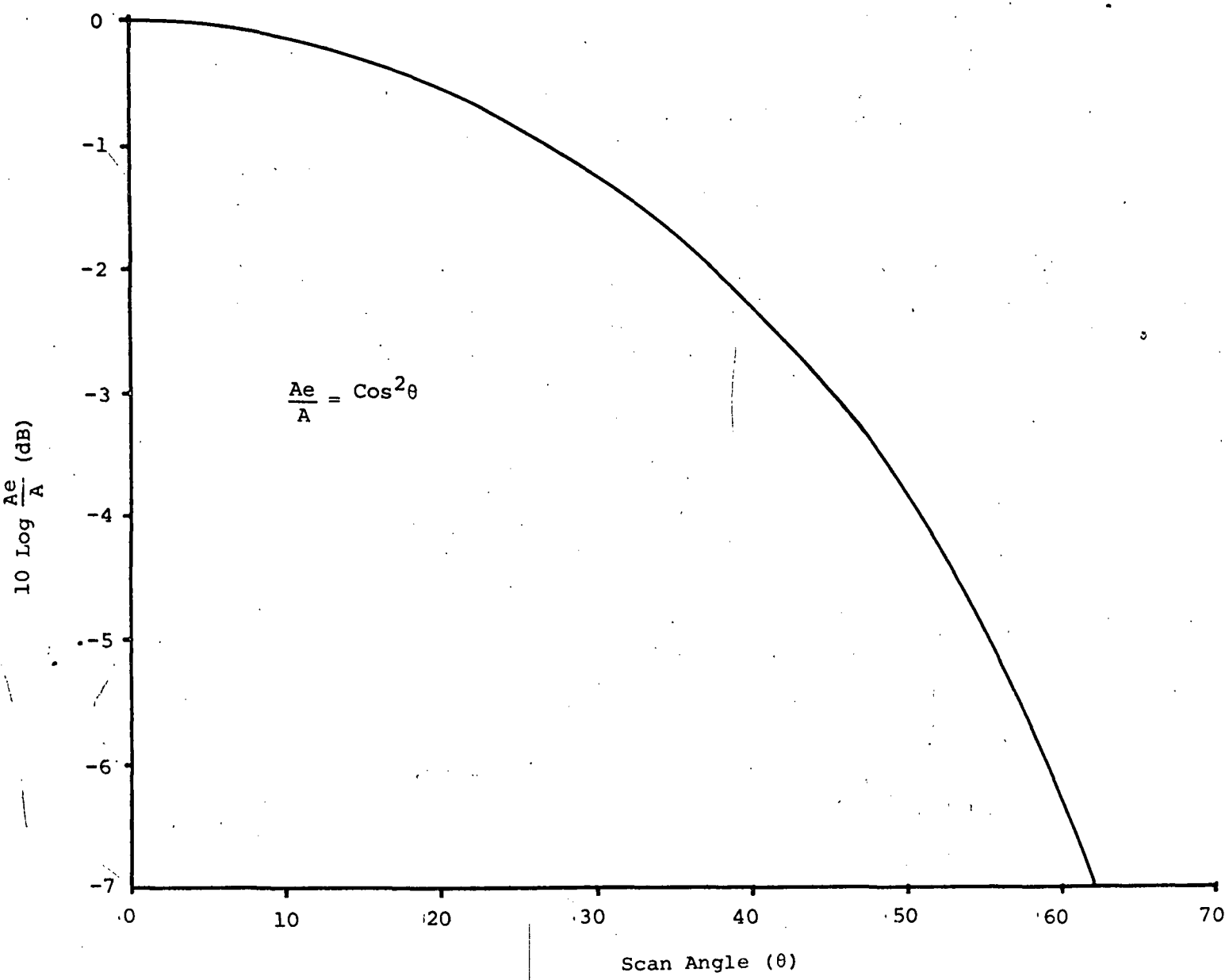

Figure 49. Relative Aperture Efficiency Versus Scan Angle for a [illegible]

efficient at widely separated frequencies, its transmission and reflection properties do not satisfy the TDRS requirements. Another non-resonant design involves the application of the metallic delay dielectric theory developed by Kock (Reference 32). The surface is comprised of an array of closely spaced conducting hexagonal plates whose size and spacing are selected to allow good transmission of low frequency energy. At the higher frequency, the plate dimensions are large compared to the wavelength, and the surface is highly reflective. In its simplest form this technique is the inverse of the wire screen and also is most efficient at widely space frequencies.

Resonant dichroic surfaces are frequency selective in that they reflect energy over a limited frequency band and pass all other frequencies above or below the resonant band; they can also be designed inversely. Therefore, resonant dichroic surfaces can be considered as band pass or band reject filters, whereas non-resonant surfaces can be considered as high and low pass filters.

Typical resonant dichroic surface designs employ an array of resonant elements embedded in the surface material. If band reject (reflection) characteristics are desired, resonant dipoles, loops, or discs are placed on a dielectric surface. If band pass (transmission) performance is required, then resonant slots are cut through a metallic surface. Reflection of circular polarization is achieved by orienting the resonant elements orthogonally to provide equal characteristics to the two orthogonal components of the circularly polarized wave.

Much activity relative to the design of various implementations of dichroic subreflectors has been reported. Schennum (Reference 33) presents design data plus experimental results of dichroic reflectors employing an array of resonant cross dipoles embedded in a dielectric surface. The geometry of his array is shown in Figure 50. He relates the parameters of the resonant elements to bandwidth and angle of incidence as shown in Figure 51. Measurements on flat sheets have verified this data; however, application of this design to a practical hyperbolic subreflector requires an optimization process that can only be done by an experimental measurement program.

L. R. Dod (NASA) and Wise (Bendix) have been conducting such an experimental program at NASA-GSFC with specific emphasis on the S- and K_u-band frequencies of the TDRSS. Although several array geometries have been considered and tested, the best choice appears to be that reported by Schennum. A K_u-band reflective test panel has been built and tested. This panel exhibits a resonance at 14.3 GHz and shows sufficient bandwidth to cover the TDRS K_u-band frequency region. Initial measurements showed an S-band transmission loss of 0.5 dB and a projected K_u-band reflection loss of 0.5 dB. The elements (S= 0.59 inch, L= 0.39 inch and W= 0.10 inch) were mounted on a G-10 grade dielectric support panel, 40 mils thick. A hyperbolic dichroic reflector is currently being fabricated using the same basic parameters.

Figure 49. Relative Aperture Efficiency Versus Beam Angle for a

can Angle (θ)

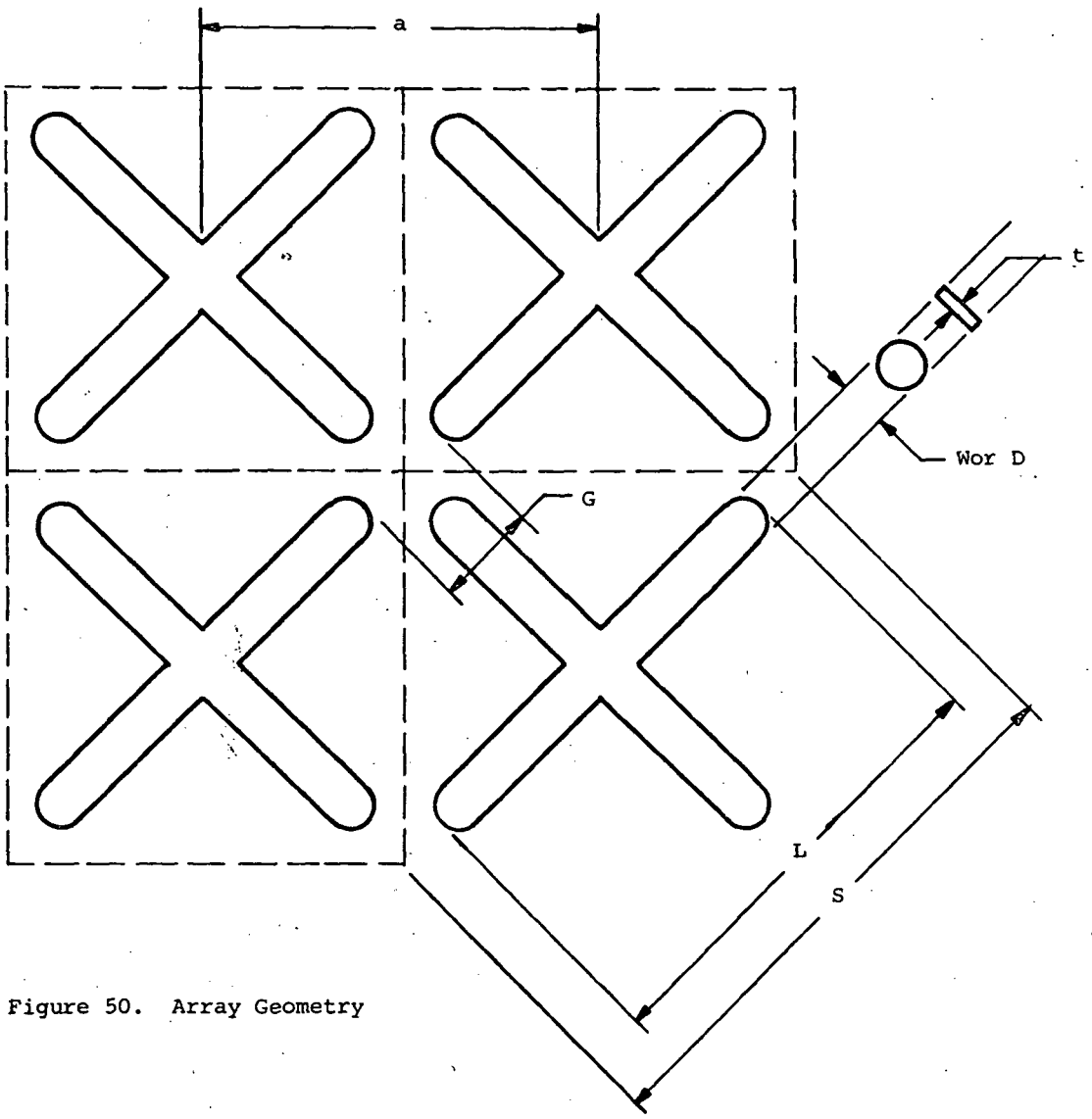

Figure 50. Array Geometry

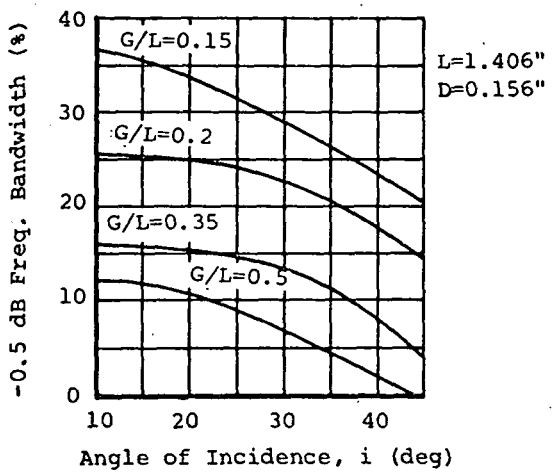

Figure 51. Bandwidth Versus Incidence Angle

4.5.3 Feed System Considerations

4.5.3.1 Non-Tracking Feeds

To illuminate the main reflector with optimum efficiency in the non-tracking/dedicated data channel mode, the RF characteristics of the feed source can be categorized. The feed source beamwidth must contain the highest amount of radiated energy possible and should contain uniform energy density in the angle subtended by the subreflector with practically zero energy radiated elsewhere.

The multi-mode feed horn, as described by Rusch and Ludwig (Reference 34), shows the radiation pattern required together with the theoretical antenna efficiency. Comparison with a dominant-mode conical horn showed that the efficiency can be improved from 76 percent to 90 percent with the multi-mode horn. Multi-mode horns derive their efficiency by reducing the characteristically high side lobes in the conical horn, together with the broadening or flattening of the main beam to form a more uniform illumination. Another advantageous characteristic of the multi-mode feed horn is its symmetry with respect to the boresight axis. This type of symmetry will produce the highest gain and equalized beamwidth in the E- and H-planes. Figure 52 shows the H-plane pattern of a multi-mode horn and the dominant mode pattern illustrating the effect of the pattern shaping through mode generation.

Potter (Reference 35) reported a method of generating these higher order modes in a conical horn configuration which resulted in 30 dB side lobe suppression, equal orthogonal plane beamwidths, orthogonal plane phase center coincidence, and high beam efficiencies. The overall measure of horn performance is the beam efficiency--the fractional radiated power between beam maximum and the first null.

Potter calculated the beam efficiencies for several types of feed horns for the E-plane, H-plane, and the 45 degree plane, and showed that the highest efficiency is obtained with the dual mode horn.

These multi-mode horns are quite large in both aperture area and length. For example, Rusch's feed antenna would have a diameter of 7 inches, and Potter's antenna would be 10λ or 8.2 inches long by 1.7 inches in diameter for the TDRS K_u-band feed. As candidate antennas for the dedicated data channel, both are too large for TDRS, since separate tracking antennas would have to be placed around the periphery, causing the tracking characteristics to deviate from the optimum. In other words, there is an optimum dimension for tracking feed location for monopulse tracking which will determine the maximum size diameter allowable. For TDRS, the element feeds are located 1.6λ apart, and the maximum diameter allowable for the central dedicated channel is 1.2 inches.

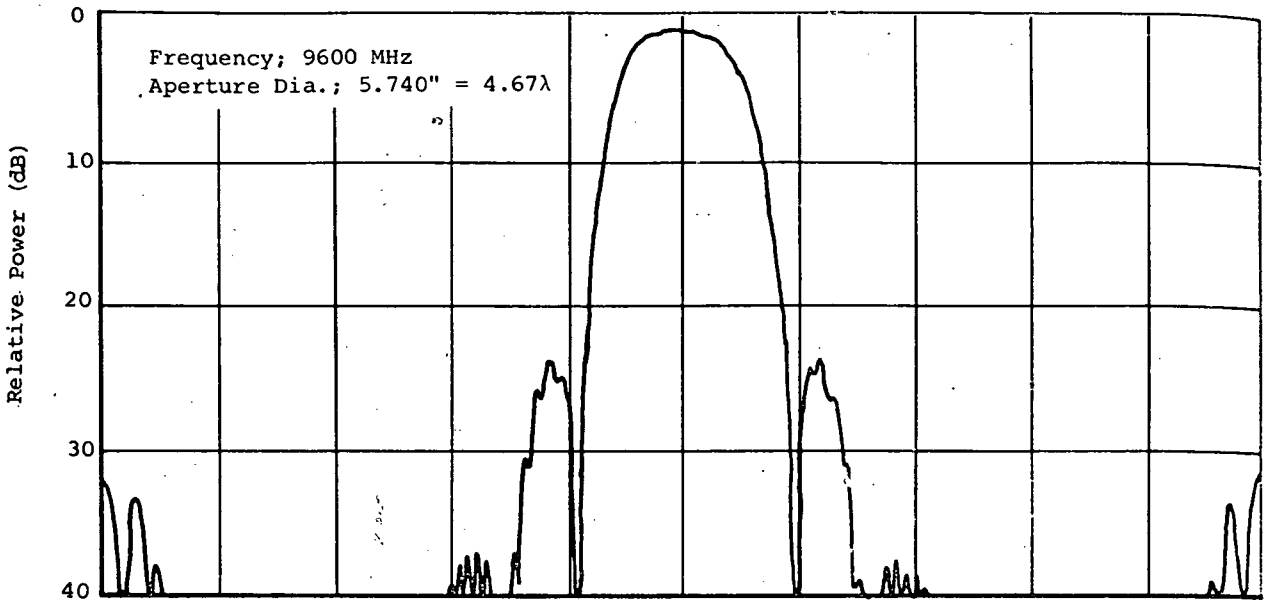

(a) Multi-Mode Horn

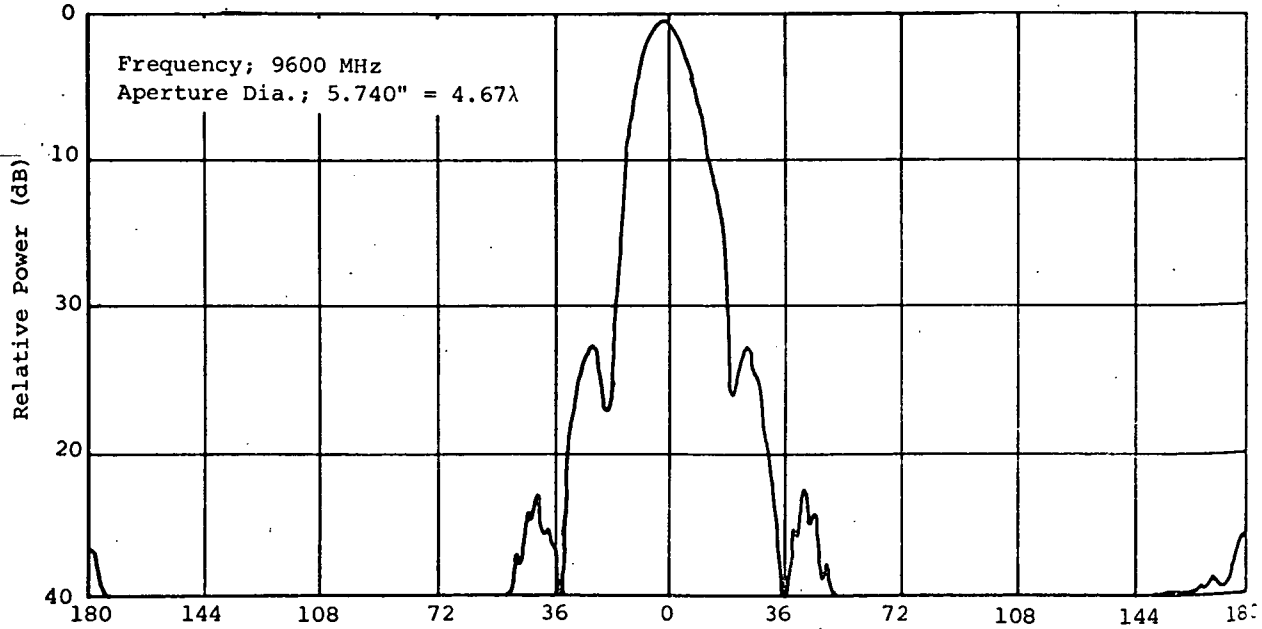

(b) Dominant Mode Horn

Figure 52. Measured Radiation Patterns

4.5.3.2 Tracking Feeds

The types of tracking feeds discussed in the following paragraphs will concentrate on the monopulse tracking feeds as applicable to the TDRS requirements. They have been selected on the basis of their high efficiency, their relative size, and reliability. The single aperture multi-mode horns provide potentially high efficiency and reliability, and the four horn configurations can be configured to sizes compatible with TDRS requirements.

For an antenna operating at a particular frequency, the maximum gain available is a direct function of the radiating aperture area, and is highest when the aperture is uniformly illuminated. However, the sidelobes are only 17.6 dB down and may be undesirable in that they can lead to multipath tracking errors. Thus, for most applications, lower sidelobes are produced by tapering the illumination from the uniform taper.

Figure 53 (Reference 36) shows the aperture efficiencies obtainable for several types of feed apertures plotted as functions of sidelobes. However, as shown in the figure, this improvement in sidelobes is obtained at the expense of lower efficiency.

The four-horn square monopulse tracking system is configured in a square. This type is preferred over the diamond shaped four horn configuration because, in the latter, the total available feed aperture is not being used to form the difference beams. Only two feed horns are used to form the elevation difference pattern as compared to all four horns in the square configuration. Consequently, the individual difference beam gain is divided by one-half, with the result that the signal at the peak of the difference pattern will be at least 6 dB below that available in the sum channel. Figure 54 shows the diamond shaped comparator network, together with the aperture division of feed horns. This type is somewhat simpler to fabricate since only three hybrids are required.

For the four horn square, Figure 55(a) shows the monopulse configuration with the comparator network, and 55(b) shows the feed excitation (Reference 37). The efficiency of this feed is only 0.58, where the sum gain is compared to a uniformly illuminated antenna of the same aperture size. This antenna suffers from high sidelobes with approximately 20 percent of the feed power radiated as H-plane sidelobes. The difference slope ratio is 0.52, which is the ratio of the difference slope to the maximum possible slope, where the maximum possible slope is the slope obtained from an odd function illumination with a linear voltage pattern. Thus, the inability of the sum gain function to be efficient will reduce the range sensitivity of the four horn monopulse feed.

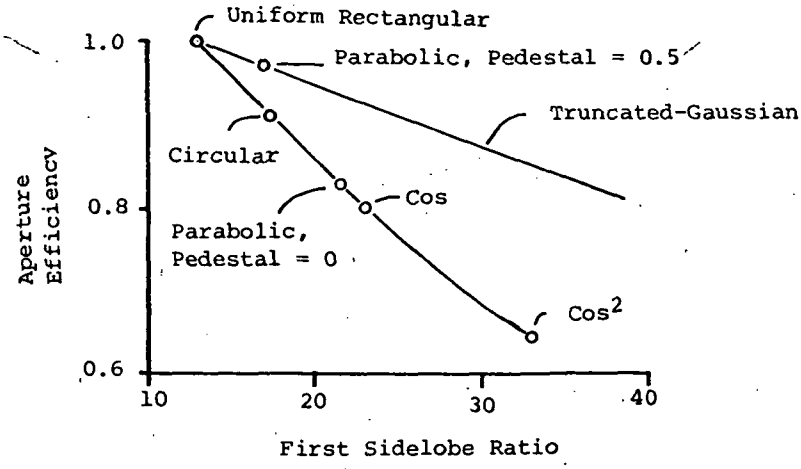

Figure 53. Aperture Efficiency as a Functional Sidelobe Ratio

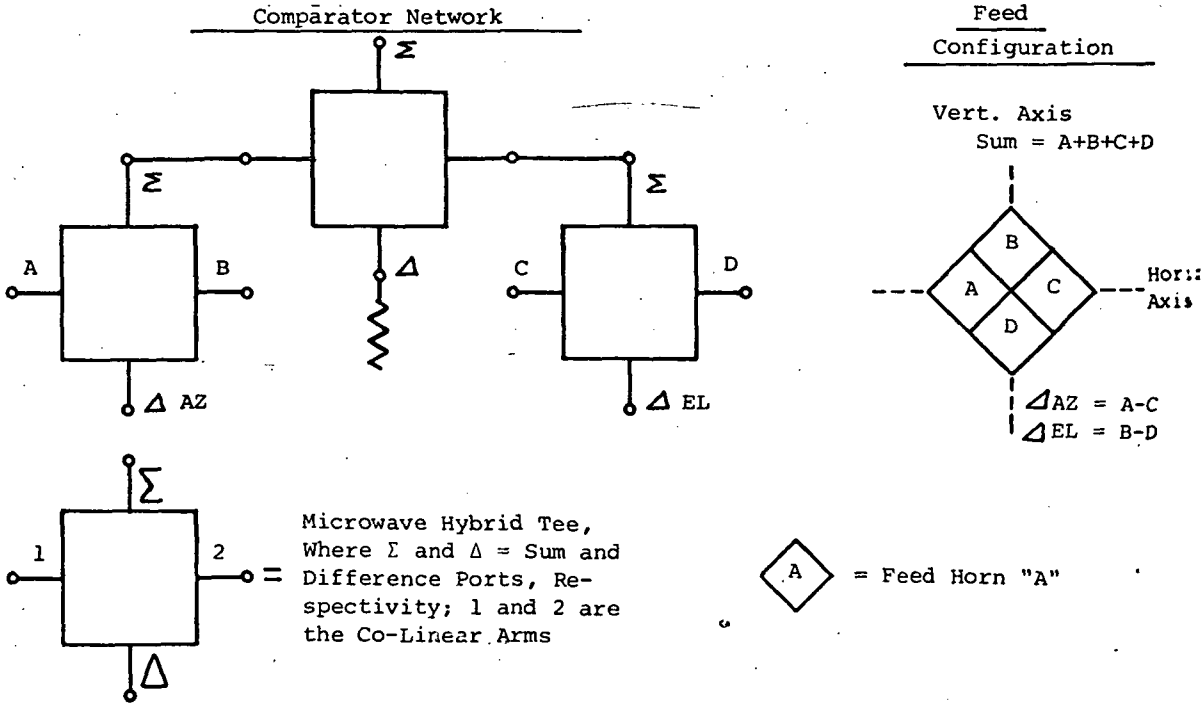

Figure 54. Diamond Shaped Monopulse Comparator

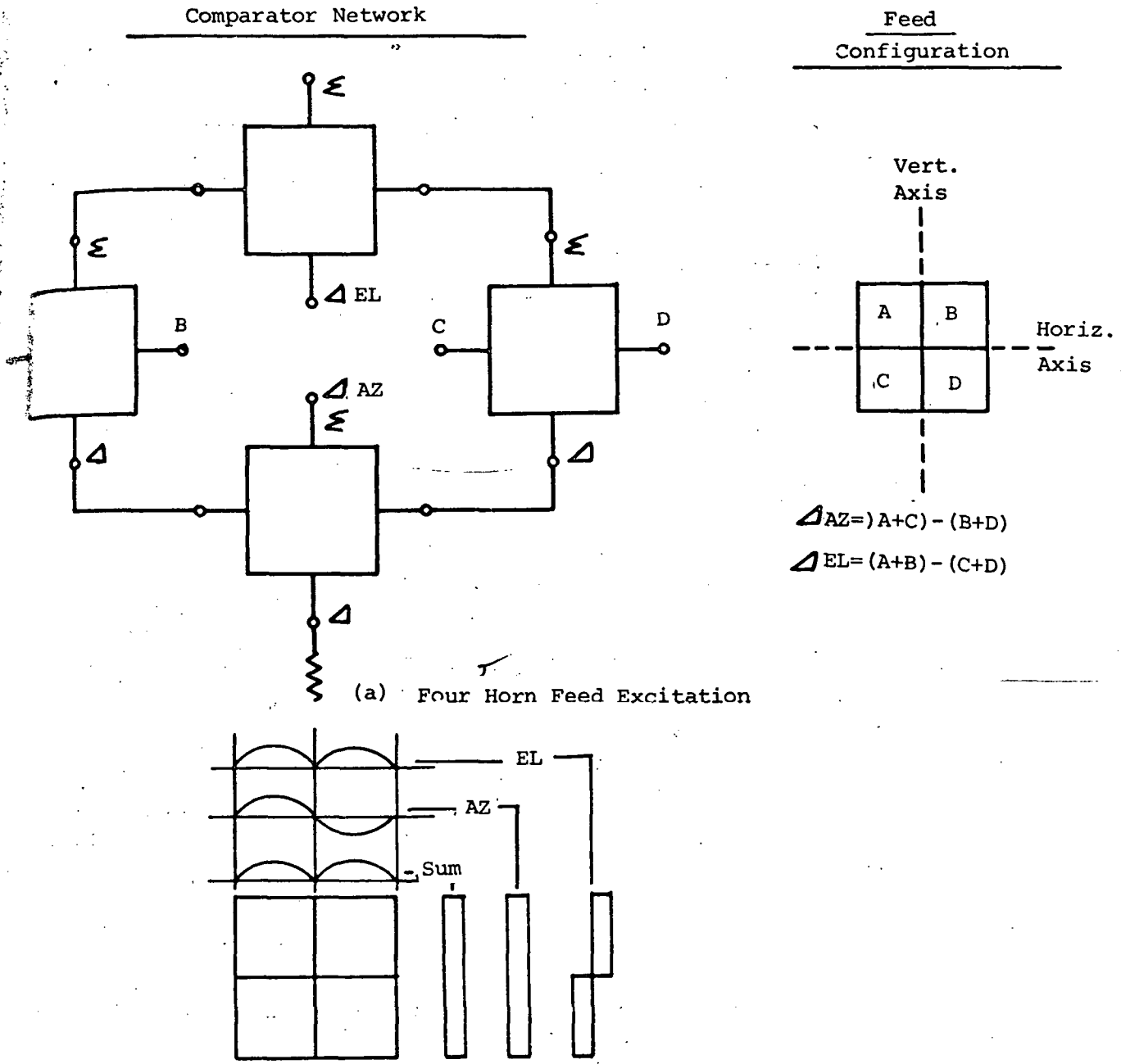

Figure 55. Square Shaped Monopulse Comparator

Plots of offset angle as a function of the feed horn dimension are presented in Figure 56(a) and the slope (volts/degree) is plotted in 56(b).

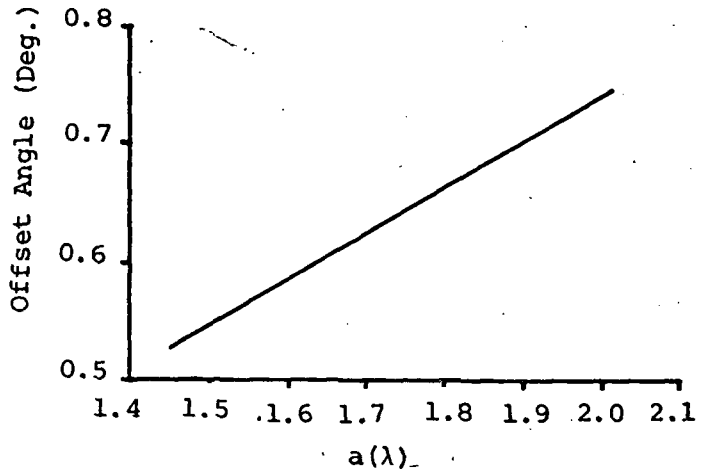

(a) Offset Angle Versus Horn Size

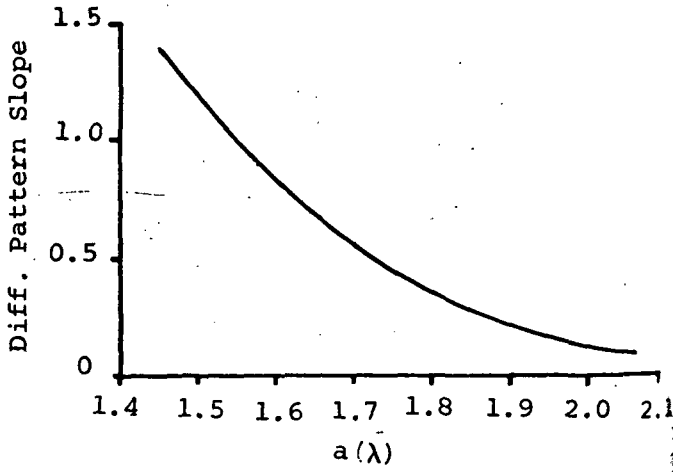

(b) Slope Versus Horn Size

Figure 56. Performance Characteristics of Square Four Horn Monopulse Cluster

Polyrod antennas belong to a class of antennas called surface wave antennas or slow wave antennas where the propagating wave is characterized by the ratios

$$\beta_z/k = \lambda/\lambda_z = \frac{c}{v_z}$$

where

β_z = phase constant along dielectric surface

k = wave number

λ = wavelength in air

λ_z = surface wavelength

c = phase velocity of light

v_z = surface phase velocity.

The ratio $\lambda/\lambda_z > 1$ means that the surface wavelength is shorter than the wavelength in air. The surface wave propagates parallel to the air-dielectric interface and decays vertically to it.

Low loss tangent dielectric materials such as teflon can be made to radiate energy in the end-fire direction when excited by a circular or rectangular waveguide. The end to which the waveguide is connected is called the feed and the opposite end which terminates abruptly in air is called the termination.

An important characteristic of the polyrod antenna is its ratio

$$\lambda/\lambda_z$$

whose variation is plotted in Figure 57. From the graph, one can see that for the selection of the dielectric material whose dielectric constant, ε, is 2.56 (for teflon $\varepsilon = 2.1$ and is considered almost identical) the surface wave velocity ratio can be adjusted by the proper choice of rod diameter. Mallach (Reference 38) has shown that for normally used dielectric materials, the feed end of the polyrod antenna should have

$$\lambda/\lambda_z \approx 1.1$$

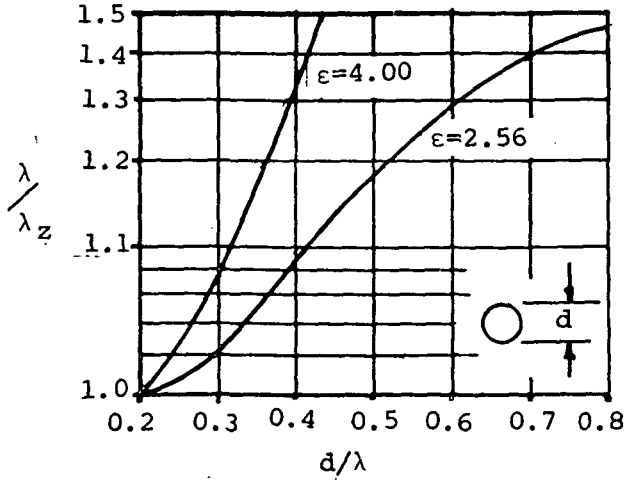

Figure 57. Relative Phase Velocity as a Function of Diameter

and the termination end should approach 1.0. Using the figure, diameters of the polyrod can be easily determined.

According to Mickey and Chadwick (Reference 39), the ratio of the diameters at the termination end to the feed end should be 0.63 for low sidelobes. This points out the fact the sidelobes can be controlled by the taper: the greater the taper length the lower the sidelobes.

The half power beamwidth is plotted in Figure 58 which demonstrates the dependence of the beamwidth upon the length of the polyrod. The proper discontinuity at the termination end will launch the surface wave for end fire radiation. The empirical design has been reported by Jasik (Reference 40) to consist of terminal taper length of 0.5λ (0.413 inch) long and a diameter of 0.23λ (0.190 inch).

When the polyrod feed element is placed in a modified four horn cluster which separates the individual horns, the tracking function can still be accomplished by the same type of comparator network. However, the separation of feed elements allows the installation of another feed element for the sole purpose of handling the data stream. Thus, the tracking feed network and the dedicated channel are separate microwave networks.

The advantage in the use of polyrods as feed elements is that they allow a more closely packed radiating area to concentrate the energy on the subreflector than conical horns in the same space. Furthermore, there is a weight saving advantage in the use of polyrods over horns. Since the tracking function requires the offset beams to crossover between the 2 dB and 3 dB point, the polyrod centers would be spaced approximately 1.6λ apart. This spacing is the same one used on the ATS 40-foot tracking antenna at the Mohave facility, in which a sub-reflector edge taper of 16 dB was obtained. This illustrates that the TDRS edge taper of 10 dB will no doubt be easily achieved by polyrod antenna beamwidth control. Figure 59 shows the crossover level as a function of the offset feed location expressed as either an offset angle or an offset from boresight in inches.

Vu and Hien (Reference 41) have reported on X-band monopulse feed using corrugated waveguide. Since the TE_{11} dominant mode pattern alone has relatively high sidelobes, the excitation of the TM_{11} mode achieves sidelobe suppression and equal beamwidths. In smooth walled waveguides, the proper phase and amplitude relationships required cannot be held over any appreciable frequency bandwidth (Reference 42). To overcome these difficulties, the corrugated waveguide is used to support the hybrid modes (hybrid modes can be thought of as linear combinations of TE and TM modes) that travel with the same velocity in the corrugated section. Thus, the HE_{11} (hybrid mode) is less frequency sensitive. Figure 60(a) shows the monopulse single aperture horn and 60(b) the measured sum and difference patterns.

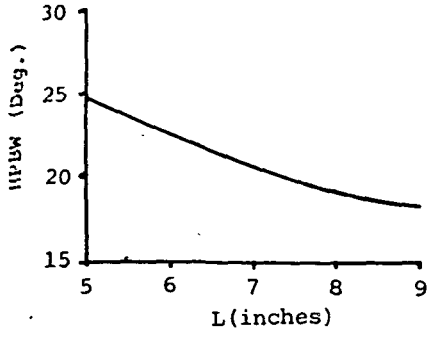

Figure 58. Half Power Beamwidth Versus the Length of the Polyrod

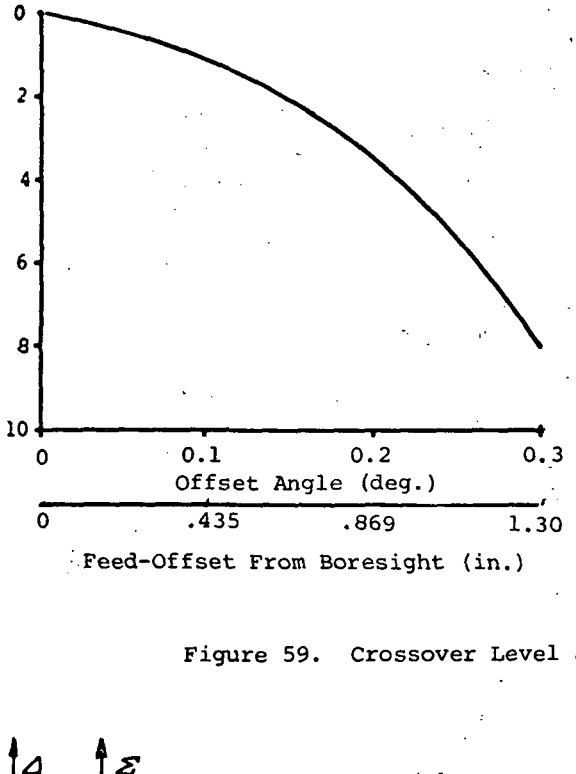

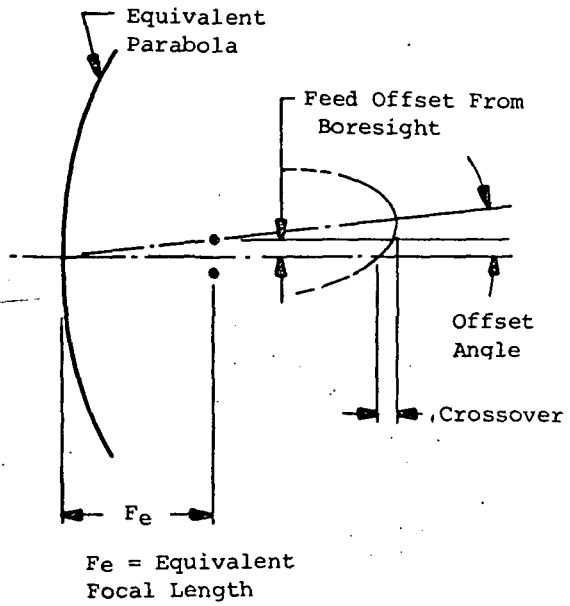

Figure 59. Crossover Level as a Function of Offset Angle

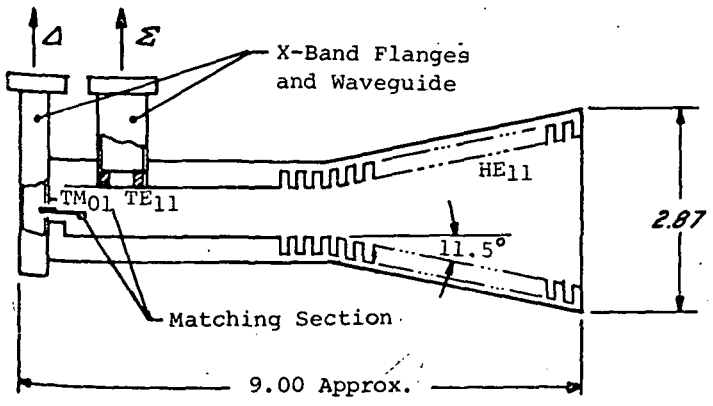

(a) Experimental Horn at X-Band

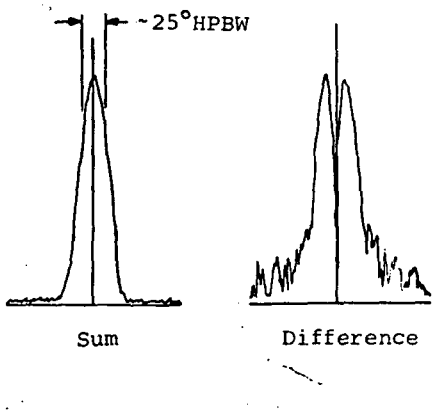

(b) Sum and Difference Patterns

Figure 60. Single Aperturn Horn

The concept of utilizing dual modes in a conical feed horn has been reported by Potter (Reference 35) in which the TE_{11} mode for sum and TM_{11} mode for sidelobe suppression control was successfully achieved. Furthermore, equality of beamwidths and symmetry of radiation patterns enabled a high level of beam efficiency to be reported.

More recently, Cooper (Reference 43) has shown that circularly polarized monopulse single aperture feed systems can be designed by using the TE_{11}, TE_{01}, and the TM_{01} modes for tracking patterns. The sum mode can be generated by the TE_{11} mode. The two other circular modes of interest are the TE_{01} and TM_{01} modes, whose radiation patterns are the same. Figure 61 shows the TE_{11} mode (for the sum mode) and the TM_{01} and TE_{01} modes (for the azimuth difference and elevation difference modes).

TM_{11} mode for sidelobe suppression was successfully achieved. Furthermore, equality of beamwidths and symmetry of radiation patterns enabled a high level of beam efficiency to be reported.

A second part studied by Cooper was the performance of such a horn when used in defocused paraboloid reflector systems. The purpose was to broaden the beamwidth of the secondary pattern to allow easier acquisition of the target. Defocusing caused the gain to drop and the beamwidths to broaden similarly to those predicted by Redlien. Smooth patterns resulted, although some problems involving the relative phase shifts of the difference signals and the sum signal may have to be corrected.

4.5.4 Wide Field of View (FOV) Techniques (Beam Broadening)

Beam broadening of the K_u-band beam is of particular interest as a designation aid. The extent of required broadening is directly related to the accuracy to which the K_u-band beam can be pointed. The object is to provide a monopulse tracking system whose FOV is sufficiently broad to insure a lock-up on the user after initial ground pointing commands. The wide FOV tracking system would then automatically refine the pointing angle so that the user is within the narrower FOV of the high gain tracking network.

There are several ways of broadening the beam of a reflector antenna system, such as:

1. Feed defocusing
2. Subreflector defocusing
3. Reflector distortion
4. Under-illumination (smaller aperture)
5. Beam spoiling.

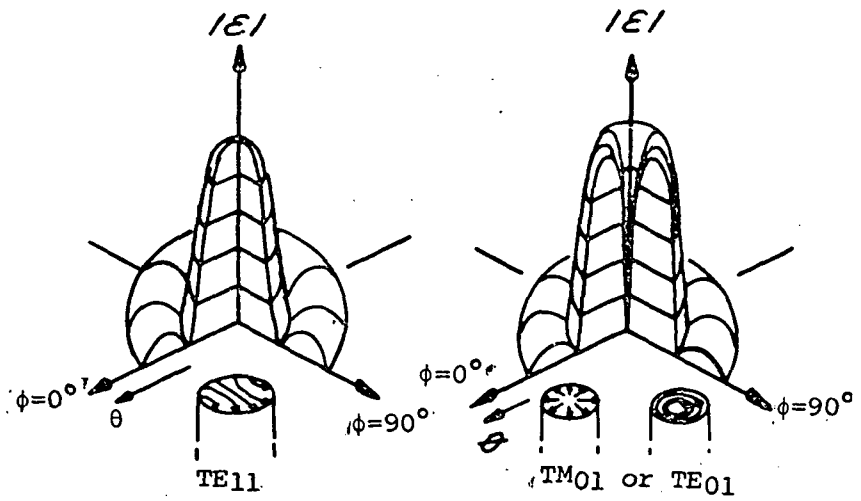

(a) Sum Mode Pattern (b) Difference Mode Pattern

Figure 61. Modal Radiation Pattern

Reflector distortion can be illustrated by considering the Radiation, Inc., reflector deployment mechanism. If this mechanism were controlled to stop short of a full deployment, the resulting surface would not be truly parabolic and would have high surface irregularities due to the looseness of the mesh cloth. Both results would lead to a broader secondary beam as compared with the fully deployed antenna. This technique suffers two obvious and significant faults which eliminate it from further consideration:

1. Repeated movement of deployment mechanism would lead to a less reliable reflector, especially in a space environment;

2. The high surface irregularities will cause greater surface accuracy losses than can be attributed to a reduction in directivity.

Under-illumination can be achieved by providing a larger aperture feed and will result in a wider secondary beam in proportion to the effective reflector aperture illuminated by the feed. This is a viable approach which can be implemented by a multi-element feed system, e.g., Figure 62. In this example, the feed aperture is doubled by the addition of an eight element ring around the basic four element monopulse feed. Typically, the feed will illuminate only half of the reflector and will produce a secondary beam twice the width of the completely illuminated reflector. Variations in the secondary beam can be achieved by increasing the number of elements or increasing the spacing between elements. The addition of variable attenuators in the outer element lines would provide control of the outer element weighting in the combined array and would then permit limited continuous adjustment of the primary illumination function, thereby controlling the secondary beamwidth.

The implementation of beam spoiling to cause beam broadening is similar to that used to achieve under-illumination. The principal difference is in the use of phase shifters and attenuators in the element lines to achieve effective aperture distributions conducive to secondary beam broadening.

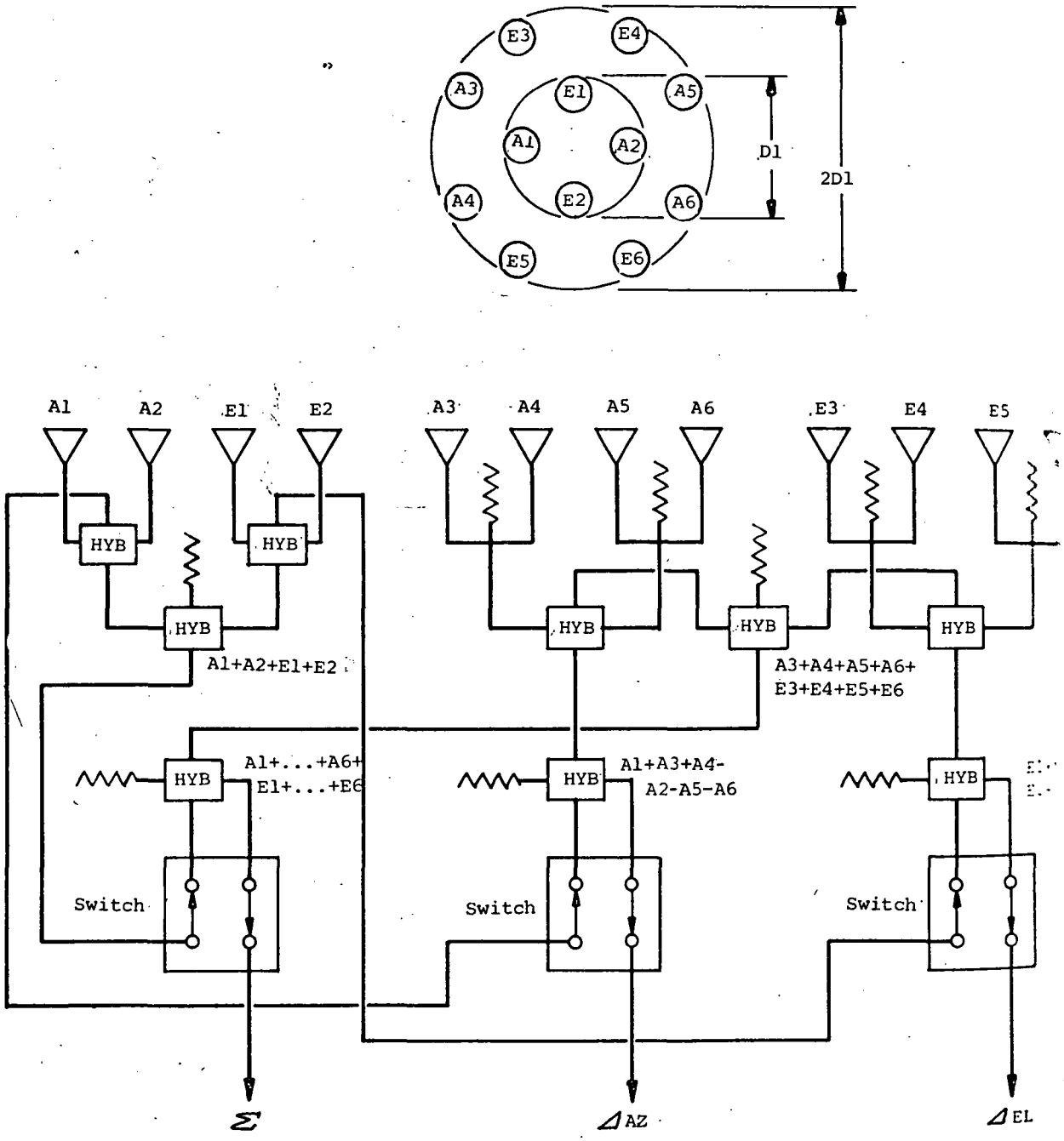

Figure 62. Feed Network for Beam Broadening by Under-Illumination

A variation of under-illumination and beam spoiling has been mathematically modeled by R.F. Schmidt of NASA-GSFC (Reference 63). The reported results have proven that the technique is valid and has excellent broadened performance characteristics. Data is not yet available for publication, pending patent disclosure.

Beam broadening by feed defocusing and subreflector defocusing is dependent on producing quadratic phase errors on the focal axis of the reflector. The effect of both implementations is essentially equal. There are many publications on this subject with respect to single surface parabolic reflectors. Of particular interest is a paper presented by Redlien (Reference 44) wherein he addresses the effect of defocusing on the performance of a monopulse tracking system. Redlien shows that in addition to the expected increase in beamwidth, defocusing also produces a relative phase shift between the sum and difference outputs. As a result, he shows that a phase shift is required to return the monopulse system to its focused phase characteristics.

Several parametric curves in Redlien's paper have been normalized to the TDRS receive frequency (14 GHz) and are presented in this section. Figure 63 shows the feed illumination functions assumed by Redlien throughout his paper. Figure 64 shows the effect of defocusing on the Σ pattern beamwidth and on the Σ and Δ pattern gain maxima. This curve shows that the beamwidth does not change significantly for the first 0.5 inch of feed movement. This results from null filling, which is the first noticeable effect of defocusing a parabolic reflector. Along with this null filling there is an immediate loss in gain, as shown in Figure 64. It can be seen that a 1.5 to 1 increase in beamwidth can be affected by 0.63 inch of defocusing and will result in a 4.3 dB loss in sum gain. As would be expected, the wide difference beamwidth produces a lower monopulse slope which is shown in Figure 65. More significant, however, is the relative phase between the sum and difference patterns as presented in Figure 66. It is also shown that the phase difference is dependent on the angle off boresight. This curve shows that a 56 degree phase shift would be needed to compensate for 0.63 inch defocusing (to achieve 1.5 to 1 beam broadening). The off axis phase shift amounts to less than 9 degrees out to the 3 dB beamwidth and should be considered in the compensation factor.

Informal correspondence with Redlien indicates the results of his paper have been successfully employed in several monopulse tracking systems wherein beam broadening was required. Furthermore, it was his understanding that another company successfully employed this analysis in the design of a cassegrain monopulse tracking system.

A series of measurements were made at Martin Marietta in an attempt to verify the application of Redlien's beam broadening data to a defocused subreflector. These measurements were made at 35.0 GHz using an 11.5-inch diameter parabolic reflector as shown in Figure 67.

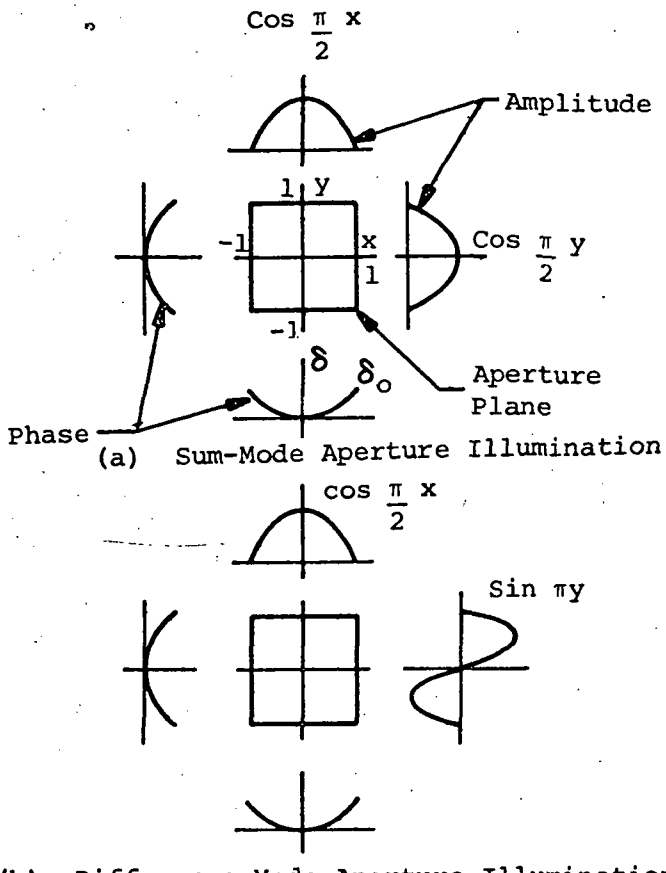

Figure 63. Aperture Illumination Assumed for Computations

Data was taken with a 10 dB and 19 dB illumination taper on the subreflector. A summary of the pattern data is shown in Figures 68 and 69. Although the data correlates in general shape with Redlien's calculations, the Martin Marietta data shows that the subreflector must be defocused more than predicted for a 2 to 1 increase in beamwidth. An explanation for this difference has not been developed to date.

Implementation of a defocused subreflector was considered for application to the TDRS antenna system. The design shown in Figure 70 illustrates a mechanism which will allow commanded defocusing for broadening the K_u-band monopulse beam (increased FOV) and then will allow for refocusing once the user has been acquired and designated. The

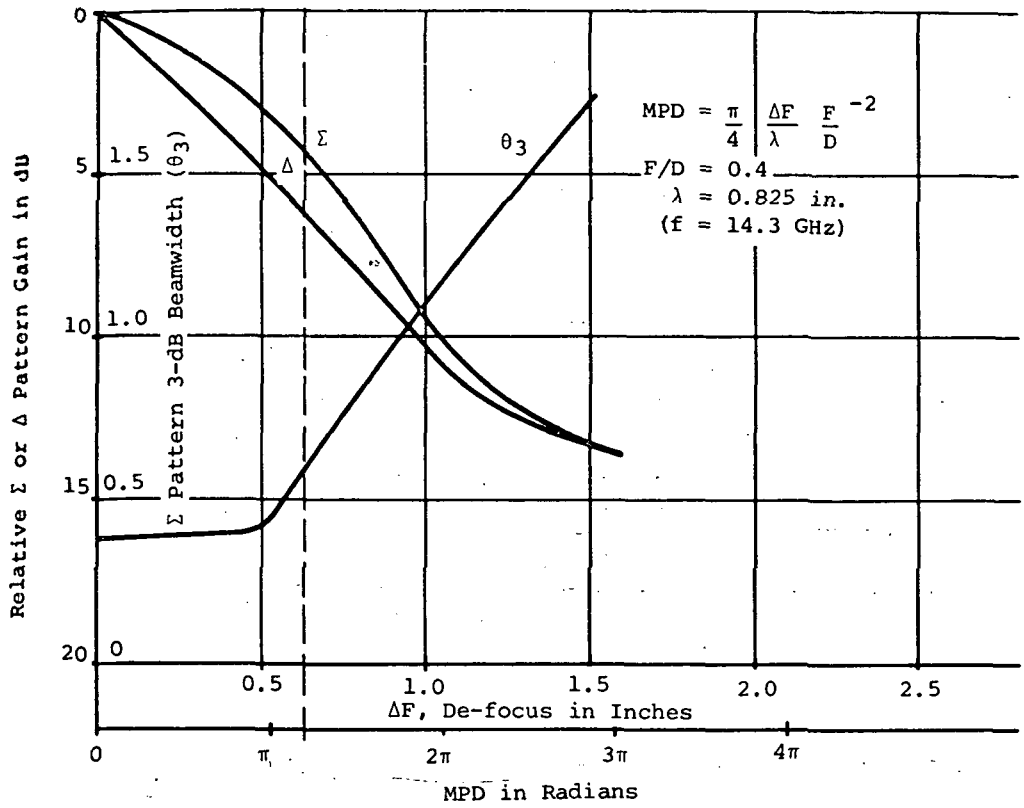

Figure 64. Pattern Gain Versus Defocus or MPD

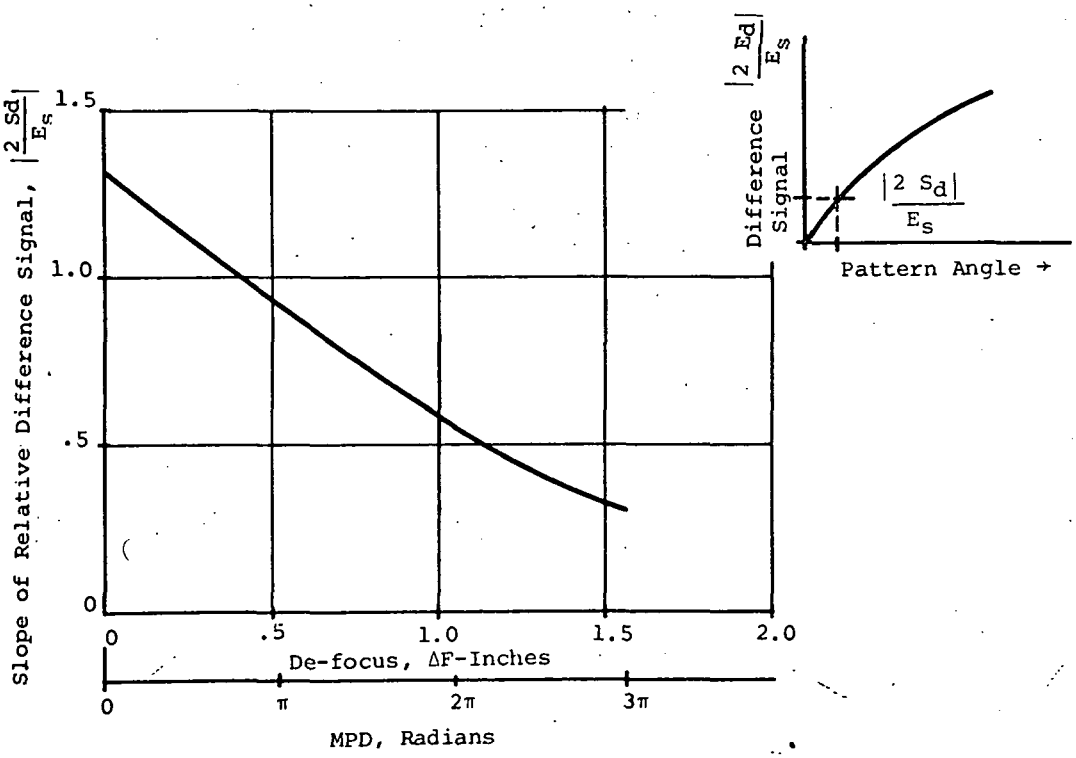

Figure 65. Slope of Relative Difference Signal as a Function of Defocus or MPD

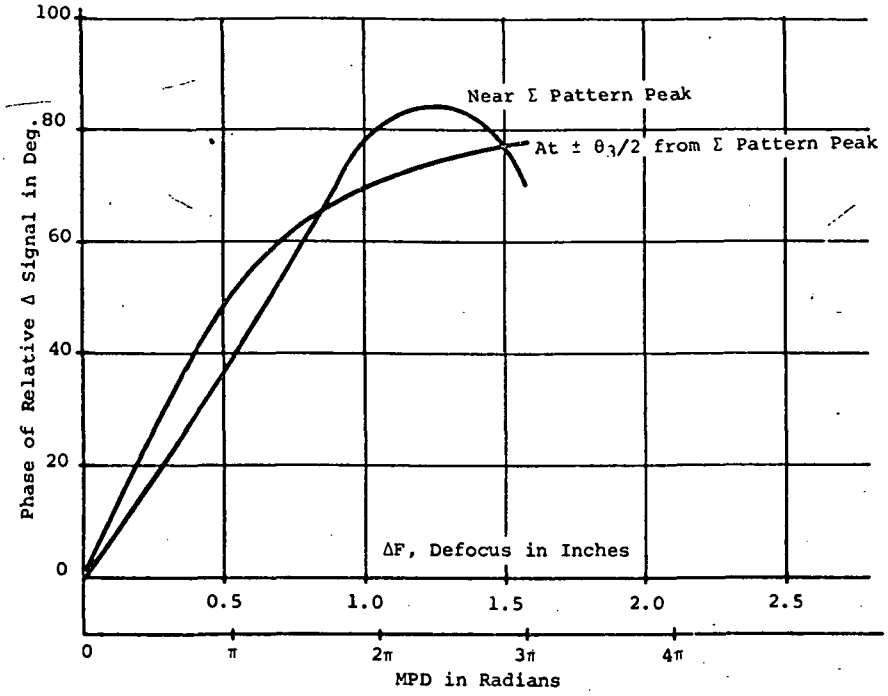

Figure 66. Phase of Relative Δ Signal Versus Δ for MPD

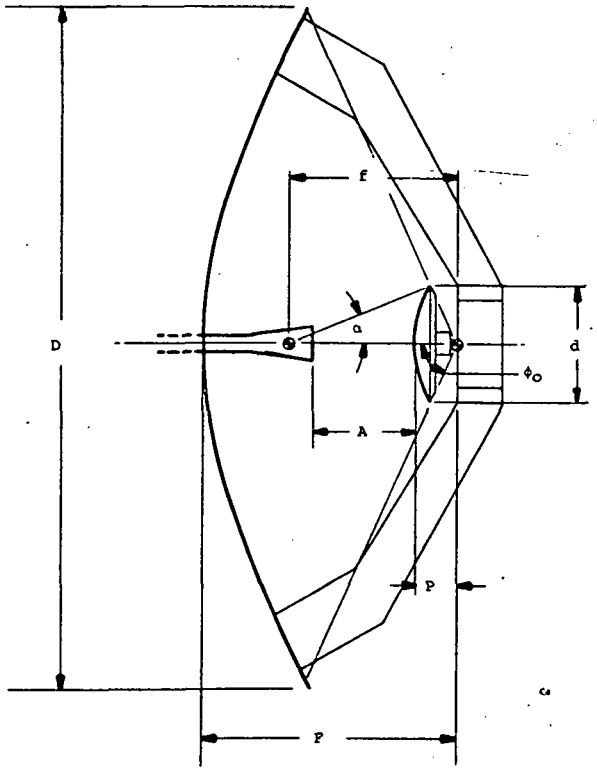

Figure 67. Cassegrain Configuration Used for Beam Broadening Measurements

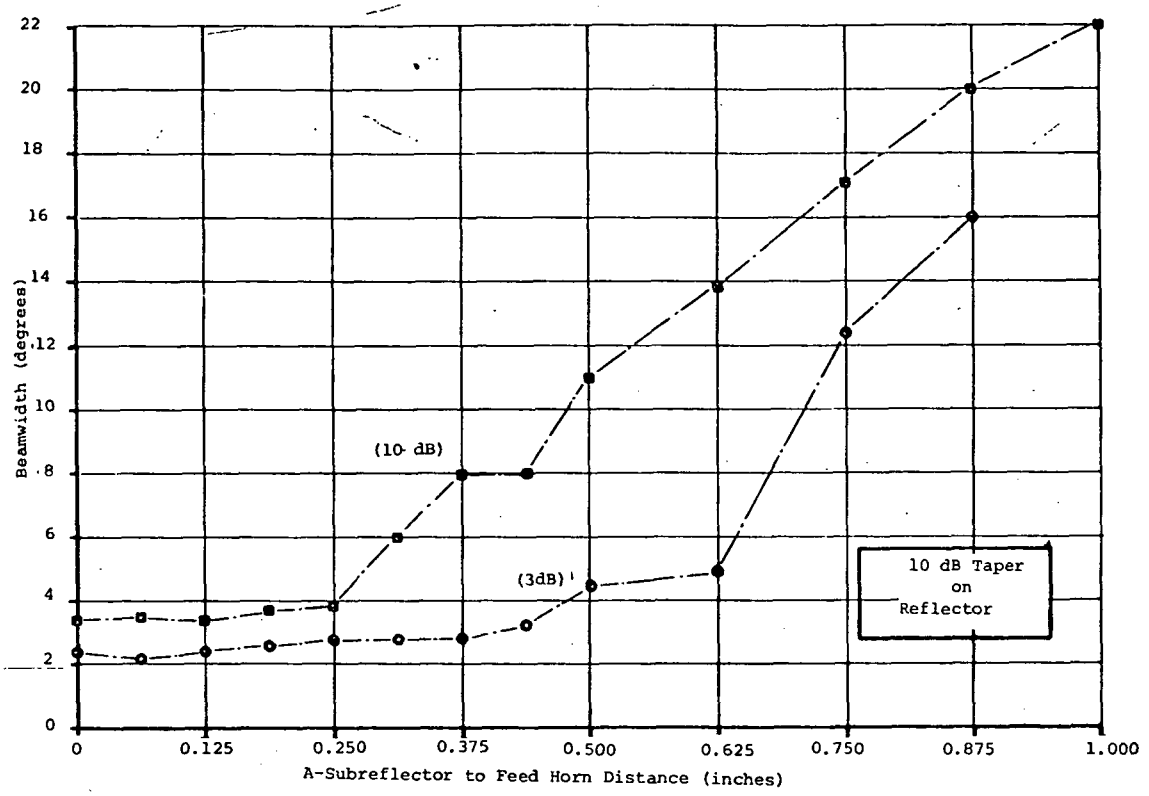

Figure 68. Beam Broadening Due to Subreflector Defocusing (35.0 GHz)

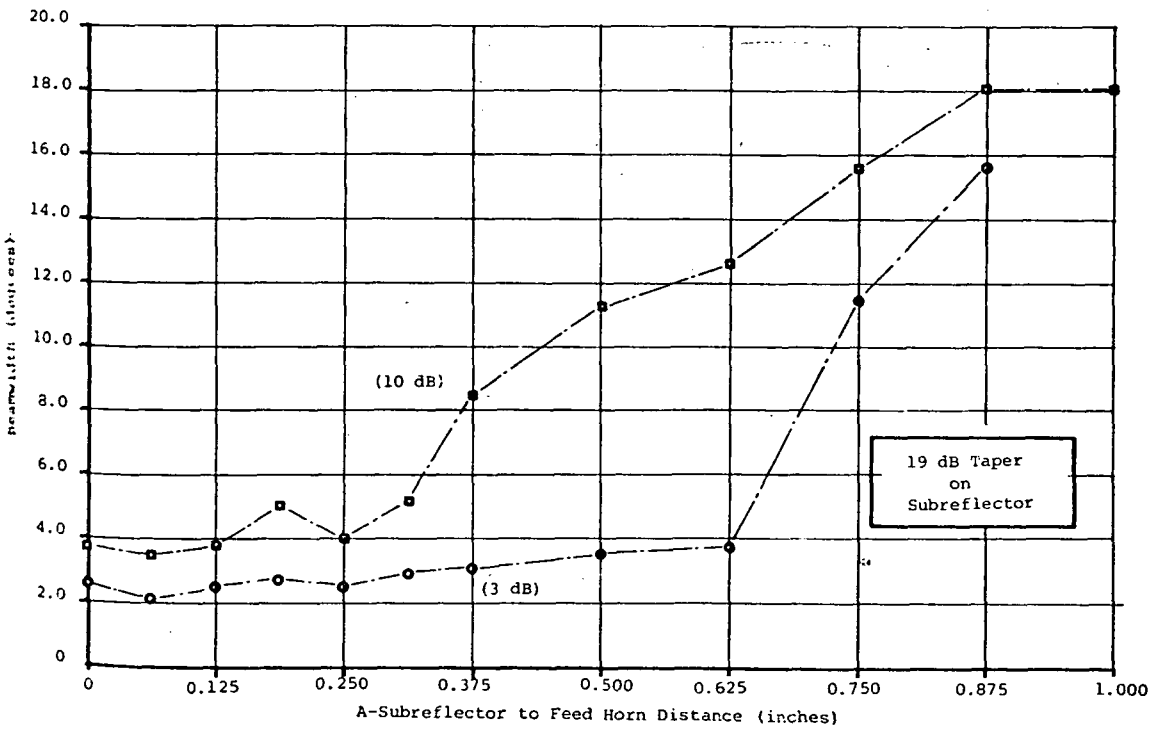

Figure 69. Beam Broadening Due to Subreflector Defocusing

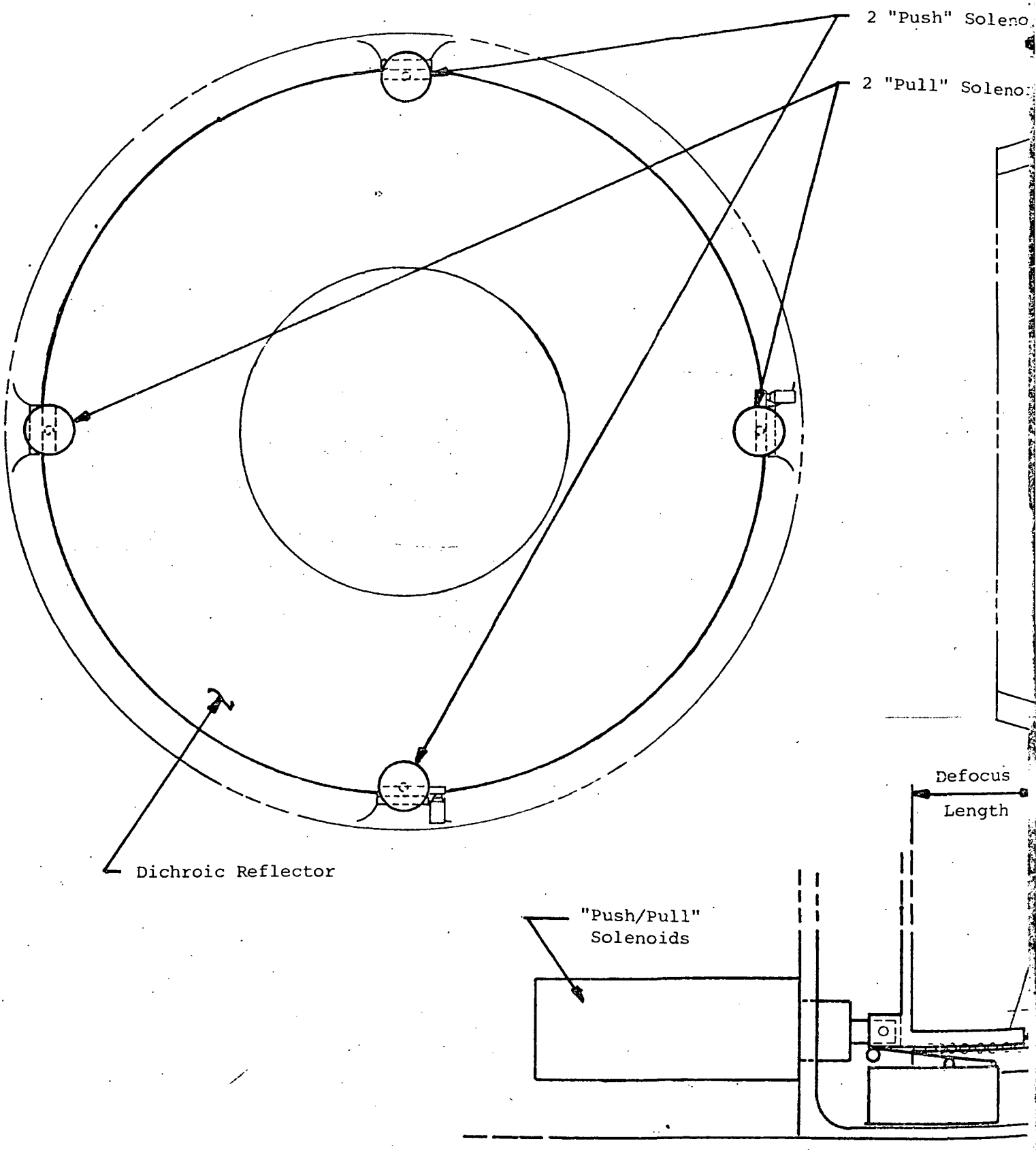

Figure 70. Dichroic Reflector Defocusing Mechanism

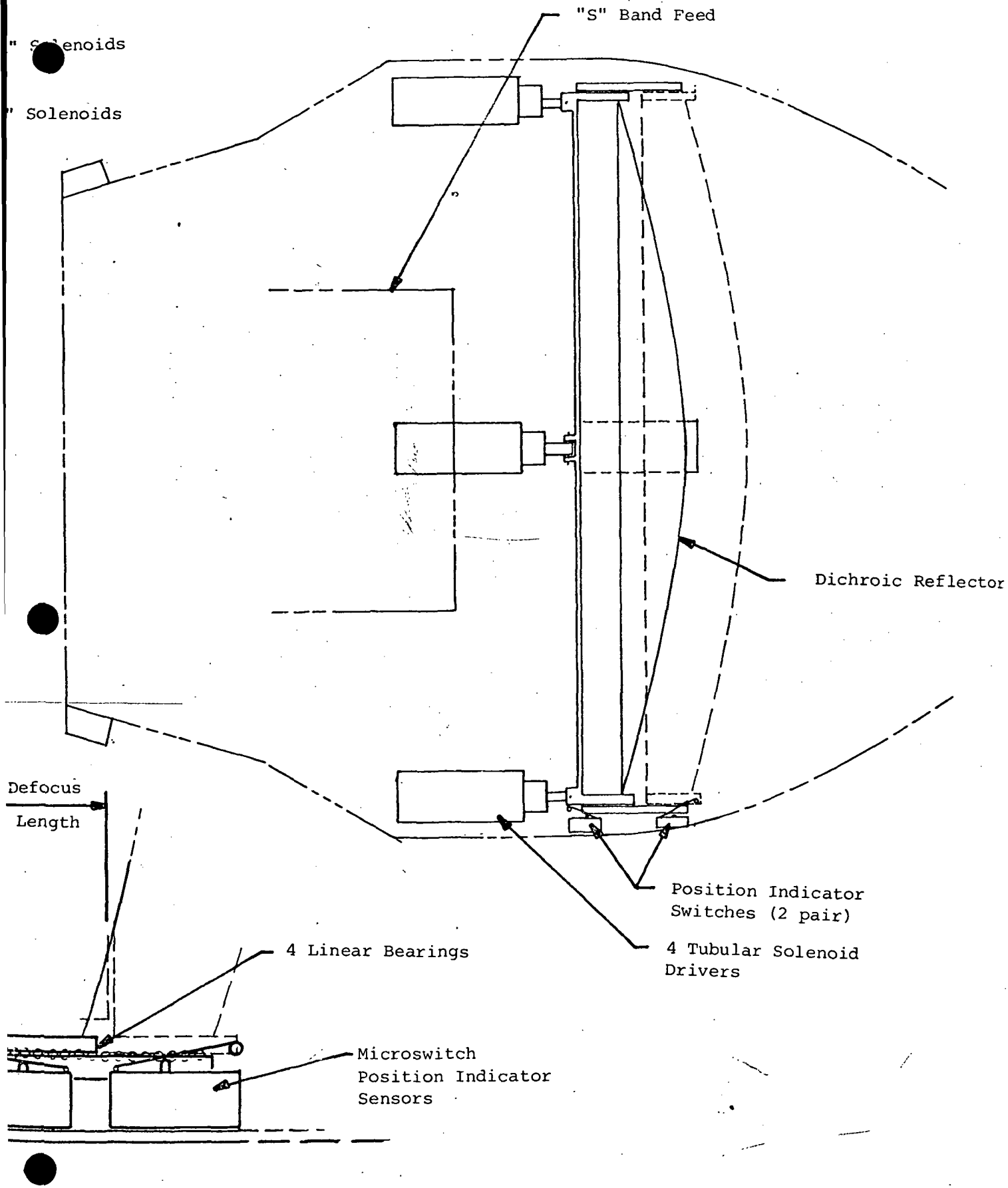
"S" Band Feed
" Solenoids
" Solenoids
Dichroic Reflector
Defocus
Length
Position Indicator
Switches (2 pair)
4 Tubular Solenoid
Drivers
4 Linear Bearings
Microswitch
Position Indicator
Sensors

mechanism provides for only two subreflector positions through push-and-pull solenoid pairs. Redundant solenoids are used to improve reliability and the mechanism is designed so that only one solinoid of each pair is sufficient to move the subreflector. Microswitches are used to sense and indicate the position of the subreflector. A fixed phase shifter would need to be switched into each of the error channel lines to compensate for the relative sum and difference phase shift caused by the defocused action. When the subreflector is refocused, this phase shift would be removed.

The preferred beam broadening technique for TDRS application is a permanent defocusing of the monopulse tracking feed to achieve a 1.5 to 1 or 2 to 1 increase in beamwidth. This can be implemented in a simple five horn feed system wherein the center horn is focused and optimized for the data link operation and four defocused peripheral horns are used to achieve monopulse auto tracking (sum and difference). Analyses in paragraph 4.8.2 show that a 1.5 to 1 FOV increase is sufficient to assure acquisition of a K_u-band user, and that the data-beam pointing error realizable with a reduced gain baseline monopulse system (paragraph 4.7.2) is adequate to assure no more than 0.5 dB reduction in the data channel peak gain level.

The preferred system offers the following advantages:

1 A dedicated data channel, optimized to achieve maximum gain

- a No comparator losses
- b No switch losses (required in under-illumination and beam spoiling)
- c No losses due to beam tilts caused by comparator unbalances.

2 Data channel reliability is higher

- a No switches required
- b No chance of subreflector jamming in defocused position
- c No dependence on monopulse network

3 Better Isolation between data transmitter and monopulse receiver

- a No coupling through comparator
- b Isolation is dependent on horn-to-horn coupling

4 Higher reliability in beam broadening
   a Fixed amount of broadening
   b No moving parts
   c No switches or phase shifters

It has been shown that the dual reflector parabolic and spherical reflectors are the only configuarations suitable for the fulfillment of all the TDRS requirements. The dichroic subreflector is a natural fit for the requirement for dual frequency operation. The combined configuration allows for independent feed designs optimized for K_u- and S-band performance. There are several companies engaged in design and development of large erectable reflector systems suitable for deployment in space. Radiation, Inc. (Division of Harris Intertype) and Lockheed Missiles and Space Company, Inc., have developed large antennas suitable for TDRS application. The Radiation 12.5-foot mesh reflector has been built and tested for mechanical and RF performance at K_u-band frequencies. Test results show an rms surface accuracy of 0.020 inch. This reflector is currently undergoing space environment testing at NASA-GSFC. A summary of the Radiation reflector is included in Appendix F. Lockheed (Reference 45) has built many mesh reflector antennas; the most recent is a 30-foot reflector currently deployed and operating on the ATS-6 spacecraft. This reflector design for X-band operation has a 0.055 inch rms surface accuracy. Private correspondence with Mr. E. L. Becker of Lockheed indicates that the same design would have a 0.025 inch surface accuracy in a 12.5-foot diameter configuration. Both the Radiation and Lockheed designs can be easily modified for spherical reflectors without sacrificing surface accuracy, weight, or space performance.

The selection of a cupped helix S-band feed for Options I and III was made because of its simplicity, low losses, reliability, low weight, inherent pattern symmetry and circular polarization. The dual mode spiral S-band feed is preferred as an auto tracking feed system because it has inherently symmetrical sum and difference patterns, good circular polarization, small size, two channel monopulse, ease of manufacture, and adequate RF performance.

Both the Radiation and Lockheed designs can be easily modified for spherical reflectors without sacrificing surface accuracy, weight, or space performance. The selection of a cupped helix S-band feed for Options I and III was made because of its simplicity, low losses, reliability, low weight, inherent pattern symmetry and circular polarization. The dual mode spiral S-band feed is preferred as an autotracking feed system because it has inherently symmetrical sum and difference patterns, good circular polarization, small size, two channel monopulse, ease of manufacture, and adequate RF performance.

Selection of the K_u-band feed system was based on tradeoffs involving the maximization of data beam gain, the provision of a reliable designation aid for K_u-band autotrack, the provision of an adequate K_u-band auto tracking system, and simplification of the TDRS equipment. The five-horn configuration, where the center horn is dedicated to the data channel (receive and transmit) and the four peripheral horns are used for auto tracking only, is preferred as the result of the above considerations. This design is basically configured

after a Sylvania feed design (Reference 46), which is used on the ATS 40-foot Electronic System ground communications antenna at the Mojave site (Figure 71). At 4.2 GHz, the ATS cassegrain antenna system is almost a direct scale model of the TDRS antenna. The primary and secondary RF performance and the tracking performance of this antenna are well known through meticulous testing of the system during a recent modification program performed by Martin Marietta Aerospace, under Contract NAS-5-21615, ATS-F&G Feed/Receiver Modification. The center feed horn of the ATS design is dedicated entirely to the transmit function. The peripheral horns are used for the sum, difference, and data reception functions.

Design calculations for the adaptation of this feed system to the TDRS show that the center horn can be used to transmit and receive data signals, and that the peripheral horns may be permanently defocused to provide adequate tracking performance. The measured data gathered during the ATS contract were used as a basis to support the FOV and tracking calculations presented in other sections of this report.

The selected K_u-band feed system offers the following advantages and characteristics:

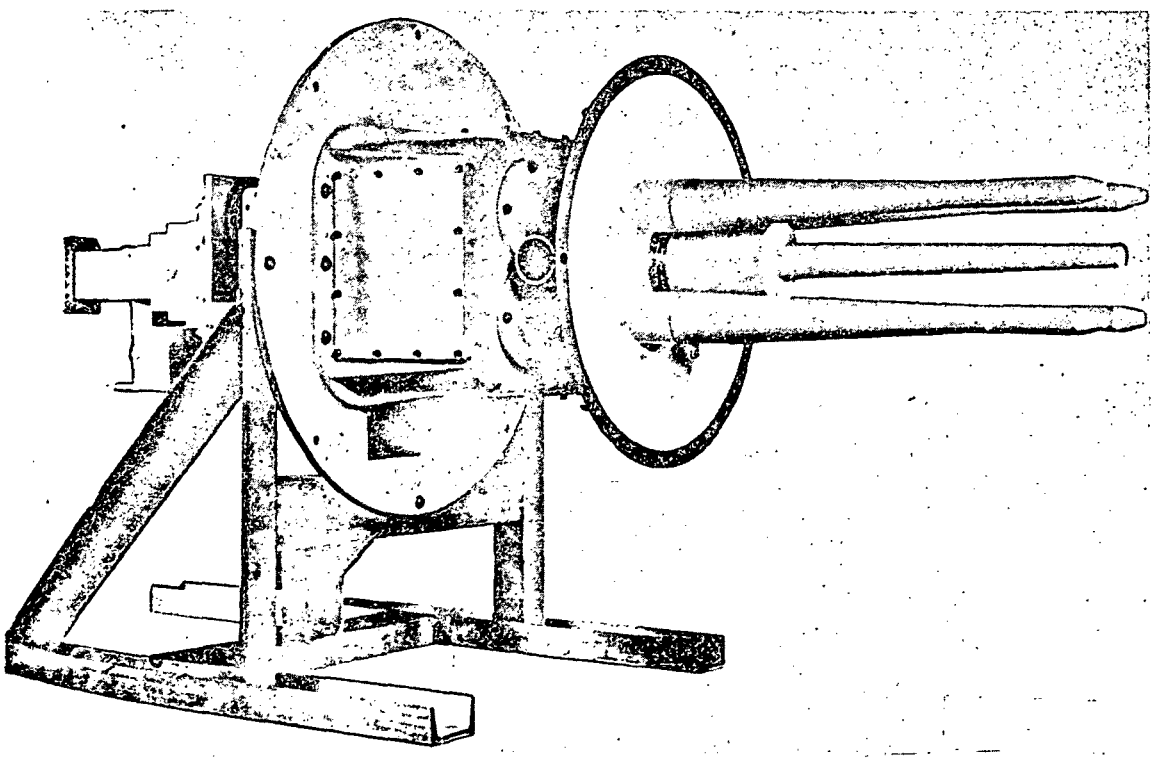

Figure 71. ATS-F&G 40-Foot Ground Antenna Feed

1 Optimized data channel

2 Simple and reliable designation aid

3 Reliable and accurate data link maintenance

4 Proven design.

Optimized Data Channel

Although a multi-mode horn can provide as much as 1 dB improvement in secondary gain, its size would preclude the employment of an effective peripheral autotrack feed system. A multi-mode auto tracking feed system would only provide a 0.5 dB (max) net increase in data channel gain due to losses in the comparator and in the higher order mode generation networks.

Simple and Reliable Designation Aid

The permanently defocused tracking feed employs a simple comparator network and requires no moving parts or electronic switches, attenuators, and phase shifters.

Reliable and Accurate Data-Link Maintenance

The analysis included in this report shows that the defocused tracking feed system has sufficient gain and tracking accuracy to maintain a maximized data link channel with less than 0.5 dB loss from peak signal level.

Proven Design

The similarity of the TDRS feed with the ATS feed is sufficient to assure that the preferred design will provide adequate performance, similar to that measured for the ATS C-band ground antennas.

4.6 Angle Tracking Receivers - Evaluation and Selection

In this section, the major physical and performance requirements of the angle sensor are first established from the contract statement of work (revised 3 April 1974), and from postulated TDRSS communications requirements. Various known angle sensing methods are then tabulated, along with their major distinguishing physical characteristics, and the estimated RF losses introduced to the data signal (when a receiver channel is common to the data and angle sensing functions). Block diagrams of the various angle sensing methods are also given, down to the major component level, assuming correlation (non-coherent) detection in all cases.

Based on the criteria of 1) data signal loss, 2) relative complexity, and 3) relative angle sensing accuracy, only several of the originally listed angle sensing techniques remain as candidates for further evaluation. These remaining candidates are then compared on the basis of their contributing angle error caused by thermal noise alone, again assuming angle sensing via non-coherent detection aboard the TDRS. Receiver thermal noise error is given as a function of signal-to-noise power ratio (SNR), referred to the IF bandwidth, for both S- and K_u- band operation. At this point in the analysis, it is observed that the specified SNR of -14 dB into the TDRS S-band receiver is insufficient to permit non-coherent angle error detection aboard the TDRS. However, the S-band angle error signals may be upconverted to K_u-band in the TDRS repeater for transmission to the ground station (GS) wherein coherent processing, e.g., using phase-locked loop (PLL) receiver techniques, may be used to detect signals well immersed in noise. The achievable improvement in angle sensing accuracy is sufficient to permit detection of SNR $\geq$ -22 dB (including 2 dB tandem link degradation) so that coherent angle sensing may be performed at the ground station or in the TDRS for the S-band user cases. Similarly, for defocused monopulse operation in the broad-beam K_u-band acquisition mode, SNR $\geq$ -20 dB may be detected with coherent angle tracking.

The component requirements (number of parts and complexity) and RF data channel losses introduced by each candidate angle sensing technique are determined and tabulated. The effects of modulation inherent in the monoscan angle sensing method are also determined.

Finally, angle tracking receivers are selected and recommended, on the basis of all the foregoing considerations, for both K_u-band and S-band. For K_u-band, both coherent and non-coherent detection methods may be used; for S-band, only coherent detection may be used because of the extremely low SNR.

4.6.1 Angle Sensor Requirements

The major physical and performance requirements for the angle tracking receiver are set forth in Table XLIV .

TABLE XLIV
Angle Sensor Requirements

Requirement	Range
Low data channel loss (transmit or receive)	$\leq$ 2 dB
Data beam pointing error (3σ)	Within $\pm$ 0.2 HPBW. (Beam on reflector axis)
Instantaneous field-of-view (FOV)	Consistent with designation accuracy
Input signal-to-noise power ratio	$\leq$ 10 dB, referred to a 1 MHz IF noise bandwidth (B_n) in K_u-band
	$\leq$ -14 dB referred to B_n = 150 KHz in S-band
Operating bandwidth (with shared data channel)	K_u-band - 950 MHz, centered at 14.875 GHz
	S-band - 100 MHz, centered at 2.250 GHz
Operating temperature range	40°F to 100°F (protected)
RF processor characteristics (monopulse operation over bandwidth and temperature limits)	
Pre-comparator phase shift	$\leq \lvert 5 \rvert$ degrees in S-band; $\leq \lvert 15 \rvert$ degrees in K_u-band
Pre-comparator amplitude unbalance	$\leq$ 0.4 dB
Post-comparator phase shift	$\leq$ 20 degrees
Sum (Σ) and difference (Δ) channel isolation	$\geq$ 40 dB
Comparator output VSWR	$\leq$ 1.50:1 (all ports)
Post comparator Σ/Δ gain differential	$\leq$ 2 dB

TABLE XLIV (Continued)

Requirement	Range
Antenna polarization	RCP or LCP
Immunity to signal fading, scintillation, etc.	
Low primary power consumption	
Adaptability to space application (space qualified components, or in development for meeting performance in TDRS environment	
Adaptability to ground station processing of angle coordinates from sensor data (coherent angle sensing must be performed at ground station)	
Hardware characteristics	
Minimum no. moving parts	
Small size and weight	
Minimum complexity maximum reliability, considering:	
No. receiver channels	
Component types and quantities	
Degree of redundancy required	
Required component uniformity (physical and performance tolerances)	
Ease of manufacturing and reproducibility	
Inherent modulation must result in negligible intermodulation products within data channel bandwidth	

4.6.2 Potential Angle Sensing Techniques and First Screening

4.6.2.1 Techniques

Various known angle sensing techniques are listed in Table XLV, where they are compared on the basis of the required number of receiver channels and insertion loss in the data channel; one of the receiver channels is used for both data transmission and angle sensing functions. The insertion loss includes beam squint, RF line, and component losses, but excludes losses caused by rotary joints, cable wrap, and feed defocusing. Other major characteristics of each technique are also given in Table XLV and each technique is referred to its corresponding block diagram (Figures 72 through 80) for greater detail. The block diagrams, except that for conical-scan (Figure 72), show the possible alternative of using an additional receiver channel for a dedicated low-loss data channel.

TABLE XLV
Angle Sensing Methods

Method	No. Receiver Channels (Shared Data Channel)	Data Channel Receive Loss K_u-Band/S-Band (dB)	Comments and Other Major Characteristics	Block Diagram
I. Conical scan	1	>3.0/2.7	Uses simple feed element Beam squint-angle causes large data channel loss and AM; no apparent way to overcome loss. Scanning requires mechanical motion in feed network; mechanical motion also required for beam broadening.	Figure 72
II. Beam switching	1	>3.0/2.7	Uses 4-element feed cluster. May use 5th element central to feed cluster for low-loss data channel (also, for beam broadening w/o mechanical motion. Beam squint-angle causes large data channel loss when sharing receiver channel.	Figure 73

TABLE XLV (Continued)

Method	No. Receiver Channels (Shared Data Channel)	Data Channel Receive Loss K_u-Band/S-Band (dB)	Comments and Other Major Characteristics	Block Diagram
II. (Cont.)			Require RF switches for beam sampling.	
III-A TDM pseudo-monopulse (monoscan)	1	1.5/1.0	Uses either multi-mode feed or 4-element feed cluster. May use 5th element central to feed cluster for low-loss data channel (also, for beam broadening w/o mechanical motion. Require RF comparator to form Σ&Δ signals AM inherent in sum channel after coupler	Figure 74
III-B FDM pseudo-monopulse	1	1.5/1.0		Figure 75
IV. Σ&Δ monopulse w/ time-shared Δ channel	2	1.5/1.0	As for monoscan (III A.) As for monoscan (III A.) As for monoscan (III A.) Require RF switch for Δ-channel signal sampling.	Figure 76
V. 2-channel Σ&Δ monopulse	2	1.5/1.0	As for monoscan (III A.) As for monoscan (III A.) As for monoscan (III A.) Inherently provides excellent null depth and sidelobe level w/use of circularly symmetrical multi-mode feed.	Figure 77

TABLE XLV (Continued)

Method	No. Receiver Channels (Shared Data Channel)	Data Channel Receive Loss K_u-Band/S-Band (dB)	Comments and Other Major Characteristics	Block Diagram
VI. 3-channel Σ&Δ mono-pulse	3	1.5/1.0	As for monoscan (III A.) As for monoscan (III A.) As for monoscan (III A.)	Figure 78
VII. amplitude monopulse	4	>2.5/2.2	Use 5-element feed cluster with central element for low-loss dedicated data channel; outer 4-elements provide beam broadening. Loss caused by beam squint-angle and RF lines. Does not require RF comparator; requires precision phase balance between channels	Figure 79
VIII. phase mono-pulse	4	1.5/1.2	As for amplitude mono-pulse (VII). Loss caused by parallax between feed beams, etc. Requires precision amplitude balance between channels; no RF comparator required, but need two quadrature RF hybrids to implement with reflector.	Figure 80

*Max. K_u-/S-band losses, excluding rotary joint, cable wrap, and/or feed defocus losses, but including other RF line and RF network losses.

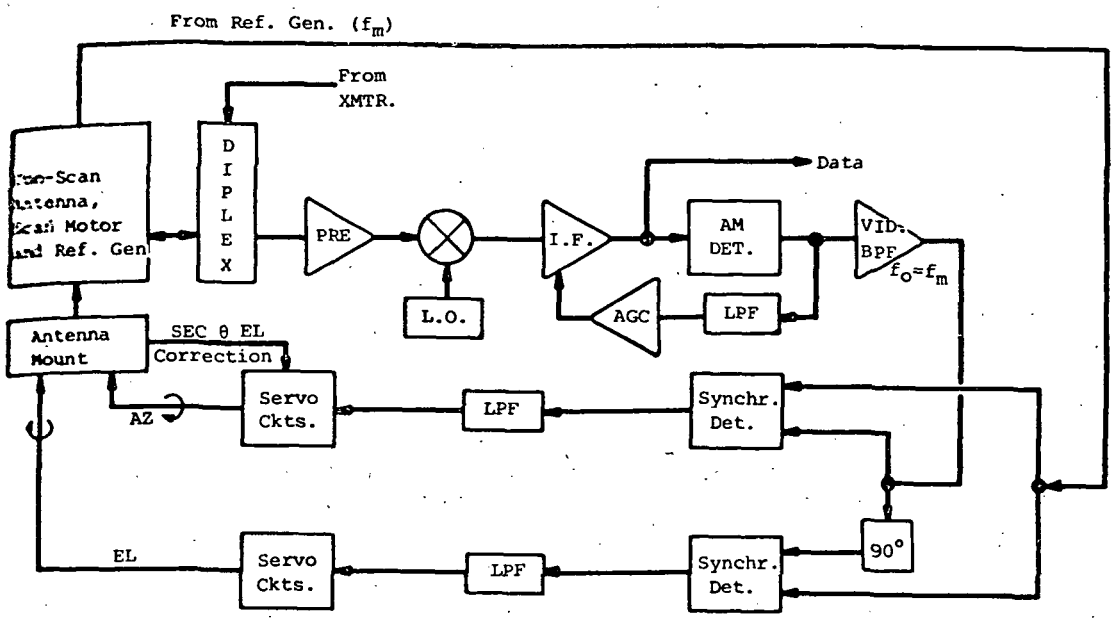

Figure 72. I. Conical Scan

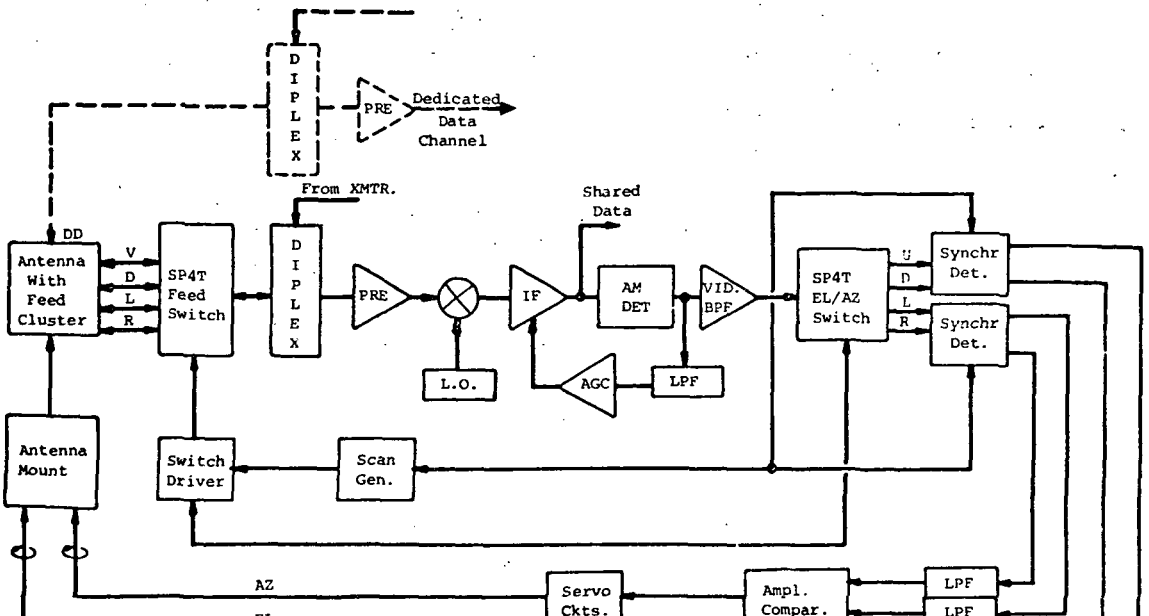

Figure 73. II. Beam Switching

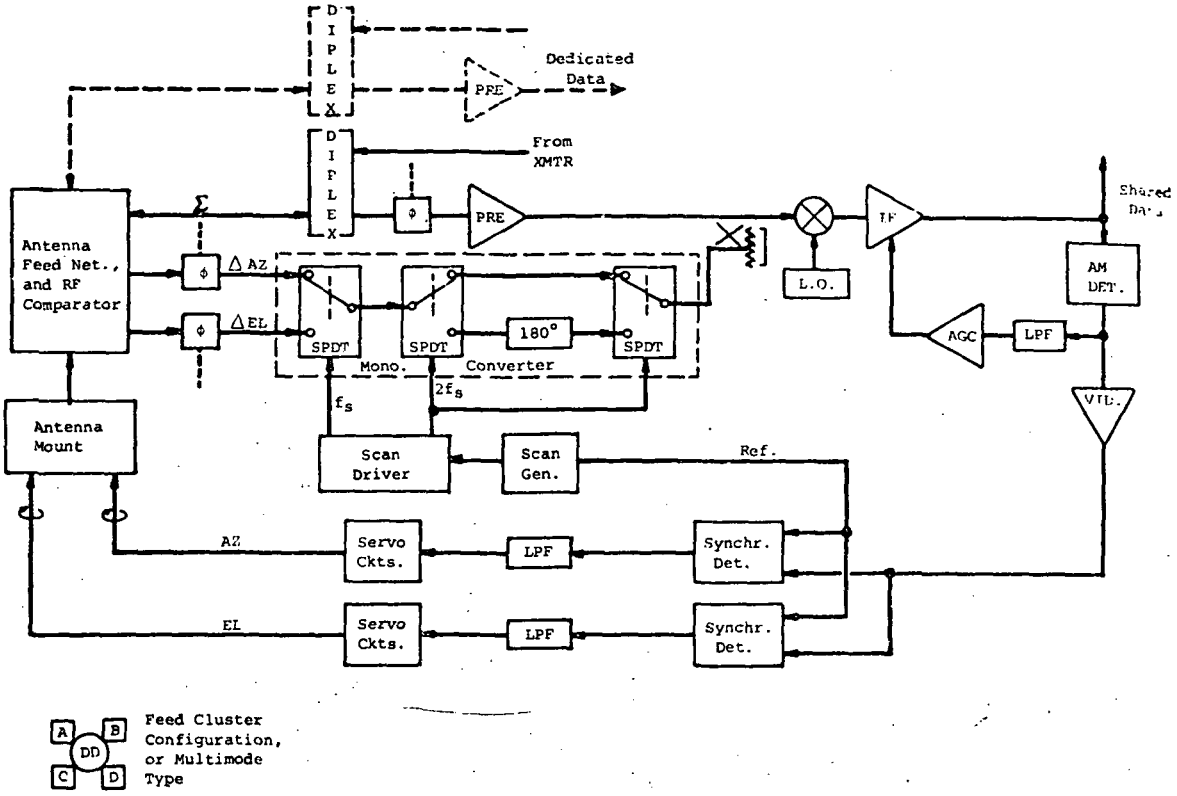

Figure 74. III-A. Monoscan (Pseudomonopulse)

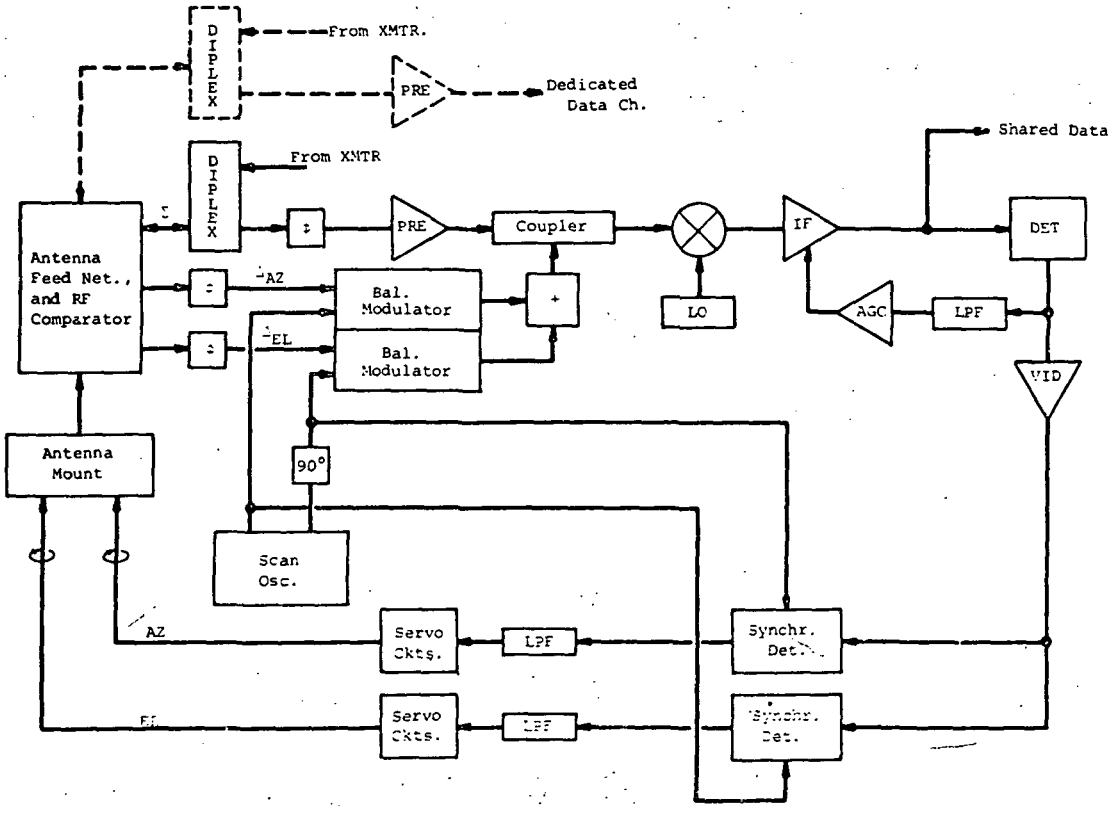

Figure 75. III-B. FDM Pseudomonopulse

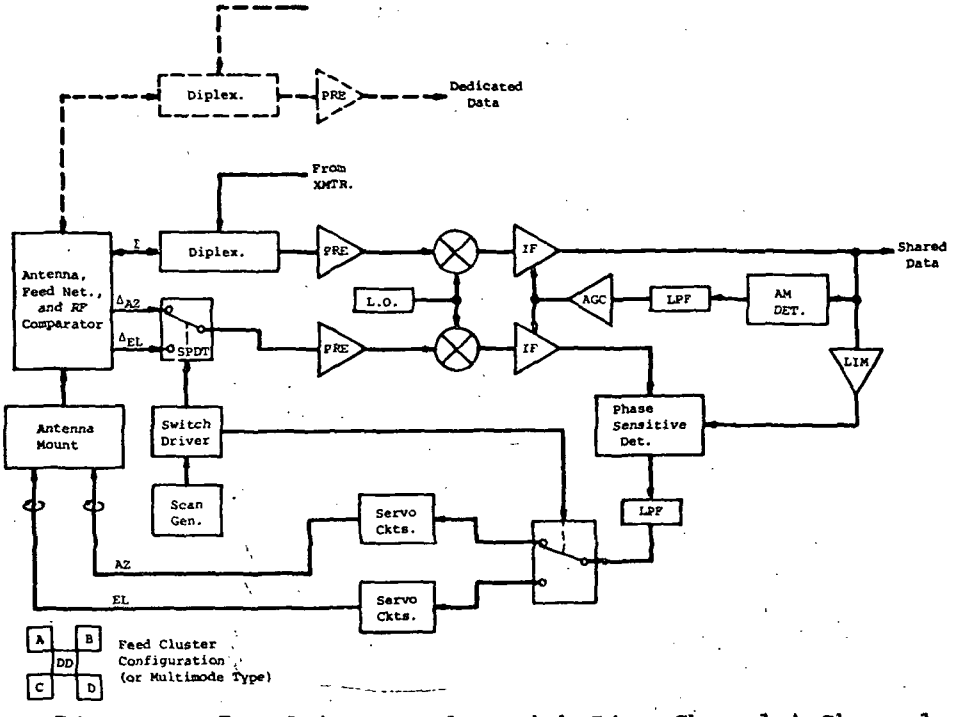

Figure 76. IV. Σ and Δ Monopulse with Time-Shared Δ Channel

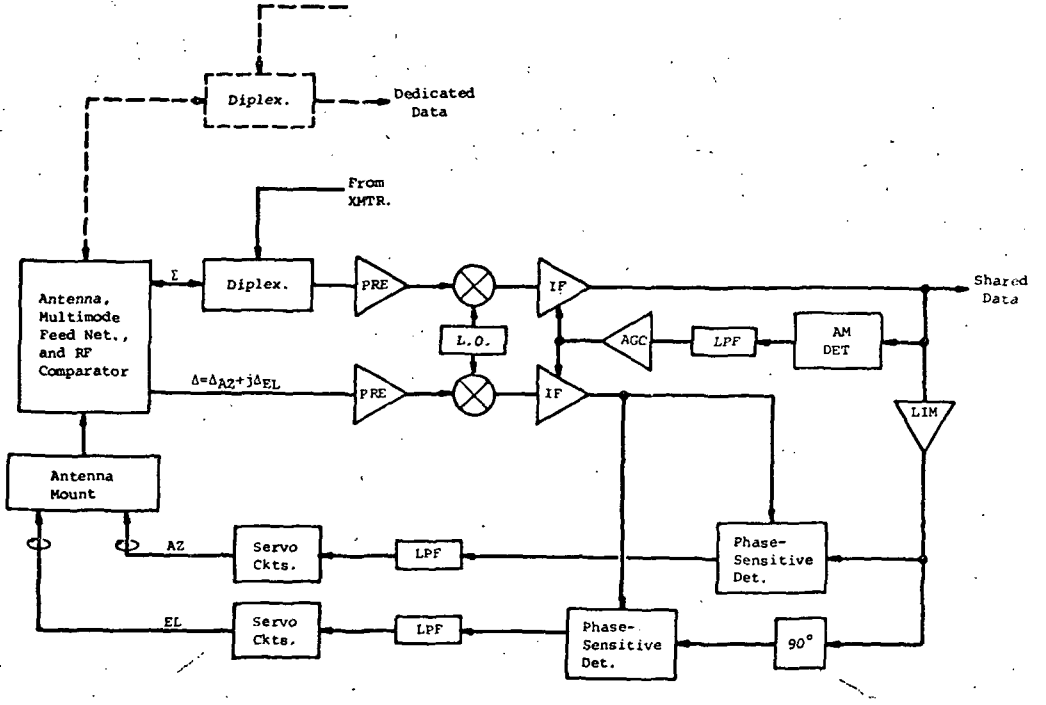

Figure 77. V. Two-Channel Σ and Δ Monopulse

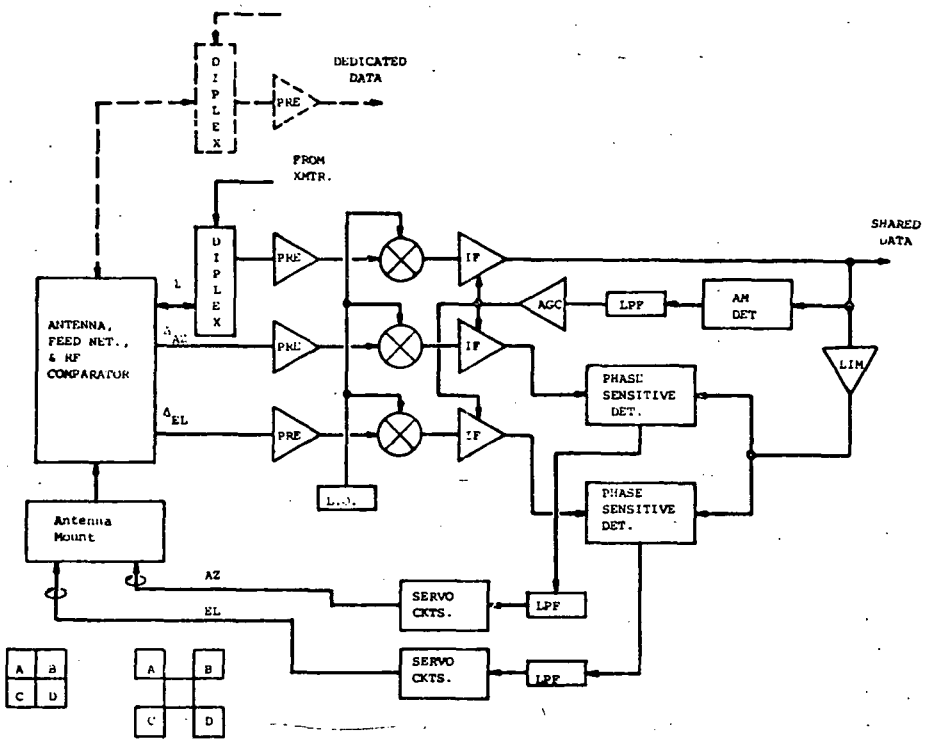

Figure 78. VI. Three-Channel Σ and Δ Monopulse

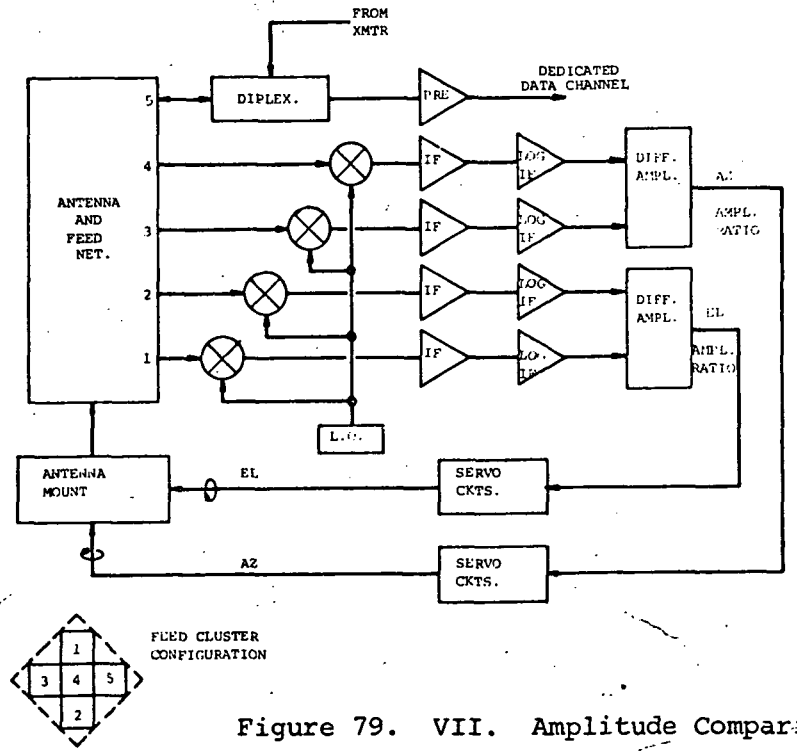

Figure 79. VII. Amplitude Comparison

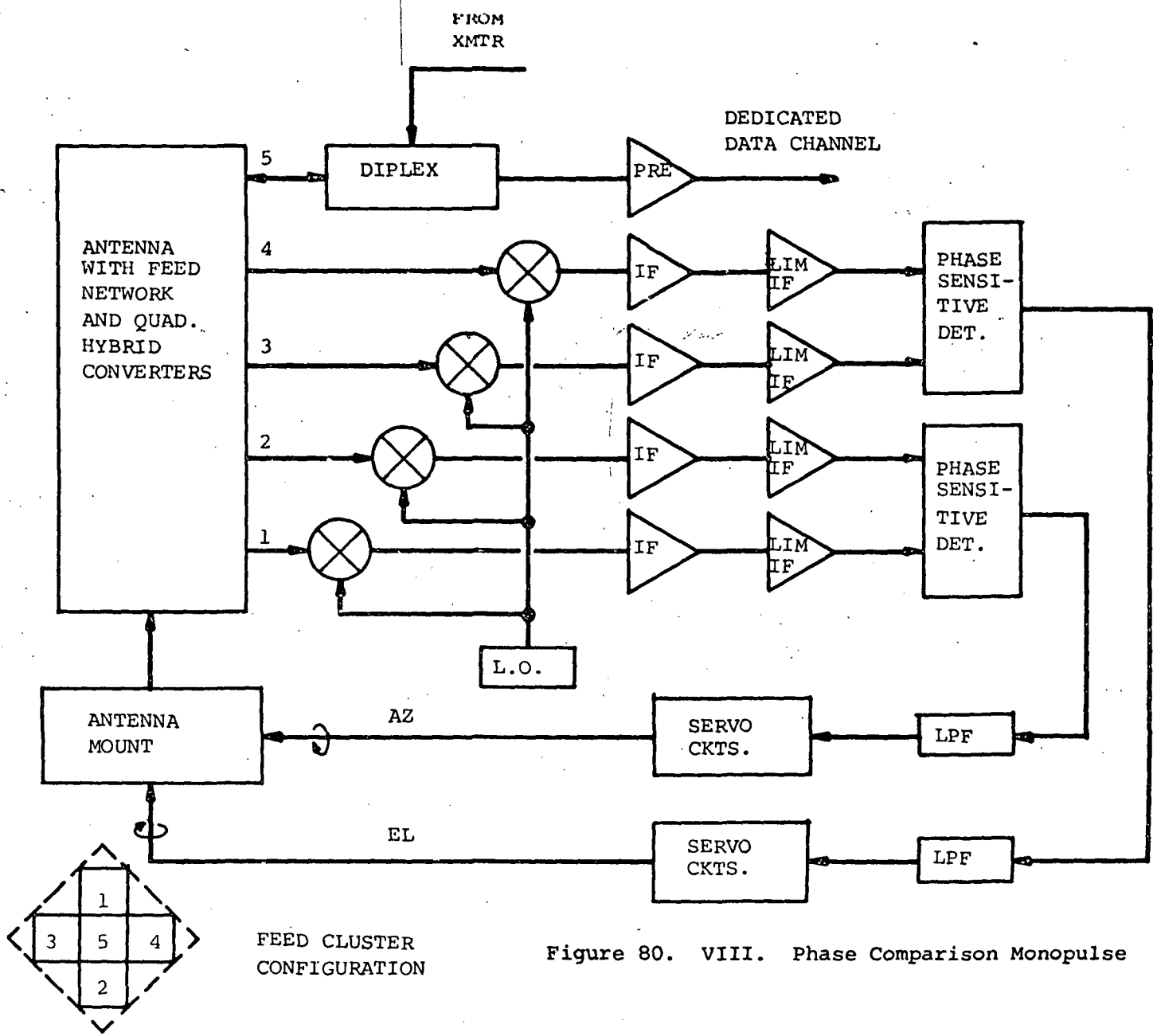

Figure 80. VIII. Phase Comparison Monopulse

4.6.2.2 First Screening

The criteria used in disqualifying certain of the angle sensing techniques of Table XLV from further consideration are as follows:

1 Data channel loss

2 Relative complexity

a No. receiver channels

b Component types and quantities

c Mechanical motion

3 Effects of losses, phase/amplitude unbalance, etc., on thermal-noise induced angle sensing error.

Applying the above criteria, angle sensing via conical-scan, beam switching, FDM pseudomonopulse, pure amplitude monopulse, and pure phase monopulse are disqualified (Table XLVI).

TABLE XLVI
Angle Sensing Methods Disqualified
by First Screening

Method	Figure No.	*Criteria Applied	Comments
I. Conical Scan	72	#1	
II. Beamswitching	73		Methods III-A and IV are refined versions of this technique, capable of less angle error and about same degree of hardware complexity.
Shared data channel		#1	
Dedicated data channel		#2 & #3	
III-B FDM pseudo-monopulse	75	#2 & #3	Method III-A is less complex and capable of less angle error.
VII. Pure amplitude monopulse	79		
Shared data channel		#1	
Dedicated data channel		#2 & #3	

TABLE XLVI(Continued)

Method	Figure No.	*Criteria Applied	Comments
VIII. Pure phase monopulse	80		
Shared data channel		#2 & #3	Capable of precision angle sensing accuracy, but requires precise control of phase and amplitude unbalances; Methods III-A, IV, V, and VI are less complex and provide sufficient angle sensing accuracy.
Dedicated data channel		#2 & #3	

*Listed in above paragraph.

The angle sensing methods remaining as candidates for further evaluation and comparison after the first screening are:

III-A. TDM pseudomonopulse (monoscan)

IV. Σ and Δ monopulse with time-shared Δ-channel

V. 2-channel Σ and Δ monopulse

VI. 3-channel Σ and Δ monopulse.

The following paragraph (4.6.3) evaluates these surviving angle sensor candidates.

4.6.3 Evaluation of Angle Sensor Candidates

4.6.3.1 Thermal Noise Angle Error -- Non-Coherent Detection

4.6.3.1.1 Monoscan and Time-Shared Δ-Channel Angle Sensors

Both the monoscan (Figure 74) and time-shared Δ-channel (Figure 76) angle sensing methods use a sequential lobing process, similar to beam switching or conical scan. Here, however, the sume (Σ) channel comparator output achieves the equivalent gain of an un-squinted beam. Therefore, the well-known receiver noise tracking error relationships for sequential

lobing may be used if properly modified to allow for differences in the sum and difference (Δ) channel losses and thermal noise power. Then, from References 47 through 49, the rms angle error for non-coherent (correlation) detection is:

$$\delta_R = \frac{\theta_3\sqrt{1 + 2\ (S/N)_\Sigma}}{\frac{k_s}{\sqrt{L_k}}\ \left(\frac{S}{N}\right)_\Sigma}\ \sqrt{\frac{\beta_n}{B_n}} \qquad (1)$$

where, k_s = error slope factor

L_k = beam crossover loss

$(S/N)_\Sigma$ = signal-to-noise power ratio in the sum channel, referred to IF noise bandwidth

β_n = servo noise bandwidth

B_n = IF noise bandwidth

θ_3 = half-power beamwidth.

The factor $K_s/\sqrt{L_k}$ must be modified by the ratio of Σ to Δ-channel signal losses, $[L_\Sigma/L_\Delta]^{1/2}$. For monoscan, these losses are incurred between the comparator output to the coupler output in each of the Σ and Δ channels. For time-shared Δ-channel monopulse, these losses are incurred between the comparator output to the preamplifier output in each of the Σ and Δ channels. It is observed that this loss ratio constitutes a post-comparator amplitude unbalance between Σ and Δ channels. Furthermore, it has been shown (Reference 50 and Appendix J) that the difference in thermal noise power levels between the common Δ channel and the Σ channel modifies $(S/N)_\Sigma$ in the denominator of Equation (1) to $\left[(S_\Sigma/N_\Sigma)\ (S_\Sigma/N_\Delta)\right]^{1/2}$.

Observing that

$$N_\Sigma = KT_{e\Sigma}B_n,$$

and $N_\Delta = KT_{e\Delta}B_n$

then, $N_\Delta = (T_{e\Delta}/T_{e\Sigma})N_\Sigma$, and

$$\delta_R = \frac{\theta_3\sqrt{1 + 2\,(S/N)_\Sigma}}{\sqrt{\frac{L_\Sigma}{L_\Delta}}\;\frac{k_s}{\sqrt{L_k}}\;\sqrt{\frac{T_{e\Sigma}}{T_{e\Delta}}}\;\left(\frac{S}{N}\right)_\Sigma}\;\sqrt{\frac{\beta_n}{B_n}} \qquad (2)$$

4.6.3.1.2 Conventional Σ and Δ Monopulse Angle Sensors

From References 47 and 49, the thermal noise rms angle error for a conventional Σ and Δ monopulse (simultaneous lobing) sensor is:

$$\delta_R = \frac{\theta_3\sqrt{1 + (S/N)_\Sigma}}{k_m\,(S/N)_\Sigma}\;\sqrt{\frac{\beta_n}{B_n}} \qquad (3)$$

where k_m is the error slope factor. When modified to account for amplitude unbalance (gain differential) and thermal noise power difference between Σ and Δ channels, Equation (3) becomes

$$\delta_R = \frac{\theta_3\sqrt{1 + (S/N)_\Sigma}}{k_m\sqrt{\frac{T_{e\Sigma}}{T_{e\Delta}}}\;\left(\frac{S}{N}\right)_\Sigma}\;\sqrt{\frac{\beta_n}{B_n}}\;\sqrt{U} \qquad (4)$$

where U is the amplitude unbalance term.

4.6.3.1.3 Error Slope Factor

The error slope factors $k_s/\sqrt{L_k}$ and k_m for sequential and simultaneous lobing cases, respectively, are treated extensively by Barton and Ward (Reference 51). For sequential lobing, $k_s/\sqrt{L_k}$ is the effective error slope factor, where L_k is the crossover loss resulting from a Δ beam offset or squint angle $k_s/\sqrt{L_k} = 1.05$ will be assumed, corresponding to a $\theta_3/2$ squint angle which results in L_K = 3 dB and no loss to the Σ beam. For simultaneous lobing, k_m = 1.57 will be assumed, corresponding to a 2-horn dual-mode monopulse feed performance.

The error slope factors are degraded (decreased) by the presence of pre- and post-comparator phase/amplitude unbalances between the Σ and Δ channels. The relationships describing the effects of these unbalances in a Σ and Δ amp... pulse system are derived in Appendix A. Using the relationships of Appendix A, and the set of amplitude and phase unbalances specified in Table XLIV, the ... slope reduction factor (S) was calculated and tabulated in Table XLVII.

TABLE XLVII

Error Slope Reduction Factor
Resulting From Comparator Unbalances

Pre-Comparator Phase Unbalance α (deg)		Post-Comparator Phase Unbalance β (deg)		Pre-Comparator Amplitude Unbalance $\lvert A_1/A_2 \rvert^2$ (dB)		Reduction in Error Slope Factor S	
S-band	K_u-band	S-band	K_u-band	S-band	K_u-band	S-band	K_u-band
+5	+15	+20	+20	0.4	0.4	0.940	0.9...
+5	+15	-20	-20	0.4	0.4	0.942	0.9...
-5	-15	+20	+20	0.4	0.4	0.942	0.9...
-5	-15	-20	-20	0.4	0.4	0.940	0.9...
+5	+15	+20	+20	-0.4	-0.4	0.942	0.9...
+5	+15	-20	-20	-0.4	-0.4	0.940	0.9...
-5	-15	+20	+20	-0.4	-0.4	0.940	0.9...
-5	-15	-20	-20	-0.4	-0.4	0.942	0.9...

From Table XLVII it is observed that the error slope reduction factor is rathe... insensitive to the various combinations of unbalance polarities. Hence, avera... values of S will be used in calculating thermal noise angle error. Specifica...

for S-band, $S_{av} = 0.941$,

and for K_u-band, $S_{av} = 0.956$.

4.6.3.1.4 Thermal Noise Angle Error Versus Signal-to-Noise, Focused Feed Case

Thermal noise angle error, normalized to $\theta_3 \times \sqrt{\beta_n}$ for K_u- and S-bands, was calculated as a function of $(S/N)_\Sigma$ for the various types of angle sensors using Equations (2) and (4). The data are plotted in Figures 81 and 82 for K_u- and S-bands, respectively. The plots of Figures 81 and 82 provide the tradeoff between thermal noise angle error (single plane) and user transmit power.

For the K_u-band (Figure 81), it was assumed that an uncooled parametric preamplifier is used only in the Σ channel*. The calculations for $T_{e\Sigma}$ and $T_{e\Delta}$ in K_u-band are shown in Table XLVIII.

TABLE XLVIII

Effective Noise Temperatures for K_u-Band

Contribution	Σ Channel	Δ Channel
Receiver noise	445°K (NF=4 dB)	1164°K(NF=7 dB)
Line loss	107°K (L=2 dB)	107°K(L=2 dB)
Earth noise	195°K	195°K
	$T_{e\Sigma}$ = 747°K	$T_{e\Delta}$ = 1465°K

It is also noted that the post-comparator unbalance used for K_u-band monoscan is the ratio L_Δ/L_Σ = 11.5 dB, based on the use of a 10 dB combining coupler and a preamplifier on the input side of the coupler (Figure 74). It was assumed that preamplifiers were not used in S-band, and that both Σ and Δ channels had about equal noise figures and line losses; hence, $T_{e\Sigma}/T_{e\Delta} = 1$ for S-band (Figure 82).

For both K_u- and S-bands, conventional Σ and Δ monopulse provides less thermal noise angle error than time-shared-Δ monopulse, which provides less error than monoscan. This is apparent from Figures 81 and 82 and from Equations (2) and (4) for the assumed conditions.

4.6.3.1.5 Broad Beam K_u-Band Noise Angle Error versus SNR, Defocused Feed Case

For the RP/K-Auto data link maintenance method, the nominal K_u-band beamwidth ($\theta_3 \approx 0.4°$) may be increased to permit reliable acquisition of the K_u-band beacon signal within the available GS command pointing accuracy. Ground Station command pointing accuracy (3σ) will be about ±0.45 degrees (paragraphs 4.4.2 and 4.7.2) so that about 1.5:1 beam broadening will be required for highly reliable acquisition (section 4.8). Methods for achieving beam broadening in the K_u-band cassegranian configuration (paragraph 4.5.2.1) include physical movement of the subreflector with respect

* It was subsequently established that although thermal noise error increases without a paramp, the K_u-band data beam pointing error results in <0.5 dB data loss for $(S/N)_\Sigma \geq -1$ dB and β_n = 1 Hz.

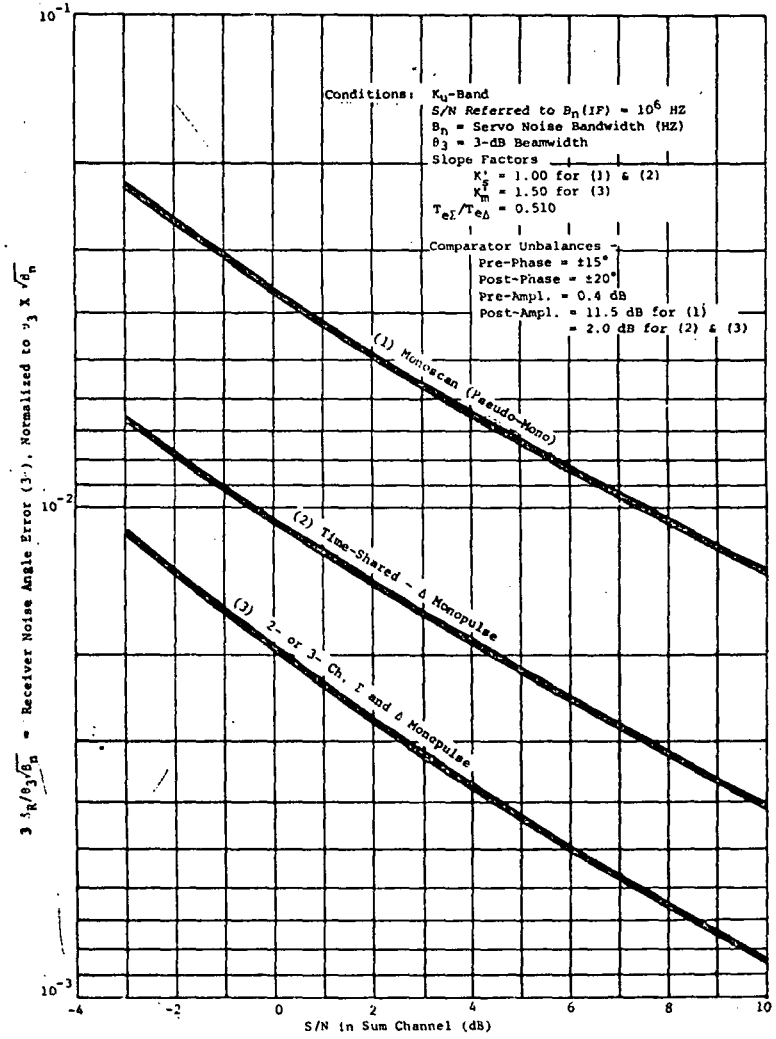

Figure 81. Thermal Noise Error Versus Signal-to-Noise, Focused Feed, K_u-Band

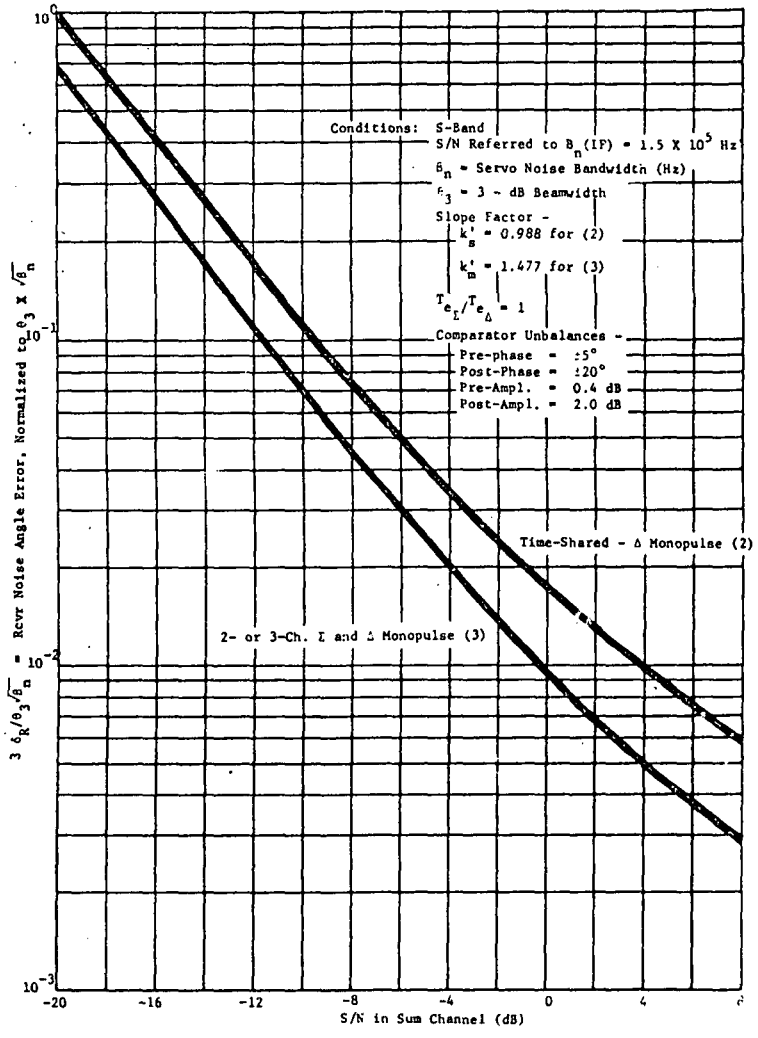

Figure 82. Thermal Noise Error Versus Signal-to-Noise, Focused Feed, S-Band

to the tracking feed, or the use of a fixed tracking feed horn outside of the focal plane with a dedicated data feed. In either case, defocused monopulse angle tracking results. To achieve monopulse operation with defocused antenna patterns, it becomes necessary to introduce 1) a fixed phase shift in the difference or sum channel to retain the required 0 or 180 degree phase difference between Σ and Δ signals and 2) a fixed gain increase in the Δ channel to compensate for a reduction of the amplitude of the relative Δ slope in the linear region about boresight. These defocusing effects have been treated by Redlien (Reference 52). Redlien's results have been applied to our beam broadening region of interest, as shown previously in Figures 64 and 66. Figure 64 shows that a shift of the feed-to-subreflector spacing of 0.63 inch relative to the focused condition provides a beamwidth increase from 0.4 degree to 0.6 degree. From Figure 64, a 0.63 inch defocusing spacing results in a 4.3 dB degradation of the Σ channel gain. Figure 66 shows that a fixed phase compensation of about 56 degrees will be required to provide maximum error signal.* The gain increase in the Δ channel required to retain the focused relative Δ signal slope will be about 3.5 dB (voltage amplification approximately proportional to beamwidth increase).

The net effect of a 1.5:1 beam broadening on thermal noise angle error will be that caused by a 4.3 dB degradation of Σ channel gain and, hence, a 4.3 dB degradation of $(S/N)_{\Sigma}$.

4.6.3.2 Thermal Noise Angle Error, Coherent Detection

4.6.3.2.1 S-Band

In Figure 82, noise angle error is plotted for small SNR because the maximum specified SNR = -14 dB, referred to B_n = 150 kHz, for S-band (refer to Statement of Work and Table XLIV). This results in appreciable noise angle error, which when combined with other angle error components, results in a marginally acceptable data beam pointing error. Furthermore, the performance of practical high-quality double-balanced mixers (used as phase detectors in the 5 to 100 MHz region) may limit the minimum SNR. Hence, a coherent angle tracking receiver is desirable for S-band. Coherent processing may be performed directly aboard the TDRS, or indirectly by translating the S-band Σ and Δ signals to K_u-band for transmission via return down-link to the ground station for processing, followed by a forward up-link servo error signal command to the TDRS. For ground station processing, an additional degradation in SNR results from TDRS repeater noise contribution.

Allowing for a 2 dB tandem link degradation in SNR, the maximum SNR at the ground station receiver input will be -16 dB, referred to B_n = 150 kHz. Allowing for an additional 6 dB reduction in user beacon power for tradeoff flexibility, the minimum SNR at the GS receiver input will be -22 dB, referred to B_n = 150 kHz. The use of a phaselock loop (PLL) as a narrowband filter in a coherent angle tracking receiver (see Appendix I) permits a minimum lock-on SNR given by (Reference 53)

* For on-boresight case; about 47° phase compensation required for off-boresight case, within required field of view achieved with 1.5:1 beam broadening.

$$\left(\frac{S}{N}\right)_{min} = \frac{32}{B_n \tau_{ec}} \quad ,$$

where τ_{ec} is the equivalent coherence time of the phase-lock oscillator (VCXO), related to the oscillator linewidth (FM noise spectrum). Typically, $\tau_{ec} \geq 0.05$ second, so that $(SNR)_{min} = 42.6 \times 10^{-4}$ (-23.7 dB) and the expected -22 dB $\leq$ SNR $\leq$ -16 dB at the ground station receiver input satisfies this limitation.

The PLL bandwidth (B_L) must be sufficiently narrow to reject enough noise spectrum, and thereby provide sufficient SNR improvement (processing gain, g) to derive an angle error signal from the PLL phase detector. If, for example, the phase detector requires a minimum SNR of about 5 dB, then for SNR $\geq$ -22 dB at the ground station receiver input,

$$g_p \leq 27 \text{ dB}$$

or, $$g_p = \frac{B_n}{B_L} \leq 500$$

and $$B_L \geq \frac{1.5 \times 10^5}{500} = 300 \text{ Hz}$$

The total spectral width dictated by the maximum doppler frequency rate, oscillator instabilities, and signal phase distortions introduced by TDRS and ground station processing circuitry, must not exceed 300 Hz for the above conditions.

It is of further interest to establish the achievable improvement (reduction) in thermal noise angle tracking error of coherent detection over that of non-coherent (correlation) detection. Using the thermal noise angle error expressions derived by Develet (Reference 47) for both coherent and correlation detection methods, it may be shown that the angle error reduction of coherent detection over non-coherent detection is

$$I_{\delta_R} = \frac{1}{\left[\prod_{k=o}^{N} J_o(\phi_k)\right] \sqrt{1+\frac{N}{S}}} = \frac{\sqrt{\frac{S}{N}}}{\left[\prod_{k=o}^{N} J_o(\phi_k)\right] \sqrt{1+\frac{S}{N}}}$$

where

ϕ_k = the $k^{\frac{th}{}}$ modulation index of the phase or frequency modulated information (radians)

S/N = signal-to-noise power ratio, referred to the IF noise bandwidth of the angle tracking receiver.

I_{δ_R} applies for simultaneous and sequential lobing types of angle sensors. It is observed that maximum improvement (minimum I) occurs when $\prod_{k=o}^{N} J_o(\phi_k)=1$, which occurs for a pure unmodulated carrier with coherent detection. For this case, the modulation index $\phi_k = 0$. Generally, however, $0 < J_o(\phi_k) \leq 1$, the lower bound $J_o(\phi_k) > 0$ occurring because noise modulating frequencies will be present in addition to the intentional modulating frequency. As the modulation index (ϕ_k) is increased and/or as the number of modulating frequencies (and modulation indices) are increased, $\prod_{k=o}^{N} J_o(\phi_k)$ will decrease (always ≤ 1), so that the achievable reduction in angle error (I_{δ_R}) degrades. This is heuristically satisfying because as the modulation bandwidth increases, noise power level also increases.

For large SNR, $I_{\delta_R} \approx \dfrac{1}{\prod_{k=o}^{N} J_o(\phi_k)}$ and

since $\prod_{k=o}^{N} J_o(\phi_k) \leq 1$, it is apparent that coherent detection offers no advantage over correlation detection in this case. For small SNR, however,

$$I_{\delta_R} \approx \frac{1}{\left[\prod_{k=o}^{N} J_o(\phi_k)\right] (N/S)^{1/2}}$$

and it is apparent that, for a fixed $\prod_{k=o}^{N} J_o\phi_k \leq 1$, I_{δ_R} decreases (improves) with decreasing SNR. The limit to which this improvement can be extended depends largely on the SNR threshold of practical coherent detection devices, as previously discussed.

As an example, consider SNR $\geq$-22 dB at the ground station receiver input, referred to B_n= 150 kHz. From Figure 82, the noise angle error with non-coherent detection will be

$$\frac{3\delta_R}{\theta_3} \leq 0.575 \text{ (assuming } B_n = 0.3 \text{ Hz and that the detector}$$

could operate with such a small SNR. From Figure 35, the data channel signal loss due to this error alone would be $\leq$ 3.98 dB, which cannot be tolerated. Using coherent detection and assuming an effective noise modulation index of ϕ_k = 1.51 ($\prod_{k=o}^{N} J_o(\phi_k) = 0.5$), the expected noise angle error will be

$$\frac{3\delta_R}{\theta_3} I_{\delta_R} \leq \frac{0.575}{5} = 0.115,$$

resulting in a data channel signal loss of $\leq$0.16 dB. This loss, when combined with other losses from other angle tracking errors, must result in an acceptable total loss of $\leq$0.5 dB (see paragraph 4.7.1). Obviously, acceptable angle tracking errors would then also result for all SNR >-22 dB.

4.6.3.2.2 K_u-Band

During the RP/K-AUTO data link maintenance mode of operation, SNR =10 dB (maximum) at the TDRS K_u-band receiver input (B_n= 1 MHz). This SNR is adequate for non-coherent angle tracking aboard the TDRS. In fact, non-coherent angle processing may be performed with an appreciable reduction of the K_u-band user beacon power, as determined by the minimum reference SNR required for correlation phase detector operation.

As discussed in paragraph 4.6.3.1.5, a 1.5:1 beam broadening for the acquisition mode results in about 4.3 dB degradation of the sum channel SNR. Therefore, coherent angle tracking (at the ground station) could be used for the broad beam K_u-band acquisition mode, thereby allowing appreciable reduction in user beacon power.

The minimum lock-on SNR for a PLL coherent angle tracking receiver (Reference 53) is

$$(SNR)_{min} = \frac{32}{B_n \tau_{ec}} = 6.4 \times 10^{-4} \ (-31.6 \text{ dB})$$

for $B_n = 10^6$ Hz and $\tau_{ec} = 0.05$ second. Allowing a 2 dB degradation for tandem operation plus a 4.3 dB degradation for antenna defocusing, it would appear that the SNR into the ground station receiver could range over -31.6 dB $\leq$ SNR $\leq$3.7 dB. However, the lowest permissible SNR will ultimately be dictated by the minimum PLL bandwidth (B_L), as determined by oscillator instabilities, maximum doppler change, and signal processing distortions, e.g., for B_L= 300 Hz, the processing gain will be

$$g_p = \frac{B_n}{B_L} = \frac{10^6}{3 \times 10^2} = 3{,}333 \ (25.2 \text{ dB}).$$

Then for a required SNR = 5 dB to the PLL phase detector, SNR $\geq$-20.2 dB and the K_u-band user beacon power may be reduced by 23.9 dB (-20.2 $\leq$SNR $\leq$+3.7 dB). It is observed that whereas only about 7.7 dB reduction in S-band user beacon power may be accommodated with coherent ground station angle tracking, much greater reduction may be accommodated for K_u-band users.

4.6.3.3 Data Channel Insertion Losses

The candidate angle sensors, remaining after the first screening (paragraph 4.6.2), are illustrated in Figures 74, 75, 76, and 77. It is observed from these candidate sensor block diagrams that each candidate introduces approximately the same insertion loss from 1) the feed input to the RF preamplifier on receive and 2) the feed input to the transmitter in each frequency band of interest. There are some minor exceptions to this, such as the additional loss of the Σ channel phase shifter used in the monoscan sensor (Figure 74) to affect channel phase balance in the shared data/tracking channel case. The contributing and total losses expected in the S- and K_u-bands are summarized in Table XLIX and L, respectively.

TABLE XLIX.

S- Band Data Channel RF Losses (All Options)

Component	Receive Loss (dB)	Transmit Loss (dB)	Source
Diplexer	0.50	0.60	Wavecom
Redundancy switch	0.30	NA	North American Rockwell TDRSS Report SD73-SA-0018-2
Rigid coaxial cable (diplexer to cable wrap, 5 foot)	NA	0.32	Times Wire and Cable (developed for GEOS) 0.065 dB foot
Rigid coaxial cable (cable wrap to transmitter, 8.25 foot)	NA	0.53	"
Flexible coaxial cable wrap 2 foot	NA	0.13	"
Coaxial connectors	0.10	0.20	
Total (dB)	0.90	1.78	

TABLE L

K_u-Band Data Channel RF Losses

Component	Receive Loss (dB)	Transmit Loss (dB)	Source
Diplexer	0.60	0.60	Sylvania and Wavecom
Redundancy switch	0.20	NA	North American Rockwell TDRSS Report SD73-SA-0018-2
Waveguide (diplexer to rotary joint, 5 foot)	NA	0.45	WR-62 at 0.09 dB/foot
Rotary joint	NA	0.10	MDL, Incorporated
Waveguide (rotary joint to transmitter, 8.25 foot)	NA	0.75	WR-62 at 0.09 dB foot
Total (dB)	0.80	1.90	

An 8.25 foot length of transmission line is assumed from the gimbal axes to the transmitter power amplifier (TWTA). This length may be changed by the designer, depending upon known reflector and transmitter proximity to the spacecraft bulkhead, using the attenuation per unit length given in Tables XLIX and L .

The feed network, polarizer, and comparator losses are included in the overall antenna efficiency and gain calculations (Tables VI, VII, XII, XVI, and XX) so that the reader is cautioned against duplicating these losses during analyses.

It is noted that data channel RF losses are identical for the shared and dedicated receiver cases, except for the shared case using a monoscan tracking receiver. As observed in paragraph 4.6.3.4, monoscan is most suitable in K_u-band; an additional 0.5 dB receive loss would be added for the calibrating phase shifter in the shared case.

Sufficient diplexer isolation must be provided to prevent degradation of paramp (preamplifier) performance, which can occur at drive levels exceeding about -45 dBm. Based on the transmitter power levels specified in Table II and a $(\sin x/x)^2$ power spectral response, it was established that diplexer isolation must be 68 dB and 40.5 dB for the S- and K_u-band, respectively. This S-band diplexer isolation will probably result in increased passband insertion loss and size and weight. This will be further investigated during Phase II.

4.6.3.4 Relative Complexity and Power Consumption

Table LI compares candidate angle sensors on the basis of their quantity of major components. Components not listed in Table LI occur in equal quantities for all candidates and in each frequency band. This comparison considers only the case where the Σ channel is common to both reference and data signals (shared); for the dedicated data channel case, the first three components would be increased by one each.

TABLE LI

Quantity of Major Components

Candidate Sensor	RF Preamp.	Mixer	IF Amp.	PSD/ LPF	RF SPDT	IF SPDT	VID. Amp.	IF LIM Amp.	Monoscan Conv.	Scan. Gen. and Switch Drive
III-A Monoscan (Figure 74)	1	1	1	2	0	0	1	0	1	1
IV Σ/Δ mono-pulse with time-shared Δ (Figure 76)	2	2	2	1	1	1	0	1	0	1
V 2-channel Σ/Δ mono-pulse (Figure 77)	2	2	2	2	0	0	0	1	0	0
VI 3-channel Σ/Δ mono-pulse (Figure 78)	3	3	3	2	0	0	0	1	0	0

Several observations may be made from TableLI: 1) candidate VI requires more components than V because of its additional IF channel (this also means additional primary power consumption and design for an additional gain/phase matched channel for VI); 2) candidates IV and V each require two IF channels (although IV uses one less phase-sensitive detector and low-pass filter (PSD/LPF), its switching and scan circuitry makes it somewhat more complex and power consuming than V); 3) when compared with candidate III-A, V requires an additional gain/phase matched IF channel. However, V does not require a monoscan converter with its switching and scan circuitry. The relative complexity of these candidates is estimated to be about equal; however, III-A will consume more primary power because of its driver and heater (for monoscan converter). From the above observations, candidates III-A and V are preferred over candidates IV and VI.

Based on the tracking feed investigation and analysis of paragraph 4.5.2.1, the dual-mode spiral (or circularly symmetric horn) provides a small, low-loss, S-band feed/comparator assembly which is inherently suitable for the 2-channel Σ/Δ monopulse sensor (candidate V); however, it exhibits a large insertion loss (about 1.3 dB for feed and comparator) in the K_u-band and does not lend itself to an assembly with a dedicated data channel. Whereas a dedicated data channel is unnecessary for the S-band, it is very desirable in the K_u-band so that the sensor feed assembly may be permanently defocused for wide FOV angle tracking capability (without mechanical motion). A five horn/comparator assembly provides a suitable low-loss K_u-band feed network with wide FOV angle tracking and high gain dedicated data channel performance. The sensor feed/comparator portion is inherently suitable for the single channel monoscan angle sensor (candidate III-A).

4.6.3.5 Intermodulation Effects Caused by TWTA Nonlinearities

The return down-link from the TDRS to the GS uses a TWTA operating at saturation for maximum power output and efficiency. TWTA saturation may be characterized by a nonlinear, limiting, input-output response. Sum and difference frequency signals (intermodulation products) will be generated in the presence of more than one frequency. If the intermodulation (IM) products occur in the data signal bandwidth and are relatively large in amplitude, data signal distortion will occur.

In the monoscan angle sensing method (Figure 74), the difference error signals are combined with the sum signal such that amplitude modulated (AM) signals result in a single RF channel. These AM signals are comprised of a carrier, upper sideband, and lower sideband frequencies, so that IM products will be present at the output of a TWTA operating at saturation. If the single RF channel is used for both the monoscan AM and data signals, data signal distortion is possible.

For small angles off boresight, the Σ and Δ RF comparator output signals are given by

$$E_\Sigma = B_1 E_m \cos w_c t ,$$

$$E_{\Delta\phi} \simeq B_2 E_m (\Delta\phi) \cos W_c t, \text{ and}$$

$$E_{\Delta\theta} \simeq B_2 E_m (\Delta\theta) \cos W_c t$$

where, E_m = RF voltage amplitude

$\Delta\phi$ and $\Delta\theta$ = angular deviations from boresight in the two orthogonal track coordinates.

$E_{\Delta\phi}$ and $E_{\Delta\theta}$ are sequentially combined with E_Σ either in-phase or 180 degree out-of-phase, resulting in a square wave AM signal. After filtering out the higher order terms caused by the square wave switching function, the resulting AM signals are:

$$E_{T\phi} = E_{\Sigma} + E_{\Delta\phi} \cos W_m t = B_1 E_m \left[1 + \frac{B_2}{B_1}(\Delta\phi) \cos W_m t\right] \cos W_c t$$

$$E_{T\theta} = E_{\Sigma} + E_{\Delta\theta} \cos W_m t = B_1 E_m \left[1 + \frac{B_2}{B_1} (\Delta\theta) \cos W_m t\right] \cos W_c t.$$

Then $E_{T\phi}$ and $E_{T\theta}$ are AM signals having modulation indices $M_{\phi} = \frac{B_2}{B_1} (\Delta\phi)$ and $M_{\theta} = \frac{B_2}{B_1} (\Delta\theta)$, respectively.

In general,

$$E_T = K [1 + m \cos W_m t] \cos W_c t$$
$$= K \cos W_c t + K \frac{m}{2} \cos (W_c + W_m)t + K \frac{m}{2} \cos (W_c - W_m)t.$$

The sideband terms $(W_c \pm W_m)$ have $m^2/4$ times the power of the carrier (W_c) term. The modulation indices are comprised of:

$\frac{B_2}{B_1}$ = ratio of Δ to Σ channel gain (or losses) from the comparator to the combining point (see Figure 74).

$\Delta\phi$ = ratio of Δ to Σ channel signal levels at the comparator output (ϕ-channel)

$\Delta\theta$ = ratio of Δ to Σ channel signal levels at the comparator output (θ-channel).

In the thermal noise angle error analyses (paragraph 4.6.3.1(4)), $B_2/B_1 = [L_{\Delta}/L_{\Sigma}]^{-1/2} = 11.5$ dB. In the vicinity of boresight, $\Delta\phi = \Delta\theta \leq -23$ dB, so that

$$20 \log_{10} M_{\phi} = 20 \log_{10} M_{\theta} \leq -34.5 \text{ dB}$$

$$\text{or } M_{\phi} = M_{\theta} \leq 1.884 \times 10^{-2},$$

i.e., the modulation indices for $E_{T\phi}$ and $E_{T\theta}$ are 1.884 percent, resulting in carrier-to-sideband power ratios greater than 35 dB. The limiting action of the saturated TWTA will cause the relatively strong carrier to contain essentially all the power when the carrier-to-noise ratio is at least 8 dB (Reference 54) i.e., the results approach the unmodulated carrier case. Also, the TWTA will cause the weak sidebands to be further suppressed by about 5 dB for the above conditions. As the noise level increases, the proportion of the total power consumed by the carrier decreases. In any case, the IM products resulting from the presence of the monoscan AM signal

alone in the saturated TWTA will be negligible. Therefore, if the beacon (carrier) frequency from the user satellite is judiciously selected with respect to the data signal spectrum, IM products resulting from the simultaneous presence of beacon and data signals will occur outside of the data signal bandwidth, and data signal distortion via IM crossproducts will be absent or negligible.

Another aspect of TWTA nonlinear operation is that signal propagation delay through the TWTA will vary with input amplitude, resulting in conversion of signal envelope fluctuations into phase modulation (AM-to-PM conversion). However, in the saturation region of TWTA operation, signal amplitude is held reasonably constant so that AM-to-PM conversion is minimum. Typical power output/phase-shift and AM-to-PM conversion response of communication type TWTA's are shown in Figures 83(a) and 83(b), respectively (Reference 55).

In conclusion, the simultaneous presence of the monoscan AM and data signals in the saturated repeater TWTA will cause negligible IM distortion and AM-to-PM conversion, while providing most efficient performance.

The monoscan AM signal could have been diverted from the Σ channel by combining Σ and Δ beacon signals in a channel exclusive of the data channel (Figure 84), thereby avoiding tracking signal effects in the TWTA. However, when compared with the original monoscan technique of Figure 74, the method of Figure 84 results in the need for some additional hardware (mixer, IF amplifier, LPF, and power divider, as indicated by asterisk).

4.6.3.6 Auto Tracking Via Signal Maximization (Step Track)

In this application, where the angular tracking sector is limited or known to several degrees, a relatively simple and inexpensive angle tracking antenna may be possible with the use of a step-track technique. With this technique (References 56 and 57), the antenna auto tracks by using a stepping algorithm and motor driven linear actuators in the two orthogonal axes of an X-Y or Az-El antenna mount. Step tracking is an automated hill climbing technique for seeking maximum received signal level. As for manual operation, the antenna is alternately moved by an incremental angle in each axis. First, the signal level is sampled and the antenna beam is stepped in one axis. The new level is integrated and compared with the preceding sample to determine the direction of the succeeding angular step. Hence, step tracking shifts the burden of constant operator attention and judgement to that of an algorithm logic circuit, which seeks the antenna beam maximum by observing signal level changes associated with a step and making decisions based on the observed changes.

Although the use of step tracking has not been thoroughly investigated for the TDRSS application, this technique has been and is being developed for various applications by Harris Intertype (Radiation/Division), Scientific Atlanta, Incorporated, and Philco (WDL). An X-band ground

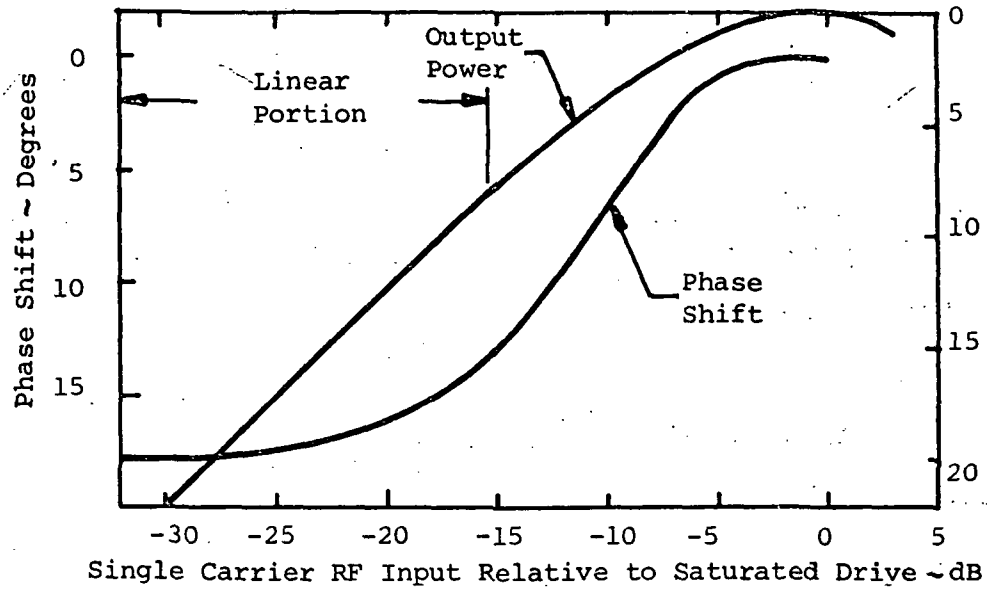

(a) Typical power output and phase shift as a function of rf input power for communication type TWT.

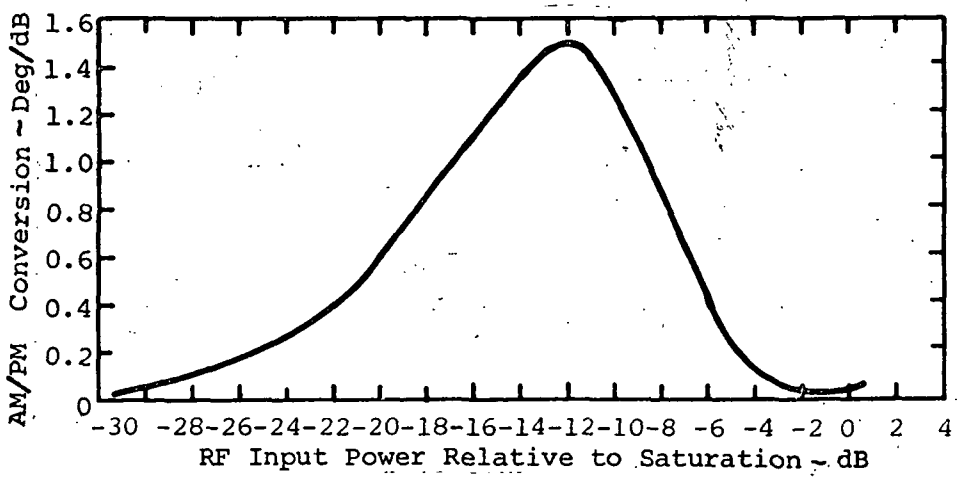

(b) Typical single carrier AM/PM conversion.

Figure 83. Characteristics of Space Communication Type TWTA's

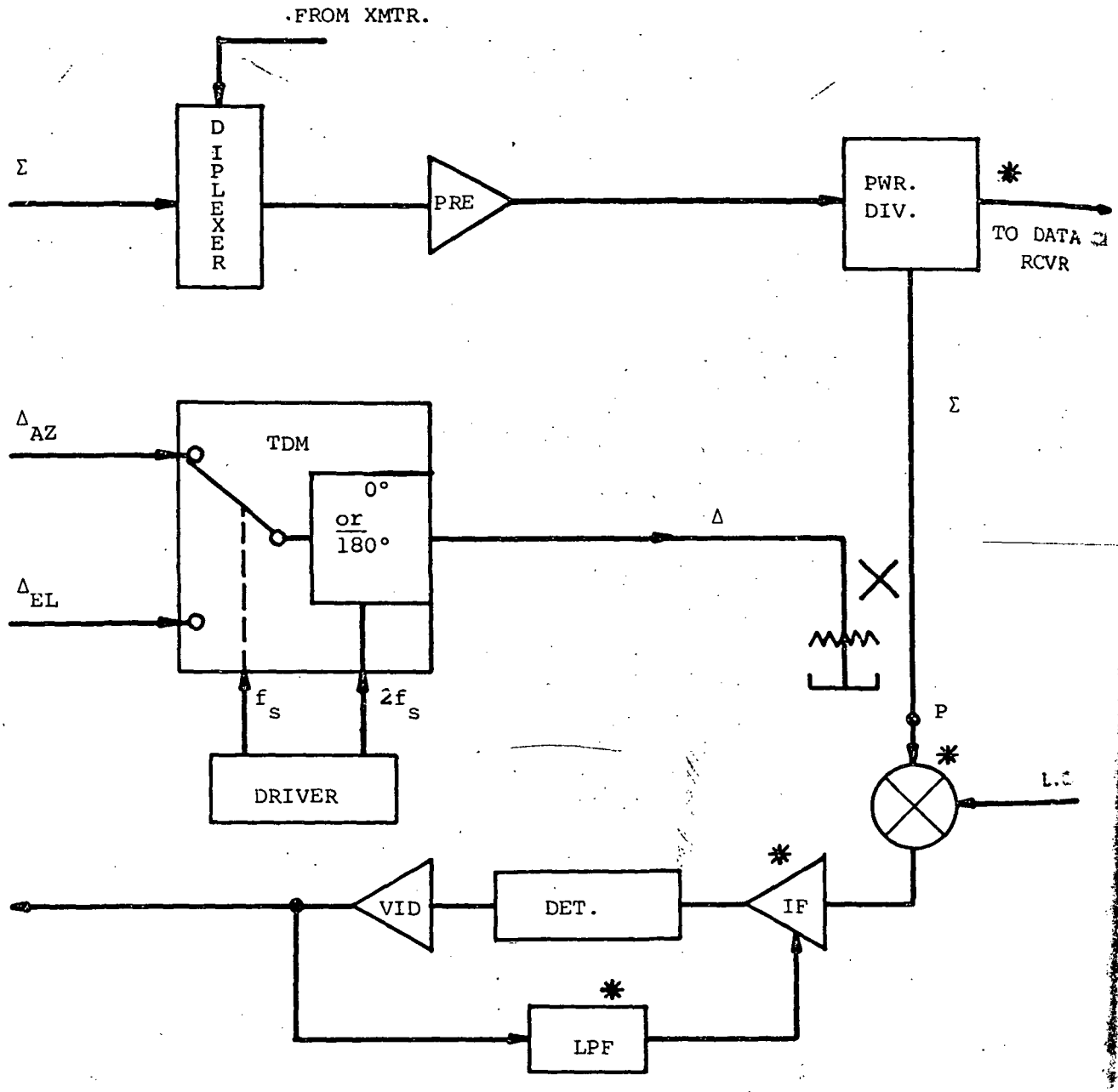

Figure 84. Alternative Monoscan Circuit with Common RF Tracking/Data Channel, for Avoiding IM Product Effects in Shared Data Channel

terminal system developed for the U.S. Army SatCom Agency has achieved a 3σ tracking accuracy corresponding to a ±0.5 dB link degradation without windloading (Reference 58). The achievable performance with step tracking depends on the selected hill climbing algorithm, the angular step size, the sampling frequency, and the integration time interval, in addition to the received SNR. The minimum sampling frequency will depend on satellite dynamics and antenna beamwidth. Integration time can be increased for improved performance with low SNR, at the expense of tracking rate. The type of ground station angle tracking receiver (correlation or coherent) will depend on received SNR level.

A block diagram of the step track servo electronics used by Radiation, Incorporated is shown in Figure 85. Here the dc voltage input to the servo electronics is the AGC voltage output of a PSK beacon receiver. The filtering (integration) time is selected to give good performance with low SNR (of the AGC monitor signal input) without introducing errors between samples. The sample-and-hold circuit samples the measurement of signal strength and holds it for comparison with the next measurement. The comparator compares successive signal strength measurements and determines the direction of antenna movement. The drive control provides selection and drive to the antenna drive motors. The tracking algorithm is the sequence of sampling signal strength, moving the antenna, and comparing that signal strength sample with the previous one to determine the direction of antenna movement to maximize signal strength. The timing circuit produces the algorithm. Radiation, Incorporation, claims (Reference 56) that a low SNR signal may be tracked with a probability of greater than 95 percent to within a tracking accuracy of 0.3 beamwidth.

Although an analysis of the achievable step tracking accuracy was not performed during this investigation, the foregoing references indicate that it may be a viable candidate for the ground and TDRS terminals. As such, its use would simplify the feed and angle sensing networks aboard the TDRS and the feed network at the ground station. It may also be possible to perform angle tracking via the data signal at the ground terminal, thereby further simplifying TDRS down-link equipment. In this application, the TDRS data beam would be pointed via program track toward the user, and step track operation would then commence about the nominal program track pointing direction.

A potential disadvantage of this technique is that short term fluctuations on the signal being tracked may result in erroneous angle tracking, as may be encountered with conical scanning. The stepping process also results in amplitude modulation on the data signal. The additional power required aboard the TDRS for stepping the antenna must also be investigated.

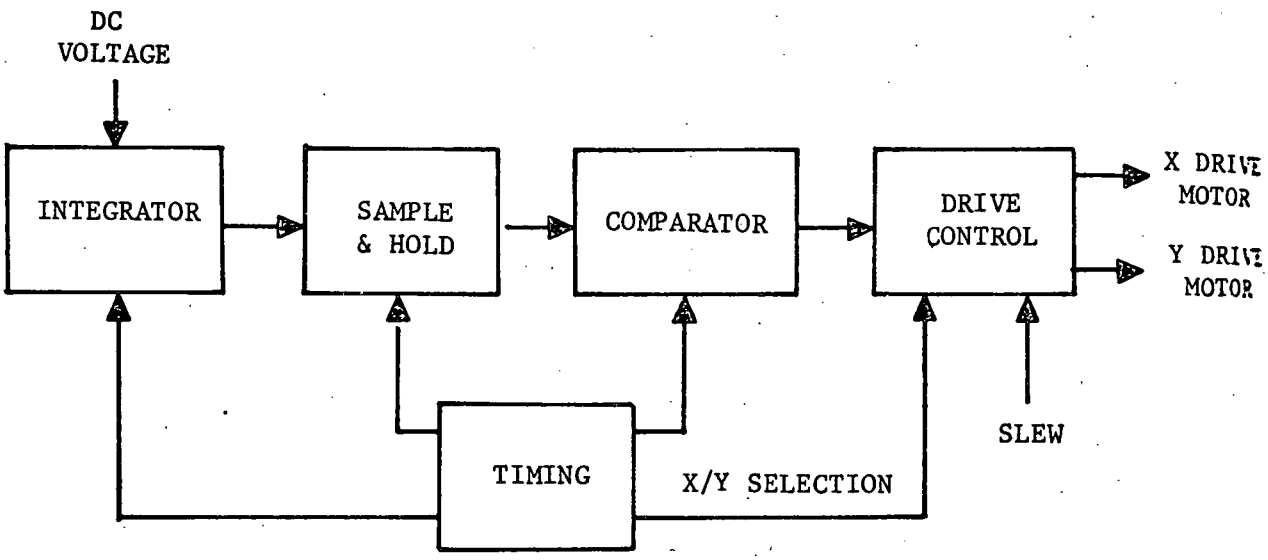

Figure 85. Step Track Servo Electornics

4.6.4 Selection of Angle Tracking Receiver

Various criteria used in evaluating the candidate angle sensors, following the first screening (paragraph 4.6.2), were:

1 Thermal noise angle error (paragraphs 4.6.3.1 and 4.6.3.2);

2 Adaptability to ground station angle tracking (paragraph 4.6.3.2 and Appendix I);

3 Data channel insertion losses (paragraph 4.6.3.3);

4 Relative complexity and power consumption (paragraph 4.6.3.4);

5 Intermodulation effects (paragraph 4.6.3.5).

The choice of baseline angle sensors, based on the above criteria, are as follows:

1 S-Band - 2-Channel Σ and Δ monopulse (candidate V, Figure 77), with a dual-mode four-arm spiral feed comparator assembly at primary focal point of reflector;

2 K_u-Band - Single channel monoscan (candidate III-A, Figure 74), with a five-horn feed/comparator assembly at secondary focal point of reflector; focused central element feeds dedicated data channel, and defocused peripheral elements for wide FOV angle sensor.

The S-band angle error signal processing must be performed with coherent receiver detection because of the small SNR received from the users. The wide FOV K_u-band feed network degrades the Σ channel SNR received from the users such that coherent processing may be desirable to permit further reduction in user power.

It is finally noted that the above selection is subject to the fact that thermal noise angle error, when combined with all other errors, results in an acceptable degradation of the data signal; this is treated in paragraph 4.7.1.

4.7 Data Signal Loss Resulting From Beam Pointing Errors

Error contributions in data beam pointing were discussed in section 4.4, and expressions for calculating these error components were derived for both auto tracking and ground command methods of data link maintenance (DLM). The calculation of data beam pointing errors, for various combinations of DLM methods and K_u-and/or S-band data links, were performed and are provided as design data in this section.

For auto tracking, design data are presented to allow the TDRSS designer the flexibility of tradeoffs between user beacon power and servo noise bandwidth, when processing either aboard the TDRS or at the ground station.

Data beam pointing errors for the various links, when using either autotrack or ground command DLM, result in a reduction of data channel antenna gain. This gain reduction is then directly translatable into a corresponding loss of data signal power.

4.7.1 Antenna Gain Reduction as Function of Data Beam Pointing Error

Figure 86 shows the antenna main lobe gain response as a function of normalized angle away from the main lobe peak for several different aperture amplitude illumination functions. Figure 86 shows that the various illuminations result in responses that are nearly equivalent to a gaussian pattern for $|\theta/\theta_3| \leq 0.6$; furthermore, a uniform illumination results in a response that is nearly equivalent to that of other representative illuminations for $|\theta/\theta_3| \leq 0.9$. The three aperture illuminations and resulting responses considered for a circular aperture (diameter D) are as follows. (References 59 and 60):

1 Uniform: $P_c(\mu) = 10 \log_{10} [\Lambda_1 (\pi D\mu)]^2$

$$= 10 \log_{10} \left[\frac{2 J_1 (\pi D\mu)}{(\pi D\mu)}\right]^2 \quad ; D_u \simeq 1.02 \frac{\theta}{\theta_3}$$

2 Bessel-on-10dB pedestal:

$$P_c(\mu) = 10 \log_{10} \left[0.3162 \quad \Lambda_1 (\pi D\mu) + \frac{1.710 \ \Lambda_0 (\pi D\mu)}{5.784 - (\pi D\mu)^2}\right]^2; \ D_u \simeq 1.14 \frac{\lambda}{D}$$

3 $0.5 + 0.5 [1 - (2\rho/D)^2]^2$:

$$P_c(\mu) = 10 \log_{10} [0.5 \Lambda_1 (\pi D\mu) + 0.1667 \ \Lambda_3 (\pi D\mu)]^2; \quad D_u \simeq 1.106 \frac{\lambda}{D}$$

Since a gaussian response is representative of those resulting from typical circular aperture illuminations in the vicinity of main lobe peak, its relatively simple analytical form may be used for accurately estimating data signal loss. The gaussian response is

$$P(\theta) = P(0) \exp [-2.77 (\theta/\theta_3)^2]$$

or

$$\frac{P(\theta)}{P(0)} = 10 \log_{10} e^{-2.77 (\theta/\theta_3)^2} \ \text{dB}$$

$$= 12.03 (\theta/\theta_3)^2 \ \text{dB}$$

Hence, if the total 3σ angle track error was $\alpha = 0.204 \theta_3$, or $\alpha/\theta_3 = 0.204$, the resulting data signal loss will be 0.5 dB; this may also be determined directly from Figure 86.

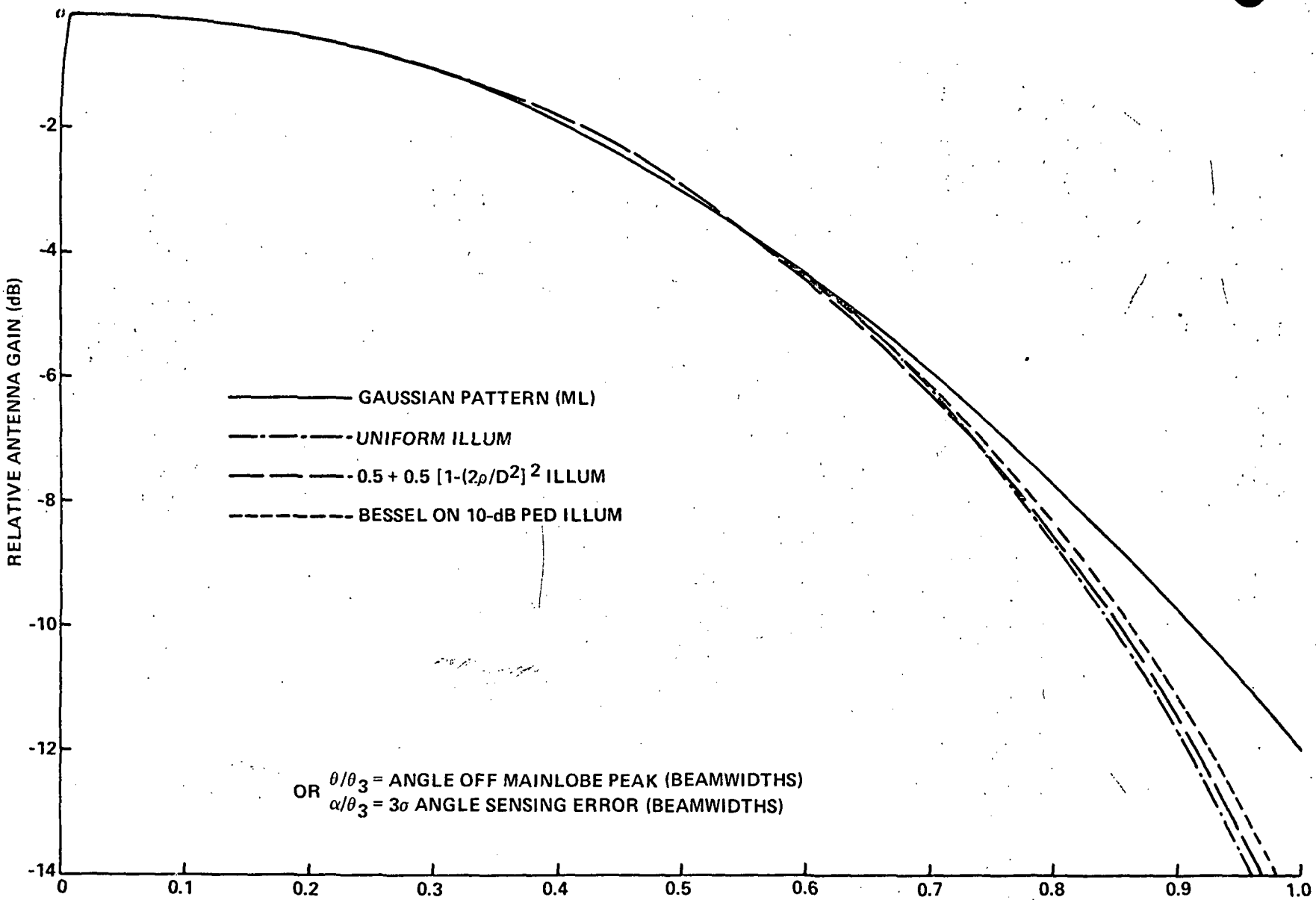

Figure 86. Antenna Gain Drop-Off Versus Angle Off Main Lobe Peak

4.7.2 Pointing Errors and Signal Loss Using DLM Via Auto Tracking

DLM via auto tracking may be performed in the K_u- and/or S-bands, as outlined in section 4.4 (Table XXIX), depending on the available user beacon frequency. The errors are defined in Table XXXI. When the data link operates in K_u-band only, or in both K_u- and S-bands, reflector pointing via K_u-band auto track (RP/K-AUTO) is applicable. The associated S-band feed configurations may take on any one of Options I, II, or III. When the data link operates in S-band only, reflector pointing must be performed via S-band auto tracking (RP/S-AUTO, Option II).

For RP/K-AUTO DLM, it is assumed that the tracking feed is permanently defocused to assure a sufficiently wide field of view (FOV) for the acquisition process. It is further assumed that a dedicated, high-gain data channel is used. For non-coherent angle processing aboard the TDRS, the monoscan angle tracking technique (paragraph 4.6.3.1, Figure 74) is used; for coherent angle processing at the ground station, the Δ and reference signals derived from the comparator are appropriately modulated and transmitted to the ground station via the K_u-band down-link. Figures 87 and 88 give the 3σ data beam pointing error for the K_u-band data link, α(DATA, K) as a function of servo noise bandwidth (β_n) for TDRS and ground station processing, respectively, with SNR as a variable. It is observed that, with TDRS processing, $10^{-7} \leq T_d/J \leq 10^{-2}$ sec^{-2} is assumed and that only the upper values are plotted in Figure 87; α(DATA, K) $\leq$ 0.08 degree ($\alpha/\theta_3 \leq 0.204$) is the maximum pointing error allowable to maintain data signal loss $\leq$ 0.5 dB.

Figures 89 and 90 give the 3σ data beam pointing error (as a function of servo noise bandwidth for an S-band data link, for TDRS and ground station processing, respectively, when using the RP/K-AUTO DLM method. For these cases, the tracking error component α(DLM, BS, K) is the same as for the K_u-band data link; however, the data beam offset/boresight error component α(DBO, BS, S) differs from that for K_u-band. The maximum data beam offset/boresight error, occurring for the Option II S-band feed configuration, was used in Figures 89 and 90. It is observed that α(DATA, S-II) $/\theta_3 << 0.204$ for either TDRS or ground station processing, so that considerable design freedom may be exercised before encountering a maximum data signal loss of 0.5 dB.

Figure 91 gives the 3σ data beam pointing error α(DATA, S-II) versus β_n, when using the RP/S-AUTO DLM method with ground station processing. It is observed, e.g., that a $\beta_n \leq 1.0$ Hz permits an α(DATA, S-II) $/\theta_3 <$ 0.204 with SNR = -22 dB and, thereby, a data signal loss of <0.5 dB.

4.7.3 Pointing Errors and Signal Loss Using DLM via Ground Command

Data beam pointing errors resulting from reflector pointing and feed positioning via ground command (RP/GC and FP/GC DLM methods, respectively) were established in paragraphs 4.4.2 and 4.4.3. The 3σ data beam pointing errors for RP/GC are summarized in Table XXXIV, the 3σ data beam pointing

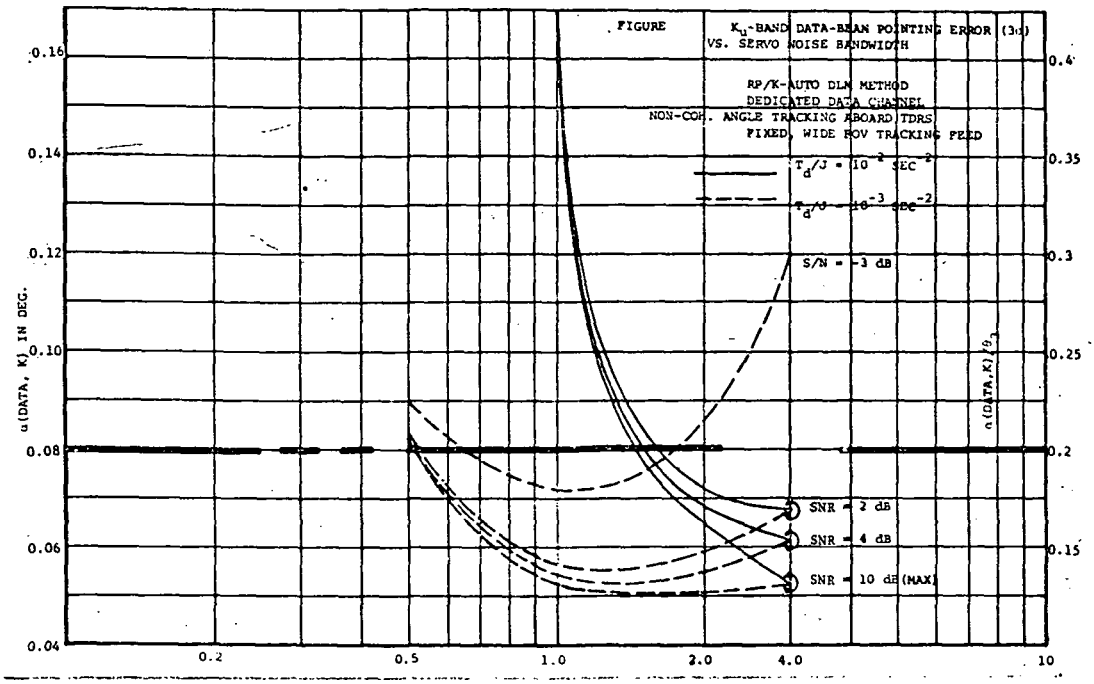

Figure 87. K_u-Band Data Beam Pointing Error (3σ) Versus Servo Noise Beamwidth - Non-Coherent Tracking Aboard TDRS

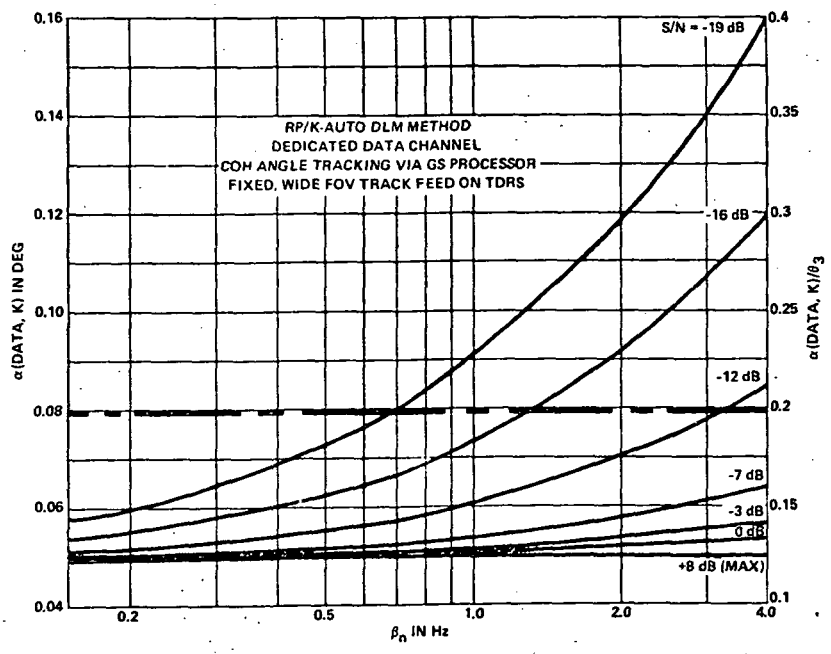

Figure 88. K_u-Band Data Beam Pointing Error (3σ) Versus Servo Noise Bandwidth - Coherent Angle Tracking Via Ground Station Processor

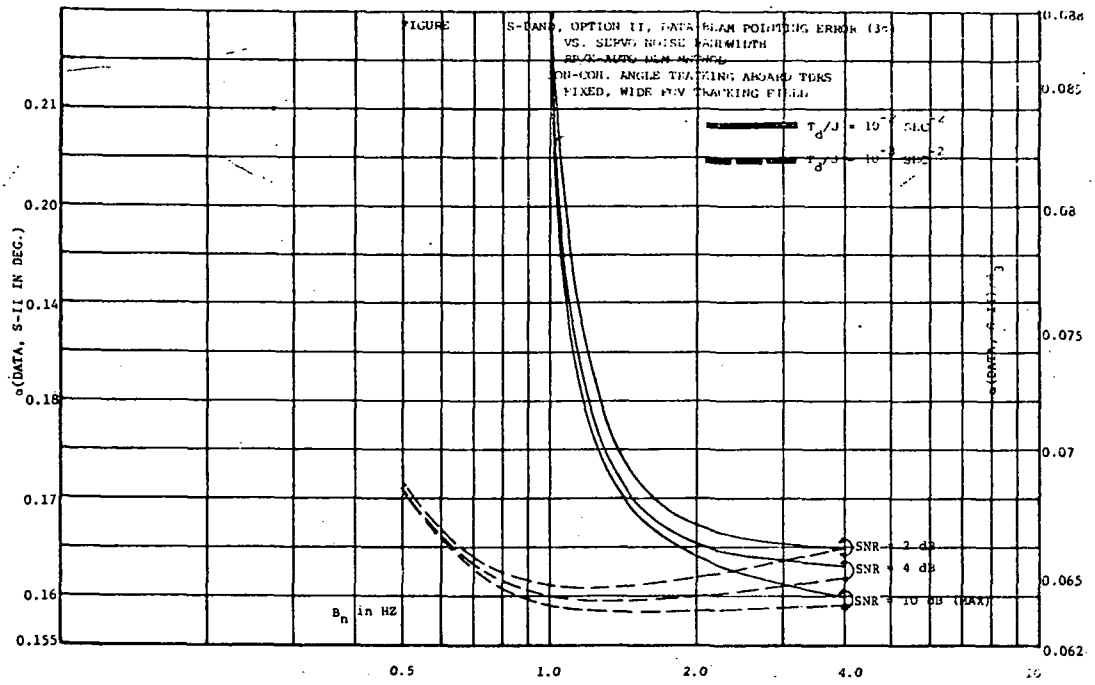

Figure 89. S-Band, Option II, Data Beam Pointing Error (3σ) Versus Servo Noise Bandwidth - Non-coherent Angle Tracking Aboard TDRS

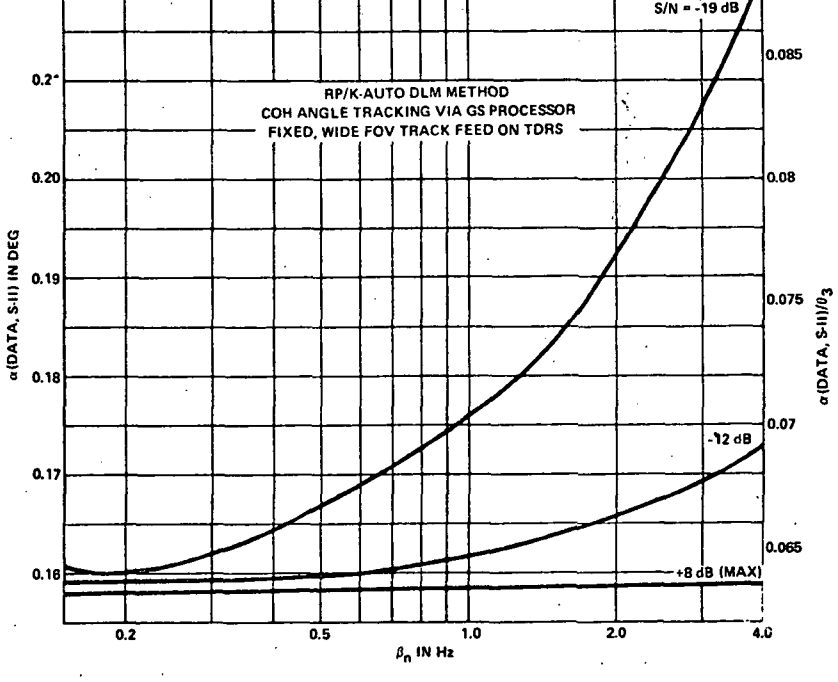

Figure 90. S-Band, Option II, Data Beam Pointing Error (3σ) Versus Servo Noise Bandwidth - Coherent Angle Tracking Via Ground Station Processor

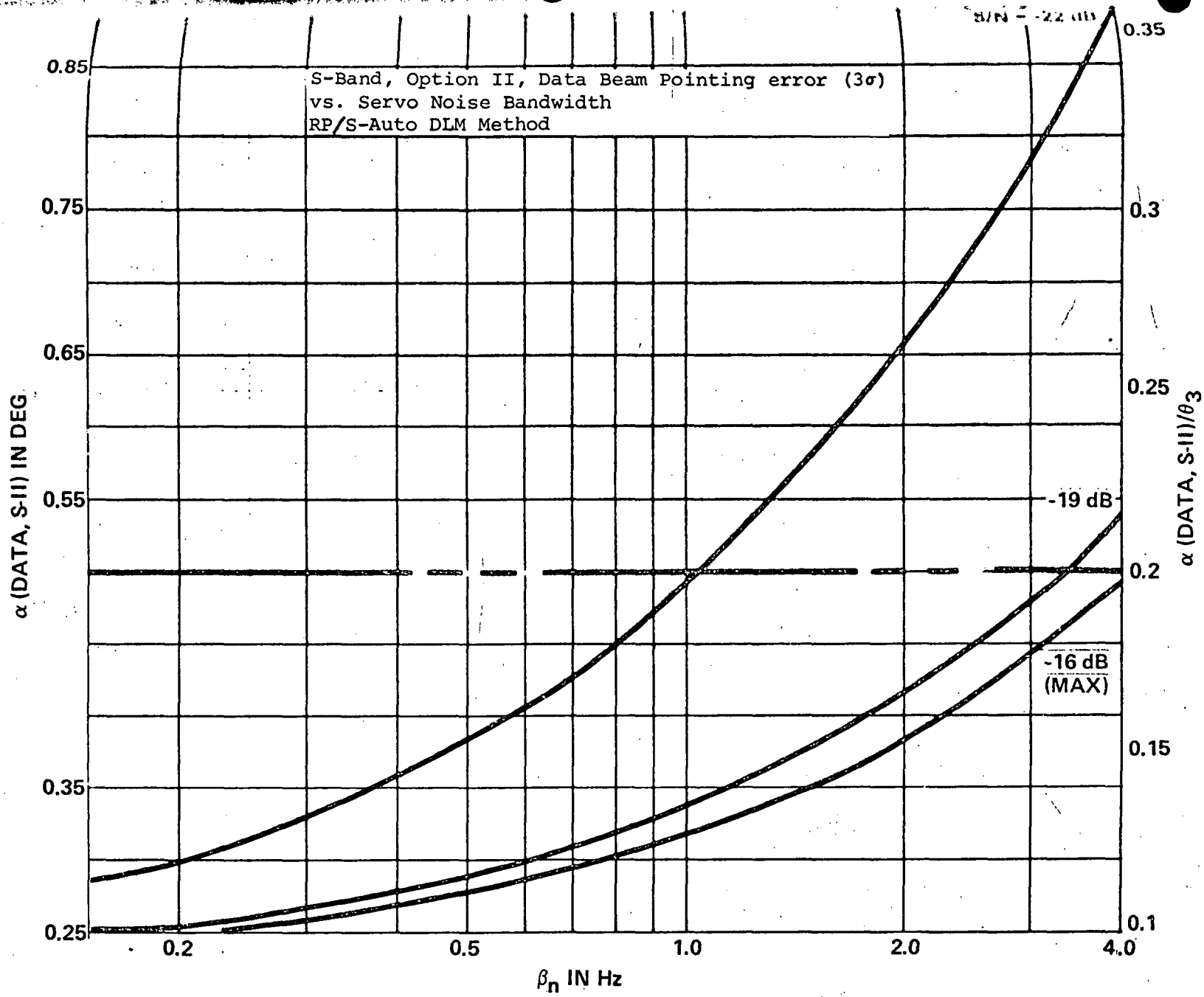

Figure 91. Coherent Angle Tracking Via Ground Station Processor

error associated with FP/GC was shown to be 0.59 degree. These errors are repeated in Table LIIalong with their associated data signal losses resulting from the effective reduction of data-channel antenna gain. The pointing error for the K_u-band data link assumes the use of a dedicated data channel (as was assumed for the auto tracking case, paragraph 4.7.2). The data signal losses of Table XXXIV; the 3 data beam pointing degree and 2.5 degrees for the K_u-band and S-band, respectively.

TABLE LII

Data Signal Loss in RP/GC and FP/GC DLM Methods

DLM Method	3σ Data Beam Pointing Error (± Degree)	Data Signal Loss (dB)
RP/GC	α(DATA, K) = 0.45	>15.22
	α(DATA, S-I) = 0.45	0.39
	α(DATA, S-II) = 0.47	0.42
RP/GC(*)	α(DATA, S-III (*) = 0.45	0.39
FP/GC	α(DATA, S-III) = 0.59(Max)	0.67 (Max)
	= 0.45(Min)	0.39 (Min)

4.7.4 Summary

When non-coherent angle auto tracking is performed aboard the TDRS with the RP/K-AUTO DLM method, minimum data beam pointing error is achieved for $\beta_\eta \simeq 1$ Hz (torque disturbance factor $T_d/J = 10^{-3}$); pointing error decreases significantly with T_d/J, and $T_d/J \lesssim 10^{-3}$ is recommended to assure $\beta_\eta \leq 2\ f_r/3$ ($f_r = 2$ to 4 Hz). Figures 87 and 89 summarize the design data for TDRS angle tracking, for RP/K-AUTO DLM of K_u-band and S-band data links, respectively. For either K_u-band or S-band links, the user beacon SNR (into the TDRS angle tracking reference channel may be significantly reduced below SNR = 10 dB (max) without exceeding $\alpha/\theta_3 \leq 0.204$, i.e., corresponding to data signal loss ≤ 0.5 dB. This means that the user beacon EIRP may be reduced correspondingly with SNR. Hence, angle tracking via ground station coherent processing need not be required with the RP/K-AUTO DLM method unless some unforeseeable advantages in TDRS and/or user hardware and/or reliability can be achieved in the total TDRSS design. Figures 88 and 90 summarize the design data for coherent angle tracking via the ground station for RP/K-AUTO DLM of K_u-band and S-band links, respectively. The maximum SNR = 8 dB at the ground station receiver input allows a 2 dB tandem link degradation and T_d/J is reduced to a negligible value by servo loop design.

With the RP/S-AUTO DLM method, the maximum user beacon SNR = -14 dB in the TDRS tracking receiver noise bandwidth (150 kHz). With non-coherent angle tracking aboard the TDRS, an SNR = -14 dB results in a marginally acceptable data beam pointing error, assuming that the phase detector could perform sufficiently well as this SNR level. Furthermore, this allows no design flexibility in reducing user beacon power. Hence, the use of coherent angle tracking via the ground station is desirable for tracking S-band (only) users. Figure 91 summarizes the design data for S-band auto tracking via the ground station. A maximum SNR = -16 dB at the ground station receiver input is used, allowing a 2 dB tandem link degradation, and T_d/J is reduced to a negligible value by servo loop design. The lowest SNR considered was -22 dB, which may be used for $\beta_\eta \lesssim 1$ Hz. This is near the minimum lock-on SNR (-23.7 dB) estimated for the S-band coherent phaselock loop receiver (paragraph 4.6.3.2).

The above data beam pointing errors occurring during autotrack do not include angular displacement between the reflector axis and the direction of the data beam maximum. However, this error (last column of TableXXXI) results in a negligible data signal loss.

From Table LII, data signal losses resulting with the RP/GC DLM method are acceptable for S-band links (all options) but are totally unacceptable for K_u-band.

The FP/GC DLM method for S-band (option III) results in a data signal loss, which is larger than the 0.5 dB design goal of Table XLIV

(3σ angle sensing accuracy $\leq \pm 0.2\ \theta_3$). This loss results from conservative estimates of error contributions (paragraph 4.4.2) and may be reduced if necessary.

Finally, when considering the total data signal losses incurred, losses resulting from both data beam pointing error and from attenuation/reflection in the RF data channel (paragraph 4.6.3.3) are of interest. From Table XLIV the combined data signal loss from both of these sources must be $\leq$ 2.5 dB. When the RF data channel losses (Tables XLIX and L are weighed in light of those resulting from data beam pointing errors, it is observed that there is adequate design margin for meeting the combined requirement of $\leq$ 2.5 dB loss.

4.8 Characterization of Designation and Aided Designation Methods

Some introductory thoughts regarding designation and aided designation were set forth in section 4.3. It was noted there that designation refers to the activities which must take place prior to the establishment of a bent pipe data link. Attention is therefore to be centered on data link maintenance methods RP/K-AUTO and RP/S-AUTO. The specific item of interest is the compatibility of the field-of-view (FOV) of the angle-sensing system and the angular uncertainty with which its boresight axis is positioned as a result of designation.

In an auto tracking antenna system, there is some value of the angular separation between the direction of signal arrival and the boresight axis such that closing the auto tracking loop will cause that angular separation to diminish, with essentially unity probability. Twice the value of that angle is defined to be the FOV of the autotracker.

According to the definitions given in section 4.3, the act of aiming the boresight axis of the auto tracking system by pointing the reflector axis in a given direction via ground command is referred to as designation. If the resulting boresight axis direction precision is unsatisfactory, then a designation-aid system must be employed. Such a system would serve to improve the boresight axis pointing accuracy to the extent required for compability with the FOV of the angle sensor.

Based on the foregoing discussion, the boresight designation accuracy is defined as the 3σ angular separation of the direction in which the boresight axis of the autotracker is pointed (as a result of designation from the ground) and a line which connects the TDRS and user spacecraft. The angular separation of the reflector axis and the TDRS/user line-of-sight associated with RP/GC was shown in paragraph 4.4.2 to be $\alpha(\text{REF,DES}) = 0.45$ degree. When this value is combined with the angular displacement of the boresight and reflector axes, the boresight designation error will result. This computation is carried out in paragraph 4.8.1, where it is concluded that the K_u- and S-band angle-sensing data link maintenance systems must exhibit an FOV of at least 0.9 degree, with 1.2 degrees as a recommended value.

It is shown in paragraph 4.8.2.1 that even for large values of sum channel SNR, the FOV of the K_u-band system is insufficient. This assertion is based upon both a theoretical prediction and experimental evidence. An increase in the FOV from 0.8 to 1.2 degrees by means of K_u-band feed system defocusing is suggested as discussed in section 4.6.

Paragraph 4.8.2.2 presents an analysis of the FOV of a sum and difference auto tracking system in which locally generated noise is present. For the case in which the user spacecraft transmits a CW signal, both non-coherent and coherent processing of the received signal is considered. It is shown that, subject to a particular product detector model, the FOV of the auto tracking system is not impaired by operation at small values of SNR. Therefore, neither the S nor the K_u-band data link maintenance schemes require aided designation.

However, it is shown in paragraph 4.8.3 that two aided designation techniques are also compatible with the FOV of the K_u-band data link maintenance system: 1) the systematic search of a given spatial region with a K_u-band pencil beam and 2) the use of the S-band autotracker employed (solely in Option II) for data link maintenance.

4.8.1 Boresight Designation Error

It was pointed out above that the boresight designation error results from the combined effect of $\alpha(REF,DES) = 0.45$ degree and the angular separation of the reflector and boresight axes. In the case of K_u-band auto tracking, the latter component was shown in paragraph 4.4.1.2 (under the heading $\alpha(DBO,BS,S\text{-}I)$) to have a 3σ value of $0.03\sqrt{1 + (2.46\theta_{3,K})^2}$. The K_u-band boresight designation error is therefore given by $\alpha(BS,DES,K) = 0.45\sqrt{1 + (0.16\theta_{3,K})^2}$, where the symbol was obtained from Figure 32. As will be seen, the values of $\theta_{3,K}$ of interest will results in $\alpha(BS,DES,K) \simeq 0.46$ degree.

When S-band auto tracking is considered, the angular separation of the reflector and boresight axes results from placement of the feed system during manufacture (0.048 degree feed deflection due to solar heating (0.008 degree) and boresight shift due to pre-comparator unbalance ($0.028\ \theta_{3,S} = 0.075$ degree). The corresponding rss value is 0.089 degree so that the S-band boresight designation error becomes $\alpha(BS,DES,S) = 0.45$ degree.

It is clear from the above results that the K_u- and S-band angle sensing data link maintenance systems must exhibit an FOV of at least 0.9 degree. Since the error, $\alpha(REF,DES) = 0.45$ degree, dominates both boresight designation errors and it has a maximum sum value of approximately 0.85 degree (see Table XXXII), it seems reasonable to require an FOV of the order of 1.2 degree with the exact value to be chosen on the basis of pertinent tracking performance characteristics.

4.8.2 Field of View of Auto Tracking System

In the material which follows, an investigation is first made of the FOV of a conventional sum/difference angle sensing system in the absence of noise. Next, the impact of feed system defocusing on the FOV is postulated. Then, receiver-generated noise is introduced into the system model, and its effect on FOV is examined for both non-coherent and coherent detection.

4.8.2.1 FOV in the Absence of Noise

The method to be employed in formulating the field of view of an angle sensing antenna is to examine the angle sensor output voltage as a function of off-boresight angle, i.e., the antenna difference pattern normalized by the sum pattern.

The antenna is modeled as a linear aperture illuminated to produce squinted far-field patterns. The aperture amplitude distribution has the form $\cos(\pi x/a)$, where a is the aperture length. The antenna pattern squint is, of course, produced by a linear phase function. Two mirror-image antenna patterns, $g(\theta)$ and $g(-\theta)$ result. The functional form of $g(\theta)$ is

$$g(\theta) = \frac{\cos\left[\frac{\pi a}{\lambda}(\sin\theta - \sin\theta_M)\right]}{1 - \left(\frac{2a}{\lambda}\right)^2 (\sin\theta - \sin\theta_M)^2} \qquad (1)$$

where θ_M is the value of θ at which $g(\theta)$ is maximized. The crossover level, i.e., the value of $g(0)$ relative to $g(\theta_M)$, was chosen to be $1/\sqrt{2}$ in keeping with typical angle sensor characteristics.

The patterns $g(\theta)$ and $g(-\theta)$ are shown in Figure 92 along with the sum pattern defined by

$$\Sigma(\theta) = \frac{1}{\sqrt{2}}(g(\theta) + g(-\theta))$$

and the angle output function $\Delta(\theta)/\Sigma(\theta)$,
where

$$\Delta(\theta) = \frac{1}{\sqrt{2}}(g(\theta) - g(-\theta)).$$

(Also, Equation (1) has been normalized so that $g(0) = 1/\sqrt{2}$ for reasons discussed below). A normalized angular scale θ/θ_3 has been used to make the results universal. The pre-comparator half-power beamwidth θ_3 is related to the aperture size and operating wavelength by $\theta_3 = 1.2(\lambda/a)$, where $a >> \lambda$.

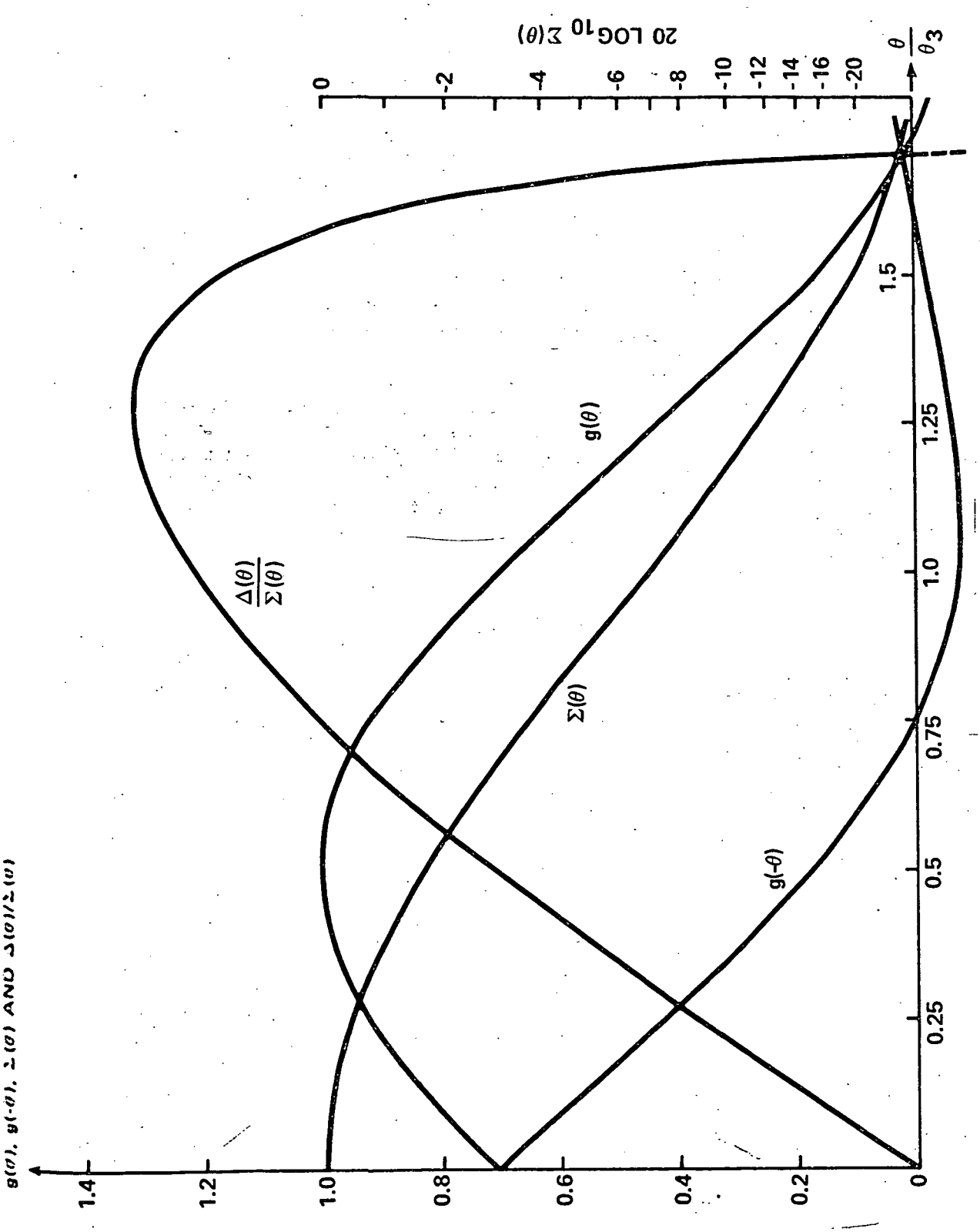

Figure 92. Pre-Comparator Antenna Patterns and Associated Sum Channel and Angle Output Functions

Several interesting observations results from an inspection of Figure 92. First, the total unambiguous range of the angle output function is seen to be $\theta \approx 3.4\theta_3$. This value results, of course, from $\Delta(\theta) = 0$. Next, it is seen that the value of $\Delta(\theta)/\Sigma(\theta)$ is a reasonably linear function of off-boresight angle over the angular region $\theta \leq 2.5\theta_3$. The latter angle is defined as the usable FOV in the noise-free case*. Also, if the sum channel signal-to-noise ratio in the boresight direction were sufficiently large to offset the ≈ 12 dB sum channel gain reduction at $\theta = 1.25\theta_3$, then the FOV would remain the same. The final observation is that the slope of the angle output function at boresight is given by

$$\frac{\partial}{\partial\theta}\left[\frac{\Delta(\theta)}{\Sigma(\theta)}\right]_{\theta = 0} = \frac{1.04}{\theta_3} .$$

Before proceeding further, it seems worthwhile to justify the use of the cosine aperture amplitude distribution on a linear aperture selected for the foregoing analysis. That is, one may question its validity in a realizable antenna system. The advantage of using the subject distribution is the relative mathematical simplicity of the resulting far-field pattern. Moreover, the far-field pattern produced by a cosine illumination function on a linear aperture closely approximates the patterns produced by a circular aperture with typical illumination, as can be seen from Figure 93.

To relate the FOV to an existing antenna system, the NASA 40-foot diameter ATS Tracking Facility at Mojave, California, was selected because of its similarity, with appropriate scaling, to the baseline TDRS concept. Table LIII compares several pertinent characteristics of the two antenna systems, both of which employ a cassegrain subreflector illuminated by a square array of polyrod antennas.

The FOV of the ATS antenna quoted in Table LIII was obtained from measurements carried out by Martin Marietta personnel and approved by members of the GSFC (Reference 61). One of the results of these measurements is shown in Figure 94, the angle sensor output voltage measured with horizontal polarization at 4.178 GHz under essentially noiseless conditions. No measured data was recorded for off-axis angles in excess of one beamwidth (of the sum channel beam), so it can be seen that the FOV is at least twice this value. Table LIII shows that the inferred FOV of the TDRS antenna, with the specified characteristics listed therein, is at least 0.79 degree. This value is consistent with the theoretical prediction of 0.91 degree made above.

*With an operating frequency of 14.3 GHz and an aperture diameter of 12.5 feet, it is the case that $\lambda/D = 5.51 \times 10^{-3}$. For a typical aperture illumination function, the pre-comparator beamwidth is $66(\lambda/D)$ degrees or, for the case of interest, 0.364 degree. The resulting FOV is 2.5 x 0.364 = 0.91 degree.

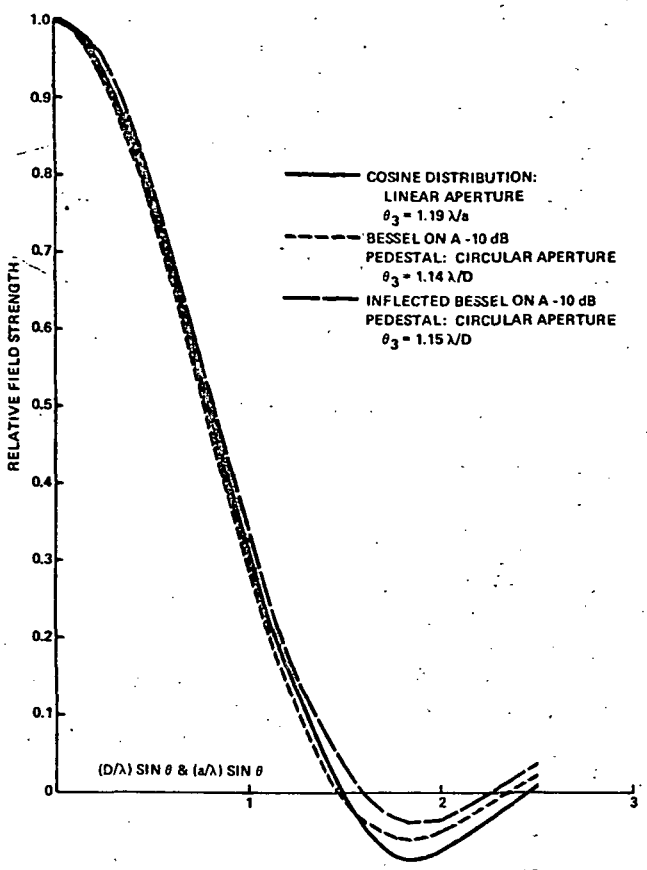

Figure 93. Far-Field Patterns Produced by Various Aperture Distributions

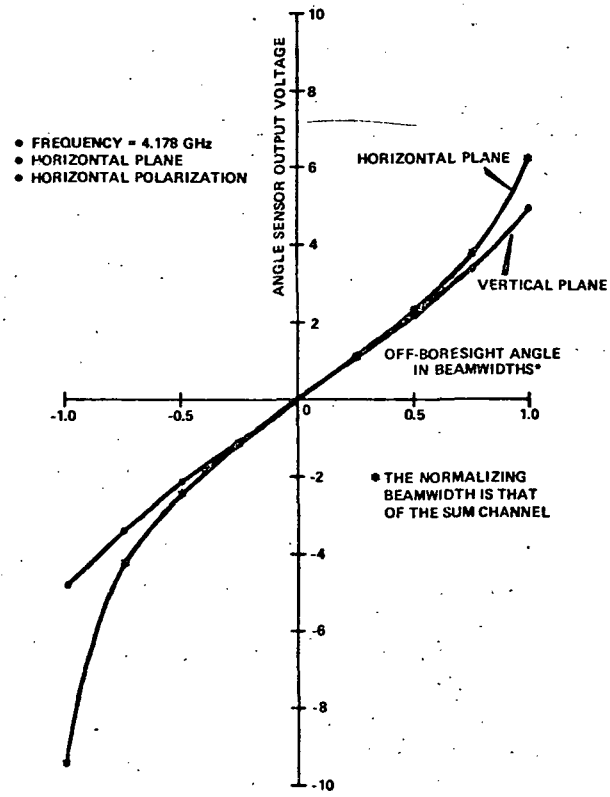

Figure 94. Angle Sensor Output Voltage as a Function of Off-Boresight Angle: ATS Tracking Facility

TABLE LIII
ATS and TDRS Antenna Systems Comparison

Characteristic	Antenna	
	ATS Tracking Facility	TDRS
Operating frequency	4.178 GHz*	14.3 GHz
Wavelength	2.83 inches	0.826 inch
Diameter	40 feet	12.5 feet
λ/D	5.89×10^{-3}	5.51×10^{-3}
f/D (main reflector)	0.4	0.4
Equivalent f/D	1.89	1.66
Sum-channel Half-power beamwidth, $\tilde{\theta}_3$	0.424 degree	$72\ (\frac{\lambda}{D}) = 0.397$** degree
$K = (\frac{D}{\lambda})\ \tilde{\theta}_3$	72	-
FOV	At least $2\tilde{\theta}_3$	$2\tilde{\theta}_3 = 0.79$**

* The ATS Tracking Facility operates over a relatively broad frequency range. The subject frequency was selected arbitrarily.

** These values are inferred from the performance of the 40-foot antenna.

The horizontal plane sum and difference patterns of the ATS antenna, measured at 4.178 GHz with horizontal polarization, are shown in Figure 95. It appears, from these data, that the angle sensor output is ambiguous at an angle slightly greater than one sum channel beamwidth from the boresight axis.

In summary, the FOV of the K_u-band auto tracking system is approximately 0.8 degree in the absence of perturbing noise. It was shown in paragraph 4.8.1 that the FOV must be at least 0.9 degree and that a value of about 1.2 degrees appears to be appropriate in terms of a reasonable safety factor. The use of defocusing of the K_u-band antenna

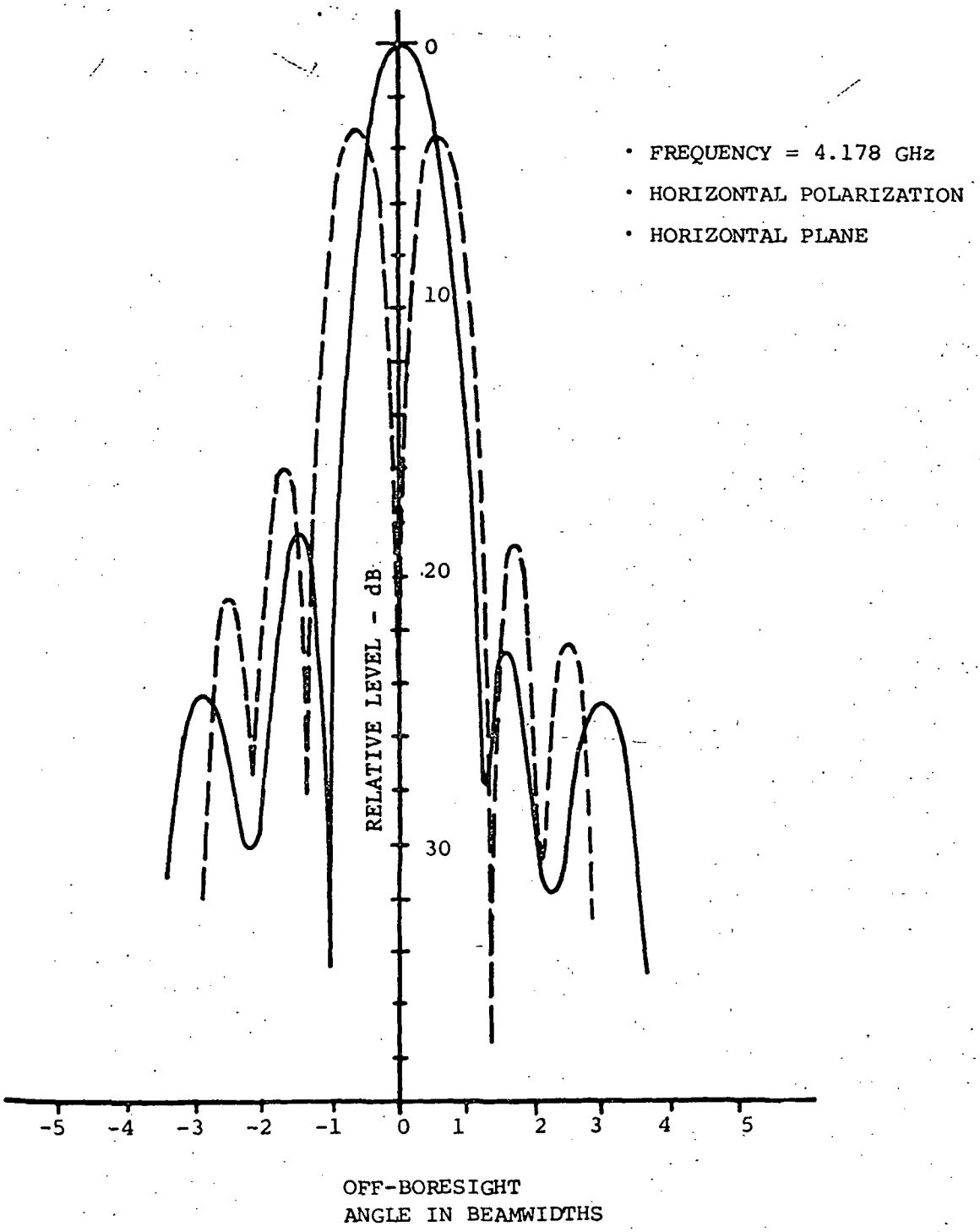

Figure 95. Sum and Difference Patterns of ATS Tracking Facility

feed to increase the FOV was discussed in section 4.6. It was shown there that a feed displacement of 0.63 inch from the nominal focal point will result in an increase of the sum channel beamwidth by a factor of 1.5. This value results from a phase error at the edge of the aperture of 1.19π radius and the theoretical work of Redlein (Reference 17). It is clear that this amount of defocusing will result in a significant increase in the FOV and is also consistent with an acceptable tracking accuracy.

A qualitative estimate of the FOV which will accompany defocused operation of the K_u-band feed system must be made, it is believed, on the basis of the detailed characteristics of the primary reflector, the cassegrainian subreflector, and the antenna feed system. Moreover, as will be seen in the material which follows, the impact on the FOV of receiver generated noise must be considered. It is therefore asserted that experimental data is required to obtain a responsible estimate of the FOV at K_u-band. This assertion is discussed in detail in section 5.0.

In terms of the S-band auto tracking system associated with data link maintenance method RP/S-AUTO, in the absence of noise, the FOV can be expected to be approximately 5.3 degrees. This estimate results from an FOV of 0.8 degree at K_u-band and a frequency ratio of 14.3/2.15 = 6.65.

4.8.2.2 FOV in the Presence of Noise

Attention is turned next to an attempt to define the FOV of a sum and difference auto tracking system in which locally generated noise is present. Two distinct cases will be considered. In one model, the angle tracking receiver is assumed to contain a phase lock loop (PLL) so that coherent processing of the received signal is employed. In the other case, there is no PLL and the processing is said to be non-coherent. Regardless of the processing method, the user is assumed to radiate a CW signal which is characterized by a particular value of signal-to-noise ratio defined in terms of the intermediate frequency bandwidth of the angle sensing receiver in the boresight direction.

4.8.2.2.1 Non-Coherent Processing

The model of the auto tracking system for which the FOV is to be determined is shown in the block diagram of Figure 96. The detailed analysis of the subject system is carried out in Appendices J and K. Only the key results of that analysis and the accompanying assumptions and conditions are reported here.

With reference to the block diagram, the antenna develops squinted single-plane sensing patterns $g(\theta)$ and $g(-\theta)$ and the comparator produces the sum and difference patterns given by

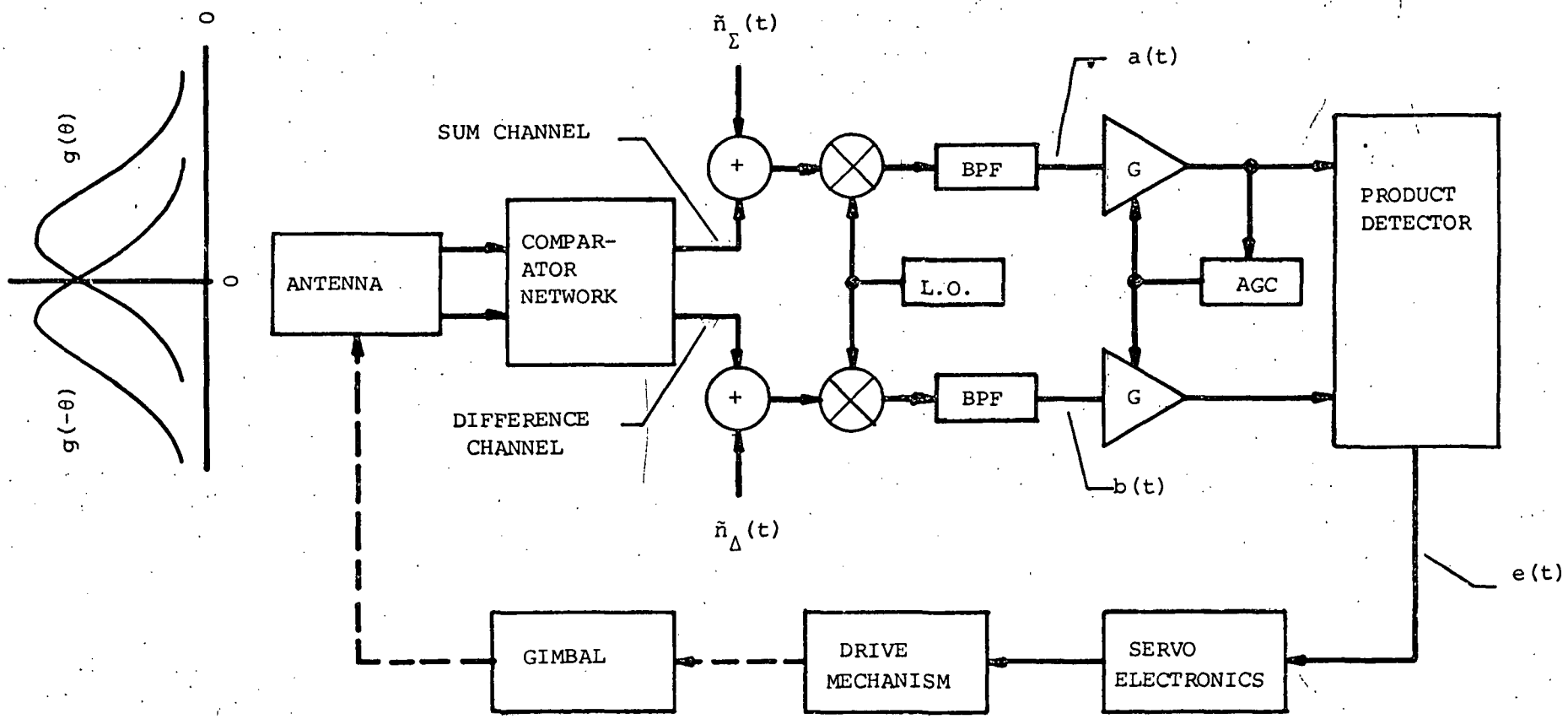

Figure 96. Angle Sensor Model: Non-coherent Processing

$$\Sigma(\theta) = \frac{A}{\sqrt{2}} (g(\theta) + g(-\theta)) \quad (2)$$

and

$$\Delta(\theta) = \frac{A}{\sqrt{2}} (g(\theta) - g(-\theta)) \quad (3)$$

where A is a constant to be defined.

The frequency of the received CW signal is slowly varying by virtue of relative motion of the user and TDRS spacecraft and the instability of various oscillators. The sum and difference channels each contain additive, wideband, gaussian noise processes $\tilde{n}_\varepsilon(t)$ and $\tilde{n}_\Delta(t)$ prior to first detection. Following frequency conversion and bandpass filtering, the processes

$$a(t) = \Sigma(\theta) \cos \omega_o t + \eta_\varepsilon(t) \quad (4)$$

and

$$b(t) = \Delta(\theta) \cos \omega_o t + \eta_\Delta(t) \quad (5)$$

are associated with the sum and difference channels respectively, where the narrowband noise processes $\eta_\varepsilon(t)$ and $\eta_\Delta(t)$ are assumed to be wide-sense stationary, uncorrelated, with mean zero and variances σ_Σ^2 and σ_Δ^2. Also, the intermediate frequency is defined as $\omega_o/2\pi$.

The antenna patterns $g(\theta)$ and $g(-\theta)$ are normalized so that $g(0) = 1/\sqrt{2}$. As a result, the received signal component at the bandpass filter output in the sum channel, at boresight, has the form $A \cos \omega_o t$. Thus, the sum channel signal-to-noise ratio has the general form

$$SNR_\varepsilon(\theta) = \frac{\Sigma^2(\theta)}{2\sigma_\varepsilon^2}, \quad (6)$$

and at boresight it has the value

$$SNR_\varepsilon(0) = \frac{A^2}{2\sigma_\varepsilon^2}, \quad (7)$$

In the material which follows, the bandpass filters are assumed to exhibit an identical, symmetrical, response centered at $f_o = \omega_o/2\pi$. The actual and noise bandwidths are, therefore, equal with values defined by

$$B_\eta = \begin{cases} 10^6 \text{ Hz at } K_u\text{-band} \\ 1.5 \times 10^5 \text{ Hz at S-band} \end{cases} \quad (8)$$

The IF amplifiers are, of course, assumed to be identical. Their frequency response is controlled by the bandpass filters which precede them, and their noise contribution is accounted for in σ_Σ^2 and σ_Δ^2. (Any difference in σ_Σ^2 and σ_Δ^2 results from amplification prior to first detection). The amplifier gain is controlled by an AGC voltage obtained from the sum channel signal (and noise) by linear detection followed by low-pass filtering. The AGC time constant is sufficiently long ($\geq 10^{-2}$ seconds) so that the IF amplifier gain is not influenced by the sum channel noise. This relatively slowly acting AGC is possible by virtue of essentially a constant value of the received signal over long periods of time, i.e., the user-to-TDRS distance changes slowly as does the angular separation of their line of sight and the TDRS coordinate frame. The IF amplifier is therefore, governed by the long time average of a(t) and has the functional form

$$G = \frac{K}{\Sigma(\theta)}$$

where K is a function of the sum channel SNR.

The receiver output waveform e(t) is assumed to be formed by the product of the signals Ga(t) and Gb(t). The voltage e_t at some time t is approximated as a gaussian random variable with an ensemble average (mean) value of

$$\langle e_t \rangle = K \left[\frac{\Delta(\theta)}{\Sigma(\theta)}\right] \tag{9}$$

and a variance of

$$\text{var } e_t = K^2 \left\{ \frac{\sigma_\Delta^2}{\Sigma^2(\theta)} + \left[\frac{\Delta(\theta)}{\Sigma \quad \theta}\right]^2 \frac{\sigma_\Sigma^2}{\Sigma^2(\theta)} + 2 \frac{\sigma_\Sigma^2 \sigma_\Delta^2}{\Sigma^4(\theta)} \right\} \tag{10}$$

The mean value is that of a noise-free system, and the variance goes to zero as σ_Σ^2 and σ_Δ^2 approach zero (and K becomes essentially $\Sigma(\theta)$).

A formulation of the correlation function of the receiver output process reveals that e(t) is wide-sense stationary. Thus, its power spectral density can be determined for use in an examination of the effect of the servo on the auto tracking system performance.

The noisiness of the product detector output waveform is defined as

$$r_e(\theta) \triangleq \frac{\text{std. dev. } e_t}{\langle e_t \rangle} . \tag{11}$$

Thus, Equation (11) defines the magnitude of the rms value of the fluctuating component of e(t) with respect to the mean value at some angle θ with respect to the boresight axis. Figure 97 illustrates the physical interpretation of Equation (11). The function $\Delta(\theta)/\Sigma(\theta)$ is modeled as a linear function of the off-boresight angle θ and the probability density function of the random variable e_t is illustrated for several values

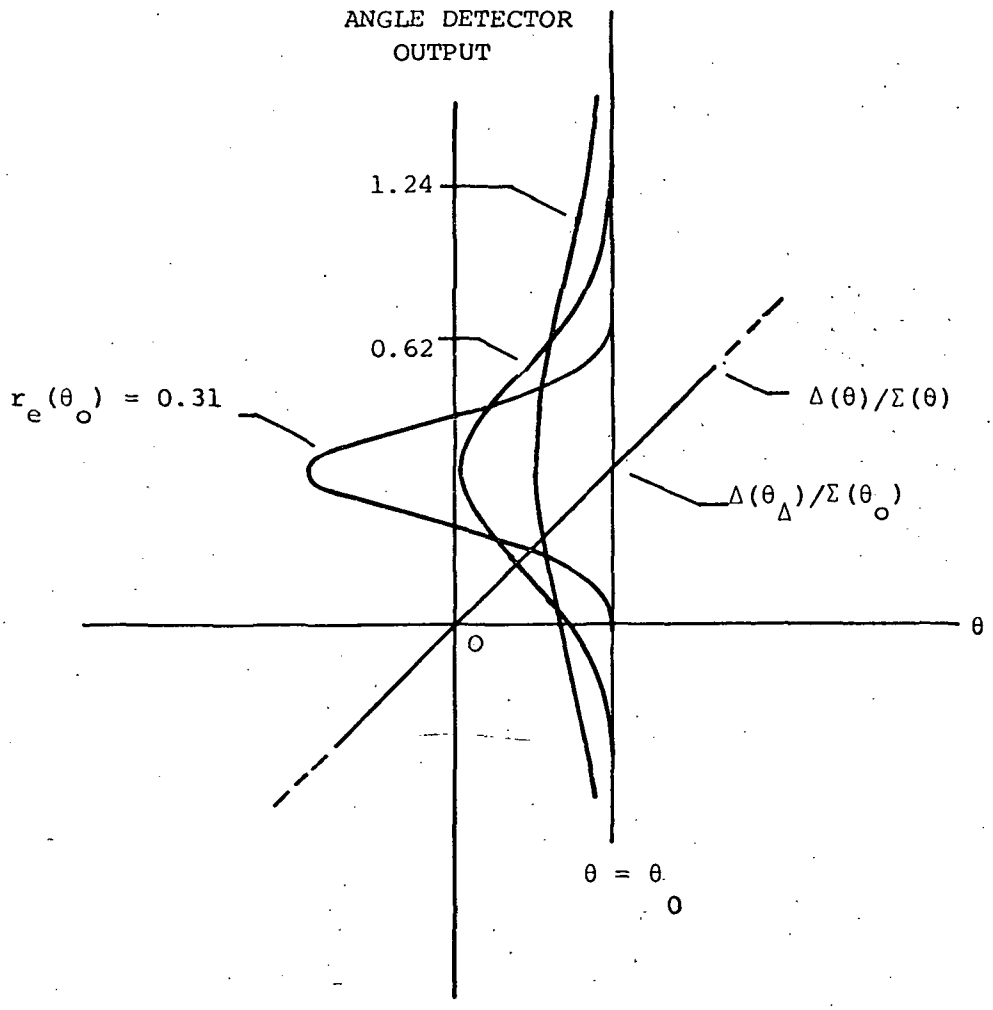

Figure 97. Angle Detector Output Voltage Distribution

of the noisiness ratio $r_e(\theta_o)$ at the angle θ_o. Clearly, even for relatively small values of r_e, the mean value of the output, $\Delta(\theta_o)/\Sigma(\theta_o)$, is a small fraction of the total excursion of the peak noise fluctuations.

To relate the ratio $r_e(\theta)$ to a realizable auto tracking system, Equations (9) and (10) are employed in (11) with the result

$$r_e(\theta) = \frac{1}{\Sigma(\theta)} \left[\frac{1}{\Delta(\theta)/\Sigma(\theta)}\right] \sqrt{\frac{1 + \left[\frac{\Delta(\theta)}{\Sigma(\theta)}\right]^2 + \frac{1}{\Sigma^2(\theta)\ SNR_\Sigma(0)}}{2SNR_\Sigma(0)}} \tag{12}$$

When the sum channel antenna pattern $\Sigma(\theta)$ and the angle sensing function $\Delta(\theta)/\Sigma(\theta)$ defined in Figure 92 are used in Equation (12), with the boresight value of SNR as a parameter, the data in Figure 98 results. It is first observed that $r_e(\theta)$ goes without bounds when $\Delta(\theta)/\Sigma(\theta)$ becomes zero at $\theta = 0$ and $1.7\theta_3$. It is also the case that for a relatively large value of boresight SNR, the rms value of the output is comparable to the dc component over the range of θ associated earlier with the FOV. However, as the value of $SNR_\Sigma(0)$ is reduced, the output becomes exceedingly noisy.

In Appendix J the tracking loop shown in the block diagram of Figure 96 is modeled as a narrowband low-pass linear filter with an output waveform q(t). When the noisiness of its output is defined in an analogous fashion as the product detector, viz.,

$$r_q(\theta) \leq \frac{\text{std. dev } q_t}{\langle q_t \rangle} \tag{13}$$

then it is the case that

$$r_q(\theta) = \sqrt{\frac{2B_n}{B_n}}\ r_e(\theta) \tag{14}$$

where B_n is the one-sided servo noise bandwidth. With B_n of the order of 1 Hz and B_n given by Equation (8), it is clear that $r_q(\theta)$ is a small fraction of $r_e(\theta)$. Thus, even for $SNR_\Sigma(0) = 0.1$, the rms value of the fluctuating component of the servo output is much less than its mean value (except, of course, in the vicinity of $\theta = 0$ and $1.7\theta_3$ degrees.

On a strictly theoretical basis, a strong case can be built for the FOV having essentially the same value for large and small values of boresight SNR. However, in a realizable system it is clear that when $SNR_\Sigma(0) \leq 1$, the angle detector output is completely dominated by noise. Therefore, for the servo to produce an accurate estimate of the mean value $\Delta(\theta)/\Sigma(\theta)$, the output dynamic range of the product detector and the input

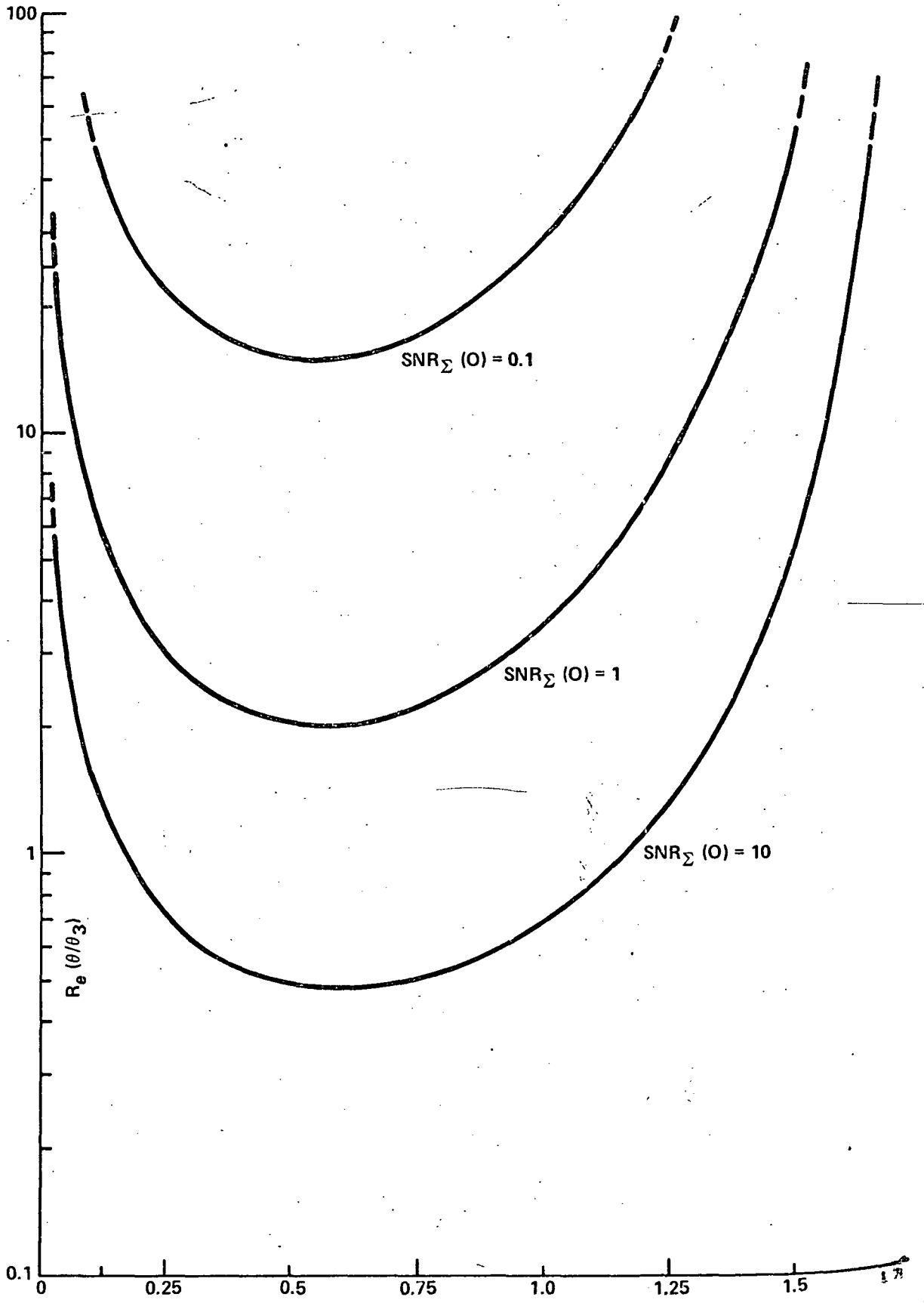

Figure 98. Noisiness of Angle Detector Output for Non-coherent Processing

dynamic range of the servo must be compatible with the fluctuation range of the waveform e(t); i.e., the excursions of the waveform about its mean value must be accurately preserved up to the $\pm 3\sigma$ level or so. For this condition to be satisfied it is clear that the mean voltage output will be extremely small and, as a result, highly susceptible to small values of offset voltage in the servo electronics.

To put these comments on a quantitative basis, define the maximum linear response output voltage from the product detector as e(max). Then, assume that noise fluctuations of $\pm$ 3 x std. dev.e_t are to be reproduced. It follows that the component has a value

$$\langle e_t \rangle = \frac{e(\max)}{3\, r_e(\theta)} .$$

The dc offset in the servo system is therefore restricted to be $<< \langle e_t \rangle$. As an example, let e(max) = 5 volts and from Figure 98 choose $\theta = 1.25\theta_3$ and $SNR_\Sigma(o) = 0.1$ so that $r_e(1.25) = 85$ and $\langle e_t \rangle = 5/3x85 \approx 0.020$ volt. It appears that an acceptable value of servo system dc offset is 1/10 of this value, or approximately 2 millivolts. This value is readily achievable in a practical system. It is also noted that if $\beta_n = 2$ Hz and $B_{if} = 10^6$ Hz, then Equation (14) yields $r_q(1.25) = \sqrt{4/10^6}(85) = 0.17$ as the 1σ noise fluctuations about the mean, i.e., the 3σ fluctuation would be approximately $\pm$ 0.010 volt, an acceptable value.

It has been shown that the FOV of the auto tracking system depicted in Figure 96 in conjunction with the antenna patterns shown in Figure 92 is not diminished as a result of operation with small values of SNR. A rigorous analysis supports this conclusion but there is reservation with regard to the precision with which the mathematical system model defines realizable hardware. Reference is made to the operation of the product detector for the case in which the sum channel SNR is small. In the foregoing material the product detector output waveform is modeled as the product of the sum and difference channel signals (followed by low-pass filtering). The accuracy of this assumption has not been verified.

When antenna feed defocusing is employed for the purpose of enlarging the FOV, the basic principles used to evaluate the focused case are, of course, applicable. However, the accompanying sum channel gain reduction illustrated in Figure 64 must be accounted for in the evaluation of $SNR_\Sigma(0)$.

Subject to the reservation stated above, it is asserted that the defocused K_u-band feed will provide an FOV on the order of 1.2 degrees with an on-boresight sum channel SNR ≥ 1, as measured in the IF bandwidth of 1 MHz. This assertion assumes the use of non-coherent processing on board the TDRS, with an AGC time constant $\geq 10^{-2}$ second.

Attention is next directed to the FOV associated with coherent processing.

4.8.2.2.2 Coherent Processing

The following material is analogous to that given above except that the auto tracking receiver model contains a phase lock loop which produces a pure sinusoidal signal at the intermediate frequency. A block diagram of the system model is shown in Figure 99 and an analysis of its performance is carried out in Appendix L. The results of this analysis are summarized in subsequent paragraphs.

As was the case for non-coherent processing, the AGC time constant is sufficiently long so that the IF amplifier gain is impervious to the fluctuations of the noise component in the sum channel. The amplifier gain is therefore defined by $K/\Sigma(\theta)$. The angle sensor output voltage e_t at some time t is a gaussian random variable with an ensemble average (mean) value

$$\langle e_t \rangle = K\left[\frac{\Delta(\theta)}{\Sigma(\theta)}\right]$$

and a variance

$$\text{var } e_t = \left[\frac{K\sigma_\Delta}{\Sigma(\theta)}\right]^2.$$

The correlation function of the process e(t) takes the simple form

$$R_e(\tau) = \left[\frac{K}{\Sigma(\theta)}\right]^2 [\Delta^2(\theta) + R_\Delta(\tau)]$$

where

$$R_\Delta(\tau) = \sigma_\Delta^2 \left[\frac{\sin \pi B_n \tau}{\pi B_n \tau}\right]$$

is the correlation function of the difference channel noise process.

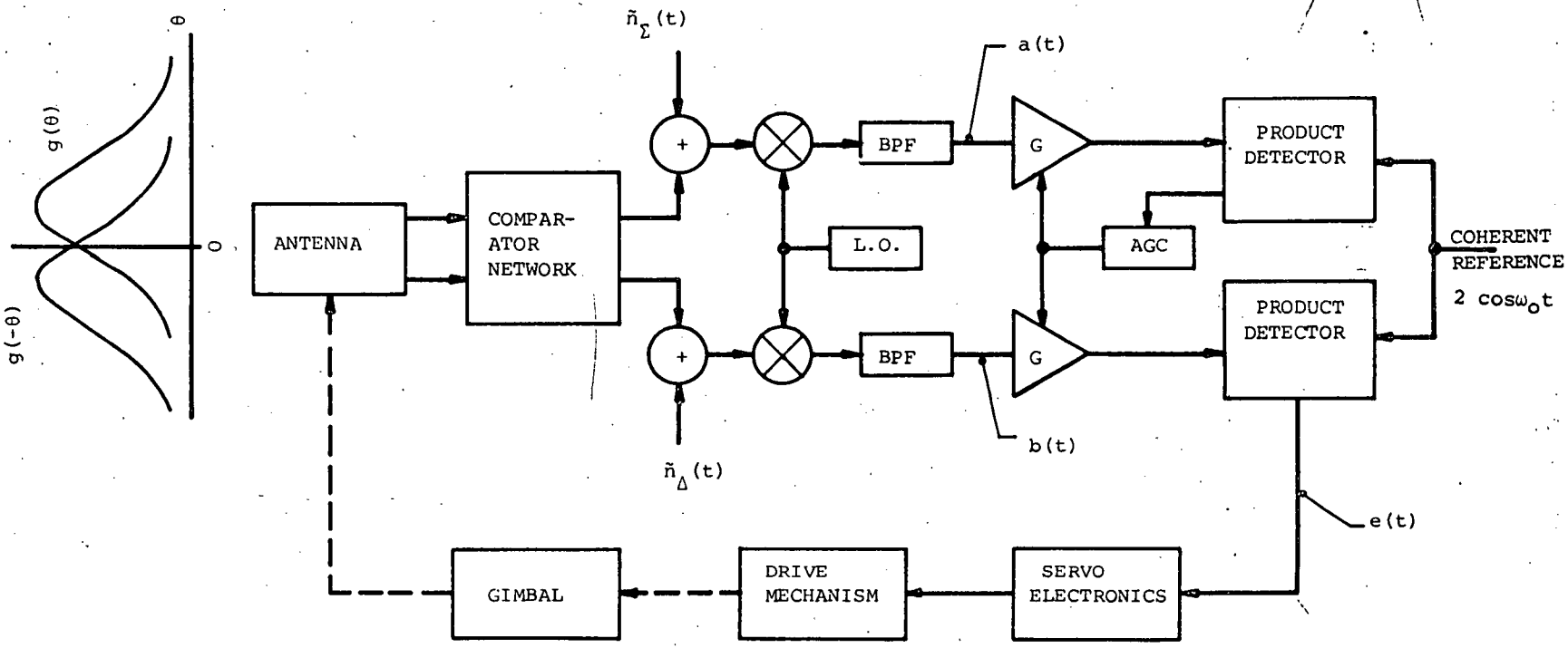

Figure 99. Angle Sensor Model: Coherent Processing

The noisiness of the angle sensor output waveform, i.e.,

$$r_e(\theta) = \frac{\text{std.dev } e_t}{\langle e_t \rangle}$$

has the form

$$r_e(\theta) = \frac{\sigma_\Delta}{\Delta(\theta)}$$

but, for purposes of computation, is rewritten as

$$r_e(\theta) = \frac{1}{\sqrt{SNR_\Delta(o)}} \quad \frac{1}{[g(\theta)+ g(-\theta)]\ [\Delta(\theta)/\Sigma(\theta)]} \tag{15}$$

where $SNR_\Delta(o)$ is the on-boresight signal-to-noise ratio referenced to the difference channel noise power, i.e.,

$$SNR_\Delta(o) \triangleq \frac{A^2}{2\sigma_\Delta^2} .$$

Equation (15) is illustrated in Figure 100 for the case of the antenna patterns defined in Figure 92. Also shown is the ratio $r_e(\theta)$ for the case of non-coherent processing. As expected, coherent processing results in a smaller value of $r_e(\theta)$ than does non-coherent processing. Moreover, the difference increases as the SNR is diminished. More specifically, for SNR $\leq$ 1, there is an improvement in the angle detector output quality on the order of 10 dB. It is therefore concluded that for a given small value of on-boresight SNR, coherent and non-coherent processing will result in approximately the same FOV when the SNR is 10 dB less for the former than for the latter method.

Next, it is noted that the reservation regarding the product detector model which was made in regard to non-coherent processing is not applicable for coherent processing. That is, when coherent processing is employed, then only one of the product detector input waveforms is noise-like. However, it is assumed that the reference signal produced by the PLL is a pure carrier at the intermediate frequency.

As a final comment on FOV, nothing has been said about the problem of transients in the tracking receiver or servo system output waveforms. It is assumed that when designation of the boresight axis of the auto tracking system is complete and the tracking loop is closed, the antenna is held in the designated position by the gimbal system for a period of

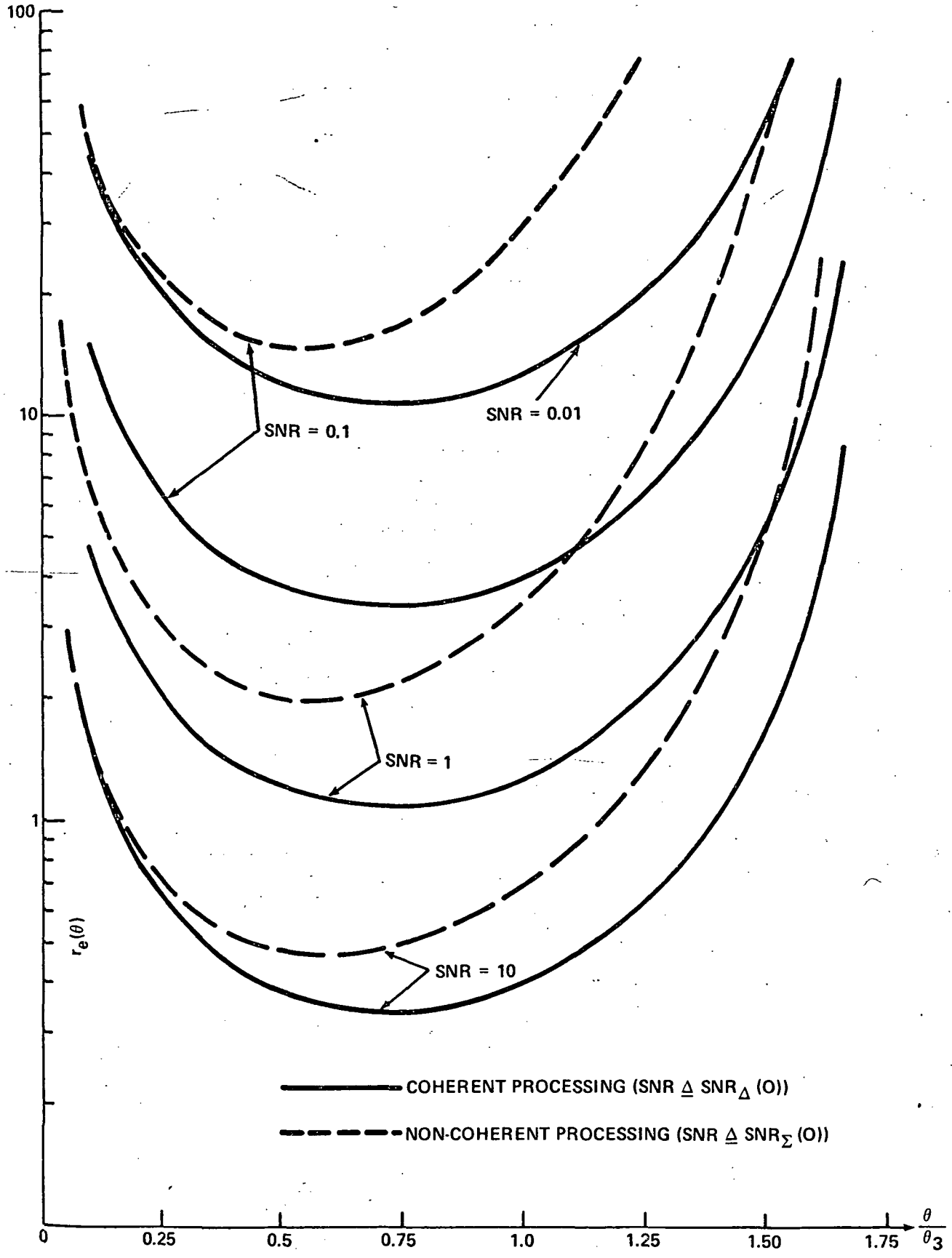

Figure 100. Noisiness of Angle Sensor Output

time equal to the reciprocal of the tracking system bandwidth. Then, when the brakes on the gimbal axes are released, if the angular difference between the TDRS/user line-of-sight and the boresight axis is less than FOV/2, that angular difference should be reduced by the action of the tracking system.

4.8.3 Aided Designation

The boresight designation error was derived in paragraph 4.8.1 for both S- and K_u-band operation. It was shown there that the 3σ angular separation between the boresight axis of the auto tracking data link maintenance system and the TDRS/user line of sight is $\alpha(BS, DES, k) = 0.45$ degree for K_u-band and $\alpha(BS, DES, S) = 0.46$ degree at S-band. These angular errors are asoociated with ground command of the reflector pointing angles.

It is of interest to determine the magnitude of the same errors for the case in which a designation aid system is employed. By definition, such a system provides more precise designation than is possible using ground command data only. Three distinct aided-designation methods were postulated in section 4.3 and are repeated below in Table LIII.

The third method, DA/K-AUTO, has already been eliminated from further consideration, i.e., rather than increasing the FOV on command from the ground, the K_u-band feed employed for RP/K-AUTO is permanently defocused. Attention is therefore to be given to the performance of aided-designation methods DA/K-SEARCH and DA/S-AUTO. It is important to note that the former method is applicable to Options I, II, and III, whereas the latter technique can be employed only in conjunction with Option II.

4.8.3.1 Aided Designation via DA/K-SEARCH

The baseline K_u-band feed system design provides two pensil beams: one associated with the data channel and the other developed in the sum channel of the auto tracking system used for data link maintenance. Either of these pencil beams can be employed to systematically search a given spatial region to estimate the direction of signal arrival from the user. A reasonable search procedure would begin with ground command of the reflector pointing angles in an attempt to align the search beam axis with the TDRS/user line of sight. The search pattern would therefore be centered on the best estimate of the user position relative to the TDRS. Next, during the search, at the time at which the decision is made that the user signal has been located, the reflector pointing angles are stored and the reflector is commanded to return to the same spatial orientation. Alternatively, the reflector can simply be stopped soon after detection occurs. The auto tracking loop of the data link maintenance system is then closed. Clearly, the FOV of the

TABLE LIII

Aided Designation Methods

Designation Technique	Designation Method
DA/K-SEARCH	Search at K_u-band with a pencil beam antenna pattern having a half-power width consistent with the feed system and reflector employed for data link maintenance.
DA/S-AUTO	Autotrack at S-band with the same feed system and angle tracking receiver employed for data link maintenance.
DA/K-AUTO	Autotrack at K_u-band with the same basic feed system and angle-tracking receiver employed for data link maintenance (RP/K-AUTO) but with modifications to increase the field-of-view, on command from the ground, by an amount to be determined.

auto tracking system must be commensurate with the angular difference between the direction in which its boresight axis is pointed (as a result of the search procedure) and the TDRS/user line of sight.

The analysis of the performance of the DA/K-SEARCH scheme begins with an examination of the precision with thich the search beam is initially pointed by command from the ground station. It is shown in Table XXXIV that the angular error of interest is

$$\alpha(\text{DA,SCH}) = \begin{cases} 0.45 \text{ degree for search with the data beam} \\ 0.45 \sqrt{1 + (0.09\,\theta_{3,K})^2} \text{ degree for search with the sum channel auto tracking beam} \end{cases}$$

where the term α(DA,SCH) is obtained from Figure 32. There are two alternatives for the half-power beamwidth of the search beam: 0.35

degree in the dedicated (receiving) data channel and 0.57 degree in the sum channel of the defocused auto tracking system. Clearly, $\alpha(DA,\overline{SCH}) = 0.45$ degree in both cases.

A detailed analysis of the performance of a spiral search system has been carried out (Reference 62) and the results obtained are now presented in summary form.

The spiral search pattern is composed of joined semicircles with an angular separation d of adjacent turns. The half-power beamwidth of the search beam and the angular separation adjacent semicircles are related by

$$\theta_{3,k} = 4d.$$

When the search region is defined by a cone with an included angle of 2Ψ, the product of the total search time T_s and the maximum antenna angular rate R (in each axis) are given by

$$T_S R = \frac{\pi\theta_{3,K}}{4}\left(\frac{8\Psi^2}{\theta^2_{3,k}} + \frac{6\Psi}{\theta_{3,k}} + 1\right)$$

And illustrated in Figure 101. For $\alpha(DA,SCH) = 0.45$ degree, a conservative choice of Ψ is 0.75 degree. Then, if R = 1.0 degree/second,

$$T_s \simeq \begin{cases} 14 \text{ seconds; } \theta_{3,k} = 0.35 \text{ degree} \\ 10 \text{ seconds; } \theta_{3,k} = 0.57 \text{ degree.} \end{cases}$$

The model of the signal detection circuit is shown in the block diagram of Figure 102. The receiver output signal is routed to a bandpass filter with bandwidth B and then detected. The detector output is sampled at a rate $\leq$ B and the average of m contiguous samples is formed by the adder. A threshold switch indicates signal detection when the adder output exceeds the threshold level.

The probability of acquisition is equal to or greater than the product of three probabilities:

1 P_A = probability that the user satellite is in the search region

2 $1-P_{fa}$ = probability that no false alarm occurs during the entire search

$= (1 - P_e)^r$

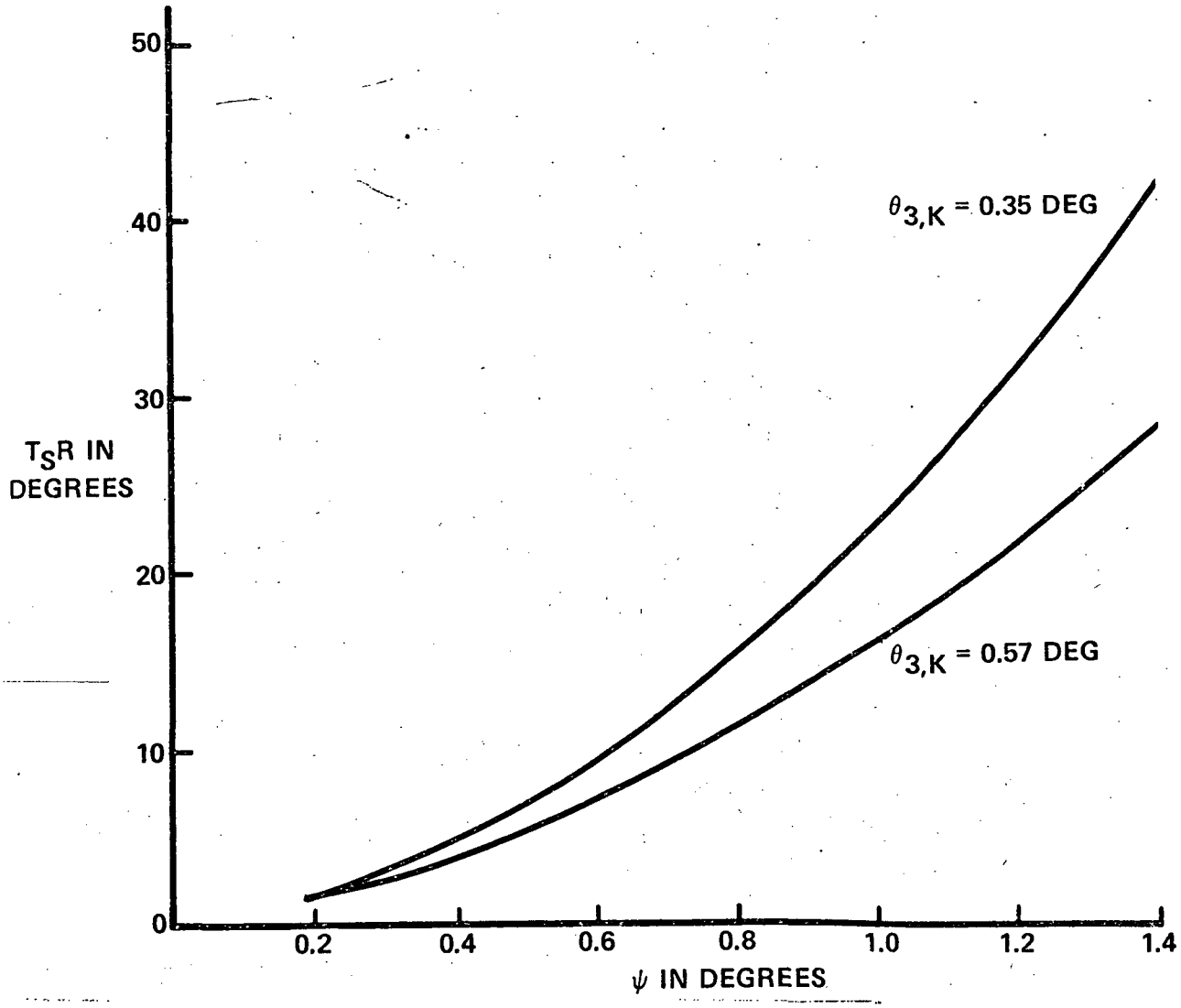

Figure 101. Required Search Time

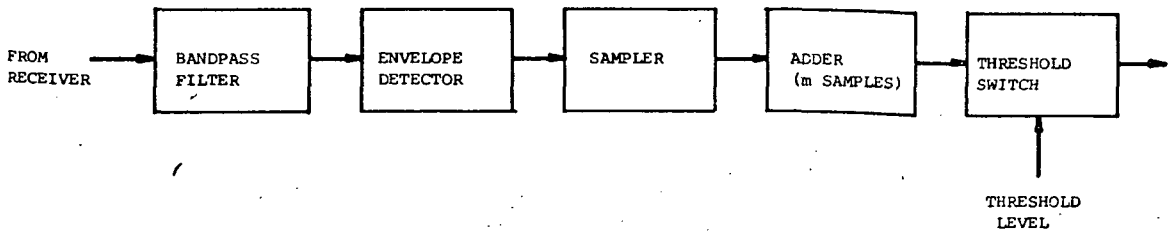

Figure 102. Signal Detection Circuit

where

P_e = probability that noise alone causes the adder output to exceed the threshold during the time t_c required for a complete sample and add cycle

r = next integer greater than T_s/t_c

3 $1-(1-P_{DC})^q$ = probability that signal detection will occur when the direction of signal arrival is within the half-power beamwidth of the search beam

where

P_{DC} = probability of detection during a time interval t_c, when the signal is present

q = total number of sample and add cycles that occur during the time the signal is within the half-power beamwidth

i.e.,

$$P_{acq} \geq P_A \, (1 - P_{fa}) \, [1 - (1-P_{DC})^q].$$

A sample performance characterization is obtained by selecting

1 $P_A = 1$

2 $P_{fa} = 10^{-6}$

3 $P_{acq} = 0.9999.$

Then,

$$P_{acq} \geq 1 - (1 - P_{DC})^q.$$

Next, with

t_{min} = minimum time during which the signal arrival direction is within the half-power beamwidth

$= 4(d/R)$

it follows that

$$q_{min} = \frac{t_{min}}{t_c} .$$

Therefore, the inequality is strengthened in the form

$$P_{acq} \geq 1 - (1 - P_{DC})^{t_{min}/t_c}.$$

Next, the time t_c is conservatively defined by

$$t_c = \frac{2m}{B}$$

so that

$$\frac{t_{min}}{t_c} = \frac{4dB}{2mR},$$

but $\theta_{3,k} = 4d$, so that

$$\frac{t_{min}}{t_c} = \frac{B\theta_{3,k}}{2mR}.$$

For K_u-band operation, $B = 10^6$ Hz and the maximum antenna angular rate has already been selected as R = 1 degree/second in each axis. If m is arbitrarily selected to be 250, then

$$\frac{t_{min}}{t_c} = 2000\,\theta_{3,k} = \begin{cases} 700;\ \theta_{3,k} = 0.35 \text{ degree} \\ 1140;\ \theta_{3,k} = 0.57 \text{ degree} \end{cases}$$

and the required probability of detection during t_c becomes

$$P_{DC} \approx \begin{cases} 0.014;\ \theta_{3,k} = 0.35 \text{ degree} \\ 0.008;\ \theta_{3,k} = 0.57 \text{ degree.} \end{cases}$$

Finally, with

$$1 - P_{fa} = 1 - 10^{-6} = (1 - P_e)^r$$

and

$$r = \frac{T_s B}{2m}$$

or, using the scan times defined earlier

$$r = \begin{cases} 2.8 \times 10^3; \ \theta_{3,k} = 0.35 \text{ degree} \\ 2.0 \times 10^4; \ \theta_{3,k} = 0.57 \text{ degree} \end{cases}$$

and therefore the SNR required at the detector input terminals is nearly -3.0 dB for both values of $\theta_{3,k}$.

Summarizing, with a maximum antenna axis rate of 1.0 degree/second over an included angle of 1.5 degrees and a SNR of at least -3 dB measured in a 1 MHz IF bandwidth, the probability that no false alarm will occur during the entire search and that detection will occur when the signal arrival direction is within the half-power beamwidth is at least 0.9999. The required search time is least for the case in which the search beam is formed in the sum channel of the auto tracking system. Moreover, that system is capable of producing the required SNR and is considered to be preferable, pending an investigation of the designation accuracy.

The next characteristic of the designation aid system DA/K-SEARCH to be determined is that accuracy with which it aims the boresight axis of the auto tracking designation aid system toward the user spacecraft. Figure 32 defines the angular error associated with the reflector pointing angles as a result of the search procedure as α(REF,DA,SCH), and attention is now directed toward the formulation of this value.

It is assumed that when detection occurs, the antenna begins to decelerate and that in order to prevent unnecessary forces on the TDRS, the deceleration period must consume 5.0 seconds. During this time, the maximum possible user angular motion is 5 x 0.013 degree/second = 0.065 degree. This value, when combined with the uncertainty in the signal arrival angle ($\theta_{3,k}/2$), yields the angular separation between the direction of the search beam maximum and the TDRS/user line of sight. The 3σ data beam offset/reflector axis error is found from Table XXXIV to be

$$\alpha(\text{DB}),\text{REF},\text{K}) = \begin{cases} 0.030 \text{ degree}; \ \theta_{3,k} = 0.35 \text{ degree} \\ 0.037 \text{ degree}; \ \theta_{3,k} = 0.57 \text{ degree} \end{cases}$$

so that the 3σ reflector/axis pointing errors become

$$\alpha(\text{REF},\text{DA},\text{SCH}) = \begin{cases} 0.19 \text{ degree}; \ \theta_{3,k} = 0.35 \text{ degree} \\ 0.30 \text{ degree}; \ \theta_{3,k} = 0.57 \text{ degree}. \end{cases}$$

The final characteristic of interest is the angular error between the boresight axis of the auto tracking data link maintenance system and the direction of signal arrival. This error will result from the just defined values of α(REF,DA,SCH) combined with the displacement of the reflector and boresight axes. The latter value is found to be

$$0.03 \sqrt{1 + (2.4\ \theta_{3,k})^2}$$

for the K_u-band autotracker.* With $\theta_{3,k}$ = 0.57 degree, the error of interest is 0.05 degree. When data link maintenance is performed with RP/S-AUTO, the corresponding value is 0.09 degree.** When these values are combined with α(REF,DA,SCH), the results are

$$\alpha(BS,K) = \begin{cases} 0.20 \text{ degree; } \theta_{3,k} = 0.35 \text{ degree} \\ 0.30 \text{ degree; } \theta_{3,k} = 0.57 \text{ degree} \end{cases}$$

$$\alpha(BS,S) = \begin{cases} 0.21 \text{ degree; } \theta_{3,k} = 0.35 \text{ degree} \\ 0.30 \text{ degree; } \theta_{3,k} = 0.57 \text{ degree} \end{cases}$$

where α(BS,K) is defined in Figure 32 as the angular displacement of the boresight axis of the K_u-band auto tracking data link maintenance system and the TDRS/user line of sight as the result of aided designation. The error α(BS,S) is similarly defined for the S-band autotracker.

These errors are required to define the FOV which the S- and K_u-band auto tracking system must exhibit if they are to be compatible with aided designation via DA/K-AUTO. The minimum acceptable value of the FOV is, of course, twice the above quoted errors. However, is αBS,K) and α(BS,S) are increased by a factor of four, the resulting values are compatible with the FOV estimates given earlier.

---

* See the material under "α(DBO,BS,S-I)" in paragraph 4.4.1.2.

** See the material under "α(DBO,BS,S-II) with RP/S-AUTO" and "α(DBO,BS,S-I)" in paragraph 4.4.1.2.

In conclusion, the concept of aided designation with a spiral search of a K_u-band pencil beam has been shown to yield a probability of acquisition of essentially unity with a -3 dB SNR in a 1.0 MHz IF bandwidth. Moreover, the pencil beams formed by either the receive data channel or the auto tracking sum channel can be employed. As expected, the former case results in greater angular designation precision to the auto tracking data link maintenance system and also imposes less stringent requirements on that system's FOV. Also, it does require a greater time for search. However, the FOV of both the S-band and K_u-band auto tracking systems is consistent with both search beamwidths.

4.8.3.2 Aided Designation Via DA/S-AUTO

When consideration is given to Option II, it is clear that the S-band auto tracking system is capable of serving a dual role. That is, in addition to maintaining the data link it can also act as a designation aid to the K_u-band autotracker.

The measure of the quality of this method of aided designation is the angular separation of the boresight axis of the K_u-band autotracker and the TDRS/user line of sight when the user spacecraft is being tracked by the S-band system. The following error components are applicable:

1 α(DLM,BS,S): the angular separation of the boresight axis of the S-band autotracker and the TDRS/user line of sight;

2 The angular displacement of the boresight axis of the S-band autotracker and the reflector axis;

3 The angular displacement of the boresight axis of the K_u-band autotracker and the reflector axis.

The first error source is obtained from the material which was used to generate Figure 91 using the relationship

$$\alpha(\text{DLM,BS,S}) = \sqrt{10^{-4} + \delta_R^2(\text{S}) + \delta_D^2}$$

given in Table XXXI.

The second error source results from the combined effect of a physical displacement of the S-band feed from the reflector axis (0.050 degree) and a boresight shift due to circuit unbalance of (0.028 $\theta_{3,S}$ = 0.07 degree). Its 3σ value is 0.09 degree.

The third error component results from the same basic sources just defined for the S-band feed system. In the case of the K_u-band feed, the

angular error of interest is $0.03 \sqrt{1 + (2.4\ \theta_{3,k})^2}$ = 0.05 degree when $\theta_{3,k}$ = 0.57 degree.

The rss combination of the above defined errors, $\alpha(BS,K)$, is given in Figure 103 as a function of the one-sided servo noise bandwidth β_n with the on-boresight value of SNR as a parameter. Also shown in the same figure is the designation error $\alpha(BS,DES,K)$ of the K_u-band boresight axis which results from ground command (paragraph 4.8.1) and the values of $\alpha(BS,K)$ associated with aided designation using DA/K-SEARCH (paragraph 4.8.3.1). Finally, for reference, the approximate value of FOV/2 of the defocused K_u-band auto tracking system is also illustrated. Clearly, there are three acceptable methods of designating the boresight axis of the K_u-band autotracker prior to the establishment of the K_u-band data link.

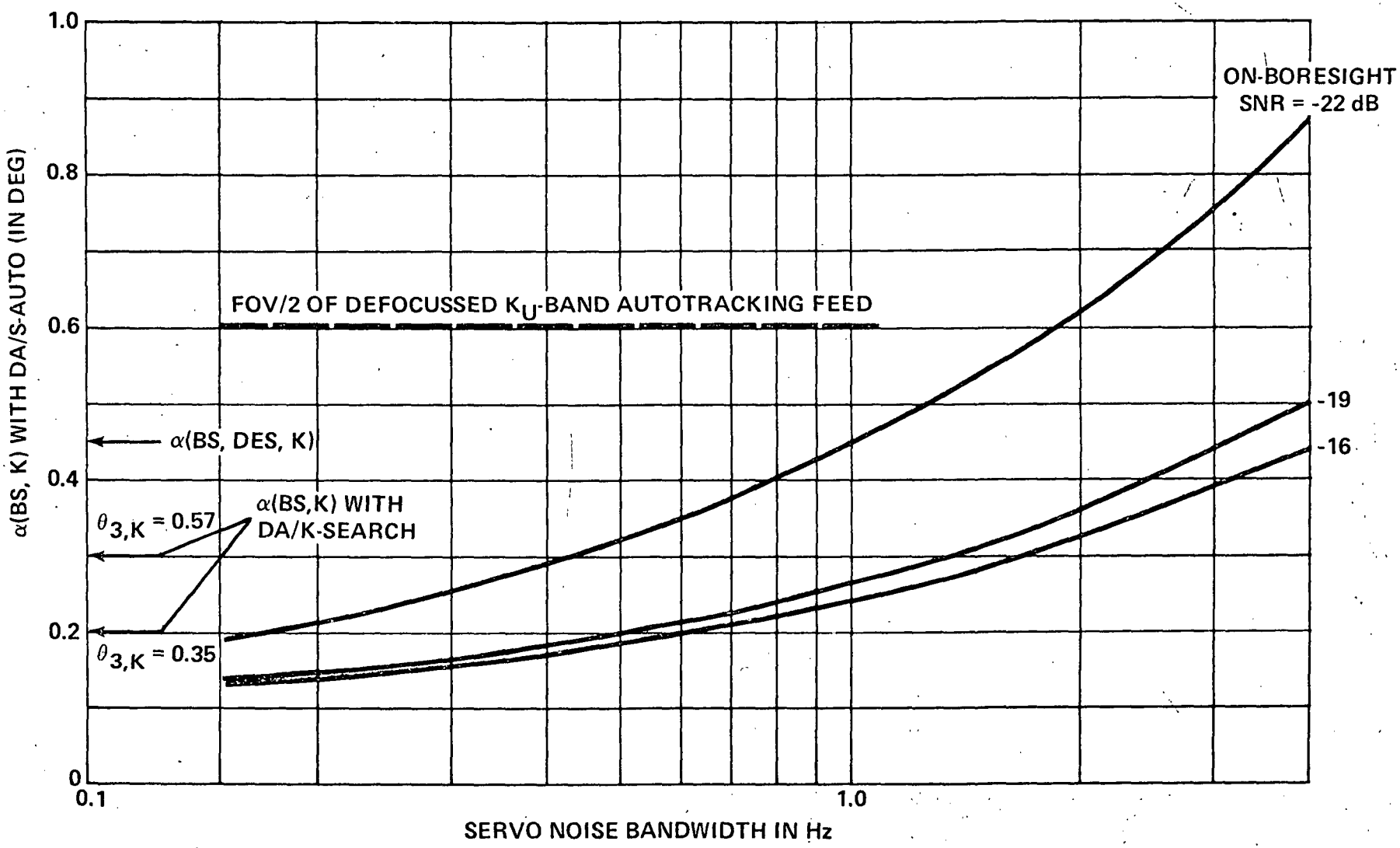

Figure 103. Error with which K_u-Band Boresight Axis is Designated as a Result of DA/S-AUTO

5.0 RECOMMENDATIONS FOR ADDITIONAL EFFORT

Based upon the material set forth above, it seems reasonable to re-examine the activities of Phase II of the subject contract to structure them more closely to the results of Phase I.

There are two fundamental areas in which Phase II measurements can be employed to support the conclusions formulated in Phase I: 1) the performance of the defocused K_u-band feed system and reflector, and 2) the off-axis characteristics of the S-band feed system in Option III.

More specifically, there are three items of interest in regard to the K_u-band feed: 1) the extent and effect of phase shift correction for defocused operation, 2) the field-of-view, and 3) the effect of mutual coupling between the data and tracking feed on the pattern and gain. With regard to the S-band feed system for illumination of a spherical reflector in Option III, the problem of minimizing the data beam loss for large angular beam offset from the reflector axis is of interest.

Clearly, the choice of the S-band feed option has an impact on the effort to be expended in Phase II. If, for example, Option III is of limited interest, then there is no motivation for the use of a spherical reflector. Phase II would logically be comprised of limited measurements of the performance of a focused S-band feed and a much more extensive determination of the characteristics associated with K_u-band operation. The reflector would, of course, be a 12.5-foot diameter paraboloid.

If, however, there is significant interest in Option III, then it seems reasonable to carry out Phase II with the use of a 12.5-foot diameter spherical reflector.

A third alternative will result from the decision that a specific option should not be selected prior to Phase II. In this event, it is suggested that two antennas be constructed and tested:

1. A 12.5-foot diameter paraboloid with a focused S-band feed, dichroic cassegrainian subreflector, and K_u-band feed (the latter device to contain a focused, dedicated data channel and a four-feed defocused auto tracking array,

2. A 3-foot diameter spherical reflector with a scanning feed scaled to approximately 9.0 GHz to simulate S-band operation.

In subsequent paragraphs, a detailed set of fundamental, recommended measurements is set forth. They are applicable, in an obvious way, to the three alternatives defined above.

Figure 103. [illegible] as a Result of DA/S-AUTO

5.1 Defocused K_u-Band Feed System

The basic problem to be solved, through a measurement program, is the determination of the compensation which must be applied to the auto tracking system to negate the deleterious effects of defocusing. The basic method selected for defocusing is to create a phase error in the aperture plane which acts to decrease the effective aperture size. (The amount of defocusing proposed will act to increase the spatial width of the pre-comparator antenna patterns without materially influencing their shape). The effect of defocusing is a departure from the 0/180 degree phase relationship between the sum and difference channel signals. For a fixed amount of defocusing, the case of interest herein, a fixed phase shift employed in each of the two tracking channels provides the desired compensation. A determination of the amount of phase shift, obtained via post-comparator phase measurements, is the objective of the proposed experiment.

5.2 Field of View of Auto Tracking System

An important result of the analysis reported in section 4.8 is that the FOV of the K_u-band auto tracking system employed for data link maintenance is compatible with ground station designation accuracy of the boresight axis of that system.

By way of review, prior to the closing of the auto tracking loop, the boresight axis of the K_u-band autotracker is indirectly aimed by ground command of the reflector pointing angles. It is shown in paragraph 4.8.1 that the resulting 3σ angular separation of the direction of signal arrival from the user and the boresight axis is 0.45 degree. Moreover, the maximum sum value of the same error is 0.85 degree. It follows that if the FOV of the K_u-band auto tracking system is of the order of 1.2 degrees, then successful closing of the auto tracking loop will result with a probability of essentially unity.

Next, it was shown theoretically that this value of FOV is achievable, even for small values of on-boresight signal-to-noise ratio. (The reduction in SNR which occurs as a result of off-boresight operation is, of course, accounted for in the analysis.) If this theoretical prediction is accurate, then the need for a systematic spatial search of the region surrounding the expected direction of signal arrival is negated. The search method of designation has teh advantage of being a proven method and subject to rather precise analysis. However, it suffers from several important disadvantages:

1. Long term gimbal component deterioration
2. Primary power needed for antenna motion
3. Thruster energy required for stabilization.

It is, therefore, asserted that elimination of the need for designation via search is a desirable goal.

In order that a sufficiently high degree of confidence be associated with direct designation of the K_u-band autotracker from the ground station, it is recommended that an experimental program be carried out for the purpose of providing measured values of FOV under carefully controlled conditions. The principal tools needed for such an investigation are a NASA ground station antenna system with an auto tracking mode of operation and the simulated TDRS reflector and feed system described above.

It is proposed that a NASA ground-based antenna which simulates, as closely as possible the TDRS antenna be defined, i.e., the two antennas must have similar properties in feed system geometry (scaled to the operating wavelength), subreflector illumination function, ratio of focal length (both actual and equivalent), and reflector diameter. (Notice that the ATS Tracking Facility at Mojave, California is an example of such an antenna, as is pointed out in paragraph 4.8.2.1.) Moreover, the NASA antenna must be equipped with a tracking receiver comparable to the type envisaged for use in the TDRS.

The recommended experimental program would be devoted to a measurement of the antenna system FOV, with the SNR as the basic variable. More specifically, the noise power with which the signal would be required to compete would be measured in the bandwidth of the IF amplifier contained in the tracking receiver.

The measured values of the radiation patterns of the ground based NASA antenna would be compared with those of the simulated TDRS antenna to obtain appropriate scaling constants. Then, measured values of the FOV of the former system would be used to infer those of the latter.

In addition to being of direct benefit to the TDRS problem, the subject experimental program would also be a useful step toward filling what has been found to be an obvious void in the published literature - substantive information on FOV.

5.3 Off-Axis S-Band Operation

The provision for a bent pipe data link at S-band using Option III requires that the antenna beam be displaced from the reflector axis to the extent necessary to deflect the antenna beam up to 30 degrees. This requirement is, of course, the motivation for the use of a spherical reflector.

The activities recommended for Phase II in this regard are directed toward maximizing the antenna gain for large angles of beam displacement from the reflector axis of symmetry. More specifically, although the feed system is constrained to move on an arc of radius one-half that of

the spherical reflector, the direction in which the feed should be pointed to maximize the gain has not been determined.

Three possibilities appear to be worthy of experimentation:

1 No pointing (feed axis normal to scan surface)

2 Feed axis parallel to reflector axis

3 Feed axis pointed toward reflector vertex.

If Phase II is so designed that the 12.5-foot diameter reflector is paraboloidal, and if there is also interest in the spherical reflector, then optimization of S-band performance using the latter device could be conveniently carried out using a 3-foot diameter reflector at approximately 9.0 GHz.

REFERENCES

1. TDRSS Definition Phase Study. NASA (GSFC) Report, December 1973.

2. Tracking and Data Relay Satellite System (TDRSS) Definition Phase Study Report. NASA (GSFC), December 1973.

3. A. F. Sciambi, Jr. Instant Antenna Patterns, Microwaves. June 1966. pp. 48-60.

4. Advanced Communication Satellite Systems Comparison Studies. Goodyear Aerospace Corporation Report N69-26435, April 1969. Volume III - Appendices, Table 5, p. D-27.

5. Advanced Communication Satellite Systems Comparison Studies. Goodyear Aerospace Corporation Report N69-26435, April 1969. Volume III - Appendices, p. D-23.

6. W. V. T. Rusch. Scattering from a Hyperboloidal Reflector in a Cassegrain Feed System. PGAP, July 1963. pp.414-421.

7. B. R. Hatcher. Graphs Estimate Feed Blockage, Microwaves. July 1971. pp. 31-32.

8. T. Wise. NASA GSFC. Unpublished information.

9. Tracking and Data Relay Satellite System, Configuration, and Tradeoff Study. Hughes Aircraft Company Report, September 1972. Volume 5, TDRS Spacecraft Design, Table 4-31.

10. Advanced Communication Satellite Systems Comparison Studies, Goodyear Aerospace Corporation Report N69-26435, April 1969. Volume III - Appendices, p. D-9

11. Critical Design Review Data Package for Advanced Applications Flight Experiment. Radiation, Inc., Report NAS1-11444, October 1972. Volume I (Basic), Table 4.3.1.1, p. 107.

12. Dr. B. C. Tankersley. Radiation, Inc., Melbourne, Florida. Unpublished data.

13. Microwave Engineer's Handbook.

14. Moreno. Microwave Transmission Design Data. p. 65.

15. D. E. Power. Antenna Pattern Shaping, Sensing, and Steering Study. Sylvania Report NASA CR72628, April 1970. pp. 39 and 43.

16. Microwave Engineers Technical and Buyers Guide Edition, Microwave Journal. February 1969. Table of Rigid Rectangular Waveguide Data and Fittings, p. 16.

17. H. W. Redlien, Monopulse Operation with Continuously Variable Beamwidth by Antenna Defocussing, PGAP. July 1968. Appendix, pp. 415-423.

18. G. C. Keller, M. S. Maxwell, L. R. Dod. Radial Rotating Antenna Feed System. NASA Technical Brief 71-10025, February 1971.

19. Critical Design Review Data Package for Advanced Applications Flight Experiment. Radiation, Inc., Report NASI-11444, Sequence No. 43118-01, October 1972. p. 79.

20. Tracking and Data Relay Satellite System Configuration and Tradeoff Study - Part II, Final Report. Hughes Aircraft Company, April 1973. Volume II, Delta Launched TDRSS - Configuration, p. 47.

21. Tracking and Data Relay Satellite System Configuration and Tradeoff Study - Part I, Final Report. North American Rockwell Report No. SD-72-SA-0133-4, October 1972. p. 6-4.

22. Critical Design Review Data Package for Advanced Applications Flight Experiment. Radiation, Inc., Report NASl-11444, Sequence No. 4318-01, October 1972. p. 76.

23. P. D. Potter. Unique Feed System Improves Space Antennas. June 1962. pp. 36-40.

24. P. W. Cramer, Jr. Large Spacecraft Antennas: Performance Comparison of Focal Point and Cassegrain Antennas for Spacecraft Applications. JPL Space Programs Summary 37-62. pp. 80-89.

25. Tingye Li A Study of Spherical Reflectors as Wide-Angle Scanning Antennas, IRE Transactions on Antennas and Propagation. July 1959. pp. 223-226.

26. A. W. Love. Spherical Reflecting Antennas with Corrected Line Sources, IRE Transaction on Antennas and Propagation. September 1962. pp. 529-537.

27. A.W. Love. Scale Model Development of a High Efficiency Dual Polarized Line Feed for the Arecibo Sperical Reflector, IEEE Transaction on Antennas and Propagation. September 1973. pp. 628-639.

28. A. D. Bresler. Multiple-Beam Spherical-Reflector Antenna Systems for Satellite Communications, IEEE International Conference on Communications. 1973. Volume I.

29. A. Ishimaru, I. Screenivisiah, and V. Wong. Durable Spherical Cassegrain Reflector Antenna, IEEE Transactions on Antennas and Propagation. November 1973. pp. 774-780.

30. J. Ashmead and A. B. Pippard. The Use of Spherical Reflectors as Microwave Scanning Aerials, J. IEEE. 1946. Volume 93, pt. 111A, No. 4. pp. 627-632.

31 P. H. Masterman. A Spherical Reflector Antenna for a Satellite-Communications Earth Station, 1973 European Microwave Conference. September 1973. Volume 2, p. c.4.2.

32. W. E. Kock. Bell System Technical Journal, 1948. Volume 27, p. 58.

33. G. H. Schennum. Frequency - Selective Surfaces for Multiple-Frequency Antennas, Microwave Journal. May 1973. p. 55.

34. W. V. T. Rusch. Analysis of Low Noise Antennas, JPL Space Programs Summary. February 1963. No. 37-19, pp. 189-196.

35. P. D. Potter. A New Horn Antenna with Suppressed Sidelobes and Equal Beamwidths, The Microwave Journal. June 1963. pp. 72-78.

36. A High Gain Autotrack Antenna System for a Low Altitude Satellite Utilizing a Data Relay Satellite System, Hughes Aircraft Company Contract No. NAS-5-11602. November 1970. pp. 3-4

37. P. W. Hannan. Optimum Feeds for All Three Modes of a Monopulse Antenna II Practice, PGAP. September 1961. pp. 454-461

38. P. Mallach. Dielectric Direcitonal Antennas for D_m and C_m Waves. Air Material Command Report, F-TS-2223-RE, February 1948.

39. L. W. Mickey and G. G. Chadwick. Closely Spaced High Dielectric Constant Polyrod Arrays, 1958 IRE National, Conv. Rec. Pt. 1.

40. H. Jasik. Antenna Engineering Handbook. McGraw-Hill Book Co., 1961. pp. 16-14.

41. T. B. Vu and N. V. Hien. A New Type of High Performance Monopulse Feed, PGAP. November 1973. pp. 855-857.

42. P. J. B. Clarricoats and P. H. Masterman. A Multimode Monopulse Feed for a Satellite Tracking Antenna, European Microwave Conference. 1969. p. 357.

43. D. N. Cooper. A New Circularly Polarized Monopulse Feed System, Proc. IEEE. September 1965. pp. 1252-1254.

44. Henry W. Redlien, Jr. Monopulse Operation with Continuously Variable Beamwidth by Antenna defucusing, Trans. IEEE. July 1968. Volume AP-16, pp. 415-423.

45. Space Deployable Large Aperture Flexible Rib Reflectors. Lockheed Missile and Space Company, Inc., LMSC-A946613-1.

46. ATS Transportable Communications Ground Station Final Report. Sylvania Electronics System-East, NASA Contract NAS5-9533(GSFC), November 1966.

47. J. A. Develet. Thermal Noise Errors in Simultaneous Lobing and Conical Scan Angle Tracking Systems, IRE Trans. June 1961. Volume SET-7, pp. 42-51.

48. G. M. Pelchat. The Effects of Receiver and Antenna Noise on the Performance of a Conical Scan Tracking System, Microwave Journal, February 1965. Volume 8, pp. 37-40, 61.

49. K. D. Barton. Radar System Analysis. Prentice-Hall, Inc., Englewood Cliffs, N. J., 1965. Chapter 9.

50. D. DeVito. Unpublished material and discussion provided by DeVito during visit to NASA(GSFC). Analysis performed for NASA(GSFC) by the Magnavox Company visit on 7-8 March 1974.

51. D. K. Barton and H. R. Ward. Handbook of Radar Measurement. Prentice-Hall.

52. H. W. Redlien. Monopulse Operation with Continuously Variable Beamwidth by Antenna Defocusing, Trans. IEEE. July 1968. Volume AP-16, pp. 415-423.

53. W. L. Nelson. Phase Lock Loop Design for Coherent Angle Error Detection in the Telstar Satellite Tracking System, Bell Technical Journal. September 1963. Volume 42, pp. 1941-1975.

54. P. D. Shaft. Hard Limiting of Several Signals and Its Effect on Communication System Perofrmance, IEEE International Convention Record. 1965. Part II, Communications II, pp. 103-112.

55. J. Benton and H. Smith. Latest Advances in Space TWT's, Progress in Aeronautics Series. MIT Press, 1971. Volume 25 (N. Feldman and C. M. Kelly, Eds.), pp. 12-13.

56. Step Track Antenna (Technical Brief I-SS-2096) and Step Track Servo Control (Technical Brief I-SS-2069). Radiation, Inc.

57. Limited Scan Antennas Cut Costs for Satellite Terminals, Microwaves. May 1974. Volume 13, p. 10.

58. Private Communication with Mr. Spencer Yawger of USASCA. Ft. Monmouth, New Jersey, 23 May 1974.

59. J. F. Ramsay. Lambda Functions Describe Antenna Diffraction Patterns, Microwaves. June 1967. Volume 6, pp. 69-107.

60. A. F. Sciambi. The Effects of the Aperture Illumination on the Circular Aperture Pattern Characteristics, Microwave Journal. August 1965. pp. 79-84.

61. Post-Mod A.T.P (Mojave), Part II - Data Sheets. Martin Marietta Aerospace Report, OR 12,035-4. January 1973.

62. Tracking and Data Relay Satellite System Configuration and Tradeoff Study - Part II, Final Report. Volume II, Delta 2914 Launched TDRSS - Configuration 2. Hughes Aircraft Company, El Segundo, California, Contract NAS5-21704, April 1973. pp. 49-60.

63. R. F. Schmidt, "Variable Beamwidth Monopulse Antenna," March 1974, NASA-GSFC, X-811-74-62.

APPENDIX A

THE EFFECTS OF PRE/POST-COMPARATOR PHASE/AMPLITUDE UNBALANCE IN A SUM AND DIFFERENCE MONOPULSE SYSTEM

There are four effects of pre/post-comparator phase/amplitude unbalance in a sum and difference monopulse system which are of interest:

1. An angular shift in the boresight axis,
2. A decrease in the slope of the angle detector output in the vicinity of boresight,
3. A sum channel gain reduction at boresight,
4. An angular shift in the sum channel maximum.

It is the purpose of this appendix to define a sum and difference monopulse system in terms of an antenna, comparator, receiver, and angle detector and then derive relationships for the four factors listed above in terms of departure of the system elements from ideal operation.

General

The monopulse system to be investigated is illustrated in Figure A-1. It represents one plane of a dual plane angle sensor. The antenna, a two port device, produces mirror image patterns characterized by $g(\theta)$ and $g(-\theta)$, where θ is the off-boresight angle. The pre-comparator phase/amplitude errors are represented by

$$A_i = |A_i| e^{j\alpha_i}; \quad i = 1,2$$

whereby the phase unbalance is $|\alpha_1-\alpha_2|$ and the amplitude unbalance is $|A_1|/|A_2|$. The phase/amplitude errors which occur between the comparator and the angle sensor are combined into the terms

$$B_i = |B_i| e^{j\beta_i}; \quad i = 1,2$$

such that the post-comparator phase and amplitude unbalances are $|\beta_1-\beta_2|$ and $|B_i|/|B_2|$, respectively. The difference and sum signals delivered to the angle detector take the form

$$\Delta(\theta) = \frac{B_1}{\sqrt{2}} [A_1 g(\theta) - A_2 g(-\theta)] \tag{1}$$

and

$$\Sigma(\theta) = \frac{B_2}{\sqrt{2}} [A_2 g(\theta) + A_2 g(-\theta)] \tag{2}$$

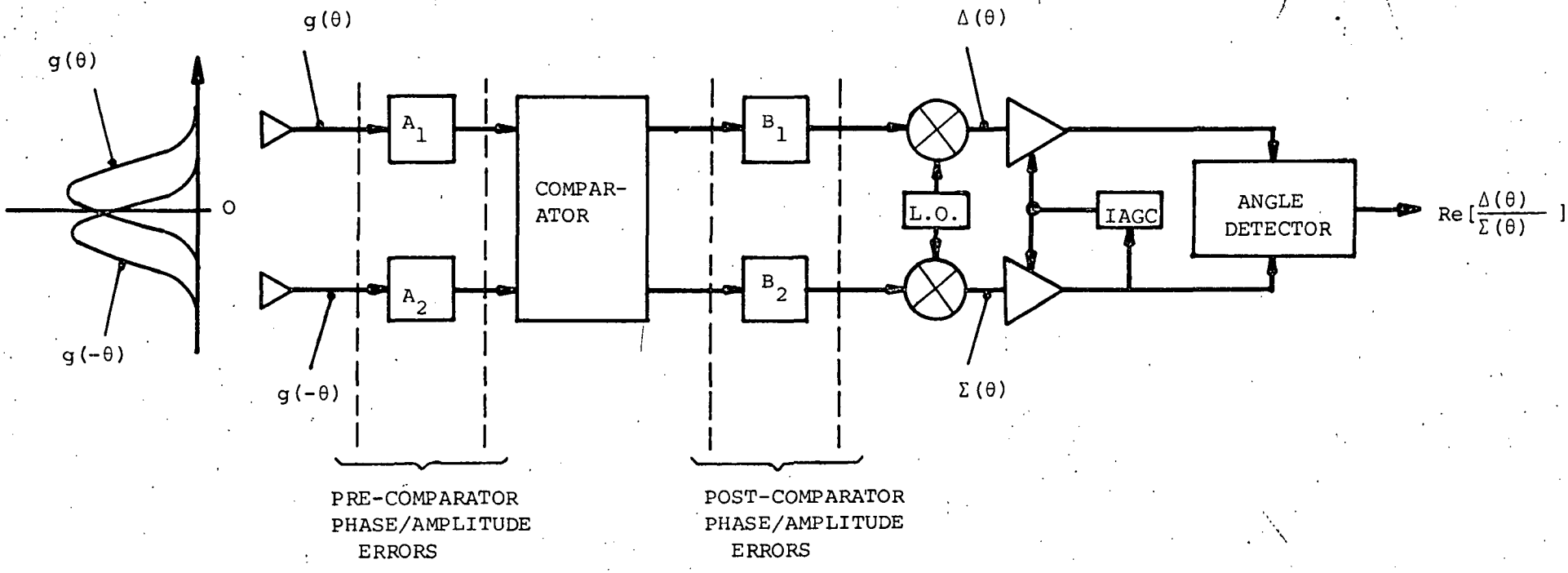

Figure A-1. Sum and Difference Monopulse System Model

Finally, the output of the angle detector can be written as Re $[\Delta(\theta)/\Sigma(\theta)]$ in accordance with the monopulse postulates set forth by Rhodes (Reference A-1). It is easy to show that this output can be expressed in terms of the real and imaginary components of the sum and difference signals by

$$\text{Re}\left[\frac{\Delta(\theta)}{\Sigma(\theta)}\right] = \frac{\Delta_R(\theta)\,\Sigma_R(\theta) + \Delta_I(\theta)\,\Sigma_I(\theta)}{|\Sigma(\theta)|^2} \tag{3}$$

The next problem is to express $\Delta(\theta)$ and $\Sigma(\theta)$ in terms of the antenna pattern functions $g(\theta)$ and $g(-\theta)$ as well as the phase/amplitude errors A_1, A_2, B_1, and B_2. Moreover, the results must bring out the real and imaginary components for use in Equation (3). Straightforward manipulations of Equations (1) and (2) lead to

$$\Delta(\theta) = \frac{g(-\theta)|A_2||B_1|}{2}\left\{R\cos(\alpha_1+\beta_1) - \cos(\alpha_2+\beta_1) + j[R\sin(\alpha_1+\beta_1) - \sin(\alpha_2+\beta_1)]\right\} \tag{4}$$

and

$$\Sigma(\theta) = \frac{g(-\theta)|A_2||B_2|}{2}\left\{R\cos(\alpha_1+\beta_2) + \cos(\alpha_2+\beta_2) + j[R\sin(\alpha_1+\beta_2) + \sin(\alpha_2+\beta_2)]\right\} \tag{5}$$

where the definitions

$$R \triangleq \left|\frac{A_1}{A_2}\right| r(\theta)$$

and

$$r(\theta) \triangleq \frac{g(\theta)}{g(-\theta)}$$

have been employed.

Next, the numerator and denominator of Equation (3) are found from Equations (4) and (5) to be

$$\Delta_R(\theta)\Sigma_R(\theta) + \Delta_I(\theta)\Sigma_I(\theta) = \frac{g^2(-\theta)|A_2|^2|B_1||B_2|}{2}[R^2\cos\beta + 2R\sin\alpha\sin\beta - \cos\beta]$$

and

$$|\Sigma(\theta)|^2 = \frac{g^2(-\theta)|A_2|^2|B_2|^2}{2}[R^2 + 2R\cos\alpha + 1] \tag{6}$$

where the phase differences

$$\alpha \triangleq \alpha_1 - \alpha_2$$

and

$$\beta \triangleq \beta_1 - \beta_2$$

have been defined. The angle detector output then takes the reasonably simple form

$$\mathrm{Re}\left[\frac{\Delta(\theta)}{\Sigma(\theta)}\right] = \left|\frac{B_1}{B_2}\right| \left\{ \frac{\left|\frac{A_1}{A_2}\right|^2 r^2(\theta)\cos\beta + 2\left|\frac{A_1}{A_2}\right| r(\theta)\sin\alpha\sin\beta - \cos\beta}{\left|\frac{A_1}{A_2}\right|^2 r^2(\theta) + 2\left|\frac{A_1}{A_2}\right| r(\theta)\cos\alpha + 1} \right\} \qquad (7)$$

As a check on the above result, if there are no phase/amplitude errors then $|A_1| = |A_2|$, $|B_1| = |B_2|$ and $\alpha = \beta = 0$, from which it follows that

$$\mathrm{Re}\left[\frac{\Delta(\theta)}{\Sigma(\theta)}\right] = \frac{g(\theta) - g(-\theta)}{g(\theta) + g(-\theta)}$$

as required.

The impact of the result stated in Equation (7) is that the slope of the error signal produced by the angle detector is reduced and the boresight direction is shifted as a result of pre/post comparator errors. These characteristics are qualitatively illustrated in Figure A-2. Equation (7) is now used to provide a quantitative evaluation of the same factors. Then, Equation (6) is employed to evaluate the effect of phase/amplitude errors on the sum channel gain.

Angular Boresight Shift

The basic problem is to determine the angle θ_o such that

$$\mathrm{Re}\left[\frac{\Delta(\theta_o)}{\Sigma(\theta_o)}\right] = 0.$$

Since the denominator of Equation (7) is obviously non-zero in the vicinity of boresight, it is only necessary to work with the numerator, i.e., to formulate the value of θ_o which yields

$$\left|\frac{A_1}{A_2}\right|^2 r^2(\theta_o)\cos\beta + 2\left|\frac{A_1}{A_2}\right| r(\theta_o)\sin\alpha\sin\beta - \cos\beta = 0$$

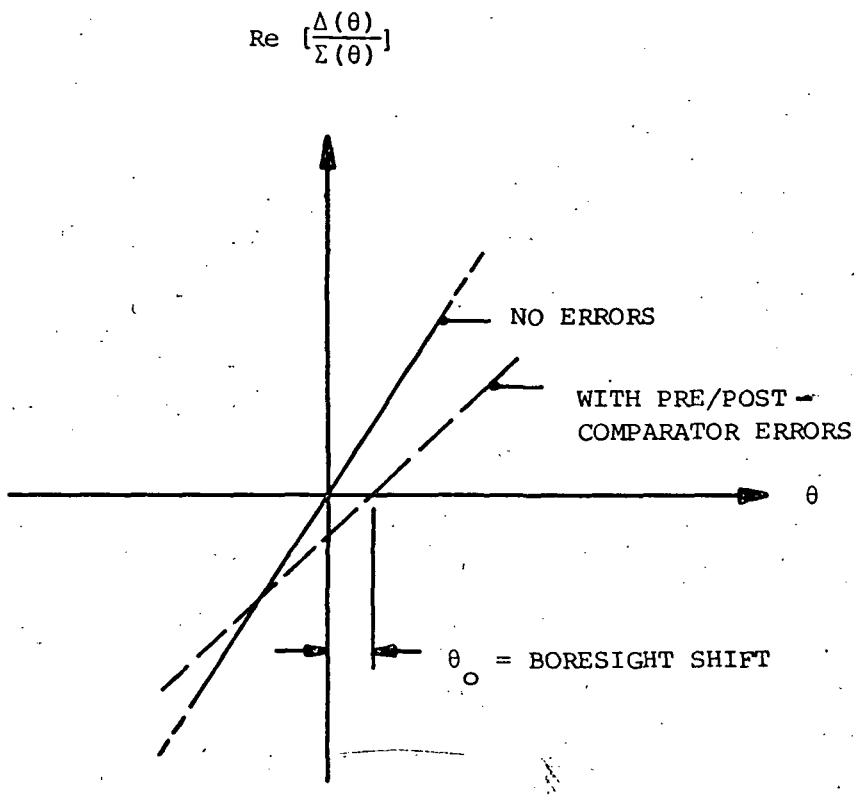

Figure A-2. Effect of Pre/Post Comparator Errors on Angle Detector Output Near Boresight

When the above equation is solved for $r(\theta_o)$, the result is

$$r(\theta_o) = \left|\frac{A_1'}{A_2}\right| \left[-\sin\alpha \tan\beta \pm \sqrt{1+\sin^2\alpha \tan^2\beta}\right]$$

In order to select the correct sign of the radical, the no-error case ($\alpha = \beta = 0$ and $|A_1| = |A_2|$) must result in $r(\theta_o) = 1$. Thus,

$$r(\theta_o) = \left|\frac{A_1'}{A_2}\right| \left[-\sin\alpha \tan\beta + \sqrt{1+\sin^2\alpha \tan^2\beta}\right] \tag{8}$$

from which it is seen that the boresight direction is shifted by all of the pre/post-comparator errors except the post-comparator amplitude unbalance. Moreover, if the pre-comparator phase and amplitude errors are reduced to zero, then $r(\theta_o) = 1$, so that $\theta_o = 0$, independent of the magnitude of β, the post-comparator phase unbalance.

In order to obtain a solution for θ_o, the ratio $r(\theta)$ must be expressed in terms of the antenna pattern functions $g(\theta)$ and $g(-\theta)$. Use is therefore made of the fact that in the neighborhood of the beam maximum, a variety of antenna patterns of the type of interest herein can be well approximated by gaussian functions. Specifically,

$$g(\theta) = g_M \exp\left[-k(\theta-\theta_M)^2\right]$$

and

$$g(-\theta) = g_M \exp\left[-k(\theta+\theta_M)^2\right]$$

where θ_M and $-\theta_M$ are the angles at which $g(\theta)$ and $g(-\theta)$ take on their maximum value g_M and the value of k is determined from

$$g\left(\theta_M \pm \frac{\theta_3}{2}\right) = \frac{g_M}{\sqrt{2}}$$

where θ_3 is defined as the half-power beamwidth of either antenna pattern. It is a simple matter to show that

$$k = \frac{\log_e 4}{\theta_3^2}$$

from which is follows that $r(\theta) \triangleq g(\theta)/g(-\theta)$ is given by

$$r(\theta) = \exp\left[\frac{4\theta\theta_M}{\theta_3^2} \log_e 4\right]$$

When θ is equated to θ_o in Equation (9) and the result used in Equation (8), the boresight shift, normalized to the antenna half-power beamwidth, becomes

$$\frac{\theta_o}{\theta_3} = \left[\frac{\theta_3}{\theta_M}\right] \frac{\log_e \left\{ \left| \frac{A_2}{A_1} \right| \left[-\sin\alpha \tan\beta + \sqrt{1+\sin^2\alpha \tan^2\beta} \right] \right\}}{5.5452} \qquad (10)$$

Notice that the factor θ_3/θ_M is related to the antenna crossover level (expressed in dB) by

$$20\log_{10}\left[\frac{g(0)}{g(\theta_M)}\right] = -12\left(\frac{\theta_M}{\theta_3}\right)^2$$

Thus, the boresight shift increases with the crossover level. Also, it is clear from an inspection of Equation (10) that the boresight shift is maximized when $|A_2|/A_1| > 1$ and either when $\alpha<0, \beta>0$ or $\alpha>0$, $\beta<0$.

Slope of Angle Detector Output

The determination of the subject quantity requires an evaluation of the slope of the angle detector output evaluated at $\theta = \theta_o$. In general,

$$\frac{d}{d\theta} Re\left[\frac{\Delta\theta}{\Sigma\theta}\right] = \frac{d}{dr} Re\left[\frac{\Delta(r)}{\Sigma(r)}\right] \cdot \frac{dr(\theta)}{d\theta} \qquad (11)$$

The formulation of the derivative with respect to r of the angle detector output is straightforward but tedious. The result is

$$\frac{d}{dr} Re\left[\frac{\Delta(r)}{\Sigma(r)}\right] = 2AB\left[\frac{r^2A^2\cos(\alpha+\beta) + 2rA\cos\beta + \cos(\alpha-\beta)}{(A^2r^2+2Ar\cos\alpha+1)^2}\right] \qquad (12)$$

where A and B have been used in place of $|A_1/A_2|$ and $|B_1/B_2|$ to simplify the notation. The next step is the evaluation of Equation (12) at $\theta = \theta_o$. In order to obtain a tractable result, it is assumed that the phase/amplitude errors are reasonably small so that the slope function defined in Equation (12) is essentially the same at $\theta = 0$ and $\theta = \theta_o$. Equation (12) then takes the form

$$\frac{d}{d\theta} Re\left|\frac{\Delta(\theta)}{\Sigma(\theta)}\right|_{\theta=0} \approx \frac{d}{dr} Re\left|\frac{\Delta(r)}{\Sigma(r)}\right|_{r=1} \cdot \left|\frac{dr(\theta)}{d(\theta)}\right|_{\theta=0}$$

or, using (12),

$$\frac{d}{d\theta} Re\left[\frac{\Delta(\theta)}{\Sigma(\theta)}\right]_{\theta=\theta_o} = 2AB\left[\frac{A^2\cos(\alpha+\beta)+2A\cos\beta+\cos(\alpha-\beta)}{(A^2+2A\cos\alpha+1)^2}\right]\cdot\left[\frac{dr(\theta)}{d\theta}\right]_{\theta=0}$$

If there are no pre/post comparator errors, then

$$\frac{d}{d\theta} Re\left[\frac{\Delta(\theta)}{\Sigma(\theta)}\right] = \frac{1}{2}\left[\frac{dr(\theta)}{d\theta}\right]_{\theta=0}$$

from which it follows that

$$\frac{d}{d\theta} Re\left[\frac{\Delta(\theta)}{\Sigma(\theta)}\right]_{WITH\ UNBAL.} \approx \frac{d}{d\theta} Re\left[\frac{\Delta(\theta)}{\Sigma(\theta)}\right]_{NO\ UNBAL} \left\{4AB\left[\frac{A^2\cos(\alpha+\beta)+2A\cos\beta+\cos(\alpha-\beta)}{(A^2+2A\cos\alpha+1)^2}\right]\right.$$

i.e., the slope of the angle detector output at boresight, in the presence of pre/post comparator phase and amplitude unbalance, is equal to the no error slope multiplied by the factor

$$SLOPE\ MOD.FACTOR = 4\left|\frac{A_1}{A_2}\right|\left|\frac{B_1}{B_2}\right|\left\{\frac{\left[\left|\frac{A_1}{A_2}\right|^2\cos(\alpha+\beta)+2\left|\frac{A_1}{A_2}\right|\cos\beta+\cos(\alpha-\beta)\right]}{\left[\left|\frac{A_1}{A_2}\right|^2+2\left|\frac{A_1}{A_2}\right|\cos\alpha+1\right]^2}\right\} \quad (13)$$

which, when there are no errors, is unity, as required.

Sum Channel Gain Reduction

The next problem is the formulation of the reduction in sum channel gain at boresight ($\theta=\theta_o$) with respect to that at $\theta=0$ in the no error case. Equation (6), repeated below, will be the principal tool.

$$|\Sigma(\theta)|^2 = \frac{g^2(-\theta)|A_2|^2|B_2|^2}{2}\left[\left|\frac{A_1}{A_2}\right|^2 r^2(\theta)+2\left|\frac{A_1}{A_2}\right| r(\theta)\cos\alpha+1\right] \quad (6)$$

A more convenient form for $|\Sigma(\theta)|^2$ is

$$|\Sigma(\theta)|^2 = \frac{|B_2|^2}{2}\left[|A_1|^2 g^2(\theta)+2|A_1||A_2| g(\theta)g(-\theta)\cos\alpha+|A_2|^2 g^2(-\theta)\right] \quad (14)$$

In the case in which there is no phase/amplitude unbalance, the boresight axis is at $\theta=0$ and the relative sum channel power is given by

$$|\Sigma(0)|^2 = \frac{|B_2|^2}{2}[4g^2(0)]$$

The sum channel gain loss therefore becomes

$$L = \frac{|\Sigma(\theta_o)|^2}{|\Sigma(0)|^2}$$

or

$$L = |B_2|^2\left[\frac{|A_1|^2 g^2(\theta_o)+2|A_1||A_2|g(\theta_o)g(-\theta_o)\cos\alpha+|A_2|^2 g^2(-\theta_o)}{4g^2(0)}\right] \quad (15)$$

When Equation (15) is used for a computation of L (or $10\log_{10}L$), it will be assumed that $B_2 = 1$. That is, dissipative post-comparator losses in the sum channel will be separately accounted for. Also, since any pre-comparator gain will not influence the result, the conditions

$$|A_1|,\ |A_2| \leq 1$$

and

$$\text{either } |A_1| = 1 \text{ or } |A_2| = 1$$

are imposed. Next, it is noted that Equation (15) can be rewritten using normalized antenna pattern functions. That is,

$$L = \frac{1}{4}\left[|A_1|^2 g_N^2(\theta_o)+2|A_1||A_2|g_N(\theta_o)g_N(-\theta_o)\cos\alpha+|A_2|^2 g_N^2(-\theta_o)\right] \quad (16)$$

where $g_N(\theta_o) \triangleq g(\theta_o)/g(0)$ and $g_N(-\theta_o) \triangleq g(-\theta_o)/g(0)$ are given by

$$g_N(\theta_o) \triangleq \exp\left[-\frac{\theta_o(\theta_o-2\theta_M)^2}{\theta_3^2}\cdot\log_e 4\right] \quad (17a)$$

and

$$g_N(-\theta_o) \triangleq \exp\left[-\frac{\theta_o(\theta_o+2\theta_M)^2}{\theta_3^2}\cdot \log_e 4\right] \tag{17b}$$

with θ_o given in Equation (10). For the case in which the phase/amplitude errors are small, Equation (17) can be simplified by using the assumptions that

$$\theta_o - 2\theta_M \approx -2\theta_M$$

$$\theta_o + 2\theta_M \approx 2\theta_M$$

whereby

$$g_N(\theta_o) \approx \exp\left[\frac{2\theta_o\theta_M}{\theta_3^2}\cdot \log_e 4\right] \tag{18a}$$

and

$$g_N(-\theta_o) \approx \exp\left[-\frac{2\theta_o\theta_M}{\theta_3^2}\cdot \log_e 4\right] \tag{18b}$$

Finally, it is seen from Equation (10) that $\theta_o = 0$ when there are no errors, so that $g_N(\theta_o) = g_N(-\theta_o) = 1$. Also $|A_1| = |A_2| = 1$ and, from Equation (16), $L = 1$, as required.

Angular Shift of Sum-Channel Maximum

In order to determine the angle $\theta = \theta_S$ at which the relative sum channel power is maximized, Equation (14) will be employed, with $|B_2| = 1$. The simplest method appears to be a trial and error examination of θ/θ_3 in

$$\left|\Sigma\left(\frac{\theta}{\theta_3}\right)\right|^2 = |A_1|^2\tilde{g}^2\left(\frac{\theta}{\theta_3}\right) + 2|A_1||A_2|\tilde{g}\left(\frac{\theta}{\theta_3}\right)\tilde{g}\left(-\frac{\theta}{\theta_3}\right)\cos\alpha + |A_2|^2\tilde{g}^2\left(-\frac{\theta}{\theta_3}\right) \tag{19}$$

where

$$\tilde{g}\left(\frac{\theta}{\theta_3}\right) \triangleq \exp\left[-\left(\frac{\theta}{\theta_3} - \frac{\theta_M}{\theta_3}\right)^2 \log_e 4\right]$$

and

$$\tilde{g}\left(-\frac{\theta}{\theta_3}\right) \triangleq \exp\left[-\left(\frac{\theta}{\theta_3}+\frac{\theta_M}{\theta_3}\right)^2 \log_e 4\right]$$

The conditions on $|A_1|$ and $|A_2|$ which precede Equation (16) should again be imposed on Equation (19).

APPENDIX B

SERVO DESIGN CONCEPT AND CHARACTERISTICS

Two servo systems are described and characterized herein. One is applicable to the case in which the tracking receiver is contained in the TDRS and the other is employed when ground station processing is utilized.

Tracking Receiver Aboard TDRS

It is the purpose of this appendix to derive expressions for the angle tracking error which results from a torque disturbance T_d in terms of pertinent characteristics of the servo system shown in Figure B-1. Although all torque disturbances are included in T_d, those of particular importance are coulomb bearing motor brush friction, slip-ring friction, and bearing/gear noise.

With reference to the block diagram, the torque attenuation can be written as

$$\frac{\theta_T}{T_d/N} = \frac{G_P}{1+G_C G_P} \tag{1}$$

At low frequencies, it is the case that

$$G_C G_P >> 1$$

so that a good approximation of the torque attenuation is

$$\frac{\theta_T}{T_d/N} \approx \frac{G_P}{G_{OL}} \tag{2}$$

where θ_T is in radians and $G_{OL} = G_P G_C$ is the open-loop transfer function.

The general form of the open-loop frequency response of the servo system of interest is shown in Figure B-2. For frequencies $<\omega_a$, the open-loop response is approximated by

$$G_{OL}(s) \approx \frac{K_a}{s^2} \tag{3}$$

where K_a is the acceleration error constant defined by

$$K_a = \omega_a^2 \tag{4}$$

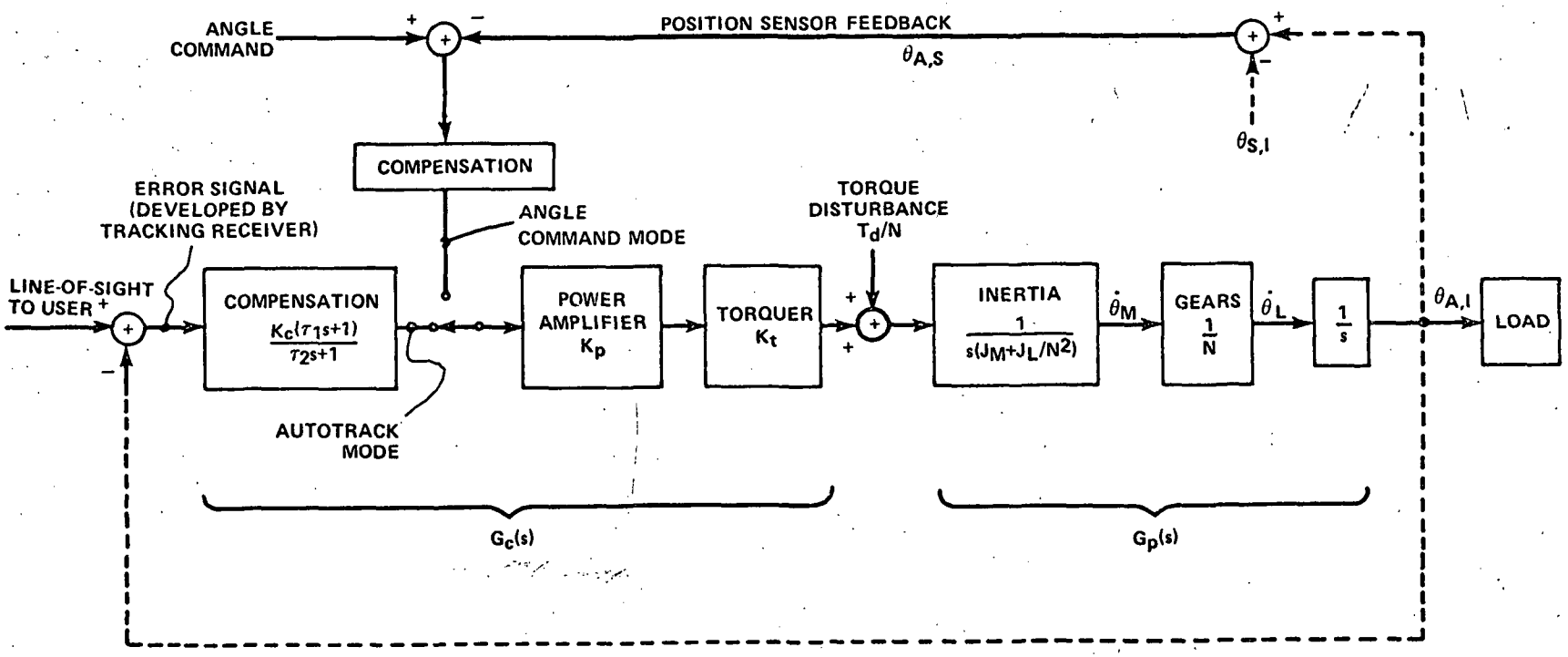

$\theta_{A,I}$ ≙ ANTENNA POSITION WITH RESPECT TO INERTIAL FRAME

$\theta_{S,I}$ ≙ SATELLITE POSITION WITH RESPECT TO INERTIAL FRAME

$\theta_{A,S}$ ≙ ANTENNA POSITION WITH RESPECT TO SATELLITE

Figure B-1. Servo System -- Tracking Receiver Aboard TDRS

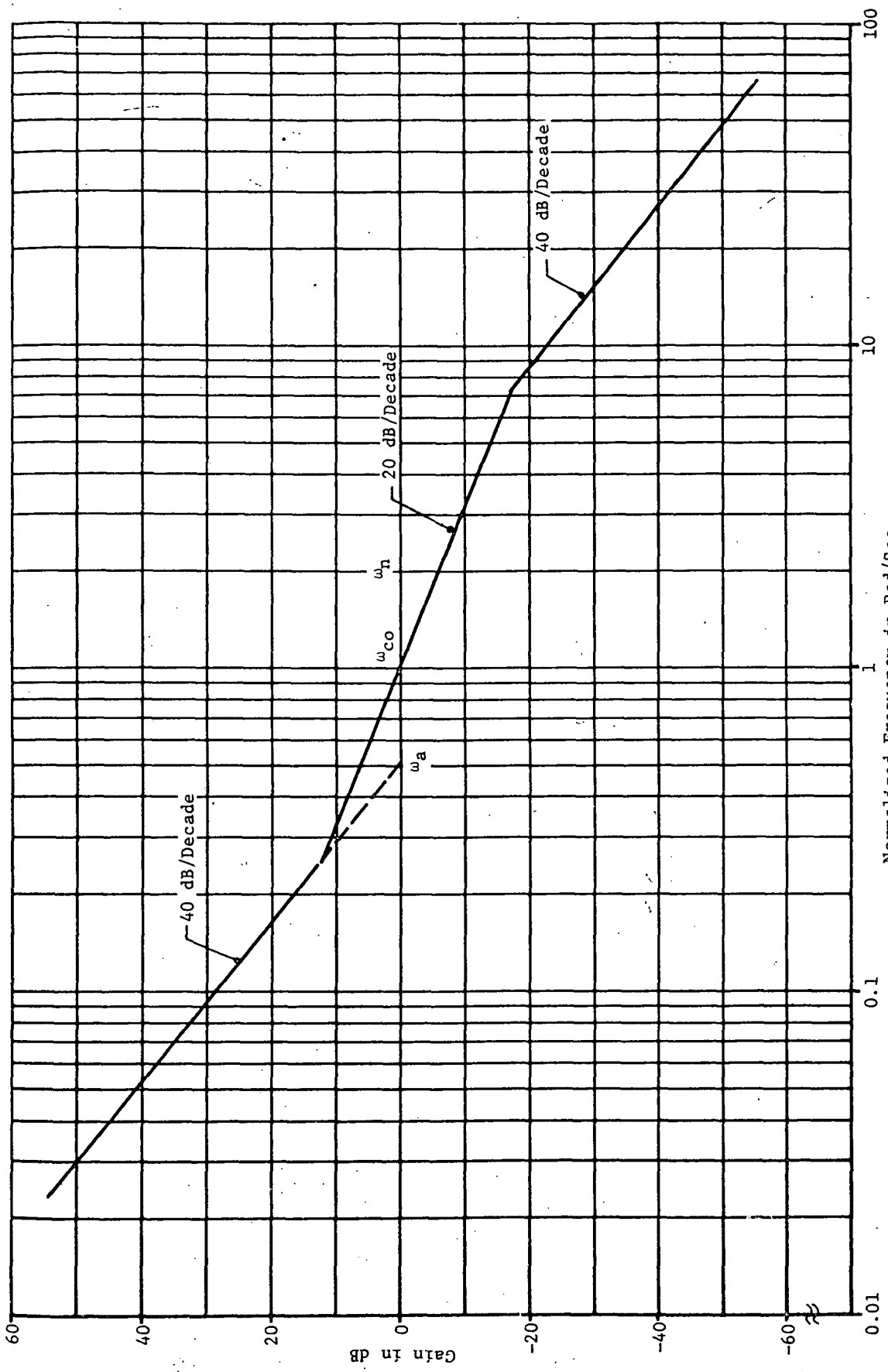

Figure B-2. Servo System Frequency Response

but

$$\omega_a^2 \approx \left(\frac{\omega_n}{4}\right)^2$$

so that

$$K_a \approx 2.5 B_n^2 \tag{5}$$

where β_n is the one-sided servo noise bandwidth in Hz. The above result is based upon a crossover frequency ω_{co} defined by $\omega_{co} \approx 2\omega_a$ for stability. Also, for a well-damped system the noise bandwidth is related to the crossover frequency by $\omega_n \approx 2\omega_{co}$. It follows then that $\omega_n = 4\omega_a$.

When Equations (3) and (5) are combined, the open-loop transfer function becomes

$$G_{OL}(s) = 2.5\left(\frac{B_n}{s}\right)^2 \tag{6}$$

Next, the transfer function $G_p(s)$ is seen from the block diagram to be

$$G_p(s) = \frac{1}{s^2 N (J_M + J_L/N^2)} \tag{7}$$

where

J_M = inertial on motor shaft

J_L = inertia on load shaft.

A substitution of Equations (6) and (7) into (2) yields the desired result, viz.,*

$$\theta_T = \frac{11.5\, T_d}{B_n^2 J}, \text{ deg.}$$

where

$$J = \frac{J_L + N^2 J_M}{2}, \text{ ft-lb-sec}^2$$

---

* In paragraph 4.4.1.1.1, the symbol δ_T is used instead of θ_T.

is a composite inertia. For the special case in which the gear ratio is selected for optimum load acceleration,

$$J_M = \frac{J_L}{N^2}$$

and, therefore

$$J = J_L.$$

Tracking Receiver at Ground Station

When the tracking receiver is relocated from the TDRS to the ground station, the servo system depicted in Figure B-1 is modified to the form shown in Figure B-3.

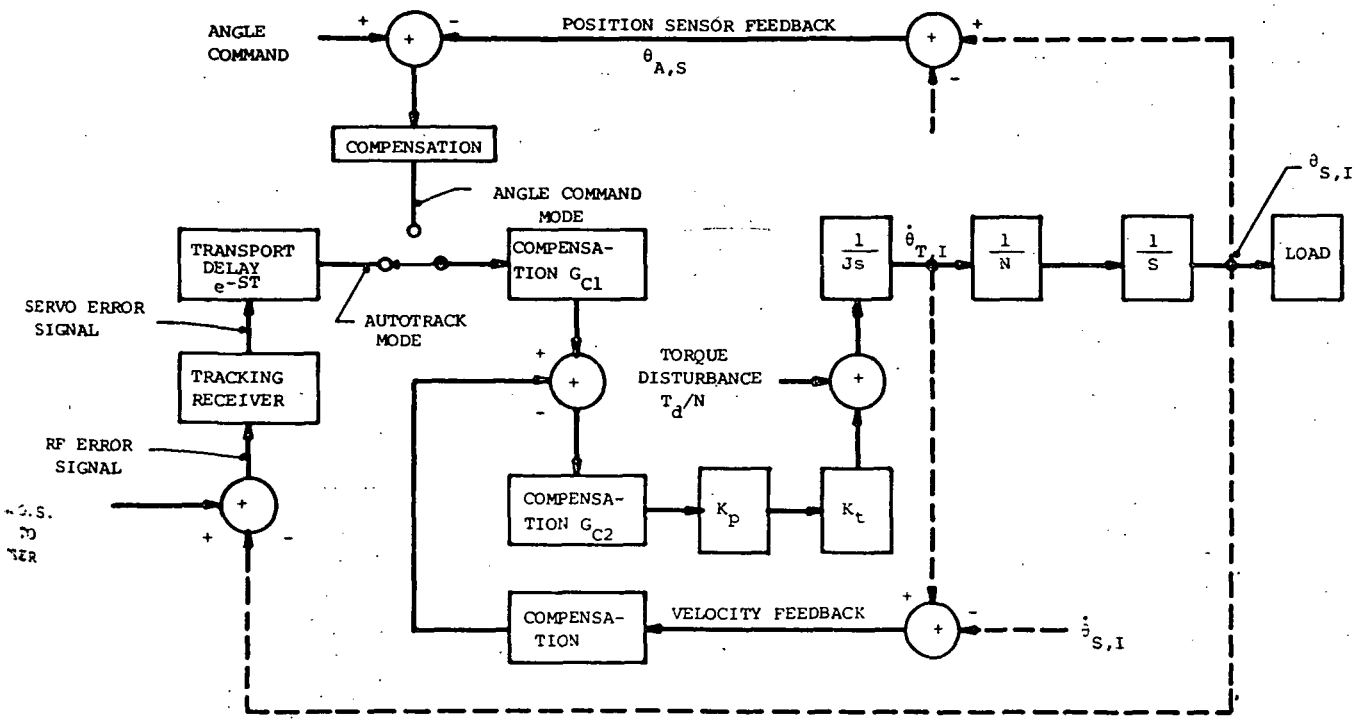

Figure B-3. Servo System -- Tracking Receiver at Ground Station

APPENDIX C

TRACKING VELOCITY AND ACCELERATION

It is the purpose of this appendix to determine the angular tracking velocity and acceleration imposed on the TDRS tracking antenna by various user spacecraft. First, general expressions will be derived for the angular velocity and acceleration of the line of sight from the TDRS to a user. Then the orbital characteristics of a variety of users will be introduced. Finally, the orientation of the gimbal axes will be defined and the tracking velocity and acceleration imposed on them by specific users will be determined.

The geometry to be employed is illustrated in Figure C-1. The user spacecraft travels on the spherical surface* shown there and the center C of that surface coincides with the center of the earth. The TDRS is assumed to be in a synchronous orbit such that a line which connects it with point C intersects the spherical surface at point A.

Consideration is given first to angular velocity. In the case of a polar user orbit, it can be shown that the maximum angular velocity of the user-to-TDRS line of sight occurs when the user intersects the equatorial plane at point B. Moreover, for all polar orbits, the one which contains point A results in the largest angular velocity, and that value obviously occurs when the user spacecraft coincides with A.

Next, it is observed that any orbit which contains point A will have the same maximum value of line-of-sight angular velocity.

When consideration is given to user orbits which are neither polar nor equatorial and do not contain point A, it is seen that the maximum angular velocity is less than that which occurs when the user coincides with point A.

Turning next to angular acceleration, attention is again first focused on polar user orbits. It is clear that the orbit defined by point A will result in some non-zero angular acceleration (except when the user is either at A or a position 180 degrees from A). Let another polar orbit be displaced from the one which contains A by 90 degrees. In this case, the angular velocity is seen to be constant so that the angular acceleration is zero. As expected, it can be shown that as point B approaches point A, the maximum angular acceleration increases, becoming largest when A and B coincide.

It follows then that maximum line-of-sight angular acceleration as well as velocity is associated with any orbit which contains point A. Thus, the determinatinon of these two quantities can be performed using the two-dimensional geometry shown in Figure C-2. The quantity of interest is the time-derivative of the angle $\theta(t)$ based upon:

---

* All of the user spacecraft to be defined subsequently exhibit a circular orbit.

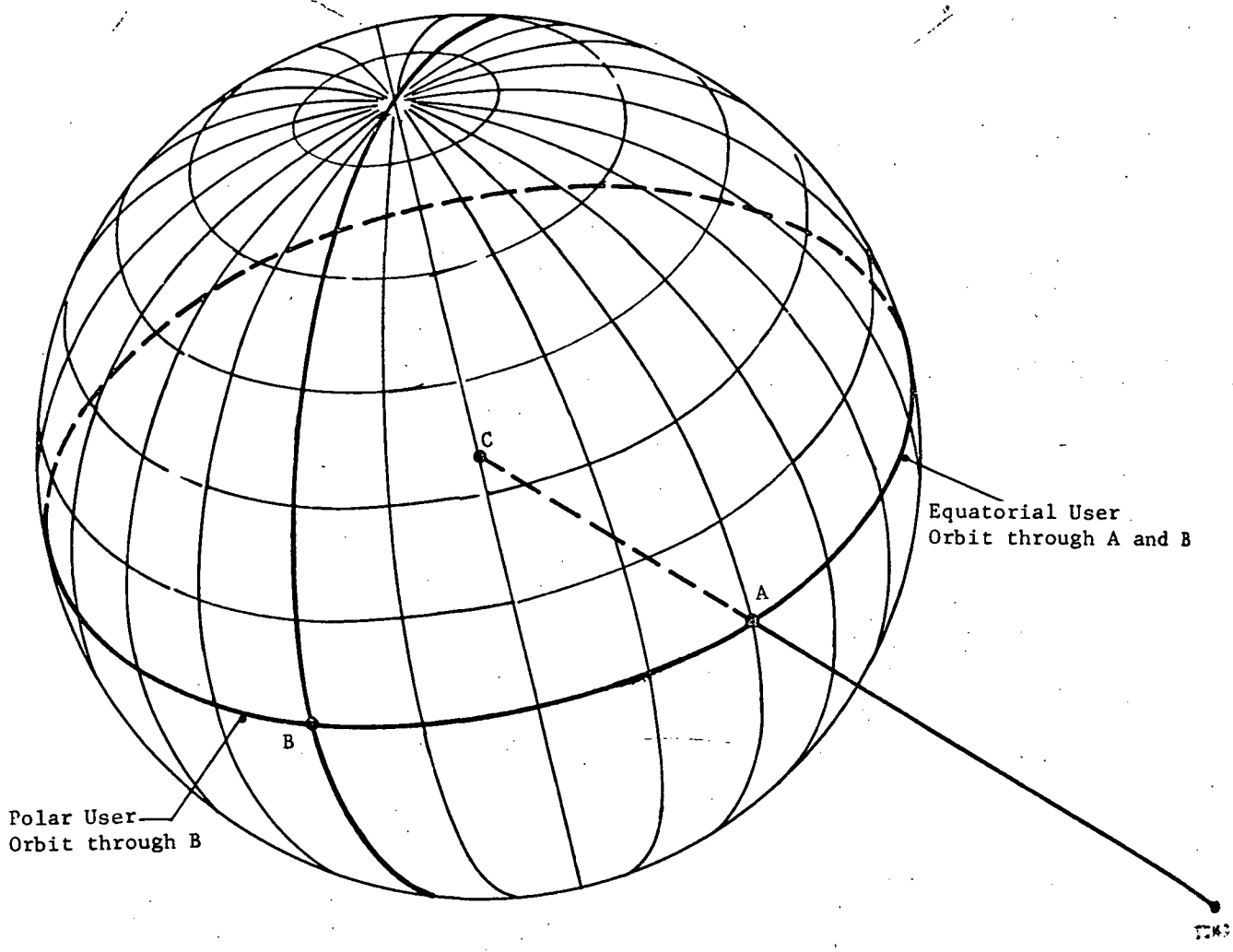

Figure C-1. Orbital Geometry of User Spacecraft

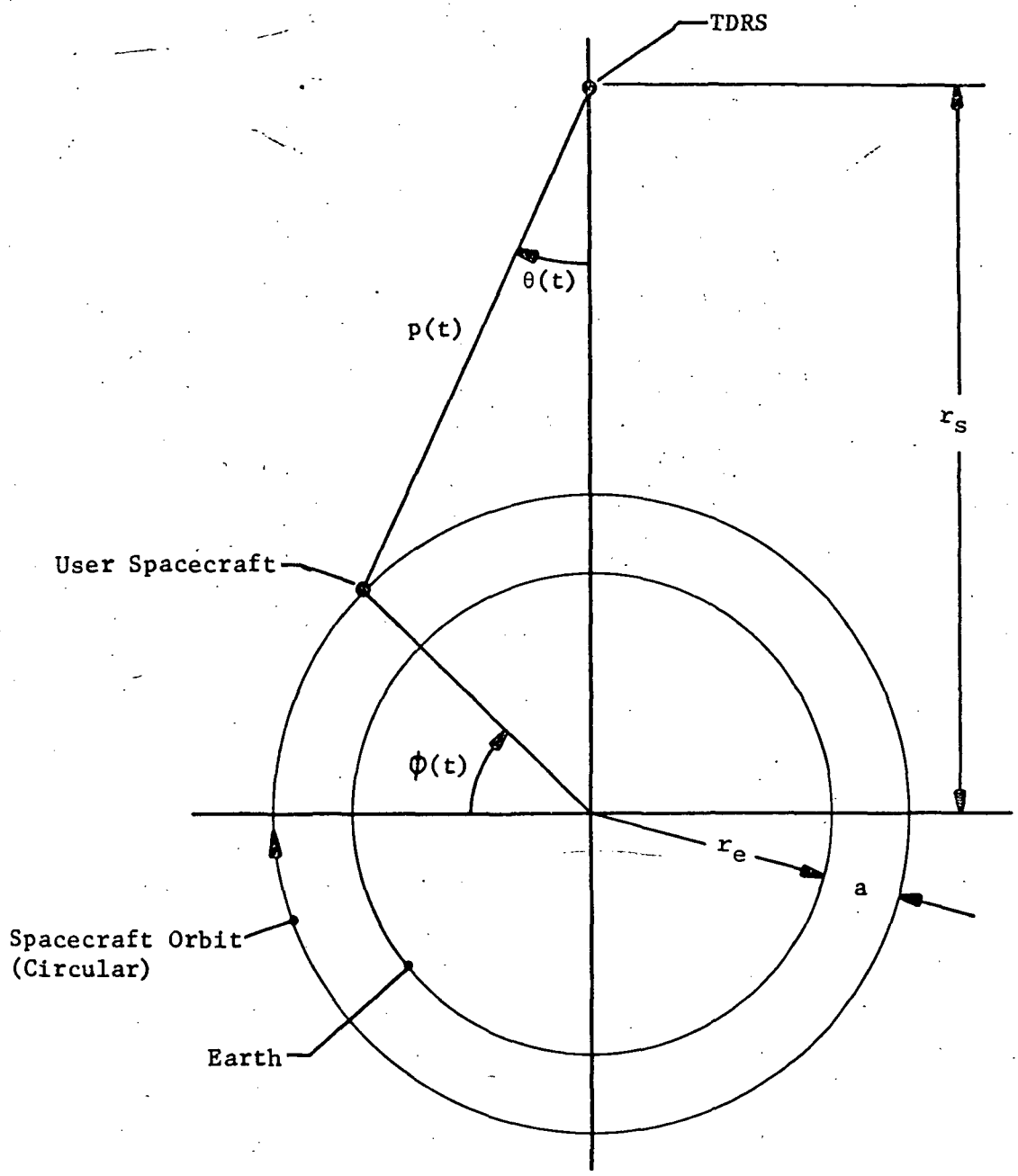

Figure C-2. Geometrical Relationship Between User, Earth and the TDRS

1 The angular position $\phi(t)$ of the user spacecraft;

2 The Earth's radius $r_E = 3{,}438$ nmi;

3 The distance $r_S = 3{,}338 + 19{,}357 = 22{,}795$ nmi from the TDRS to the Earth's center;

4 The satellite altitude a.

The derivation of angular velocity is straightforward and will now be summarized. The line-of-sight angle $\theta(t)$ is defined by

$$\theta(t) = \sin^{-1}\left[(r_e + a)\frac{\cos\phi(t)}{\rho(t)}\right]$$

where $\rho(t)$ is the TDRS-to-user distance given by

$$\rho(t) = \left[(r_e + a)^2 + r_s^2 - 2r_s(r_e + a)\sin\phi(t)\right]^{\frac{1}{2}}$$

The user motion is governed by the relationship

$$\phi(t) = \omega t$$

where $\omega = 2\pi/T$ and T is the orbital period. The time derivative of $(\theta)(t)$ is defined by

$$\frac{d\theta}{dt} = \frac{1}{\sqrt{1 - f^2(t)}}\frac{df}{dt} \qquad \begin{cases} 0 \le \phi(t) \le \pi/2 \\ 3\pi/2 \le \phi(t) \le 2\pi \end{cases}$$

where

$$f(t) \triangleq (r_e + a)\left[\frac{\cos\omega t}{\rho(t)}\right]$$

After carrying out the indicated operations, the result is

$$\frac{d\theta}{dt} = \frac{\omega\lambda(\lambda - \sin\omega t)}{1+\lambda^2 - 2\lambda\sin\omega t}$$

using the definition

$$\lambda \triangleq \frac{r_e + a}{r_s}$$

The maximum value of the line-of-sight angular velocity, which occurs when $\omega t = \pi/2, 5\pi/2, 9\pi/2, \ldots$, is simply

$$\left|\frac{d\theta}{dt}\right|_{max.} = \frac{\omega\lambda}{1-\lambda}$$

Table C-I presents values for the maximum angular velocity based upon the orbital user characteristics supplied by the NASA.

TABLE C-I

Maximum Angular Velocity for Various Users

User Spacecraft	Altitude (km)	Period (min)	$\left\|\frac{d\theta}{dt}\right\|_{max}$ (deg/sec)
AE	600	130	0.00912
EOS	1000	100	0.0127
HEAO	400	90	0.0127
Nimbus F	1000	100	0.0127
OSO	500	95	0.0123
SAS	550	96	0.0122
SATS	500	100	0.0117
TIROS-N	1700	120	0.0118

In order to estimate maximum line-of-sight angular acceleration, the characteristics of the EOS, SAS, and TIROS-N spacecraft were employed in a computation of angular velocity as a function of ωt, i.e., the orbits of these users were assumed to contain point A in Figure C-1. The results, shown in Figure C-3, indicate that the maximum angular acceleration occurs at approximately $\omega t = 40, 360 + 40, 720 + 40, \ldots$ degrees and is largest for EOS and SAS.

The angular acceleration, easily shown to be given by

$$\frac{d^2\theta}{dt^2} = \frac{-\omega^2\lambda(1-\lambda^2)\cos\omega t}{(1+\lambda^2-2\lambda\sin\omega t)^2}$$

yields virtually the same value, viz.,

$$\left|\frac{d^2\theta}{dt^2}\right|_{max} = 1.25 \times 10^{-5}\ deg/sec^2$$

for both cases.

The final step is to relate the velocity and acceleration of the gimbal axes to the corresponding line-of-sight values. In this regard, the assumption is made that the two gimbal axes, which are, of course, orthogonal to one another, are also orthogonal to the line connecting the Earth's center with the TDRS. As a result, the maximum combined angular velocity and acceleration for both axes is 0.013 degree/second and 1.25×10^{-5} degree/second^2, respectively.

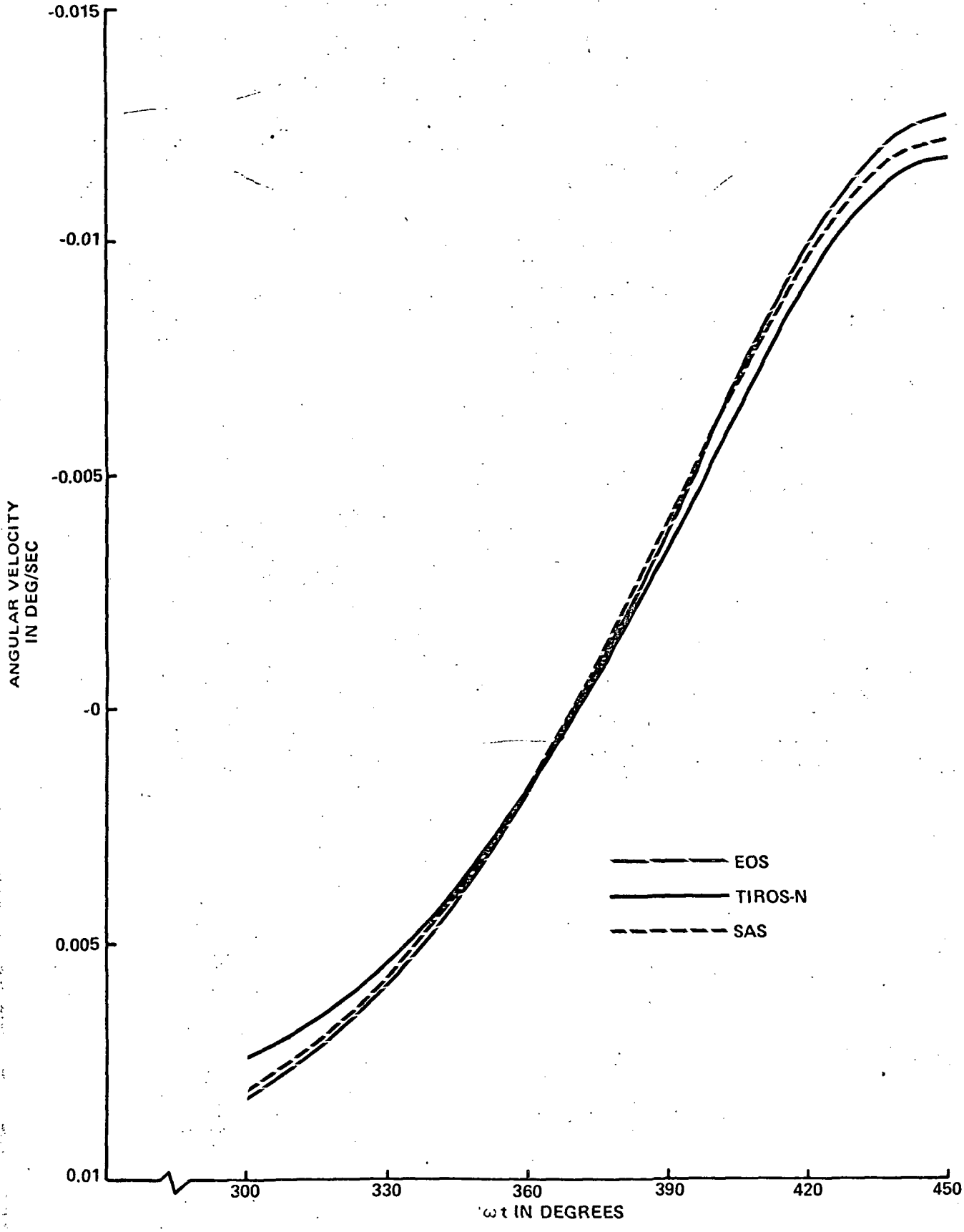

Figure C-3. Time History of Angular Velocity for Typical User Spacecraft

APPENDIX D

ANGULAR BEAM POINTING ERROR WHICH RESULTS FROM S-BAND FEED POSITIONING ERROR

The quantity to be determined is the change in the angular position of the beam maximum as a result of mispositioning of the phase center of the S-band feed. Reference is made to Figure D-1 which illustrates the coordinate system in which the reflector and feed focal surface are located.

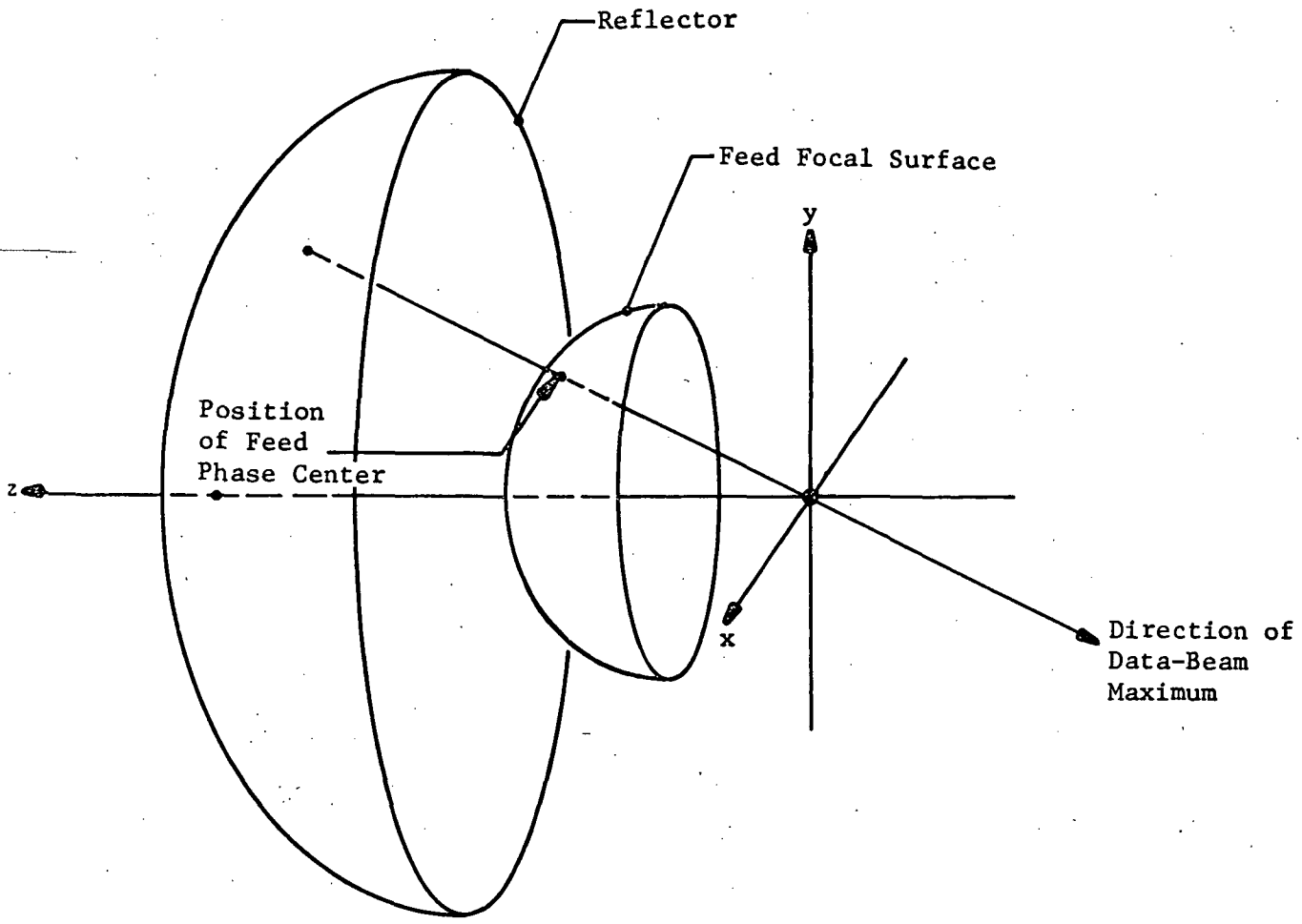

Figure D-1. Coordinate System of Reflector and Feed Focal Surface

The origin of the x, y, z coordinate frame is the center of the spherical reflecting surface of radius R. The feed focal surface is also spherical, with radius R/2, and centered at (0, 0, 0). The direction of the maximum of the data beam radiation pattern is defined by the line which contains the point (0, 0, 0) and the feed phase center.

In order to determine the relationship between the feed positioning errors and the data beam pointing direction, the geometry of Figure D-2 will be employed.

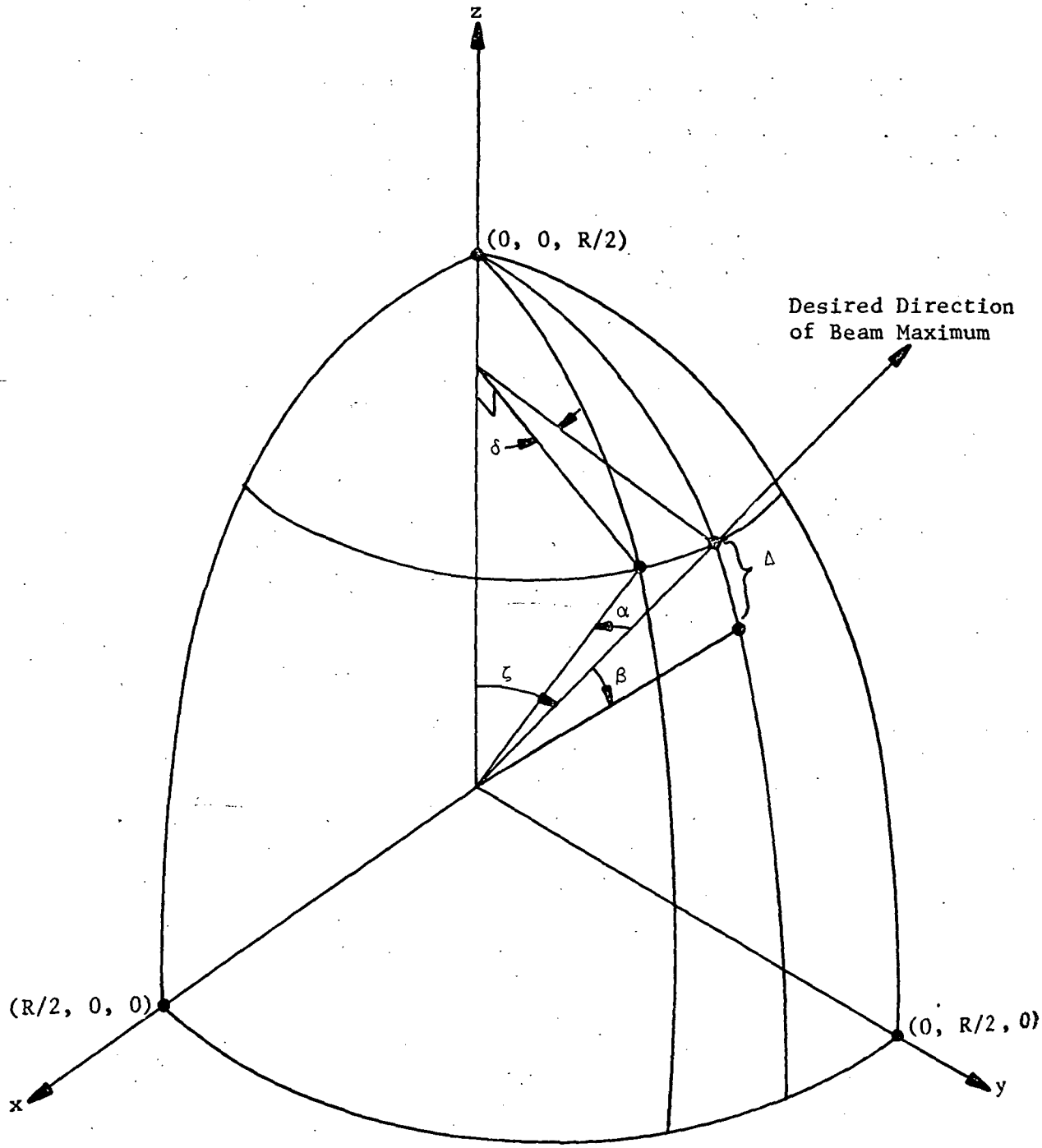

Figure D-2. Geometry of Beam Pointing Errors

The positioning of the feed is modeled in terms of two errors: an angular error δ with respect to rotation about the z-axis and a displacement error Δ. The angular feed error δ gives rise to an angular beam error α obtained from

$$\delta\left(\frac{R}{2}\sin\xi\right)=\left(\frac{R}{2}\right)\alpha$$

where ξ is the desired angular beam displacement from the reflector axis. Thus,

$$\alpha=\delta\sin\alpha$$

Next, a physical feed displacement of Δ in a plane which contains the reflector axis results in a beam deflection β defined by

$$\beta\approx\frac{\Delta}{R/2}$$

Since the beam position errors occur in orthogonal directions and with $\alpha,\beta \ll 1$ rad, it is clear that the total error is simply

$$\sqrt{\alpha^2+\beta^2}=\sqrt{(\delta\sin\xi)^2+(360\Delta/\pi R)^2}$$

where δ is expressed in degrees and Δ and R are in the same units. For the case in which the 3σ values of δ and Δ are 0.5 degree and 0.25 inch respectively, and with ξ = 30 degrees and R/2 = 60 inches, it is the case that

$$\sqrt{\alpha^2+\beta^2} = 0.35 \text{ degree}$$

APPENDIX E

A SURVEY OF REFLECTOR ANTENNAS

Configuration	Advantages	Disadvantages
I. Single Reflectors (In general)	1. Simplicity; aligment involves fewer parts. 2. Design principles and procedures are widely known (axially fed cases). 3. Approach has low weight potential since no subreflector is required.	1. The low weight potential dims somewhat when the weight of the focal-point-mounted receiver front end and cable run is considered.
A. Axially Fed		
1. Paraboloid Reflector	1. This is the most common widely used and well-known type of reflector antenna. 2. Prevailing reflector fabrication technology is adequate.	1. Some radiated energy is reflected back into the feed. 2. The feed partially blocks the radiating aperture. (This causes a loss in gain and an increase in sidelobes.) 3. The receiver front end has to be mounted at the focal point to avoid the long waveguide run to the back of the dish. This is not convenient. 4. Beam scan by feed movement is limited to a few beamwidths before there is excessive gain loss. 5. Spillover is highest in rearward direction.
2. Spherical Reflector	1. This type of structure allows excellent wide angle scanning even as much as ± 15 degrees by a simple rotation of the feed about the center of the sphere. (More conservatively one could expect a scan capability of 25 beamwidths with less than 1 dB gain loss.)	1. Some radiated energy is reflected back into the feed. 2. The feed partially blocks the radiating aperature. 3. The receiver has to be mouned at the focal point to avoid the long waveguide run to the back of the dish.

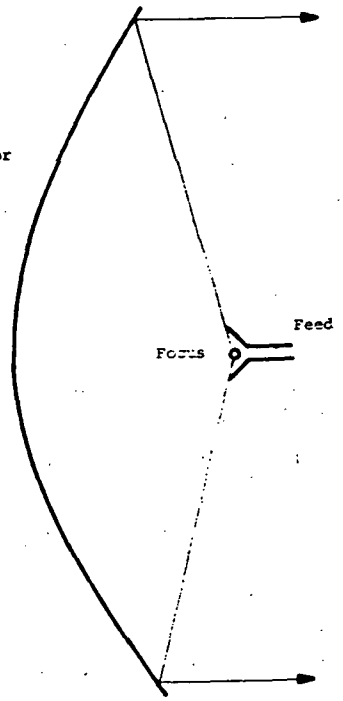

Configuration	Advantages	Disadvantages
	2. When configured for scanning this type of antenna has very low spillover. 3. Some simplicity of this approach stems from the fact the reflector structure can be derived from an inflatable device. 4. With a very wide scan design, sufficient angular coverage could be provided to greatly simplify satellite and/or reflector pointing.	4. The reflector has no true focal point; it suffers from spherical aberration. This causes a gain loss. 5. When the antenna is configured to minimize the aberration gain loss, the maximum effective radiating diameter is significantly less than the physical diameter. (About 0.6 D for a simple horn feed and 0.8 D with a line source corrector. Other efficiency factors must be included in addition to this.)
B. Offset Fed (In general)		

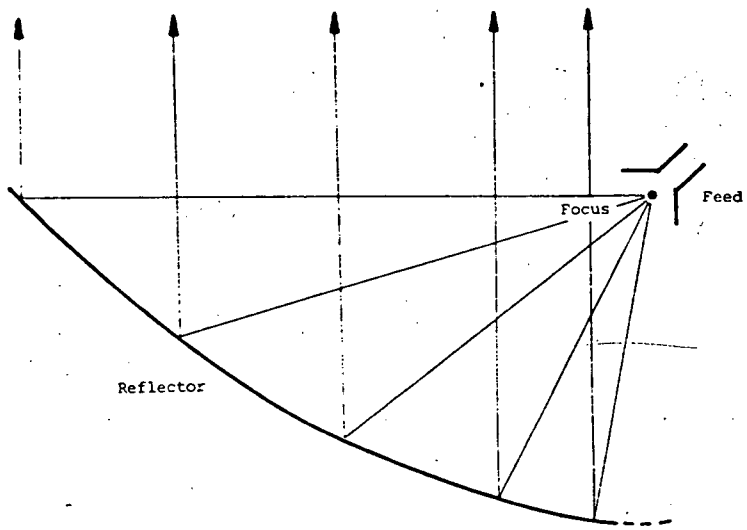

	1. There is no feed blockage (and usually no support blockage too). 2. No radiated energy is reflected back into the feed. 3. Spillover is directed neither forward or backward. (This could be a disadvantage too.)	1. Beam scanning by movement of the feed is not widely documented. It appears from geometrical considerations, that since the feed is not co-axial with the far-field beam, the axes of scan (beam and feed) are not orthogonal; requiring perhaps some angular coordinate conversion. 2. In one plane the beam tends to be asymmetrical. 3. Design principles and procedures are not widely known.
Others	Most published data involves paraboloid reflectors; none with an offset fed spherical reflector.	

Configuration	Advantages	Disadvantages
II. Dual Reflectors (In general)	1. The feed is near the main reflector vertex, therefore, a long waveguide run to the receiver may conveniently be eliminated and certain structural advantages are obtained. 2. The antenna beam may be scanned by subreflector motion. This very nicely eliminates the need for rotary joints when scanning. 3. The spillover past the subreflector is in the forward direction (axially fed cases).	1. The subreflector with its associated scanning drive motor and gearing is potentially a weight penalty. 2. While scanning by subreflector movement is convenient, there is additional loss due to spillover past the subreflector. This effect is more troublesome than for a single reflector because of the high gain (narrower beam) feed antenna.
A. Axially Fed		
1. Paraboloidal Main Reflector		
a. Cassegrain (Hyperboloid Subreflector)	1. This is the most common, widely used and well-known dual reflector antenna. 2. The design principles and procedures are widely known.	1. The blockage effects are slightly greater than for a single reflector. (Subreflector diameter > 10 λ and the main reflector diameter > 100 λ for efficient operation).

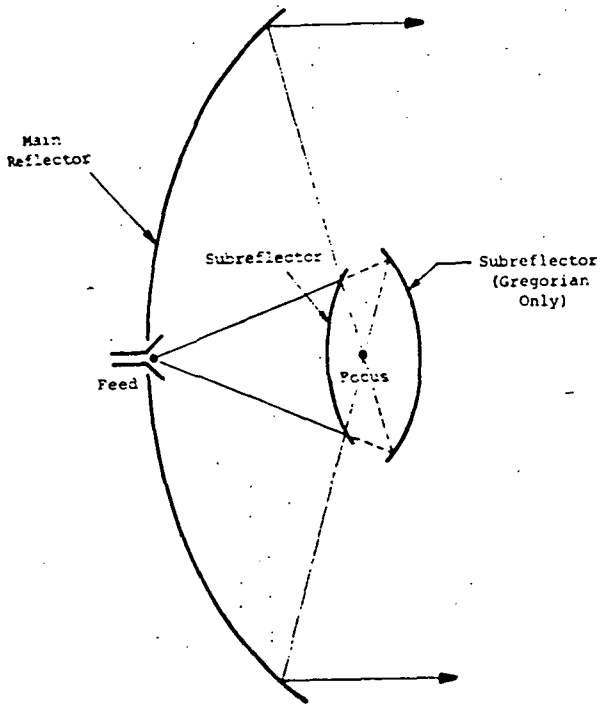

	3. The bulk of the subreflector is inside the main reflector focal point; spar length as well as potential inertia problems are reduced.	2. Some radiated energy is reflected back into the feed.

APPENDIX F

SUMMARY AND CRITIQUE OF RADIATION, INC.'S REPORT ON A 12.5-FOOT DEPLOYABLE REFLECTOR

Reference: "Critical Design Review Package for Advanced Applications Flight Experiment," (NAS1-11444) prepared for Langley Research Center by Radiation, Inc., a Division of Harris Intertype, 3 October 1972.

The Radiation, Inc. reflector is a deployable 12.5-foot parabolic dish suitable for operation in the K_u-band frequency range. It is a candidate for the TDRS High Data Rate and Medium Data Rate (HDR/MDR) antennas. It consists of two major parts: the mesh reflector consisting of 12 ribs for shaping the parabolic reflecting surface, and the cone structure consisting of the RF feed network and the mechanical deployment system. These parts are illustrated in Figure F-1.

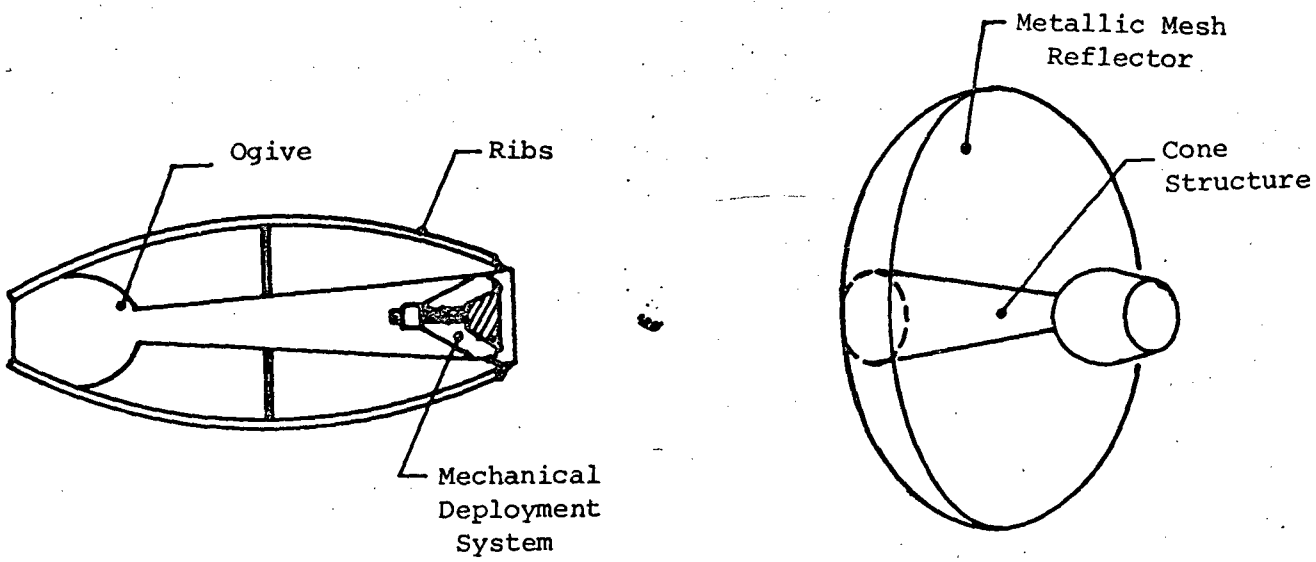

(a) Stowed Configuration (b) Deployed Antenna

Figure F-1. Radiation, Inc.'s 12.5-Foot Deployable Reflector

The parabolic reflecting surface consists of 12 aluminum ribs which support and shape the metallic dish. The metallic dish is built on a "double mesh" technique, where the parabolic reflecting surface side is comprised of closely knit strands. The second mesh is a coarsely knit surface on the opposite backside of the ribs. The reflector utilizes the second mesh as a drawing surface for contouring the front reflector mesh. This second mesh is attached to the back of the ribs and is tied to the front mesh by tensioned wires. By applying proper tension to these tie wires, the reflector surface can be contoured to the desired parabolic shape. The mesh is constructed from 5-strand bundles of 0.007 inch Chromel-R wire knitted into a wire screen. The mesh is plated with electroless nickel and gold, which provide the RF reflectivity.

The cone structure, housing the mechanical deployment system and the RF network, was chosen because its aperture blockage is no more severe than that of a spar support. It is the primary structural member of the stowed antenna. The ogive geometry of the radome was selected because of its high electrical efficiency over other geometries.

The mechanical deployment system at the base of the cone structure provides a controlled deployment of the reflector from the stowed to the fully deployed position. It is comprised of a torque motor which drives a disk-shaped carriage mounted to the moving section of a recirculating ball unit on a ball screw shaft. The movement of the carriage is connected to linkages which transmit the force and motion required for deployment to the ribs.

The RF reflectivity of the mesh at K_u-band frequencies is 98 percent, according to Radiation, Inc., and the cross-polarization efficiency is 99.0 percent. The total surface error budget is broken down in Table F-1.

TABLE F-1
Surface Error Budget

Error Source	Magnitude (inches)
Thermal distortion	0.008
Manufacturing (mesh attachment, adjustment, and bulge)	0.015
Gravity error	0.006
Total error	0.018
Measurement error effects on total rms error	$\pm$0.001

The surface error loss due to 0.019 rms surface tolerance can be calculated from the following equation:

$$n_{\phi S} = 10 \log\{\exp[-4\pi\varepsilon/\lambda^2]\} ,$$

where $n_{\phi S}$ = surface error loss in dB

ε = RMS surface error

λ = frequency of operation.

For K_u-band (14 GHz) the loss is 0.4 dB and at S-band (2.3 GHz) the loss is 0.01 dB. Although the loss at K_u-band is high when compared to a solid reflector, 0.4 dB loss is tolerable.

A maximum of 0.25 dB loss is allowed for linear displacement of the feed due to a nominal sun angle of 60 degrees to antenna boresight and is equivalent to an axial defocusing of 0.15 inch. A loss of 0.25 dB is attributed to beam mispointing, which is equivalent to a feed offset angle of 0.07 degree. The physical size of the stowed antenna is given by a maximum package envelope dimension of a right circular cylinder 75 inches high and 30 inches in diameter.

APPENDIX G

S-BAND BEAM STEERING IN A PARABOLIC REFLECTOR

The purpose of this investigation is to calculate the performance degradation experienced when steering a monopulse feed off the axis of a parabolic reflector. This investigation was conducted using a computer program supplied by NASA-GSFC. This program calculates the radiation patterns from parabolic, spherical, elliptical, hyperbolic, or conical single reflectors with various feed and polarization configurations and options. The program is based on the Kirchoff-Huygens diffraction theory. The source language is Fortran IV and the machine used was the IBM 370 located at Martin Marietta Orlando.

Inputs to the program are as follows:

1. Antenna radius
2. Focal length
3. Vertex displacement from origin
4. Frequency
5. Type of reflector surface
6. Number of feeds
7. Field of observation
8. Source strength
9. Source starting phase
10. Electric field polarization
11. Exponent for the illumination function $\cos^N(\sigma)$
12. Feed translations $(x_\varepsilon, y_\varepsilon, z_\varepsilon)$
13. Feed rotations (α, β, γ)
14. Control constants and bookkeeping data.

Outputs are:

1. A restatement of certain input parameters
2. Antenna reflector radius
3. Angular coordinate of the field point
4. Phase and amplitude of the electrical field in spherical coordinates
5. Phase and amplitude of the electrical field in rectangular coordinates.

The investigation was conducted assuming a 12.5-foot diameter parabolic reflector with a 50-inch focal length ($f/d = 0.4$). The S-band feed was assumed to be a dual mode spiral antenna. The simulation of the spiral was made by a two-element in-phase array separated by $\lambda/3$ to generate the sum beam and a two-element, 180 degree out-of-phase array separated by $2\lambda/3$ to generate the difference beam. Circular polarization was simulated by selecting crossed dipoles in phase quadrature for each array element. All beam steering was implemented by moving the feed off-axis in a line perpendicular to the focal axis.

The plots of Figure G-1 show the reduction in gain due to steering the sum beam off-axis. Both cos and $\cos^2$ distributions were considered. The additional points plotted at 10 degree scan angle represent an attempt to find a higher gain level by moving the feed forward and backward from the scan line, which is perpendicular to the focal axis. As is evident from the graph, no improvement was realized. In addition, the feed was tilted to point at the vertex of the parabolic reflector, but no apparent improvement in gain was observed. The reduction in gain due to beam steering showed up as an increase in beamwidth (Figure G-2) and an increase in coma-lobe level (Figure G-3).

The composite pattern plots shown in Figure G-4 show the effect of beam steering on a monopulse feed system. These patterns have not been normalized to the on-axis peak level and do not show the attendant reduction in gain. These patterns were reduced to S-curves (Figure G-5) by plotting the angle off boresight (θ) against $10^{x/20} \cos(\Delta\phi)$ where $x = (\Sigma-\Delta)$ dB and $\Delta\phi$ is the phase angle between the sum and difference at a given θ.

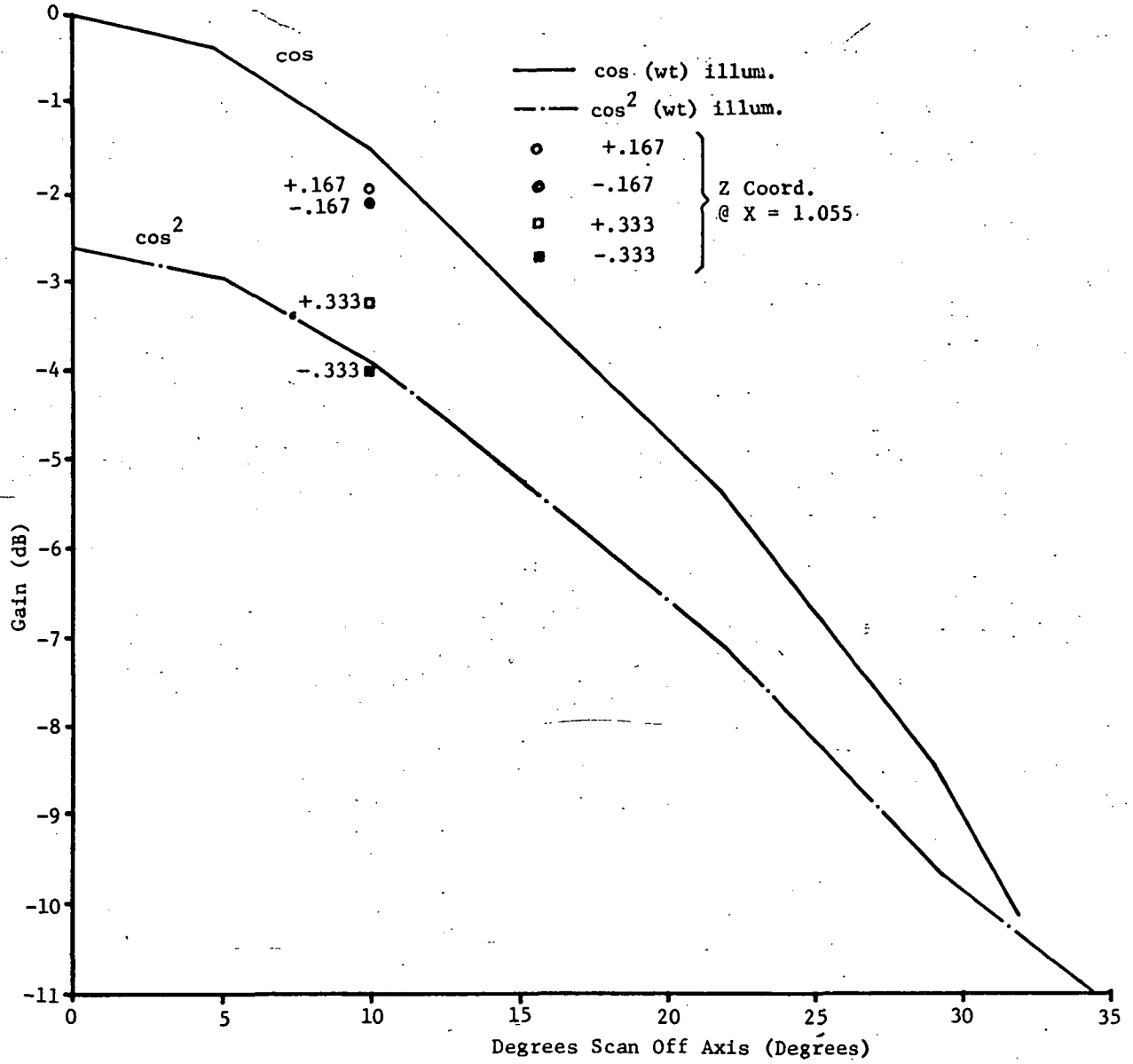

Figure G-1. Computerized Plots of Gain Loss as a Function of Scan Degrees

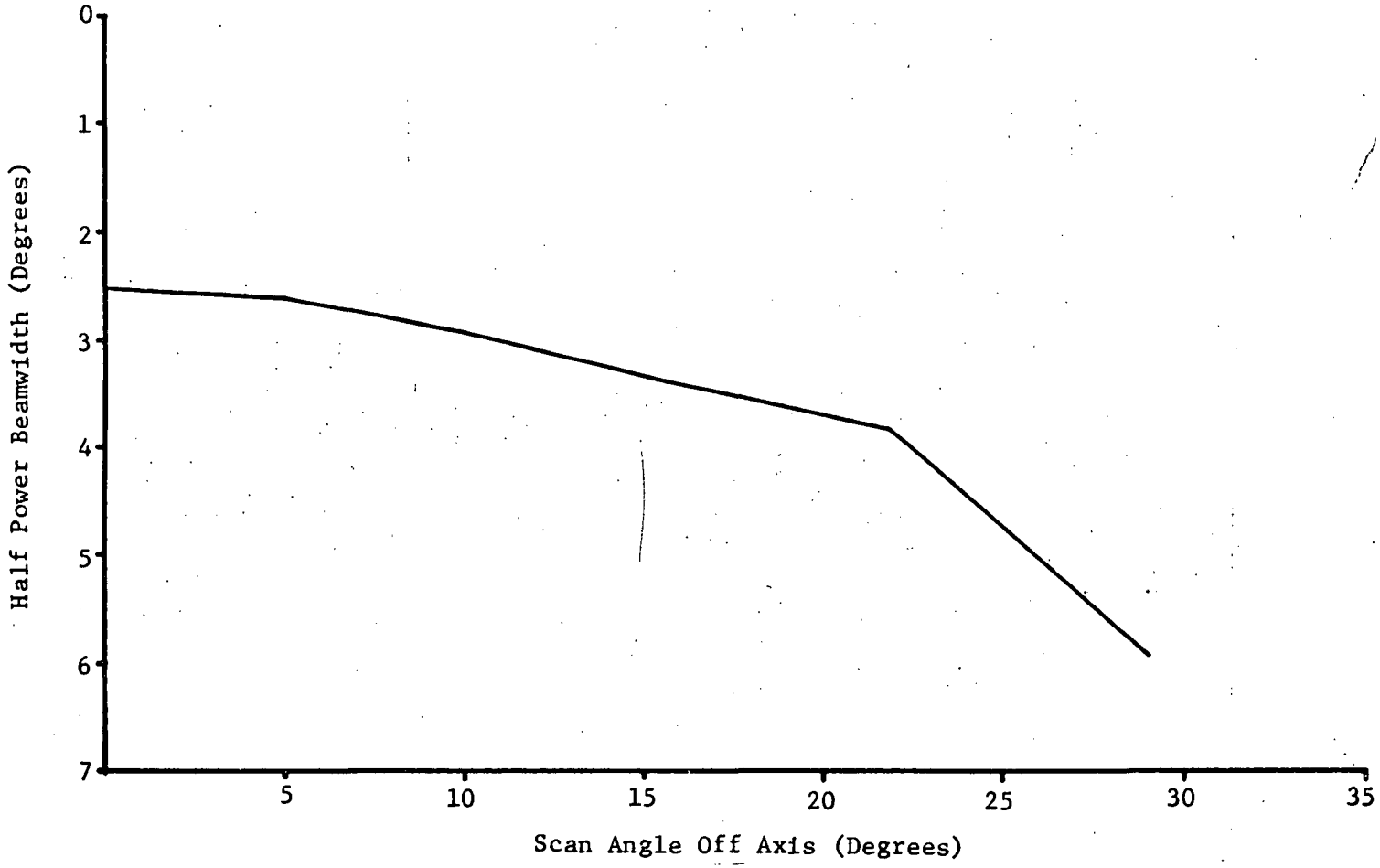

Figure G-2. Computerized Plots of Half Power Beamwidth as a Function of Scan Angle

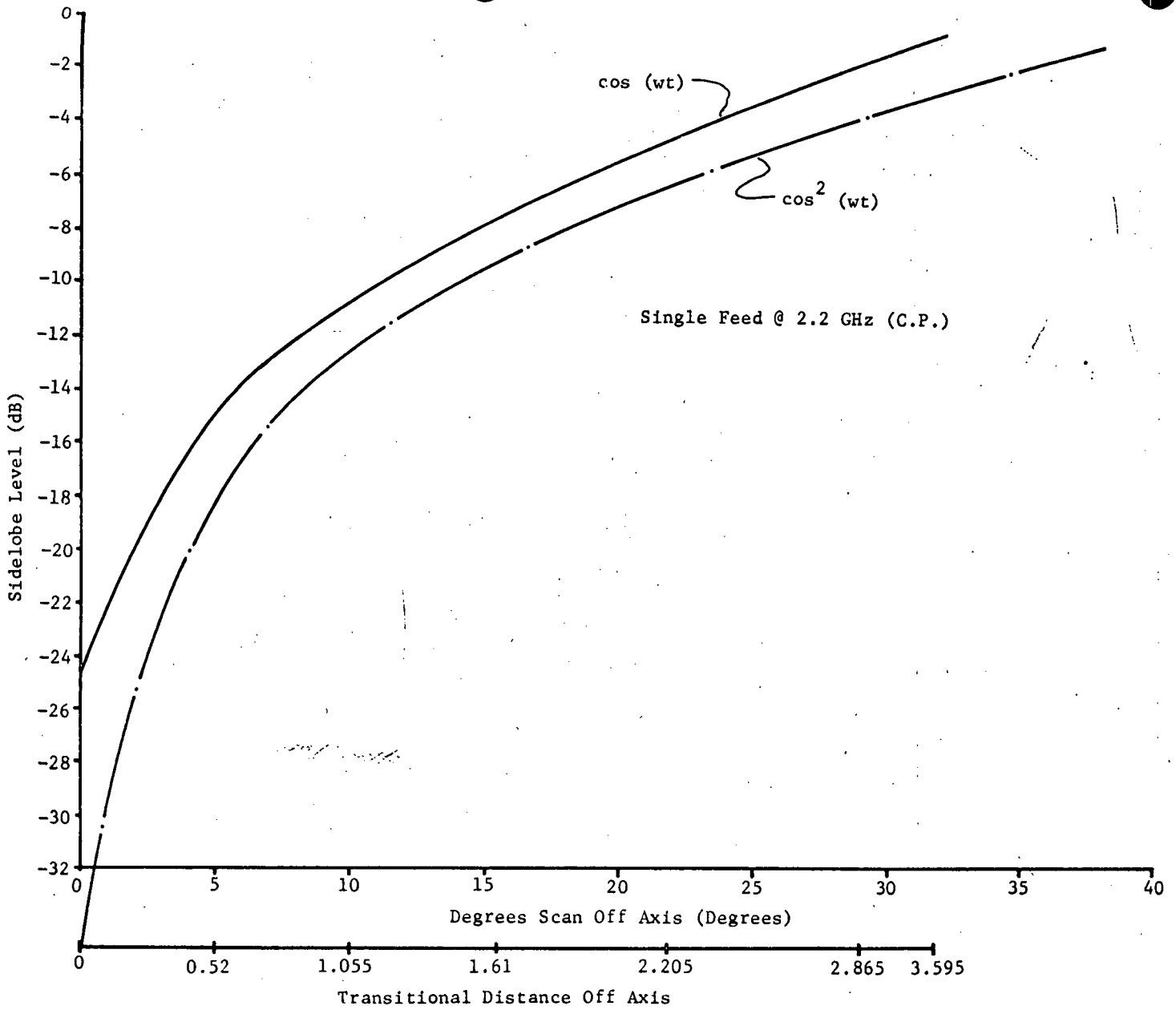

Figure G-3. Computerized Plots of Sidelobe Level as a Function of Scan Angle

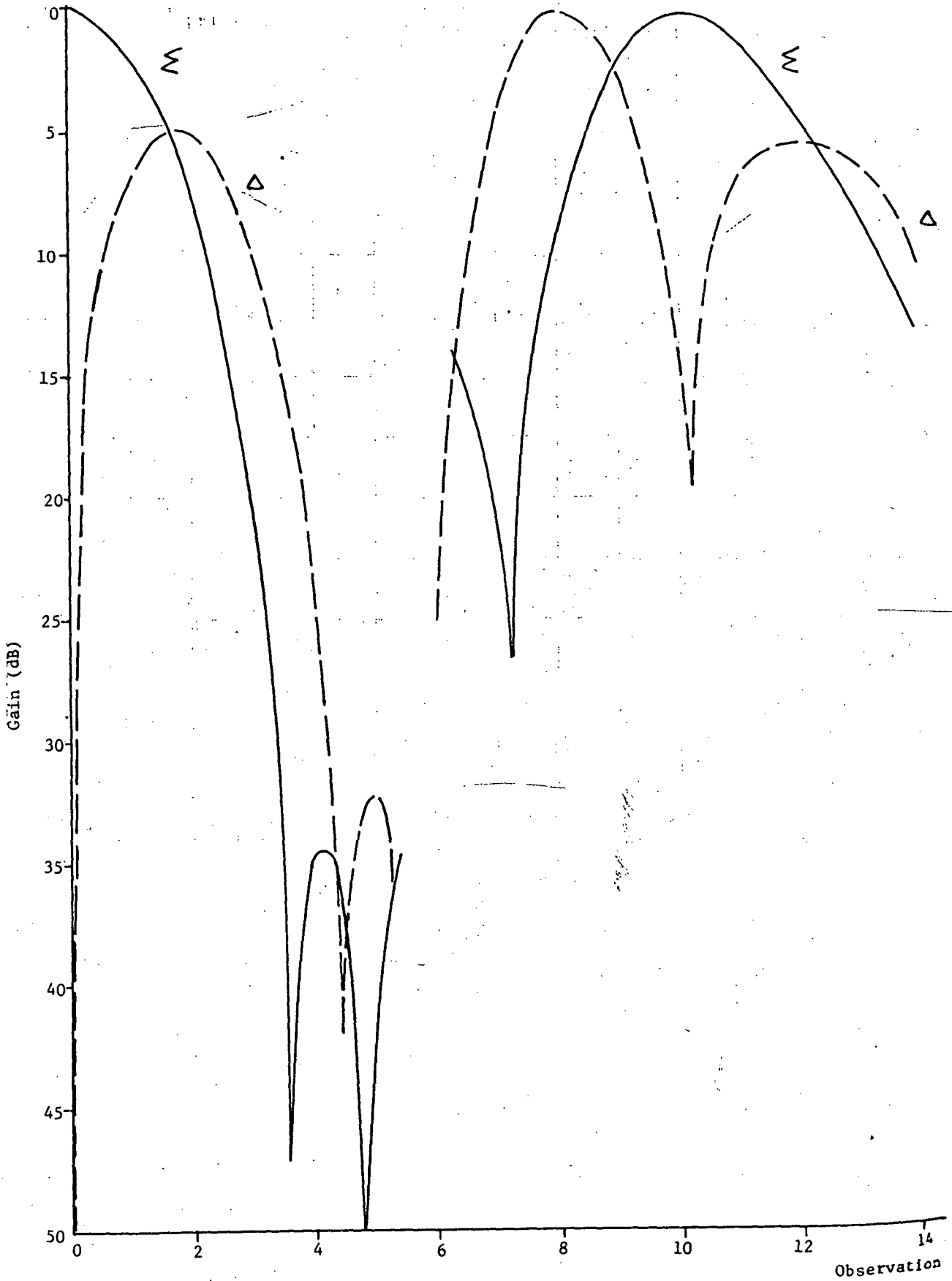

Figure G-4. Sum and Difference Patterns

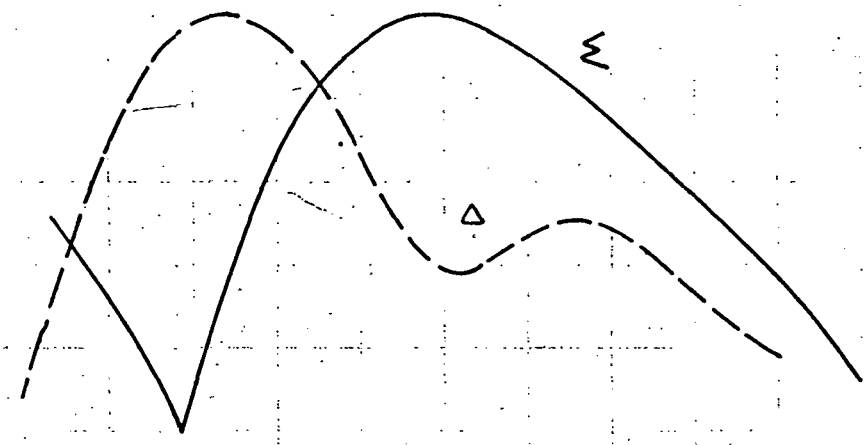

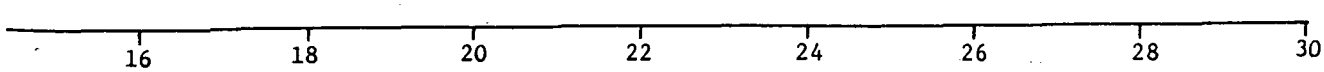

Angle (Degrees)

as a Function of Scan Angle

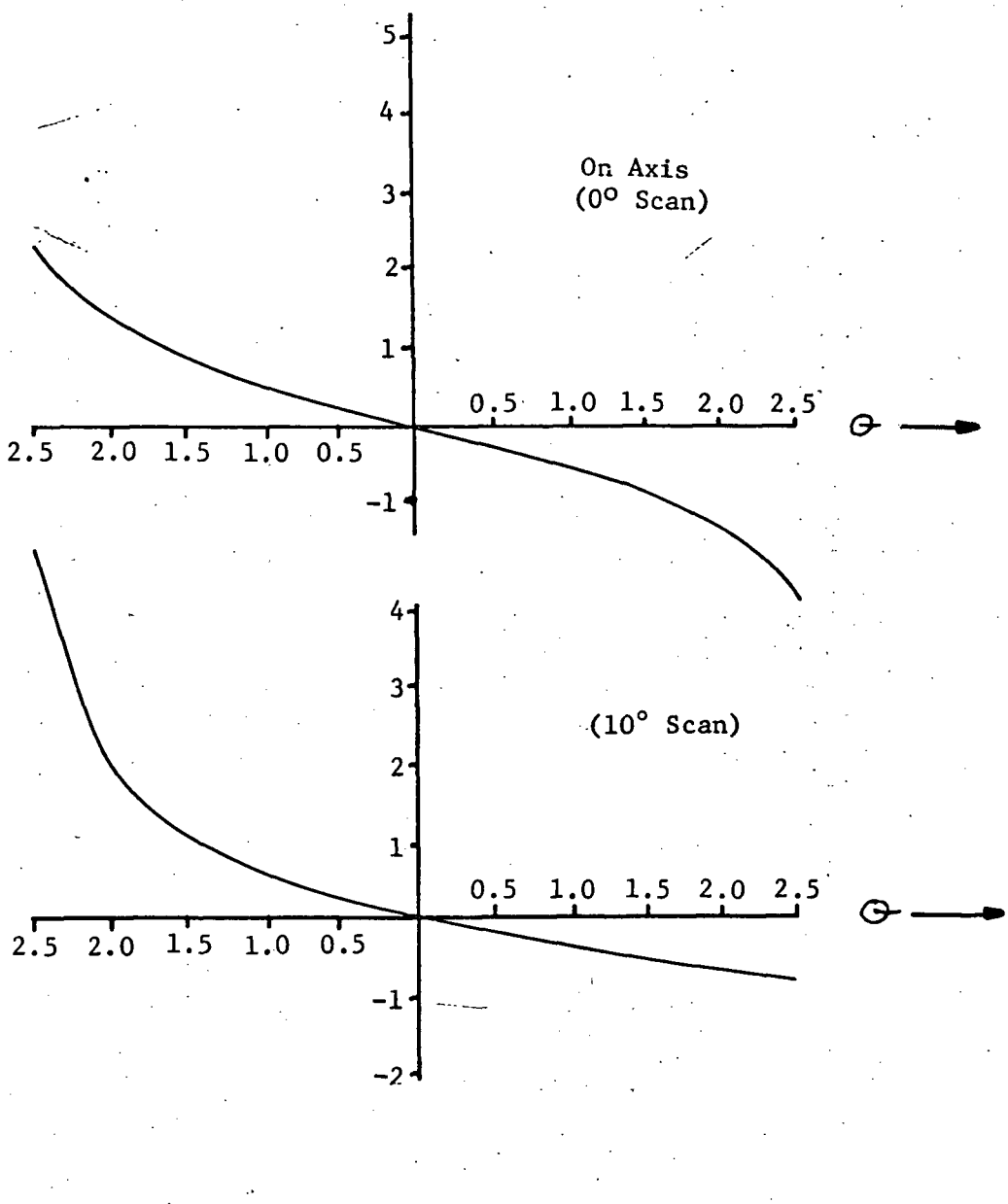

Figure G-5. S-Curves For Off-Axis Scan Angles of 0, 10, 20 Degrees

APPENDIX H

OPTIMUM DESIGN OF LARGE CASSEGRAIN ANTENNAS FOR SPACECRAFT APPLICATIONS

The usual method of designing cassegrain antennas has been guided by the geometric optics procedure. In this procedure, the curvature of the reflectors is dictated by the optical path differences in which the individual rays propagating from the feed focal point will form a plane wavefront when they emerge from the main reflector. This appendix will show that optimum pattern efficiency is not achieved in this case, and that some alterations should be made to improve the efficiency of large cassegrain antennas.

This appendix follows the work by Cramer (Reference H-1) of JPL, where comparison was made for spacecraft antennas between prime focus paraboloids and cassegrains of the same diameters. A feed efficiency computer program was used to calculate the overall antenna efficiency for combinations of diameters, F/D ratios, and illumination tapers. The computations were carried out for diameter variations of 68λ to 257λ in X-band (TDRS = 182λ), F/D variations of 0.35 to 0.5, and illumination tapers from 7 to 17 dB. To facilitate computations, the feed pattern was expressed as a mathematical function of $\cos^2\theta$ illumination, and the results are valid for actual feed patterns that do not substantially deviate from this assumed pattern.

The cassegrain configuration is shown in Figure H-1, where the optical rays define the minimum blockage feed aperture. The hyperbola's focal length uniquely determines the location of the primary feed since the phase center of the primary feed is located at one hyperbolic focus and the focus of the parabola is located at the other hyperbolic surface. The results showed that the axial location of the primary feed is not critical and means that the feed location can be determined by physical considerations, such as best location for the mounting requirements and transmission line constraints. Also, the size of the feed can be optimized for best overall feed performance, without concern that the feed dimension or beamwidths chosen will force the feed to be at a point where the antenna system efficiency will suffer. This investigation showed that even subreflector subtended angles up to 80 degrees can be utilized without becoming a factor in antenna efficiency. The results of cassegrain efficiency as a function of edge taper is shown in Figure H-2 and is labeled B. It was found that the efficiency could be increased by reducing the parabola diameter, and that the amount of reduction was approximately 13 percent (optimum diameter) with an increase in efficiency of 4.6 percent. This was attributed to the effect of diffraction from the subreflector edge; however, since the antenna diameter is generally fixed according to the overall system gain and/or the beamwidth required, the increase in efficiency can be achieved by increasing the subreflector diameter. This effect can be

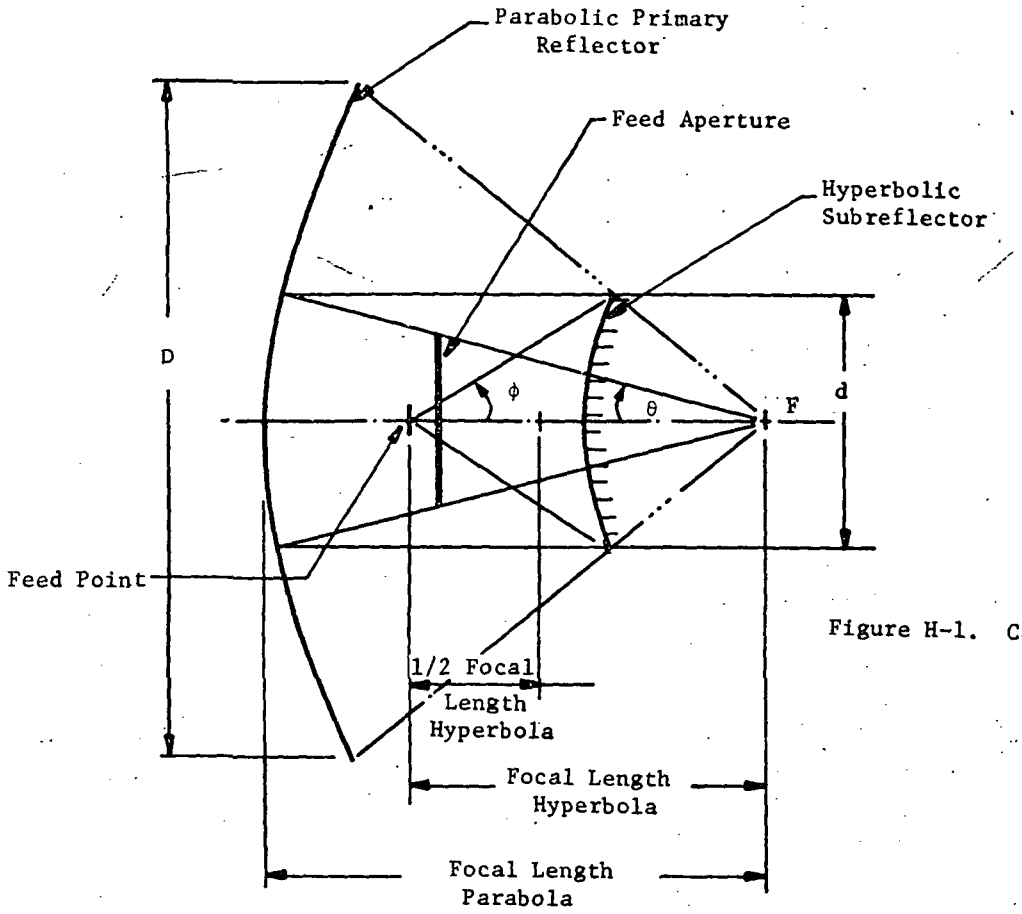

Figure H-1. Cassegrain Configuration

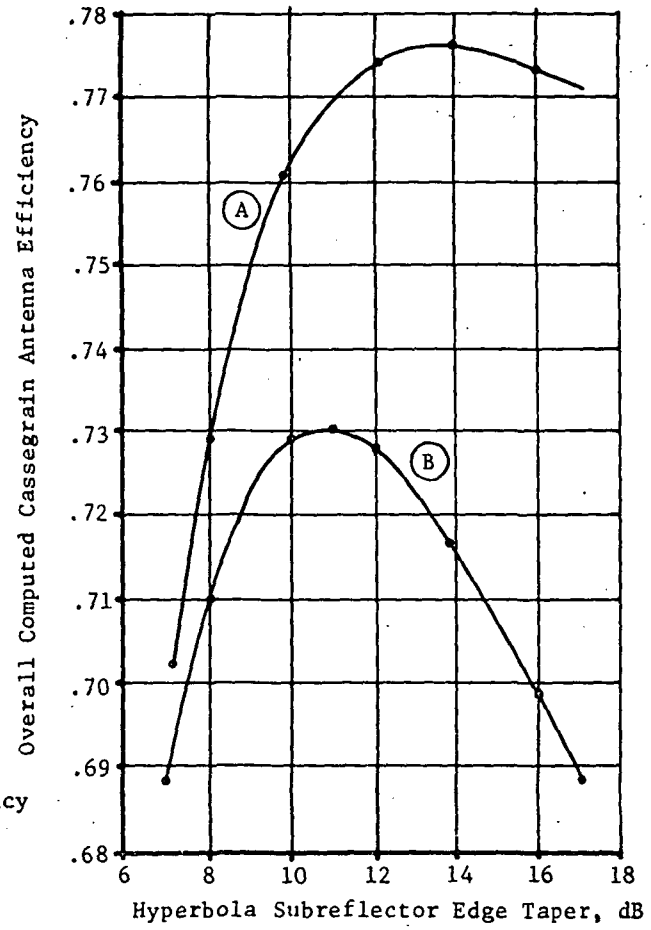

Figure H-2. Cassegrain Efficiency as a Function of Edge Paper

shown by referring to Figure H-3 where the geometric diameter and the geometric subreflector diameter are shown together with the equivalent subreflector diameter and the optimum diameter. The equivalent subreflector diameter is that diameter based on the optimum diameter, and the equivalent taper is the level of the illuminating feed pattern at the subreflector's equivalent diameter. Figure H-4 shows the new overall efficiency as a function of the hyperbola subreflector equivalent taper, where the maximum efficiency occurs for an edge taper of 9.2 dB. The steps to design the large cassegrain antenna would be to:

1 Determine parameters based upon a geometric configuration

2 Adjust the edge taper on the subreflector to approximately 9.2 dB

3 Extend the subreflector to a new diameter approximately 18 percent larger than that for the geometric case.

The exact amount of increase of the diameter is dependent upon the F/D ratio, and was determined to be 1.18 for the TDRS antenna diameter of 150 inches. Thus, the resultant subreflector dish must be 1.18 x 13.2 or 15.58 inches.

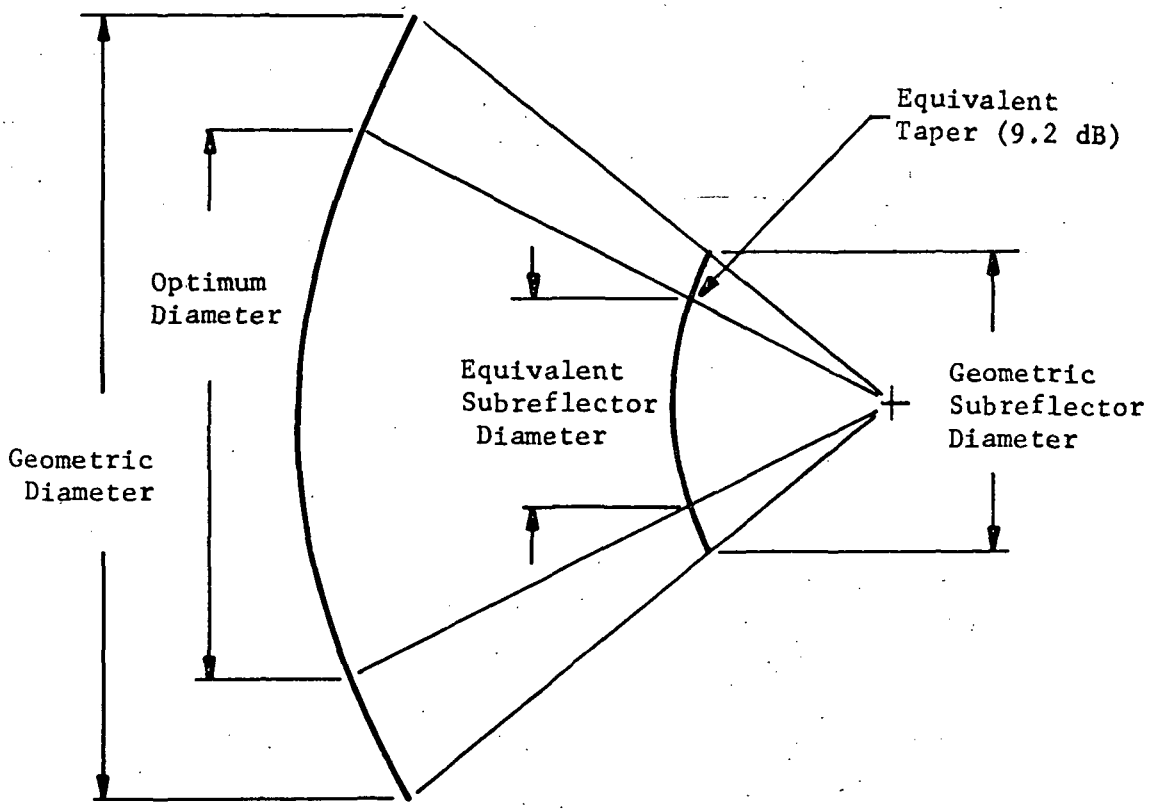

Figure H-3. Improved Cassegrain Configuration

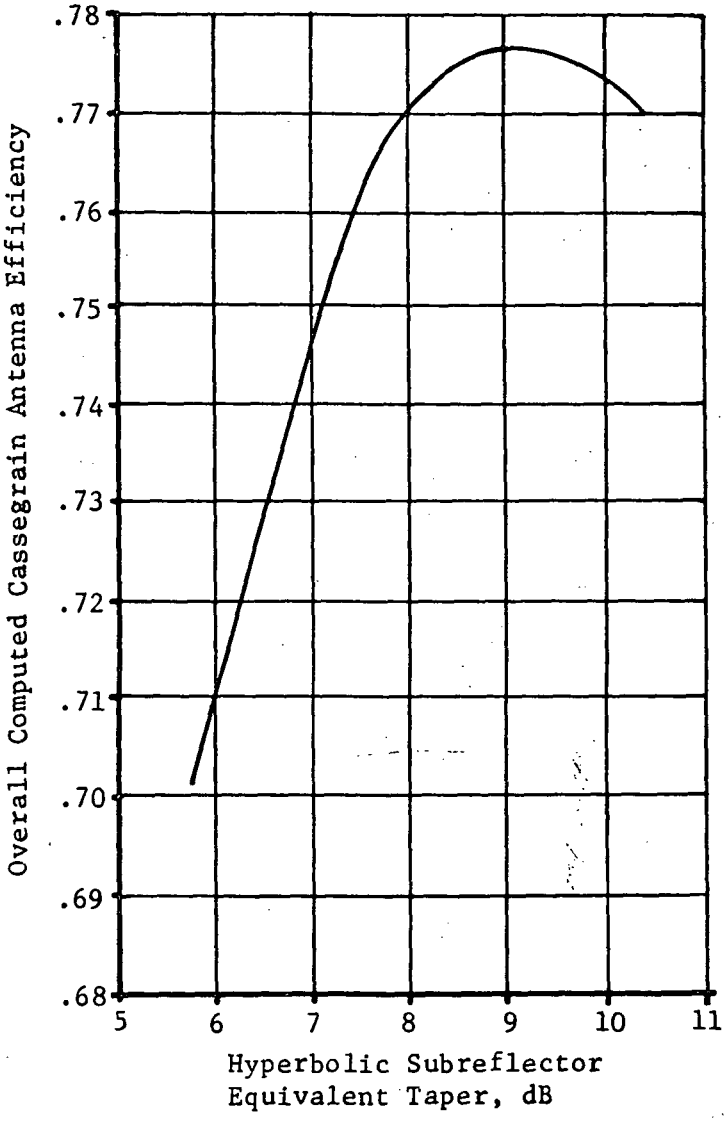

Figure H-4. New Overall Efficiency as a Function of Hyperbolic Subreflector Equivalent Taper

APPENDIX I

THE USE OF COHERENT DETECTION FOR ANGLE TRACKING

A significant decrease in the signal-to-noise ratio required for angle tracking can be obtained if coherent detection is used. The use of such detection requires the use of a coherent source in the receiver, which in the case of TDRSS - as in most cases - must be obtained through the use of a phase-locked loop. A simplified block diagram of how a phase-locked loop might work for angle detection in a single plane is shown in Figure I-1. The RF signal, which arrives at some angle other than boresight of the two antennas, causes the hybrid to produce a sum signal (Σ) which is greatest when the RF signal is normal to the antennas, and a difference signal (Δ) which is minimum when the RF signal is normal to the antennas. The sum signal is fed to the phase detector of the phase-locked loop (PLL) where it is mixed with the output of the voltage controlled oscillator operating at the same frequency. The output of the phase detector, which is proportional to the phase difference of the two signals, is filtered and amplified to produce an error signal to correct the phase of the VCO so that the output of the phase detector is zero or nearly so. The detector output, E_D, is given by

$$E_D = 2E_i \text{Sin } \theta$$

where

E_i = the input signal

θ = the phase difference between the input signal and the VCO output.

It is assumed that the VCO output is much greater than the input signal. It can be seen from the equation above that the output will be the minimum (zero) where $\theta = 0$.

The VCO output can now be used to coherently detect the difference signal. To maximize the output of the phase detector, the output of the VCO is shifted by 90 degrees. Thus, the phase detector output is a function only of the input signal amplitude, since the θ of the equation is now equal to 90 degrees.

In determining the performance which a PLL might give in the TDRS system, it is necessary to determine the maximum doppler and the maximum rate of change of doppler as the range between the user satellite and the TDRS changes. Figure I-2 shows the relationship between the two satellites. K is the distance between the TDRS and the center of the earth; D is the distance between the orbit of the user satellite and the center of the Earth; and r is the instantaneous range between the

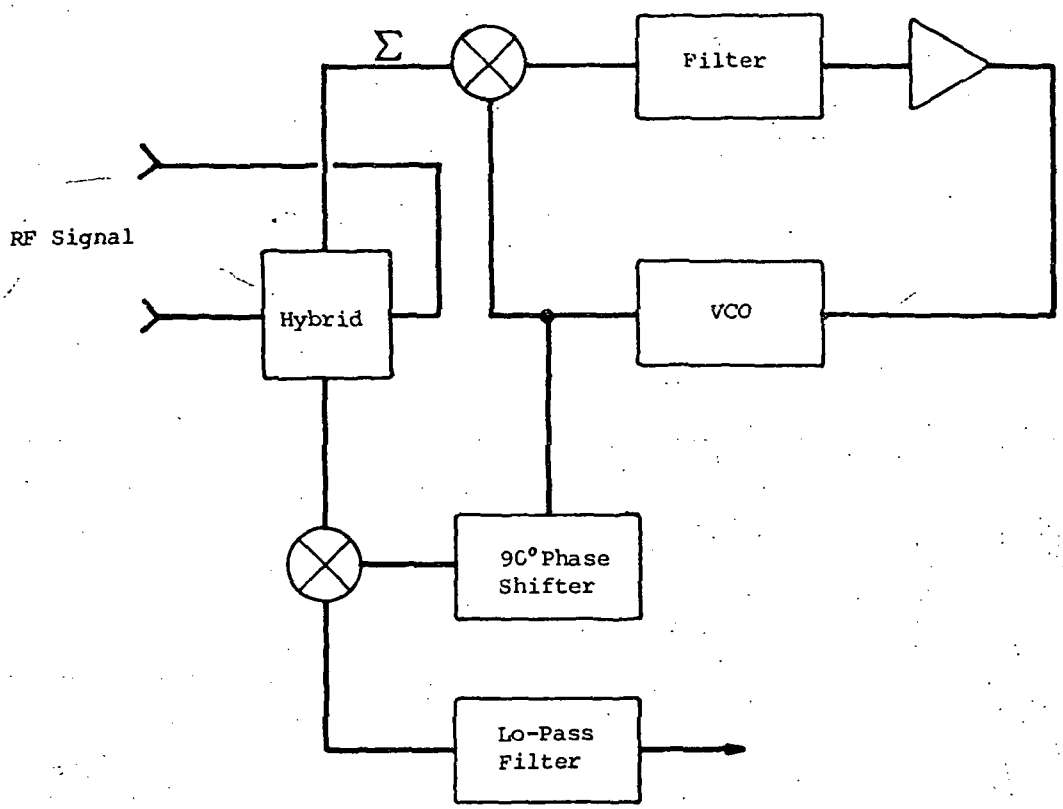

Figure I-1. Simplified Block Diagram of Coherent Deletion Method

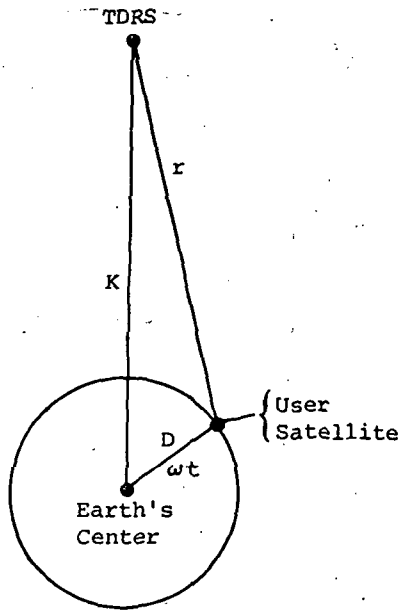

Figure I-2. Relation of TDRS to User Satellite Orbit

two satellites. The range can then be expressed as

$$r = \sqrt{K^2 + D^2 - 2KD \sin \omega t}$$

Taking the first derivative of r, the instananeous relative velocity, v, is

$$v = \frac{-KD\omega \cos \omega t}{\sqrt{K^2 + D^2 - 2KD \sin \omega t}}$$

Taking the second derivative of r yields the acceleration, a:

$$a = \frac{KD\omega^2 \sin \omega t}{\sqrt{K^2 + D^2 - 2KD \sin \omega t}} - \frac{(KD\omega \cos \omega t)^2}{(\sqrt{K^2 + D^2 - 2KD \sin \omega t})^3}$$

If it is assumed that the altitude of TDRS is 22,500 statute miles, that the altitude of the lowest user satellite is 150 statute miles, and that the radius of the earth is 6,378 km, then K = 42,588 km and D = 6618 km. It is further assumed that the period of the orbit of the lowest satellite is 90 minutes, so that $\omega = 1.164 \times 10^{-3}$ radians per second. Setting the expression for acceleration equal to zero and solving for ωt, the velocity is found to be maximum when $\omega t = 8.87$ degrees, at which point v = 7.7 km/s. The acceleration is a maximum when $\omega t = 90$ degrees where a is equal to .01061 km/s^2. With these values of maximum velocity and acceleration, the maximum doppler and maximum doppler rate can be determined from the following equations:

$$\text{Doppler } (\Delta f) = \frac{f_b V_{max}}{C} \text{ Hz}$$

$$\text{Doppler rate } (\dot{\Delta f}) = \frac{f_b A_{max}}{C} \text{ Hz/s}$$

where

f_b = beacon frequency of user satellite

C = velocity of light.

For S-band (2250 MHz),

Δf_s = 57.750 kHz

$\dot{\Delta f}_s$ = 79.6 Hz/s

and for K_u-band (15.008 GHz)

Δf_{Ku} = 385 kHz

$\dot{\Delta f}_{Ku}$ = 530 Hz/s.

The receiver bandwidth must be wide enough to accommodate twice the doppler (since it has both negative and positive exclusions) plus make allowance for various frequency instabilities in oscillators and filters. At S-band, the receiver bandwidth must be about 150 kHz, and at K_u-band, a bandwidth of about 1 MHz is required.

The use of a phase-locked loop may be implemented in either of two ways: 1) by placing the PLL in the satellite, or 2) by transmitting the undetected sum and difference information to the ground and accomplishing the coherent detection there. The advantage of the latter method is that the PLL is available for repair or modification to alter its characteristics, if necessary.

Figures I-3 and I-4 show simplified block diagrams of how the phase-locked loop can be located in the ground station. Though these diagrams purport to represent both the S- and K_u-band case, the S-band is actually slightly different in that the azimuth and elevation errors are combined orthogonally on a single carrier which must eventually be resolved into the two components. In such an implementation, almost one-third of the equipment shown could be eliminated. However, the figures are still representative of the methods involved in accomplishing coherent detection in the ground station.

Figure I-3 shows the simplified block diagram of the angle sensing equipment in the satellite. A four-horn monopulse scheme is shown in which sum, azimuth difference, and elevation difference signals are generated. Those signals are immediately down-converted, filtered, amplified, and down-converted a second time. As will be shown, it is necessary that the intermediate frequencies be as low as possible, but that cannot be accomplished in one step because of the image frequency. In the K_u-band, where the final IF is 1 MHz, a single conversion receiver would place the image frequency only 2 MHz away which is still in the middle of the user-to-TDRS link. The use of a 300 MHz first IF and high-side injection places the image at 15608.5 MHz, where no radiation is present. Low side injection with a higher IF would place the image frequency between the TDRS receiver and transmit bands, but interference from the transmitter might cause some problems because of the low received signal levels. The same basic arguments hold true for S-band where high-side injection is also recommended.

In each frequency translation in both the satellite and ground station, the same oscillator (or phase-locked oscillators) must be used in all three channels to preserve the phase information so that coherent detection can be accomplished.

Following the second IF amplifier, an AGC signal is derived from the sum channel and fed to all three channels. The two difference channels contain amplitude information and must not be allowed to saturate.

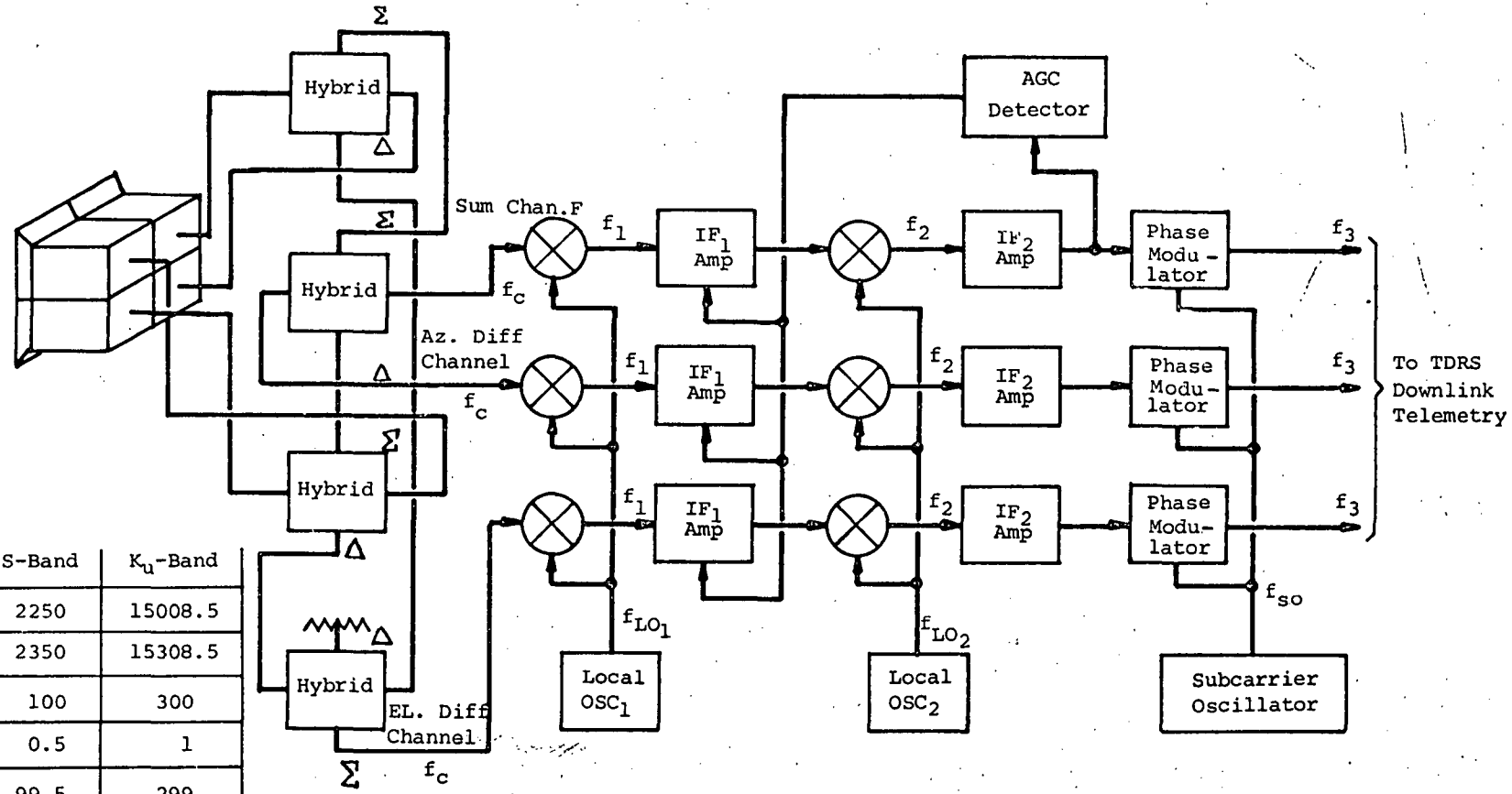

	S-Band	K_u-Band
f_c	2250	15008.5
f_{LO_1}	2350	15308.5
f_1	100	300
f_2	0.5	1
f_{LO_2}	99.5	299
f_{SO}	1	4
f_3	1	4

Figure I-3. Simplified Block Diagram of Angle Sensing Equipment in Satellite

	S-Band	K_u-Band
f_3	1	4
f_{SO}	1	4
f_2	0.5	1
f_{LO_3}	4.5	9
f_4	5.0	10

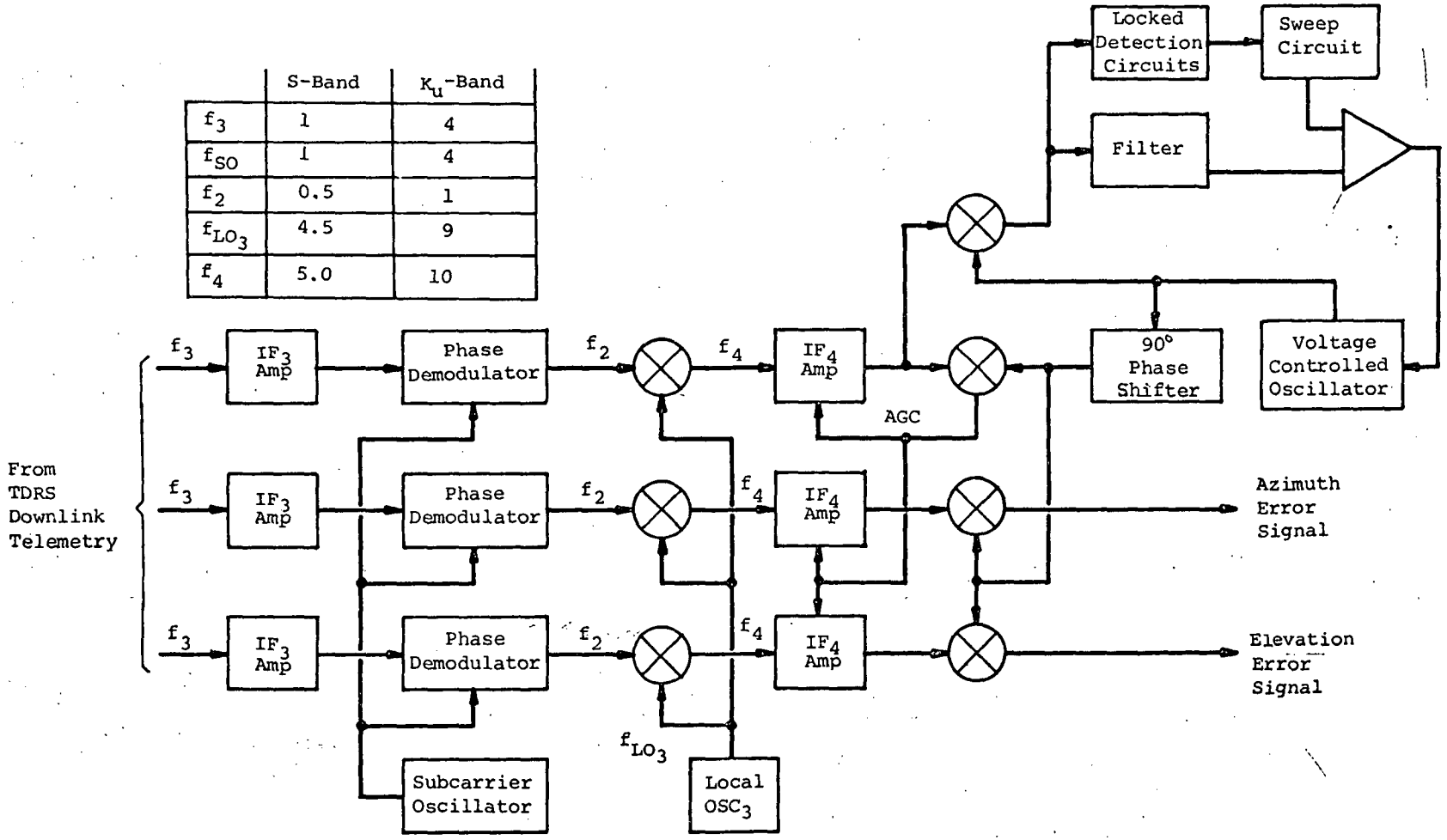

Figure I-4. Simplified Block Diagram of Angle Sensing Equipment in Ground Station

The second intermediate frequency must be kept as low as possible to preserve bandwidth in the telemetry channels. Because the amplitude as well as phase information in f_2 must be preserved, each channel must be transmitted by phase modulation. The bandwidth of the output of the phase modulator follows Carson's rule which states

$$BW = 2(f_{mod} + \Delta f)$$

where

BW = the bandwidth

f_{mod} = the modulating frequency

Δf = the deviation.

Although f_2 contains low speed data, the intermediate frequency itself becomes f_{mod}. At K_u-band, if f_2 is set at 1 MHz with a bandwidth of 1 MHz ($\pm$ 500 kHz), the maximum value of f_2 will be 1.5 MHz. The bandwidth of the modulator output will then be 3.0 MHz because of the f_{mod} term alone, or about 3.5 MHz ($\pm$ 1.75 MHz) when both terms are considered. To achieve some degree of linearity, the unmodulated subcarrier must be about 4 MHz. When modulation is added, the maximum value of f_3 will be 4 + 1.75 or 5.75 MHz of bandwidth for each of the three channels. A single subcarrier oscillator is used to preserve the coherence of the three signals.

S-band presents similar problems, although correspondingly lower frequencies and narrower bandwidths could be used. Alternatively, the same frequencies could be used to obtain better linearities, or as shown in the frequency tables, some combination of the two. f_2 might be 500 kHz with a bandwidth of 150 kHz. The highest value of f_2 would then be 500 plus 75 or 575 kHz. A reasonable bandwidth out of the phase modulator would then be 1.5 MHz. If a subcarrier oscillator of 1 MHz were used, the maximum value of f_3 would be 1.75 MHz. However, as pointed out previously, only two channels need to be transmitted since both azimuth and elevation information are transmitted in one difference channel.

The three (or two) channels are then transmitted over existing telemetry channels, and recovered in the ground station from the telemetry equipment at the same frequency, f_3, in the same form. Figure I-4 is a simplified block diagram of the necessary ground station equipment. IF amplifiers may or may not be needed prior to recovery of the phase modulation. The modulation, f_2, which is the same value of f_2 in the satellite, is obtained from the phase demodulators (phase detectors) and are immediately up-converted to a new intermediate frequency, f_4. This is the same frequency at which the VCO must operate, and it must be at some frequency at which the VCO can achieve the necessary bandwidth. For example, in the K_u-band the VCO must deviate $\pm$ 500 kHz, or

a total of 1 MHz. At a center frequency of 10 MHz, this represents a bandwidth of 10 percent, which is a realizable number. At a center frequency of 1 MHz, it represents a bandwidth of 100 percent, which is an impossible value. A center frequency which is even higher - perhaps 50 MHz - might be better. At S-band, a center frequency of 5 MHz and a bandwidth of 150 kHz represents only 3 percent bandwidth, which is easily obtained. Additional IF amplifiers - mainly for gain control - are included prior to the PLL and the coherent detection circuits. Again, the control for all three channels is derived from the sum channel. The operation of the loop detection of the difference channels is the same as pointed out earlier, except that a sweep circuit has been included. To assure that the loop will lock onto the beacon signal and to decrease the time required to obtain lock, a sweep circuit generates a ramp signal which is added to the error signal to change the output frequency of the VCO. When the VCO frequency is close enough to that of the reference channel, the loop will lock. It is possible to detect when the loop is locked and to then disable the sweep circuit. If lock is lost for any reason, the sweeping will resume until lock is once again obtained.

In analyzing the performance of the PLL, several characteristics are of importance: 1) the minimum input signal-to-noise ratio $(SNR)_{IN}$ at which the loop will lock, 2) the output SNR in the difference channels, and 3) the time to acquire lock.

The phase jitter, or mean square phase error, of the loop is given by (Reference I-1):

$$\sigma^2 = \frac{\left(1+\frac{1}{4\zeta^2}\right)}{8\tau_{CE} B_L} + \frac{1}{(SNR)_{IN}}\left(\frac{B_L}{B_{IF}}\right) \text{rad}^2$$

where

σ^2 = mean square phase error

ζ = damping ratio

τ_{CE} = equivalent coherence time of the system oscillators

B_L = loop noise bandwidth

$(SNR)_{IN}$ = input signal-to-noise ratio

B_{IF} = bandwidth of input signal

If σ^2 is differentiated with respect to B_L, the minimum value σ^2 as a function of B_L will be obtained. The optimum value of B_L is given by

$$B_L = \sqrt{\frac{B_{IF}\left(1+\frac{1}{4\zeta^2}\right)}{8\tau_{CE}\left(\frac{1}{SNR}\right)_{IN}}}$$

Substituting this expression for B_L into the equation for σ^2, the expression for the minimum σ^2 is obtained

$$\sigma^2_{MIN} = \sqrt{\frac{1}{(SNR)_{IN}} \cdot \frac{1}{2B_{IF}\tau_{CE}}\left(1+\frac{1}{4\zeta^2}\right)}$$

Using the values from Table I-I, expressions for σ^2_{MIN} as a function of only $(SNR)_{IN}$ may be obtained. For both S- and K_u-bands

$$\sigma^2_{MIN} = \frac{8.16 \times 10^{-3}}{\sqrt{(SNR)_{IN}}}$$

TABLE I-I

Typical Parametric Values

Parameter	S-Band	K_u-Band
B_{IF}	150 kHz	1.0 MHz
τ_{CE}	0.1 second	0.015 second
ζ	0.5	0.5

The expression for σ^2 is the same for both bands because B_{IF} and τ_{CE} for both bands are related by the same factor. Figure I-5 shows a plot of σ^2 MIN as a function of $(SNR)_{IN}$. The proper operation of the PLL depends on the magnitude of the phase error remaining less than $\pi/2$ radians, which is to say that the loop will unlock at values of $\pi/2$ or greater. For the phase error due to random fluctuations, it can only be required that the probability of its exceeding $\pi/2$ radians be very small. A criterion for this which has been chosen as a realistic measure of the threshold of the PLL is that the value of σ^2 be restricted by

$$\sigma^2_{MIN} \leq 1/8 \text{ rad}^2$$

This value is shown in Figure I-5 and indicates that the minimum $(SNR)_{IN}$ threshold for acquiring lock in either band is -23.7 dB.

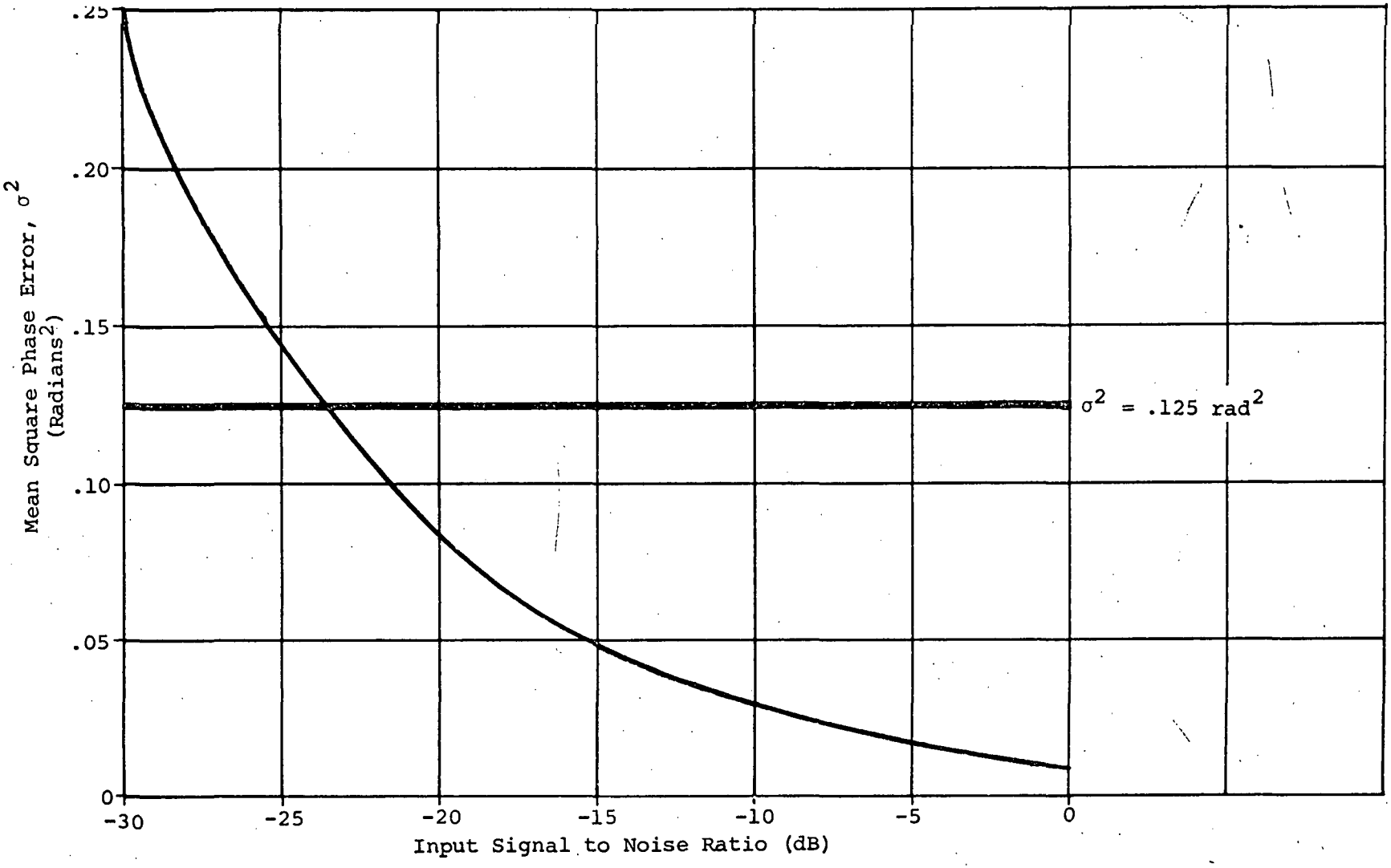

Figure I-5. Mean Square Phase Error vs Input Signal-To-Noise Ratio

Because the minimum (SNR) at which the loop can work is so heavily dependent on τ_{CE} (which can be increased through the use of more stable oscillators), an expression for $(SNR)_{IN}$ as a function of τ_{CE} when $\sigma^2_{MIN} = 0.125$ rad^2 is useful. For S-band

$$(SNR)_{IN} = -33.7 - 10 \log \tau_{CE} \text{ dB.}$$

For K_u-band

$$(SNR)_{IN} = -41.9 - 10 \log \tau_{CE} \text{ dB.}$$

Figure I-6 plots the minimum permissible $(SNR)_{IN}$ as a function of τ_{CE} for the S- and K_u-bands.

From the previous expression for B_L, the value of B_L can be obtained using the values in Table I-I and an $(SNR)_{IN}$ of -23.7 dB.

For S-band

$$B_L = 40 \text{ Hz.}$$

For K_u-band

$$B_L = 266.8 \text{ Hz.}$$

B_L is related to the loop natural frequency, ω_n, by

$$\omega_n = \frac{2B_L}{(\zeta + \frac{1}{4\zeta})} \text{ rad/s.}$$

For the case where $\zeta = 0.5$

$$\omega_n = 2B_L \text{ rad/s.}$$

For S-band

$$\omega_n = 80 \text{ rad/s}$$

and for K_u-band

$$\omega_n = 533.6 \text{ rad/s.}$$

The dynamic phase error, θ_a, in a second order loop is given by

$$\sin \theta_a = \frac{\Delta\dot{\omega}}{\omega_n^2}$$

where $\Delta\dot{\omega}$ is the doppler rate expressed in radians and has previously been shown to be $2\pi(79.6)$ or 500.1 rad/s^2 for S-band and $2\pi(530)$ or

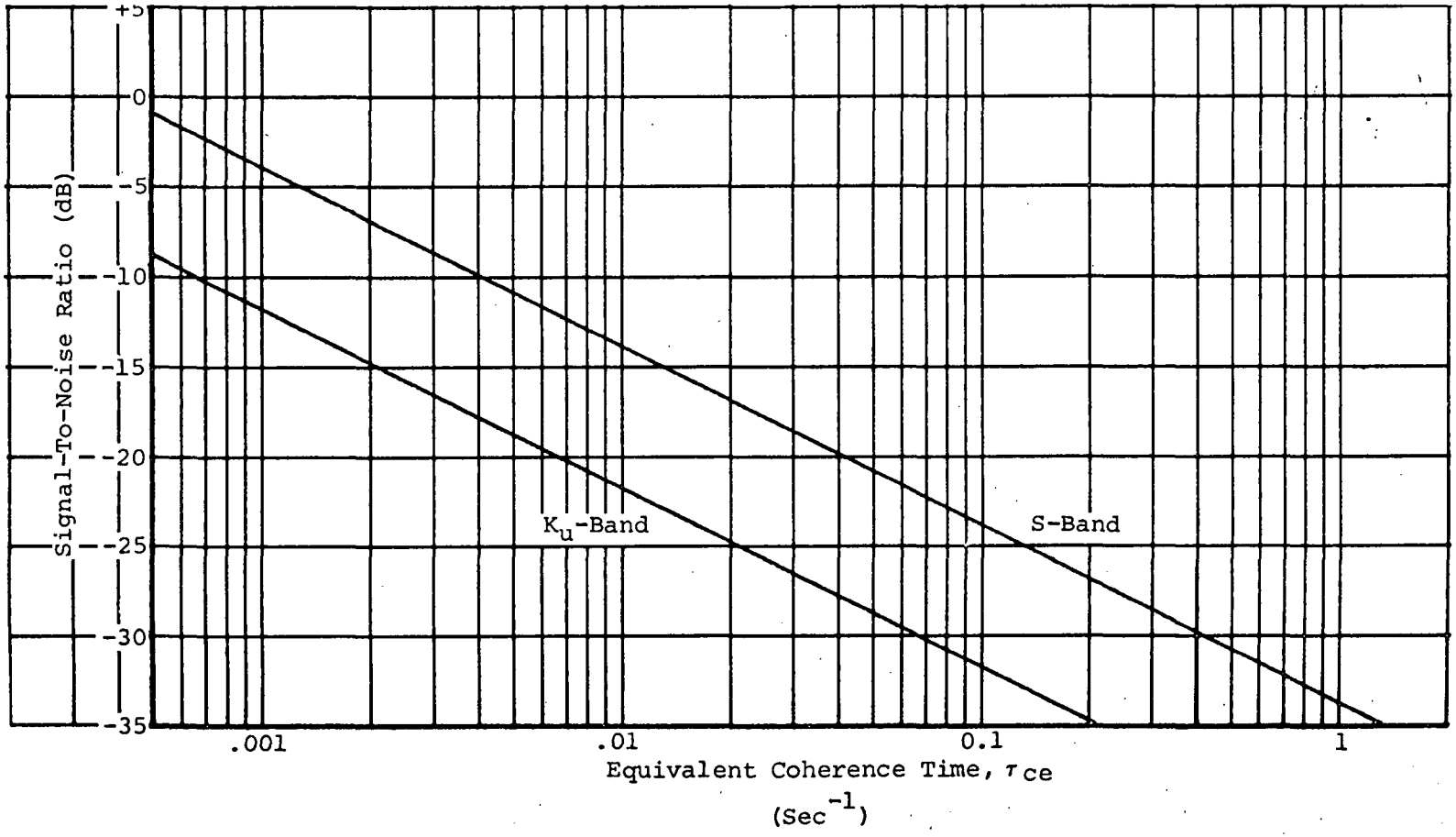

Figure I-6. Input Signal-To-Noise Ratio Required For $\sigma^2 = .125$ vs Equivalent Coherence Time

3330 rad/s^2 for K_u-band. Therefore, θ_a = 0.078 radian for S-band and θ_a = 0.0117 radian for K_u-band. It has been pointed out previously that θ_a must not exceed $\pi/2$ radians. The values listed here show that even in the worst case (S-band), θ_a has a 20 to 1 safety factor.

The maximum theoretical sweep rate can be calculated by letting $\theta_a = \pi/2$, in which case $\Delta\dot{\omega} = \omega_n^2$ where $\Delta\dot{\omega}$ now represents the sweep rate. Acquisition under these circumstances is questionable, especially if the input signal is noisy. $\Delta\dot{\omega}$ should be reduced by a factor of

$$\left[1-\left(\frac{(SNR)_{IN}\,B_{IF}}{B_L}\right)^{-\frac{1}{2}}\right]$$

The maximum sweep rate then becomes

$$\Delta\dot{\omega} = \omega_n^2\left[1-\left(\frac{(SNR)_{IN}\,B_{IF}}{B_L}\right)^{-\frac{1}{2}}\right]$$

For S-band

$$\Delta\dot{\omega} = 4.80 \times 10^3 \text{ rad/s}^2 \text{ or } 763 \text{ Hz/s.}$$

For K_u-band

$$\Delta\dot{\omega} = 213.5 \times 10^3 \text{ rad/s}^2 \text{ or } 34 \text{ kHz/s.}$$

If it is assumed that the maximum difference between the frquency of the input signal and the VCO is 150 kHz in the S-band and 1.0 MHz in the K_u-band, then the maximum time to acquire in each band is 196.6 seconds and 29.4 seconds, respectively. The time to acquire in the S-band is probably excessive and can be overcome by widening the loop bandwidth. However, the wider bandwidth will result in increased phase jitter (σ^2).

To determine the output signal-to-noise ratio, $(SNR)_o$, it is necessary to determine the improvement factor achieved through coherent detection. In a non-coherent system, the bandpass of the components prior to the detector must be wide enough to pass the entire doppler range - 1 MHz in the case of K_u-band. In the detection process, all of the noise power in that bandwidth is added to the output signal, which in fact is very narrow. In coherent detection, the phase-locked loop has tracked the frequency of the input signal so that when the VCO output is mixed with the input signal in the phase detector, the noise in the output will be determined by the bandwidth of the output filter. The output filter need only be wide enough to assure the passage of all or most of the signal information. In the present case, that bandwidth is $\frac{1}{\tau_{CE}}$.

Thus, in either coherent or non-coherent detection, the signal power is the same, but the noise power is related directly to the noise bandwidths

involved. Thus, the improvement factor may be expressed

$$K_i = 10 \log (B_{IF}\, \tau_{CE}).$$

In both bands

$$K_i = 41.8 \text{ dB}.$$

As has been shown, the minimum acceptable $(SNR)_{IN}$ is -23.7 dB. $(SNR)_o$, then, is 18.1 dB.

The above results are modified slightly by the fact that detection occurs on the ground. The input SNR is degraded by 2 dB because of the transmission to the ground, so that to obtain 18.1 dB at the output, an input to satellite antenna of -21.7 dB is required. Hence, the method proposed here actually results in an improvement of 39.8 dB.

APPENDIX J

ANALYSIS OF ANGLE SENSOR CHARACTERISTICS FOR NON-COHERENT PROCESSING

It is the purpose of this appendix to define a model of a single-plane angle sensor, which utilizes non-coherent processing, and then to:

1. Characterize the sensor output function,
2. Relate the sensor characteristics to the field of view,
3. Derive an expression for the angular tracking error due to receiver noise.

The sensor model is shown in block diagram form in Figure J-1. The antenna develops the squinted antenna patterns $g(\theta)$ and $g(-\theta)$, and the comparator network produces sum and difference patterns. The received signal is assumed to be an unmodulated carrier with a slowly varying frequency due to relative motion of the TDRS and user spacecraft. The sum and difference channel signals are perturbed by wideband gaussian noise which is assumed to be uncorrelated between channels. Frequency conversion is followed by bandpass filtering which results in the processes

$$a(t) = \Sigma(\theta)\cos\omega_o t + \eta_\Sigma(t) \tag{1}$$

in the sum channel and

$$b(t) = \Delta(\theta)\cos\omega_o t + \eta_\Delta(t) \tag{2}$$

in the difference channel

where

$$\Sigma(\theta) \triangleq \frac{A}{\sqrt{2}}[g(\theta)+g(-\theta)] \tag{3}$$

and

$$\Delta(\theta) \triangleq \frac{A}{\sqrt{2}}[g(\theta)-g(-\theta)] \tag{4}$$

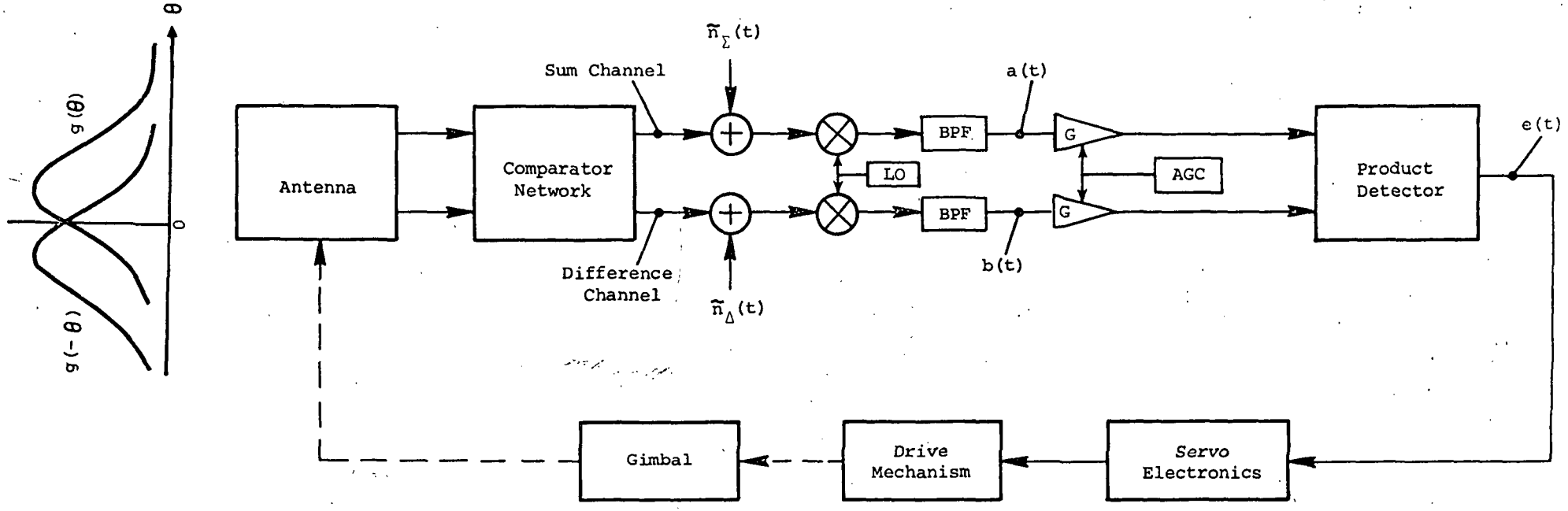

Figure J-1. Angle Sensor Model: Non-Coherent Processing

The antenna patterns $g(\theta)$ and $g(-\theta)$ are normalized so that at boresight, $g(0) = 1/\sqrt{2}$. Therefore, the signal component at the bandpass filter output in the sum channel, at boresight, is simply $A \cos \omega_o t$, where $\omega_o/2\pi$ is the intermediate frequency.

The bandwidth of the bandpass filters is, of course, commensurate with the doppler shift and any frequency instability which characterizes the received signal.

The noise waveforms $n_\Delta(t)$ and $n_\Sigma(t)$ are assumed to be wide-sense stationary, narrowband, gaussian processes with mean values of zero and variances σ_Δ^2 and σ_Σ^2. Moreover, the variances are related to the receiver characteristics by

$$\sigma_\Sigma^2 = k T_o B_n F_\Sigma \tag{6a}$$

and

$$\sigma_\Delta^2 = k T_o B_n F_\Delta \tag{6b}$$

where

k = Boltzman's constant

B_n = noise bandwidth of bandpass filter

F_Σ = noise figure of sum channel

F_Δ = noise figure of difference channel

T_o = reference temperature at which F_Σ and F_Δ are measured.

The bandpass filters are followed by identical (wideband) IF amplifiers, the gains of which are controlled by an AGC voltage obtained from the sum channel. The normalized sum and difference channel signals (and noise) are then delivered to a product detector. Its output, $e(t)$, is an error signal which is applied to the servo system for positioning the antenna.

Clearly, the signal-to-noise ratio at the output terminals of the sum channel bandpass filter is

$$SNR_\Sigma\ (\theta) = \frac{\Sigma^2(\theta)}{2\sigma_\Sigma^2} \tag{7}$$

In the boresight direction, this value becomes

$$SNR_{\Sigma}(0) = \frac{\Sigma^2(0)}{2\sigma_{\Sigma}}$$

$$= \frac{A^2}{2\sigma_{\Sigma}^2} \qquad (8)$$

since, as noted earlier, $g(0) = 1/\sqrt{2}$, and therefore $\Sigma(0)$ A.

Characterization of Sensor Output

Attention is given next to a detailed examination of the nature of the error signal e(t) which is developed at the output of the product detector. The first step is to characterize the noise processes $n_{\Sigma}(t)$ and $n_{\Delta}(t)$ in a conventional fashion as

$$n_{\Sigma}(t) = n_{\Sigma c}(t) \text{ Cos } \omega_o t - n_{\Sigma s}(t) \text{ sin } \omega_o t \qquad (9)$$

and

$$n_{\Delta}(t) = n_{\Delta c}(t) \text{ Cos } \omega_o t - n_{\Delta s}(t) \text{ sin } \omega_o t \qquad (10)$$

where $n_{\Sigma c_t}$, $n_{\Sigma s_t}$, $n_{\Delta c_t}$ and $n_{\Delta s_t}$ are Gaussian random variables with

$$\langle n_{\Sigma c} \rangle = \langle n_{\Sigma s} \rangle = \langle n_{\Delta c} \rangle = \langle n_{\Delta s} \rangle = 0,$$

$$\langle n_{\Sigma c} n_{\Sigma s} \rangle = \langle n_{\Delta c} n_{\Delta s} \rangle = 0,$$

$$\langle n_{\Sigma c}^2 \rangle = \langle n_{\Sigma s}^2 \rangle = \sigma_{\Sigma}^2$$

and

$$\langle n_{\Delta c}^2 \rangle = \langle n_{\Delta s}^2 \rangle = \sigma_{\Delta}^2$$

where <•> denotes expectation and the time subscript has been deleted. It is also recalled that $n_{\Sigma}(t)$ and $n_{\Delta}(t)$ were earlier assumed to be uncorrelated so that their components are also uncorrelated with each other.

The sum and difference channel signals are now written from Equations (1), (2), (9), and (10) as

$$a(t) = [\Sigma(\theta) + \eta_{\Sigma c}(t)]\cos\omega_o t - \eta_{\Sigma s}(t)\sin\omega_o t \qquad (11)$$

and

$$b(t) = [\Delta(\theta) + \eta_{\Delta c}(t)]\cos\omega_o t - \eta_{\Delta s}(t)\sin\omega_o t \qquad (12)$$

The model of the detector output to be employed here results in an output e(t) which is the product of a(t)G(t) and b(t)G(t) with appropriate filtering to remove frequency components of $2\omega_o/2\pi$. Now, from Equations (11) and (12), it is seen that

$$a(t)b(t) = \frac{1}{2}\{[(\Sigma+\eta_{\Sigma c})(\Delta+\eta_{\Delta c}) - \eta_{\Sigma s}\eta_{\Delta s}](1+\cos 2\omega_o t) + \eta_{\Sigma s}\eta_{\Delta s} - [\eta_{\Delta s}(\Sigma+\eta_{\Sigma c}) + \eta_{\Sigma s}(\Delta+\eta_{\Delta c})]\sin 2\omega_o t\}.$$

When coefficients of $\cos 2\omega_o t$ and $\sin 2\omega_o t$ are equated to zero, the product detector output takes the form

$$e(t) = \frac{G^2(t)}{2}[\Sigma(\theta)\Delta(\theta) + \Sigma(\theta)\eta_{\Delta c}(t) + \Delta(\theta)\eta_{\Sigma c}(t) + \eta_{\Sigma c}(t)\eta_{\Delta c}(t) + \eta_{\Sigma s}(t)\eta_{\Delta s}(t)] \qquad (13)$$

where signal x signal, signal x noise, and noise x noise terms are readily discernible.

The next problem is the formulation of G(t) in terms of the nature of the sum channel signal a(t). The value of G(t) is, of course, determined by the AGC voltage which is modeled as being derived from linear detection of the process a(t)G(t) followed by amplification and low-pass filtering. The signal component of a(t) is assumed to exhibit a constant amplitude over long periods of time by virtue of the slow temporal changes in both the user/TDRS distance and the angular separation of their line of sight with respect to the TDRS coordinate frame. Therefore, a long AGC time constant will be used to prevent fluctuations in G(t) being induced by the sum channel noise.

Two characteristics of the AGC voltage are of interest - the mean value and the fluctuations about the mean. The linear detector at the input to the AGC circuit acts to extract the envelope of the signal G(t)a(t). Since the value of G(t) will change slowly compared to a(t),

the linear detector output v(t) is characterized by a(t). Since a(t) is the sum of a sinusoid and narrowband gaussian noise, the probability density function of the random variable v_t has the well-known form (Reference J-1)

$$f_{v_t}(v_t) = \begin{cases} \frac{v_t}{\sigma_\varepsilon^2} \exp\left[-\frac{v_t^2 + \Sigma^2(\theta)}{2\sigma_\varepsilon^2}\right] I_o\left(\frac{v_t \Sigma(\theta)}{\sigma_\varepsilon^2}\right); & v_t \geq 0 \\ 0; & v_t < 0 \end{cases}$$

The mean value and second moment of v_t are given by

$$\langle v_t \rangle = \sqrt{\frac{\pi\sigma_\varepsilon^2}{2}}\, {}_1F_1\left(-\frac{1}{2}, 1; -SNR_\varepsilon(\theta)\right) \tag{14}$$

and

$$\langle v_t^2 \rangle = 2\sigma_\varepsilon^2 (1 + SNR_\varepsilon(\theta)). \tag{15}$$

When $SNR_\varepsilon(\theta) >> 1$, it is the case that

$$\langle v_t \rangle \approx \Sigma(\theta)\left[1 + \frac{1}{4SNR_\varepsilon(\theta)}\right]$$

and

$$\langle v_t^2 \rangle = \Sigma^2(\theta)\left[1 + \frac{1}{SNR_\varepsilon(\theta)}\right]$$

so that the mean value of the AGC voltage is nearly $\Sigma(\theta)$ and its variance is essentially zero. In the subject case, however, attention is to be concentrated on small values of sum channel signal-to-noise ratio.

It has been shown that if

$$0 \leq SNR_\varepsilon(\theta) \leq 2.5$$

then the mean value of the envelope is well approximated by (Reference J-2)

$$\langle v_t \rangle = \sqrt{\frac{\pi\sigma_\varepsilon^2}{2}}\left[1 + 0.4\, SNR_\varepsilon(\theta)\right] \tag{16}$$

The ratio of the variance to the square of the mean value can therefore be expressed as

$$\frac{\text{var } v_t}{\langle v_t \rangle^2} = \frac{2(1+SNR_\Sigma(\theta)) - \frac{\pi}{2}(1+0.4\,SNR_\Sigma(\theta))^2}{\frac{\pi}{2}(1+0.4\,SNR_\Sigma(\theta))^2}$$

and, in the limit $SNR_\Sigma(\theta) \to 0$, it is the case that

$$\frac{\text{var } v_t}{\langle v_t \rangle^2} = 0.27.$$

Thus, even for small values of sum channel SNR, the fluctuations about the mean are rather small. Moreover, these fluctuations will be further diminished by the factor $1/T_{AGC}B_{IF}$ where B_{IF} is defined by

$$B_{IF} = \begin{cases} 10^6 \text{ Hz at Ku-band} \\ 1.5\times10^5 \text{ Hz at S-band} \end{cases}$$

and T_{AGC} is the AGC time constant. Clearly, if $T_{AGC} \geq 10^{-2}$ seconds, the variation of the AGC voltage about its mean value will be negligible. That mean value, defined by Equation (16), can be rewritten in the form

$$\langle v_t \rangle = \frac{\Sigma(\theta)}{2}\sqrt{\frac{\pi}{SNR_\Sigma(\theta)}}\left[1+0.4\,SNR_\Sigma(\theta)\right]$$

provided that $0 < SNR_\Sigma(\theta) \leq 2.5$, i.e., the IF amplifier gain controlling voltage is:

1. Directly proportional to the sum channel signal level, $\Sigma(\theta)$,
2. Not influenced by noise,

over any time interval of duration T_{AGC}. The amplifier gain therefore takes the form

$$G = \frac{K}{\Sigma(\theta)} \tag{17}$$

where $K = K(SNR_\Sigma(\theta))$.

Returning now to the product detector output process, Equations (13) and (17) yield

$$e(t) = K\left[\frac{\Delta(\theta)}{\Sigma(\theta)} + \frac{\eta_{\Delta C}(t)}{\Sigma(\theta)} + \frac{\Delta(\theta)}{\Sigma(\theta)}\cdot\frac{\eta_{\Sigma C}(t)}{\Sigma(\theta)} + \frac{\eta_{\Sigma C}(t)\eta_{\Delta C}(t)+\eta_{\Sigma S}(t)\eta_{\Delta S}(t)}{\Sigma^2(\theta)}\right] \tag{18}$$

where the signal x signal, signal x noise, and noise x noise terms are still clearly visible and $K=K(SNR_\Sigma(\theta))$. In the absence of noise, $e(t) = K[\Delta(\theta)/\Sigma(\theta)$, as expected.

All of the information needed for characterizing the process e(t) is now available. This activity is conveniently carried out by rewriting Equation (18) in the form

$$e(t) = \frac{K}{\Sigma^2(\theta)}\left[\Delta(\theta)\Sigma(\theta) + \eta_{\Delta c}(t)\Sigma(\theta) + \eta_{\Sigma c}(t)\Delta(\theta) + \eta_{\Sigma c}(t)\eta_{\Delta c}(t) + \eta_{\Sigma s}(t)\eta_{\Delta s}(t)\right] \quad (19)$$

Next, it is noted that the covariance of the random variables

$$\Sigma(\theta)n_{\Delta c_t},\ \Delta(\theta)n_{\Sigma c_t},\ n_{\Sigma c_t},\ \text{and}\ n_{\Sigma s_t}n_{\Delta s_t}$$

is zero when they are considered pairwise in every possible combination. (The details will not be carried out.) Therefore, a good approximation to the probability density function of the random variable e_t is obtained by invoking the central limit theorem, whereby e_t becomes gaussian. Its mean value is

$$\langle e_t \rangle = K\left[\frac{\Delta(\theta)}{\Sigma(\theta)}\right] \quad (20)$$

and it is a simple matter to show that its variance is

$$\text{var}\, e_t = K^2\left\{\frac{\sigma_\Delta^2}{\Sigma^2(\theta)} + \left[\frac{\Delta(\theta)}{\Sigma(\theta)}\right]^2\frac{\sigma_\Sigma^2}{\Sigma^2(\theta)} + 2\frac{\sigma_\Sigma^2\sigma_\Delta^2}{\Sigma^4(\theta)}\right\} \quad (21)$$

For the special (but typical) case $\sigma_\Sigma^2 = \sigma_\Delta^2$,

$$\text{var}\, e_t = \frac{K^2}{2SNR_\Sigma(\theta)}\left\{1 + \left[\frac{\Delta(\theta)}{\Sigma(\theta)}\right]^2 + \frac{1}{SNR_\Sigma(\theta)}\right\} \quad (22)$$

Since a gaussian random variable is defined by its mean and variance, the first order properties of the process e(t) have been determined. The next step is the formulation of one of the second order properties, viz., the correlation function. This tedious process is carried out in Appendix K, where it is shown that

$$R_e(\tau) = \left[\frac{K}{\Sigma^2(\theta)}\right]^2\left[(\Delta(\theta)\Sigma(\theta))^2 + \Sigma^2(\theta)R_\Delta(\tau) + \Delta^2(\theta)R_\Sigma(\tau) + 2R_\Sigma(\tau)R_\Delta(\tau)\right] \quad (23)$$

where

$$R_\Sigma(\tau) = \int_{-\infty}^{\infty} S_\Sigma(f)\cos\left[2\pi(f-f_0)\tau\right]df \quad (24)$$

and

$$R_\Delta(\tau) = \int_{-\infty}^{\infty} S_\Delta(f)\cos\left[2\pi(f-f_0)\tau\right]df \quad (25)$$

The quantitities $S_\Sigma(f)$ and $S_\Delta(f)$ are the power spectral densities associated with the noise processes $n_\Sigma(t)$ and $n_\Delta(t)$ and both are required to be even functions with respect to f_o for Equation (23) to be valid. If $S_\Sigma(f) = S_\Delta(f)$, then $R_\Sigma(\tau) = R_\Delta(\tau)$ and therefore

(19)

$$R_e(\tau) = \left[\frac{K}{\Sigma^2(\theta)}\right]^2 \left\{(\Delta(\theta)\Sigma(\theta))^2 + R_\xi(\tau)\left[\Sigma^2(\theta)+\Delta^2(\theta)+2R_\xi(\tau)\right]\right\}. \quad (26)$$

It has been concluded that the sensor output process e(t) is characterized by:

1. e_t closely approximates a gaussian random variable with a mean and variance defined by Equations (20) and (21),

2. Wide-sense stationarity with a correlation function given by Equation (23), provided that the just stated conditions on the power spectral density are satisfied,

for any non-zero value of sum channel SNR and an AGC time constant of the order of 10^{-2} seconds or greater.

Sensor Field-of-View

It has been shown above that when a signal arrives at the angle sensing antenna from some arbitrary angle θ, the sensor output voltage waveform consists of the sum of signal and noise. The mean value of that output has the same value that would result from a noise free system, viz., $K\Delta(\theta)/\Sigma(\theta)$. The additive noise has an rms value given by the square root of the variance, defined in Equation (22), i.e.,

$$\text{std. dev. } e_t = \frac{K}{\sqrt{2SNR_\xi(\theta)}}\sqrt{1+\left[\frac{\Delta(\theta)}{\Sigma(\theta)}\right]^2+\frac{1}{SNR_\xi(\theta)}} \; ; \begin{cases} SNR_\xi(\theta) \neq 0 \\ \sigma_\xi^2 = \sigma_\Delta^2 \end{cases} \quad (27)$$

It seems reasonable to define the FOV of the angle sensor in terms of the noisiness of the output waveform. To this end, the ratio

$$r_e(\theta) = \frac{\text{std. dev. } e_t}{\langle e_t \rangle}$$

is defined. A useful "working" relationship for $r_e(\theta)$ in terms of the antenna characteristics and the value of the sum channel SNR at boresight, i.e., $SNR_\Sigma(0) = A^2/2\sigma_\Sigma^2$ (see Equation (8)), is

$$r_e(\theta) = \frac{\Sigma(0)}{\Sigma(\theta)}\left[\frac{1}{\Delta(\theta)/\Sigma(\theta)}\right]\sqrt{\frac{1+\left[\frac{\Delta(\theta)}{\Sigma(\theta)}\right]^2+\frac{\Sigma^2(0)}{\Sigma^2(\theta)SNR_\xi(0)}}{2SNR_\xi(0)}} \quad (28)$$

where

$$\Sigma(0)/\Sigma(\theta) = \sqrt{2}/\left(g(\theta)+g(-\theta)\right)$$

The tracking loop will act to materially reduce the value of $r_e(\theta)$ by virtue of its very small bandwidth. To obtain a quantitative measure of the reduction, the tracking loop is modeled as a linear low-pass filter with an impulse response h(t). The waveform at the servo output terminals is defined as q(t) in response to the input process e(t) from the angle sensor. The total power at the servo system output can therefore be written as

$$R_q(0) = \int_{-\infty}^{\infty} S_e(f) |H(f)|^2 df$$

where $R_q(\tau)$ is the correlation function of the waveform q(t), $S_e(f)$ is the power spectral density at the angle sensor output terminals and H(f) is the Fourier transform of h(t). Before proceeding, it is noted that the servo system output voltage q(t) at some instant of time t is a gaussian random variable since e_t is gaussian.

The dc component of the power represented by $R_q(0)$ is simply the product of the dc component of $R_e(0)$ and the dc response of the servo. That is

$$R_q(0)\big|_{DC} = |H(0)|^2 R_e(0)\big|_{DC}$$

or, using Equation (23),

$$R_q(0)\big|_{DC} = K^2 |H(0)|^2 \left[\frac{\Delta(\theta)}{\Sigma(\theta)}\right]^2 \tag{29}$$

Since the bandwidth of the servo is very small compared to the IF bandwidth, it follows that the sensor output spectrum is essentially constant over the non-zero response of |H(f)|. Therefore, the ac component of servo output power is

$$R_q(0)\big|_{AC} \approx S_e(0)\big|_{AC} \int_{-\infty}^{\infty} |H(f)|^2 df, \tag{30}$$

but

$$S_e(0)\big|_{AC} = \int_{-\infty}^{\infty} R_e(\tau)\big|_{AC} \, d\tau \tag{31}$$

where, from Equation (23)

$$R_e(\tau)\big|_{AC} = \left[\frac{K}{\Sigma^2(\theta)}\right]^2 \left[\Sigma^2(\theta) R_\Delta(\tau) + \Delta^2(\theta) R_\Sigma(\tau) + 2 R_\Sigma(\tau) R_\Delta(\tau)\right] \tag{32}$$

with $R_\Sigma(\tau)$ and $R_\Delta(\tau)$ defined by

$$R_\varepsilon(\tau) = \int_{-\infty}^{\infty} S_\varepsilon(f)\cos[2\pi(f-f_o)\tau]\,d\tau \tag{24}$$

and

$$R_\Delta(\tau) = \int_{-\infty}^{\infty} S_\Delta(f)\cos[2\pi(f-f_o)\tau]\,d\tau. \tag{25}$$

The spectral shapes $S_\Sigma(f)$ and $S_\Delta(f)$ are now defined to be rectangular, centered at f_o and having a width B_{IF}, from which it follows that

$$R_\varepsilon(\tau) = \sigma_\varepsilon^2\left[\frac{\sin \pi B_{IF}\tau}{\pi B_{IF}\tau}\right] \tag{33}$$

and

$$R_\Delta(\tau) = \sigma_\Delta^2\left[\frac{\sin \pi B_{IF}\tau}{\pi B_{IF}\tau}\right]. \tag{34}$$

Under the assumed conditions regarding $S_\Sigma(f)$ and $S_\Delta(f)$, it is clear that B_{IF} is the noise bandwidth as well as the actual IF bandwidth.

From Equations (31), (32), (33), and (34), it is seen that

$$S_e(0)\big|_{AC} = \left[\frac{K}{\Sigma^2(\theta)}\right]^2\int_{-\infty}^{\infty}\left[\Sigma^2(\theta)\sigma_\Delta^2\left(\frac{\sin\pi B_{IF}\tau}{\pi B_{IF}\tau}\right)+\Delta^2(\theta)\sigma_\varepsilon^2\left(\frac{\sin\pi B_{IF}\tau}{\pi B_{IF}\tau}\right)+2\sigma_\varepsilon^2\sigma_\Delta^2\left(\frac{\sin\pi B_{IF}\tau}{\pi B_{IF}\tau}\right)^2\right]d\tau$$

which becomes, after carrying out the indicated integration

$$S_e(0)\big|_{AC} = \frac{1}{B_{IF}}\left[\frac{K}{\Sigma^2(\theta)}\right]^2\left[\Sigma^2(\theta)\sigma_\Delta^2+\Delta^2(\theta)\sigma_\varepsilon^2+2\sigma_\varepsilon^2\sigma_\Delta^2\right]. \tag{35}$$

Next, Equation (30) is rewritten in the form

$$Rq(0)\big|_{AC} = S_e(0)\big|_{AC}\,|H(0)|^2\int_{-\infty}^{\infty}\left|\frac{H(f)}{H(0)}\right|^2 df$$

where the integral is now recognized as the two-sided servo noise bandwidth, to be defined as 2 β_n. Thus,

$$Rq(0)\big|_{AC} = 2|H(0)|^2 \beta_n Sc(0)\big|_{AC}$$

or, when Equation (35) is employed

$$Rq(0)\big|_{AC} = 2K^2|H(0)|^2\left(\frac{\beta_n}{B_{IF}}\right)\left[\frac{\sigma_\Delta^2}{\Sigma^2(\theta)} + \frac{\Delta^2(\theta)}{\Sigma^2(\theta)}\cdot\frac{\sigma_\Sigma^2}{\Sigma^2(\theta)} + \frac{2\sigma_\Sigma^2\sigma_\Delta^2}{\Sigma^4(\theta)}\right]. \quad (36)$$

The ratio of the ac and dc servo output power is found from Equations (29) and (36) to be

$$\frac{Rq(0)\big|_{AC}}{Rq(0)\big|_{DC}} = 2\left(\frac{\beta_n}{B_{IF}}\right)\left\{\frac{\left[\frac{\sigma_\Delta}{\Sigma(\theta)}\right]^2 + \left[\frac{\Delta(\theta)}{\Sigma(\theta)}\right]^2\cdot\left[\frac{\sigma_\Sigma}{\Sigma(\theta)}\right]^2 + \frac{2\sigma_\Sigma^2\sigma_\Delta^2}{\Sigma^4(\theta)}}{\left[\frac{\Delta(\theta)}{\Sigma(\theta)}\right]^2}\right\}; \Delta(\theta)/\Sigma(\theta) \neq 0. \quad (37)$$

For the case $\sigma_\Sigma^2 = \sigma_\Delta^2$, the term in braces is recognized as $r_e^2(\theta)$. It is reasonable to define the noisiness of the servo system output as

$$rq(\theta) \triangleq \frac{\text{std. dev. } q_t}{\langle q_t \rangle}$$

whereby

$$r_q(\theta) = \sqrt{\frac{2\beta_n}{B_{IF}}}\, r_e(\theta). \quad (38)$$

It is not surprising to find that the ratio of the rms and dc components at the output of the servo system is less than the same ratio at the angle sensor output terminals by the bandwidth factor shown in Equation (38).

Angular Tracing Error Due to Receiver Noise

The final problem is the formulation of the shift in the boresight direction of the antenna system which results from noise generated in the receiver. The derivations performed above make this a simple matter. The definition of the rms value of the angle tracking error is

$$\delta_{rms} \triangleq \frac{\text{Standard Deviation of } q_t \text{ at Boresight}}{\text{Slope of } \langle q_t \rangle \text{ at Boresight}}$$

or, symbolically

$$S = \frac{\sqrt{VAR\, \varepsilon_t}}{\left.\frac{d\langle \varepsilon_t \rangle}{d\theta}\right|_{\theta=0}} . \tag{39}$$

The numerator, obtained from Equation (36), is

$$\left.\sqrt{VAR\, \varepsilon_t}\right|_{\theta=0} = K|H(0)|\sqrt{\left(\frac{2B_n}{B_{IF}}\right)\left[\left(\frac{\sigma_\Delta}{\Sigma(0)}\right)^2 + \frac{2\sigma_\varepsilon^2\sigma_\Delta^2}{\Sigma^4(0)}\right]} \tag{40}$$

and the denominator is obtained from

$$\begin{aligned}\langle \varepsilon_t \rangle &= |H(0)|\langle c_t \rangle \\ &= K|H(0)|\frac{\Delta(\theta)}{\Sigma(\theta)}\end{aligned}$$

using Equation (20). Now

$$\frac{d\langle \varepsilon_t \rangle}{d\theta} = K|H(0)|\frac{d}{d\theta}\left[\frac{\Delta(\theta)}{\Sigma(\theta)}\right]$$

from which it follows that

$$\left.\frac{d\langle \varepsilon_t \rangle}{d\theta}\right|_{\theta=0} = K|H(0)|\left\{\frac{\left.\frac{d\Delta\theta}{d\theta}\right|_{\theta=0}}{\Sigma(0)}\right\} .$$

The term in braces is recognized as the angle sensor slope factor which is defined herein as

$$M \triangleq \frac{1}{\Sigma(0)}\left.\frac{d\Delta(\theta)}{d\theta}\right|_{\theta=0} . \tag{41}$$

The rms tracking error is now obtained from Equation (39) with the use of (40) and (41) as

$$S_{RMS} = \frac{\frac{\sqrt{2}\sigma_\Delta}{\Sigma(0)}\sqrt{\left(\frac{B_n}{B_{IF}}\right)\left[1 + \frac{2\sigma_\varepsilon^2}{\Sigma^2(0)}\right]}}{M} . \tag{42}$$

Recalling the definition of the sum channel SNR ratio at boresight

$$SNR_{\Sigma}(0) = \frac{\Sigma^2(0)}{2\sigma_{\Sigma}^2} = \frac{A^2/2}{kT_0 B_n F_{\Sigma}}$$

from Equation (8), and defining an equivalent difference channel SNR as

$$SNR_{\Delta}(0) = \frac{\Sigma^2(0)}{2\sigma_{\Delta}^2} = \frac{A^2/2}{kT_0 B_n F_{\Delta}}$$

results in (with $B_n = B_{IF}$, as shown earlier),

$$\delta_{RMS} = \frac{1}{M}\sqrt{\frac{B_n}{B_n}}\cdot\sqrt{\frac{1+SNR_{\Sigma}(0)}{SNR_{\Sigma}(0)\cdot SNR_{\Delta}(0)}}\,. \qquad (43)$$

When $\sigma_{\Sigma}^2 = \sigma_{\Delta}^2$, Equation (43) reduces to a value obtained by others, viz.,

$$\delta_{RMS} = \frac{1}{M}\sqrt{\frac{B_n}{B_n}}\cdot\sqrt{\frac{1+SNR_{\Sigma}(0)}{SNR_{\Sigma}(0)}}\,.$$

APPENDIX K

FORMULATION OF CORRELATION FUNCTION OF ANGLE SENSOR OUTOUT: NON-COHERENT DETECTION

It is shown in Appendix J that the process at the output of the angle sensor modeled there is given by

$$c(t) = \frac{K}{\mathcal{E}^2(\theta)}\left[\Delta(\theta)\mathcal{E}(\theta)+\eta_{\Delta c}(t)\mathcal{E}(\theta)+\eta_{\mathcal{E}c}(t)\Delta(\theta)+\eta_{\mathcal{E}c}(t)\eta_{\Delta c}(t)+\eta_{\mathcal{E}s}(t)\eta_{\Delta s}(t)\right] \quad (1)$$

It is the purpose of the material which follows to formulate the correlation function defined by

$$R_c(t,t+\tau) = \langle c(t)c(t+\tau)\rangle .$$

Clearly,

$$\left(\frac{\mathcal{E}^2}{K}\right)^2 R_c(t,t+\tau) = \langle\left[\Delta\mathcal{E}+\eta_{\Delta c}\mathcal{E}+\eta_{\mathcal{E}c}\Delta+\eta_{\mathcal{E}c}\eta_{\Delta c}+\eta_{\mathcal{E}s}\eta_{\Delta s}\right] \times\left[\Delta\mathcal{E}+\eta'_{\Delta c}\mathcal{E}+\eta'_{\mathcal{E}c}\Delta+\eta'_{\mathcal{E}c}\eta'_{\Delta c}+\eta'_{\mathcal{E}s}\eta'_{\Delta s}\right]\rangle \quad (2)$$

where Σ and Δ have been written for $\Sigma(\theta)$ and $\Delta(\theta)$ and the notation has been simplified by defining

$$\eta_t \triangleq \eta$$

and

$$\eta_{t+\tau} \triangleq \eta' .$$

The first step is to rewrite Equation (2) in the form

$$\left(\frac{\mathcal{E}^2}{K}\right)^2 R_c(t,t+\tau) = \langle(\Delta\mathcal{E})^2+\Delta\mathcal{E}\left[\eta_{\Delta c}\mathcal{E}+\eta_{\mathcal{E}c}\Delta+\eta_{\mathcal{E}c}\eta_{\Delta c}+\eta_{\mathcal{E}s}\eta_{\Delta s}\right] +\Delta\mathcal{E}\left[\eta'_{\Delta c}\mathcal{E}+\eta'_{\mathcal{E}c}\Delta+\eta'_{\mathcal{E}c}\eta'_{\Delta c}+\eta'_{\mathcal{E}s}\eta'_{\Delta s}\right] +\left[\eta_{\Delta c}\mathcal{E}+\eta_{\mathcal{E}c}\Delta+\eta_{\mathcal{E}c}\eta_{\Delta c}+\eta_{\mathcal{E}s}\eta_{\Delta s}\right] \times\left[\eta'_{\Delta c}\mathcal{E}+\eta'_{\mathcal{E}c}\Delta+\eta'_{\mathcal{E}c}\eta'_{\Delta c}+\eta'_{\mathcal{E}s}\eta'_{\Delta s}\right]\rangle .$$

Based upon the conditions imposed on the noise processes in Appendix J, the second and third of the four terms shown above vanish. Therefore.

$$\left(\frac{\mathcal{E}}{K}^2\right)^2 Re(t,t+\tau)-(\Delta\mathcal{E})^2 = \Big\langle \mathcal{E}\left[\mathcal{E}\,\eta_{ac}\eta'_{ac}+\Delta\,\eta_{ac}\eta'_{ec}+\eta_{ac}\eta'_{ec}\eta'_{ac}+\eta_{ac}\eta'_{es}\eta'_{as}\right]$$
$$+\Delta\left[\mathcal{E}\,\eta_{ec}\eta'_{ac}+\Delta\,\eta_{ec}\eta'_{ec}+\eta_{ec}\eta'_{ec}\eta'_{ac}+\eta_{ec}\eta'_{es}\eta'_{as}\right]$$
$$+\mathcal{E}\,\eta_{ec}\eta_{ac}\eta'_{ac}+\Delta\,\eta_{ec}\eta_{ac}\eta'_{ec}+\eta_{ec}\eta_{ac}\eta'_{ec}\eta'_{ac}+\eta_{ec}\eta_{ac}\eta'_{es}\eta'_{as}$$
$$+\mathcal{E}\,\eta_{es}\eta_{as}\eta'_{ac}+\Delta\,\eta_{es}\eta_{as}\eta'_{ec}+\eta_{es}\eta_{as}\eta'_{ec}\eta'_{ac}+\eta_{es}\eta_{as}\eta'_{es}\eta'_{as}\Big\rangle.$$

In all of those cases in which there is the product of three (gaussian) random variables, it can be shown that the expectation of that product is zero since the random variables all have mean zero. Also, when the product of two random variables occurs and they are associated with the sum and the difference channel, then their expectation is also zero. The following simplification results:

$$\left(\frac{\mathcal{E}}{K}^2\right)^2 Re(t,t+\tau)-(\Delta\mathcal{E})^2 = \Big\langle \mathcal{E}^2\eta_{ac}\eta'_{ac}+\Delta^2\eta_{ec}\eta'_{ec}+\eta_{ec}\eta'_{ec}\eta_{ac}\eta'_{ac}$$
$$+\eta_{ec}\eta_{ac}\eta'_{es}\eta'_{as}+\eta_{es}\eta_{as}\eta'_{ec}\eta'_{ac}$$
$$+\eta_{es}\eta_{as}\eta'_{es}\eta'_{as}\Big\rangle. \qquad (3)$$

Next, since the variables are all gaussian, it can be shown that

$$\langle \eta_{ec}\eta'_{ec}\eta_{ac}\eta'_{ac}\rangle = \langle \eta_{ec}\eta'_{ec}\rangle\langle \eta_{ac}\eta'_{ac}\rangle \qquad (4a)$$

$$\langle \eta_{ec}\eta_{ac}\eta'_{es}\eta'_{as}\rangle = \langle \eta_{ec}\eta'_{es}\rangle\langle \eta_{ac}\eta'_{as}\rangle \qquad (4b)$$

$$\langle \eta_{es}\eta_{as}\eta'_{ec}\eta'_{ac}\rangle = \langle \eta_{es}\eta'_{ec}\rangle\langle \eta_{as}\eta'_{ac}\rangle \qquad (4c)$$

$$\langle \eta_{\varepsilon s}\, \eta_{\Delta s}\, \eta'_{\varepsilon s}\, \eta'_{\Delta s} \rangle = \langle \eta_{\varepsilon s}\, \eta'_{\varepsilon s} \rangle \langle \eta_{\Delta s}\, \eta'_{\Delta s} \rangle \quad \text{(4d)}$$

with the use of the definitions

$$\langle \eta_{\Delta c}\, \eta'_{\Delta c} \rangle \triangleq R_{\Delta c}(\tau)$$
$$\langle \eta_{\varepsilon c}\, \eta'_{\varepsilon c} \rangle \triangleq R_{\varepsilon c}(\tau)$$
$$\langle \eta_{\Delta s}\, \eta'_{\Delta s} \rangle = R_{\Delta s}(\tau)$$
$$\langle \eta_{\varepsilon s}\, \eta'_{\varepsilon s} \rangle = R_{\varepsilon s}(\tau)$$

where the just-defined correlation function depends only on τ because the basic processes are stationary. With the use of Equation (4), Equation (3) then becomes

$$\left(\frac{\Sigma}{K}\right)^2 R_e(t, t+\tau) - (\Delta\varepsilon)^2 = \Sigma^2 R_{\Delta c}(\tau) + \Delta^2 R_{\varepsilon c}(\tau) + R_{\varepsilon c}(\tau) R_{\Delta c}(\tau) + \langle \eta_{\varepsilon c}\, \eta'_{\varepsilon s} \rangle \langle \eta_{\Delta c}\, \eta'_{\Delta s} \rangle + \langle \eta_{\varepsilon s}\, \eta'_{\varepsilon c} \rangle \langle \eta_{\Delta s}\, \eta'_{\Delta c} \rangle + R_{\varepsilon s}(\tau) R_{\Delta s}(\tau) .$$

Next, it can be shown that (Reference K-1)

$$\langle \eta_{\varepsilon c}\, \eta_{\varepsilon s'} \rangle = -\langle \eta_{\varepsilon s}\, \eta'_{\varepsilon c} \rangle$$

and

$$\langle \eta_{\Delta c}\, \eta'_{\Delta s} \rangle = -\langle \eta_{\Delta s}\, \eta'_{\Delta c} \rangle .$$

Also, it is the case that (Reference K-1)

$$R_{\Sigma c}(\tau) = R_{\Sigma s}(\tau) \triangleq R_{\Sigma}(\tau)$$

and

$$R_{\Delta c}(\tau) = R_{\Delta s}(\tau) \triangleq R_{\Delta}(\tau)$$

Therefore, Equation (5) can be written as

$$\left(\frac{\Sigma}{K}^2\right)^2 R_c(t, t+\tau) - (\Delta\Sigma)^2 = \Sigma^2 R_{\Delta}(\tau) + \Delta R_{\Sigma}(\tau) + 2R_{\Sigma}(\tau)R_{\Delta}(\tau) + 2\langle n_{\Sigma c} n'_{\Sigma s}\rangle\langle n_{\Delta c} n'_{\Delta s}\rangle .$$

A definition of all of the terms contained in Equation (6) is available (Reference K-1). Specifically,

$$R_{\Sigma}(\tau) = \int_{-\infty}^{\infty} S_{\Sigma}(f)\cos[2\pi(f-f_o)\tau]df$$

$$R_{\Delta}(\tau) = \int_{-\infty}^{\infty} S_{\Delta}(f)\cos[2\pi(f-f_o)\tau]df$$

$$R_{\Sigma,cs}(\tau) = \int_{-\infty}^{\infty} S_{\Sigma}(f)\sin[2\pi(f-f_o)\tau]df$$

$$R_{\Delta,cs}(\tau) = \int_{-\infty}^{\infty} S_{\Delta}(f)\sin[2\pi(f-f_o)\tau]df$$

where the definitions

$$R_{\Sigma,cs}(\tau) \triangleq \langle n_{\Sigma c} n'_{\Sigma s}\rangle$$

and

$$R_{\Delta,cs}(\tau) \triangleq \langle n_{\Delta c} n'_{\Delta s}\rangle$$

have been used. Also $S_{\Sigma}(f)$ and $S_{\Delta}(f)$ are the power spectral densities in the sum and difference channels. In most cases of interest, these spectral densities are even functions with respect to f_o, so that

$$R_{\Sigma,cs}(\tau) = R_{\Delta,cs}(\tau) = 0 .$$

Subject to this restriction, the correlation function of the process e(t) becomes

$$R_e(t, t+\tau) = R_e(\tau)$$

$$= \left(\frac{K}{\mathcal{E}^2}\right)^2 \left\{(\Delta\mathcal{E})^2 + \mathcal{E}^2 R_\Delta(\tau) + \Delta^2 R_\mathcal{E}(\tau) + 2R_\mathcal{E}(\tau)R_\Delta(\tau)\right\}.$$

APPENDIX L

ANALYSIS OF ANGLE SENSOR CHARACTERISTICS FOR COHERENT PROCESSING

The objectives of this appendix are identical to those of Appendix J except that the angle sensor model contains a phase-lock loop (from which the term coherent processing results). Specifically, this Appendix will:

1 Characterize the sensor output function

2 Relate the sensor characteristics to the field of view

3 Derive an expression for the angle tracking error due to receiver noise.

The sensor model, shown in Figure L-1, is identical to that employed for non-coherent processing except that: 1) the AGC voltage is derived from a product detector for which the inputs are the sum channel signal and the coherent reference signal, and 2) the error signal delivered to the servo system is obtained from a product detector which utilizes the same reference as well as the difference channel signal.

The AGC voltage, considered first, is related to the product of the sum channel signal and the coherent reference signal, i.e.,

$$u(t) = 2a(t) \cos \omega_o t \tag{1}$$

where

$$a(t) = \Sigma(\theta) \cos \omega_o t + \eta_\Sigma(t) \tag{2}$$

and the sum channel noise process has the form

$$\eta_\Sigma(t) = \eta_{\Sigma C}(t) \cos \omega_o t - \eta_{\Sigma S}(t) \sin \omega_o t. \tag{3}$$

When Equations (2) and (3) are inserted into (1) and the coefficients of the frequency terms $2\omega_o/2\pi$ are equated to zero, the result is

$$u(t) = \Sigma(\theta) + \eta_{\Sigma C}(t).$$

The first and second moments of the random variable u_t are seen to be

$$\langle u_t \rangle = \Sigma(\theta)$$

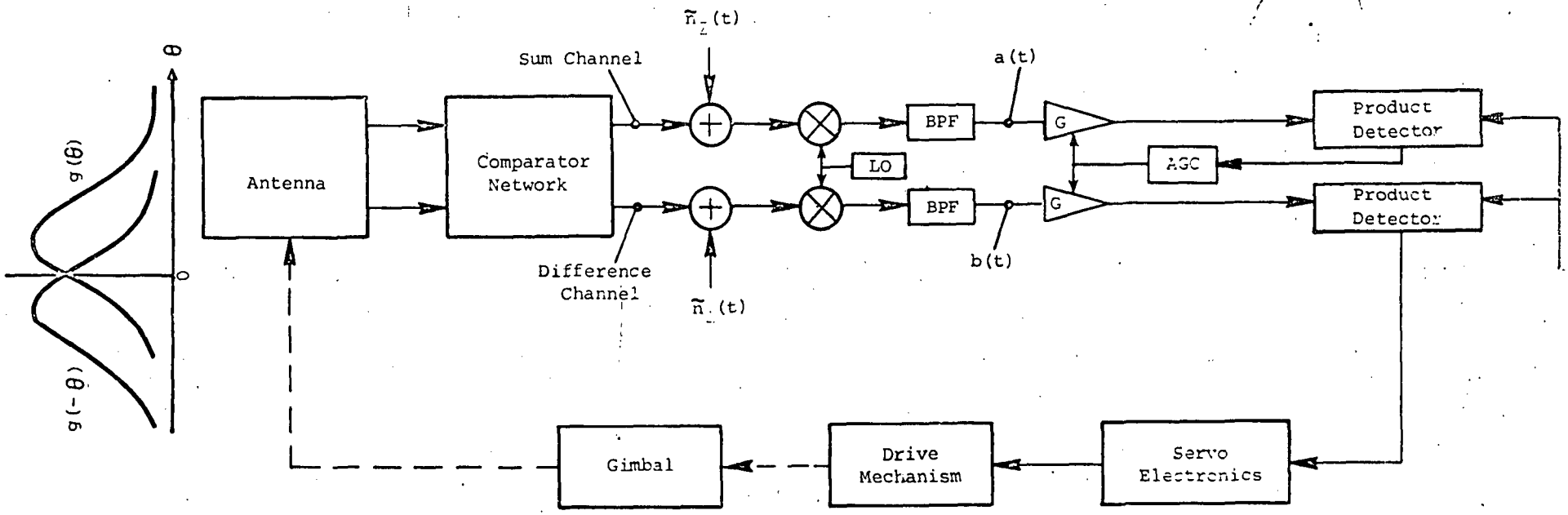

Figure L-1. Angle Sensor Model: Coherent Processing

and

$$\langle u_t^2 \rangle = \Sigma^2(\theta) + \sigma_\Sigma^2$$

from which it follows that

$$\text{var } u_t = \sigma_\Sigma^2 .$$

The smoothing action of the AGC filter will cause the variance to be reduced by a factor of $1/T_{AGC}\, B_{IF}$ to a negligibly small value with respect to u_t. (The use of a large AGC time constant has already been discussed in conjunction with non-coherent processing.) Therefore, the IF amplifier gain is not influenced by the sum channel noise fluctuations and it is the case that

$$G = \frac{K}{\Sigma(\theta)} .$$

Consideration is now given to the formulation of the error signal e(t) which is the product of the difference channel signal,

$$b(t) = \Delta(\theta) \cos \omega_o t + \eta_\Delta(t),$$

the IF amplifier gain, and the coherent reference signal. With frequency terms $2\omega_o/2_\pi$ removed, it is the case that

$$e(t) = K \left[\frac{\Delta(\theta) + \eta_{\Delta c}(t)}{\Sigma(\theta)} \right] .$$

Thus, e(t) consists of the desired output $K\Delta(\theta)/\Sigma(\theta)$ plus the additive noise waveform $KN_{\Delta c}(t)/\Sigma(\theta)$. Since $\eta_{\Delta c_t}$ is a gaussian random variable with mean zero and variance σ_Δ^2, it follows that e_t also exhibits a gaussian distribution with a mean value

$$\langle e_t \rangle = K \left[\frac{\Delta(\theta)}{\Sigma(\theta)} \right] \tag{4}$$

and a variance

$$\text{var } e_t = \left[\frac{K\sigma_\Delta}{\Sigma(\theta)} \right]^2 \tag{5}$$

The correlation function

$$R_e(t, t + \tau) = \langle e(t) e(t + \tau) \rangle$$

of the process e(t) is readily found to be

$$R_e(\tau) = \left[\frac{K}{\Sigma(\theta)}\right]^2 \left[\Delta^2(\theta) + R_\Delta(\theta)\right] \tag{6}$$

where

$$R_\Delta(\tau) = \sigma_\Delta^2 \left[\frac{\sin \pi B_{IF} \tau}{\pi B_{IF} \tau}\right]. \tag{7}$$

This complete the characterization of the angle sensor output process.

Sensor Field-of-View

As in the case of non-coherent processing, the noisiness of the sensor output

$$r_e(\theta) \triangleq \frac{\text{std. dev. } e_t}{\langle e_t \rangle} \tag{8}$$

is again employed as a tool in the determination of the sensor FOV. When Equations (4) and (5) are substituted into (8), the result is

$$r_e(\theta) = \frac{\sigma_\Delta}{\Delta(\theta)}$$

which can be put in the more convenient form

$$r_e(\theta) = \frac{1}{\sqrt{2\ SNR_\Delta(\theta)}} \left[\frac{1}{\Delta(\theta)/\Sigma(\theta)}\right]$$

where the difference channel SNR is defined in terms of the sum signal antenna pattern as

$$SNR_\Delta(\theta) \triangleq \frac{\Sigma^2(\theta)}{2\sigma_\Delta^2}.$$

If $\sigma_\Delta^2 = \sigma_\Sigma^2$, then $SNR_\Delta(\theta) = SNR_\Sigma(\theta)$. The form of $r_e(\theta)$ best suited for computation is

$$r_e(\theta) = \frac{1}{\sqrt{SNR_\Delta(o)}} \frac{1}{[g(\theta) + g(-\theta)]\ [\Delta(\theta)/\Sigma(\theta)]}$$

where $SNR_\Delta(\theta)$ is the on-boresight signal-to-noise ratio

$$SNR_\Delta(o) = \frac{A^2}{2\sigma_\Delta^2} .$$

Following the method utilized in Appendix J, the noisiness of the servo system output is defined as

$$r_q(\theta) \triangleq \frac{\text{std. dev } q_t}{\langle q_t \rangle}$$

and found to have the same functional form, viz.,

$$r_q(\theta) = \left(\frac{2\beta_n}{B_{IF}}\right) r_e(\theta) .$$

Angular Tracking Error Due to Receiver Noise

The procedures adopted in Appendix J are again employed in the formulation of the subject quantity for which the definition is

$$\delta_{rms} = \frac{\text{Standard Deviation of } q_t \text{ at Boresight}}{\text{Slope of } \langle q_t \rangle \text{ at Boresight}}$$

With

$$\text{var } q_t = K^2 \left(\frac{2\beta_n}{B_{IF}}\right) |H(o)|^2 \left[\frac{\sigma_\Delta^2}{\Sigma^2(\theta)}\right]$$

and

$$\frac{d\langle q_t \rangle}{d\theta} = KM|H(o)|$$

it follows that

$$\delta_{rms} = \frac{1}{M} \sqrt{\frac{\beta_n}{B_{IF}}} \cdot \frac{1}{SNR_\Delta(o)} .$$

REFERENCES

A-1 D. R. Rhodes. Introduction to Monopulse, McGraw-Hill Book Company, Inc., New York, 1959. p. 50.

H-1 P. W. Cramer. Large Spacecraft Antennas: Performance Comparison of Focal Point and Cassegrain Antennas for Spacecraft Applications, JPL Space Programs Summary No. 37-62. pp. 80-89.

I-1 W. L. Nelson. Phase-Lock Loop Design for Coherent Angle-Error Detection in the Telstar Satellite Tracking System. September 1963. BSTJ, Volume 42, pp. 1941-1976.

J-1 W. B. Davenport and W. L. Root. An Introduction to the Theory of Ramdom Signals and Noise. McGraw-Hill Book Company, Inc., New York, 1958. p.166.

J-2 A. Grumet. Demodulation Effect of an Envelope Detector at Low Signal-to-Noise Ratios, Proc. IRE. October 1962. pp.2133-2134.

K-1 W. B. Davenport and W. L. Root. An Introduction to the Theory of Random Signals and Noise. McGraw-Hill Book Company, Inc., New York, 1958. p. 162.